

# **WIND EFFECTS OF TALL BUILDING HAVING DIFFERENT CORNER CONFIGURATION USING CFD**

**Ph.D. THESIS**

*by*

**RAHUL KUMAR MEENA**



**DEPARTMENT OF CIVIL ENGINEERING  
DELHI TECHNOLOGICAL UNIVERSITY  
DELHI – 110042 (INDIA)  
DECEMBER, 2022**





# **WIND EFFECTS OF TALL BUILDING HAVING DIFFERENT CORNER CONFIGURATION USING CFD**

**A THESIS**

*Submitted in partial fulfilment of the  
requirements for the award of the degree*

*of*

**DOCTOR OF PHILOSOPHY**

*in*

**CIVIL ENGINEERING**

*by*

**RAHUL KUMAR MEENA**



**DEPARTMENT OF CIVIL ENGINEERING  
DELHI TECHNOLOGICAL UNIVERSITY  
DELHI – 110042 (INDIA)  
DECEMBER, 2022**

**©DELHI TECHNOLOGICAL UNIVERSITY, DELHI-2022  
ALL RIGHTS RESERVED**



# DELHI TECHNOLOGICAL UNIVERSITY DELHI

## CANDIDATE'S DECLARATION

I hereby certify that the work which is being presented in the thesis entitled “**WIND EFFECTS OF TALL BUILDING HAVING DIFFERENT CORNER CONFIGURATION USING CFD**” in partial fulfilment of the requirements for the award of the Degree of Doctor of Philosophy and submitted in the Department of Civil Engineering of the Delhi Technological University, Delhi is an authentic record of my own work carried out during a period from August, 2018 to April, 2022 under the supervision of Dr. Ritu Raj, Assistant Professor and Dr. S.Anbukumar, Professor, Department of Civil Engineering, Delhi Technological University, Delhi, India.

The matter presented in this thesis has not been submitted by me for the award of any other degree or any other Institution.

**(RAHUL KUMAR MEENA)**

This is to certify that the above statement made by the candidate is correct to the best of my (our) knowledge.

**(Prof. S. Anbukumar)**  
**Joint-Supervisor**

**(Dr. Ritu Raj)**  
**Supervisor**

Date: December 20, 2022

## ACKNOWLEDGEMENT

I would like to express my great pleasure and acknowledgement to those people who have supported me and extended their help to complete this thesis. The completion of this thesis was possible with the support of several people. I would like to express my feeling of grateful acknowledgment for them in the following lines.

First of all, I would like to express my deepest sense of gratitude, special thanks and appreciation to my supervisor **Dr. Ritu Raj, Assistant Professor** for his kind support, I will never forget your incredible support during my PhD journey, especially on days when I felt directionless and lethargic since you were there for me like a big brother. You are an excellent motivator, a strong leader, and a man who is always seeking new passions and endeavors. No words could possibly explain how grateful I am to him for his support and cooperation. I would also like to express my heartfelt gratitude to my joint supervisor, **Dr. S. Anbukumar, Professor**, Department of Civil Engineering, Delhi Technological University, Delhi, for their expert guidance, valuable suggestions, unwavering cooperation, and assistance throughout the research. Once again, I want to express my gratitude to my supervisor **Dr. Ritu Raj** for providing the necessary and unwavering guidance that greatly aided into my thesis and made it possible for it to be presented in its current form.

I truly appreciate the assistance received by the department head, Prof. V.K. Minocha, during my PhD journey. I am always respectful to him. The cooperation and help extended by the Heads and faculty members, Department of Civil Engineering, Delhi Technological University, Delhi is gratefully acknowledged. I also want to express my special thanks to SRC members Prof. Mehtab Alam, Department of Civil Engineering, Jamia Milia Islamia, Delhi and Prof. Munish Bharadwaj, Department of Civil Engineering, IGNOU, New Delhi. Dr. P.K. Goyal, Associate Professor, Department of Civil Engineering, and Dr. M. S. Niranjana Associate Professor, Department of Mechanical Engineering at Delhi Technological University, Delhi for proving me insightful and constructive comments.

I would like to express my great appreciation and thanks to the staff in the Earthquake Engineering laboratory and Computer Aided Design Laboratory, Department of Civil Engineering. I especially thank my lab-assistant Mr. Sanjay, Mr. Mahesh and also Mr. Pankaj for their continuous assistance during the course of simulation work.

I would also like to thank all my fellow friends Dr. Manvendra Verma, Dr. Supriya Pal, Dr. S. K. Nagar, Dr. Deepak Singh, Mr. Arun Sinha, Mr. Abhishek Prakash Paswan, Mr. Harshit

Kumar Jayant, Mr. Indrajeet Singh, Ms. Shamabalid Ahedy, Mrs. Arti Rhea, Mrs. Kiran Cholak, Mr. Rahul Kumar, Mr. Mohit Gupta, Mr. Vikash, Mr. Prashant C. Ramateke, Mr. Nitin Lambha, Ms. Istuti Singh, Mr. Parvesh Kumar, and Mr. Sushant Kumar for providing their valuable suggestions and help whenever they were approached.

I want to express my gratitude to Ms. Chitrakshi Meena, a research scholar in the department of environmental engineering, for her warm words of appreciation. I also like to express my gratitude to Dr. Shailendra Yadav for his insightful advice.

I would also want to thank my juniors Mrs. Kiran Cholak, Mr. Prateek Roshan, Mr. Dharmendra, Mr. Vijay Kaushik, Ms. Payal devi, Mr. Deepak Sharma, Ms. Noopur, Mr. Aniket Sharma, Mr. Rishbah Tyagi and Mr. Amit Ram Ahirwar for their unwavering support.

Last but not least, I am grateful to few of my juniors, Nikhil Gaur, Hemant Gautam, and Sonia Kumari, for giving brilliant ideas at the start of my research work , which have always helped me throughout the Journey.

Last but not least, I would want to express my heartfelt thanks to Mr. Prasenjit Sanyal for constantly assisting me at each level of my journey in resolving the major problem in my numerical simulation and answering all of my doubts whenever I contacted him.

**Ms. Bhagya Jayant**, who makes a special effort to detect typographical errors, and numerous b. tech. students Particular thanks should be extended to Mr. Shrey Srivastav, Ms. Dharishti Thappa, and M. Tech. student Ms. Daisy Singh for completing the thesis on time.

I am thankful from the core of my heart to my reverend parents, **Shri Lala Ram Meena** and **Smt. Dholi Devi Meena** for their blessing to see this day. My thanks are also to my sister **Asha Meena** and **Aparna Meena** and my brother **Mr. Ramavtar Meena**, also to my bhabi Mrs. Sunita Meena for their moral and emotional support. A special thanks for my cousins Mr. Dinesh Meena, Rythem Meena, Nirma Meena and my Friend Mr. Goverdhan Lal Meena and Mr. Ramakant Saini supported me every time during the journey. I shall always be grateful to my friend **Mr. Abhishek Prakash Paswan** for his efforts and support during this Ph.D. Journey. At the end, I am thankful and grateful to all those who supported me for bringing this day in my life.

**(RAHUL KUMAR MEENA)**

## ABSTRACT

Population is increasing at an exponential rate and availability of the land in the regular shape is limited. Hence structural designer needs the developed the irregular plan shape tall buildings also because of the huge population, now a days structural designers are shifting to develop the tall buildings. Tall building which are coming up all around the world is serving the purpose of residential and commercial. Tall building is best suitable for residential, institutional, industrial and assembly purposes. These buildings are constructed in regular and irregular shape this is mainly due to the constraint in the availability of regular shape land. Because of irregular land the building at present time is constructed in irregular cross-sectional shape, tall building need investigation of wind effects on such irregular shape buildings. Available information regarding wind pressure coefficients on different type of building is not updated in the codal provision and international standards are silent about the various type of irregular cross-sectional shape. As the height increase the wind load increases and wind load becomes the governing criteria for the design of tall buildings hence the investigation of wind effects is necessary for such tall buildings.

As the flow pattern around the tall building is generally varies as per the plan cross sectional shape and thus creating the change in pressure distribution. Also, a quantum of change in the wind angle changes the distribution of pressure on a high-rise building. Investigation of wind effects is required for high rise buildings, as shape changes and since there is very few numbers of studies are available for equal area building having the regular and irregular shape. Wind tunnel tests and computational fluid dynamic (CFD) are the only possible solution as on today to evaluate the wind loads on a high-rise building. Aim of the present study is to investigate the wind effects on tall building models with varying cross-sectional shape in CFD simulation to measure wind generated effects.

In the present study, high-rise buildings with eight types of building models are considered and the available information about corner modification of equal dimensions is very limited. In this entire study the comparison of equal area building having “rectangular” and “Y” shape is performed and the modification of same corners such as corner cut, chamfer and fillet of equal dimensions is applied in plan cross sectional shape. Wind effect are investigated using ANSYS CFX, 2020 and results are presented in various forms like pressure is represented in the form of contours while the pressure distribution along the

peripheral distance of building and pressure on the vertical center line of each face is represented using graphs. Many more results are depicted in various graphical forms and critical values are tabulated.

In this numerical study, the models of high-rise buildings with different corner configuration are made at a scale of 1:200. These models are numerically investigated for wind effects in the domain having the dimension as, from top of the building model to top of the domain is at 5H, while both sides are kept at 5H, inlet is placed at 5H from the building model and the outlet is provided as 15H, where H is the height of the building model. The numerical simulation is done using k- $\epsilon$  turbulence model. The pressure data is exported by ANSYS CFX post processing, the data of pressure is exported by the creating the set of lines which act as pressure tapping and are configured with the experimental procedure adopted in the wind tunnel testing.

The models are investigated in a numerical simulation having a total length of domain as 20 H such domain dimensions are kept so that the wind flow recirculation can be prevented. The prototype buildings are considered to be situated in a sub urban terrain with well scattered objects having height between 1.5 m to 10 m, defined as Terrain Category 2 in IS: 875 (Part-3) 2015. Turbulence is defined as medium turbulence and wind speed is modelled according to power law which is applied at the inlet of the domain.

Wind pressure distribution on the surface of all eight model is measured using ANSYS CFX post processing for varying wind incidence angle starting from  $0^{\circ}$  to  $180^{\circ}$  at an interval of  $15^{\circ}$ . The various corner configuration such as corner cut, chamfer and fillet are having the same dimensions in both (regular and irregular buildings) type of high-rise building model. Wind pressure on each surface is represented in the form of contours with label so that the designer can use such pressure contours while designing the corresponding type of building.

Values of mean wind pressure coefficients ( $C_p$ ) are evaluated from the measured values of wind pressures at each surface of the tall building. Results of the study are presented in the form of contours and cross-sectional variation of  $C_p$  for each building model. The results are also presented in the graphical form for peripheral distribution of pressure around the model at top one third which is at 500 mm height from the base of the model and second is presented at mid height of the model which is at 375 mm from the base of the model while the pressure along the peripheral distance at bottom one third which is at 250 mm from the

ground is presented. The result of pressure along the vertical center lines at each face is also presented in the graphical form while the result of wind force and moment coefficient is presented for eight building models for varying wind incidence angle starting from  $0^{\circ}$  to  $180^{\circ}$  at the interval of  $15^{\circ}$ .

The results presented in the present study can be used in future for the revision of codal recommendations about wind loads on high-rise buildings with different corner configuration. These can also be used by the architects and structural designers while designing such building of equal cross-sectional area.



# LIST OF CONTENTS

## 1. Contents

CANDIDATE’S DECLARATION .....	i
ACKNOWLEDGEMENT .....	ii
ABSTRACT .....	iv
LIST OF CONTENTS .....	vii
LIST OF FIGURES .....	xii
LIST OF TABLES .....	xx
LIST OF PHOTOGRAPHS .....	xxi
NOTATIONS AND SYMBOLS .....	xxii
CHAPTER 1 .....	1
INTRODUCTION .....	1
1.1 General .....	1
1.2 Wind Load.....	1
1.3 Modelling .....	3
1.4 Experimental Study .....	4
1.5 CFD .....	4
1.6 Need of The Study .....	5
1.7 Objective of Study .....	6
1.8 Outline of thesis .....	8
CHAPTER 2 .....	9
LITERATURE REVIEW .....	9
2.1 General .....	9
2.2 Codal Provision.....	9
2.2.1 American Standards (ASCE 7-16).....	9
2.2.2 Indian Standards (IS 875:part-3:2015) .....	9
2.2.3 Australia and New Zealand Standards (AS/NZS 1170.2:2011) .....	10
2.2.4 The European Union (EN 1991-1-1:2005 (E)).....	10
2.2.5 Ethiopian Standards (ES ISO 4354:2012 (E)) .....	12

2.2.6	Hong Kong Standards (HK CP WIND).....	12
2.3	Recent Research Study.....	12
2.3.1	Experimental Studies.....	12
2.3.2	CFD studies.....	24
2.4	Limitations.....	44
CHAPTER 3	.....	45
Methodology.....	.....	45
3.1	General.....	45
3.2	Numerical Simulation.....	45
3.2.1	Computational Fluid Dynamics (CFD).....	45
3.2.1.1	Governing Flow equation.....	45
3.2.1.2	Navier Stokes Equation.....	46
3.2.2	Turbulence model.....	47
3.2.2.1	Zero-Equation Model.....	48
3.2.2.2	Two- Equation Model.....	48
•	k- $\epsilon$ turbulence model.....	48
•	k- $\omega$ Turbulence model.....	50
•	Shear Stress Transport (SST).....	51
3.3	Geometry.....	52
3.4	Meshing.....	56
3.5	CFX Pre.....	58
3.5.1	Grid Independent Test.....	58
3.5.2	Velocity profile.....	59
3.5.3	Turbulent Intensity.....	61
3.5.4	Boundary Conditions.....	62
3.6	Solver.....	64
3.7	CFD Post.....	65
3.8	Validation.....	71
3.8.1	Validation model:.....	72

CHAPTER 4.....	79
Results and Discussion on Rectangular Shape with Corner Configuration .....	79
4.1 General .....	79
4.2 Rectangle Shape with Simple Corners.....	79
4.2.1 Pressure contours .....	79
4.2.2 Vertical Pressure Distribution along the height of Building.....	83
4.2.3 Horizontal Pressure Distribution along the peripheral Distance of Building .....	89
4.2.4 Force Coefficients.....	93
4.2.5 Moment Coefficients .....	94
4.2.6 External Pressure Coefficients.....	95
4.3 Rectangle Shape with Corner cuts .....	97
4.3.1 Pressure contours .....	97
4.3.2 Vertical Pressure Distribution along the Height of Building.....	105
4.3.3 Horizontal Pressure Distribution along the Peripheral Distance of Building.....	110
4.3.4 Force coefficients.....	114
4.3.5 Moment coefficients .....	115
4.3.6 External Pressure Coefficient .....	116
4.4 Rectangle Shape with Chamfer Corners .....	118
4.4.1 Pressure contours .....	118
4.4.2 Vertical Pressure Distribution along the Height of Building.....	122
4.4.3 Horizontal Pressure Distribution along the Peripheral Distance of Building.....	127
4.4.4 Force Coefficients.....	131
4.4.5 Moment Coefficients .....	132
4.4.6 External Pressure Coefficients.....	133
4.5 Rectangle Shape with Fillet in Corners.....	134
4.5.1 Pressure contours .....	134
4.5.2 Vertical Pressure Distribution along the Height of Building.....	138
4.5.3 Horizontal Pressure Distribution along the Peripheral Distance of Building.....	143
4.5.4 Force Coefficients.....	147

4.5.5	Moment Coefficients .....	148
4.5.6	External Pressure Coefficients .....	149
4.6	Comparative study of $C_{fx}$ at $0^0$ and $90^0$ wind incidence angles .....	150
CHAPTER 5	.....	151
Results and Discussion Y-Shape with Corner Configuration	.....	151
5.1	General .....	151
5.2	Y-shape with simple Corners .....	151
5.2.1	Pressure Contours .....	151
5.2.2	Vertical Pressure Distribution along the Height of the Building .....	165
5.2.3	Horizontal Pressure Distribution along the Peripheral Distance of Building .....	173
5.2.4	Force Coefficients .....	179
5.2.5	Moment Coefficients .....	180
5.2.6	External Pressure Coefficients .....	181
5.3	Y-shape with Corner Cuts .....	183
5.3.1	Pressure Contours .....	183
5.3.2	Vertical Pressure Distribution along the Height of the Building .....	197
5.3.3	Horizontal Pressure Distribution along the Peripheral Distance of Building .....	205
5.3.4	Force Coefficients .....	211
5.3.5	Moments Coefficients .....	212
5.3.6	External Pressure Coefficients .....	213
5.4	Y-shape with Chamfer Corners .....	215
5.4.1	Pressure Contours .....	215
5.4.2	Vertical Pressure Distribution along the Height of the building .....	229
5.4.3	Horizontal Pressure Distribution along the Peripheral Distance of Building .....	237
5.4.4	Force Coefficients .....	243
5.4.5	Moment Coefficients .....	244
5.4.6	External Pressure Coefficients .....	245
5.5	Y-shape with Fillet in Corners .....	247
5.5.1	Pressure Contours .....	247

5.5.2	Vertical Pressure Distribution along the Height of the Building.....	261
5.5.3	Horizontal Pressure Distribution along the Peripheral Distance of Building.....	269
5.5.4	Force Coefficients.....	275
5.5.5	Moment Coefficients .....	276
5.5.6	External Pressure Coefficients.....	277
5.6	Comparative Study of $C_{fx}$ at $0^0$ and $180^0$ wind incidence angle .....	279
CHAPTER 6 .....		281
Conclusion .....		281
6.1	Pressure measurement.....	281
6.2	Force measurement .....	285
6.3	RECOMMENDATIONS TO CODE OF PRACTICE .....	288
6.4	RECOMMENDATIONS FOR FUTURE RESEARCH.....	288
REFERENCES .....		289
LIST OF PUBLICATIONS .....		300

## LIST OF FIGURES

<b>Figure No.</b>	<b>Description</b>	<b>Page No.</b>
Figure.1.1	Isometric view of building models	7
Figure:2.1	Force coefficient for rectangular clad buildings in uniform flow	11
Figure.3.1	Plan View of regular shape model	52
Figure.3.2	Plan View of Irregular Y- shape model	53
Figure.3.3	Isometric View of regular shape model	54
Figure.3.4	Isometric View of irregular Y-shape model	55
Figure 3.5	Different Meshing; (a) Building Meshing; (b) Domain Meshing and (c) Inflation	57
Figure 3.6	Variation of velocity profile with height	60
Figure 3.7	Variation of Turbulent intensity with height	62
Figure 3.8	Isometric view of domain used in the numerical simulation	63
Figure 3.9	Plan view of domain used in the numerical simulation	64
Figure 3.10	Isometric view of the regular shape building model having vertical centre line	66
Figure 3.11	Isometric view of the irregular shape building model having vertical centre line	67
Figure 3.12	Isometric view of the regular shape model having horizontal peripheral lines	69
Figure 3.13	Isometric view of the irregular shape model having horizontal peripheral lines	70
Figure 3.14	Plan Cross sectional shape of validation model	72
Figure 3.15	Mean pressure coefficient comparison with various international standards and experimental studies on the rectangular shape model	74
Figure 3.16	Mean pressure coefficient comparison with various international standards and experimental studies on the corner cut model	75

Figure 3.17	Mean pressure coefficient comparison with various international standards and experimental studies on the irregular Y- shape model	76
Figure 3.18	Square shape validated model	77
Figure 4.1	Distribution of wind pressure coefficient on the rectangle with simple corners at $0^0$ wind incidence angle	80
Figure 4.2	Distribution of wind pressure coefficient on the rectangle with simple corners at $15^0$ wind incidence angle	80
Figure 4.3	Distribution of wind pressure coefficient on the rectangle with simple corners at $30^0$ wind incidence angle	81
Figure 4.4	Distribution of wind pressure coefficient on the rectangle with simple corners at $45^0$ wind incidence angle	81
Figure 4.5	Distribution of wind pressure coefficient on the rectangle with simple corners at $60^0$ wind incidence angle	82
Figure 4.6	Distribution of wind pressure coefficient on the rectangle with simple corners at $75^0$ wind incidence angle	82
Figure 4.7	Distribution of wind pressure coefficient on the rectangle with simple corners at $90^0$ wind incidence angle	83
Figure 4.8	Mean pressure distribution on the vertical center line for rectangle with simple corners	88
Figure 4.9	Mean pressure distribution along the peripheral distance of the rectangle with simple corners	92
Figure 4.10	Wind force coefficient for the rectangle with simple corners	93
Figure 4.11	Wind moment coefficient for the rectangle with simple corners	94
Figure 4.12	Distribution of wind pressure coefficient on the rectangle with corner cut at $0^0$ wind incidence angle	98
Figure 4.13	Distribution of wind pressure coefficient on the rectangle with corner cut at $15^0$ wind incidence angle	99
Figure 4.14	Distribution of wind pressure coefficient on the rectangle with corner cut at $30^0$ wind incidence angle	100
Figure 4.15	Distribution of wind pressure coefficient on the rectangle with corner cut at $45^0$ wind incidence angle	101
Figure 4.16	Distribution of wind pressure coefficient on the rectangle with corner cut at $60^0$ wind incidence angle	102

Figure 4.17	Distribution of wind pressure coefficient on the rectangle with corner cut at $75^0$ wind incidence angle	103
Figure 4.18	Distribution of wind pressure coefficient on the rectangle with corner cut at $90^0$ wind incidence angle	104
Figure 4.19	Mean pressure distribution on the vertical center line for rectangle with corner cut	109
Figure 4.20	Mean pressure distribution along the peripheral distance of the rectangle with corner cut	113
Figure 4.21	Wind Force coefficient of the rectangle with corner cut	114
Figure 4.22	Moment coefficient of the rectangle with corner cut	115
Figure 4.23	Distribution of wind pressure coefficient on the rectangle with chamfer corner cut at $0^0$ wind incidence angle	119
Figure 4.24	Distribution of wind pressure coefficient on the rectangle with chamfer corner cut at $15^0$ wind incidence angle	119
Figure 4.25	Distribution of wind pressure coefficient on the rectangle with chamfer corner cut at $30^0$ wind incidence angle	120
Figure 4.26	Distribution of wind pressure coefficient on the rectangle with chamfer corner cut at $45^0$ wind incidence angle	120
Figure 4.27	Distribution of wind pressure coefficient on the rectangle with chamfer corner cut at $60^0$ wind incidence angle	121
Figure 4.28	Distribution of wind pressure coefficient on the rectangle with chamfer corner cut at $75^0$ wind incidence angle	121
Figure 4.29	Distribution of wind pressure coefficient on the rectangle with chamfer corner cut at $90^0$ wind incidence angle	122
Figure 4.30	Mean pressure distribution on the vertical centre line for rectangle with chamfer corner cut	126
Figure 4.31	Mean pressure distribution along the peripheral distance of the rectangle with chamfer corner cut	130
Figure 4.32	Wind Force coefficient of the rectangle with chamfer corner	131
Figure 4.33	Wind moment coefficient of the rectangle with chamfer corner	132
Figure 4.34	Distribution of wind pressure coefficient on the rectangle with fillet corner at $0^0$ wind incidence angle	135
Figure 4.35	Distribution of wind pressure coefficient on the rectangle with fillet corner at $15^0$ wind incidence angle	135



Figure 4.36	Distribution of wind pressure coefficient on the rectangle with fillet corner at $30^{\circ}$ wind incidence angle	136
Figure 4.37	Distribution of wind pressure coefficient on the rectangle with fillet corner at $45^{\circ}$ wind incidence angle	136
Figure 4.38	Distribution of wind pressure coefficient on the rectangle with fillet corner at $60^{\circ}$ wind incidence angle	137
Figure 4.39	Distribution of wind pressure coefficient on the rectangle with fillet corner at $75^{\circ}$ wind incidence angle	137
Figure 4.40	Distribution of wind pressure coefficient on the rectangle with fillet corner at $90^{\circ}$ wind incidence angle	138
Figure 4.41	Mean pressure distribution on the vertical centre line for rectangle with fillet corner	142
Figure 4.42	Mean pressure distribution along the peripheral distance of the rectangle with fillet corner	146
Figure 4.43	Wind Force coefficient of the rectangle with fillet corners	147
Figure 4.44	Wind Moment coefficient of the rectangle with fillet corners	148
Figure 4.45	Figure 4.45 $C_{fx}$ for the regular shape building model	150
Figure 5.1	Distribution of wind pressure coefficient on the Y-shape with simple corner at $0^{\circ}$ wind incidence angle	152
Figure 5.2	Distribution of wind pressure coefficient on the Y-shape with simple corner at $15^{\circ}$ wind incidence angle	153
Figure 5.3	Distribution of wind pressure coefficient on the Y-shape with simple corner at $30^{\circ}$ wind incidence angle	154
Figure 5.4	Distribution of wind pressure coefficient on the Y-shape with simple corner at $45^{\circ}$ wind incidence angle	155
Figure 5.5	Distribution of wind pressure coefficient on the Y-shape with simple corner at $60^{\circ}$ wind incidence angle	156
Figure 5.6	Distribution of wind pressure coefficient on the Y-shape with simple corner at $75^{\circ}$ wind incidence angle	157
Figure 5.7	Distribution of wind pressure coefficient on the Y-shape with simple corner at $90^{\circ}$ wind incidence angle	158
Figure 5.8	Distribution of wind pressure coefficient on the Y-shape with simple corner at $105^{\circ}$ wind incidence angle	159

Figure 5.9	Distribution of wind pressure coefficient on the Y-shape with simple corner at $120^0$ wind incidence angle	160
Figure 5.10	Distribution of wind pressure coefficient on the Y-shape with simple corner at $135^0$ wind incidence angle	161
Figure 5.11	Distribution of wind pressure coefficient on the Y-shape with simple corner at $150^0$ wind incidence angle	162
Figure 5.12	Distribution of wind pressure coefficient on the Y-shape with simple corner at $165^0$ wind incidence angle	163
Figure 5.13	Distribution of wind pressure coefficient on the Y-shape with simple corner at $180^0$ wind incidence angle	164
Figure 5.14	Mean pressure distribution on the vertical centre line for Y shape with simple corner	172
Figure 5.15	Mean pressure distribution along the peripheral distance of the Y-shape with simple corner	178
Figure 5.16	Wind force coefficient of the Y-shape with simple corners	179
Figure 5.17	Wind moment coefficient of the Y-shape with simple corners	180
Figure 5.18	Distribution of wind pressure coefficient on the Y-shape with corner cut at $0^0$ wind incidence angle	184
Figure 5.19	Distribution of wind pressure coefficient on the Y-shape with corner cut at $15^0$ wind incidence angle	185
Figure 5.20	Distribution of wind pressure coefficient on the Y-shape with corner cut at $30^0$ wind incidence angle	186
Figure 5.21	Distribution of wind pressure coefficient on the Y-shape with corner cut at $45^0$ wind incidence angle	187
Figure 5.22	Distribution of wind pressure coefficient on the Y-shape with corner cut at $60^0$ wind incidence angle	188
Figure 5.23	Distribution of wind pressure coefficient on the Y-shape with corner cut at $75^0$ wind incidence angle	189
Figure 5.24	Distribution of wind pressure coefficient on the Y-shape with corner cut at $90^0$ wind incidence angle	190
Figure 5.25	Distribution of wind pressure coefficient on the Y-shape with corner cut at $105^0$ wind incidence angle	191
Figure 5.26	Distribution of wind pressure coefficient on the Y-shape with corner cut at $120^0$ wind incidence angle	192

Figure 5.27	Distribution of wind pressure coefficient on the Y-shape with corner cut at 135 <sup>0</sup> wind incidence angle	193
Figure 5.28	Distribution of wind pressure coefficient on the Y-shape with corner cut at 150 <sup>0</sup> wind incidence angle	194
Figure 5.29	Distribution of wind pressure coefficient on the Y-shape with corner cut at 165 <sup>0</sup> wind incidence angle	195
Figure 5.30	Distribution of wind pressure coefficient on the Y-shape with corner cut at 180 <sup>0</sup> wind incidence angle	196
Figure 5.31	Mean pressure distribution on the vertical centre line for Y shape with corner cut	204
Figure 5.32	Mean pressure distribution along the peripheral distance of the Y-shape with corner cut	210
Figure 5.33	Wind force coefficient of the Y-shape with corner cut	211
Figure 5.34	Wind moment coefficient of the Y-shape with corner cut	212
Figure 5.35	Distribution of wind pressure coefficient on the Y-shape with chamfer corner at 0 <sup>0</sup> wind incidence angle	216
Figure 5.36	Distribution of wind pressure coefficient on the Y-shape with chamfer corner at 15 <sup>0</sup> wind incidence angle	217
Figure 5.37	Distribution of wind pressure coefficient on the Y-shape with chamfer corner at 30 <sup>0</sup> wind incidence angle	218
Figure 5.38	Distribution of wind pressure coefficient on the Y-shape with chamfer corner at 45 <sup>0</sup> wind incidence angle	219
Figure 5.39	Distribution of wind pressure coefficient on the Y-shape with chamfer corner at 60 <sup>0</sup> wind incidence angle	220
Figure 5.40	Distribution of wind pressure coefficient on the Y-shape with chamfer corner at 75 <sup>0</sup> wind incidence angle	221
Figure 5.41	Distribution of wind pressure coefficient on the Y-shape with chamfer corner at 90 <sup>0</sup> wind incidence angle	222
Figure 5.42	Distribution of wind pressure coefficient on the Y-shape with chamfer corner at 105 <sup>0</sup> wind incidence angle	223
Figure 5.43	Distribution of wind pressure coefficient on the Y-shape with chamfer corner at 120 <sup>0</sup> wind incidence angle	224
Figure 5.44	Distribution of wind pressure coefficient on the Y-shape with chamfer corner at 135 <sup>0</sup> wind incidence angle	225

Figure 5.45	Distribution of wind pressure coefficient on the Y-shape with chamfer corner at $150^0$ wind incidence angle	226
Figure 5.46	Distribution of wind pressure coefficient on the Y-shape with chamfer corner at $165^0$ wind incidence angle	227
Figure 5.47	Distribution of wind pressure coefficient on the Y-shape with chamfer corner at $180^0$ wind incidence angle	228
Figure 5.48	Mean pressure distribution on the vertical centre line for Y shape with chamfer corner	236
Figure 5.49	Mean pressure distribution along the peripheral distance of the Y-shape with chamfer corner	242
Figure 5.50	Wind force coefficient of the Y-shape with chamfer corner	243
Figure 5.51	Wind moment coefficient of the Y-shape with chamfer corner	244
Figure 5.52	Distribution of wind pressure coefficient on the Y-shape with fillet corner at $0^0$ wind incidence angle	248
Figure 5.53	Distribution of wind pressure coefficient on the Y-shape with fillet corner at $15^0$ wind incidence angle	249
Figure 5.54	Distribution of wind pressure coefficient on the Y-shape with fillet corner at $30^0$ wind incidence angle	250
Figure 5.55	Distribution of wind pressure coefficient on the Y-shape with fillet corner at $45^0$ wind incidence angle	251
Figure 5.56	Distribution of wind pressure coefficient on the Y-shape with fillet corner at $60^0$ wind incidence angle	252
Figure 5.57	Distribution of wind pressure coefficient on the Y-shape with fillet corner at $75^0$ wind incidence angle	253
Figure 5.58	Distribution of wind pressure coefficient on the Y-shape with fillet corner at $90^0$ wind incidence angle	254
Figure 5.59	Distribution of wind pressure coefficient on the Y-shape with fillet corner at $105^0$ wind incidence angle	255
Figure 5.60	Distribution of wind pressure coefficient on the Y-shape with fillet corner at $120^0$ wind incidence angle	256
Figure 5.61	Distribution of wind pressure coefficient on the Y-shape with fillet corner at $135^0$ wind incidence angle	257
Figure 5.62	Distribution of wind pressure coefficient on the Y-shape with fillet corner at $150^0$ wind incidence angle	258

Figure 5.63	Distribution of wind pressure coefficient on the Y-shape with fillet corner at $165^{\circ}$ wind incidence angle	259
Figure 5.64	Distribution of wind pressure coefficient on the Y-shape with fillet corner at $180^{\circ}$ wind incidence angle	260
Figure 5.65	Mean pressure distribution on the vertical centre line for Y shape with fillet corner	268
Figure 5.66	Mean pressure distribution along the peripheral distance of the Y-shape with fillet corner	274
Figure 5.67	Wind force coefficient of the Y-shape with fillet corner	275
Figure 5.68	Wind moment coefficient of the Y-shape with fillet corner	276
Figure 5.69	Figure 5.69 $C_{fx}$ for the irregular shape building model	279

## LIST OF TABLES

Table No.	Description	Page No.
Table: 2.1	Wind Pressure Coefficients on Rectangular Clad Building	10
Table 3.1	Grid convergence test result for model-A	59
Table 3.2	Comparison of average face pressure coefficient ( $C_p$ ) on the Rectangular Tall Building	77
Table-4.1	External Pressure Coefficients for model-A (Rectangle Simple)	96
Table-4.2	External Pressure Coefficients for model-B (Rectangle Corner-Cut)	117
Table: -4.3	External Pressure Coefficient for Building Model-C (Rectangular Chamfer)	133
Table: 4.4	External Pressure Coefficient for Building Model-D (Rectangular Fillet)	149
Table: 5.1	External Pressure Coefficients for model-E (Y-Shape)	182
Table: 5.2	External Pressure Coefficient for Building Model-F (Y-shape having Chamfer)	214
Table:5.3	External Pressure Coefficient for Building Model-G (Y-shape Fillet)	246
Table: 5.4	External Pressure Coefficient for Building Model-H (Y-shape Chamfer)	278

## LIST OF PHOTOGRAPHS

<b>Image. No.</b>	<b>Description</b>	<b>Page No.</b>
Image. 1.1	Image. 1.1 Various Type of Tall Buildings	2

## NOTATIONS AND SYMBOLS

A	Effective frontal area of building
B	Breadth of building
h	Height of the building
$P_d$	Design wind velocity pressure
s	Spacing between buildings
V	Mean velocity of wind at any height
$V_d$	Design wind velocity
$V_b$	Basic wind speed
$V_{ref}$	Mean wind velocity measured at boundary layer depth in the wind tunnel
$\alpha$	Power law index
$\rho$	Density of air
$\theta$	Wind direction
$\nu$	Kinematic viscosity of air
$C_{pe}$	External wind pressure coefficients
$C_p$	Mean Wind Pressure Coefficients
FST	Free Stream Turbulence
k- $\epsilon$	k-epsilon turbulence model
SST	Shear stress transport turbulence model
k- $\omega$	k-omega turbulence model
DNS	Direct numerical simulation
BAF	Building amplification factor
LES	Large eddy simulation
FEM	Finite element method
TTU	Texas tech university building
GVE	Global venturi effect
LVE	Local venturi effect
CAARC	Commonwealth advisory aeronautical council building
RANS	Reynold average Navier stock
PSD	Power spectrum density
CFD	Computational fluid dynamics



# CHAPTER 1

## INTRODUCTION

### 1.1 General

There is a rapid increase in population and land availability in regular shape is reducing at very fast rate. To cope with this problem high rise buildings are designed. Tall buildings need special attention on design loads in case of wind load. Estimation wind effects on tall buildings is to be investigated using wind tunnel test and CFD tests. Wind engineering for the tall building involves complex turbulent flow conditions around bluff bodies.

### 1.2 Wind Load

Wind load is a force acting on a building's elevations when the wind blows against the building. Wind load is frequently the main load in case of the designing tall buildings, and it is primarily a horizontal force. The shape and size of the building, as well as the wind velocity, affect the wind load. On the windward side, the wind causes overpressure, whereas on the leeward side, the wind creates suction. Because wind tunnel tests are time-consuming and expensive, computational fluid dynamics is now a valuable tool for estimating wind loads on tall buildings.

Computational fluid dynamics can be used in many aspects of building design, offering accurate and fast simulations of a building's performance in terms of wind flow, pressure, and other variables. To assess a variety of field factors such as wind velocity, pressure, and turbulence intensity, wind tunnel testing necessitates a pricey equipment and sophisticated sensors. The fact that such measurements are limited to a few selected points inside the test section, severely unstable complicated phenomena like vortex shedding and turbulence wake, is a major constraint.

Modeling of buildings involves a considerable number of variables, including height, plan cross sectional shape, building shape, distance between nearby structures, wind incidence angles, topographical factors, and many metrological conditions. There is a common misperception that wind loads on a building are less severe when it is surrounded by other structures than when it is isolated. Many works done earlier in the field of wind engineering include wind pressure characteristics, wind flow, dynamic response, interference effect etc. for tall as well as low rise buildings. Various tall buildings are shown in Image. 1.1 Various Type of Tall Buildings.



**Petronas Twin**



**Park Avenue**



**The 42 Kolkata**



**Willis Tower**



**Zifeng Tower**



**Burj Khalifa**



**KK 100**



**Wuhan Center**



**CITIC Tower**

**Image. 1.1 Various Type of Tall Buildings**

### 1.3 Modelling

Investigation of wind effects on high rise structures is possible through two available methods that is wind tunnel test and CFD. Wind load is evaluated using the following expressions provided in the Indian Standards [IS: 875 (part-3): 2015]

Design wind speed

$$V_z = V_b K_1 K_2 K_3 K_4 \quad (1)$$

Where;

$V_b$  = Basic wind speed;

$K_1$  = Probability factor;

$K_2$  = Terrain, height and structure size factor;

$K_3$  = Topography factor and

$K_4$  = Importance factor for cyclonic region.

Design wind pressure

$$P_z = 0.6 \times V_z^2 \quad (2)$$

Where;

$P_z$  = Wind pressure at height Z, in N/m<sup>2</sup>

$V_z$  = Design wind speed at height Z in m/s

$$P_d = K_d K_a K_c P_z \quad (3)$$

Where;

$K_d$  = Wind directionality factor;

$K_a$  = Area averaging factor and

$K_c$  = Combination factor.

The value of  $P_d$  shall not be taken less than 0.70  $P_z$

Force and pressure method

$$F = (C_{pe} - C_{pi})AP_d \quad (4)$$

Where;

$F$  = Wind force

$C_{pe}$  = External pressure coefficient

$C_{pi}$  = Internal pressure coefficient

$A$  = Effective area of structure

$P_d$  = Design wind pressure

$$F = C_f AP_d \quad (5)$$

Where;

$F$  = Wind force

$C_f$  = Force coefficient

$A$  = Effective area of structure

$P_d$  = Design wind pressure

#### **1.4 Experimental Study**

Investigation of wind effects on tall building is necessary because the available international wind standards and past studies are limited for regular structures. The present study compares the wind effects on tall building by keeping the equal ratio of corner configuration such as corner cut, chamfer and fillet for exactly same plan area and height for both (regular and irregular) tall buildings model. Such investigation of wind effects can be performed using wind tunnel test or by CFD technique.

#### **1.5 CFD**

Computational fluid dynamics (CFD) analyses the wind effects on tall building of various cross sections while this numerical simulation needs the validation of results with experimental data as well as with different international standards. CFD is generate the solution after dividing the

building geometry into elements. Elements are of different shape which depends on the type of meshing, meshing independent test are the pre-requisite of the numerical simulation, the solution obtained using the numerical simulation is mainly dependent on the definition of flow parameters which are set before the starting of the numerical simulation.

CFD simulation also require to monitor the output during the simulation using display monitors where the imbalances are plotted in the form of residual in x, y and z- direction. The observation of Reynold's number and various other parameter are made at this stage. Once the simulation is performed the results can be presented using CFD post some results are then exported and the procedure explained as in the wind tunnel manual and report no 67 is followed to present the results.

## **1.6 Need of The Study**

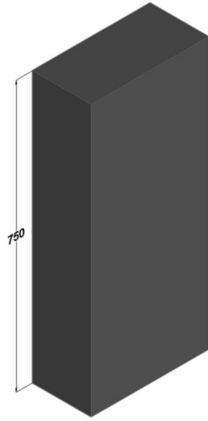
Wind load is varying as per the shape and size of high-rise structure, with the increment in the hight of the structure wind load becomes critical for tall building, hence for each type of tall building wind effects need to be investigated. For this purpose, wind tunnel test and CFD simulation is performed on such structures. Most of the structural designer use the data available in the international standards and past studies where there is no comparison is present for equal area building having the regular and irregular shape. Most of the available studies are either compare the effect on regular or irregular shape structure while the present studies compare the results of wind generated effects on both type of building model. Available literature till date discusses the effect of equal ratio of modification provided into the tall building to reduce the wind effects.

The present study investigates the wind effects on the building having corner configuration of recessed, fillet and chamfer corner and the ratio of modification are kept same for regular and irregular shape model. Most of the available land is not in the regular shape so such studies will be provided the designer a confidence of selecting the shape of building as it compares the two-shape having same area and height of the model. The unique "Y" shape mainly serves to redirect the wind flow, save material, and improve antithetic. The tri axial symmetry of Y-shape is best suited model for the commercial purposes as this provides the maximum view to the out-side area and the area between the limbs is can facilitate for various other utilities. That is why the shape of structure are selected as Y and rectangular.

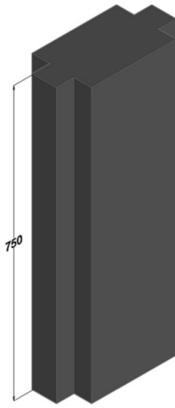
## 1.7 Objective of Study

The current study is about investigating the wind effects on tall building having different corner configuration. In this study wind effects are investigated on equal area building with same height. The tall building models having regular and irregular shape are considered. To analyse the result of wind effects on tall building having equal cross-sectional area and equal ratio of corner modification such as corner cut, chamfer and fillet are examined. The available international standards are limited for the regular shapes only that is why in this study the analysis of wind effect is performed on regular and irregular shape building model using computational fluid dynamic (CFD). The shape of the evaluated models is depicted in Figure. 1.1 Isometric view of building models. The objective of the present study is in the following points.

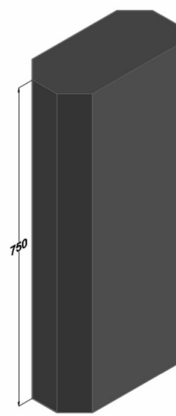
- To study the effects of different corner configuration on Y plan shaped building and same plan area building on different corner configuration on rectangular building will be compared.
- To obtain Wind forces including base shear and base moments acting on all models by numerical simulation using ANSYS.
- To find the flow field around the Y-plan shape and rectangular plan shape building models with different corner configuration
- To measure the drag and force coefficients from the values of forces.
- To study the effect of wind incidence angle and wind forces by allowing the wind to hit the models at many angles.
- To study the wind pressure distribution on the surface of all building models.



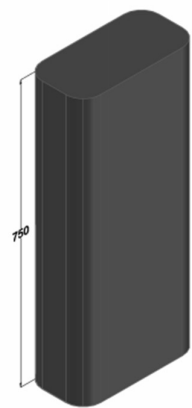
**Model-A**



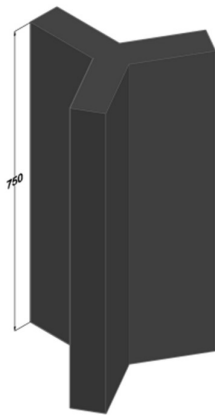
**Model-B**



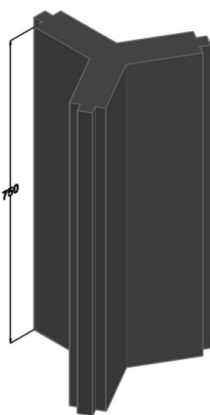
**Model-C**



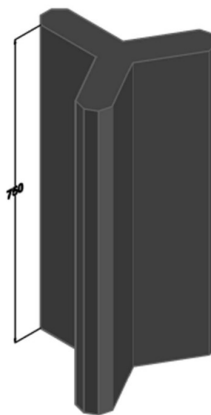
**Model-D**



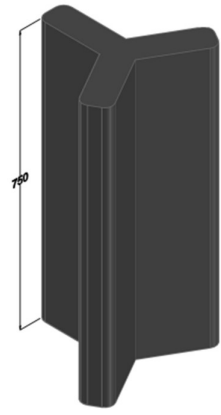
**Model-E**



**Model-F**



**Model-G**



**Model-H**

(All dimensions are in mm)

**Figure. 1.1 Isometric view of building models**

## 1.8 Outline of thesis

- The current research work is explained in 6 chapters in this thesis.
- **CHAPTER 1** gives a brief introduction to wind induced response on high rise structure with the objective and scope of the present study.
- Knowledge regarding numerical and experimental studies for determining wind force, pressure and responses of structure on tall building of various shape are enumerated in **CHAPTER 2**.
- **CHAPTER 3** cover the details of model and numerical simulation of investigating the wind effects on tall buildings using CFD.
- **CHAPTER 4** present the result of numerical simulation performed on a rectangular plan shape structure having different corner configuration.
- **CHAPTER 5** presents the result of numerical simulation performed on an irregular Y-shape having different corner configuration.
- The observation and conclusions drawn from the present study are summarized in **CHAPTER 6**. Scope of future research work is also included in this chapter.
- Publications made during the present study are listed in the end of the thesis.



# CHAPTER 2

## LITERATURE REVIEW

### 2.1 General

Objective of the present research work is to find the effect of wind on the tall building model having corner modification in the equal area building and same height model. The investigation of wind effects is performed using numerical simulation ANSYS CFX for the varying wind incidence angle starting from  $0^0$  to  $180^0$  at an interval of  $15^0$ . The validation of numerical result is performed in this study while the results of external  $C_p$  is compared with the data available in various international standards and different experimental results.

### 2.2 Codal Provision

Various international standards are available for wind load to investigate the wind effects on the tall building but such standards are having impediment of regular shapes. The present study investigates the wind effects on corner configuration of regular and irregular shape building.

#### 2.2.1 American Standards (ASCE 7-16)

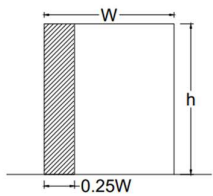
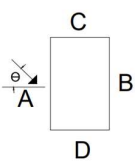
The American standards [1] discuss the important steps in the modelling of wind for low rise and high rise building. Code is silent about the skewed wind angles and the corner effects are also not evaluated by the standards. Although various data for the wind design is available for low rise buildings. However, the code is not discussing about the irregularity of the building model.

#### 2.2.2 Indian Standards (IS 875:part-3:2015)

Indian standards [2] is used for the present study to model the wind speed and the explanatory hand book [3] available on this international standards is utilized for the depth understanding of the wind behaviour. Clause 6.3 provides the design wind speed while Table: 5 (clause 7.3.3.1) discusses about the external pressure coefficient for various types of building models. Such available data for pressure is used for numerical verification and this is also used to validate the study. The pressure coefficient for the wind incidence angle  $0^0$  and  $90^0$  is available and for the rectangular model is presented in tabular form. The data is also presented in the present code in the form of force coefficient in clause 7.4.2.1, typical values are presented in the Table: 2.1 Wind Pressure Coefficients on Rectangular Clad Building. The force coefficients are explained in the

Figure:2.1 Force coefficient for rectangular clad buildings in uniform flow [2] for the isolated building.

**Table: 2.1 Wind Pressure Coefficients on Rectangular Clad Building**  
**[Clause 7.3.3.1, IS 875(part-3,2015)]**

Building Height Ratio	Building Plan Ratio	Elevation	Plan	Wind Angle $\Theta$	C <sub>p</sub> for Surface				Local C <sub>pe</sub>
					A	B	C	D	
$\frac{3}{2} < \frac{h}{w} < 6$	$\frac{3}{2} \leq \frac{l}{w} < 4$			0	+0.7	-0.4	-0.7	-0.7	-1.2
				90	-0.5	-0.5	+0.8	-0.1	

### 2.2.3 Australia and New Zealand Standards (AS/NZS 1170.2:2011)

The external pressure coefficient is also presented for rectangular building in this international standards [4], however the codal provisions are limited and do not specify the values but recommends the use of linear interpolation for the intermittent data.

### 2.2.4 The European Union (EN 1991-1-1:2005 (E))

The international standards [5] provides many important parameters which need to be considered before the modelling of wind such as terrain category, roughness length etc. which considerably affect the distribution of wind loads on tall and low rise building.

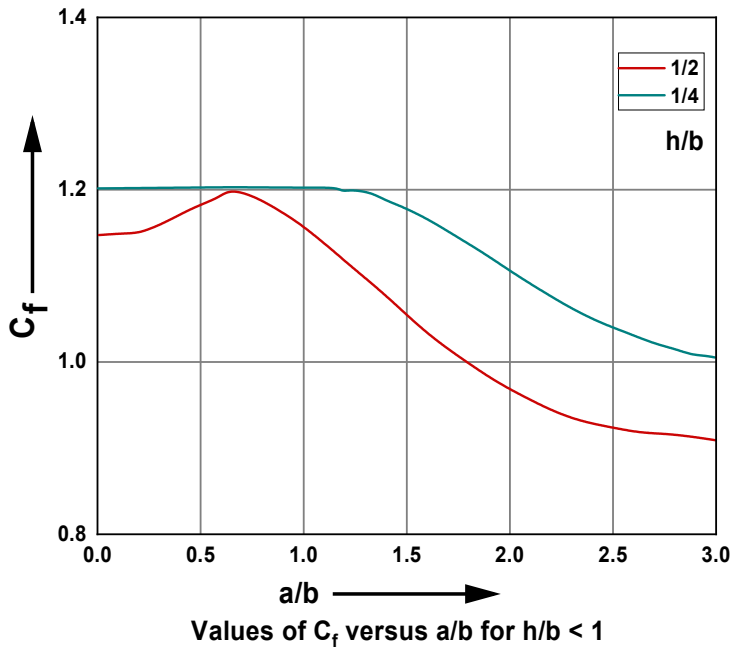
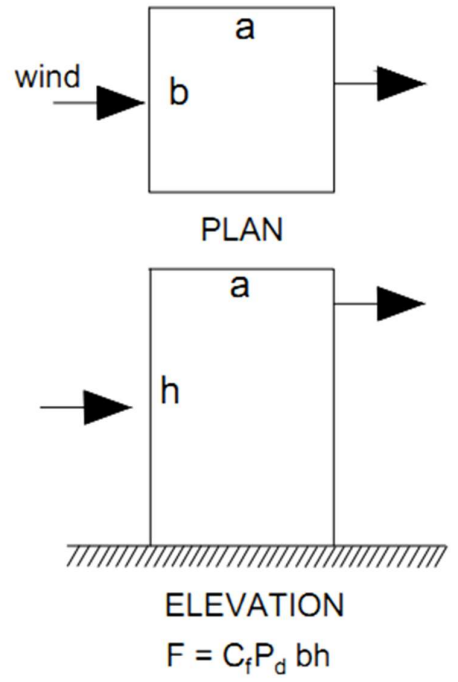
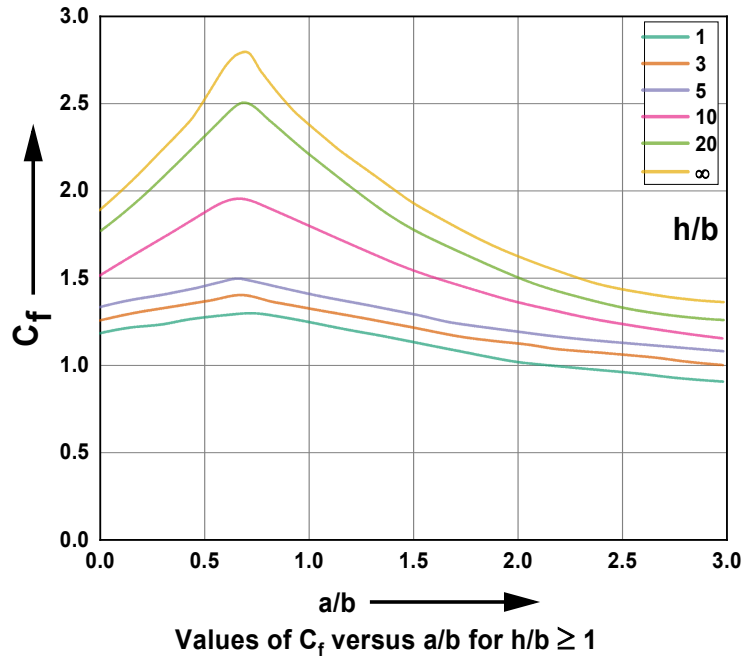


Figure:2.1 Force coefficient for rectangular clad buildings in uniform flow [2]  
 [(Clause 7.4.2.1, Fig. 4), IS: 875 (part-3); 2015]

### **2.2.5 Ethiopian Standards (ES ISO 4354:2012 (E))**

Ethiopian standards [6] also discuss the external pressure coefficient for wind load design which can further be used to validate the study. The study deals with wind load design factor which needs calibration of the flow physics and for the same purpose different international standards prove to be good. Present standards provide details on the terrain roughness and dynamic response.

### **2.2.6 Hong Kong Standards (HK CP WIND)**

The Hong Kong standard [7] on wind suggest the requirement of wind tunnel testing to obtained the response of structure with respect to wind along with some important features of wind dynamic behaviour. The effect of proximity on the instrumented model affects the behaviour pattern for wind pressure. Although this international standard suggested the model scale limitations on the geometric scale and velocity scale. A general guideline is that the building model with sharp corners will have the Reynold number based on the typical breadth of the building and it should not be less than  $1 \times 10^4$ .

## **2.3 Recent Research Study**

### **2.3.1 Experimental Studies**

**Sheng et al. [8]** conducted the experiment using wind tunnel at a scale of 1: 300 on high rise building and investigated the pressure load under atmospheric boundary layer flow, it was observed that inlet conditions are effecting the velocity and turbulent intensity profile. Front face is always under the effect of upstream flow while the lateral faces are in vortex shedding, wind behaviour is different for different ground conditions.

**Sun et al. [9]** wind tunnel tests were performed to investigate the pressure distribution on super high rise building and numerical simulation is also performed on same model, the grid study was performed by accounting the upstream wind velocity, interval and blockage ratio. Upstream wind speed and grid blockage ratio is affected by downstream wind speed while interval is mainly influencing the turbulence intensity. With the increase in the height, largest peak positive pressure increases while the smallest peak negative pressure decreases.

**Li et al. [10]** conducted the experiment using wind tunnel test on “L” shape model and observed that terrain category has little effect on the mean torque coefficient in all wind directions, RMS torque coefficient increases with increase in the wind velocity. The mean and RMS base torsional moment coefficients varying with approaching wind direction are in consistent patterns with that of torque coefficient. The mean base torsional moment coefficient ranges from -0.14 to 0.28 and the RMS base torsional moment coefficient vary from 0.009 to 0.065 in all wind directions.

**Mooneghi and Kargarmoakhar [11]** presented a review on reducing wind load using shape optimization because generally shape of building is influenced by architectural drawing, aerodynamic modification are applied to reduce the wind effects by breaking the flow streamlines around the building model or by changing the flow patterns in the downstream wind. The wind effects can be reduced by using the various available methods to reduce the effect of wind such as by changing the external shape of the building so that the flow patterns in the downstream of wind can be changed and because of this the wake is reduces in the downstream wind direction.

**Yi and Li [12]** presented and analysed the result for a combined wind tunnel test and full scale study of the wind effects on super tall building and point out that the interference effect from the surrounding buildings were significantly dependent on the incident wind directions. The magnitude of the mean force coefficients in the along wind direction are greater than across wind direction and the effect of shielding can be reduced by increasing the height of the tall building. Mean wind force coefficient decreases as the ground roughness increases and dynamic response of wind increases with the increase in the mean wind speed.

**Carassale et al. [13]** experimentally investigated the aerodynamic behaviour of square cylinder with rounded corners and measured the Reynold number, varies from  $1.7 \times 10^4$  to  $2.3 \times 10^5$ . The introduction of rounded and chamfered corner has often positive effect to reduce the drag and fluctuations in the transverse force generated due to the vortex shedding. Sharp corner square cylinder, produce separate flow conditions.

**Kwon and Kareem [14]** investigated the overall loads and generally consistent in the along wind response, but more scattered in the across wind response, as explained the causes of the variations and similarities in the wind loads and their consequences on tall buildings. The discrepancy among the result provided in various international standards can be eliminated by using same velocity profile.

**Bandi et al. [15]** experimentally investigated the aerodynamic characteristics on six high rise building model in boundary layer wind tunnel. The values for mean wind force is higher for triangular model in comparison to square section model. The local wind force coefficient of  $180^0$  helical and  $360^0$  helical models varied greatly with height, which helps to reduce the total wind force coefficient for helical models.

**Tanaka et al. [16]** experimentally evaluated the aerodynamic force and wind pressure acting on a tall building with various unconventional configurations, Reynold number also varied based on the mean wind velocity and width of the square model. For the corner cut model large negative wind pressures occurs at the leading edge of the side surface and their distribution varies greatly from the leading edge and trailing edge. For  $180^0$  helical model, weak vortices with wide band are shed irregularly throughout the height and this result in the better aerodynamic behaviour.

**Merrick and Bitsuamlak [17]** investigated the shape effect on the wind induced response of high-rise building of various shape like square, circular, triangular, rectangular and elliptical. Some shapes are highly prone to adverse wind effects such as vortex shedding which can generate the high dynamic load which controls the design parameters. Elliptical, triangular and rectangular shaped buildings were found highly susceptible to high torsion loading.

**Irwin [18]** experimentally evaluated the wind effects on bluff body and concluded that the flow around the bluff bodies is due to the formation of strong vortices in their wakes, also this is largely influenced the impact of the wind on tall buildings. The base moment and base shear at the base can be reduced up to 25 % by modifying the corner shape of the building model. The opening reduces the negative pressure in the wake region in fair amount and that generate significant saving in the structure due to reduced wind loads in both drag and across wind directions.

**Kawai [19]** investigated the corner modification on tall building in wind tunnel test, various corner modification such as corner cut, recession and roundness was investigated. Corner roundness is effective to increases the aerodynamic damping to suppress the instability. Building with square or rectangular sections are generally susceptible to aero elastic instabilities in turbulent boundary layer flow, because approaching flow separates from the windward corner of the building and forms strong vortices by rolling up of the separated shear layer. Modification of windward corner is very effective to reduce the drag and lift by changing the flow patterns which effects various flow characteristics such as reattachment and thus narrowing the width of the wake generated in the downstream of wind. The suppression of the aero elastic instability by the

small corner cut and recession does not come from the suppression of the vortex shedding but from the increases of the aerodynamic damping.

**Zaki et al.** [20] investigated the wind flow inside a two side wind catcher building. The test is performed experimentally as well as the numerically and the simulation is performed using the k- $\epsilon$  turbulence model. The effect of two different surface terrains and two different locations of the wind catcher building, above the tunnel floor were investigated. The effect of the terrains on the pressure coefficients inside the windward and leeward ducts were found to be insignificant. The numerical turbulence model k- $\epsilon$  model shows the better results with the experimental results.

**Miyashita et al.** [21] estimated the wind induced response of high rise buildings of square shape with chamfer corner was investigated using wind tunnel test. Wind induced vibration are controlled by cutting the corners and making the effective opening in model. The across wind fluctuating wind force coefficient of a model with corner cuts or opening is smaller than the model having square plan shape in the case of  $0^\circ$  wind incidence angle. The combined value for the displacement which was obtained using the wind force correlation is large than the combined value of the maximum value plus standard deviation in the case of the angle for the wind incidence angle  $10^\circ$ .

**Hayashida and Iwasa** [22] effect of building plan shape on aerodynamic forces and displacement response have been studied for super high rise building with an height of 600 m in a wind tunnel using rigid model. The square shape of corner cutting shows the smaller peak of power spectrum in comparison to normal square shape. Vortex shedding can be controlled using the corner cutting and a large displacement were obtained in the model having the square plan shape in comparison to other type of plan shape minimum displacement were found in the case of the model having the triangular plan shape.

**Kwok et al.** [23] investigated the effect of edge configuration using experimental method of wind tunnel and obtained the wind induced response on tall building model. Slotted corner and chamfered corner and combination of these two caused the significant reduction in both the along wind and across wind responses. It was concluded that the slotted corner and in particular chamfered corner are effective in reducing both the along wind and cross wind responses of a tall building with a rectangular cross-sectional shape. Strength of vortex shedding for chamfer corner is reduced in comparison of slotted corner in the case of the cross-wind direction.

**Bhattacharya et al.** [24] presented the pressure distribution on various face of “E” plan shaped tall buildings under wind load and conducted the experimental and numerical study. The obtained pressure is different from square plan shape model. The maximum positive pressure of 0.8 is obtained in the case of  $180^{\circ}$  wind while the largest negative pressure of -0.68 is found in the case of  $90^{\circ}$  wind. Numerical results may vary for different meshing properties and different meshing sizes. The pressure distribution is largely depending on the plan shape of those tall buildings.

**Bhattacharyya and Dalui** [25] performed experimental and numerical analysis on “E” shape tall building, symmetrical faces are having the same pressure distribution pattern. Error calculated between numerical simulation result and experimental result and found under the permissible limit. Proposed a general equation of pressure distribution for the particular face of the building model in case of “E” shape model. The similar pressure distribution observed on similar face for these two-wind incidence angle. A change in flow pattern is observed in the case of  $30^{\circ}$  and  $120^{\circ}$  wind incidence angle. Generated flow pattern in such case is directly influencing the pressure variation in the wake region of building.

**Zaki et al.** [26] performed the wind tunnel experiment on a single zone building with a two side wind catcher and a window. Mean and fluctuating surface pressure are measured to investigate the effect of the turbulent on set flows on a building ventilation. The building exterior could significantly affect the inlet flow through roof top wind catchers openings. The window is essential when operating windcatchers as it enhances the flow rates significantly.

**Kwok** [27] conducted a wind tunnel test to investigate the effect of the wind on the tall building having rectangular cross section shape. It was found that horizontal slots, slotted corners and chamfered corners caused a significant reduction in both along and across wind response. With the incident wind is on wide face of the building, the cross-wind force spectra will have high peak at the critical location. Reduced wind speed in case of the incident wind is normal to the narrow face of the building the peak in the cross-wind force spectra were broadened and much less prominent. For the building with chamfered corner this peak cease to exist. The modified building shape were tested to reduce the considerable amount of the magnitude of cross wind excitation force.

**Stathopoulos** [28] experimental investigation of ground level wind conditions around building with chamfered corner was performed in boundary layer wind tunnel. Experiment was performed on two shapes of tall building of square and chamfer corner by varying the height of the model. Chamfering of corner at  $45^{\circ}$  were result in greater reduction in the size of strong wind area in the



corner region. Chamfer corner has little effect on the turbulence condition in the corner region and chamfer corner affects the flow separation and reduce the turbulence on the windward face. As the height of the building is increases wind velocities and the size of the strong wind area in the corner stream of both square and chamfers building increases whereas turbulence conditions are not much affected.

**Lam and Lam** [29] presented a comparative study of the wind pressure distribution on a full scale building and a wind tunnel model. With low-speed wind tunnels it is difficult to simulate atmospheric turbulence to an acceptable scale, which is essential in determining the fluctuating wind force acting on a structure. Nevertheless, low speed wind tunnel testing without elegant turbulence simulation can yield useful design information on time averaged wind loads. Most of the essential characteristics such as the position of maximum mean wind pressure and special features due to shielding effects of adjacent obstruction, can be reproduced in the wind tunnel.

**Raj and Ahuja** [30] An open circuit boundary wind tunnel test was conducted to investigate the effects of wind loads on cross shape tall buildings with varied cross sectional shapes on equal floor area buildings. Wind load on a building is maximum when it experiences maximum exposed area to direct wind incidence. The cross-sectional shape of the building alters the wind loads acting on the building. The rise in the values of these forces as compared to square section reflects on the cross-sectional shape of the building. Wind loads also changes as the wind incidence angle varies.

**Lam and Lam** [31] performed the assessment of wind loading on the cladding of high rise buildings, In the design of cladding for a multistorey building it would appear that the gust speed method of the British code is likely to provide lower pressure values than the mean wind approach of the Canadian Code. These lower pressure values are likely to be close to the actual average values of local pressure or suction applied to the cladding. Higher pressure values may occur at isolated positions in the cladding caused by the influence of nearby building or other obstacles. These localized higher values are of the order of magnitude predicted by the Canadian code. For the present, a design method based on  $C_p$  would seem to be suitable on the understanding that isolated positions of higher pressure represent a modest encroachment on the factor of safety inherent in the design of the cladding.

**Jozwiak et al.** [32] presented the wind tunnel investigations of the aerodynamic interference effects on pressure distributions on a building adjacent to another one. Tests were carried out on the model at the length scale of 1: 100 scale, were set up behind a turbulent flow development.

It has been found that for some wind direction local values of the external pressure coefficient on the leeward wall in case of interfering building, may be 2.5 times higher than on isolated building. This may also lead to reverse draught in natural ventilation system of apartment buildings. Significant difference in pressure distribution with and without modelling of the boundary layer, as well as the demonstrated strong interference between neighbouring building, confirm the need for this type of research and indicate the necessity of not only modelling the boundary layer, but also the close surroundings are required.

**Blackmore** [33] the role of wind tunnel testing in the design of building structures was examined. Wind forces are dynamic and fluctuate in nature, and their magnitude and position are constant. Wind loads are expressed as assumed uniform static loads for generic building types in most recent wind codes. These standardised values are sufficient for the majority of building structures. In certain situations, the code expressly recommends the use of experimental methods, which include the results of correctly conducted wind tunnel testing. When wind loading data is necessary in greater depth than the system allows, experimental approaches should be used.

**Blessmann and Riera** [34] conducted the extensive wind tunnel study of wind effects on two square prisms with a height to base length equal to six. In comparison to the isolated building, buffeting causes a 30 % increase in the maximum force coefficient. Because of the upwind structure, the maximum torsional moment coefficient can be enhanced threefold.

**Amin and Ahuja** [35] presented a review on aerodynamic modification to the building for reduce the wind load, in case of high rise structure a tall building oscillation are observed in across wind and along wind. The wind effects on the tall building are reduced by various type of aerodynamic modification techniques are applied as active and passive devices. Buildings openings at top significantly reduces the along wind and cross wind forces. Tapering effect is more effective to reduce the across wind effects than the along wind response. The roundness in the corner is more effective to reduce the aero elastic instability for the square building.

**Tamura and Miyagi** [36] investigated the effect of the corner modification on aerodynamic forces, the separated shear layer approach on the side surface with corner cutting and corner rounding thus promoting reattachment and reduction of drag forces. For uniform flow the value of RMS is have some reduction in the values for two-dimensional cylinder in the comparison of three-dimensional cylinder. The effect of Karman vortices and the resulting lift force are not so large for three-dimensional cylinder. Reattachment of the separated shear layers is promoted by

corner modification and the behaviour of the shear layers separated from modified corners is more sensitive to turbulence intensity than for a square cylinder.

**Verma et al.** [37] experimentally investigated the wind effects on the square plan tall building by varying the wind incidence angle. The pressure increased with height for most of the wind incidence angle in case of positive pressure. The negative pressure increased from windwards edge to leeward edge in the case of  $0^0$  wind incidence angle. Face average  $C_p$  and pressure distribution on the face is significantly varies from the international standards values.

**Sharma et al.**[38] presented the review on mitigation of wind load on tall building through various modification. Chamfering, rounding, recession, and slotted corners, for example, are effective techniques for reducing wake of approximately to 30%. Alteration of the flow structure depends on the type and extent of modification it is well known that the corner modification alters the flow structure depends on the type of type and extent of modification. Flow pattern is also modified by the variation in the cross section at mid height. The upper region of the octagon plan shape cross section reduces the wake as compared to the square plan cross section. Strong wind produced excitation is particularly vulnerable to bluff-shaped tall structures, which can be regulated either structurally or aerodynamic technique.

**Tieleman** [39] conducted the wind tunnel test to investigate the mean wind effects and various turbulence characteristics. Observed that the peak wind effects are non-stationary in nature for short time periods and cannot be included in hourly averages. Better predictions of the wind speed can be obtained with a single layer model when the actual velocity, not the potential wind speed, is used instead of the two-layer model with potential velocity, and the regional roughness length based on land use maps is reduced to values commensurate with the local terrain.

**Ahmad et al.** [40] through the use of an experimental method, study examined into the effect of geometry on wind pressure on low-rise hip roof buildings. On the TTU building model, the  $C_p$ , mean and  $C_p$ , rms are often found to be quite near to the prototype values for the roof as well as the experimental data. the  $C_p$ , min is nearly half for the corner roof of the building model in the case of  $180^0$  and  $270^0$  wind incidence angel. The critical wind angle is  $120^0$  is found for all the wind effects.

**Bandi et al.** [41] investigated the peak pressure acting on tall building with various configuration, among all the model having shape triangular, square, pentagon, hexagon, octagon, dodecagon, circular and clover, the helical and corner cut combination shows much reduction in

$C_p$  max. The tri-corner cut model has a smaller maximum strongest negative peak pressure coefficient than the triangle model, but the square corner cut model has a larger maximum largest negative peak pressure coefficient than the square model.

**Kim et al.** [42] investigated the shape effects on aerodynamic and response characteristics of tall and super tall buildings, efficiency of corner modification, setback, taper, helical and so on in reducing aerodynamic forces is clearly demonstrated. Polygon buildings with five or more sides show excellent aerodynamic performance. The aerodynamic performance of triangular models including a clover shape (Y-shape) is not good under the conditions of same height and same volume. Tapered and setback building with larger bottom widths show larger speed-up area, thus causing adverse effects on pedestrian-level winds.

**Bearman and Morel** [43] conducted the test on bluff bodies by varying the free stream turbulence and measured high Reynolds number for bluff bodies, Reynold number of the flow mainly effect the drag force that is also effected by subcritical and supercritical flow over cylinders. Increasing Reynold number reduces boundary layer skin friction while free stream turbulence increases it. The effect of drag is not easily detected and sometime FST acts to increases drag, sometimes to decreases it and it might have no effects at all.

**Verma et al.** [44] estimated the coefficient of pressure in high rise buildings using the artificial neural network. The ANN-BPNN model was used to estimate the mean value of the pressure in terms of  $C_p$  at various points with varying wind incidence angle. The ANN was trained with wind tunnel experimental data of varying wind incidence angle.

**Tominaga and Shirzadi** [45] conducted the wind tunnel test on the low rise and high rise building, the surrounding of the building models can reasonably reproduce the developed urban flow consisting of several rows of urban blocks. The downwash flow caused by the high rise building drastically changed the flow direction in the upwind street canyon flow. A strong time averaged velocity occurred due to flow separation at the upwind corner and the corner stream at the side of the high-rise building. The static pressure difference between the windward and leeward walls below the street canyon level was greatly increased by the high-rise construction. This can contribute to an increase in the driving force of natural ventilation in the lower part of the building.

**Maruta et al.** [46] evaluated the effects of surface roughness for wind pressure on glass and cladding of buildings, increase of surface roughness restrains the transmission of disturbances

with approaching flows to the side wall face. Also eliminates or weakens the severity of the fluctuating pressure induced by separation bubbles near the leading edge. The fluctuating pressure affected by separated flows which had only weak turbulent components that is acting uniformly on the whole surface of the side walls.

**Chakraborty et al.** [47] experimentally investigated the wind effects using wind tunnel test, change in wind direction may induce different pressure on various surfaces of a “+” plan shape building and the pressure may either increase or decrease depending on the location of a surface. The symmetrical faces are having identical pressure distribution due to symmetry in wind flow for both wind angle.

**Kim et al.** [48] concluded that the peak normal stress reduces and approaches the quasi-static value as the damping ratio increases in a wind tunnel test on 13 super tall building models with unconventional building geometries under urban area flow. The increase in bending moment for the across wind direction becomes large as the damping ratio decreases, and the helical and multiple modification models peak normal stresses were less sensitive to damping ratio and wind directions than the other models. In the time histories of normal stress, the impacts of damping ratio were also examined.

**Allegrini and Lopez** [49] investigated the flow between two buildings with different angular configuration and conducted the test using the wind tunnel test. The wind speed in the passage between two buildings are for all cases and all heights above the ground is higher for diverging compared to converging configurations. The wind speed at all height above the ground in the passage between two buildings can be found for diverging configurations with small angles between the buildings. For parallel configurations the wind speed is lower compared to diverging cases with small angles.

**Nagar et al.** [50] performed the experiment on interfering building to check the effect of different wind incidence angle, the distribution of mean pressure coefficient on the front face of “H” plan tall building is very similar to those of the square plan tall building with a slightly higher magnitude but at  $90^0$  wind incidence, the magnitude of mean pressure is less. At full blockage condition, the front face of the principal building is immersed in the wake of upwind interfering building and thus  $C_p$ , mean on the front face of both principal building model is negative. The wake is generated because wind separates at the upwind interfering building. In the case of interfering building the magnitude of mean pressure is reduced than those with the isolated building.

**Kushal et al.** [51] experimentally investigated the effect of interference on wind loads on tall buildings. Torsional moments decreased rapidly with increase in spacing between the instrumented and interfering building blocks up to a specific distance and becomes constant thereafter. Wind force on rectangular building block is maximum under isolated conditions. Interference effect will be vanished if the spacing between the blocks becomes 20 times in the dimension of the interfering building blocks.

**Pal et al.** [52] comparative study of wind induced pressure of mutual interference effects on twin square and fish plan shape building model. With similar volume, it is discovered that the dominance of drag and lift force for the fish plan shape model at isolated conditions of  $0^0$  and  $180^0$  wind incidence is greater than the isolated wind at  $0^0$  on the square shape model. Interference effects improve overall efficiency in terms of base shear of primary buildings, with back-to-back wind interference conditions exhibiting the highest efficiency when only the fish-plan shape model is examined. In comparison to the fish plan shape model, the square model performed best in terms of resisting base shear.

**Ahmad et al.** [53] the experiment was conducted on a Texas Tech University (TTU) building model that was created at a 1:50 geometric scale and tested in simulated wind environment to compare the pressure results to full scale results. Different placements of a single interfering building showed significant augmentation and shielding. Maximum enhancement was observed in the rms value of the pressure while maximum shielding was observed in the mean value.

**Nagar et al.** [54] investigated the proximity effect between two plus plan shape high rise building on mean and RMS pressure coefficients. On the windward side face near the recessed corners, interference effects on local wind pressure are much larger. Suction was created on the walls facing the gap to the interfering building due to the complete obstruction. Half-blockage and no-blockage conditions cause more severe interference than full-blockage conditions. Wind load on the side face and the leeward side is lowered due to interference effects. Suction at side faces reduced approximately by half percentage than the full condition.

**Yahyai et al.** [55] performed the experiment in boundary layer wind tunnel on a multistoreyed rectangular building. The responses of the aeroelastic model were record in the two principal direction that is along wind and across wind by a set of strain gauge transducers. The effect of the interference is much more pronounced when the interfering building is located on the up-stream side compared to the when the building situated in the down stream side. When a building

is located in the wake of another building in its vicinity, it experiences a shielding effect which reduces the static wind loads.

**Kar and Dalui** [56] conducted the test to evaluate the effects of square plan shaped tall buildings on an octagonal plan shaped tall structure. The effect of the interference building on shielding and channelling on the octagonal plan shaped building is also explored. If the coefficient of pressure ( $C_p$ ) for each face of the octagonal plan shaped building in each interfering case is multiplied by the interference factor with the  $C_p$  in the isolated case, the coefficient of pressure ( $C_p$ ) for each face of the octagonal plan shaped building in each interfering case can be easily found. The flow patterns are symmetrical because the plan shape is symmetrical, yet such symmetries are maintained until the development of vortices. In the event of a symmetrical wind incidence angle, symmetrical faces will have identical or at least similar pressure distributions. Diverse interference circumstances will result in different wind flow patterns. As the distance between the principle and interfering buildings or between the interfering buildings changes, so will the wind flow pattern be also changes.

**Pal and Raj** [57] wind induced pressure on square and fish-plan shapes was investigated experimentally under various interference conditions. The tests were conducted in a 1:300 scale boundary layer wind tunnel for 100 percent obstruction between twin interfering models. The distance between the twin building models is set at 10% of the building model's height. Because the Average  $C_p$  values of the fish-plan shape building model differ from those of the square and rectangular plan shape building models, structural and cladding design investigation from regular plan shape buildings under identical working conditions will not suffice. Because the model has an unusual cross sectional plan shape, there is very high turbulence at some faces of all interference conditions when the cross-sectional plan of the fish plan shape building model is gradually increased and then decreased, as opposed to square plan shape building model and any other interference studies.

**Pal et al.** [58] at various interference environments, an experimental study of square plan shape and remodel triangular shape building model was conducted. The analysis was carried out in a boundary layer wind tunnel at a length scale of 1:300 for full blockage circumstances. The result of structural and cladding design from a regular plan shape building at similar working conditions will not suffice because the  $C_p$  values of the RTS building model differ from those of the square and rectangular shape building models. Because the orientation of duplicate models attracts the greatest overturning moments in both the along wind and cross wind directions of all interference

situations tested in this investigation, back-to-back interference of an RTS model should be avoided.

**Yu et al.** [59] investigated the interference effects on wind pressure distributions between two building with various configurations in tandem, oblique and parallel arrangements were studied. Because of the shielding, the mean pressure was typically advantageous, however the peak pressure of the lateral façade near to the interfering building was mostly enhanced. For maximal interference factor, the channelling effect must be taken into account in parallel configurations.

**Hajra and Dalui** [60] the interference factor was numerically studied by varying the separation between the two interfering buildings and between the interfering and major buildings. A number of CFD simulations are performed at various spacing values to determine the best distance between the interfering building and the major building. When 10 percent height spacing is used, the interfering building has no effect on the major building, and the principal octagonal building behaves as if it were an isolated structure.

**Amin and Ahuja** [61] investigated the mean interference effects between two rectangular building located in close proximity in a geometrical configuration of “L” and “T” plan shape through wind tunnel test on a length scale of 1:300. The wind pressure distribution and its magnitude on inner walls depends on the arrangement of building models, wind directions and their relative dimensions due to the mutual interference of wind flow by both the models.

**Paul and Dalui** [62] numerically computed the wind effects on “Z” plan shape tall building under varying wind directions. The leeward face is subjected to suctions as a result of frictional flow separations and the production of vortices. The streamlines clearly show flow separation characteristics and vortices. The combination of pressure on the windward side and suction on the leeward side creates vortices in the wake region, causing the body to deflect. Suction can occur even on the windward face due to the separation of flow in the structure with the limbs, as well as uplift, side wash, and backwash from the wind.

### **2.3.2 CFD studies**

**Sanyal and Dalui** [63] studied the wind load and response of the structure for designing the tall building by varying the width to breadth ratio of “Y” shape building. Analysis was performed by ANSYS CFX using two turbulence model SST and k- $\epsilon$ . with the increase in the length to width ratio the horizontal force coefficient and the overturning moment coefficient increases significantly. The lower value of length to width ratio has also some negative impact on the



corner suction. So far, the cladding design of a “Y” plan shaped building with lower value of length to width ratio, the corner regions must be checked properly for the suction pressure.

**Bairagi and Dalui** [64] simulated the wind environment around the setback building model, investigated the flow behavior and concluded that, double side double set back building can reduce the 30 % velocity in front and 70 % velocity in downstream wind. Velocity speed at the recirculation zone over the roof is increases. Also studied the variation of velocity, spectral density, frequency and building amplification factor (BAF) at the pedestrian level of building for isolated building case. This study mainly concerted on pedestrian level wind comfort. The model scale for high rise building is kept in between 1:100 to 1:600 and for low rise building this could be 1:20 to 1: 50, generally for high rise building it is 1:200 and above is used by several researchers. Scale study is done to save the time and computational resources.

**Tominaga et al.** [65] Compared the various model using different turbulence model such as  $k-\epsilon$ , LK model and MMK model among all  $k-\epsilon$  performed better and result obtained are found similar with experimental result.

**Chan et al.** [66] concluded that  $k-\epsilon$  turbulence model generated result are similar with wind tunnel results. The gradient diffusion hypothesis is used in the  $k-\epsilon$  model to relate Reynold stresses to mean velocity gradients and turbulence intensity. The separation and reverse flow at the roof top of the building model cannot be reproduced by this  $k-\epsilon$  model. Doesn't accommodate the strong flow separation, large pressure gradient, large streamline condition.

**Goyal et al.** [67] investigated the wind loads effects on “Y” shape tall building using CFD, at the edge of the windward side, the wind velocity is maximum, and at the leeward side, it is lowest. Following the addition of corner modification, the rounded corner on the windward side shows the highest speed. In the case of a spherical model, the smaller size of eddy makes it more stable. Due to direct wind flow, the windward face is subjected to positive pressure distribution, whereas the leeward face is subjected to negative pressure distribution due to flow separation and vortex generation.

**Sanyal and Dalui** [68] compared the aerodynamic coefficient of various types of “Y” plan shape building and different types of helical, tapered, setback and corner modification are applied on this tall building. Three independent wings are joined to a central core component of a Y plan building, which is often triaxially symmetrical in shape. This style of structure is ideal for hotel, corporate, or residential use since it provides the best possible outside view without affecting the

resident's privacy. This form is also suggested since it allows for good airflow. The greatest way to reduce wind loads and overturning moment coefficient is to create a setback building with fully rounded corners.

**Kumar and Raj** [68] the pressure distribution pattern on an irregular octagonal plan oval plan shape building was quantitatively analysed using CFD. On the upwind faces, the length to width ratio effects the formation of up wash, down wash, and stagnation zones, and this phenomenon has a large impact on the flow characteristics surrounding the model. The model's ground level upwind vortex is responsible for the deposition of dust and debris close to the ground level, thus obstructing air passage.

**Bairagi and Dalui** [69] estimated the wind load on stepped tall building using CFD on a 1 : 300 length scale, studied the external pressure coefficient and force variation on roof and face of the building model at  $0^0$  and  $90^0$  wind angles. Maximum pressure develops at 90 % of building height from the base of the building models. Negative pressure develops at the building roof top. Turbulence is mainly influence by the steps provided in the building model. For transient analysis, 3.0 second gust is considered and it takes nearly 22 hours for single simulation. BAF (Building amplification factor) defines the maximum ground level concentration with building to the maximum concentration at the same source in the absence of the building.

**Raj et al.** [70] investigated the wind effect on "H" shape tall building using CFD. In isolated conditions for  $0^0$  wind incidence angle, the "H" plan shape building experiences symmetrical pressure distribution. Positive pressure occurs on the windward sides of the building due to undeviated wind impact and negative values occurs at the leeward side of the building due to suction pressure. Principal building has major interference effects and these effects are highly dependent upon the orientation of the building, the relative distance between the building, the terrain and the wind incidence angle.

**Sanyal and Dalui** [71] numerically investigated the effects of courtyard and opening on a rectangular plan shaped tall building under wind load using ANSYS CFX. Because the model's exposed wind ward surface receives an undeviating wind force, the wind ward faces experience positive pressure coefficients. The leeward and side faces are exposed to suction pressure due to frictional flow separation and the creation of vortices. The formation of vortices in the wake zone occurs when there is a windward side pressure force and a leeward side suction force, causing the body to deflect.

**Amin and Ahuja** [72] in the wind tunnel, the study examined rectangular building models with the same plan area and height but varied side ratios of 1, 1.56, 2.25, 3.06, and 4. The building's side ratio has a big impact on the wind pressure on the leeward and sidewalls, but the wind pressure on the windward wall is essentially unaffected. Wind incidence angle and side ratio of structures have a considerable impact on mean displacements and torque.

**Gaur et al.** [73] performed the numerical study on aerodynamic mitigation by corner modification on square model under wind loads employing CFD and wind tunnel at a length scale of 1: 100. The corner-cutting (Chamfer and Fillet) in building plan can be effective in aerodynamic mitigation but requires a complete understanding of the building aerodynamic and wind response. Streamline study and pressure field of the models shows suction near the corner cuts. The reduction in the drag force is obtained this is because of the walls and the modification made in the high-rise building model. The reattachment of separated flow in corner cut models may results in a more stable wake region than the square model.

**Sanyal and Dalui** [74] studied the effect of corner modification on “Y” plan shape tall building under wind load. Corner modification is one of the most commonly used minor shape modification which significantly reduces the wind loads and responses. Symmetry in flow patterns has resulted in identical pressure distribution on symmetrical faces for  $0^0$  and  $60^0$ ,  $90^0$  wind angle. However, no such symmetry is present for  $90^0$  wind angles. Good agreement has been observed among the numerical and experimental results. Overall accuracy of k- $\epsilon$  model is better as compared to SST model. However, SST model predicts pressure in high turbulence zone with higher degree of accuracy.

**Raj et al.** [75] investigated the response analysis of plus shaped tall building with different bracing system under wind load. The axial force values were lower in the single diagonal bracing system. The axial force values show a gradual decline from the bottom to 30% of the building's height, followed by a quick decrease to the top. Twisting moments were found to be insignificant in all bracing systems, with the exception of inverted V-bracing on the leeward side when the wind incidence angle was  $60^0$ .

**Amin and Ahuja** [76] conducted the investigation on effects of side ratio on wind induced pressure distribution on rectangular buildings using wind tunnel. At  $0^0$  wind incidence angle, the magnitude and distribution pressure coefficient on windward wall of the rectangular models are almost independent of model depth and side ratio. As side ratio of model increases the absolute value of mean pressure coefficients on side face decreases from leading edge region at  $0^0$  wind

incidence angle. The highest peak suction may occur practically at any location of the model side face.

**Raj et al.** [77] investigated the response of square and plus shape building on varying wind loads, when wind flow is perpendicular to the windward face, pressure occurs on it and suction occurs on all other faces. The positive wind pressure observed on windward face increase from bottom to near top edge of the face due to increase in wind velocity with height. Entire wind ward face including cut corners are subjected to pressure due to long length of cut corners, when wind hits perpendicular to long wall. At skew angles and also when wind hits perpendicular to a short wall, most of the surfaces are subjected to suction.

**Kumar and Raj** [78] numerically studied the “L” shape building using CFD, numerical simulation performed with standard k- $\epsilon$  model shows a good agreement in case of normal wind incident angle. Denser mesh arrangement in the particular flow region and improved modelling for mapping the three-dimensional non isometric unsteady flow could enhance the quality of the result. The results can provide useful information about wind pressure on re-entrant wing faces of “L” shape buildings for practical engineering calculations.

**Thordal** [79] performed wind tunnel test on “CAARC” high rise building with large eddy simulation. The DWT mean wind profile, turbulence intensity profiles and power spectral densities were in good agreements with EWT results. The DWT stream wise components of the power spectral density coincided with the EWT spectrum up until a frequency of 0.79 Hz in full scale, which was higher than the first three fundamental model of the high-rise buildings. The CFD simulations are capable of predicting the peak responses of a high rise building with high accuracy for most wind angles of attack. The spatial correlation coefficients of the DWT were overall consistent with the EWT results.

**Shao** [80] evaluated the wind pressure coefficient using CFD methods to prediction. The leeward negative pressure of the upper part reduces due to the introduction of slot and this reduction more compensates for the increase of windward pressure. So, the slot is beneficial to the upper part of the building while designing such buildings. The pressure profile along the wind ward and leeward facade vertical centre line of both building. Pressure on both windward side and leeward is reduced by providing the slot in the building plan cross sectional area.

**Franke et al.** [81] provided the guidelines for the use of CFD in wind engineering the main guide lines are as, the blockage of the flow by the built area should be below 3% and the outflow

boundary far enough away from the built area in a developed flow. The minimal grid resolution should be 10 cells per cube root of a building volume and 10 cells per building separation. Hexahedra or at least prism should be used at wall. Pedestrian wind speed should not be analysed in the first cell on the ground. Use of the local grid refinement in the region of interest to check for grid dependence of the results generally systematic grid convergence study performed before the simulation is started. The result obtained using the numerical simulation result should be identical in nature with the experimental result this is necessary for the better simulation and for the validation purposes.

**Thordal et al.** [82] presented the important aspect which are needed when employing the CFD simulation for the determination of wind load on high rise building. A large deviation of between the result of CFD and wind tunnel result is largely depending on the inflow conditions. Results of CFD can be compared with wind tunnel result if the exact same boundary conditions are used in the simulation otherwise it can lead to critical error and misleading results. The fluctuating pressure coefficient are more inclined to be dependent on the velocity profile and turbulent intensity profile while the turbulence intensity mainly influencing the fluctuating pressure coefficient. Isolated building which are generally slender and have smaller width to depth ratio, the separation point of the flow will occur at the leading edge and the flow will not reattached to the side surfaces.

**Meng et al.** [83] performed the sensitivity analysis of wind pressure coefficient on “CAARC” tall building using CFD simulation. Maximum positive wind pressure coefficient found around 0.8-0.85 H of wind ward surface, while maximum negative once occurred at foreside of top surface. Turbulence model has also significant effect on the numerical results and grid resolution has more effect on negative pressure distribution. An increase in wind speed leads to a gradual decrease in mean wind pressure coefficient while the blockage ratio is affecting the negative pressure zone. In numerical simulation wind pressure coefficients on windward surface are stable, although they slightly vary with wind direction, turbulence model, approaching flow speed and grid resolution.

**Kumar and Dalui** [84] conducted the numerical investigation to find the effect of internal angles between limbs of cross plan shaped tall building under wind load. The effect of mutual interference between faces on the side of limbs, the side faces of regular rectangular or square plan shaped building are generally subjected to a suction while the side faces of the frontal limbs of cross plan shaped building undergo a positive pressure caused by the flow slowing down due

to wind striking on the other surface. Angular cross plan shaped building, having lowest force coefficient is more efficient compared to regular and square plan shaped building. k- $\epsilon$  turbulence model shows the better agreement with experimental results.

**Tominaga** [85] evaluated the performance of the unsteady Reynold averaged Navier-Stokes (URANS) turbulence modelling of the flow field around high rise building with a 1:1:2 shape. A modified equation of  $\epsilon$  was introduced into the RNG k- $\epsilon$  model to enable it is use to reproduce the periodic fluctuation and more accurately predict the flow separation on the roof of the building. The k- $\omega$  and SST turbulence model significantly underestimated the turbulent kinetic energy around the building, and the flow separation around the building corner was therefore significantly over-estimated, despite the reproduction of the periodic fluctuation.

**Keerthana and Harikrishna** [86] investigated the wind effects on rectangular and “H” section using CFD. The result obtained using CFD and wind tunnel shows the better agreement of results. As the angle of wind incidence changes there is more deviation in result of mean lift coefficients between the numerical and experimental results. Wind ward pressure coefficients are well predicted for both the turbulence model while some deviation is observed in the wake region in downstream of wind.

**Yahyai et al.** [87] numerically performed on investigation of wind effects on Milad tower. Reynold observed in the flow is  $10^5$ . The RANS model with the standards turbulence model can present acceptable result and have the advantage of providing the fast solutions. The flow pattern is simulated and presented pictorially for the better understanding of flow around the tower using the CFD.

**Dagnew and Bitsuamlak** [88] presented a review on computational evaluation of wind loads on building, computational result are effected by the type of turbulence modelling, inflow boundary conditions, roughness consider for ground surface, near wall treatment and quantification of wind loads. Validation in this study shows good results for wind ward face while there was some discrepancy reported in the side wall and lee ward wall. The along wind and cross wind response using LES turbulence model predicted well.

**Revuz et al.** [89] provided the guidelines for the size of the domain in the steady state, low rise building are generally free from the blockage ratio while the high rise building model are considered the domain size that solely depends on the height of the building model. The domain

of approximately 10 % of the volume could be used to predict the results with a loss of 10%. There is no formal restriction on the size of the parallel direction in RANS simulation.

**Blocken et al.** [90] carried out the numerical simulation of wind speed conditions in passage between parallel building has been conducted for a wide range of passage width. The results are compromised by the use of wall roughness coefficient to predict the result of atmospheric boundary layer flow. The simulation result indicates that, at least for the cases studied in this study, the increase in wind speed in passage is only pronounced at the pedestrian level and that the flow rate through the passage is only 8% higher than the free field flow rate, indicating that the venturi-effect is weak in such situations.

**Gomes et al.** [91] performed the experimental and numerical study of wind pressure on irregular shape of “L” and “U” shape model. The experiment was carried out in closed circuit wind tunnel at a length scale 1:100, as the angle of incident flow increases the pressure field turn out to be negative and almost uniformly distributed, which is characteristics of a recirculation area. CFD result for RNG k- $\epsilon$  turbulence model for  $0^0$  wind incidence was is better agreement with wind tunnel result.

**Huang et al.** [92] carried out the numerical simulation of wind effects on a tall building using CFD, LES turbulence model was adopted to predict the wind load and wind flow around the building model. The velocity profile of the approaching wind flow mainly influences the mean pressure coefficients on the building and the incident turbulent intensity profile has a significant effect on the fluctuating wind force. Flow filed around the bluff body in atmospheric boundary layers such as recirculating flow region contraction in the building back zone due to base suction were captured by the simulation. Instantaneous flow patterns showed that the detailed flow fields predicted by the LES were irregular and complex when the Reynolds number was larger than the  $10^5$ .

**Okajima et al.** [93] Numerically studied the blockage effects on aerodynamic characteristics on an oscillating cylinder, the k- $\epsilon$  turbulence model was considered and Reynold number lies around  $4 \times 10^3$ , for stationary cases, the lift and drag forces and vortex shedding, Strouhal number all are increases with the increases of blockage ratio. The flow streamlines and vorticity contours show the conspicuous feature of a wake under high blockage ratio. Reynold number changes because of the changes into the reattachment of separated shear layer to reattachment of wind flow by the blockage effects.

**Stahopoulos** [94] presented the reviewed on computational wind engineering, the roof and the leeward wall area appear problematic regarding the numerical results. LES model does not perform well and does not show a very significant improvement. Numerical result obtained with the k- $\epsilon$  turbulence model for the same point show drastic difference from both the full scale and the wind tunnel values, particularly from the critical wind azimuths ranging from  $170^0$  to  $280^0$  wind incidence angle. The pressure coefficients on the windward face scatter very much both in experimental and numerical calculation, as far as the roof and the leeward face is concerned, refined turbulence models although turbulence model modification are unlikely to perform well beyond the specific flow conditions for which wind tunnel test is carried out.

**Tsuchiya et al.** [95] investigated the various parameter of k- $\epsilon$  turbulence model which influences the flow field and pressure fields around bluff body. It was observed that the roof pressure distribution from wind tunnel test was varied from wind ward side as small and negative pressure is gradually decreases towards the leeward side. In comparison with the experimental result, the wind pressure coefficient obtained by the standard k- $\epsilon$  turbulence model is greatly overestimated in the vicinity of the impinging region. The result of pressure distribution on the windward corner of the side faces for the MMK model are slightly larger than the wind tunnel results.

**Yu and Kareem** [96] numerically simulated the flow around the rectangular prism using LES turbulence model. In a direct numerical simulation of turbulent channel flow the computational time step substantially influences the statically results. The result obtained from numerical simulation were in a closer agreement with wind tunnel results. a grid refinement study was revealed that sufficient resolution is very important in 3D LES simulation.

**Meng et al.** [97] performed a numerical study of the wind field in a boundary layer flow. The velocity profile of wind speed in the typhoon boundary layer flow can be satisfactorily stated by the power law expression. The vorticity influences the velocity profile which influences the gradient height. The gradient height is a function of the length scale and modified surface number. The value of the gradient height is strongly dependent on the large length scale of the atmospheric boundary layer flow. The power law can be related with small length scale. A comparison of wind speed and wind direction using the numerical results and observed data, wind speed profile is normalized by the wind speed at a height of 200 m (top of tower). The result of numerical analysis is found in a better agreement with wind tunnel test result.

**Uchida and Ohya** [98] conducted a numerical study for a wide range of K ( $0 \leq K \leq 3.0$ ), as K increases the recirculating eddy behind the hill is suppressed and its length is shortened. The



lee wavelength is shortened as  $K$  increases. For the case of  $0 \leq K \leq 1.0$ , the time series of the drag coefficient  $C_d$  suggests that the flow around the hill under weak stratification reaches an almost steady condition. For the case of  $K$  is 1.75 and 2, the flow around the hill reaches a steady condition because of the appearance of the distribution at node. The changes into the high and low  $C_d$  are because of the eddy distribution in the upstream.

**Cowan et al.** [99] presented the computational simulation result of flow and distribution around the tall building model. The result based on the numerical simulation are not only based on the boundary condition while these results are also based on the quality of the meshing and numerical methods. The result for course meshing might be closer to the experimental value than the finer meshing. Result obtained by one numerical simulation might not be same if the solution obtained by different CFD user this divergence is because of the variable degree of controlled.

**He and Song** [100] conducted the comparative study using wind tunnel test and numerical simulation for studying the flow patterns around the Texas technical university building model and a details were presented for the roof corner vortex. The mean value is in better state as such values are in the closer agreement with the wind tunnel result while the RMS are not very close to the experimental results this is because of the small eddies and same can also be resolved by using the finer meshing. The low-pressure regions also obtained in the corner regions.

**Kawamoto** [101] provide the guidelines for the cost effective and accurate turbulence model to estimate the wind load on building, the  $k$ - $\epsilon$  turbulence model predicts well for bluff body problem. The error obtained in the standard  $k$ - $\epsilon$  turbulence model is because of the over production of the turbulence kinetic energy at the impinging area which is strongly favourable for the pressure gradient area. The helical flow field generated if the simulation is performed using the  $k$ - $\epsilon$  turbulence model and same can be removed using  $k$ - $\epsilon$ - $\Phi$  turbulence model.

**Richards and Hoxey** [102] studied the appropriate boundary condition for the  $k$ - $\epsilon$  turbulence model, the coefficient use to solve the numerical equation will predict result closer to the experimental values. The  $k$ - $\epsilon$  turbulence model constant such as  $k$  is 0.42,  $C_\mu$  is 0.013. The boundary conditions used should be capable of producing a homogeneous boundary layer flow in the absence of the object. The boundaries defined in the numerical simulation should be located sufficiently at remote distance from the object so that they have negligible effect in the region of interest. At the ground, a retarding shear stress will exist, but in order to allow this to adapt to changes caused by a building or other obstruction this should be calculated on a local basis.

**Lee and Bienkiewicz** [103] presented the finite element formulation of the large eddy simulation to calculate two dimensional turbulent flow for the square plan shape building model, the Reynold number is 40,000. The fully developed flow is imposed as inflow and no slip condition is enforced on the surface of the solid walls. The simulated results are compared with the numerical and experimental studies while the result of both the testing were in closer match with each other. The combination of LES and FEM can capture the mean properties of high Reynolds number separated flow. The time averaged separation and reattachment characteristics are well reproduced using the LES and FEM approach.

**Selvam** [104] numerically investigated the wind flow around the Texas Technical University building model. The turbulence generated by numerical dispersion using central difference has a considerable effect over the vortex shedding over a circular cylinder while the flow caused by central difference and up wind pressure computed same mean pressure around the square plan shape building. The variation of turbulence in the lateral direction at the inflow, the variation of flow direction with time and proper modelling of inflow turbulence can greatly improve the results.

**Wiik et al.** [105] performed the numerical simulation for the assessment of wind loads on roof overhang in the case of low rise building. The mean pressure coefficient in most of the part is same as with the experimental values while in the corners there is larger differences were observed. Numerical simulation with the basic k- $\epsilon$  turbulence model predicts well the pressure at the wind ward side of the building model. At the edges with flow separation, the numerical simulation seems to underestimate the pressure at the windward side of the edge and overestimate the negative pressure at the leeward side of the edge. The effect of a long roof overhang will change the pressure distribution on the low standing wall. The pressure will increase at the upper part of the wall compared with no overhang.

**Robertson et al.** [106] conducted the full scale measurements and predicted the result of wind load using the computational methods. The full-scale result has shown clearly the strong dependence of wind loads effects in incident wind direction and on position along the wall. Maximum loads occur at the wind ward end of the wall in the case of  $40^0$ - $45^0$  wind from normal to the wall.

**Leitl et al.** [107] investigated the flow distribution around the “U” shape building model and presented the comparative result with wind tunnel result and computational result. Large discrepancies were also obtained for most of the ground level release situations. Even if the

roughness height was chosen to give similar inflow and outflow profile for calculation of rough surface. The k- $\epsilon$  turbulence model was used to provide the turbulent closure during the simulation.

**Alminhana et al.** [108] performed a numerical investigation to study the aerodynamic performance of building cross section using corner modifications. The flow patterns in the simulation changes as the extension of corner modification is increased. Moreover, corner modification tends to reduce recirculation zone along the side edges of the building model. The streamlines for chamfered corner configuration presented a more aerodynamic pattern, with the streamline attached to the side of the model. While cross sections with recessed corner showed zones of recirculation at the frontal and backward corners.

**Chakraborty et al.** [109] presented the result of the wind tunnel studies and numerical studies done on the “+” shape building model. The experimental study was performed in open circuit boundary layer wind tunnel on a 1:300 scale of rigid model while the numerical studies were performed using ANSYS. The pressure on the leeward side for both the wind incidence angles are almost same and the pressure distribution for the symmetric faces has the symmetrical pressure distribution. The nature of wind pressure is positive for the wind ward face while for the leeward face and side face the pressure distribution in negative in nature.

**Hoxey et al.** [110] provided the geometrical parameter that effect the wind loads on low rise building and full scale test is done in the CFD. A region extending from the windward eaves up to the roof slope to a distance of  $h/2$ , in this region, the effect of the separated flow generates large negative pressures, the magnitude of which are inversely related to span shape and size. A central region, applicable to long roof slopes, in which there is a slowly changing pressure, the magnitude of which is similarly inversely related to span size. The suction generated near the ridge of the building is dependent on the combined parameter of height to span ratio. The pressure distribution over the roof is significantly non uniform and dependent on the geometrical parameter of roof. The averaged pressure on the leeward roof slope is relatively in sensitive to geometry and can be assigned a constant value in the range -0.6 to -0.8 depending on the height.

**Chauhan and Ahuja** [111] studied the response of tall building subjected to wind loads under interference conditions. Peak value of axial force, displacement in along wind direction and bending moment caused by the along wind force are noted to reduce for both columns, with the increase in height of interfering building due to shielding effect. Peak value of twisting moment,

displacement in across wind direction and bending moment caused by across wind force are detected to enhance significantly for both columns with increase in height of interfering building.

**Bairagi and Dalui** [112] investigated the distribution of wind pressure around different shape of tall building. The extensive amount of suction matured at leeward side due to the decrease in the number of setback roof for  $90^0$  wind angles. The models have single and double type setback at different elevations. The pressure calculation was conducted in the analytical study. Some amount of pressure bulb was observed on the leeward side due to the setback model, which mean the increase of suction on that particular region. The excessive amount of suction envelops recognized at the top roof of the setback model compared to square model.

**Zhang et al.** [113] performed the numerical simulation of investigation of wind field around different building arrangement. The model length scale was 1:150, it was also found that the wind environment for two improved arrangements with lower interval to height ratio is better than that for the reference layout with higher aspect ratio in terms of the natural ventilation. The interference effect is more obvious for two improved arrangements than the reference one. The numerical result shows that changing in wind direction from perpendicular to the building facades to a  $45^0$  wind incidence angle has significant effect on the flow filed for different configuration. The result predicted using the numerical simulation is relatively more economical and faster tool to evaluate the wind environment.

**Tang et al.** [114] numerically investigated the wind load on tall building. Multiple wind direction and BESO algorithm was used to optimize the shape of the building model. Putting fewer bracing elements at the upper levels will also provide the additional benefits of the lowering the centre of gravity of the whole building. For such a slender structure, considerable costs will be involved in constructing an appropriate anchor system in the foundation. When the centre of gravity is lowered, such costs could be significantly reduced. The dynamic effect of the wind loading on the building topology can be considered by conducting transient CFD analysis.

**Bairagi and Dalui** [115] computed the spectral density at roof of setback tall building due to time variant wind load. The frequency of the roof due to wind also affects the pressure fluctuation on neighbour faces. Most of the pressure fluctuation develop at 0.06 sec from the initial time and maximum pressure difference occurred at the setback roof for along wind conditions. Maximum pressure has been developed on the top roof of the setback model at the initial time for along wind conditions. However, the square model without any set back has less pressure effect than that of the setback model if the simulation is performed at the same time series.

**Shahab et al.** [116] performed the comparative study of aerodynamic coefficients of prismatic and twisted tall buildings with various cross section using CFD. Twisted model is best among the other building model and also it performs well to resist the wind generated force and moments. In the comparative study among the pentagon, hexagon and square building model, it was found that the hexagonal model is best to resist the drag and moment. All prismatic model has the well-defined wake region and vortices are created in a large volume as compared to the twisted model which have discontinues wake regions with small volume affected by the vortices.

**Wahrhaftig and Silva** [117] numerically computed the drag for tall building under wind load. Pressure acting on structure is the function of terrain category. CFD can effectively simulate the drag force and the resultant forces in the direction of the flow as well as the vortices that result during coating detachment and other types of damages. The result obtained in this study are in a closer match with the different codal values.

**Zidan et al.** [118] investigate the effect of the domain size using CFD simulation. Four distinct sources of domain error are identified which include wind blocking error caused by short upstream length, flow recirculation error due to insufficient downstream length, global venture effects (GVE) due to large blockage ratios, and local venturi effects (LVE) caused by insufficient clearance between the building and top and lateral domain boundaries.

**Bairagi and Dalui** [119] presented the comparative study of the pressure coefficient between square and setback tall building due to wind load. The surface pressure and roof pressure on unconventional tall building are quite different compared to the regular plan shape high rise building. The roof of the setback tall building has large pressure difference compare to the top roof of that building. The designer must consider the positive pressure on setback wind ward roof and negative pressure for top roof and leeward roof.

**Zheng et al.** [120] evaluated the impact of building balcony on wind speed on balcony space and wind induced mean surface pressure for generic high rise building. Balcony geometry can greatly affect the mean wind speed on balcony spaces and the local and façade averaged mean pressure coefficient. The presence of balconies can increase the façade averaged  $C_p$  over the wind ward and lee ward facades by 5.2 % and 8.9 % receptively. Adding five partition walls can reduce the overall area averaged wind speed on balcony spaces by 68 % compared to the case without partition walls. These finding can be useful in developing, designing and constructing building with façade geometrical details that improve building ventilation, air quality and wind comfort.

**Li et al.** [121] performed the wind tunnel test to study the effect the aerodynamic characteristics of the leeward vertical cylinder with ice shape. The ice thickness had a greater impact on the lift coefficients of “D” shape ice leeward cylinder at the same angle of attack. The aerodynamic characteristics of the iced leeward cylinder were stable the ratio of cylinder spacing was within the range of 4.8 to 6.2. The change of flow field should be considered in the stability analysis of two circular vertical cylinder. The drag coefficient of the iced leeward cylinder varied significantly due to the shielding effect, especially within the range of  $9^0$  attack angle and a cylinder spacing of  $L < 6.2D$ .

**Li et al.** [122] investigated the reduction of wind loads on rectangular tall building with different taper ratio. The tapered model can reduce the mean wind pressure and RMS wind pressure on the surface of rectangular tall buildings. As the taper ratio increase, the absolute value of the mean wind pressure and RMS wind pressure coefficient on the surface of rectangular tall building decrease. The increasing of the taper ratio will lead to the reduction of mean and RMS drag force coefficient, as well as the RMS lift force coefficient. As the taper ratio increase, the bandwidth of the power spectral of across wind force expands and the peak value of the power spectrum decrease. The power spectra peak of tapered models with ratio 15% and 20% are even not obvious anymore.

**Bairagi and Dalui** [123] numerically investigated the aerodynamic effect on setback tall building using CFD simulation. Normal building design and step building is quite different as wind load distribution pattern is different from the conventional type of structure. The pressure distribution, turbulence and spectral density are higher on the setback roof comparing to the normal square roof building model. The spectral density is more in the inner part of setback roof. High positive pressure developed in the setback roof compare to the top roof due to high turbulence. Maximum spectral frequency developed at the extreme location of setback roof, where the turbulence is also maximized.

**Gunaydin** [124] examined the wind pressure distribution on “U” plan shape building having four different depth ratio. The increase in the wind velocity did not considerably changes the pressure coefficient values, however it was noticed that all positive pressure coefficient decreased with the increase in the wind velocity value. The vertical centre line of pressure shows that the there is no regular increase or decrease in the pressure coefficient to half of the height of the building according to the distance from the re-entrant corner, however it was noticed that the distance from the re-entrant corners have great influence on the pressure coefficient.

**Li et al.** [125] conducted the wind tunnel experiment to study the wind effects on 90° helical and square tall building and measure the pressure. Due to the different flow separation characteristics, the mean local force coefficients of helical model show different trends along the height for different wind directions. The RMS wind force coefficient of the helical model are obviously smaller than those of the square model under all wind directions, especially for across wind direction. The variation trends of mean and RMS base moment coefficient with wind direction for the two models are in good agreement with those of the local wind forces. The helical treatment can reduce the mean and RMS wind load of square tall building effectively. The power spectral densities of base moment coefficient of two model vary gently and almost keep the same pattern at along wind direction. The peak value of the power spectrum of base RMS acceleration at across wind direction is much smaller than that of the square model.

**Jendzelosky and Antal** [126] performed the experimental and CFD wind pressure distribution on the high rise building on the shape of an equilateral acute triangle. The result obtained by CFD are validated with the experimental studies and found that if the proper flow physics is defined in the CFD simulation than it is not mandatory to conduct the experimental test. When a better accuracy of the CFD result is required than time dependent variable is necessary and for same purpose the direct numerical simulation turbulence model and large eddy simulation turbulence model should be used. However, CFD result are predicting the wind effects up to the good extent but in the case of irregular building it is recommended to perform the experimental test.

**Germi and Kelehsar** [127] evaluated the upstream and downstream interference effect of two CAARC (Commonwealth Advisory Aeronautical Research Council) standard tall building using computational fluid dynamics (CFD). Large eddy simulation turbulence model is used for this numerical simulation. In most of the interfering case, the shielding effect of the interfering building results in lower mean drag coefficient of the principal building. In comparison of isolated building depending upon location of the interfering building, the fluctuating lift coefficient either increase or decrease, while the mean pressure coefficient at the windward surface is not significantly sensitive to the interference states, it is strongly influenced by the different states of the interference at the lateral and leeward surface.

**Rocchio et al.** [128] performed the numerical simulation on a rectangular cylinder and different values of the edge radius of curvature is considered. It was found that the sharp edge can introduces the higher level of turbulent fluctuation in the shear layer separation. Turbulent kinetic

energy growth along the shear layer is affected by the shape of the building and shape of corner configuration. The investigation of corner rounding varying in the spanwise direction.

**Du et al.** [129] investigated the effect of turbulence integral scale and four rectangular model were tested in grid generated turbulence flows. An empirical result of turbulence integral length scale and model depth were provided to reduce the error in the numerical simulation. Turbulence integral scale is a key parameter in assessing the fluctuating pressure, especially the peak pressure, the fluctuating pressure must be modified by considering the effect of the turbulence scale.

**Daniels at al.** [130] numerically investigated the freestream turbulence effect on the vortex induced vibration of a rectangular cylinder. With respect to the free stream turbulent flows, the increase of turbulent intensity less than 12 % and with the integral length scales in the same order of magnitude of the bridge width  $B$  has significant effect to diminish the amplitude of the oscillation. The increase of turbulent length scale of the freestream flow moderately enhances the amplitude of oscillation of both heaving and pitching motions. The enhanced amplitudes are less than those in smooth flows. The investigation of spanwise correlation of surface pressure confirms that the increase of the integral length scale of the free turbulence enhances the spanwise correlation and subsequently enhances the amplitude of oscillation within the lock in regime.

**Tian et al.** [131] investigated the unsteady RANS simulation of flow around rectangular cylinders with different aspect ratios. The Reynolds number based on the free stream velocity and height. The values of Strouhal number are not sensitive to the aspect ratio, and the calculated Strouhal number obtained in from the numerical simulation is agreed well. The drag force acting on the cylinder with high aspect ratio are well predicted however, the drag forces are overpredicted for low aspect ratio. The vortex shedding frequency are not sensitive to the aspect ratio.

**Ikegaya et al.** [132] experimental investigation on the interaction between turbulent boundary layer and wake behind various types of two dimensional cylinder. The velocity distribution of the wake flow within the boundary layer has similar characteristics to the two-dimensional wake. Moreover, these sustain phenomena of wake within the boundary layer were observed regardless of the cylinder shapes and diameters. In addition, the monotonic increase of the wake half width within the boundary layer also supports the speculation that the wake flow expansion in the spanwise direction hardly occurs once the wake flow and boundary layer flow start interacting.



**Yang et al.** [133] studied the modification of aerodynamic force characteristics on high rise building arrangement of vertical plates. The testing results indicate that vertical plates can greatly affect the mean and fluctuating pressure on the building, the along wind and across wind layer forces and base moment. Continuous and stagger arranged vertical plates can significantly decrease the layer forces at the  $0^0$ -wind direction and the largest decrement of fluctuating across wind layer force can reach 60 %. It was also found that the back-to-back arrangement of vertical plates has the best effects on reducing fluctuating across wind base moment with largest decrement of 50 %.

**Diez et al.** [134] investigated the drag reduction on a three dimensional blunt body with different rear cavities under cross wind conditions. When the free stream is aligned with the body, the curved cavity provides a stronger attenuation of the fluctuating nature and the bi stable dynamics of the wake than the straight one. besides, the reduced size of the near wake, which is provoked by flow reorientation and the reduced span between the rear edges of the curved cavity, leads to an important base pressure recovery, that translates into relative reduction of the drag of 10 % in comparison with the straight cavity. The cross-wind response is considerably improved since the increase with the yaw angle of the force is particularly intense for the body with the straight cavity and attenuated for the model with the curved cavity.

**Li at al.** [135] presented a comprehensive investigation on the along wind response of base isolated tall building with a built tall building. For the base isolated building, GRFs increase on the whole. The GRF of the base bending moment is close to that of the top displacement, and those two are smaller than the GRF of the base shear force. Variation of GRFs of the shear force and bending moment along the height become small, compared with those of the fixed base building. The analysis for the isolation layer indicated that the increase of the additional damping and isolation layer stiffness can suppress responses. For the top displacement, the stiffness is very effective, and for the acceleration, the additional damping is superior. In order to reduce to make the wind induced shear force not exceed the design yielding force at the base isolation layer, the scheme of choosing the proper stiffness and damping for the reduction of the base shear force provides a useful guidance.

**Kataoka et al.** [136] investigated the applications and prospects of CFD for wind engineering fields. Initially CFD was used for environmental task for predicting the pedestrian wind environment since than CFD application is extending for predicating the dust dispersion from construction site. These predictions are based on the Reynold Average Navier Stock simulation

another model large eddy simulation is used to predict high temperature exhaust gas flows inside the urban canopy, where the unsteady flow field affects the scalar transport phenomena.

**Stathopoulos and Alrawashdeh** [137] presented a review on wind loading of building from a codal perspective. The building height plays a dominant role in impacting the values of pressure coefficient, the distribution patterns of roof wind pressure are also affected by the building plan dimension. It was found that the area averaged pressure coefficient prescribed in the codal provision are relevant to large roof but the edge and corner zones shall be limited to the 80 % of the building height. Codal provision are absent in the case of wind load in the case of the roof, top solar panel and wind loads on canopies are needed to provide in the international standards. CFD is using now days but for the structural wind engineering yet it needs so many developments.

**Cui and Caracoglia** [138] examined the wind loading uncertainty for structural fragility analysis of tall building in the context of wind engineering. The experiments were conducted in a small-scale wind tunnel under the homogeneous turbulence flow. The power spectrum density equation was developed and found that it may be difficult and cumbersome when several wind directions need to be investigated. The concept of model equation of power spectrum density enables the generation of a statistically consistent set of synthetic PSD function by Monte-Carlo sampling and Copula method and the interdependence among the parameters of the model curves should be considered during the modelling.

**Hangan et al.** [139] presented the novel technique in wind engineering. One approach, the gust front factor method is essentially a time domain analysis approach that extends the ASCE-7 approach and address the dynamic loading effects arising from thunderstorm events by introducing a generalized gust front factor. This gust front factor is determined as a superposition of kinematic effects, dynamics rise effects, turbulence and transient aerodynamic effects.

**Hou and Sarkar** [140] investigated a time domain method for predicting wind induced buffeting response of tall buildings. The procedure of the method is discussed and a section model with a cross section of B/D of 1.5 was built and tested in a wind tunnel to identify the parameters. The aerodynamic static mean load coefficient, buffeting indicial derivative function, and flutter derivatives effects were considered. Aeroelastic model test, which shows the effectiveness of the proposed method in the simulation of wind induced response of tall building subject to buffeting loads. However, limitations to linear aerodynamic load response regime only precludes it from

predicting response in wind flow regimes attributed to divergent response when the damping of the tall building.

**Ahmad et al.** [141] numerically predicted the wind loads effects on low rise building. The simulation is performed in ANSYS Fluent using k-  $\epsilon$  turbulence model on TTU building model. The similarity was observed among the numerical and experimental results. The discrepancies in the pressure coefficient variations of TTU building model with wind tunnel testing results are due to the improper simulation performed in the numerical simulation.

**Tse et al.** [142] investigated the aerodynamic characteristics of tall buildings with corner modification. A small corner modification ratio was more effective in reducing local along wind and cross wind force than a large ratio. Corner modification reduced vortex shedding and considerably reduced the cross-wind force acting on the side surface. However, in the evaluation of extreme local pressures of buildings, a substantial amount of extreme pressure occurred on the surface as a result of the corner modification.

**Bhattacharya and Dalui** [143] numerically evaluated the force coefficient of “V” plan shape tall building. The numerical simulation is performed using the computational fluid dynamics tool. Aerodynamic modification is less effective to reduce the structural vibration while the passive devices are more effective for reducing the same wind generated vibration in the tall building. The vibration is reduced by using the tuned mass damper techniques.

**Quan et al.** [144] investigated the aerodynamic interference effects on a high rise building in the presence of the another tall building. The most unfavourable positive and negative local wind pressures at certain locations on the windward façade of the target building are likely to be increased by the influences of the upstream nearby proposed super tall building. In the case of the even when half of the wind ward façade of the target building is shielded by the upstream high-rise building, two adjacent locations on its windward façade suffer tremendous positive and negative wind pressures for the same wind directions.

**Behera et al.** [145] conducted the boundary layer wind tunnel test on the effect of plan ratio on wind interference of two tall buildings. The interference zones extend over a larger area as the building plan ratio increases. The minimum interference factor depends on the plan ratio of the interfering building especially in the case of the oblique direction of the wind incidence angle. When the interfering building is located near the principal building, interference effects for the maximum positive pressures were generally beneficial due to shielding, but the minimum negative peak pressure significantly increased due to interference.

**Deng et al.** [146] performed an experimental study on the wind pressure distribution of tapered super high rise building. Chamfered modification can significantly increase the peak negative pressure at the chamfered locations. For the square model, the distribution of the peak wind pressure on side surfaces is nearly uniform, and the peak wind pressure coefficient is larger at the bottom of side surfaces. The peak negative pressures decrease with an increase of the tapering ratio of the model. For chamfered models, the maximum peak negative pressures coefficients of side surfaces, which occur at leading edge, increase significantly and increases with an increase of the tapering ratio.

## **2.4 Limitations**

It is observed from above studies that the wind load effects are available for various type of tall building but almost all studies are mainly performed on same type of plan cross sectional shape. Generally, the past studies are either performed on regular plan shape or irregular plan cross sectional shape while the aim of the present study was to investigate the wind effects on equal area building have plan cross sectional shape in the form of regular and irregular tall building. For the case of irregular building model, the present study is performed on “Y” shape model. The wind incidence angle varies from  $0^0$  to  $180^0$  wind at an interval of  $15^0$  wind. The various corner modification such as corner cut, chamfer and fillet are applied by keeping the equal ratio of corner modification in each type of tall building model.

# CHAPTER 3

## Methodology

### 3.1 General

As explained earlier in chapter-1, the main aim of the present study is to investigate the wind effects on the building model having equal area and same height of regular and irregular shape building model. This chapter explains the methodology adopted for the investigation of wind effects on tall building model using the numerical simulation.

### 3.2 Numerical Simulation

Numerical simulation is performed into this study and boundary condition used into this simulation are kept as the boundary condition used by Raj in the experiment performed in the boundary layer wind tunnel at IIT Roorkee, India. For the simulation a prerequisite is that the result should be validated with either to the experimental result or with some international standards. The domain is kept as per the various recommendation provided by different studies based on the numerical investigation. The numerical simulation performed into this study is performed using ANSYS CFX and uses the k- $\epsilon$  turbulence model.

#### 3.2.1 Computational Fluid Dynamics (CFD)

Computational fluid dynamics is the branch of engineering where various fluid dynamics equation are solved using finite element method technique where the numerical equation are solved for each element. Elements are making together different type of meshing pattern.

Basics problems of fluid dynamics are based on the Navier-stock equation and this is based on the three conservation laws; conservation of mass, conservation of momentum and conservation of energy.

##### 3.2.1.1 Governing Flow equation

Fluid flow in general is turbulent in nature and when the flow passes to the cars, planes and building it creates the high turbulence near the walls. A general definition in the case of turbulent flow is not possible because this involves a larger parameter. The basis of the fluid flow governing equation are as follows.

### 3.2.1.2 Navier Stokes Equation

The continuity equation is given in equation (1);

$$\dot{\rho} + \rho v_{i,i} = 0 \quad (1)$$

Change of notation into continuity equation become equation (2)

$$\frac{d\rho}{dt} + \rho \frac{\partial v_i}{\partial x_i} = 0 \quad (2)$$

For incompressible flow ( $\rho = \text{constant}$ )

$$\frac{\partial v_i}{\partial x_i} = 0$$

The momentum equation is as follows.

The momentum equation is based on the constative law for Newtonian Viscous fluids

$$\sigma_{ij} = -P\delta_{ij} + 2\mu S_{ij} - \frac{2}{3}\mu S_{kk}\delta_{ij} \quad (3)$$

$$\tau_{ij} = 2\mu S_{ij} - \frac{2}{3}\mu S_{kk}\delta_{ij} \quad (4)$$

This Newtonian equation modified form

$$\rho \frac{du_i}{dt} = -\frac{\partial P}{\partial x_i} + \frac{\partial \tau_{ji}}{\partial x_j} + \rho f_i = -\frac{\partial P}{\partial x_j} + \frac{\partial}{\partial x_j} \left( 2\mu S_{ij} - \frac{2}{3}\mu \frac{\partial v_k}{\partial x_k} \delta_{ij} \right) + \rho f_i \quad (5)$$

Where;

$\mu$  = dynamic viscosity

The above equation is the Navier Stokes equation (sometimes the continuity equation is also included in the name of “Navier-Stokes”).

The above equation is also known as the transport equation for momentum. Here the stress tensor  $\sigma_{ij}$  depend only on the symmetric part (i.e.,  $S_{ij}$ ) of the velocity gradient.  $S_{ij}$  is the only part of the velocity gradient which deforms the fluid. Also, the rotating part of the fluid doesn't account in the stress tensor.

For incompressible flow, the last term in the diffusion term is zero because of the continuity equation.

$$\rho \frac{du_i}{dt} = -\frac{\partial P}{\partial x_i} + \frac{\partial}{\partial x_j} \left[ \mu \left( \frac{\partial u_i}{\partial x_j} + \frac{\partial u_j}{\partial x_i} \right) \right] = \rho f_i \quad (6)$$

If the viscosity,  $\mu$  is constant equation is re-written as

$$\frac{\partial}{\partial x_j} \left[ \mu \left( \frac{\partial u_i}{\partial x_j} + \frac{\partial u_j}{\partial x_i} \right) \right] = \mu \frac{\partial}{\partial x_j} \left( \frac{\partial u_i}{\partial x_j} + \frac{\partial u_j}{\partial x_i} \right) = \mu \frac{\partial^2 u_i}{\partial x_j \partial x_j} \quad (7)$$

As per the continuity equation, i.e.

$$\mu \frac{\partial}{\partial x_j} \left( \frac{\partial v_j}{\partial x_i} \right) = \mu \frac{\partial}{\partial x_i} \left( \frac{\partial v_j}{\partial x_j} \right) = 0 \quad (8)$$

For constant  $\mu$  and incompressible flow it can be re written as

$$\rho \frac{dv_i}{dt} = -\frac{\partial P}{\partial x_i} + \mu \frac{\partial^2 u_i}{\partial x_j \partial x_j} + \rho f_i \quad (9)$$

The viscous stress tensor then becomes

$$\tau_{ij} = 2\mu S_{ij} = \mu \left( \frac{\partial v_i}{\partial x_j} + \frac{\partial v_j}{\partial x_i} \right) \quad (10)$$

For inviscid (potential) flow, there are no viscous (friction) forces, In that case the Navier-Stokes equation reduces to Euler equations

$$\rho \frac{dv_i}{dt} = -\frac{\partial P}{\partial x_i} + \rho f_i \quad (11)$$

### 3.2.2 Turbulence model

Various types of turbulence models are available to solve fluid problems but most of the past studies done in the field of wind engineering recommend that the for complex fluid problem of tall building should be solved by utilizing the k- $\epsilon$  turbulence model while the problem related to low rise building should be solved by using SST and k- $\omega$  turbulence model. These all-turbulence model provide the solution based on Reynold Average Naiver-Stokes (RANS) equation.

The laminar flow is governed by the unsteady characteristics of Navier-Stokes equation, this typically applies in the case of low Reynold number if by mistake the simulation is solved for the low Reynold number then solution might not converge and simulation will not provide an accurate result.

### 3.2.2.1 Zero-Equation Model

When the complex fluid problem of turbulent flow is solved using the zero- equation model in CFX, no doubt that solution will generate the results very quickly also it helps in trial and error for setting the real boundary condition. Generally, zero equation model uses the constant eddy viscosity for the entire fluid problem unless it is changed.

### 3.2.2.2 Two- Equation Model

Various turbulence model like k-ε, SST and k-ω are two equation model, where the numerical simulation generate the solution after solving two different equations.

- **k-ε turbulence model**

This method is generally used to solve complex fluid problem and it is two equation model. Solution is generated after solving two different equations during the entire numerical simulation. This model performs nearly equivalent to experimental problem and k-ε model also uses the scalable wall-function to increase the efficiency of the solver and this model perform more robustness in the case of the fine mesh.

It is very less expensive and mostly used to simulate the turbulent flow characteristics. K-ε turbulence model is two-equation model and provides the solution by using two transport equations, i.e., turbulent kinetic energy (k) and turbulent dissipation rate (ε). It has positive advantage of not including any geometry-related parameters in the modelling. The turbulent kinetic energy and the turbulence dissipation rate are two variables introduced into the system of equations for the model. The values for turbulence are calculated according to turbulence eddy dissipation using

The inlet value of turbulence kinetic energy (k) is given by Eq. (1)

$$k = \frac{3}{2} (U_{avg} I)^2 \quad (12)$$

$$\epsilon = \frac{c_{\mu} k^2}{v(\mu_{\tau}/\mu)} \quad (13)$$

Where;

$c_{\mu}$  = a non-dimensional constant

K = is the turbulent kinetic energy



$\nu$  = is the kinematic viscosity

$\mu_t/\mu$  = eddy viscosity ratio

The standard  $k$ - $\epsilon$  model uses the following equations;

The continuity equation

$$\frac{\partial \rho}{\partial t} + \frac{\partial}{\partial x_j}(\rho U_j) = 0 \quad (14)$$

Momentum equation

$$\frac{\partial(\rho U_i)}{\partial t} = -\frac{\partial(\rho U_i U_j)}{\partial x_j} - \frac{\partial P}{\partial x_i} + \frac{\partial}{\partial x_j} \left[ \mu_{eff} \left( \frac{\partial U_i}{\partial x_j} + \frac{\partial U_j}{\partial x_i} \right) \right] + S_M \quad (15)$$

$S_M$  is the sum of body force,  $\mu_{eff}$  is the effective viscosity accounting for turbulence, and  $p'$  is the modified pressure as defined in equation (4)

$$P + \frac{2}{3} \rho k + \frac{2}{3} \mu_{eff} \frac{\partial U_k}{\partial k} \quad (16)$$

The term in equation (4)  $+\frac{2}{3} \mu_{eff} \frac{\partial U_k}{\partial k}$  Represent the divergence of velocity. It is ignored in ANSYS CFX solver, so this hypothesis is valid for incompressible fluids.

The  $k$ - $\epsilon$  model depends on the eddy viscosity concept so that

$$\mu_{eff} = \mu + \mu_t \quad (17)$$

Where

$\mu_t$  Turbulence viscosity.

The  $k$ - $\epsilon$  model uses the turbulence viscosity is linked to the turbulence kinetic energy and dissipation via the relation:

$$\mu_t = \rho c_\mu \frac{k^2}{\epsilon} \quad (18)$$

Where  $c_\mu$  is the dimensionless constant of value 0.09

The values of  $k$  and  $\epsilon$  taken directly from the differential transport equations for the turbulence kinetic energy and turbulence dissipation rate:

$$\frac{\partial(\rho k)}{\partial t} + \frac{\partial}{\partial x_j}(\rho U_j k) = \frac{\partial}{\partial x_j} \left[ \left( \mu + \frac{\mu_t}{\sigma_k} \right) \frac{\partial k}{\partial x_j} \right] + P_k - \rho \varepsilon + P_{kb} \quad (19)$$

$$\frac{\partial(\rho \varepsilon)}{\partial t} + \frac{\partial}{\partial x_j}(\rho U_j \varepsilon) = \frac{\partial}{\partial x_j} \left[ \left( \mu + \frac{\mu_t}{\sigma_k} \right) \frac{\partial \varepsilon}{\partial x_j} \right] + \frac{\varepsilon}{k} (C_{\varepsilon 1} P_k - C_{\varepsilon 2} \rho \varepsilon + C_{\varepsilon 1} P_{\varepsilon b}) \quad (20)$$

Where  $C_{\varepsilon 1}$ ,  $C_{\varepsilon 2}$ ,  $\sigma_k$  and  $\sigma_\varepsilon$  are constant.

$P_{kb}$  and  $P_{\varepsilon b}$  Represent the influence of the buoyancy forces, which are described in equation (10).

$P_k$  Turbulence production due to viscous forces, which is modeled using.

$$P_k = \mu \left( \frac{\partial U_i}{\partial x_j} + \frac{\partial U_j}{\partial x_i} \right) \frac{\partial U_i}{\partial x_j} - \frac{2}{3} \frac{\partial U_k}{\partial x_k} \left( 3\mu_t \frac{\partial U_k}{\partial x_k} + \rho k \right) \quad (21)$$

### Advantages

- Performs best for boundary layer separation fluid problem.
- Most use turbulence model for validation purposes.
- Generally, use by industrialist to solve complex fluid problem.
- Provided the solution based on the boundary conditions.

### Disadvantage

- Doesn't perform well in the case where flow is changing instantaneously.
- Unable to generate the accurate solution for rotating fluid problem.
- Not able to generate the accurate solution for low Reynold number.
- Cannot reproduce the separation and reverse flow at the roof top of building model.

### • k- $\omega$ Turbulence model

This model provides the solution after solving the transport variable k, turbulence kinetic energy and turbulence dissipation rate. Sometimes k- $\omega$  turbulence model performs better than the k- $\varepsilon$  turbulence model. It may also provide the solution near-wall treatment and generate solution for problem based low Reynold – number.

This turbulence model, first proposed by Kolmogorov in 1941, it was in fact the first model of turbulence. The advantage of this turbulence model over the k- $\varepsilon$  turbulence model is that it

utilizes the  $\varepsilon$ - equation with the  $\omega$ - equation which is easy for the numerical simulation to generate the simulation.[147]

Eddy viscosity

$$\mu_t = \rho \frac{k}{\omega} \quad (22)$$

Turbulent kinetic energy

$$\rho \frac{\partial k}{\partial t} + \rho \bar{u}_i \frac{\partial k}{\partial x_j} = \tau_{ij} \frac{\partial \bar{u}_i}{\partial x_j} - \beta^* \rho \omega^2 + \frac{\partial}{\partial x_j} \left[ (\mu + \sigma^* \mu_t) \frac{\partial k}{\partial x_j} \right] \quad (23)$$

Specific dissipation rate

$$\rho \frac{\partial \omega}{\partial t} + \rho \bar{u}_j \frac{\partial \omega}{\partial x_j} = \alpha \frac{\omega}{k} \tau_{ij} \frac{\partial \bar{u}_i}{\partial x_j} - \beta \rho \omega^2 + \frac{\partial}{\partial x_i} \left[ (\mu + \sigma \mu_t) \frac{\partial \omega}{\partial x_j} \right] \quad (24)$$

- **Shear Stress Transport (SST)**

Standard k- $\varepsilon$  turbulence model some time unable to provide accurate solution in the case of turbulent flow and some time it may not provide the exact location of flow separation point. The SST turbulence model mostly used to get the solution for the problem which are based on low rise building. SST model also perform most optimum near the wall region and it also enable to generate the solution in the case of adverse pressure gradient. Major drawback which are not addressed with the help of k-  $\varepsilon$  turbulence model are addressed using SST model. SST model is giving the most efficient solution in the case of flow separation and to get the solution of aerodynamic related problem like aeroplane where lift is controlled. SST model provided more conservative data for problem related to air foil. This model is performing better as the effect of transport of wind are accounted in calculating the effect of wind. SST model recommended for the problem related to boundary layer simulation. For free shear flow mathematically, this model is nearly equivalent to k- $\varepsilon$  model.

The transport equation for k to generate the solution in SST turbulence model are as follows;

$$\frac{\partial(\rho k)}{\partial t} + \frac{\partial}{\partial x_j} (\rho U_j k) = \frac{\partial}{\partial x_j} \left[ \left( \mu + \frac{\mu_t}{\sigma_k} \right) \frac{\partial k}{\partial x_j} \right] + P - \beta \rho k \omega \quad (25)$$

The transport equation for  $\omega$  to generate the solution in SST turbulence model are as follows;

$$\frac{\partial(\rho \omega)}{\partial t} + \frac{\partial}{\partial x_j} (\rho U_j \omega) = \frac{\partial}{\partial x_j} \left[ \left( \mu + \frac{\mu_t}{\sigma_\omega} \right) \frac{\partial \omega}{\partial x_j} \right] + \alpha \frac{\omega}{k} P - \beta \rho \omega^2 + 2(1 - F_1) \frac{\rho \sigma}{\omega} \frac{\partial k}{\partial x_j} \frac{\partial \omega}{\partial x_j} \quad (26)$$

Where;

$2(1 - F_1) \frac{\rho \sigma \omega_2}{\omega} \frac{\partial k}{\partial x_j} \frac{\partial \omega}{\partial x_j} =$  cross diffusion term and  $F_1$  is a blending function.

### Advantages

- SST turbulence model work near wall using the k- $\omega$  turbulence model while it works away from the wall using the standard k- $\epsilon$  turbulence model.
- This two-turbulence model works on the basis of cross-diffusion derivative term.
- Turbulent viscosity takes into account for the transport of turbulent shear stress.

### 3.3 Geometry

Most of the studies available is either for regular shape or irregular shape while in this study the investigation of wind effects is done on both type of equal area and same height building model. The main objective of this study is about the corner configuration for these purposes different type of corner such as corner cut, chamfer and fillet of equal ratio is considered. Plan cross sectional shape model having the shape of rectangular with variation in the corner configuration is presented in Figure.3.1 Plan View of regular shape model and irregular shape model is depicted in the Figure.3.2 Plan View of Irregular Y- shape model.

#### Plan Shape: -

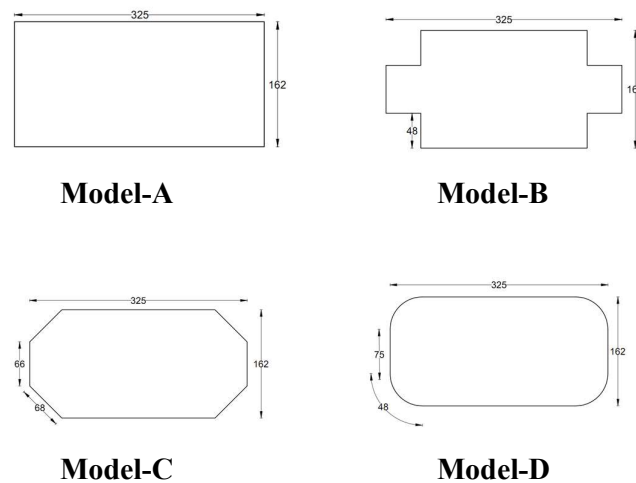


**Figure.3.1 Plan View of regular shape model**

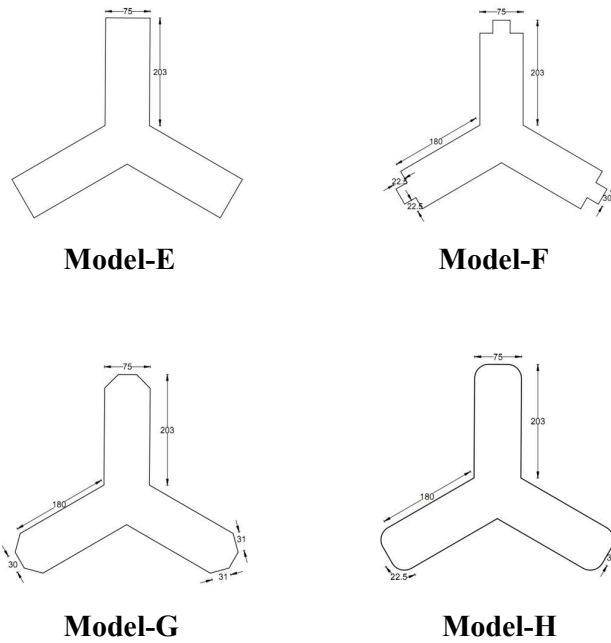


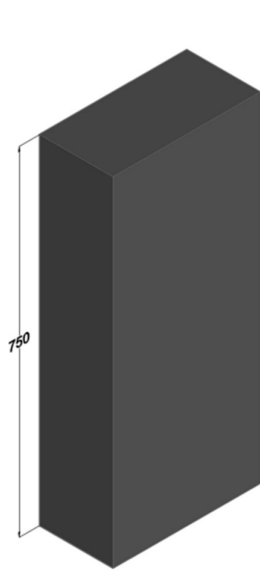
**Figure.3.2 Plan View of Irregular Y- shape model**

Isometric view is for the regular shape of rectangular shape model-A, model-B, model-C and model-D is illustrated in the Figure.3.3 Isometric View of regular shape model and the dimension along the height is also depicted in the figure. Model which is having triaxial symmetry is presented in the isometric view in Figure.3.4 Isometric View of irregular Y-shape model.

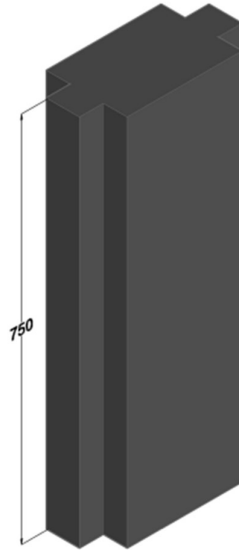
The main objective of the present study was to compare the wind generated effects on the equal area building it is because of the most of the past available studies are concentrated either on the regular shape or on the irregular shape. The present study not only studied the equal area building model while the modification in the corner configuration was also equal so that the structural designer can check the suitability of the type of the building model.

The present study is depicting the variation in the pressure in the form of pressure contours, pressure along the central line of the surface of the building model with the height and pressure along the peripheral distance. The drag and lift force are depicted in the graphical form for the wind incidence angle varies from  $0^0$  to  $180^0$  at the interval  $15^0$ .

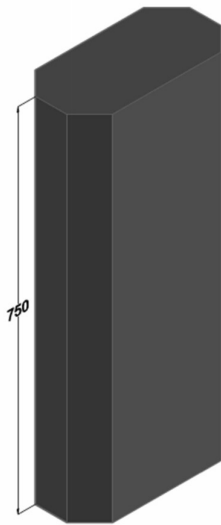
**Isometric Model:-**



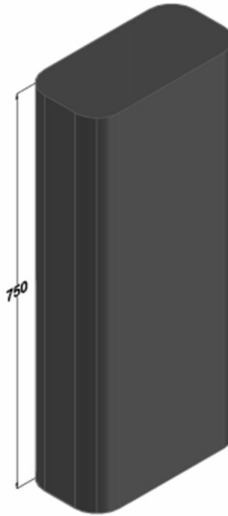
**Model-A**



**Model-B**

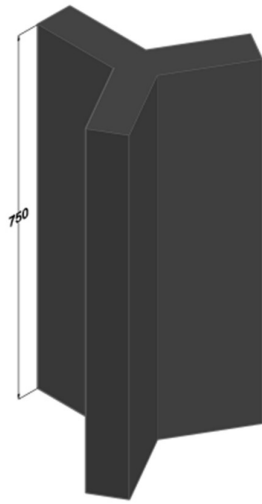


**Model-C**

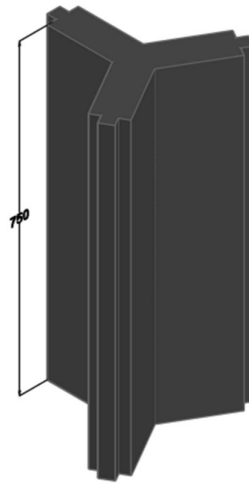


**Model-D**

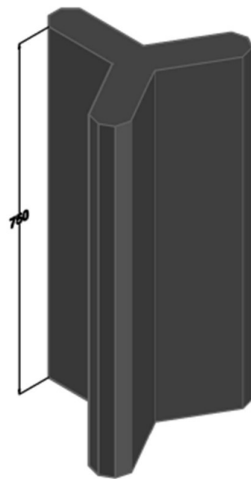
**Figure.3.3 Isometric View of regular shape model**



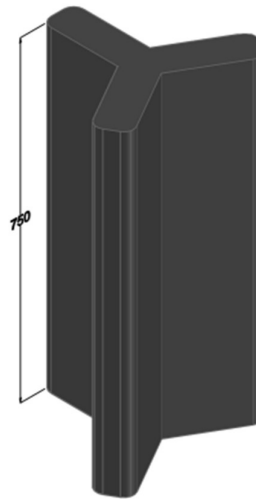
**Model-E**



**Model-F**



**Model-G**



**Model-H**

**Figure.3.4 Isometric View of irregular Y-shape model**

### 3.4 Meshing

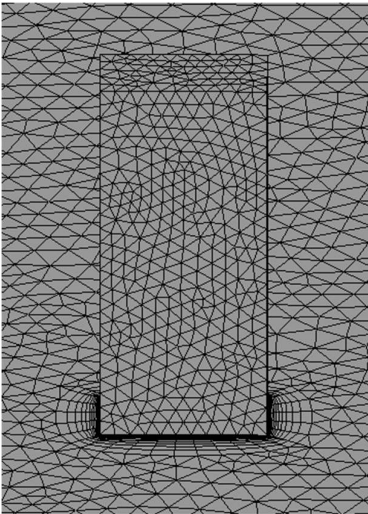
Meshing should be well designed to solve the numerical problem and for these purposes various CFD tools are available. Meshing contains important flow features which are dependent upon the flow parameters such as grid refinement inside the wall boundary layer. Steps for the meshing are as first draw the geometry as per the need after the geometry into the design modular or any other tool the model can be imported in to the design modular, the name selection for each part of geometry are required to understand the CFX pre about the geometrical configuration of the building model. The name selection is required to define flow physics. It is better to provide the name selection before the meshing so that the surface mesh exactly matches with nodes on the two sides of the boundary which allow more accurate fluid solution. Name selection also helps the program to controlled the inflation i.e., will automatically select for wall and inflation automatically provided during the auto mesh generation i.e., inflation.

The mesh generation steps are automatically work into the program however this can be controlled by varying the element size, type of mesh to generate and where and how the mesh should be refined. Meshing is of different types and ANSYS allow the tetra dominant meshing for the model that are directly imported into ANSYS and having a clean CAD geometry mostly this uses the large size of mesh. Tetra dominant meshing which is patch independent is suitable for CAD model having many surface patches and if the geometry is having the small edges than this is suitable. Hex meshing is uses the both general sweep and thin sweep, it is also recommended for the model which are having the clean cad geometry. Mapped and free meshing is adopted where the fluid problem needs different type of meshing like structured (mapped) and unstructured (free) however this is suitable for the problem where sweeping method not work without extensive geometry decomposition.

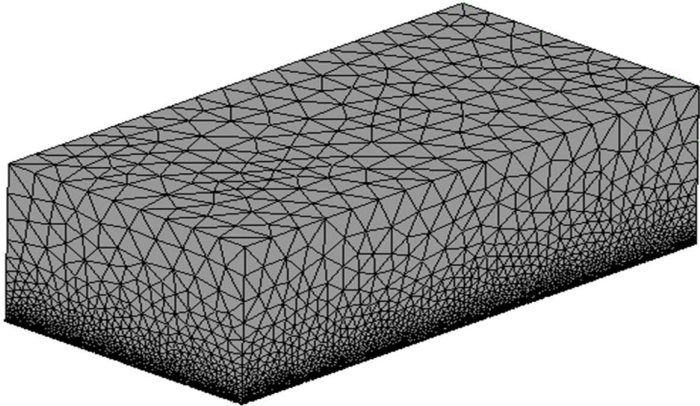
Inflation is provided to capture the flow properly at the interface and same can be provided by various method available into the CFD. Smooth transition this is the default option and it uses the local tetrahedron elements size to compute each local height and total height so that the rate of volume change is smooth, each triangle that is being inflated will have an initial height that is computed with respect to it is area, averaged at the nodes. This means that for the uniform mesh, the initial heights will be roughly same, while for a varying mesh, the initial height will vary. Increment in the value of growth rate control the reduction in the total height of the inflation layers. The total height of the inflation layers is the asymptotic value with respect to the number of the inflation layers. Total thickness option creates the constant inflation layers using the values



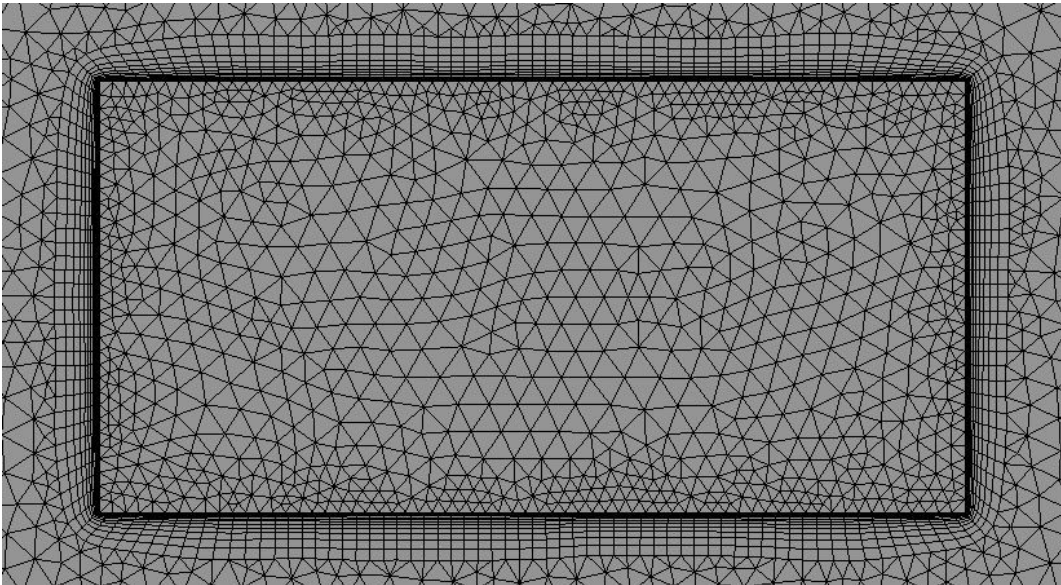
of the number of layers and growth rate controls to obtain the total thickness as defined by the value of the maximum thickness controls. First layer thickness creates the constant inflation layers using the values of the first layer height, maximum layers and growth rate can be control to generate the inflation mesh. Meshing done in the numerical simulation is presented in Figure 3.5 Different Meshing; (a) Building Meshing; (b) Domain Meshing and (c) Inflation.



(a)



(b)



(c)

**Figure 3.5 Different Meshing; (a) Building Meshing; (b) Domain Meshing and (c) Inflation**

Transition ratio controls the rate at which adjacent elements grow, it is the volume-based size change between the layer of elements in the inflation layer and the first elements in the tetrahedron region. The value of transition ratio is an ideal value and should produce accurate size change for inflation from a planar body. However, it is be aware that area of strong curvature will introduce an accuracy into the size change. Also, this transition ratio controls is only applicable in the case of smooth transition. Numerical simulation solves the problem based on the finite volume method in which the geometry is discretises into the elements and fluid flow is passes through this element so that result can be produces after CFD post.

### **3.5 CFX Pre**

#### **3.5.1 Grid Independent Test**

In this study a grid convergence study was performed on model - A . Grid convergence study is essential requirement for a CFD programming because it suggest, the meshing pattern for entire numerical simulation. For the present study GC-3 is selected for various cases of wind incidence angle that are varies in the range of  $0^0$  to  $90^0$  at an interval of  $30^0$  each. In this study the grid convergence is performed on the basis of procedure provided by Celik et al.[148] and Derakhshandeh and Alam [149]. The percentage error is reported in the Table-3.1 Grid Convergence Test result for model -A and GC-3 is adopted because of the less percentage error reported in the mean  $C_p$  compared with the IS: 875 (part-3): 2015 [2] for  $0^0$  wind incidence angle. Reynold number varies from  $3.56 \times 10^6$  to  $3.90 \times 10^6$  for all the models which signifies that flow is turbulent flow for the entire numerical simulation. The grid convergence study is performed on five different cases by varying the meshing type namely coarse, medium and fine. Number of elements for coarse, medium and fine meshing are 957324, 1439589 and 2497236 respectively. It is clearly demonstrated from the table-1 that the medium mesh performed most optimum for GC-3 and the error is calculated with respect to IS 875 (part-3): 2015. When the solution is obtained using the numerical simulation the geometry of the building is divided into the small elements and these elements are of many shapes for the present study the tetrahedron meshing is adopted for the domain. The flow is computed into these grids and stiffness matrix is solved for each grid and these is the procedure adopted for obtained the solution for the wind engineering problem solved through the computational fluid dynamics tool in the present study.

**Table-3.1 Grid Convergence Test result for model -A**

Name	Type of Meshing	No of Elements	Mean External Pressure				% Error				Reynold No
			Face				A	B	C	D	
			A	B	C	D	A	B	C	D	
GC-1	Coarse	957324	0.59	-0.49	-0.24	-0.49	36%	32%	26%	32%	3.56×10 <sup>6</sup> to 3.90×10 <sup>6</sup>
GC-2	Medium-1	1284687	0.73	-0.56	-0.27	-0.56	10%	16%	12%	16%	
<b>GC-3</b>	<b>Medium-2</b>	<b>1439589</b>	<b>0.78</b>	<b>-0.64</b>	<b>-0.30</b>	<b>-0.64</b>	<b>3%</b>	<b>2%</b>	<b>0%</b>	<b>2%</b>	
GC-4	Medium-3	1561140	0.81	-0.69	-0.32	-0.69	1%	5 %	6 %	5 %	
GC-5	Fine	2497236	1.02	-0.98	-0.43	-0.98	33%	33%	30%	33%	

### 3.5.2 Velocity profile

Wind flow over the tall building involves the complex flow patterns, wind flow generally separated from the surface, where the flow is mostly recirculating. Flow patterns are unsteady and thus these are creating the turbulence that is why the investigation of wind effects are the main objective of this study. These turbulences are also developing because of the rough surface and blockage of wind. Such effects are accounted into the boundary layer flow which states that the wind up to the gradient height is increasing and after that it becomes constant. This is known as boundary layer depth and wind speed is also called free stream velocity. Wind velocity variation is presented in Figure 3.6 Variation of velocity profile with height.

Numerical simulation solution of complex fluid problem depends upon the number of parameters, basically finite element-based solution is dependent on the boundary condition. That is why in this entire numerical simulation for the better accuracy the boundary condition is kept same as that done in the experiment performed by Raj[150] in the boundary layer wind tunnel (BLWT). However, the boundary and the guidelines provided in the wind tunnel manual and report no 67 were kept in the consideration during the modelling of the setup before the starting of the solution.

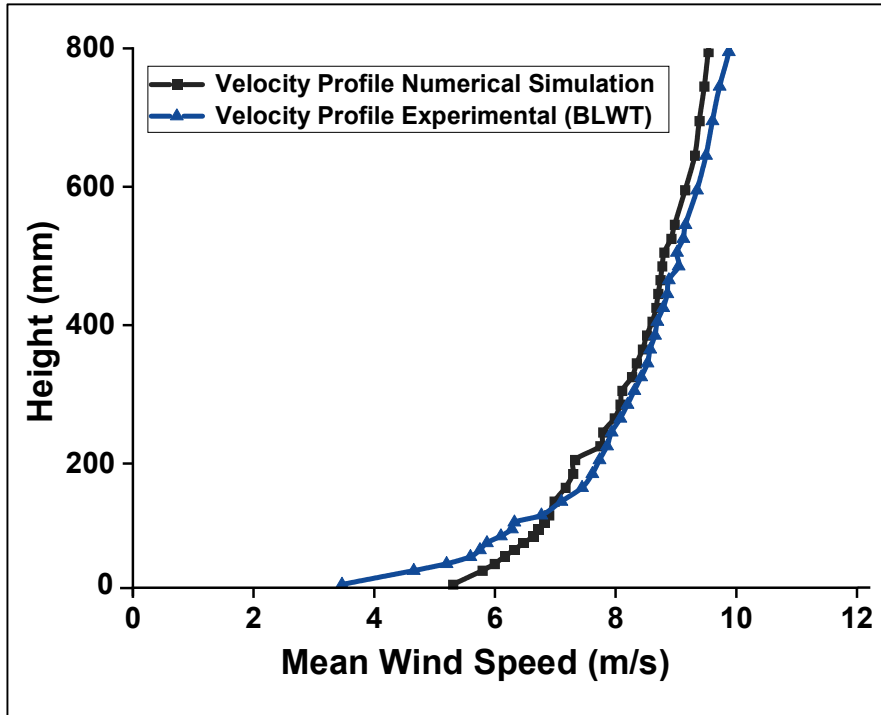


Figure 3.6 Variation of velocity profile with height

Mean wind speed defines in the CFX Pre is represented in the Figure 3.6 Variation of velocity profile with height , this the variation in the form of a power law between height and mean wind speed is as follows;

$$\frac{U(Z)}{U(Z_{ref})} = \left(\frac{Z}{Z_{ref}}\right)^n \quad (27)$$

Where

$U(Z)$  = mean velocity at height  $Z$ ;

$U(Z_{ref})$  = mean velocity at reference height  $Z_{ref}$ ; and

$n$  = power law exponent, a measure of ground roughness; varies between 0.13 to 0.15 in open terrain

The variation in the mean wind speed with height is generally expression in alternate form in logarithmic form.

$$\frac{U(Z)}{U_*} = \left(\frac{1}{k}\right) \ln\left(\frac{Z}{Z_0}\right) \quad (28)$$

Also a simplification of this logarithmic equation is as followed;

$$\frac{U(z)}{U(z_{ref})} = \frac{\ln\left(\frac{z}{z_o}\right)}{\ln\left(\frac{z_{ref}}{z_o}\right)} \quad (29)$$

Where;

$U_*$  = the shear velocity;

$k$  = von karman constant, 0.4;

$\ln$  = natural log function; and

$Z_o$  = effective roughness length, another measure of ground roughness; 0.01 to 0.05 meters in an open terrain.

The log law is less accurate at the lower altitude of more than the 100-200 m height while the power law predicts most appropriate results but log law is also suitable for tall buildings.

### Deves and Harris model

The log-law predicts good result where the ground roughness is not accounted and also this is not allowing the different wind characteristics. The Deaves and Harris model (Deaves and Harris 1978) overcome this problem by accounting the downwind characteristics in roughness profile.

$$\bar{V} = \frac{1}{K} u_* \left( \ln \left[ \frac{(z-d)}{z_o} \right] + 5.75 \left( \frac{z}{d} \right) / z_g \right) \quad (30)$$

Where;

$z_g$  = gradient height

### 3.5.3 Turbulent Intensity

Generally, turbulence intensity for the smooth terrain is less than the turbulence intensity for rough terrain. Turbulence intensity is a non-dimensional quantity derived from the variance and for the mean wind speed. The variation of turbulent intensity is presented in Figure 3.7 Variation of Turbulent intensity with height.

$$I_z = \frac{\sigma_z}{U(z)} \quad (31)$$

Where;

$I_z$  = turbulence intensity at height  $z$ ;

$\sigma_z$  = standard deviation of the wind speed at height  $z$ ; and

$U(z)$  = mean wind speed at reference height

An expression for turbulence is explain by Simu and Scanlan, 1986 [151]

$$T_u = \frac{(B)(U_*)}{U(z)} \quad (32)$$

Where;

$B$  = a constant, approximately 2.5 for open terrain.

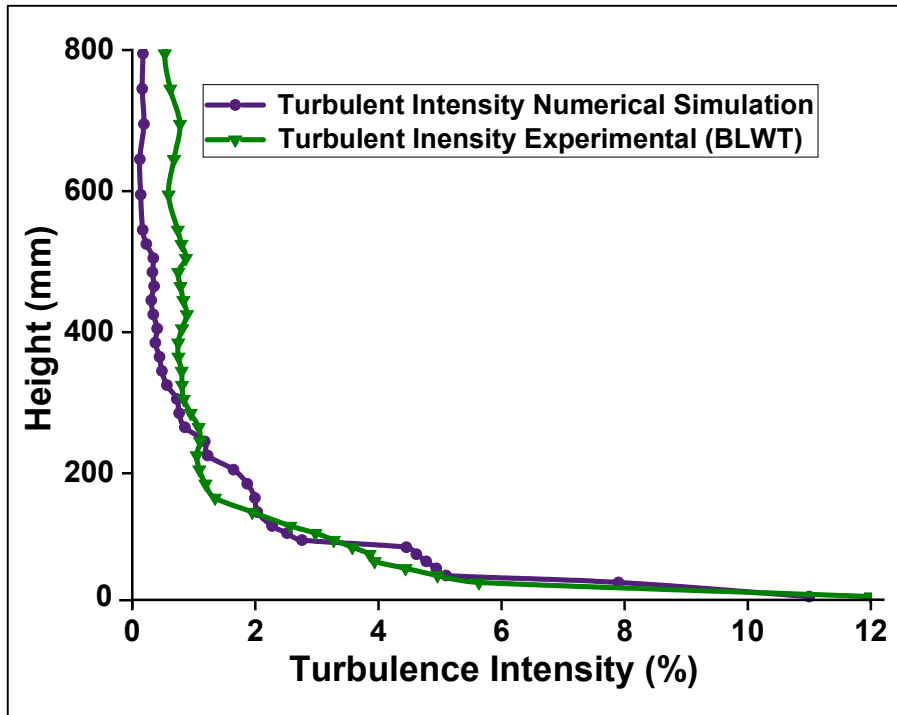


Figure 3.7 Variation of Turbulent intensity with height

### 3.5.4 Boundary Conditions

Numerical simulation predicts the result based on the boundary conditions as the finite element method work well with boundary conditions. In this entire study the boundary condition is kept similar with experiment performed by Raj.[150] in the boundary layer wind tunnel at IIT Roorkee. Inlet wind speed is provided as power law where the reference height in the simulation is considered as 1m while the reference velocity is defined as 10 m/s. The wall of the domain is

considered as free slip wall while the ground of the domain is rough wall. The faces of the model are considered as no slip. The iteration is kept same for each wind incidence angle and these are kept same as with the validation model. Wall function defines that if a coarse mesh near the wall than it assumes that the logarithmic law applies as wall function. While the fine mesh near the wall and various turbulence model account for low Reynolds number. Wall function are useable to low Reynolds number problems. The domain is depicted in Figure 3.8 Isometric view of domain used in the numerical simulation and Figure 3.9 Plan view of domain used in the numerical simulation.

In general, if the fine mesh is defined near the wall than the gradient changes are considered automatically by the solver.

### **No slip wall**

This is the most common type of wall boundary condition. The fluid immediately next to the wall assumes the velocity of the wall, which is zero by default.

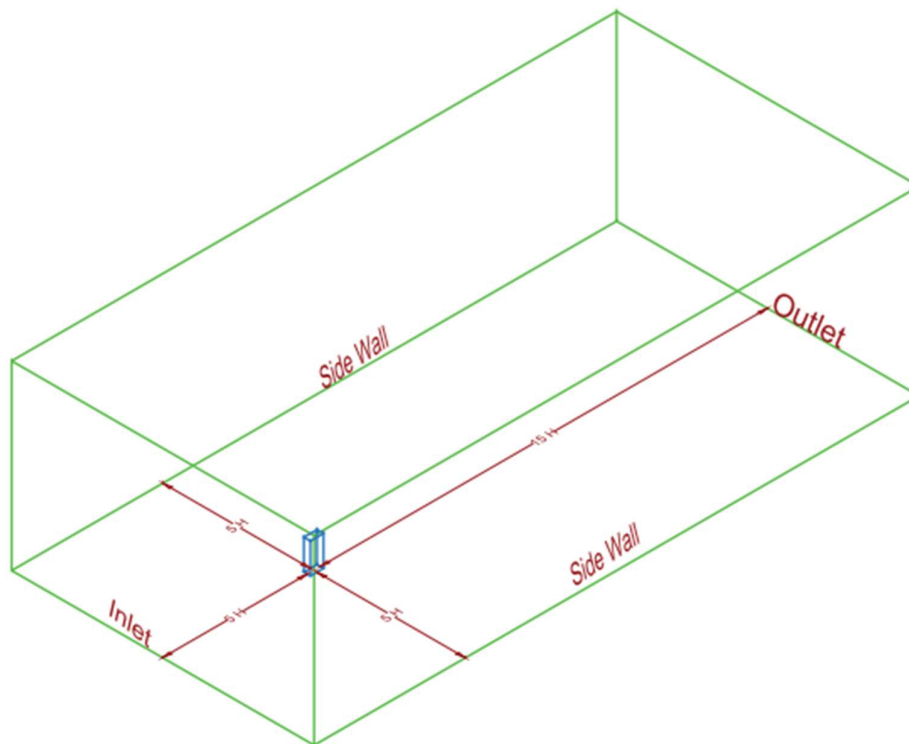


**Figure 3.8 Isometric view of domain used in the numerical simulation**

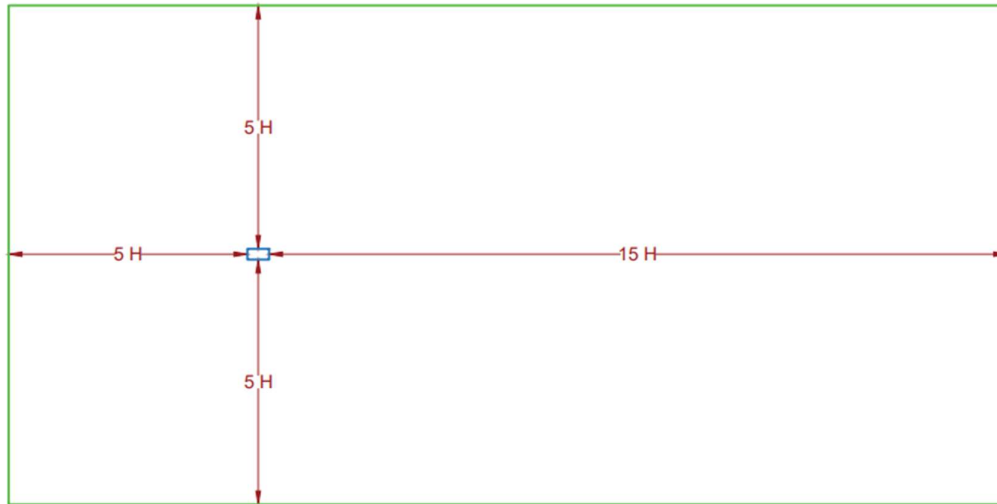


**Figure 3.9 Plan view of domain used in the numerical simulation**

### **Free slip wall**

Free slip wall, where the shear stress at the wall is zero and the velocity of the fluid near the wall is not retarded by the wall friction effects.

### **Wall roughness**

For simulation using the various turbulence model, smooth or rough type of wall can be provided. For rough wall, the equivalent sand grain roughness is required as an input parameters. High roughness is valuable for SST turbulence model.

Outlet boundary condition is used where the flow is predominantly directed out of the domain. The hydrodynamic boundary condition for a subsonic outlet involves some constraint on the boundary static pressure, velocity or mass flow. For all other transport equation, the outlet value of the variable is part of the solution.

### **3.6 Solver**

Numerical simulation is performed in ANSYS CFX and the wind is applied as power law. Generally, the tall building is affected by atmospheric boundary layer flow and where wind speed is varying with height. After a fixed height velocity becomes as free stream velocity and the height as which the velocity becomes as constant is known as gradient height. As per the recommendation available into different international standards this gradient is generally 10m



for the case of terrain category-II. Power law is modelled and the reference height in this numerical simulation is considered as 1m while the reference velocity is considered as 10 m/s. The convergence criteria is adopted as more than the residual criteria. The analysis of wind is done in the steady state only by utilizing the medium intensity of 5 %. The grid independent test is also performed on rectangular model-A which don't have any corner modification in the plan cross sectional shape.

### 3.7 CFD Post

CFD post helps to visualizes and analysis the wind effects into various type of graphical form. The result in the form of pressure distribution on vertical centre line of each face of the model considered in this study are evaluated for wind incidence angle varies from  $0^0$  to  $180^0$  at the interval of  $15^0$ . The result of pressure distribution along the peripheral distance of model are depicted into the graphical form. Result of pressure along the face as per the shape and size are depicted into the contour form with label. The result of wind response is also depicted into graphical form for wind force and moment coefficient. The building model are presented in Figure 3.11 Isometric view of the irregular shape building model.

The result of external pressure coefficient is found after drawing the lines on the model face, these lines are acting as pressure tapping and for each face the coordinate frame is also provided into the CFD post. Lines drawn for the purpose of vertical centre line are depicted in the isometric view in Figure 3.10 Isometric view of the regular shape building model having vertical centre line and Figure 3.11 Isometric view of the irregular shape building model having vertical centre line These lines pressure data is exported after the numerical simulation and then after performing the required calculation the average of each face is reported as external pressure coefficient. The formulas which are required to calculate the pressure is represented in equation (33)

The external pressure coefficient '  $C_p$  ' is calculated using the equation (33).

$$C_p = \frac{p-p_o}{\frac{1}{2}\rho U_H^2} \quad (33)$$

Where;

$p$  = pressure derived from the external lines plotted on the model;

$p_o$  = static pressure at reference height;

$\rho$  = air density (1.225 kg/m<sup>3</sup>);

$U_H$  = mean wind velocity at the building reference height.

The pressure on vertical centre line of each face for every model, the pressure is exported on that line and after that this data is also processed and represented along the height of the model.

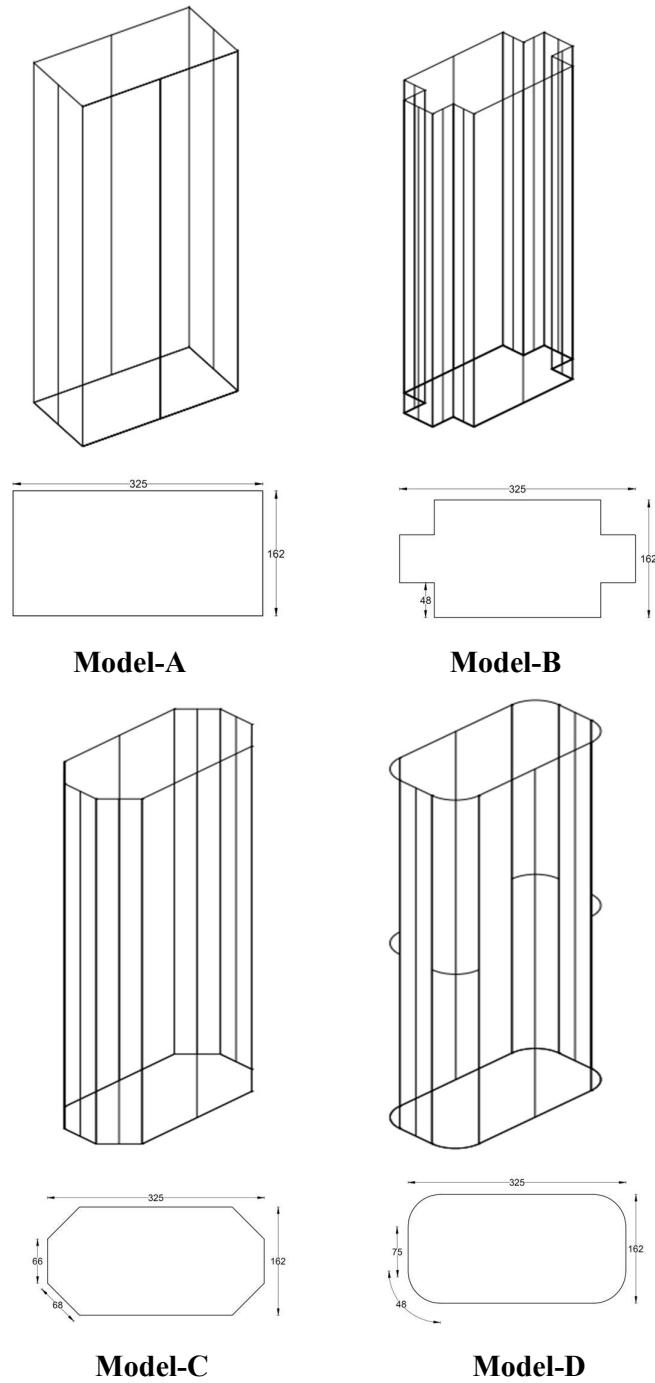
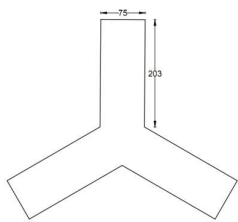
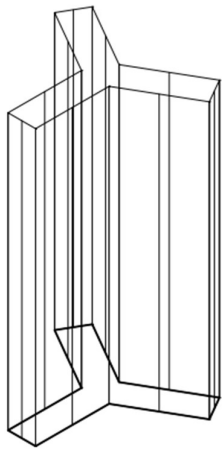
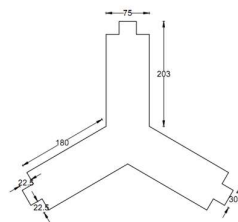
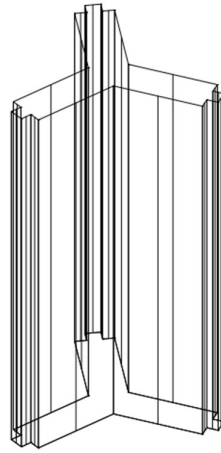


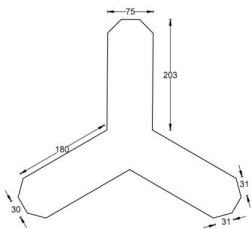
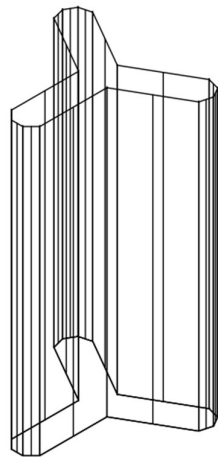
**Figure 3.10** Isometric view of the regular shape building model having vertical centre line



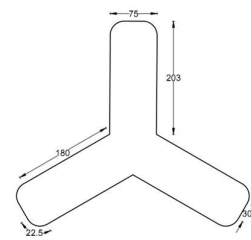
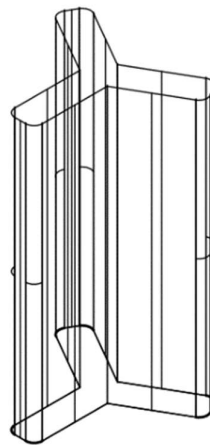
**Model-E**



**Model-F**



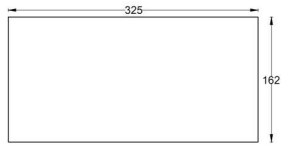
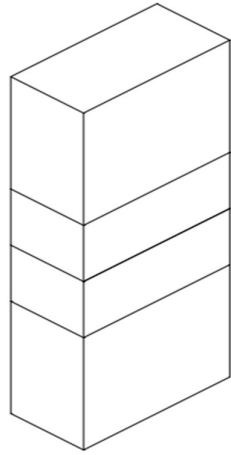
**Model-G**



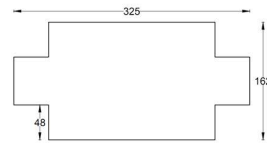
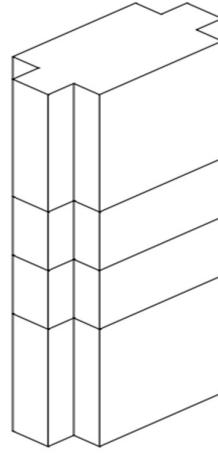
**Model-H**

**Figure 3.11 Isometric view of the irregular shape building model having vertical centre line**

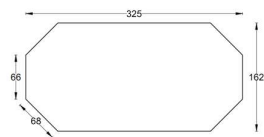
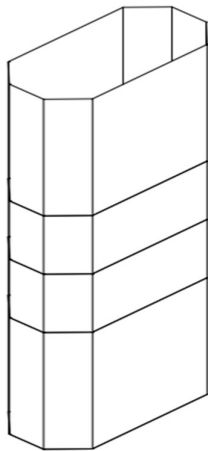
The pressure along the peripheral distance is also observed and process after the export. The pressure along the peripheral distance is found at three different level such as bottom one third (i.e. at 250 mm from the base of the model), mid height of the model (i.e. at 375 mm form the base of the model) and top one third (i.e. at 500 mm from the base of the model). The isometric view of the model having the horizontal peripheral distance are presented in Figure 3.12 Isometric view of the regular shape model having horizontal peripheral lines and Figure 3.13 Isometric view of the irregular shape model having horizontal peripheral lines. These pressure along the peripheral distance of the building model is depicted to provide the better understanding of the flow parameters such as reattachment, vortex shedding, wake in the downstream of wind. Presented the comparison for corner configuration building models and the pressure effects like along the model is presented so that the nature of pressure at each level for regular and irregular building model can be visualized clearly with the help of such figures where the variation of the pressure along the peripheral distance is depicted.



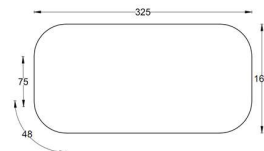
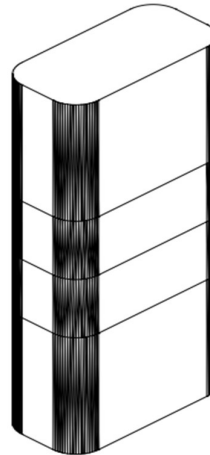
**Model-A**



**Model-B**

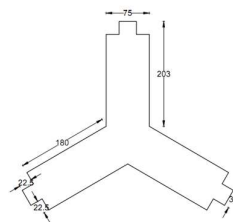
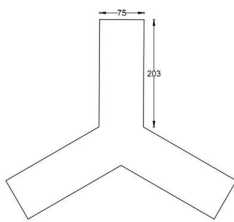
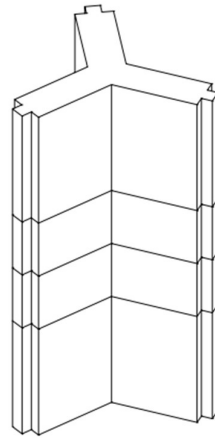
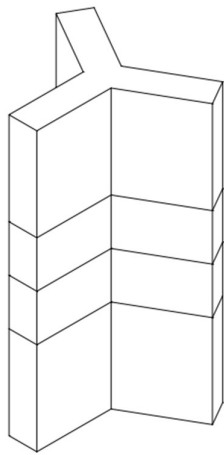


**Model-C**



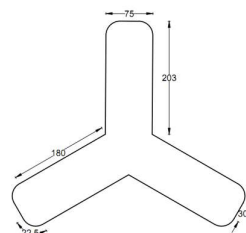
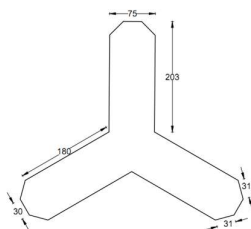
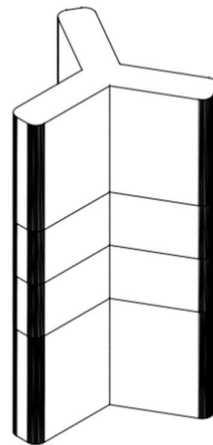
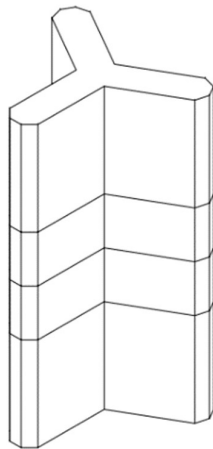
**Model-D**

**Figure 3.12 Isometric view of the regular shape model having horizontal peripheral lines**



**Model-E**

**Model-F**



**Model-G**

**Model-H**

**Figure 3.13 Isometric view of the irregular shape model having horizontal peripheral lines**

The wind generated effect in the form of wind force coefficient and moment coefficient are evaluated after the numerical simulation performed on building model. The value of Force in X and Y direction are obtained using CFD post while the projected area is calculated for each model at every wind incidence angle. Reference speed is considered as found during the velocity modelling. Density of air already described in the previous part. Likewise, the moment coefficient is also investigated in X and Y direction i.e., along and across wind direction. The equation used to find the force and moment coefficient are represented in equation 34 to equation 37.

$$C_{f_x} = \frac{F_x}{(0.5\rho U_h^2.A_p)} \quad (34)$$

$$C_{f_y} = \frac{F_y}{(0.5\rho U_h^2.A_p)} \quad (35)$$

$$C_{m_x} = \frac{M_x}{(0.5\rho U_h^2.A_p.H)} \quad (36)$$

$$C_{m_y} = \frac{M_y}{(0.5\rho U_h^2.A_p.H)} \quad (37)$$

### 3.8 Validation

Validation is performed on the rectangular building model which do not have any type of corner modification. Validation is pre-requisite of the numerical simulation for these purposes the four different model are considered in this study and rectangular model is selected because the data already available to validate this study is limited that is why rectangular and square model are selected. While a few studies are also available for corner cut model of rectangular shape and Y-shape which don't have any corner modification this is why such model are choose and compared the external  $C_p$  with all such models. The main objective of this study was the investigation of wind effect on the corner configuration model which is having the regular and irregular shape. This is also clearly depicted that the result obtained in this numerical simulation are showing nearly identical result for the pressure coefficient. The result of present CFD study is also compared with the other available CFD and experimental study.

### 3.8.1 Validation model:

The result plotted for rectangular model, rectangular model having corner cut and Y-shape model are representing a very close match with the results therefore the result obtained in this study are very much accurate for designing the model which are considered in this study. The square shape model is also investigated for wind load so that further pressure coefficient is compared with the available international standards and such values are tabulated in the table. The magnitude and nature are also obtained same with the available data for pressure coefficient. The model used for the validation is presented in Figure 3.14 Plan Cross sectional shape of validation model.

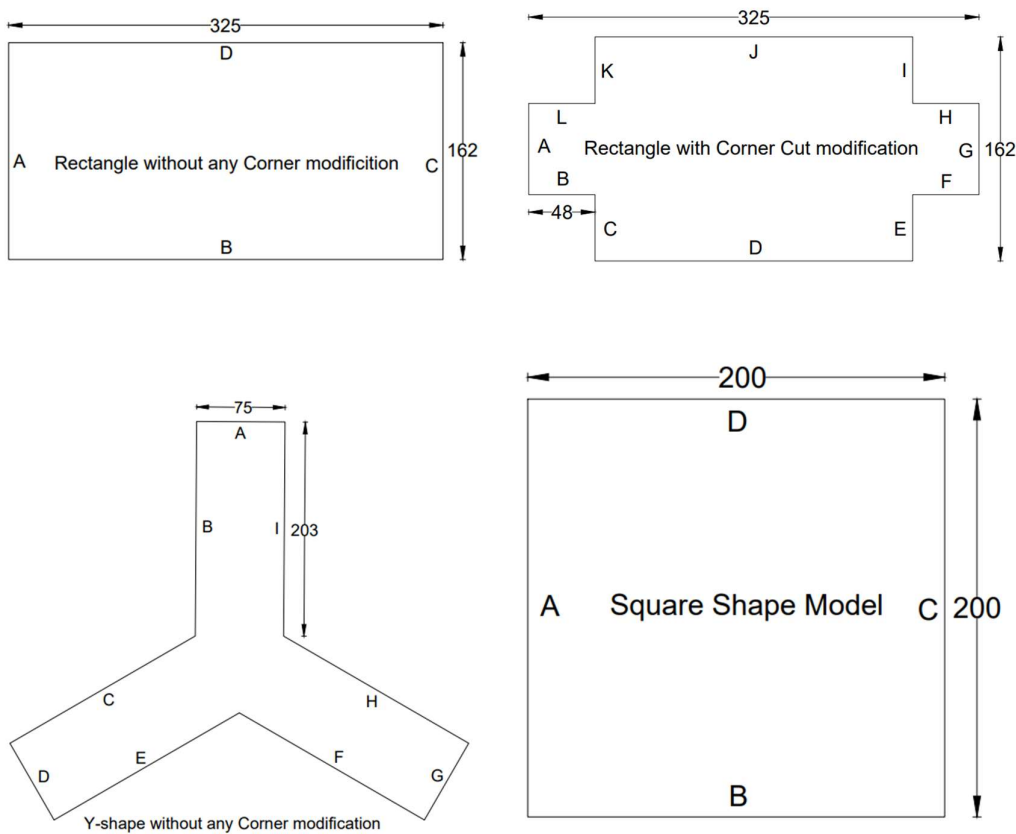


**Figure 3.14 Plan Cross sectional shape of validation model**

The available international standards are having the values of the regular shapes model and because of that the model having regular shape of rectangular and square shape model result of mean pressure on wind ward face, side face and lee ward face are compared and the result are more or less identical with the values of the pressure coefficient provided in the various international standards. Figure 3.15 Mean pressure coefficient comparison with various international standards and experimental studies on the rectangular shape model, Figure 3.16



Mean pressure coefficient comparison with various international standards and experimental studies on the corner cut model, Figure 3.17 Mean pressure coefficient comparison with various international standards and experimental studies on the irregular Y- shape model and Figure 3.18 Square shape validated model are presented. The mean values of pressure on square shape are tabulated in Table 3.2 Comparison of average face pressure coefficient ( $C_p$ ) on the Rectangular Tall Building.

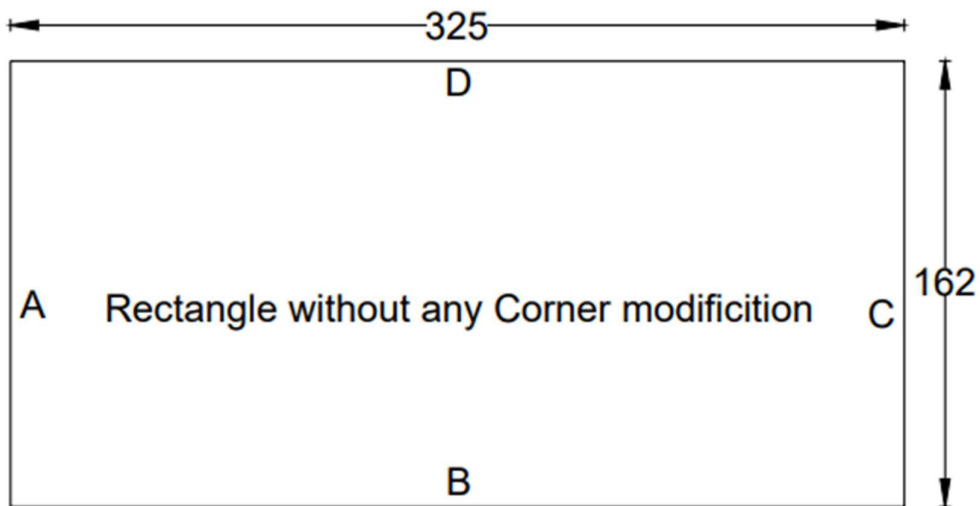
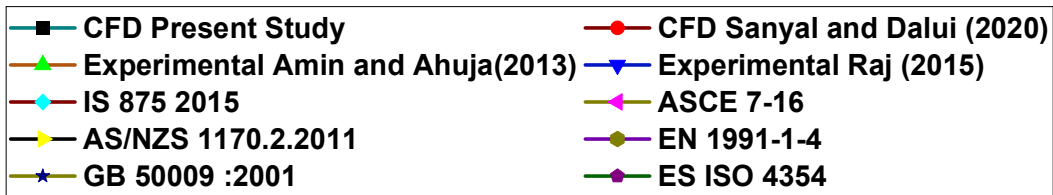
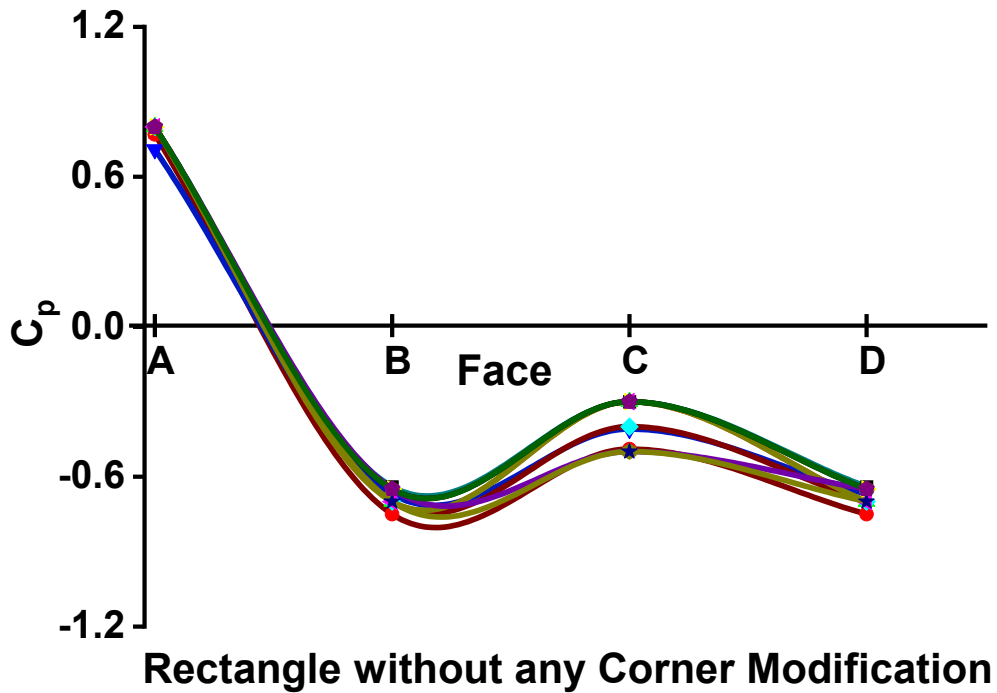
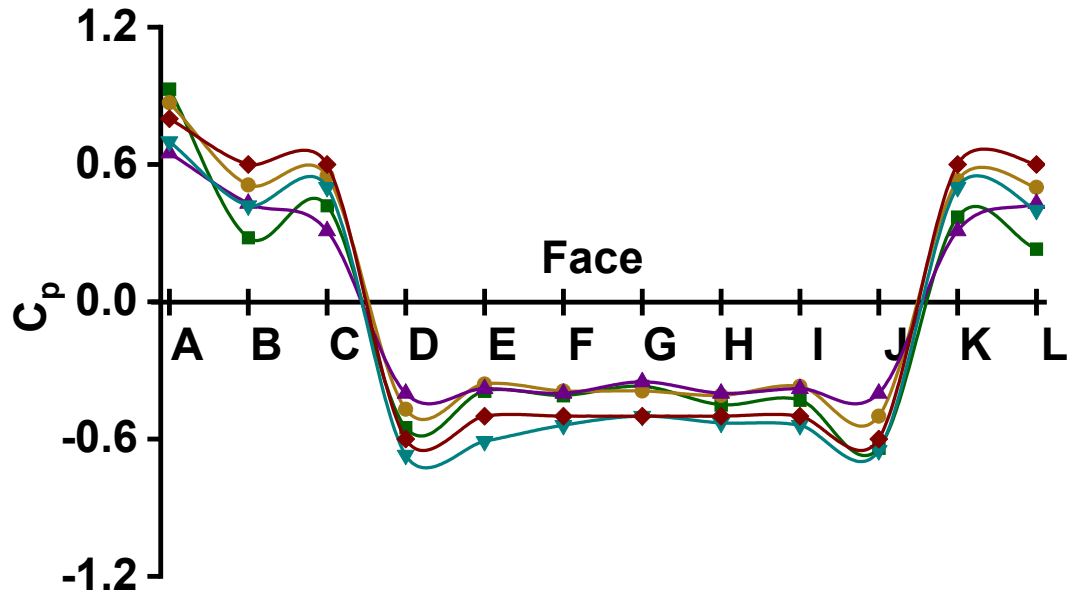


**Figure 3.15 Mean pressure coefficient comparison with various international standards and experimental studies on the rectangular shape model**



**Rectangular shape model with corner cut**

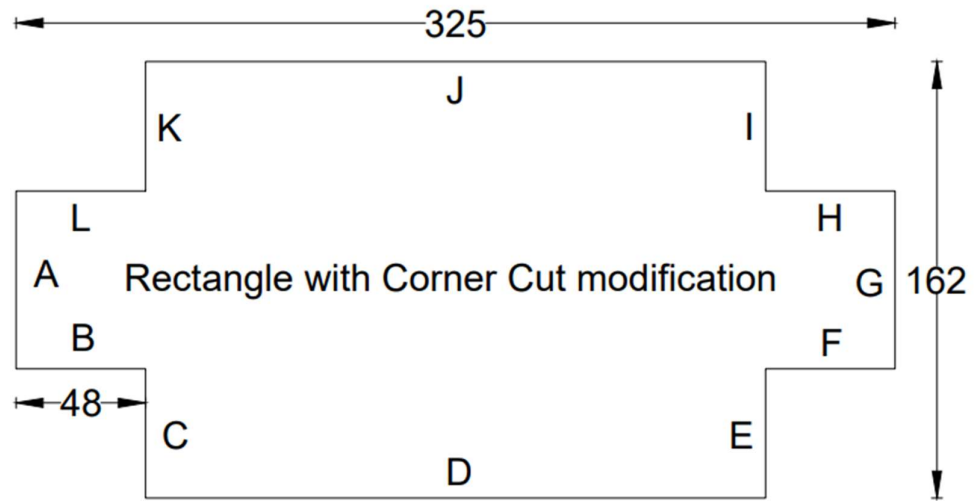


**Figure 3.16 Mean pressure coefficient comparison with various international standards and experimental studies on the corner cut model**

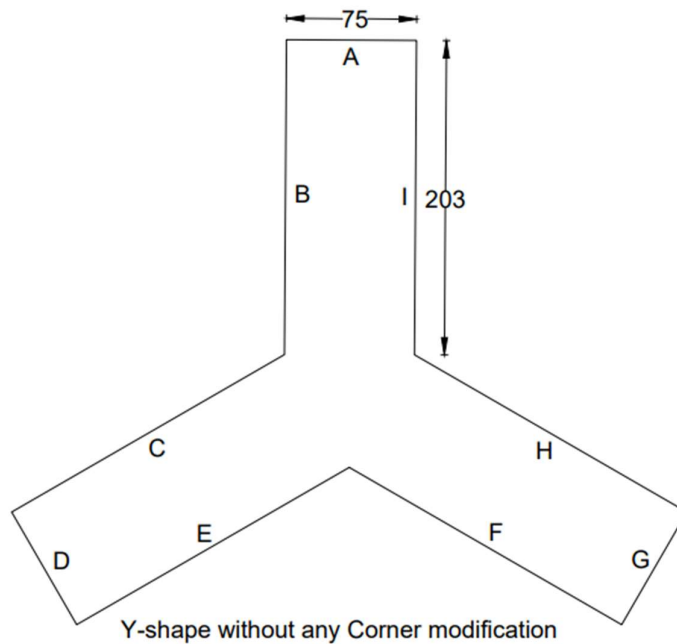
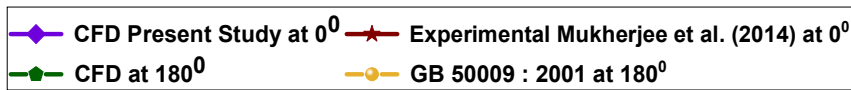
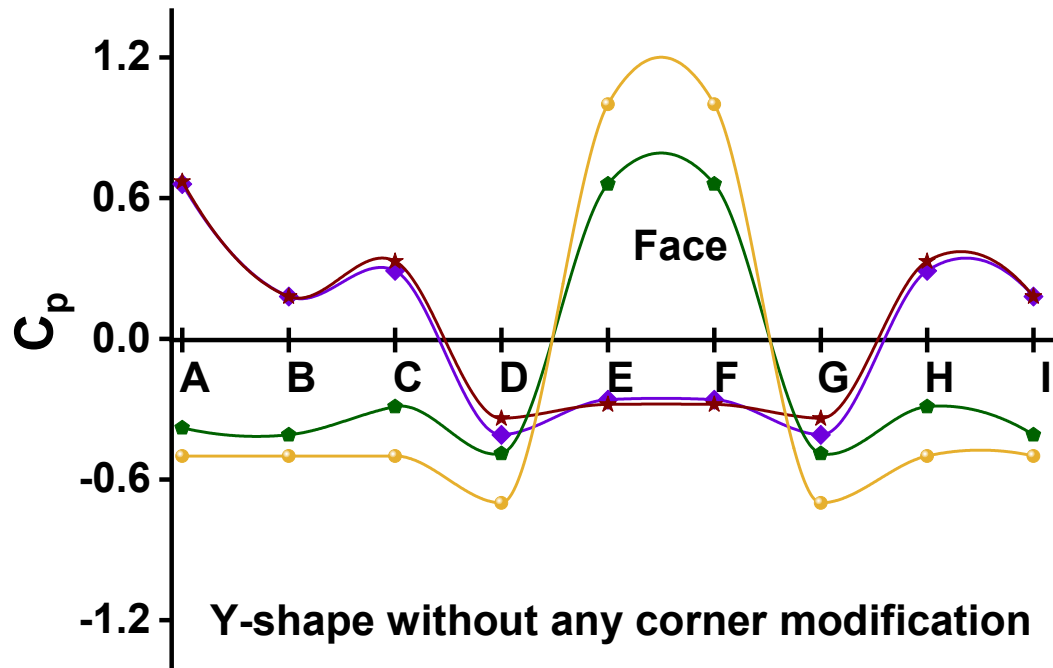


**Figure 3.17 Mean pressure coefficient comparison with various international standards and experimental studies on the irregular Y- shape model**

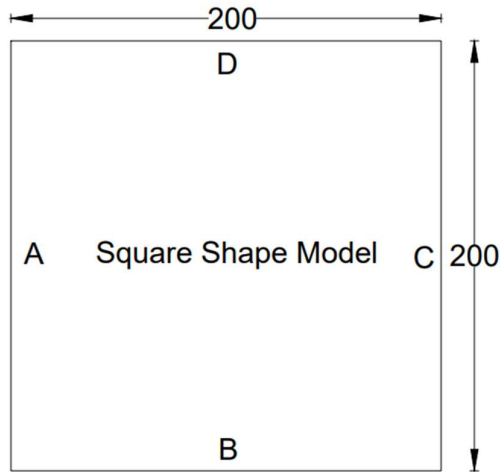


**Figure 3.18 Square shape validated model**

**Table 3.2 Comparison of average face pressure coefficient ( $C_p$ ) on the Rectangular Tall Building**

<b>International Code</b>	<b>Wind Angle</b>	<b>Windward Side</b>	<b>Side Wall</b>	<b>Leeward side</b>
<b>CFD Results</b>	<b>0<sup>0</sup></b>	0.78	-0.64	-0.30
	<b>90<sup>0</sup></b>	0.70	-0.61	-0.45
<b>IS 875 (Part 3)</b>	<b>0<sup>0</sup></b>	0.7	-0.7	-0.4
	<b>90<sup>0</sup></b>	0.8	-0.5	-0.1
<b>ASCE/SEI 7-16</b>	<b>0<sup>0</sup></b>	0.8	-0.7	-0.5
	<b>90<sup>0</sup></b>	0.8	-0.7	-0.5
<b>AS/NZS 1170.2.2011</b>	<b>0<sup>0</sup></b>	0.8	-0.65	-0.5
	<b>90<sup>0</sup></b>	0.8	-0.65	-0.5
<b>EN 1991-1-4</b>	<b>0<sup>0</sup></b>	0.8	-0.5	-0.7
	<b>90<sup>0</sup></b>	0.8	-0.5	-0.7
<b>BS 6399-2</b>	<b>0<sup>0</sup></b>	0.8	-0.5	-0.7
	<b>90<sup>0</sup></b>	0.8	-0.5	-0.7
<b>GB 50009-2001</b>	<b>0<sup>0</sup></b>	0.8	-0.5	-0.7
	<b>90<sup>0</sup></b>	0.8	-0.5	-0.7
<b>NSCP 2015</b>	<b>0<sup>0</sup></b>	0.8	-0.5	-0.7
	<b>90<sup>0</sup></b>	0.8	-0.5	-0.7
<b>ES/ISO 4354: 2012</b>	<b>0<sup>0</sup></b>	0.8	-0.65	-0.7
	<b>90<sup>0</sup></b>	0.8	-0.65	-0.7

Validation is a prerequisite part of numerical simulation and total four different models are considered in this study to validate the study with the available international standards and experimental studies. Regular shape three buildings models having plan cross sectional shape such as square, rectangle without any corner modification and rectangle having corner cut or plus shape is considered and external  $C_p$  compared with the available results. In case of irregular plan shape only “Y” shape without any corner modification is considered because of the limitations of the data availability thus in this case  $C_p$  values are compared with the experimental values. This is also clearly depicted in Figure 3.17 Mean pressure coefficient comparison with various international standards and experimental studies on the irregular Y- shape model and the result obtained in this numerical simulation show nearly identical result for the pressure coefficient.

## CHAPTER 4

### Results and Discussion on Rectangular Shape with Corner Configuration

#### 4.1 General

Due to limited land tall buildings are very common structural engineers need to design tall building such that it faces less amount influence because of the wind. Now a day's population growth is at a faster rate worldwide, that is why the demand of such high-rise projects is increasing. The high-rise projects which contain the sky scrapper and high building tower needs their evaluation against wind as the it influences the structural parameters like the shape and openings. Wind effects investigation of wind effects is possible through different techniques like wind tunnel test and by some computational fluid dynamics tool.

As the incident wind that come into contact with structure is atmospheric boundary layer flow that is why the knowledge of boundary layer flow, wake field, stagnation zone is needed for complete understanding of the flow interaction with structure. The fluid structure interaction study is also required before configuring the model into the numerical simulation. The numerical simulation for the present study is performed using k- $\epsilon$  turbulence model. The k- $\epsilon$  turbulence model is a two-equation model.

#### 4.2 Rectangle Shape with Simple Corners

Regular shape structure is very common in tall buildings but since last few decades due to load of use of land availability use of the regular shapes is deciding so now days structures in the form of irregular shape are used all around the globe. In this research a rectangular building which is having the plan cross sectional area of 2080 m<sup>2</sup> and 150 m height of building are considered. The study is done on the wind incidence angle ranging from of 0<sup>0</sup> to 90<sup>0</sup> at as interval of 15<sup>0</sup> each.

##### 4.2.1 Pressure contours

The various parameters of wind effects are obtained through the numerical simulation and presented into graphical forms. The pressure contours with respect to the height of the building model is depicted for rectangular models having the corner configuration.

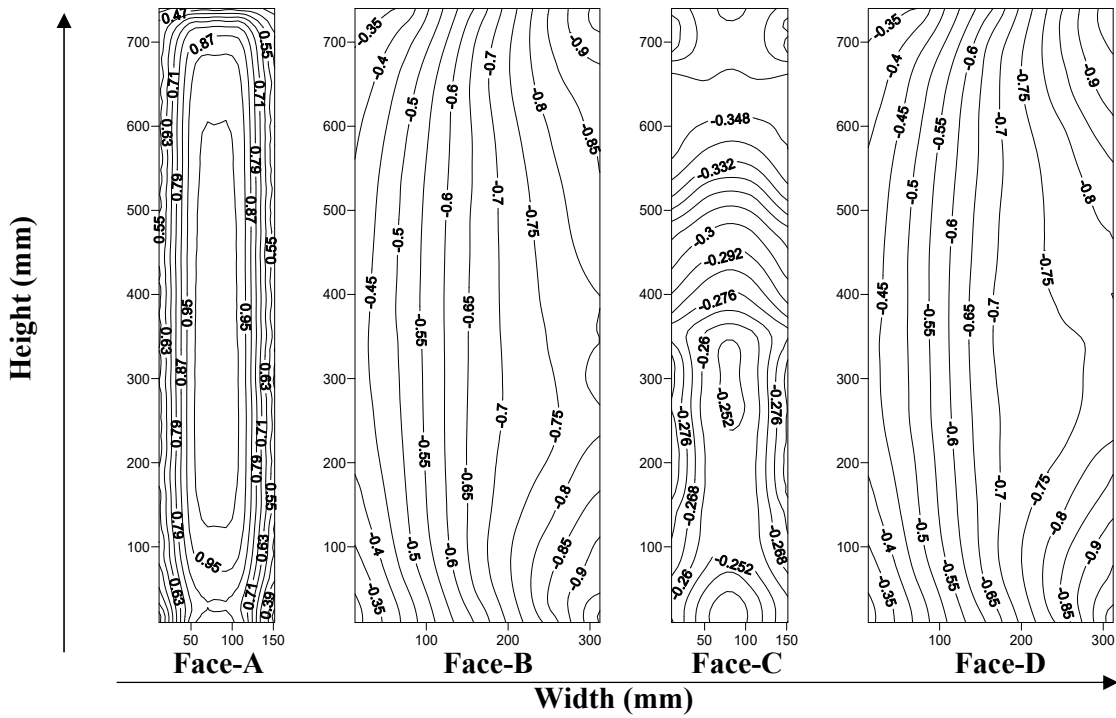


Figure 4.1 Distribution of wind pressure coefficient on the rectangle with simple corners at  $0^\circ$  wind incidence angle

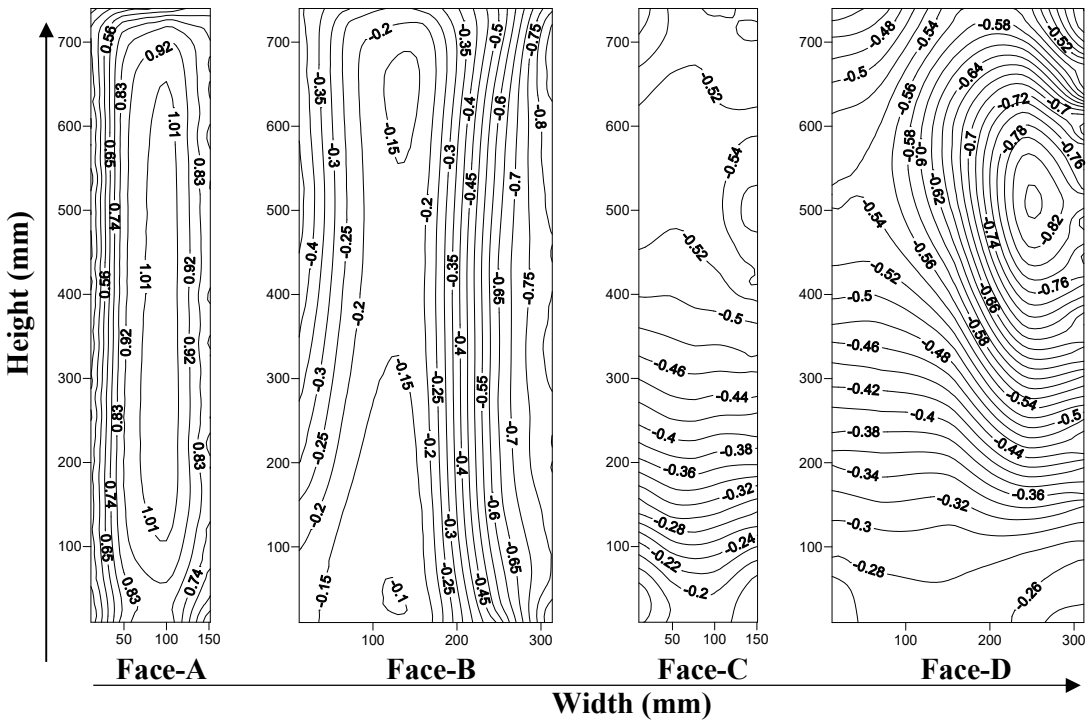


Figure 4.2 Distribution of wind pressure coefficient on the rectangle with simple corners at  $15^\circ$  wind incidence angle



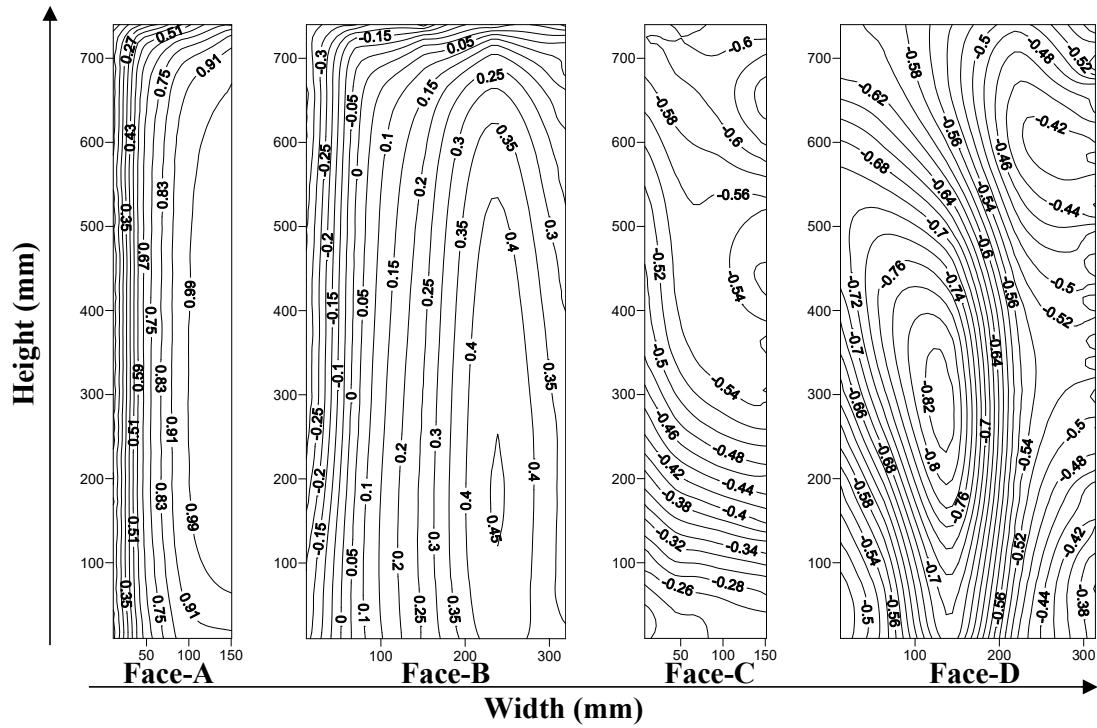


Figure 4.3 Distribution of wind pressure coefficient on the rectangle with simple corners at  $30^\circ$  wind incidence angle

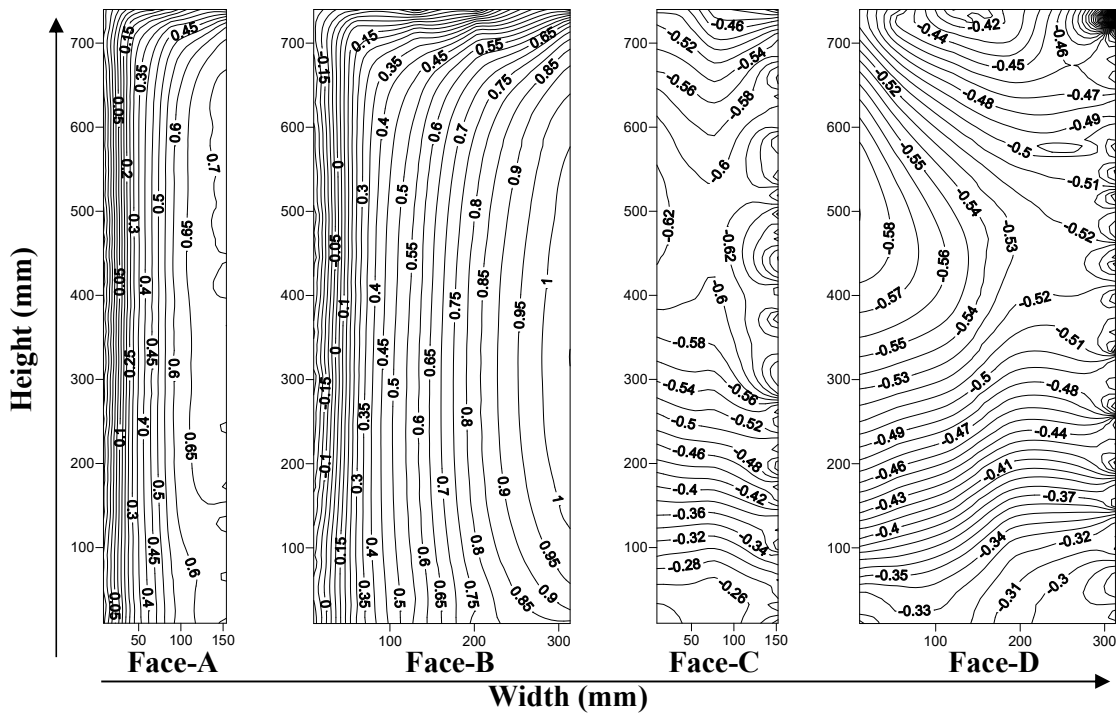


Figure 4.4 Distribution of wind pressure coefficient on the rectangle with simple corners at  $45^\circ$  wind incidence angle

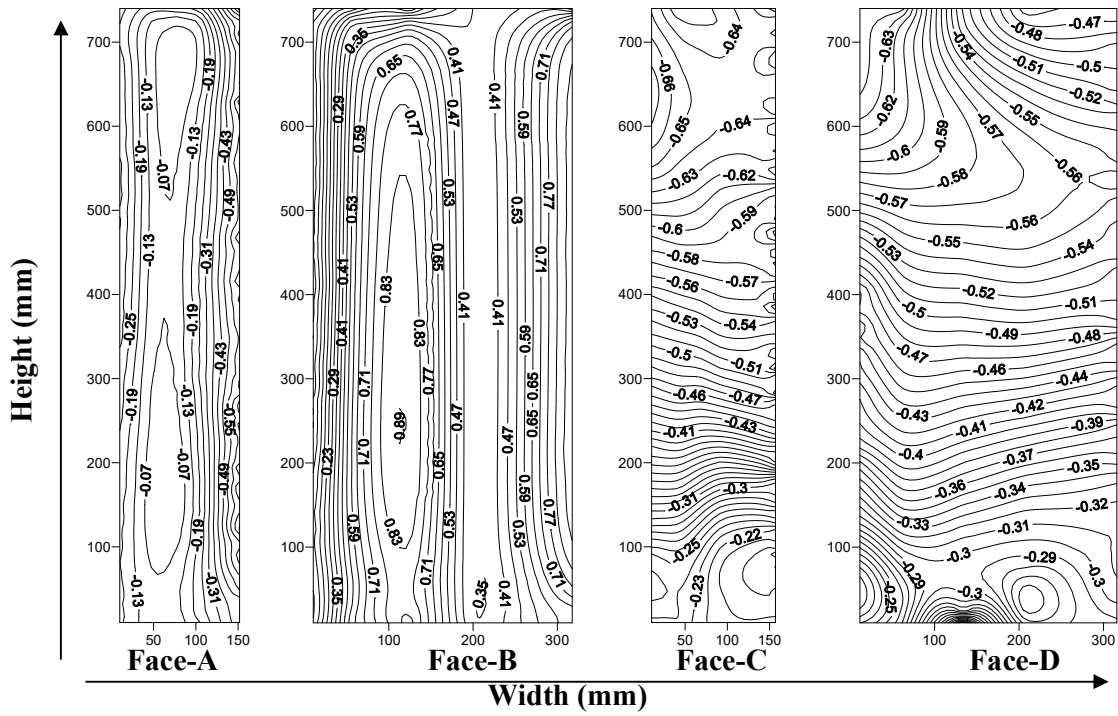


Figure 4.5 Distribution of wind pressure coefficient on the rectangle with simple corners at  $60^\circ$  wind incidence angle

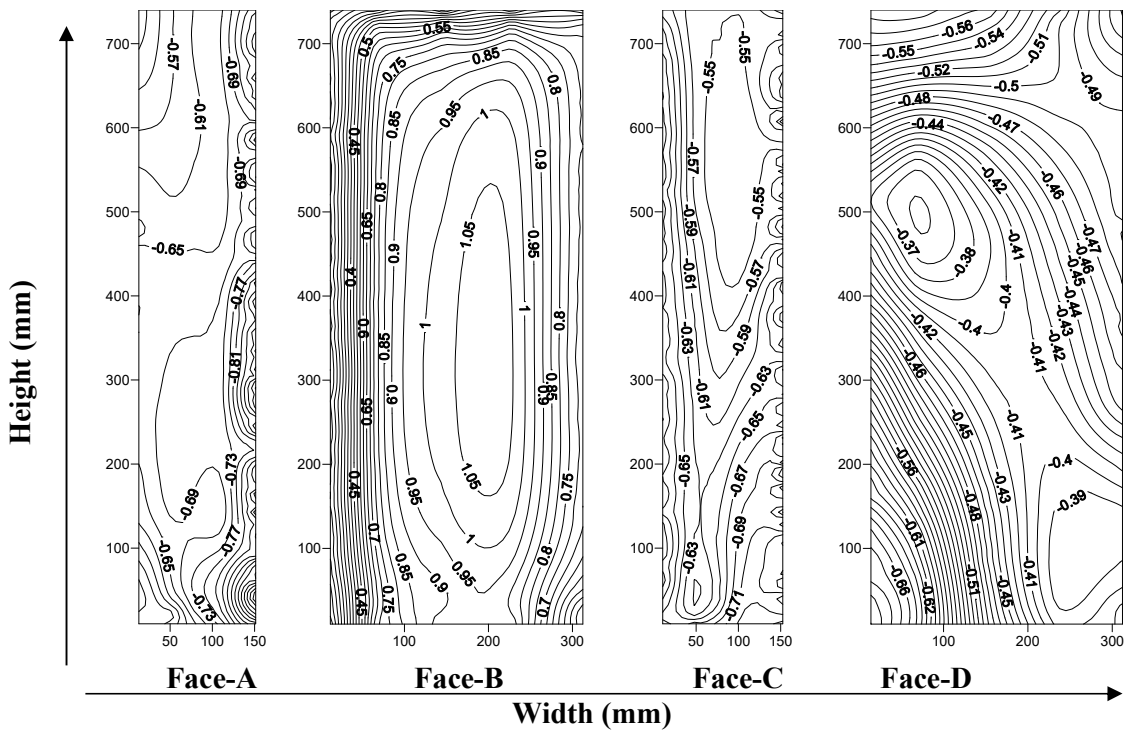
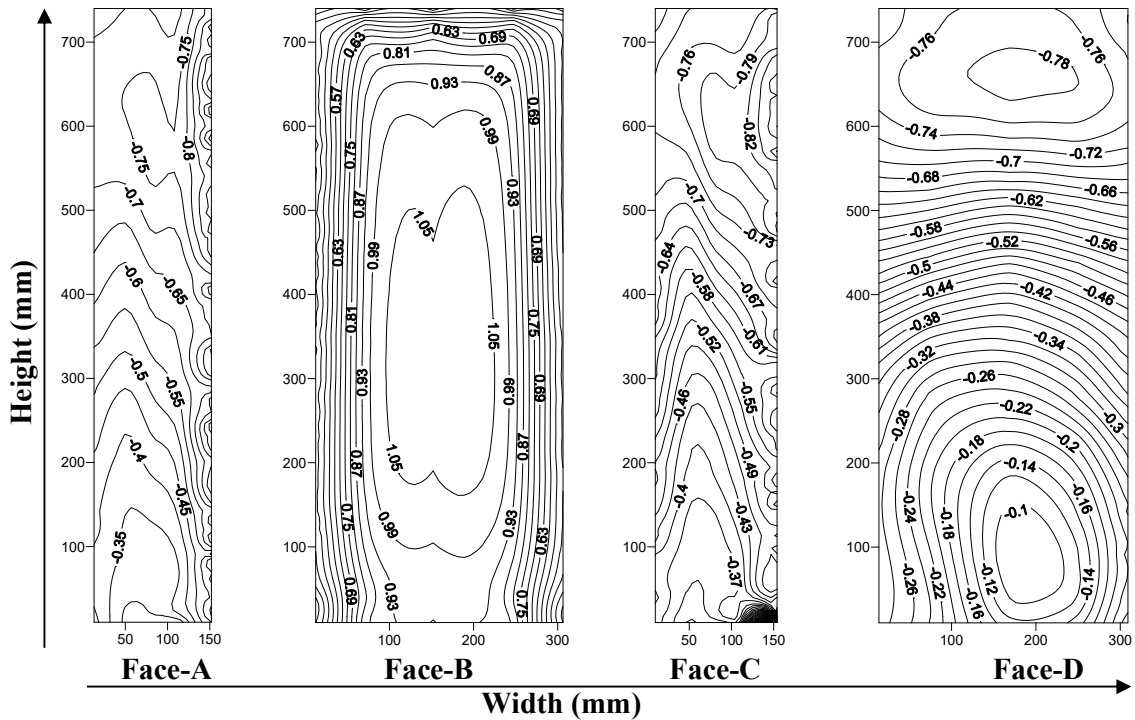


Figure 4.6 Distribution of wind pressure coefficient on the rectangle with simple corners at  $75^\circ$  wind incidence angle



**Figure 4.7 Distribution of wind pressure coefficient on the rectangle with simple corners at  $90^{\circ}$  wind incidence angle**

The pressure contours at  $0^{\circ}$  wind incidence angle are depicted in Figure 4.1 Distribution of wind pressure coefficient on the rectangle with simple corners at  $0^{\circ}$  wind incidence angle, at  $15^{\circ}$  in Figure 4.2 Distribution of wind pressure coefficient on the rectangle with simple corners at  $15^{\circ}$  wind incidence angle, at  $30^{\circ}$  in Figure 4.3 Distribution of wind pressure coefficient on the rectangle with simple corners at  $30^{\circ}$  wind incidence angle, and in the case of  $45^{\circ}$  wind Figure 4.4 Distribution of wind pressure coefficient on the rectangle with simple corners at  $45^{\circ}$  wind incidence angle at  $60^{\circ}$  wind in Figure 4.5 Distribution of wind pressure coefficient on the rectangle with simple corners at  $60^{\circ}$  wind incidence angle, for wind incidence angle at  $75^{\circ}$  wind Figure 4.6 Distribution of wind pressure coefficient on the rectangle with simple corners at  $75^{\circ}$  wind incidence angle and at of  $90^{\circ}$  wind Figure 4.7 Distribution of wind pressure coefficient on the rectangle with simple corners at  $90^{\circ}$  wind incidence angle are presented.

#### **4.2.2 Vertical Pressure Distribution along the height of Building**

Mean pressure distribution in terms of  $C_{p,mean}$  is presented in graphical form in Figure 4.8 Mean pressure distribution on the vertical centre line for rectangle with simple corners on the centre line of the face. The centre line  $C_{p,mean}$  suggest the pattern followed by the pressure with respect to the height of the building model places and width of opening for different purposes

can be provide on the places where the less amount of wind is found for that particular face. The  $C_{p, \text{mean}}$  on vertical centre line for regular shape model, the model without any corner configuration is presented for various wind incidence angle from  $0^0$  to  $90^0$  at as interval of  $15^0$ . The values of  $C_{p, \text{mean}}$  lies between positive 1.06 to negative 0.69 for  $0^0$  wind incidence angle, while for  $15^0$  the range of  $C_{p, \text{mean}}$  on vertical center line + 0.89 to - 0.58. The  $C_{p, \text{mean}}$  on vertical center line at  $30^0$  wind is varied form + 0.82 to - 0.69. The mainly  $C_{p, \text{mean}}$  on vertical center line is lies from positive to negative and the pressure distribution on this vertical center line that is  $C_{p, \text{mean}}$  is presented into graphical form at  $0^0$ ,  $15^0$ ,  $30^0$ ,  $45^0$ ,  $60^0$ ,  $75^0$  and  $90^0$  wind incidence angle. The pressure distribution is found after drawing the center line into CFD post and the number of sample point on this line is defined at different intervals as per the experimental guide lines provided into the wind tunnel testing manuals. Figure 4.8 Mean pressure distribution on the vertical centre line for rectangle with simple corners are presented for the wind incidence angle from  $0^0$  to  $90^0$ .

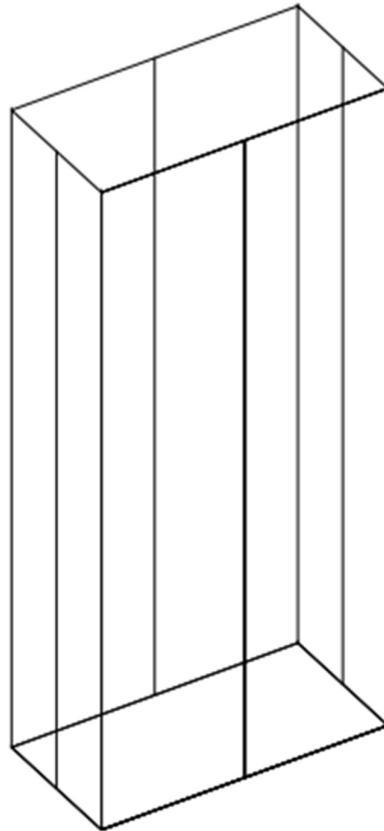
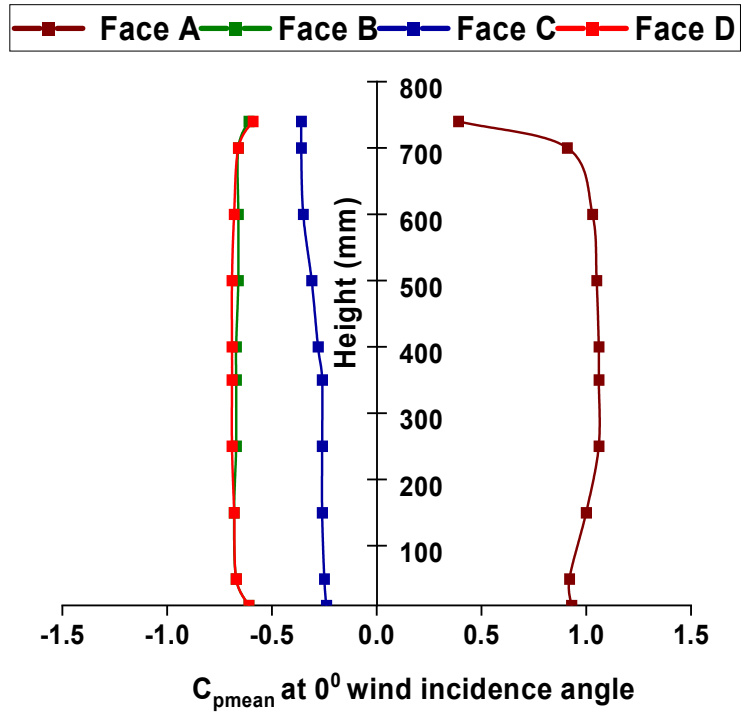


Figure 4.8(contd.) Mean pressure distribution on the vertical centre line for rectangle with simple

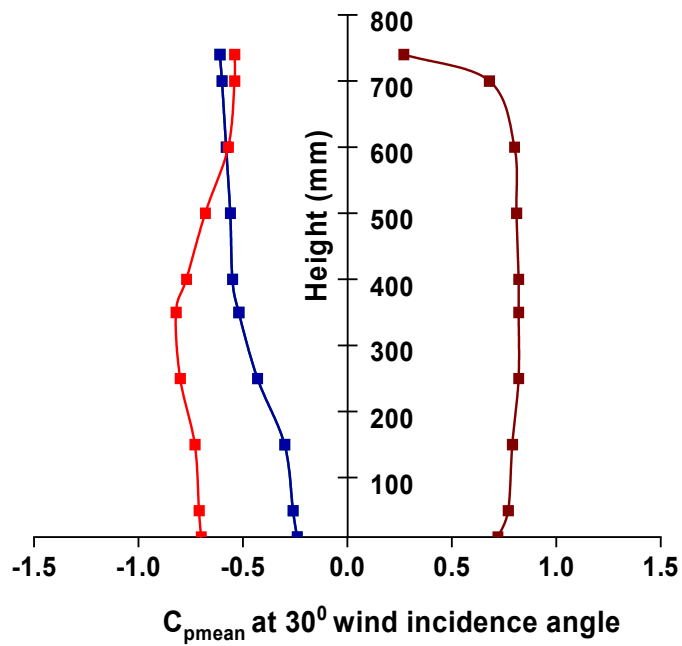
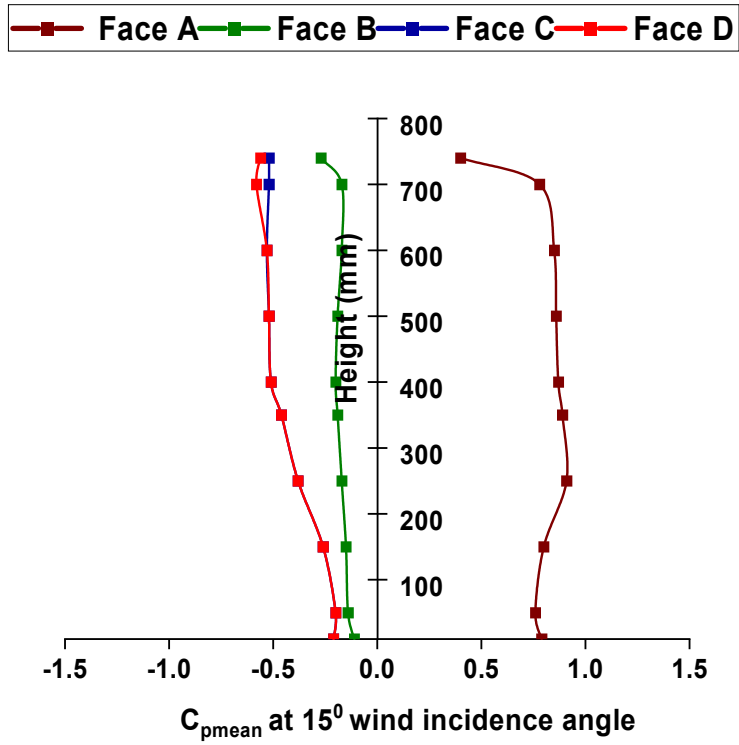


Figure 4.8 (contd.) Mean pressure distribution on the vertical centre line for rectangle with simple corners

■ Face A
 ■ Face B
 ■ Face C
 ■ Face D

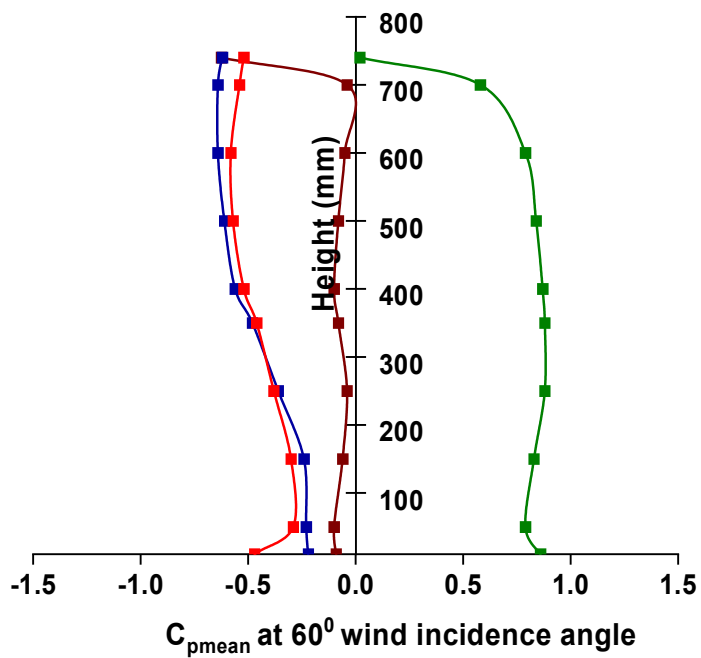
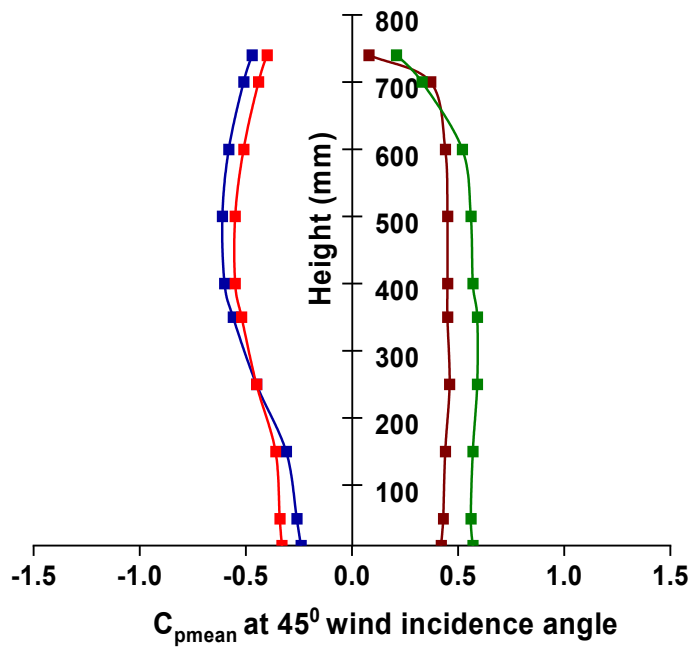


Figure 4.8 (contd.) Mean pressure distribution on the vertical centre line for rectangle with simple corners

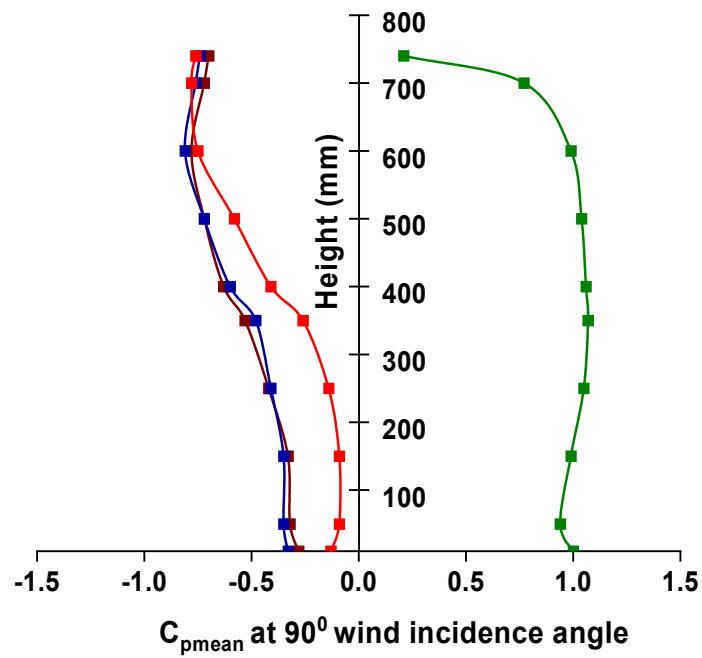
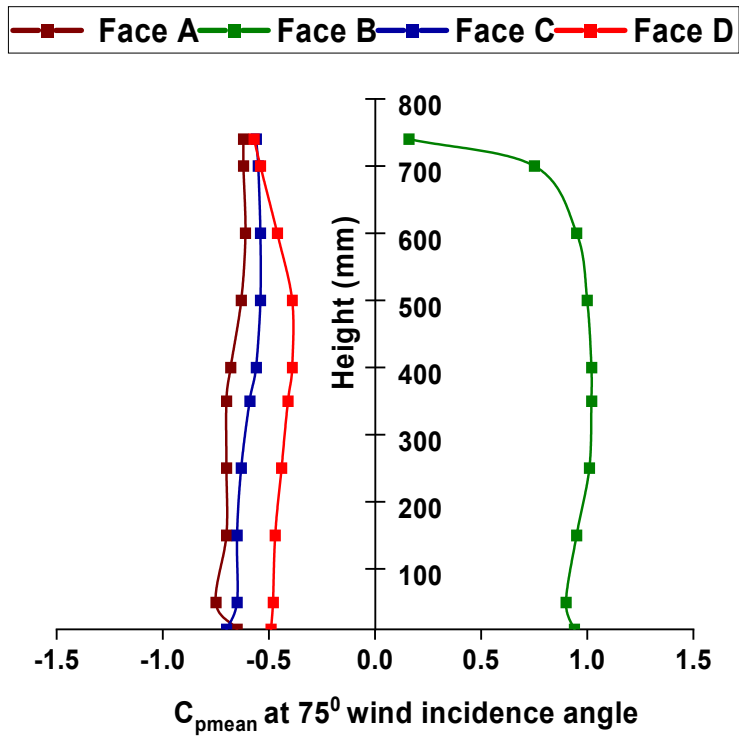


Figure 4.8 Mean pressure distribution on the vertical centre line for rectangle with simple corners



### **4.2.3 Horizontal Pressure Distribution along the peripheral Distance of Building**

The  $C_{p,mean}$  is plotted along the peripheral distance of various building models at various heights starting from 250 mm height from the base of the model which is at one third height of the model. The second line of  $C_{p,mean}$  that is drawn in the post CFX and drawn at 375 mm height of the building model which is at mid height of building model. Another line along the perimeter is plotted at 500 mm height from the base of the model which is at the two third height of the building model. Figure 4.9 Mean pressure distribution along the peripheral distance of the rectangle with simple corners is presented.

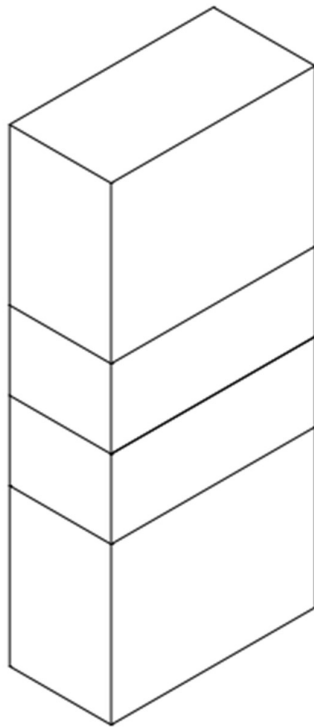
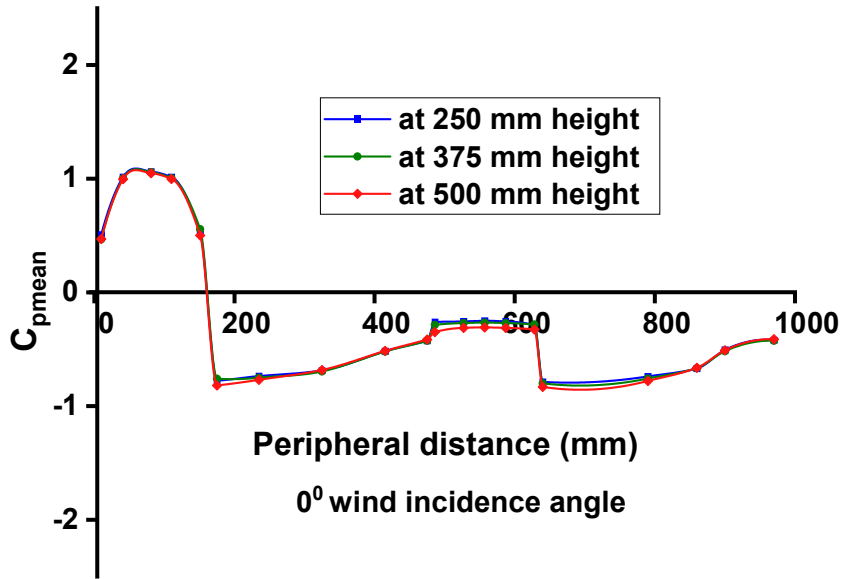


Figure 4.9(contd.) Mean pressure distribution along the peripheral distance of the rectangle with simple corners

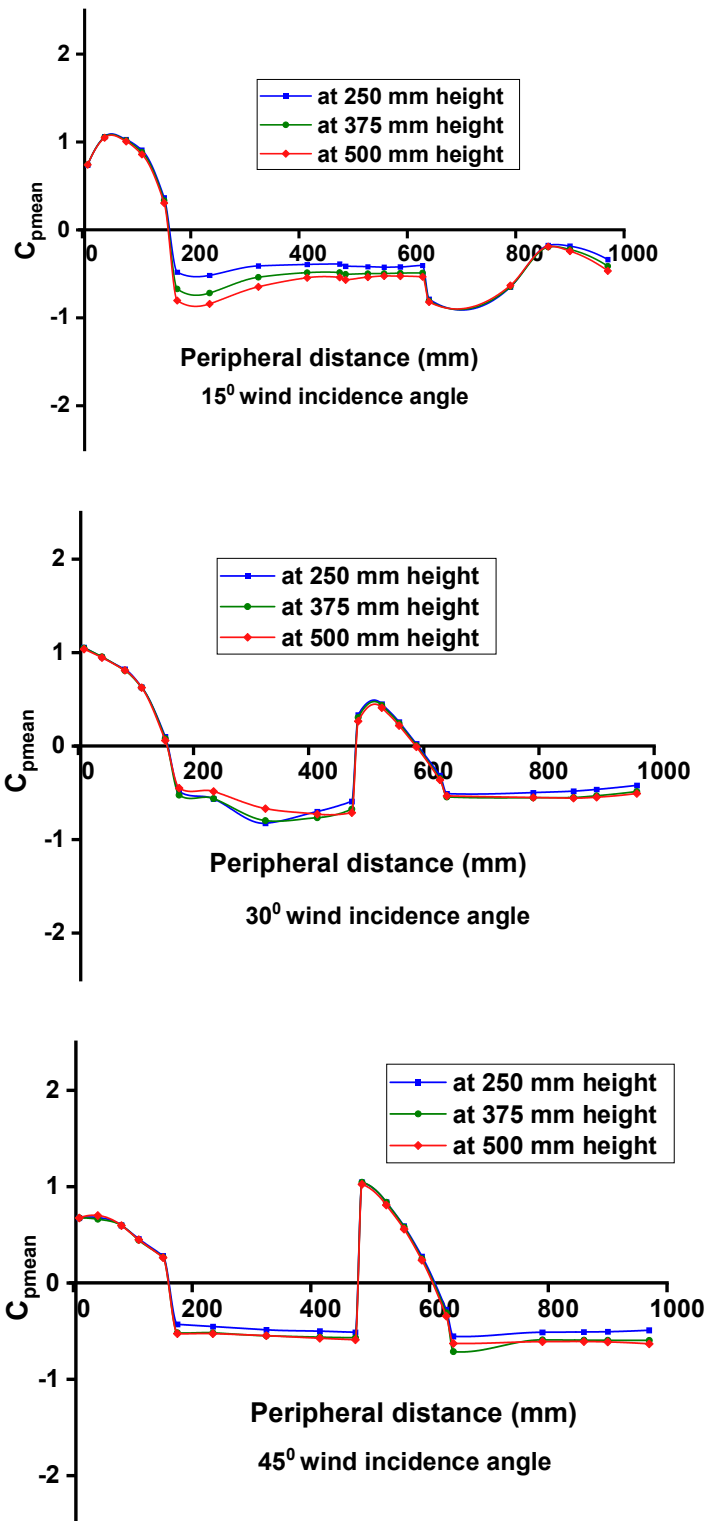


Figure 4.9(contd.) Mean pressure distribution along the peripheral distance of the rectangle with simple corners

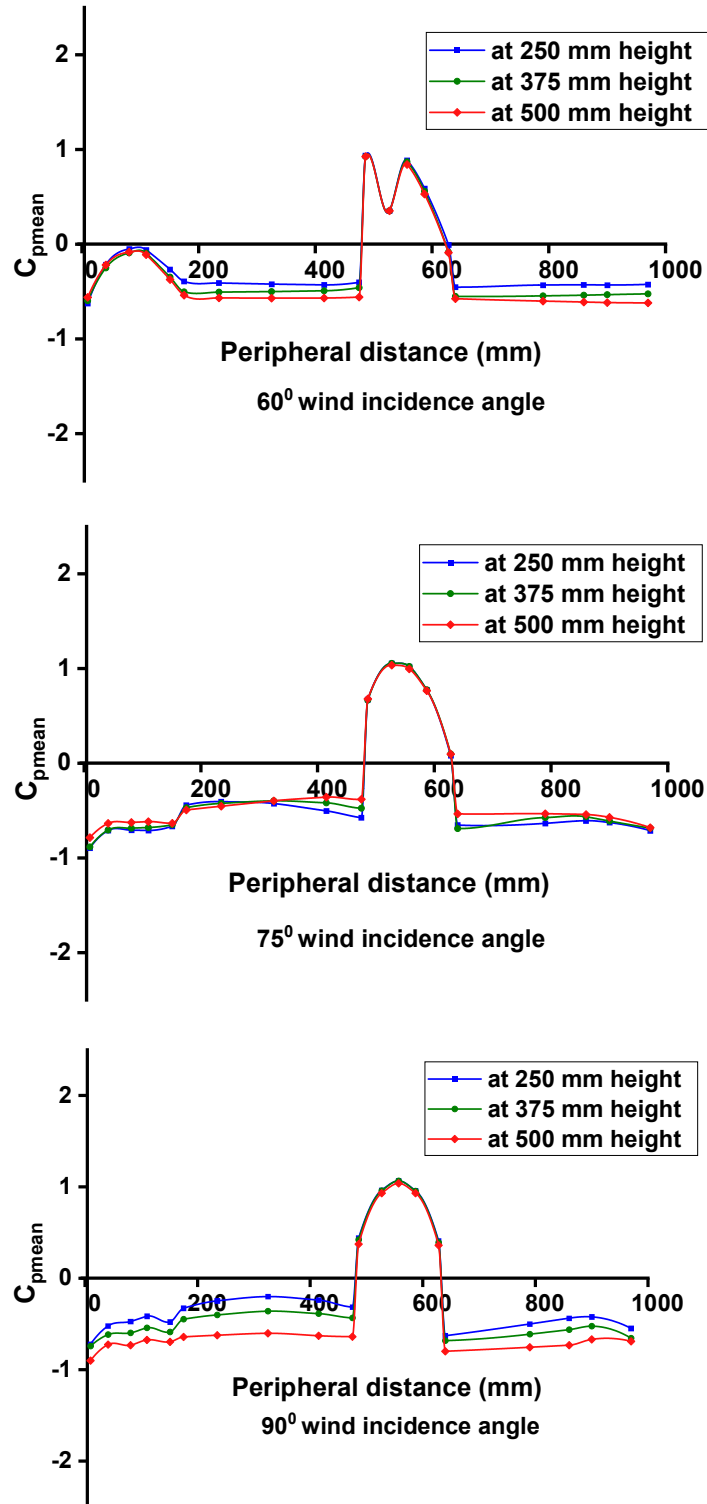


Figure 4.9 Mean pressure distribution along the peripheral distance of the rectangle with simple corners

### 4.2.4 Force Coefficients

Force coefficient are computed from the numerical simulation performed in ANSYS, CFX. The data generated through the CFD simulation is exported from CFD post and then the calculation is done as per the procedure explained into the various research paper and as explained earlier in the methodology section of this thesis. The drag coefficient is called as  $C_{Fx}$  and the lift coefficient is calculated in terms of  $C_{Fy}$ . The variation of drag and lift forces are depicted in the graphical from in Figure 4.10 Wind force coefficient for the rectangle with simple corners. The value for drag coefficient varies from 0.08 to 0.92 for model without any corner configuration while the lift force coefficient lies in between 0 to 0.31 for model having no corner configuration. The value of drag and lift coefficient are plooted graphically for angle ranging from  $0^{\circ}$  to  $90^{\circ}$  at an interval of  $15^{\circ}$  wind.

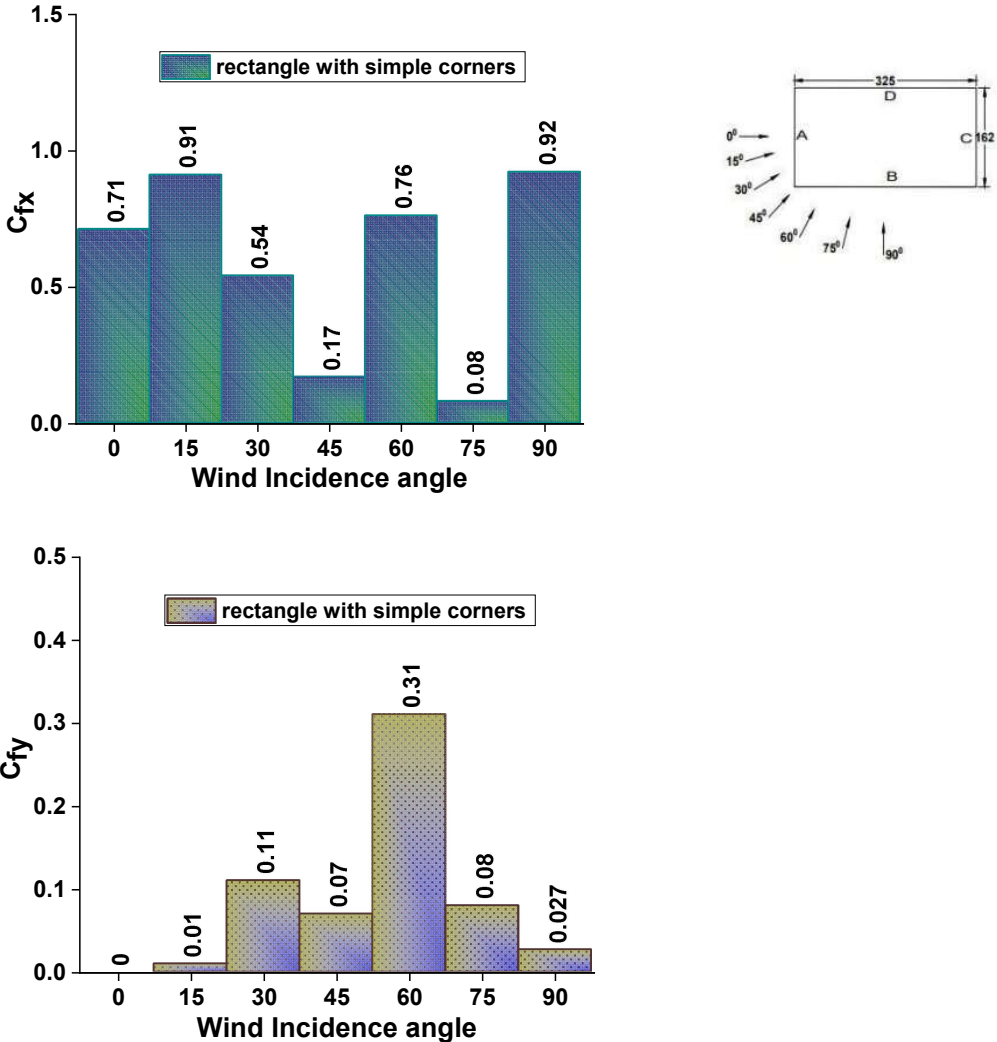


Figure 4.10 Wind force coefficient for the rectangle with simple corners

### 4.2.5 Moment Coefficients

The base shear and base moments is obtained using ANSYS CFX post processing. The data of base shear and base moments is exported and calculated as per the procedure explained in the wind tunnel manual. The formulas used to calculate the base shear and base moments is explained in the methodology chapter of this thesis. The base shear and base moments are graphically plotted into the form of bar chart for various wind incidence angles and presented in Figure 4.11 Wind moment coefficient for the rectangle with simple corners. The base shear range from 0.02 to 0.62 for the model without any corner configuration of rectangular shape while the base moment ranges from 0.14 to 0.99 for wind angle from  $0^{\circ}$  to  $90^{\circ}$  at the interval of  $15^{\circ}$ .

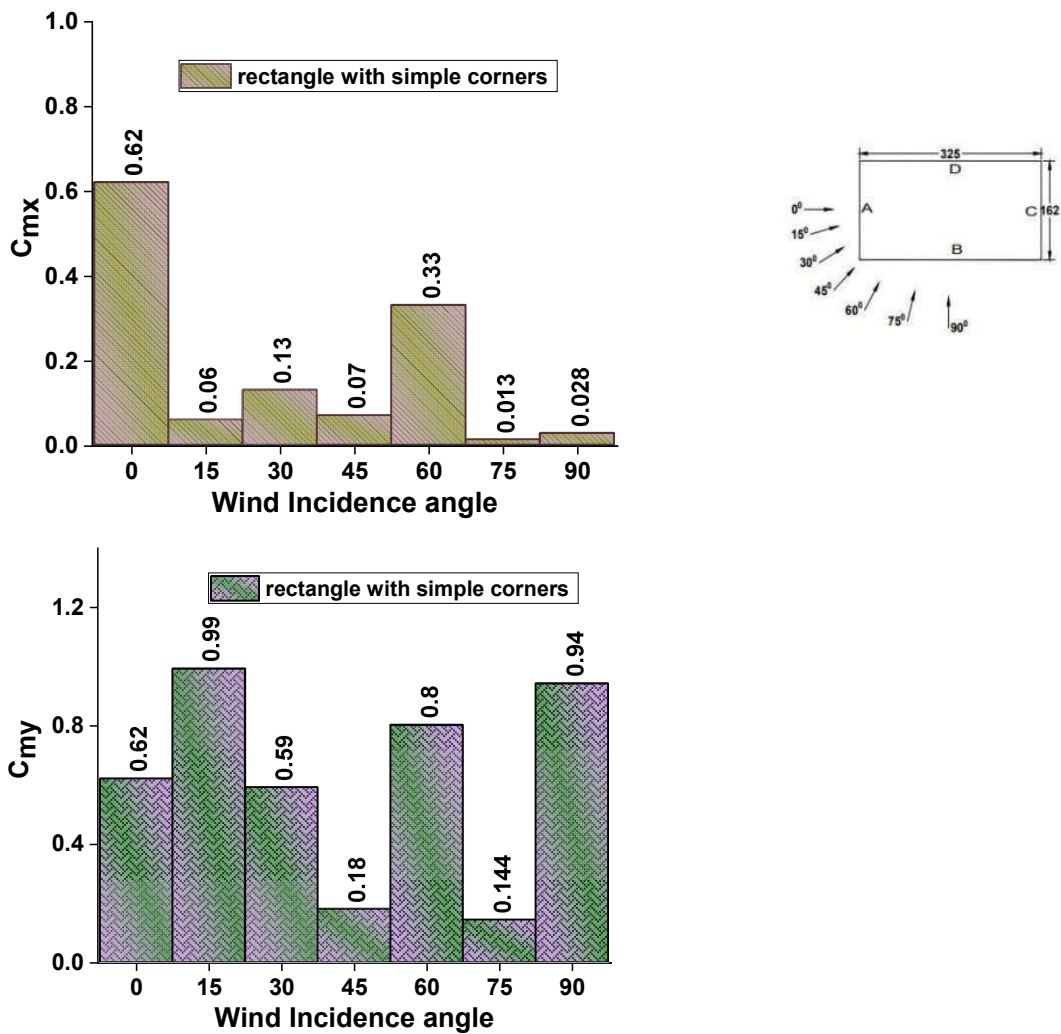


Figure 4.11 Wind moment coefficient for the rectangle with simple corners

#### 4.2.6 External Pressure Coefficients

The experimental methods such as wind tunnel test is quite superior but require heavy equipment and is costly. Wind tunnel test take a lot of time and resources while the same investigation is possible through the different available CFD tools. CFD gives the result in very less time with a quite clear pictorial view of the flow characteristics. There also some limitation in CFD simulation like the person who configure the model into simulation needs the adequate amount of knowledge of wind flow parameter like the flow patterns and power law.

The data from ANSYS CFX post is exported into the csv format which is then processed as per the guide lines and procedure presented by various researchers. The processed data is then graphically plotted on the center line with respect to the increment in the height of the building model.

The pressure coefficient in terms of external pressure coefficient is tabulated in the Table-4.1 External Pressure Coefficients for model-A (Rectangle Simple). The maximum external pressure coefficient for model without any corner configuration is 0.78 at  $0^{\circ}$  and  $15^{\circ}$  wind incidence angles while the least pressure coefficient is obtained as -0.69 for  $75^{\circ}$  wind incidence angle. The external pressure coefficient for rectangular model is tabulated in the table for each face at every  $15^{\circ}$  intervals for the wind incidence angles ranging between  $0^{\circ}$  to  $90^{\circ}$ . The external pressure coefficient is the sum of pressure of the lines drawn on each face. The data in the form of pressure is exported and the calculation is preformed and external pressure coefficient on each face at every angle is tabulated in table for rectangular model without any corner configuration.

**Table-4.1 External Pressure Coefficients for model-A (Rectangle Simple)**

<b>Model-A (Rectangle Simple)</b>							
<b>Face</b>	<b>0°</b>	<b>15°</b>	<b>30°</b>	<b>45°</b>	<b>60°</b>	<b>75°</b>	<b>90°</b>
<b>A</b>	<b>0.78</b>	<b>0.78</b>	<b>0.68</b>	0.35	-0.25	<b>-0.69</b>	<b>-0.61</b>
<b>B</b>	<b>-0.64</b>	-0.43	0.11	<b>0.45</b>	<b>0.50</b>	<b>0.67</b>	<b>0.70</b>
<b>C</b>	-0.30	-0.43	-0.48	<b>-0.51</b>	<b>-0.49</b>	-0.62	<b>-0.61</b>
<b>D</b>	<b>-0.64</b>	<b>-0.50</b>	<b>-0.59</b>	-0.48	-0.46	-0.47	-0.45



### **4.3 Rectangle Shape with Corner cuts**

The investigation of wind effect is the primary aim to conduct this study and for this purpose corner configuration of different shapes is applied such as corner cut, fillet and chamfer etc. The wind generated pressure is more prominent on the structure and to curtail the pressure there are a number of modifications is applied in the high-rise structure. The model without any corner configuration and corner cut model has the identical area and same height of the building. Investigation is performed on the model having cut in each corner of equal ratio of side length. Various parameters are studied like  $C_p$  distribution on vertical centre line,  $C_p$  distribution along the peripheral distance of building model at different levels, mean  $C_p$  is also studied and presented in the form of table at every face of the building model for the wind incidence angle ranging from  $0^\circ$  to  $90^\circ$  at an interval of  $15^\circ$ .

#### **4.3.1 Pressure contours**

The pressure distribution in the form of contours is depicted by considering the width and height of the face, the variation in the pressure in exact distribution is depicted. The negative pressure that is suction is observed on the lee ward and side faces of building model because of the various flow characteristics like flow reattachment, separation and other different phenomena.

The rectangular model which is having corner cuts, the pressure distribution pattern is depicted into contours at each wind incidence angle. The pressure distribution nature varies from positive to negative. The positive pressure is mainly found on the wind ward face where the wind is directly acting on the model while the other faces have different variation. Symmetrical nature of pressure distribution is observed for symmetrical faces and same can be validated through the pressure contours at every face for  $0^\circ$  to  $90^\circ$  wind incidence angles ranging from at every  $15^\circ$  intervals. Pressure contours for corner cut rectangle are represented from Figure 4.12 Distribution of wind pressure coefficient on the rectangle with corner cut at  $0^\circ$  wind incidence angle to Figure 4.18 Distribution of wind pressure coefficient on the rectangle with corner cut at  $90^\circ$  wind incidence angle for the wind incidence angle varies from  $0^\circ$  to  $90^\circ$  wind.

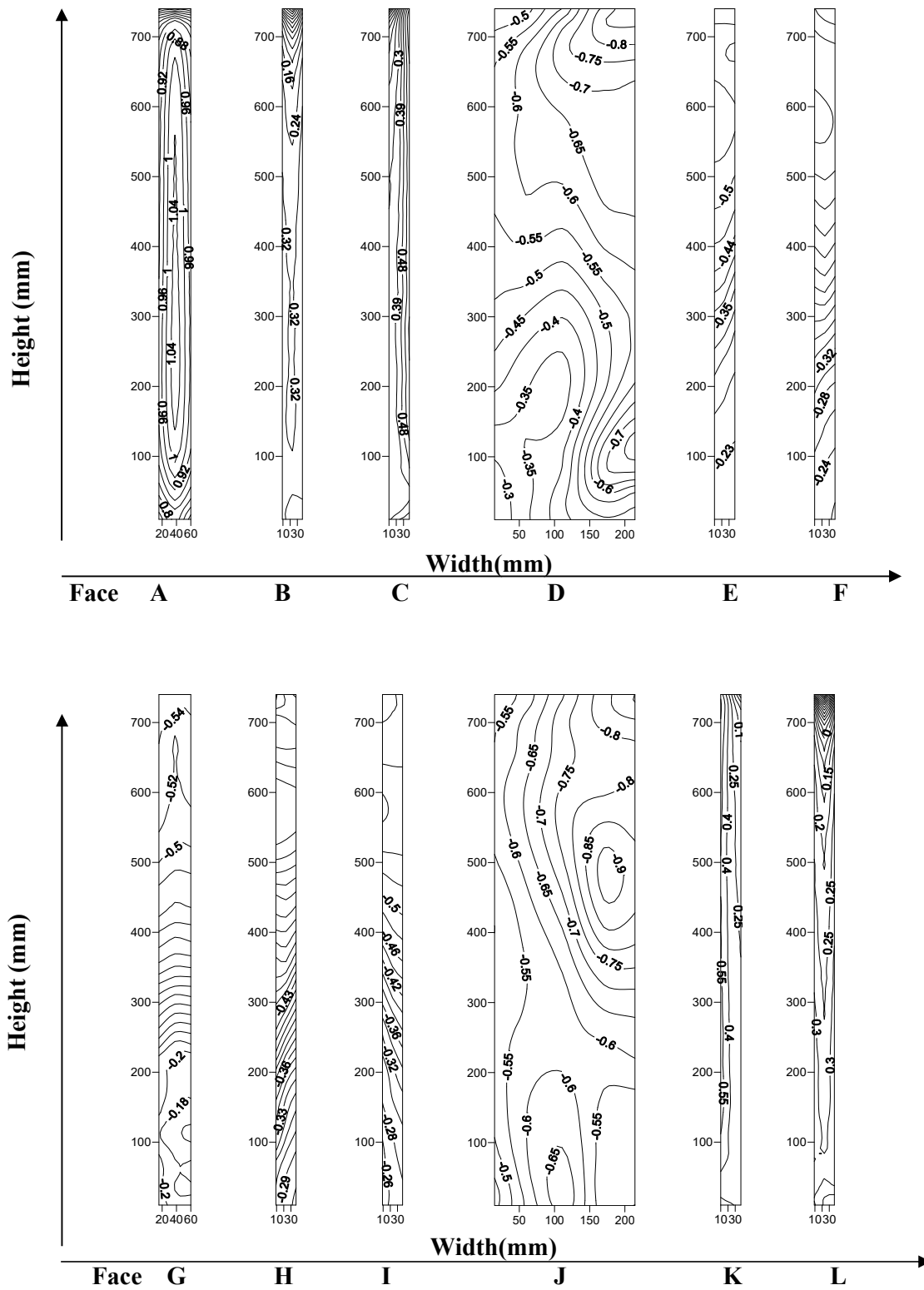


Figure 4.12 Distribution of wind pressure coefficient on the rectangle with corner cut at  $0^\circ$  wind incidence angle

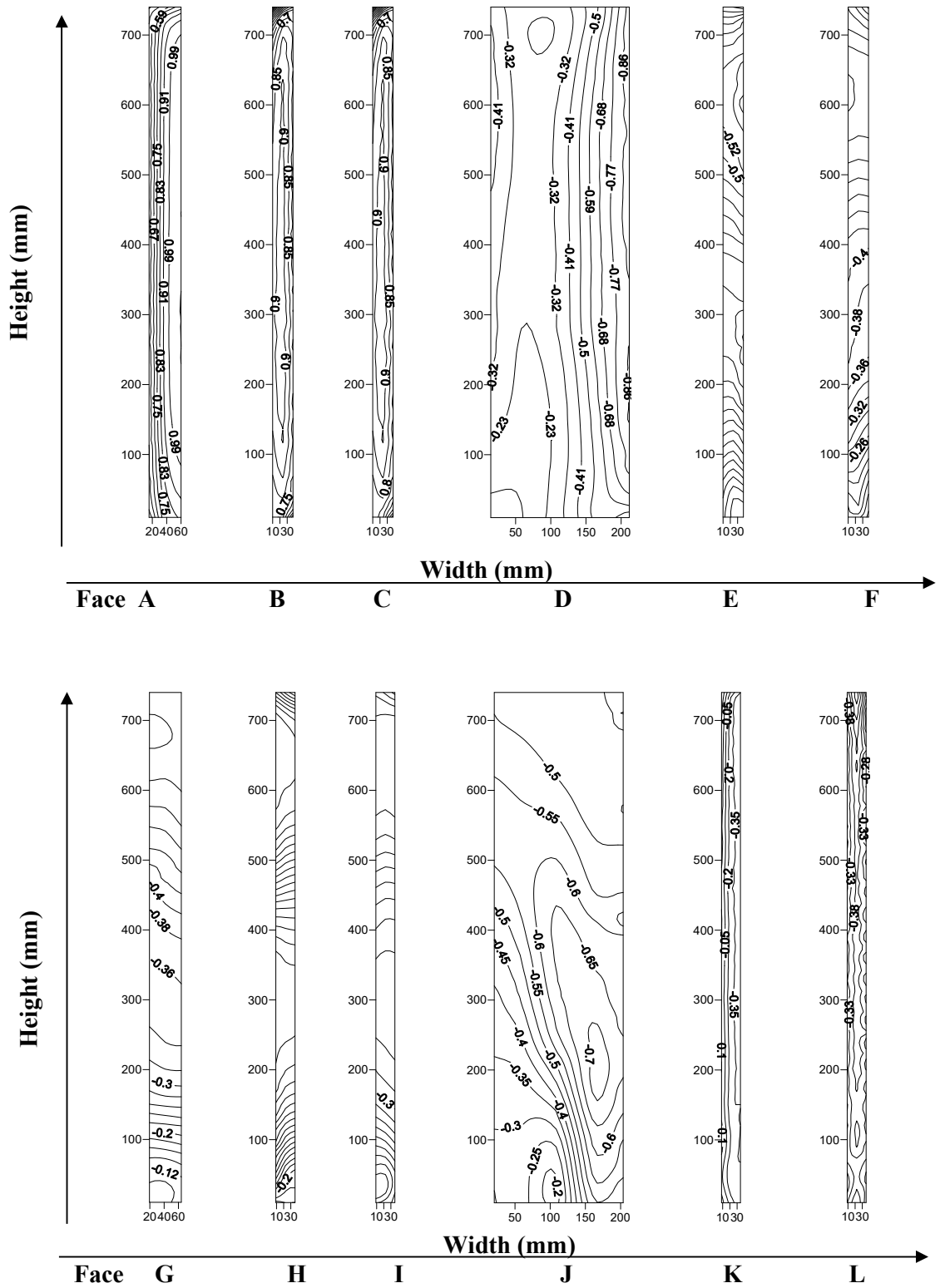


Figure 4.13 Distribution of wind pressure coefficient on the rectangle with corner cut at 15° wind incidence angle

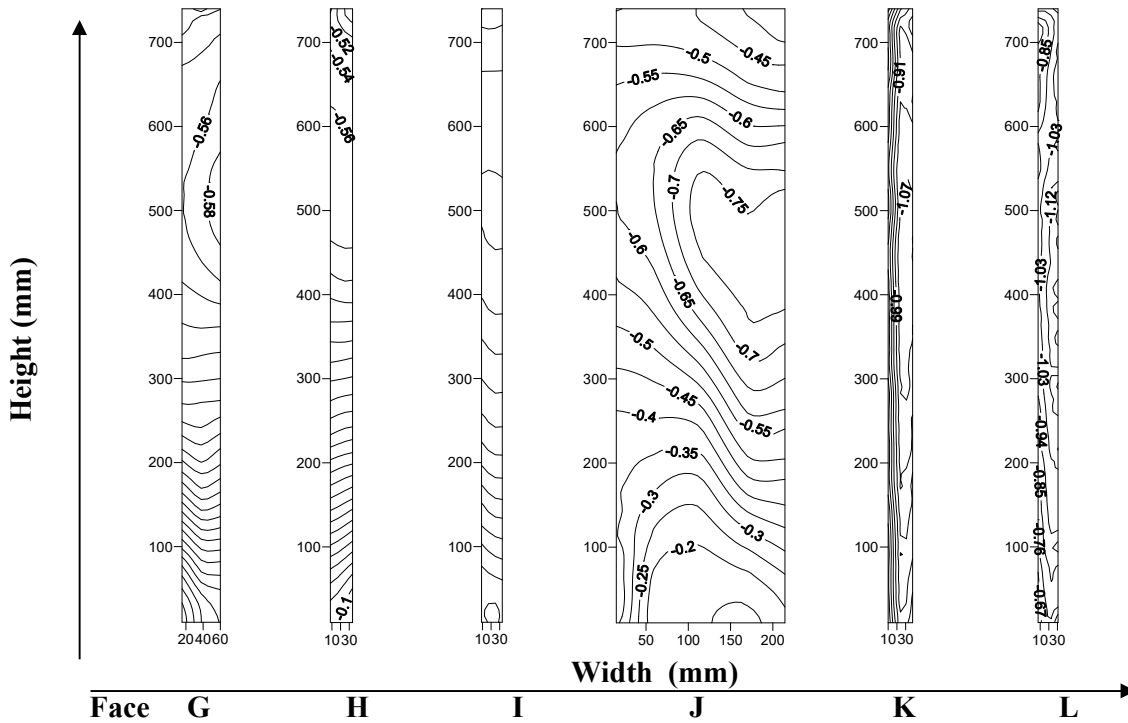
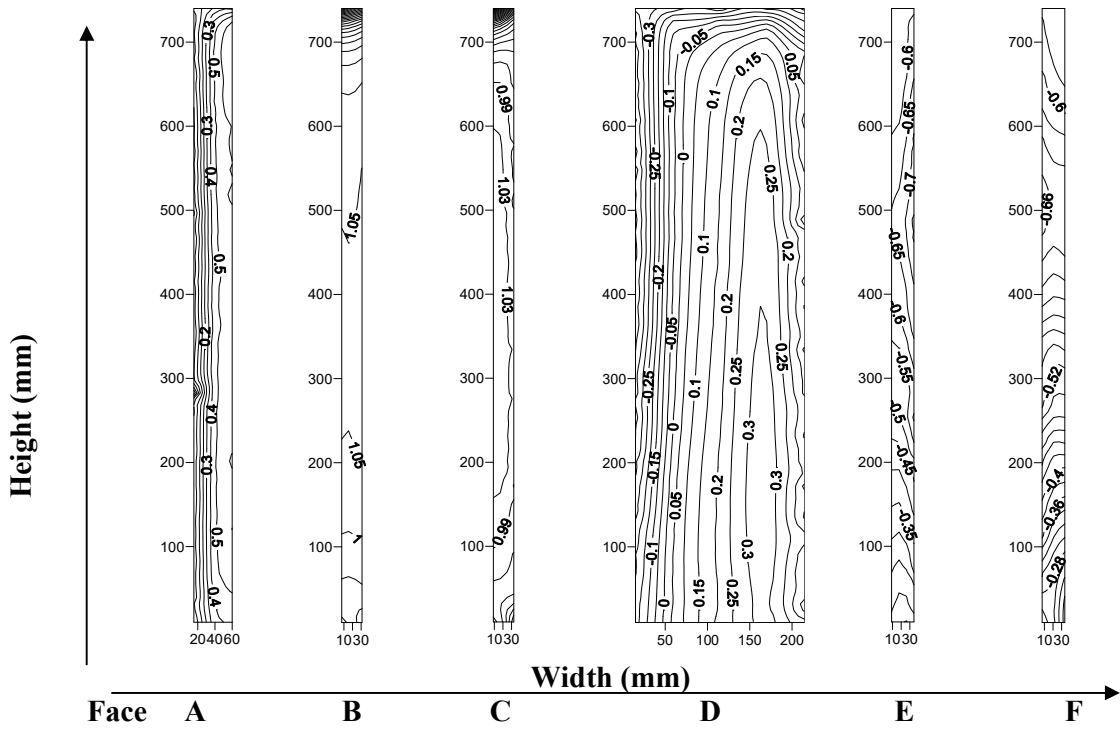


Figure 4.14 Distribution of wind pressure coefficient on the rectangle with corner cut at  $30^\circ$  wind incidence angle

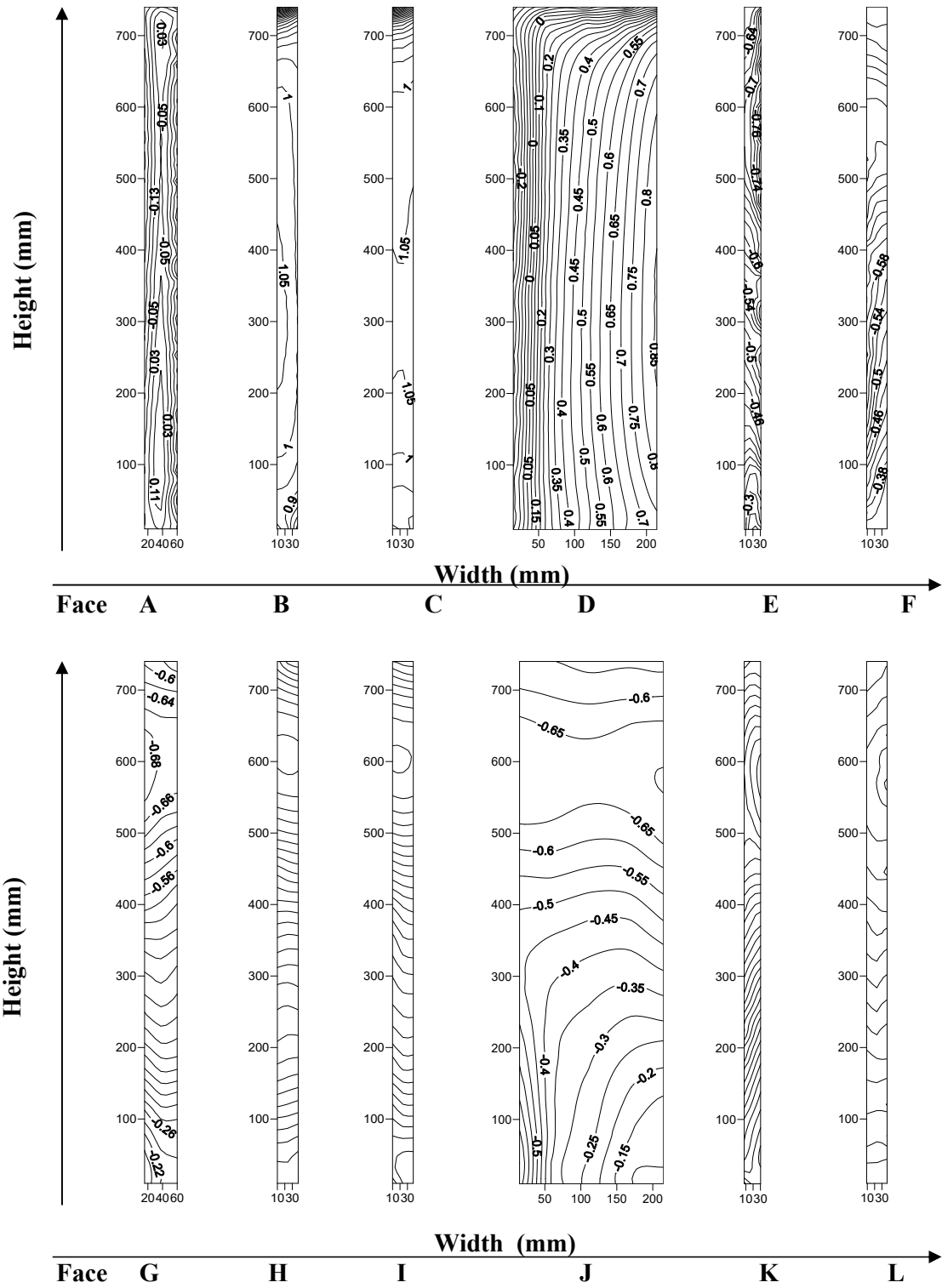


Figure 4.15 Distribution of wind pressure coefficient on the rectangle with corner cut at 45° wind incidence angle

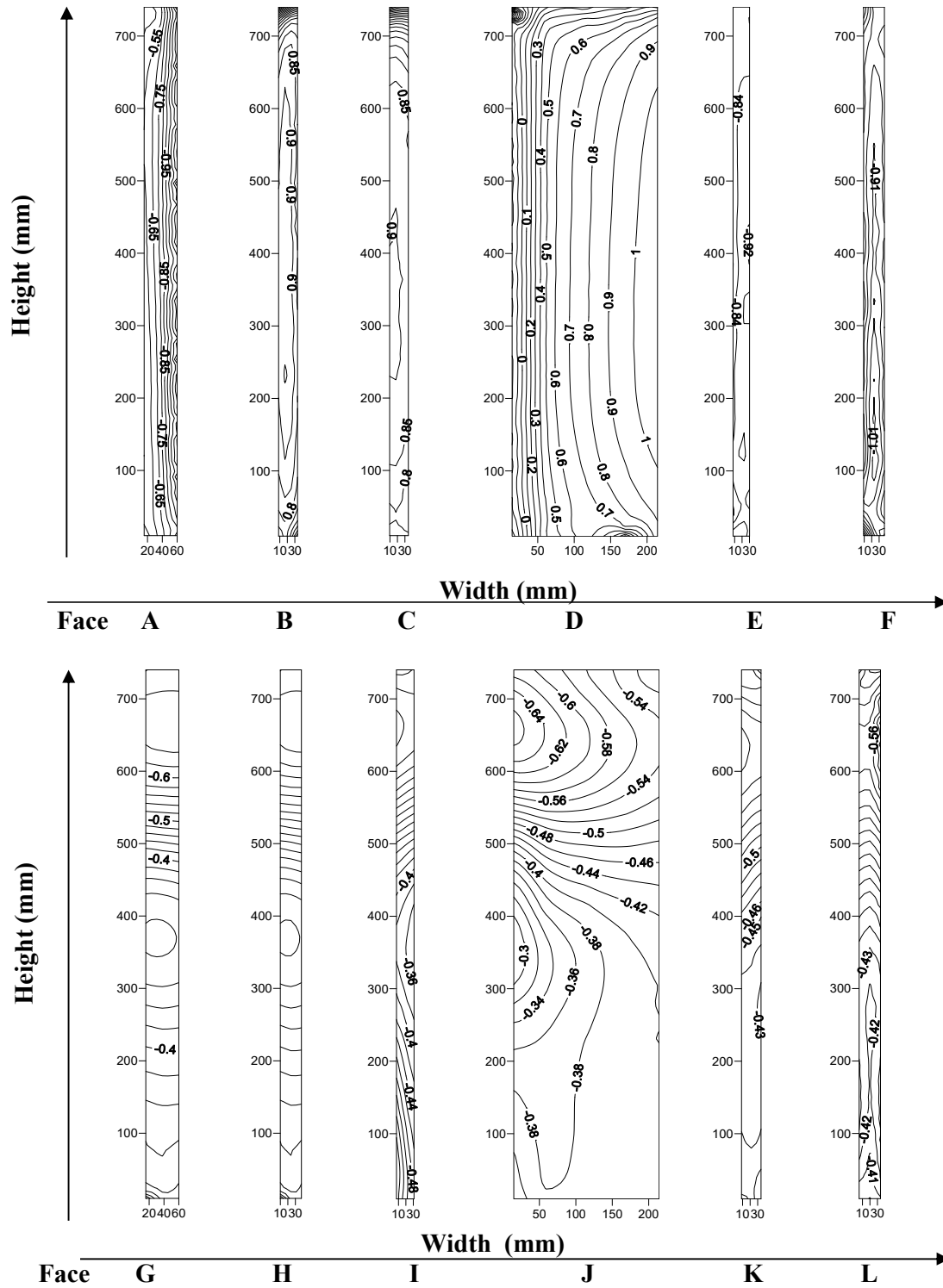


Figure 4.16 Distribution of wind pressure coefficient on the rectangle with corner cut at 60° wind incidence angle

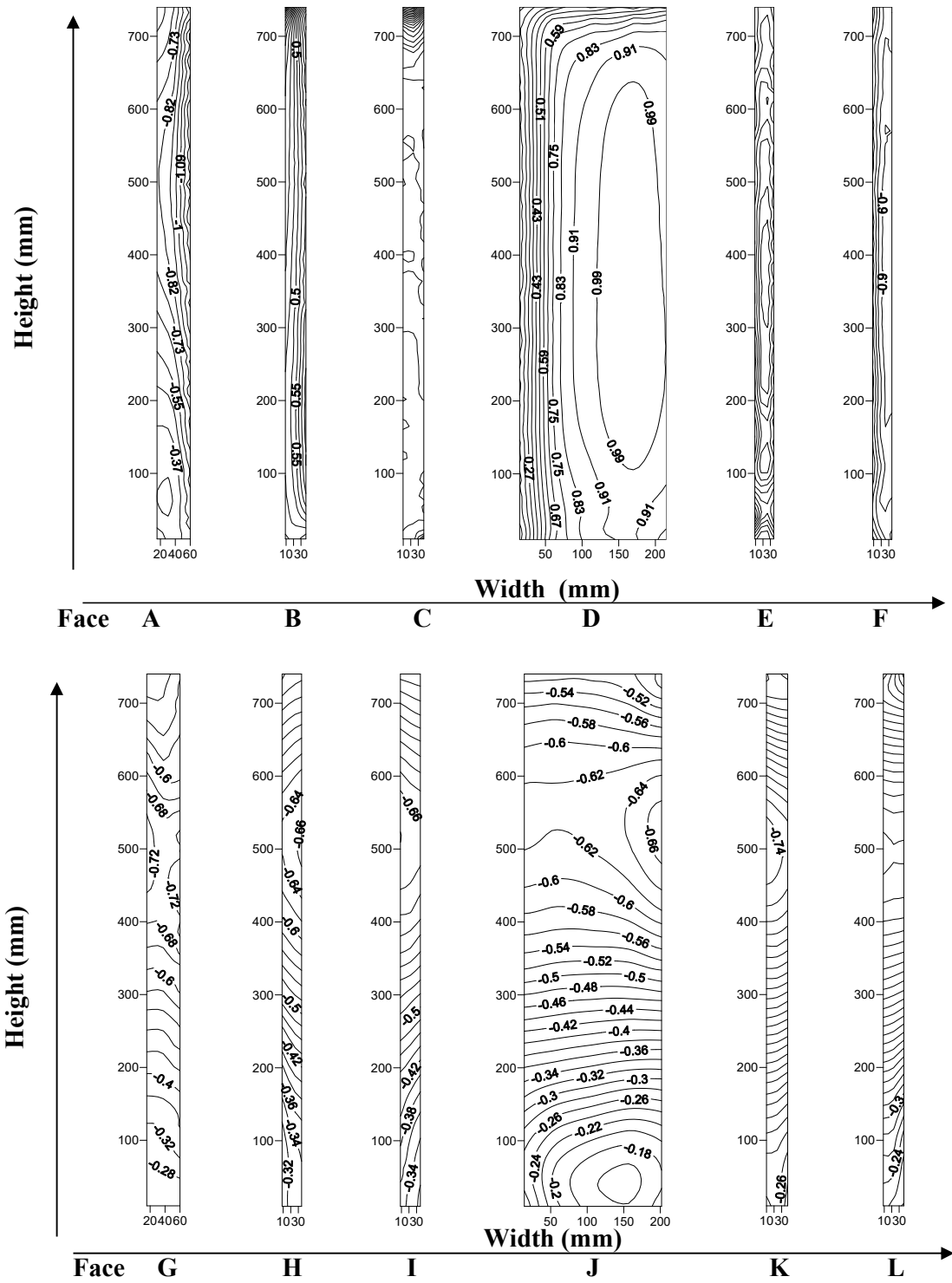


Figure 4.17 Distribution of wind pressure coefficient on the rectangle with corner cut at 75° wind incidence angle

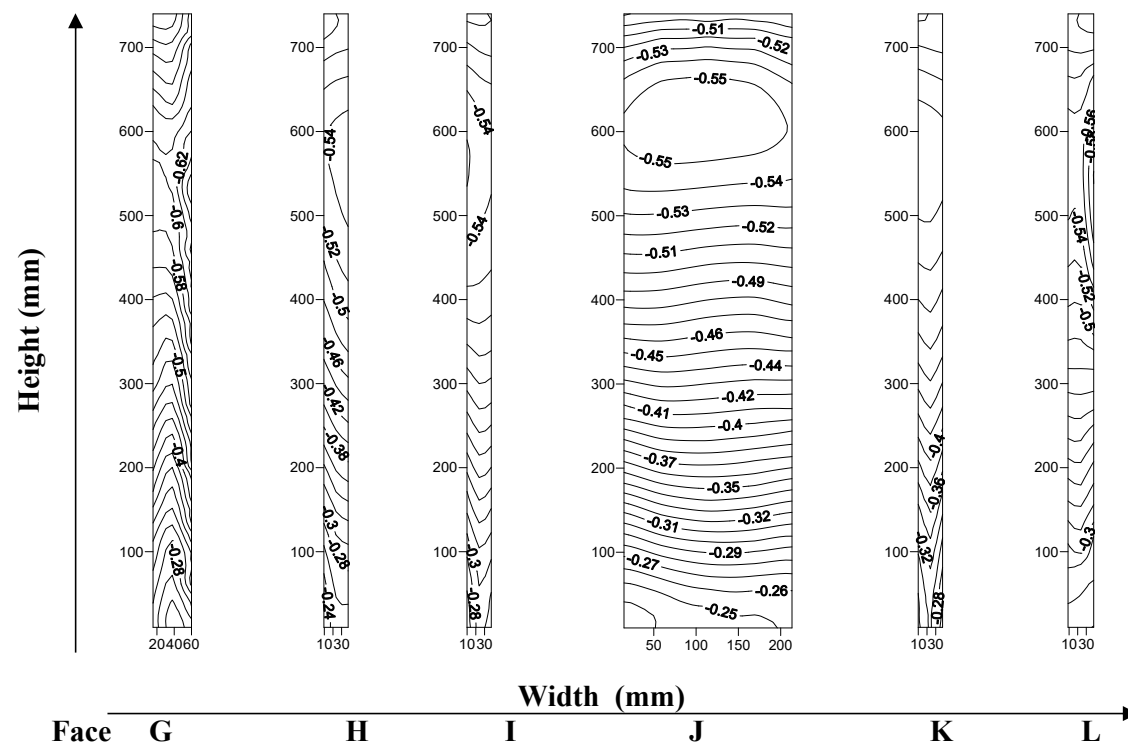
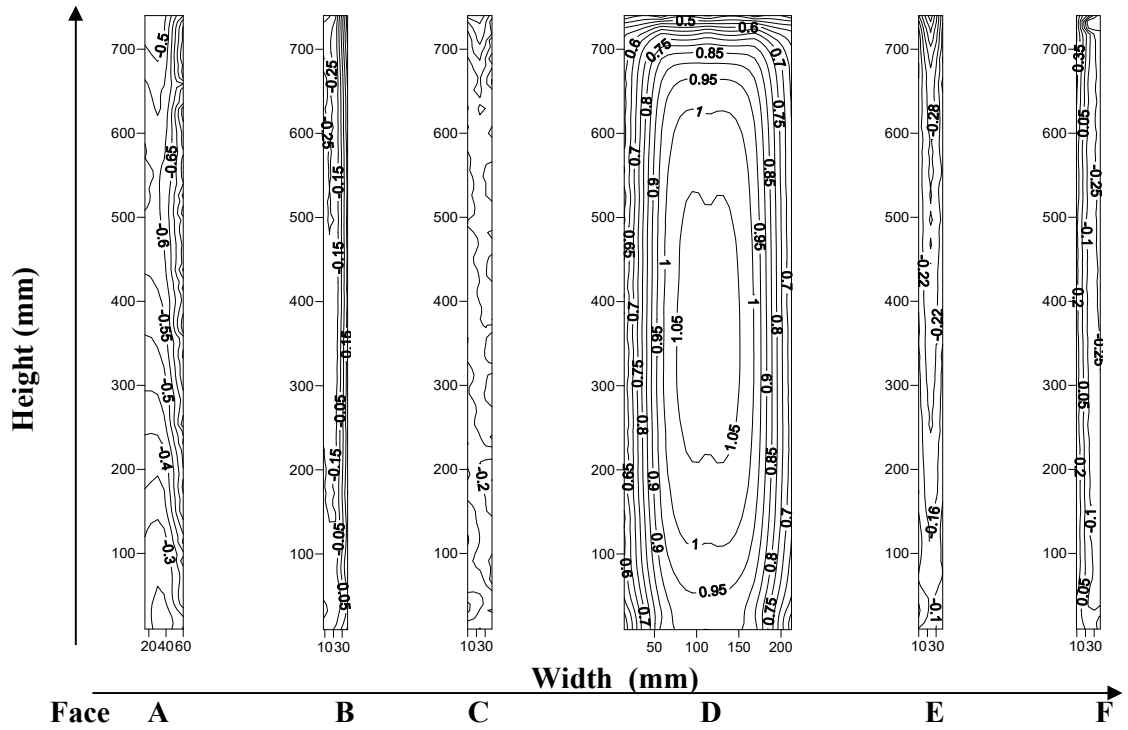


Figure 4.18 Distribution of wind pressure coefficient on the rectangle with corner cut at 90° wind incidence angle



### **4.3.2 Vertical Pressure Distribution along the Height of Building**

The distribution of  $C_{p, \text{mean}}$  on vertical centre line of each face is graphically plotted and represented in Figure 4.19 Mean pressure distribution on the vertical centre line for rectangle with corner cut, for the building model which is having corner cut. The distribution of pressure along the height of the building model is investigated for wind angle ranging from  $0^0$  to  $90^0$  at an interval of  $15^0$ . Face-E, Face-F, Face-G, Face-H, Face-I, and Face-J is subjected to negative pressure on all wind incidence angle. Face-B and Face-C are subjected to negative pressure at  $90^0$  wind incidence angles and subjected to positive pressure at  $0^0$  to  $75^0$  wind incidence angles. Face D is subjected to negative pressure at  $0^0$  and  $15^0$  wind incidence angles. Rest of the angles, are subjected to positive pressure. Face-K and Face-L are under the effect of positive pressure at  $0^0$  wind incidence angle for the rest of the angle, and it is subjected to negative pressure. The variation in  $C_{p, \text{mean}}$  on the vertical centre line is plotted and presented.

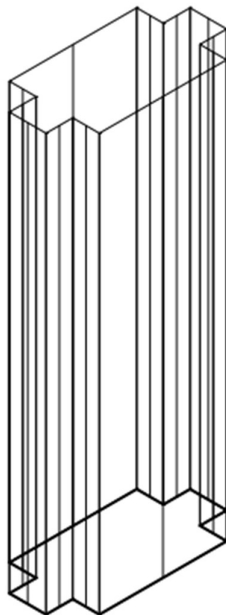
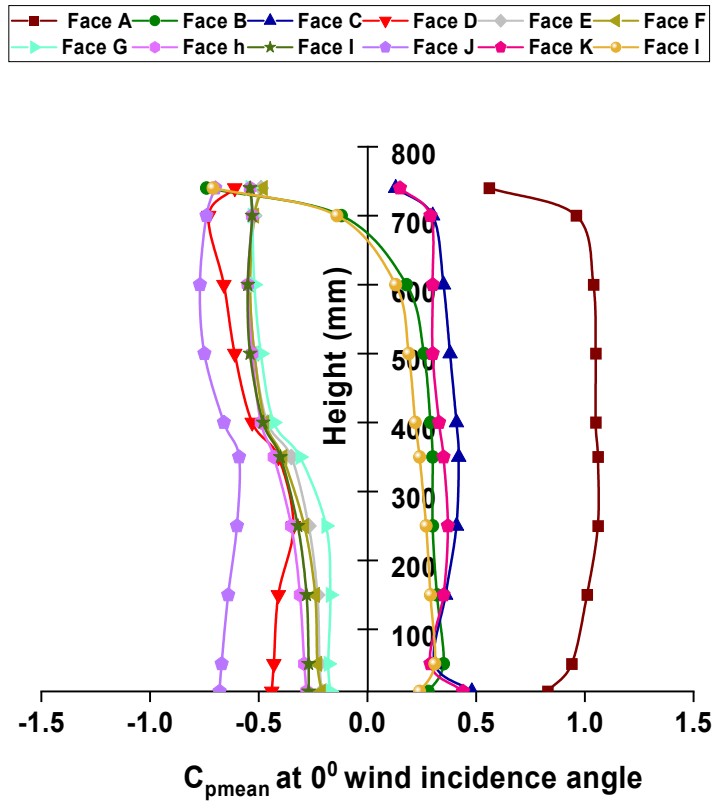


Figure 4.19 (contd.) Mean pressure distribution on the vertical centre line for rectangle with corner cut

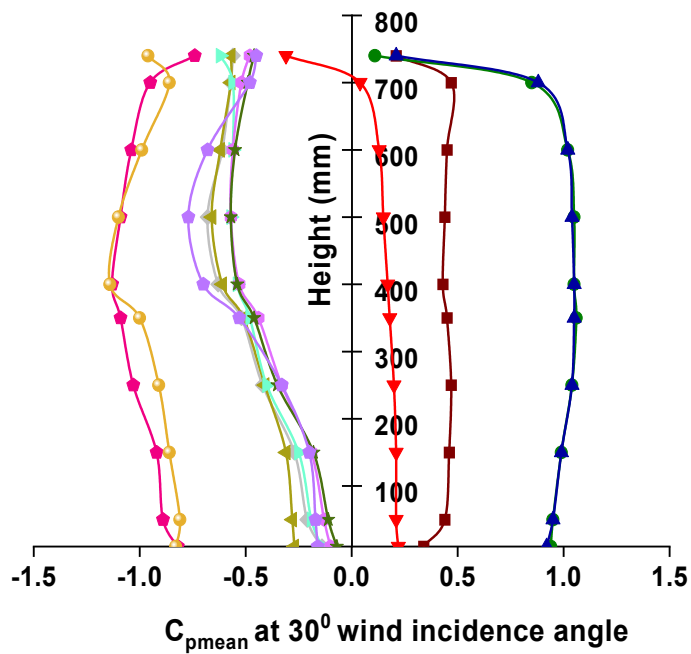
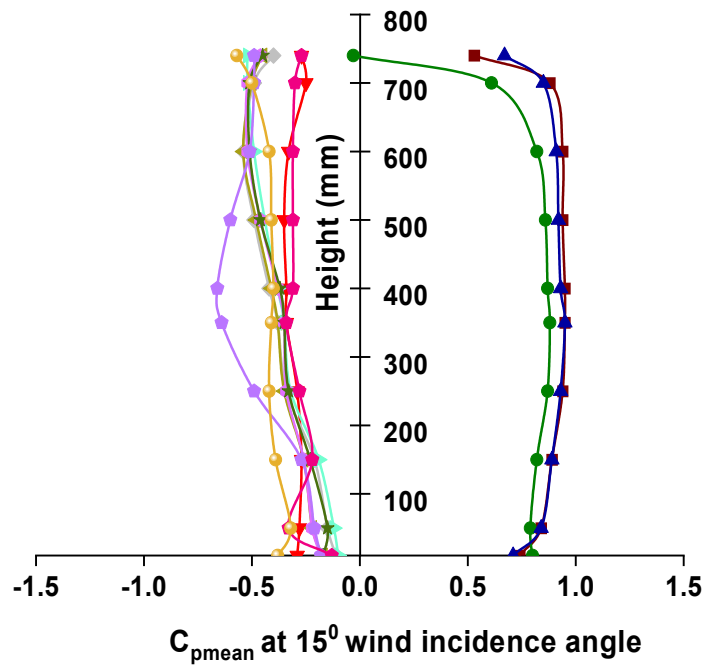
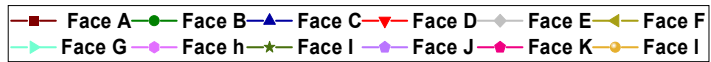


Figure 4.19 (contd.) Mean pressure distribution on the vertical centre line for rectangle with corner cut

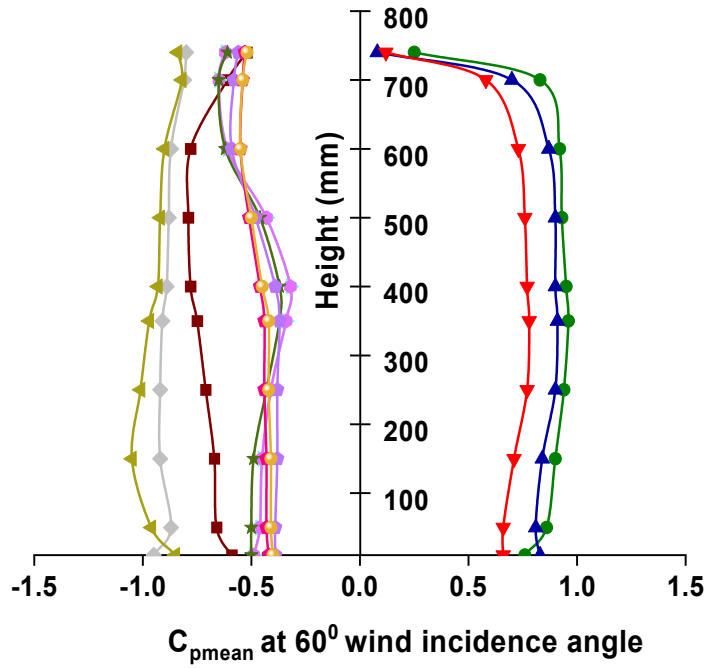
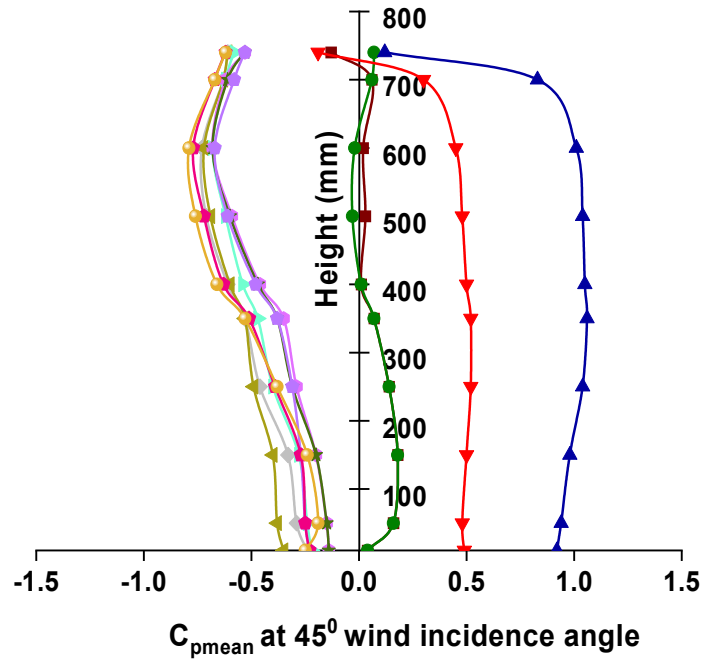
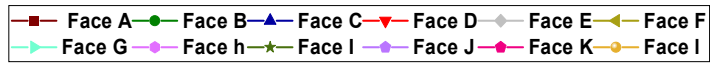


Figure 4.19 (contd.) Mean pressure distribution on the vertical centre line for rectangle with corner cut

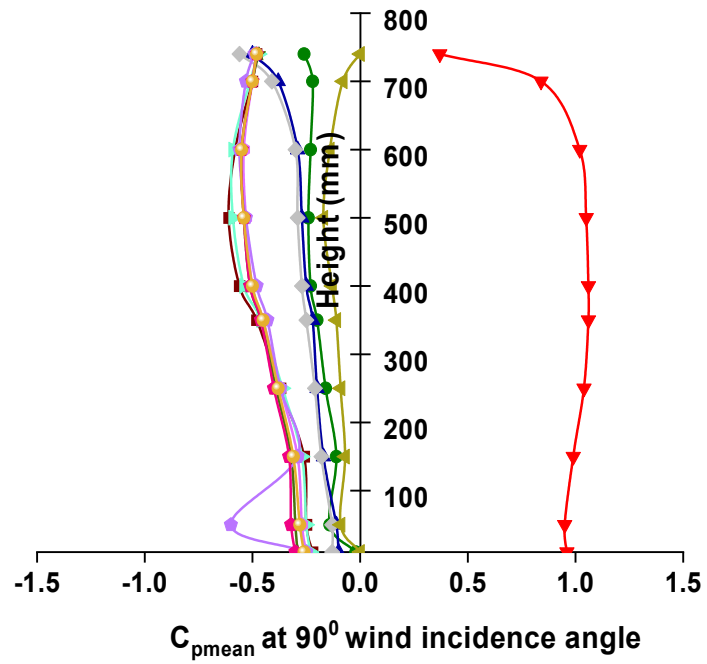
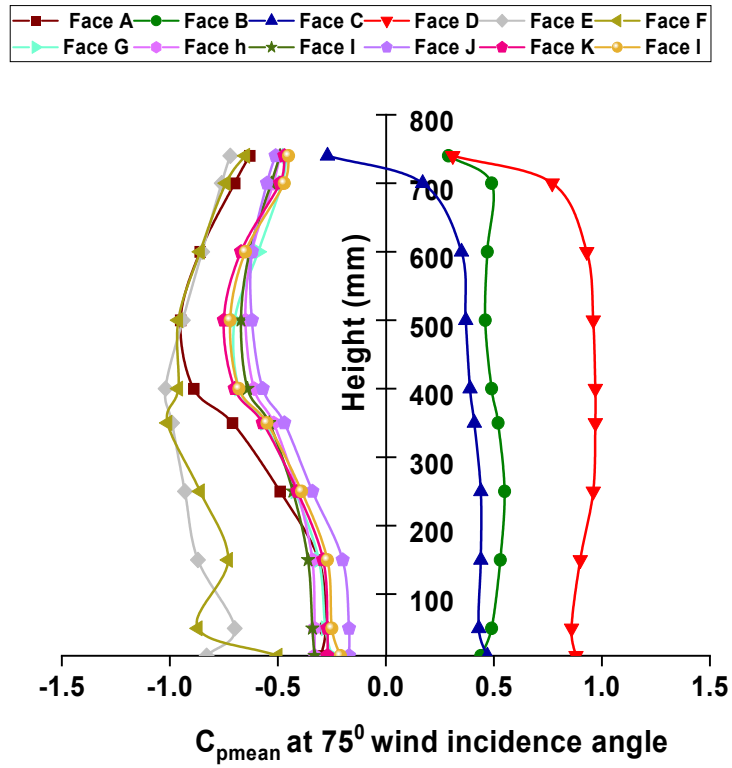


Figure 4.19 Mean pressure distribution on the vertical centre line for rectangle with corner cut

### 4.3.3 Horizontal Pressure Distribution along the Peripheral Distance of Building

The Pressure distribution around the peripheral distance of the building models are depicted graphically in Figure 4.20 Mean pressure distribution along the peripheral distance of the rectangle with corner cut at three different height from base of the model. The distribution of pressure around the building is a function of shape and size of the building and it depends on the speed of the building model. The maximum pressure of 1.05 is observed at  $0^\circ$  wind near 90 mm and minimum is -0.63 around 830 mm distance. The maximum pressure of 1.05 is noted at 33 mm distance at 375 mm height of the model while the least of -0.79 is observed at 805 mm distance at mid height of building. The variation of pressure around the peripheral distance at three different heights is plotted and depicted in the graphical form for rectangular model having the corner cut.

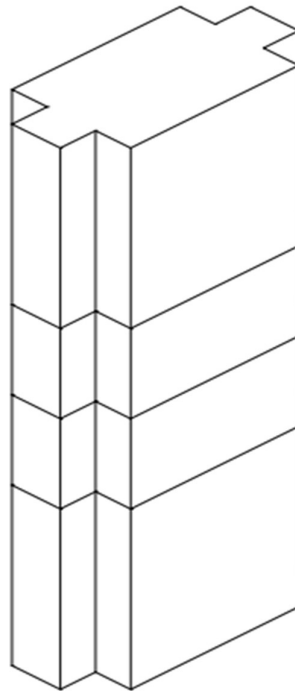
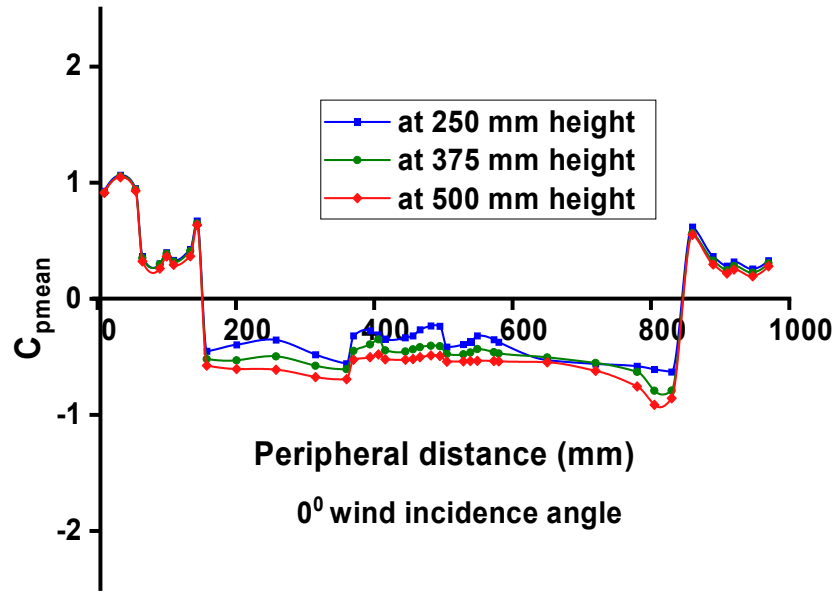


Figure 4.20 (contd.) Mean pressure distribution along the peripheral distance of the rectangle with corner cut

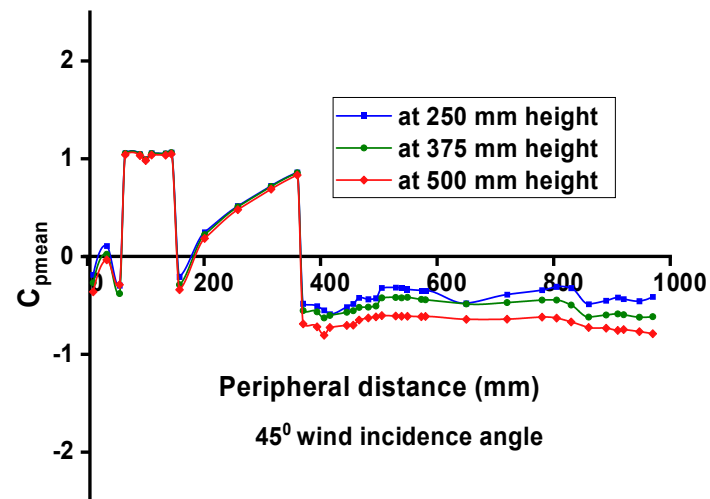
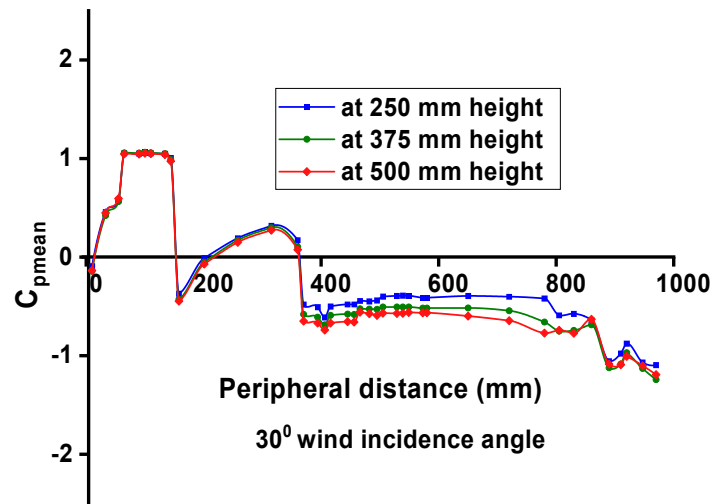
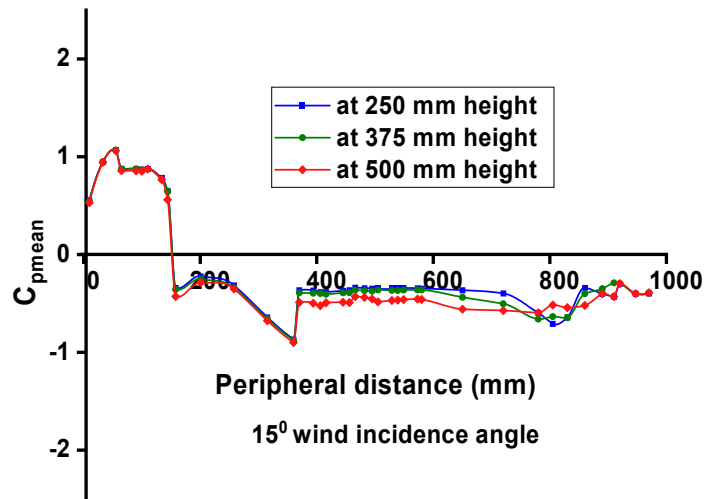


Figure 4.20 (contd.) Mean pressure distribution along the peripheral distance of the rectangle with corner cut



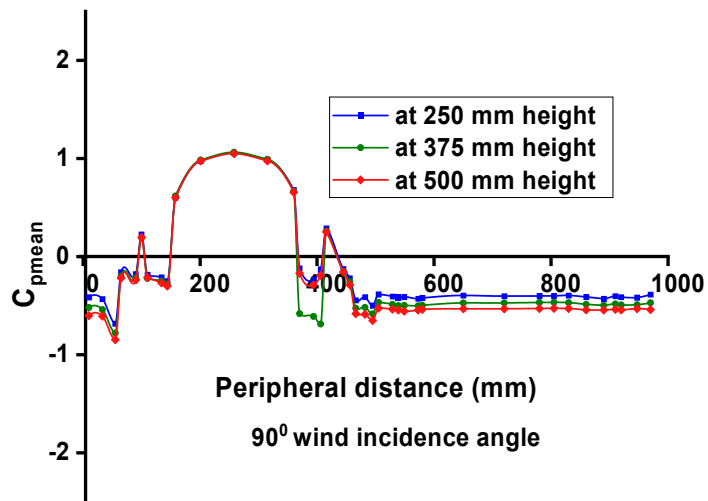
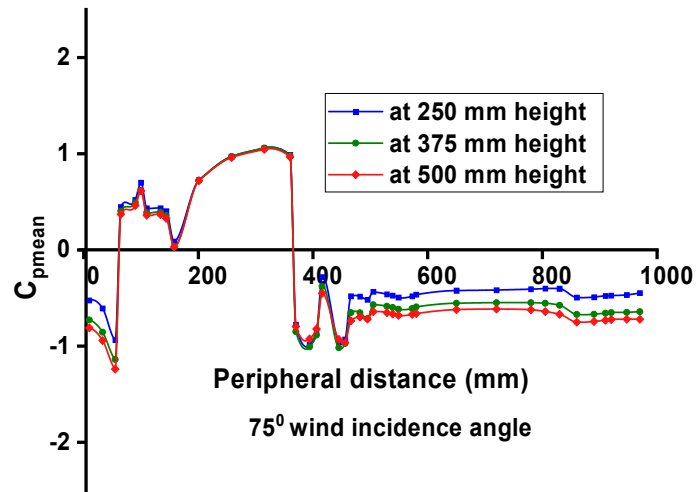
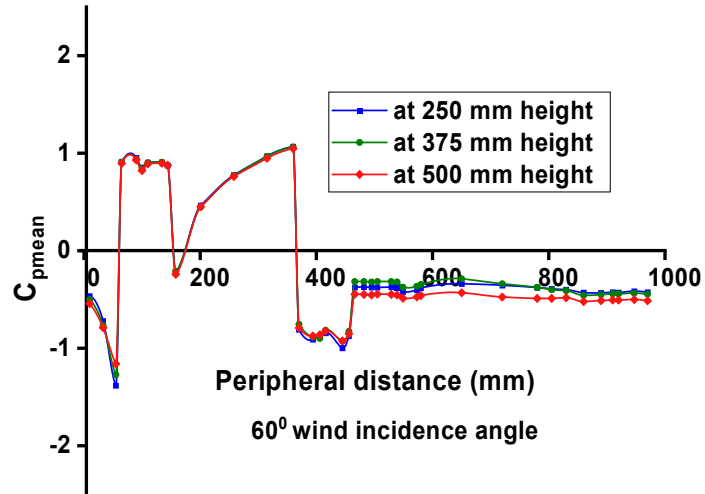


Figure 4.20 Mean pressure distribution along the peripheral distance of the rectangle with corner cut

### 4.3.4 Force coefficients

The force coefficients are investigated for wind incidence angle ranging from  $0^{\circ}$  to  $90^{\circ}$  wind angle at an interval of  $30^{\circ}$ . The data force coefficient is depicted in Figure 4.21 Wind Force coefficient of the rectangle with corner cut and it is obtained from the numerical simulation in the form of force in x and y direction and after calculating the projected area the force coefficient in different direction is evaluated. The  $C_{fx}$  varies from 0.46 to 1.59. The maximum  $C_{fx}$  is 1.59 at  $0^{\circ}$  wind incidence angle because drag is maximum while minimum  $C_{fx}$  is noted at  $45^{\circ}$ . The max  $C_{fy}$  is 0.082 at  $15^{\circ}$  wind incidence angles while the min  $C_{fy}$  of -0.84 is observed at  $30^{\circ}$ .

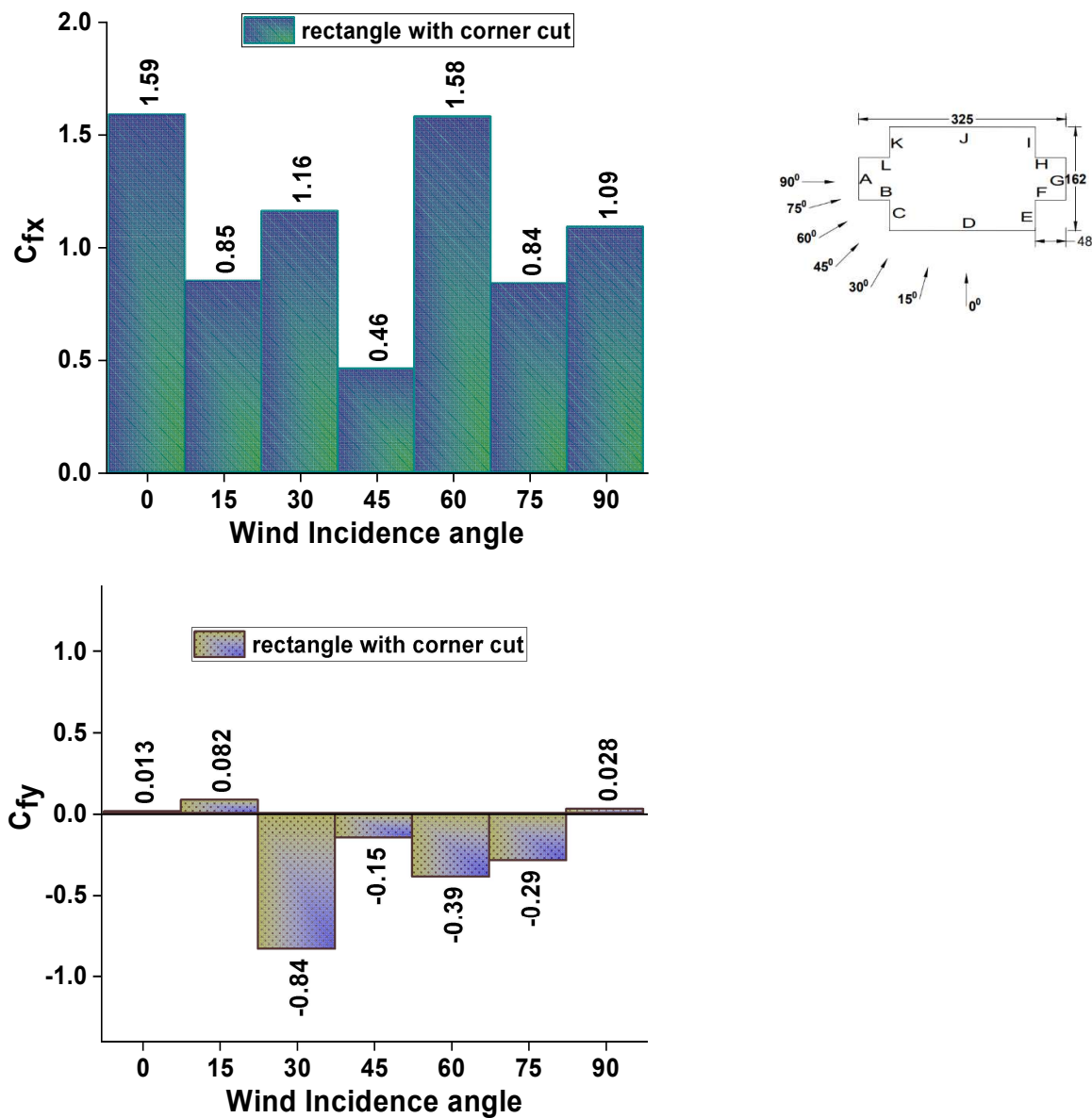


Figure 4.21 Wind Force coefficient of the rectangle with corner cut

### 4.3.5 Moment coefficients

The moment coefficient is calculated and presented for rectangular model with corner cut. The maximum  $C_{mx}$  of 0.438 is observed at  $60^\circ$  wind angles while the smallest  $C_{mx}$  of -0.16 is noted in the case of  $30^\circ$  wind angle. The highest  $C_{my}$  of 1.74 is noted at  $0^\circ$  and  $60^\circ$  wind angles while the smallest  $C_{my}$  of 0.5 is noted at  $45^\circ$  wind angles. The  $M_x$  and  $M_y$  is obtained from computational simulation and  $C_{mx}$  and  $C_{my}$  is graphically plotted in Figure 4.22 Moment coefficient of the rectangle with corner cut.

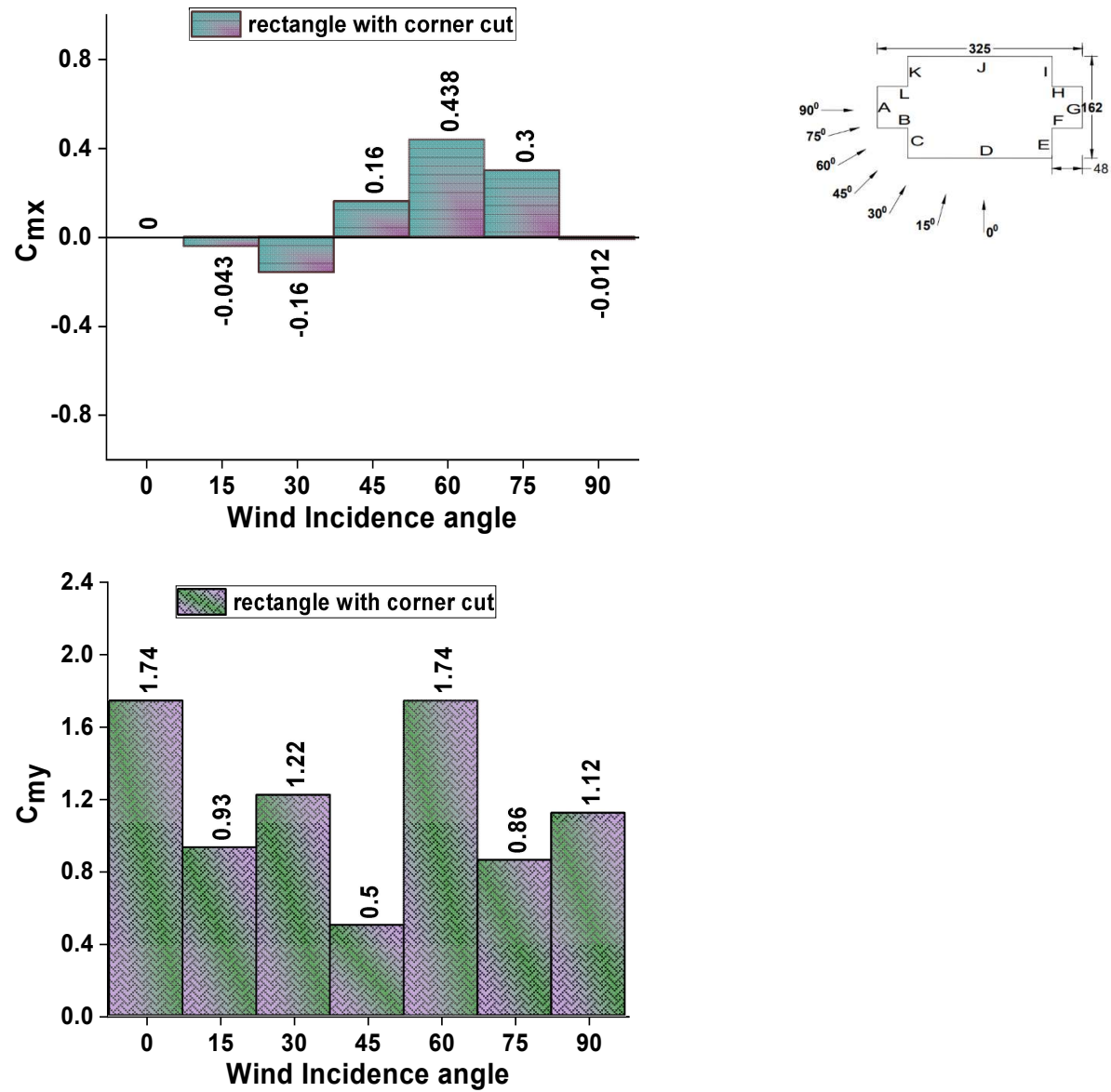


Figure 4.22 Moment coefficient of the rectangle with corner cut

#### 4.3.6 External Pressure Coefficient

The external pressure coefficient is tabulated for all faces of rectangular model which is having cuts in each corner. The values are tabulated in Table-4.2 External Pressure Coefficients for model-B (Rectangle Corner-Cut). This model is having the 12 number faces and the maximum mean  $C_p$  of 0.99 on face-B and face-C is spotted at  $30^\circ$  and  $45^\circ$  wind incidence angles while the minimum  $C_p$  of -0.98 is found on face-L at  $300^\circ$  wind angles. The external  $C_p$  ranges from +0.99 to -0.98 for wind incidence angle ranging from  $0^\circ$  to  $90^\circ$ . The external  $C_p$  is calculated after drawing the external lines on each face and defining the local coordinate frame for each face. The data provided by numerical simulation is then processed as per the procedure explained in the wind tunnel manual and then the mean external  $C_p$  is reported into the tabular form to every  $15^\circ$  intervals from  $0^\circ$  to  $90^\circ$  wind incidence angles. The external pressure coefficient is found positive on wind ward face while the external pressure coefficient is found negative in nature for leeward face and side faces.

**Table-4.2 External Pressure Coefficients for model-B (Rectangle Corner-Cut)**

<b>Model-B (Rectangle Corner-Cut)</b>							
<b>Face</b>	<b>0°</b>	<b>15°</b>	<b>30°</b>	<b>45°</b>	<b>60°</b>	<b>75°</b>	<b>90°</b>
<b>A</b>	<b>0.93</b>	0.82	0.31	-0.15	-0.81	-0.75	<b>-0.51</b>
<b>B</b>	0.26	0.81	<b>0.99</b>	0.97	<b>0.85</b>	0.51	-0.12
<b>C</b>	0.40	<b>0.83</b>	0.98	<b>0.99</b>	0.83	0.37	-0.21
<b>D</b>	<b>-0.60</b>	-0.47	0.02	0.37	0.56	<b>0.72</b>	<b>0.82</b>
<b>E</b>	-0.41	-0.39	-0.53	-0.56	-0.85	<b>-0.81</b>	-0.21
<b>F</b>	-0.43	-0.40	-0.51	<b>-0.57</b>	<b>-0.87</b>	-0.70	-0.12
<b>G</b>	-0.37	-0.36	-0.46	-0.49	-0.46	-0.53	<b>-0.51</b>
<b>H</b>	-0.43	-0.39	-0.42	-0.43	-0.47	-0.51	-0.44
<b>I</b>	-0.41	-0.38	-0.42	-0.44	-0.49	-0.53	-0.45
<b>J</b>	<b>-0.60</b>	<b>-0.50</b>	-0.51	-0.48	-0.44	-0.47	-0.44
<b>K</b>	0.40	-0.18	-0.86	-0.54	-0.48	-0.53	-0.45
<b>L</b>	0.26	-0.33	<b>-0.98</b>	-0.55	-0.47	-0.51	-0.44

#### **4.4 Rectangle Shape with Chamfer Corners**

Wind effects are investigated using numerical simulation for tall building of different configuration and also in this study the different corner configuration is applied such as recessed, chamfer and fillet for both regular shape and irregular shape building. The regular shape is modified because sometimes the available land is having different types of condition and wind effects may generate very critical effects. To reduce this wind load on the tall building modifications in the corners can be applied. The angle varies from  $0^{\circ}$  to  $90^{\circ}$  at an interval of  $15^{\circ}$  while irregular Y-shape model is investigated for  $0^{\circ}$  to  $180^{\circ}$  at an interval of  $15^{\circ}$ .

In this study the result is plotted for the distribution of pressure on each surface of the model and pressure distribution pattern is studied at the centre line of each face and the pressure along the peripheral distance is also studied at three different level of 250 mm, 375 mm and 500 mm height from the base of the model.

Investigation of wind effects are done in the numerical simulation performed by varying the wind as per the power law which states that the wind speed attains free stream velocity above the gradient height and after the gradient height mean wind speed becomes constant. Mean wind speed and turbulent intensity are kept same for the experiment performed in the boundary layer wind tunnel and it is also presented for the validation of result with the experimental values and various international standards.

##### **4.4.1 Pressure contours**

Pressure distribution is depicted in the form of pressure contours for rectangular model-C. The pressure contours are studied for  $0^{\circ}$  to  $90^{\circ}$  wind incidence angle and the pressure varies from positive to negative and the impact of this is more or less dependent on the behaviour of wind flow characteristics. If the wind is acting directly on the wind ward face then there will be positive pressure while if the flow is reattaching on the surfaces of the building model then some nature of pressure distribution will be obtained. The pressure lies in the range of 1.15 to -0.98 and it is also observed that the identical faces have the same type of pressure distribution while some critical faces also have more suction. The pressure contours that are depicted from the Figure 4.23 Distribution of wind pressure coefficient on the rectangle with chamfer corner cut at  $0^{\circ}$  wind incidence angle to Figure 4.29 Distribution of wind pressure coefficient on the rectangle with chamfer corner cut at  $90^{\circ}$  wind incidence angle.

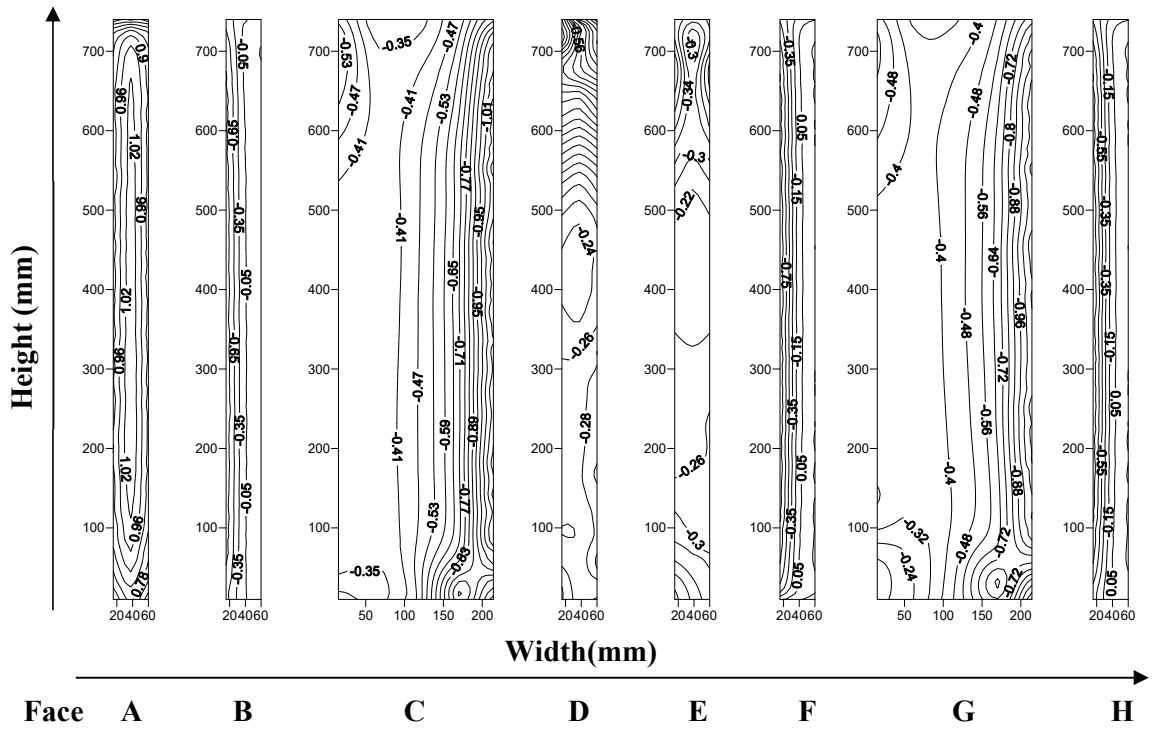


Figure 4.23 Distribution of wind pressure coefficient on the rectangle with chamfer corner cut at  $0^\circ$  wind incidence angle

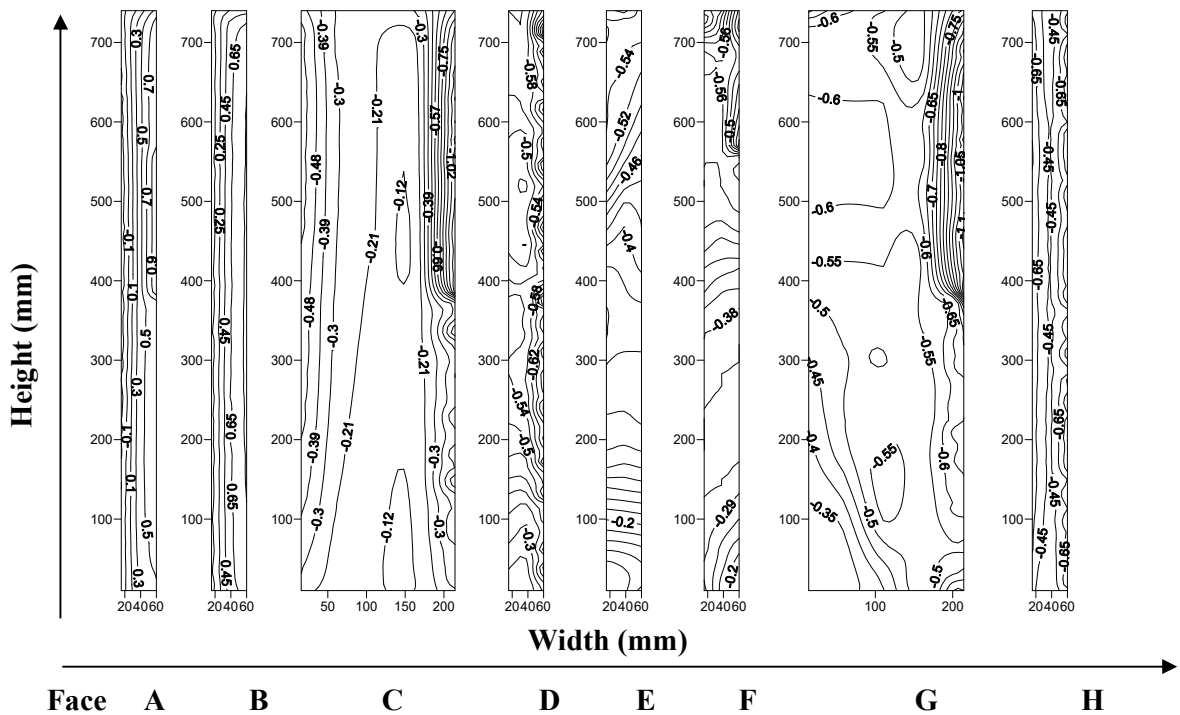


Figure 4.24 Distribution of wind pressure coefficient on the rectangle with chamfer corner cut at  $15^\circ$  wind incidence angle

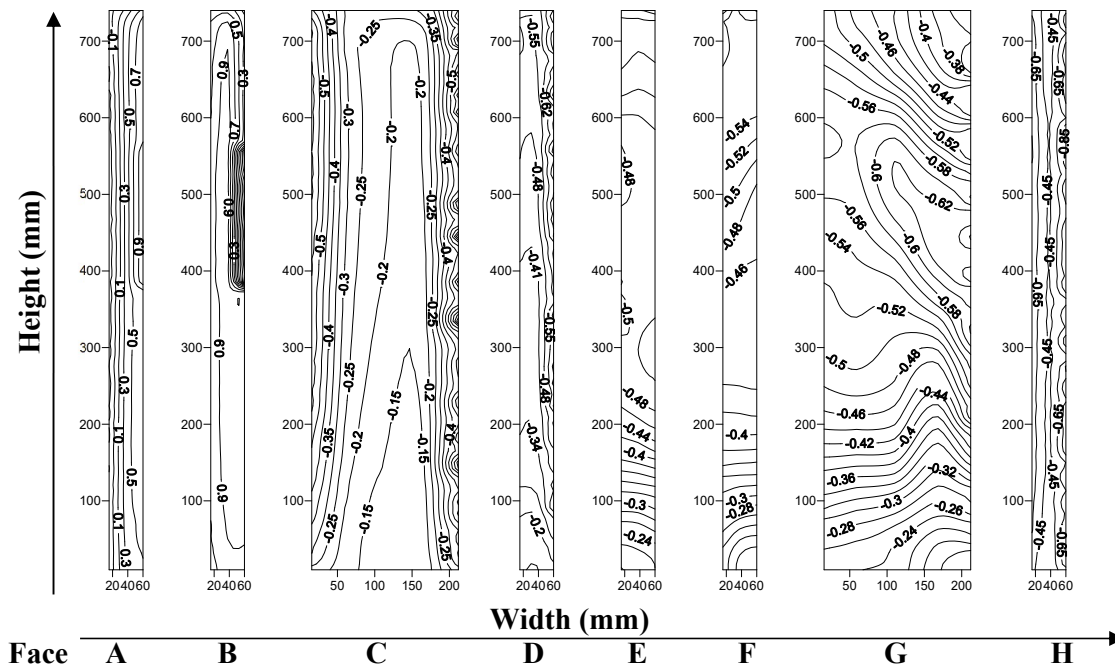


Figure 4.25 Distribution of wind pressure coefficient on the rectangle with chamfer corner cut at 30° wind incidence angle

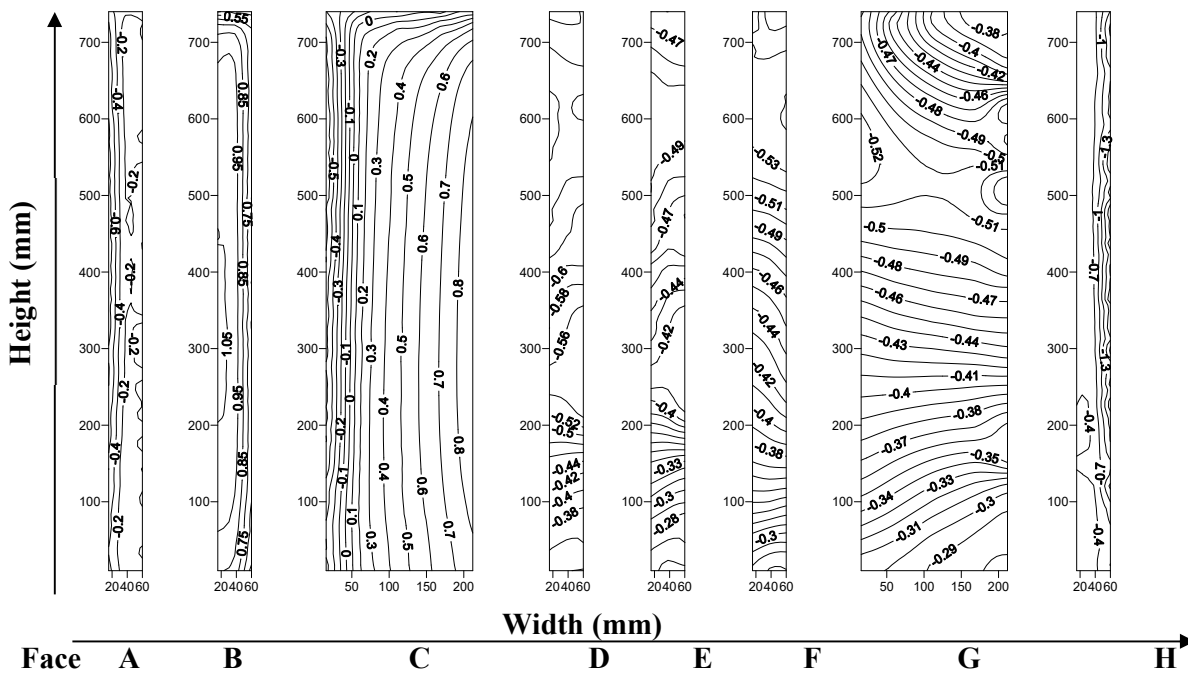


Figure 4.26 Distribution of wind pressure coefficient on the rectangle with chamfer corner cut at 45° wind incidence angle



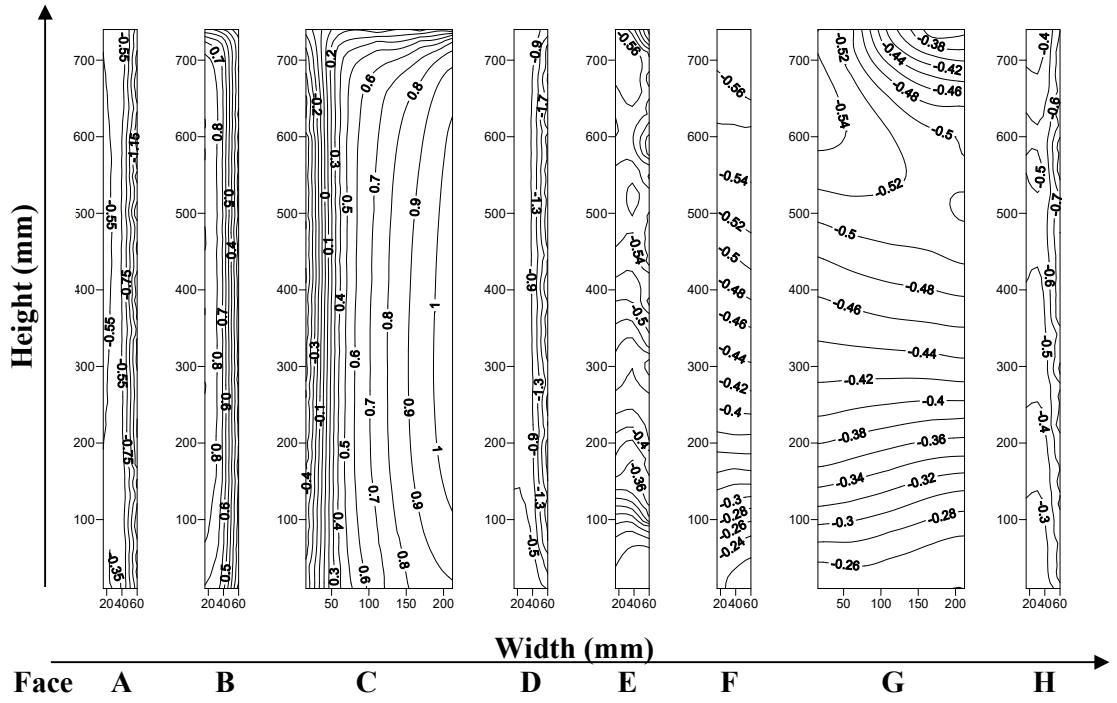


Figure 4.27 Distribution of wind pressure coefficient on the rectangle with chamfer corner cut at  $60^\circ$  wind incidence angle

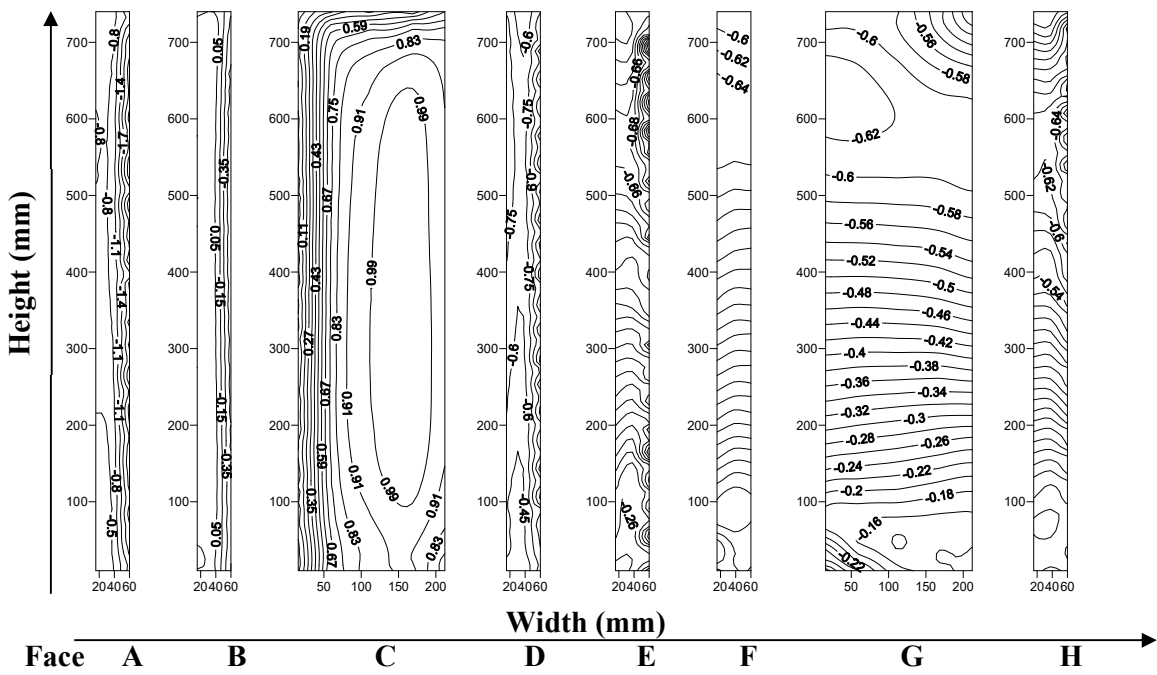
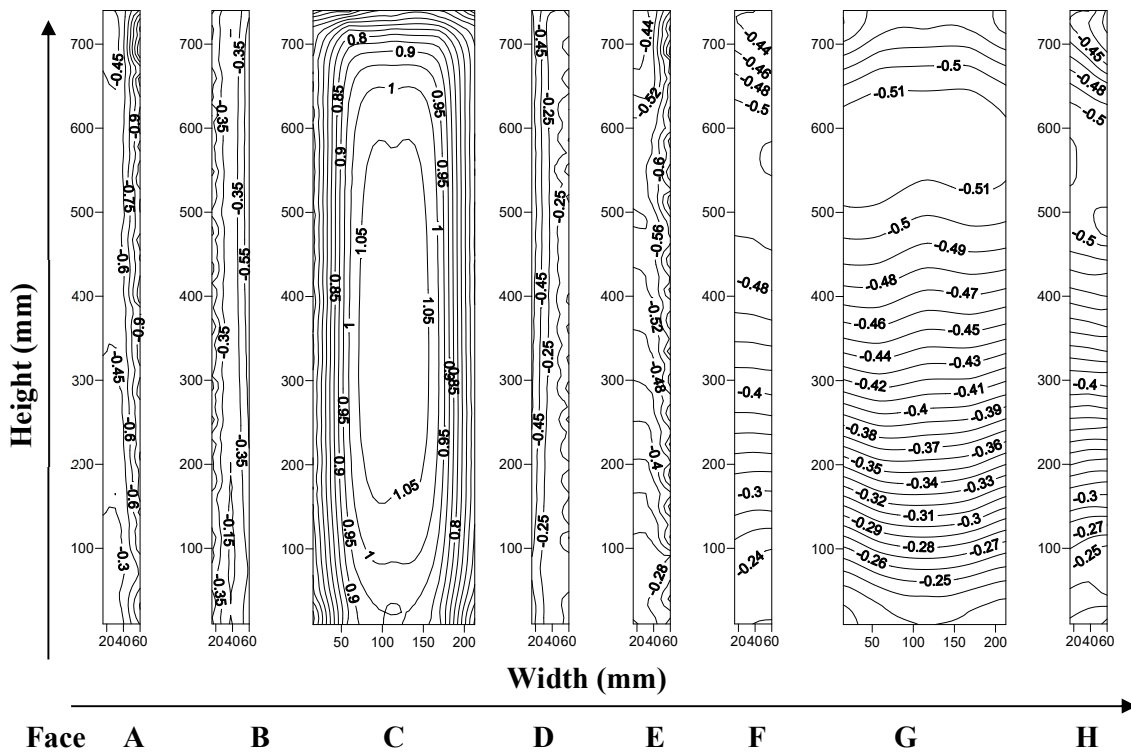


Figure 4.28 Distribution of wind pressure coefficient on the rectangle with chamfer corner cut at  $75^\circ$  wind incidence angle



**Figure 4.29 Distribution of wind pressure coefficient on the rectangle with chamfer corner cut at  $90^\circ$  wind incidence angle**

It is also clearly represented that if the nature of pressure along the surface is positive, it means that pressure acting on the surface is more than the static pressure. If the pressure is less than the static pressure than the pressure contours is negative and it is calculated after accounting the various types of wind flow characteristics like vortex shedding, flow reattachment etc.

#### 4.4.2 Vertical Pressure Distribution along the Height of Building

Vertical pressure distribution on the vertical centre line of each face is depicted in Figure 4.30 Mean pressure distribution on the vertical centre line for rectangle with chamfer corner cut and the pressure flow characteristics are depicted along the centre line where this is clearly demonstrated the flow characteristic like vortex shedding in the downstream of wind is observed. It is also observed that in the case of  $0^\circ$  wind incidence angle only face-A has positive pressure while the other faces are under the impact of negative pressure and when wind is incidence on model is  $15^\circ$  two faces are under the impact of positive pressure while the other faces of the building model are under the effect of suction that is why the centre line pressure on other surfaces of building model is under the effect of negative pressure. Likewise, the centre line pressure along the height of the model is studied and depicted.

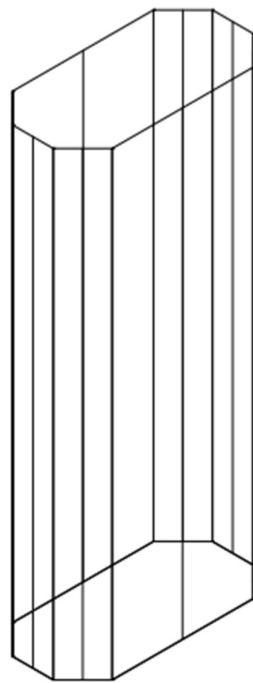
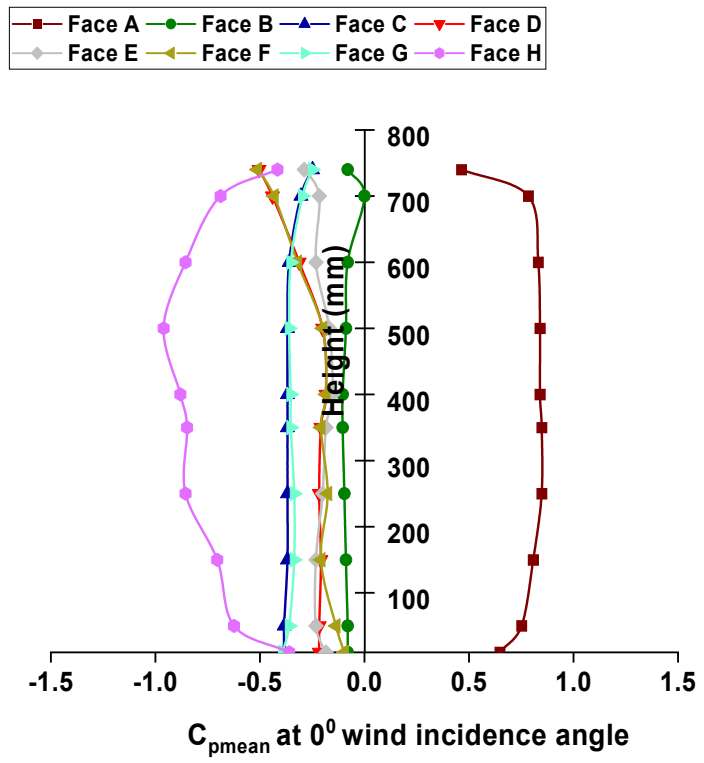


Figure 4.30 (contd.) Mean pressure distribution on the vertical centre line for rectangle with chamfer corner cut

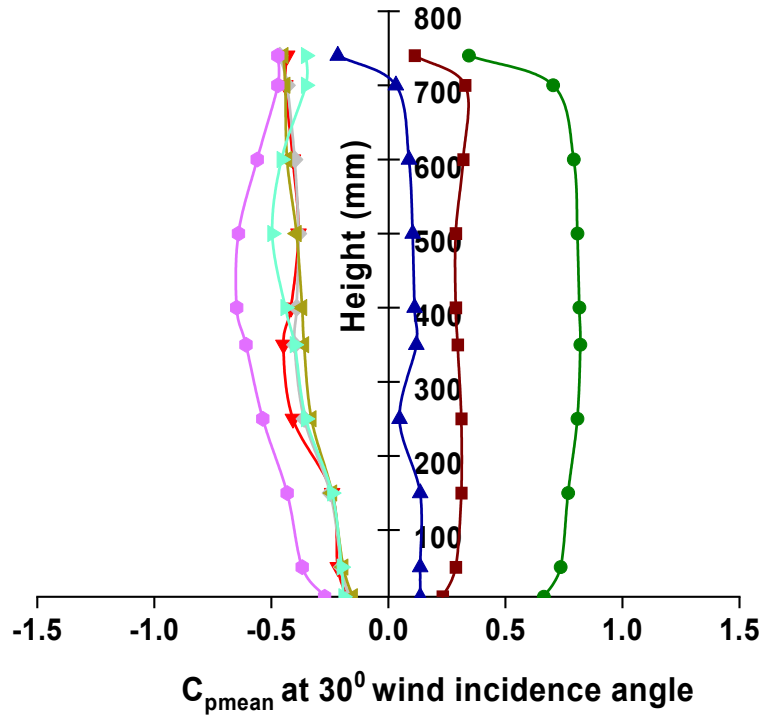
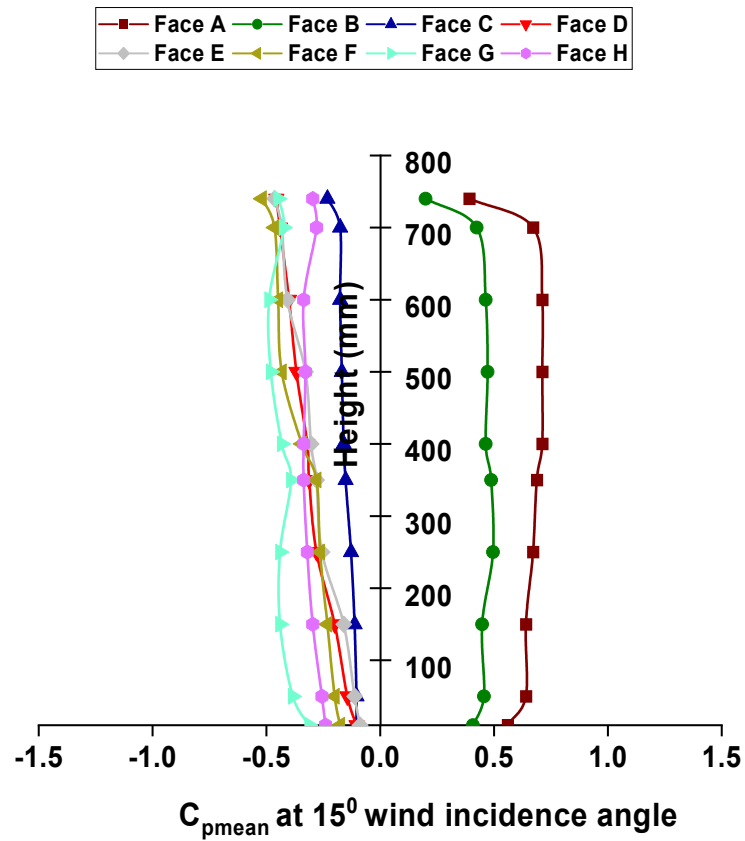


Figure 4.30 (contd.) Mean pressure distribution on the vertical centre line for rectangle with chamfer corner cut

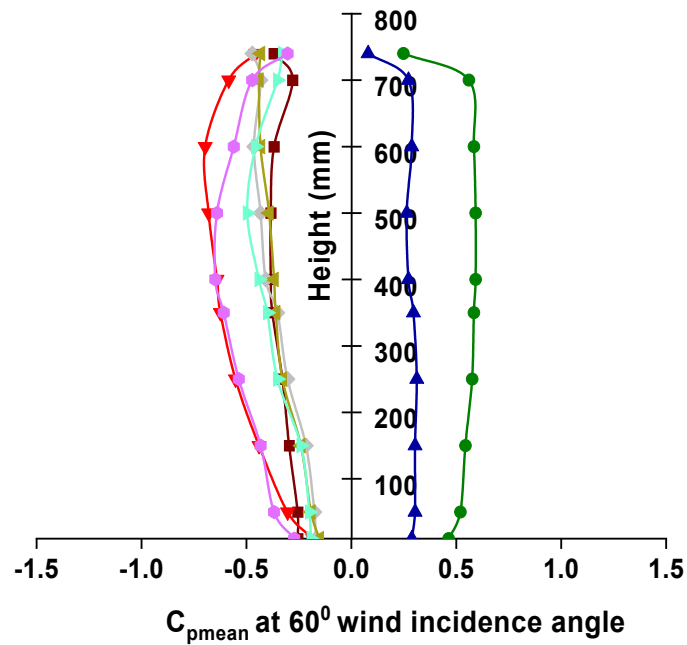
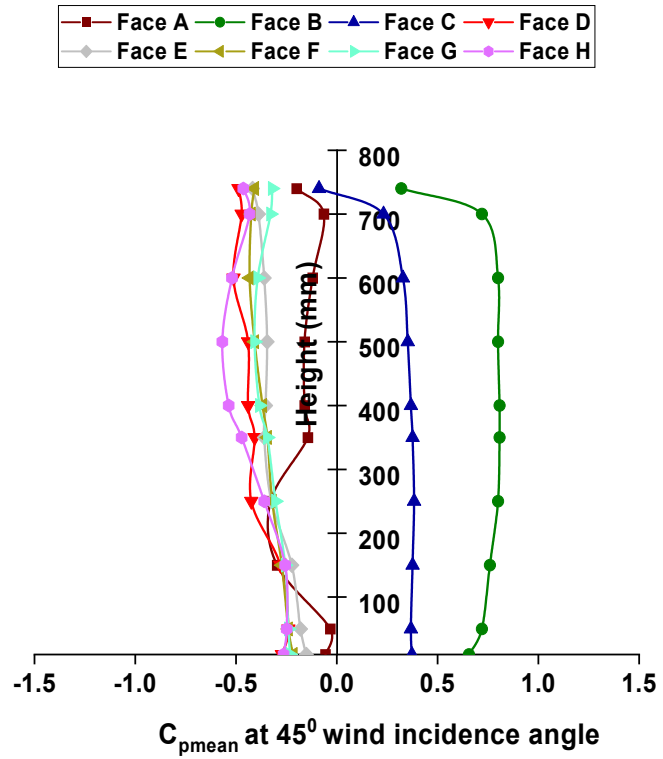


Figure 4.30 (contd.) Mean pressure distribution on the vertical centre line for rectangle with chamfer corner cut

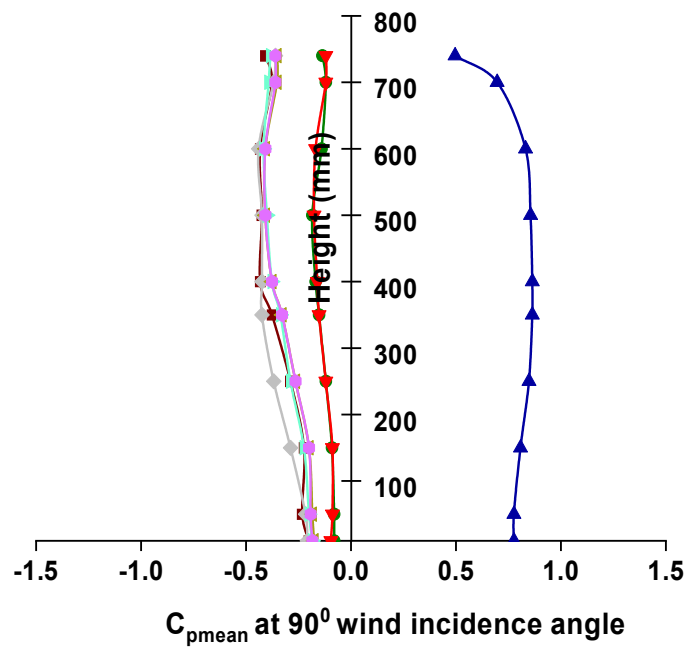
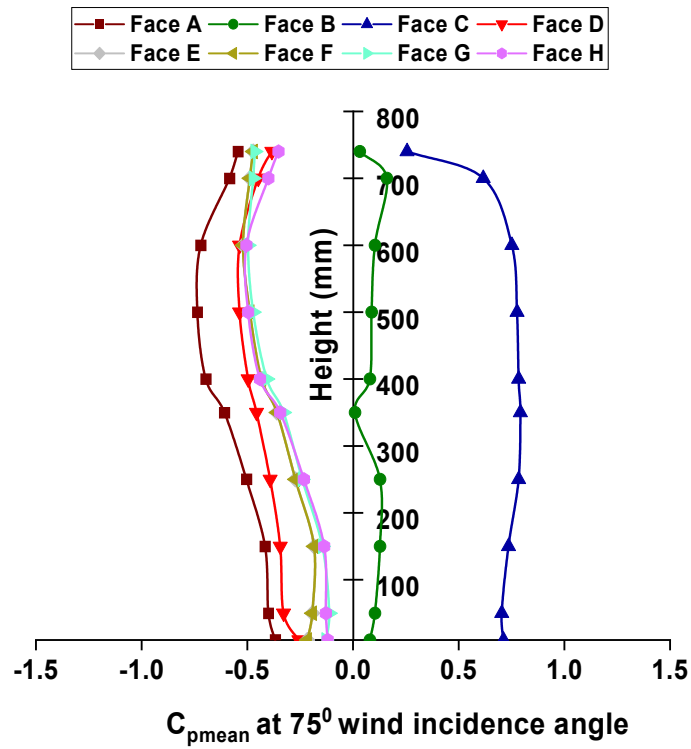


Figure 4.30 Mean pressure distribution on the vertical centre line for rectangle with chamfer corner cut

#### **4.4.3 Horizontal Pressure Distribution along the Peripheral Distance of Building**

Pressure distribution along the peripheral distance of model is graphically plotted in Figure 4.31. Mean pressure distribution along the peripheral distance of the rectangle with chamfer corner cut at three different levels such that one level is located at 250 mm from the base of the model while the second level is at mid height of the model and the last level that is the third level is located at 500 mm height from the base of the model. More or less the pressure distribution pattern is same for all building models while at some of the angles some deviation is observed at all three levels. The pressure distribution along the peripheral distance for rectangular building model that is model-C is depicted in graphical form. The variation is observed because of the flow reattachment characteristics.

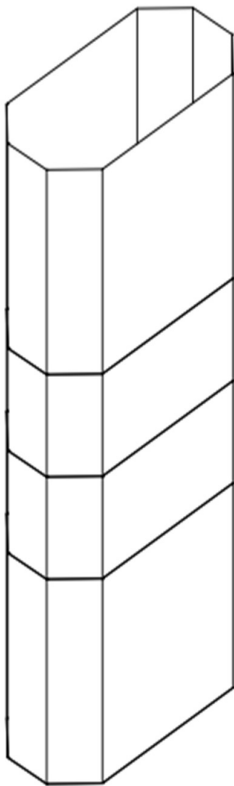
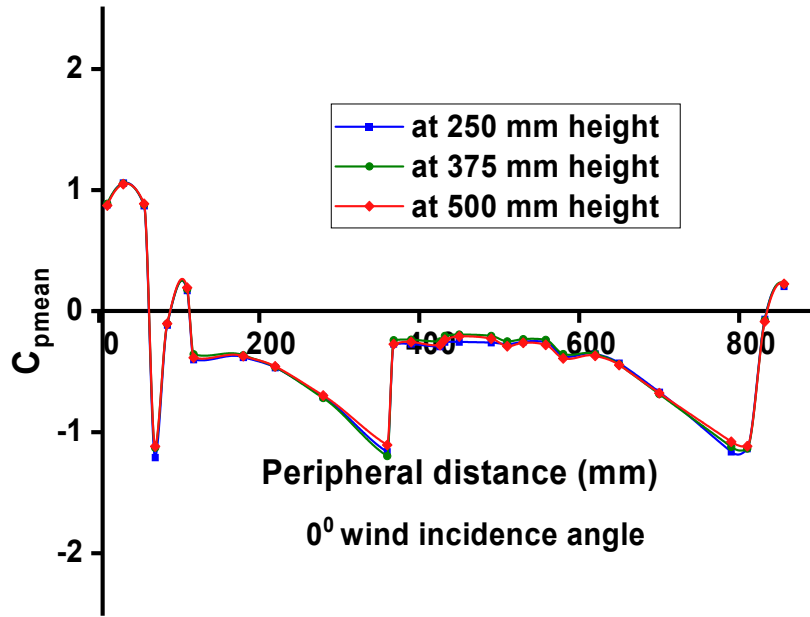


Figure 4.31 (contd.) Mean pressure distribution along the peripheral distance of the rectangle with chamfer corner cut



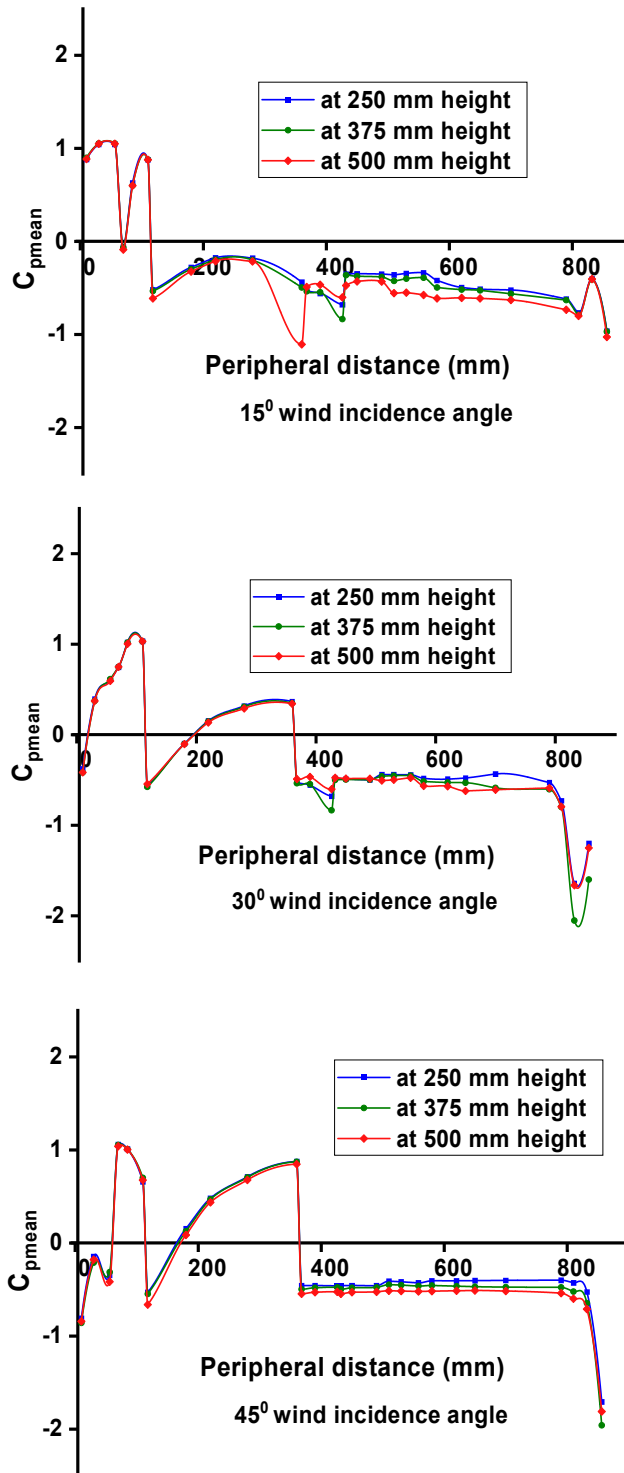


Figure 4.31 (contd.) Mean pressure distribution along the peripheral distance of the rectangle with chamfer corner cut

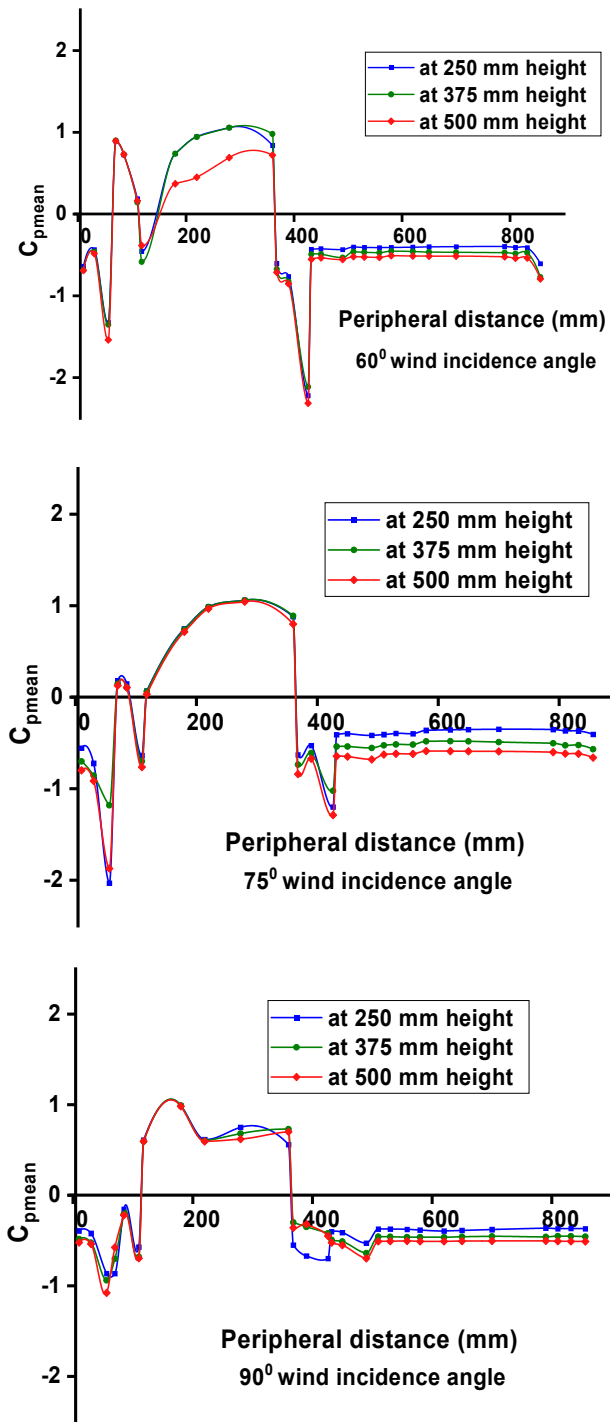


Figure 4.31 Mean pressure distribution along the peripheral distance of the rectangle with chamfer corner cut

### 4.4.4 Force Coefficients

The wind force coefficients in x and y direction are computed and plotted in Figure 4.32. Wind Force coefficient of the rectangle with chamfer corner, it is found the force coefficient in x-direction is  $C_{Fx}$  while in y-direction is  $C_{Fy}$  and it is also observed that force coefficient in x-direction is drag force and the force coefficient in y-direction is lift force. The  $C_{Fx}$  is varies from 0.43 to 1.8 with the min  $C_{Fx}$  is found at  $75^\circ$  wind incidence angle while the max  $C_{Fx}$  is spotted in the case of  $45^\circ$  because at these angles due to the corner configuration wind effects are changing and max drag is observed. Likewise, the  $C_{Fy}$  is computed and graphically plotted for the wind incidence angle ranging from  $0^\circ$  to  $90^\circ$ . The  $C_{Fx}$  is drag while the  $C_{Fy}$  is lift.

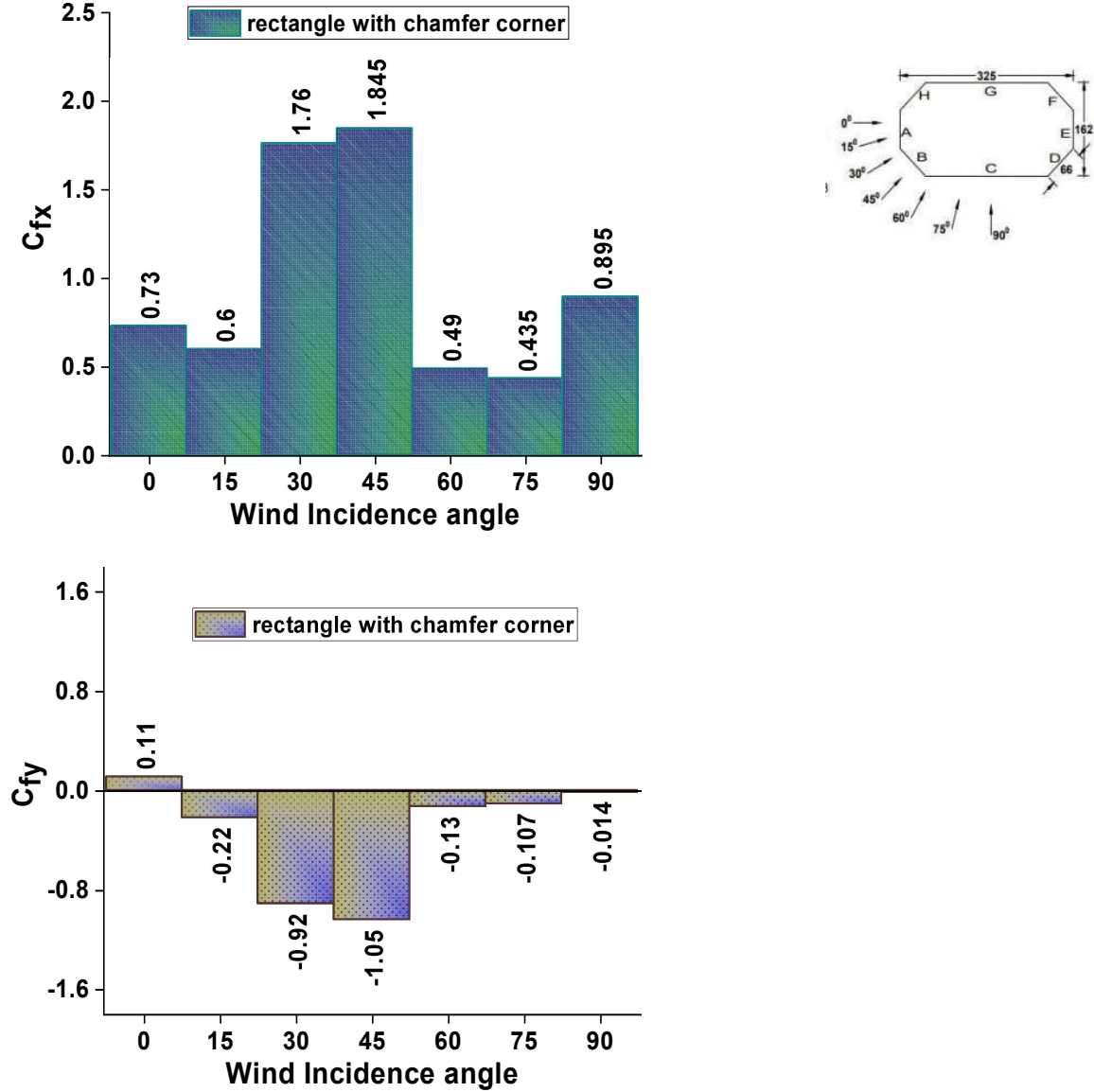


Figure 4.32 Wind Force coefficient of the rectangle with chamfer corner

#### 4.4.5 Moment Coefficients

The moments are calculated for building model having the chamfer corners the moment coefficients in x-direction is  $C_{mx}$  and moment calculated in y-direction is  $C_{my}$ . The  $C_{mx}$  varies from -0.062 to 1.63 with the maximum  $C_{mx}$  observed at  $30^\circ$  and least moment  $C_{mx}$  is found at  $0^\circ$ . The  $C_{my}$  is varies from 0.53 to 1.95 with max  $C_{my}$  is at  $45^\circ$  while minimum is at  $75^\circ$  wind incidence angle. The moment coefficients in x and y direction are calculated for the wind incidence angles ranging from  $0^\circ$  to  $90^\circ$  wind and the flow characteristics are accounted to calculate the wind effects on the chamfer corner of rectangular building model and presented in Figure 4.33 Wind moment coefficient of the rectangle with chamfer corner.

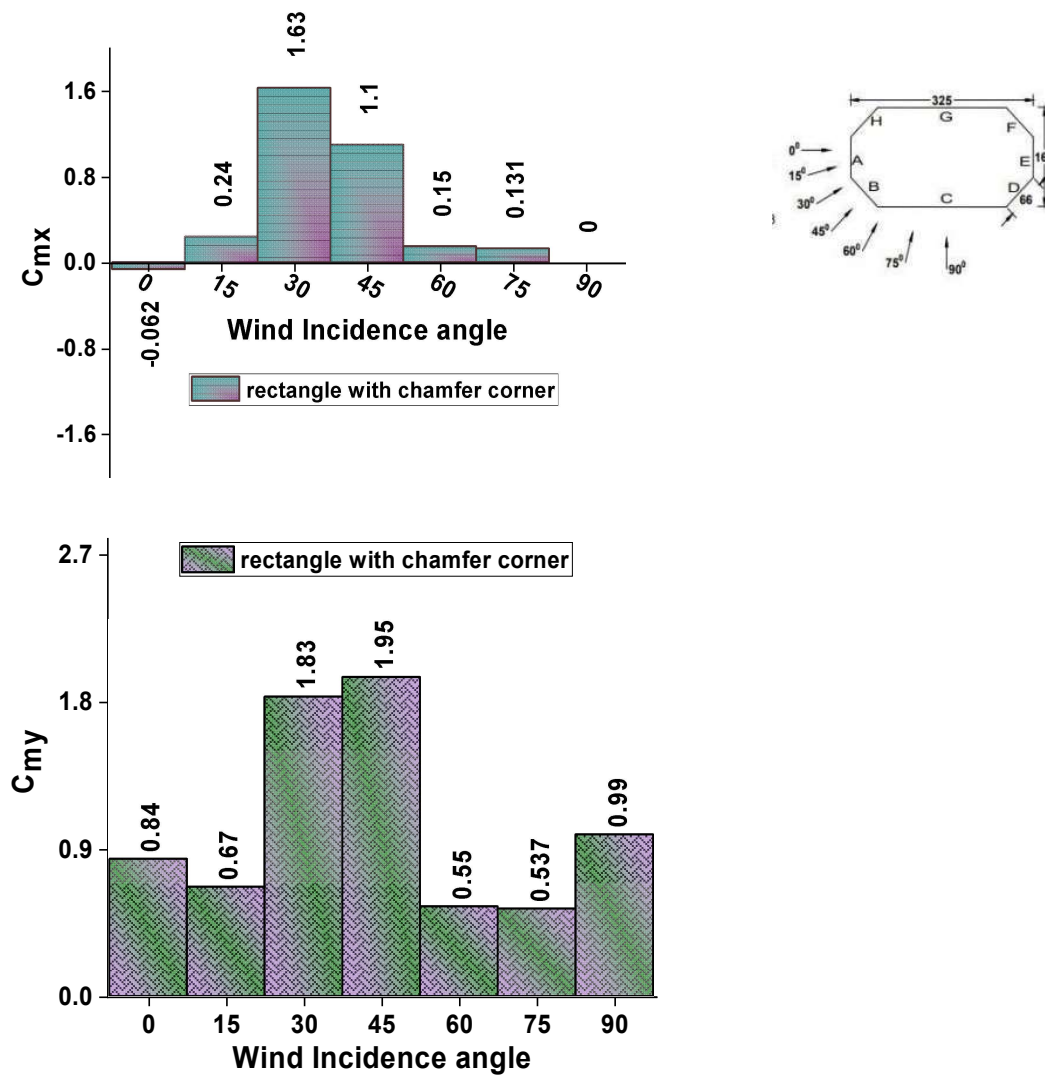


Figure 4.33 Wind moment coefficient of the rectangle with chamfer corner

#### 4.4.6 External Pressure Coefficients

External pressure coefficient is determined on each surface of building model which is having the chamfer corner for the wind incidence angle ranging  $0^{\circ}$  to  $90^{\circ}$ . The maximum pressure coefficient of 0.91 is observed on face-A in the case of  $0^{\circ}$  while the minimum pressure of -1.12 is observed on face- D when wind incidence angle is  $60^{\circ}$ . The external pressure coefficient is useful for the structural design engineer when they are accounting such chamfer corner in the rectangular building model. The external pressure coefficient ranges from positive to negative in the specific ranges, and same is depicted in the tabular form in Table:-4.3 External Pressure Coefficient for Building Model-C (Rectangular Chamfer).

**Table:-4.3 External Pressure Coefficient for Building Model-C (Rectangular Chamfer)**

<b>Model-C (Rectangular Chamfer)</b>							
<b>Face</b>	<b><math>0^{\circ}</math></b>	<b><math>15^{\circ}</math></b>	<b><math>30^{\circ}</math></b>	<b><math>45^{\circ}</math></b>	<b><math>60^{\circ}</math></b>	<b><math>75^{\circ}</math></b>	<b><math>90^{\circ}</math></b>
<b>A</b>	<b>0.91</b>	<b>0.83</b>	0.21	-0.36	-0.78	<b>-1.11</b>	<b>-0.50</b>
<b>B</b>	-0.30	0.46	<b>0.89</b>	<b>0.87</b>	<b>0.57</b>	-0.12	-0.45
<b>C</b>	<b>-0.59</b>	-0.32	0.02	0.29	0.19	<b>0.71</b>	<b>0.82</b>
<b>D</b>	-0.32	-0.46	-0.52	<b>-0.69</b>	<b>-1.12</b>	-0.76	-0.45
<b>E</b>	-0.28	-0.37	-0.45	-0.46	-0.46	-0.51	<b>-0.50</b>
<b>F</b>	-0.32	-0.42	-0.44	-0.45	-0.4	-0.48	-0.41
<b>G</b>	<b>-0.59</b>	-0.54	-0.47	-0.43	-0.42	-0.44	-0.42
<b>H</b>	-0.30	<b>-0.65</b>	<b>-0.99</b>	-0.83	-0.50	-0.45	-0.41

## 4.5 Rectangle Shape with Fillet in Corners

Rectangle shape with fillet corner is a type of modification which helps to reduce the wind effects on the high-rise structures. As the height increases the wind effect also become more critical and such effects are investigated either by the experimental method (Wind tunnel testing) or by using the numerical techniques such as computational fluid dynamics tool like ANSYS CFX. Numerical tool is provides for the stability and response of the structure that can be obtained using different software. Most of the numerical tools are provide the solution based on the boundary condition. The boundary conditions of fluid problem mainly depend on the turbulence model because it contains a large number of variables that are interdependent on each other and because of that the basic of the boundary layer and fluid mechanics is thoroughly very clear to the person who is setting the flow physics.

Numerical simulation results also varies on the basis of mesh sizes. There are various methods available for meshing and because of that mesh independent test is prerequisite. Too fine mesh will not always provide an accurate solution, because sometimes it may happen that flow intermixing can be present if too fine mesh is applied and stiffness matrix will not generate for the provided mesh and because of that the solution might get the divergence. That is why for the solution based upon the numerical methods are first investigate the mesh independent solution are checked. The convergence and residuals are checked. The rectangular shape building is investigated for the wind effects and the modifications in the corners are applied to reduce the wind effects, and the result of wind generated pressure are depicted in various graphical forms like pressure contours, centre line pressure of each face along the height of the model, horizontal pressure distribution at three different level along the peripheral distance of the building model.

### 4.5.1 Pressure contours

The pressure distribution in the form of pressure contours is depicted for the rectangular model which is having the fillet corners. Fillet corner building is having the eight surfaces of the building model. Pressure contours are depicted in Figure 4.34 Distribution of wind pressure coefficient on the rectangle with fillet corner at 0° wind incidence angle to Figure 4.40 Distribution of wind pressure coefficient on the rectangle with fillet corner at 90° wind incidence angle for the wind incidence angle from 0° to 90° wind at an interval of 15°.

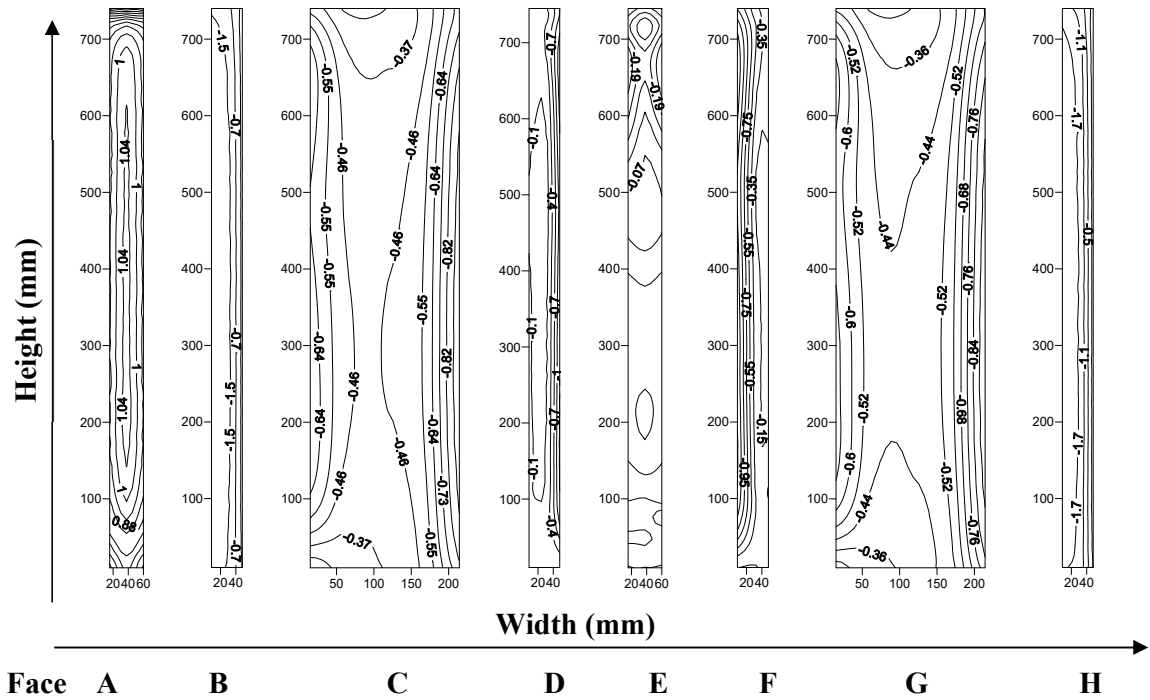


Figure 4.34 Distribution of wind pressure coefficient on the rectangle with fillet corner at  $0^\circ$  wind incidence angle

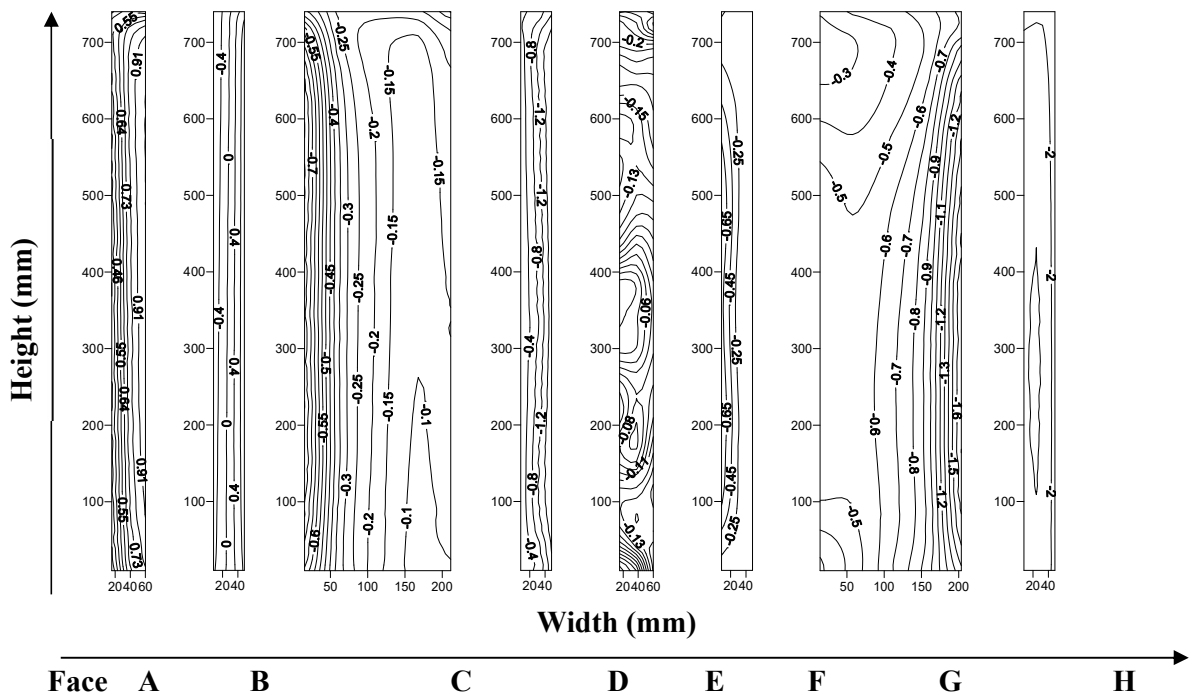


Figure 4.35 Distribution of wind pressure coefficient on the rectangle with fillet corner at  $15^\circ$  wind incidence angle

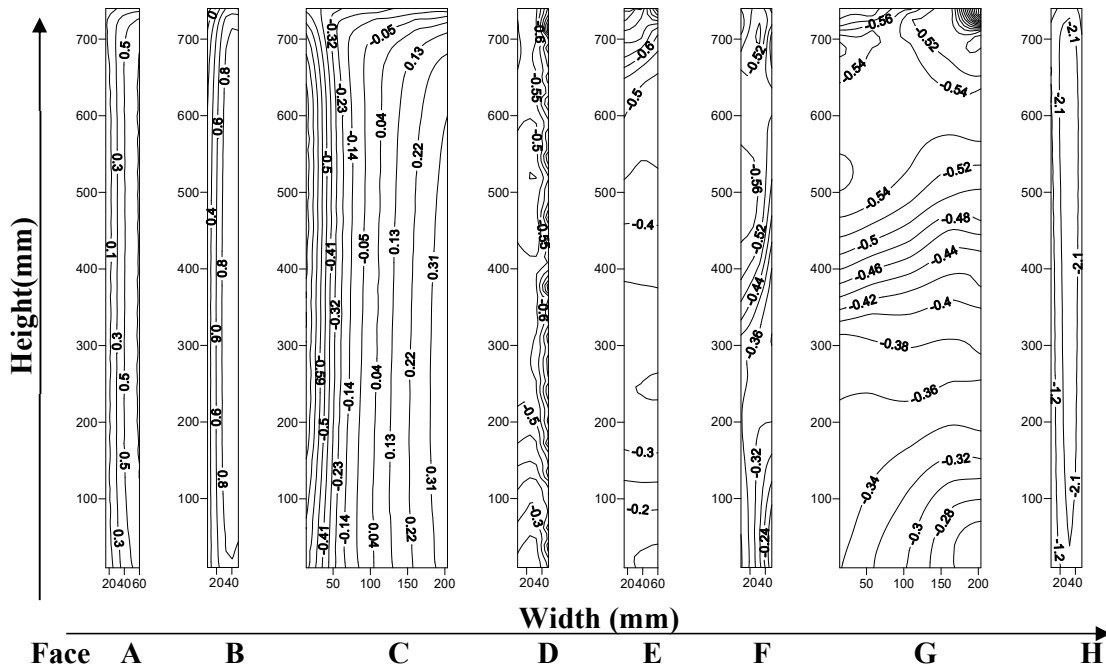


Figure 4.36 Distribution of wind pressure coefficient on the rectangle with fillet corner at  $30^\circ$  wind incidence angle

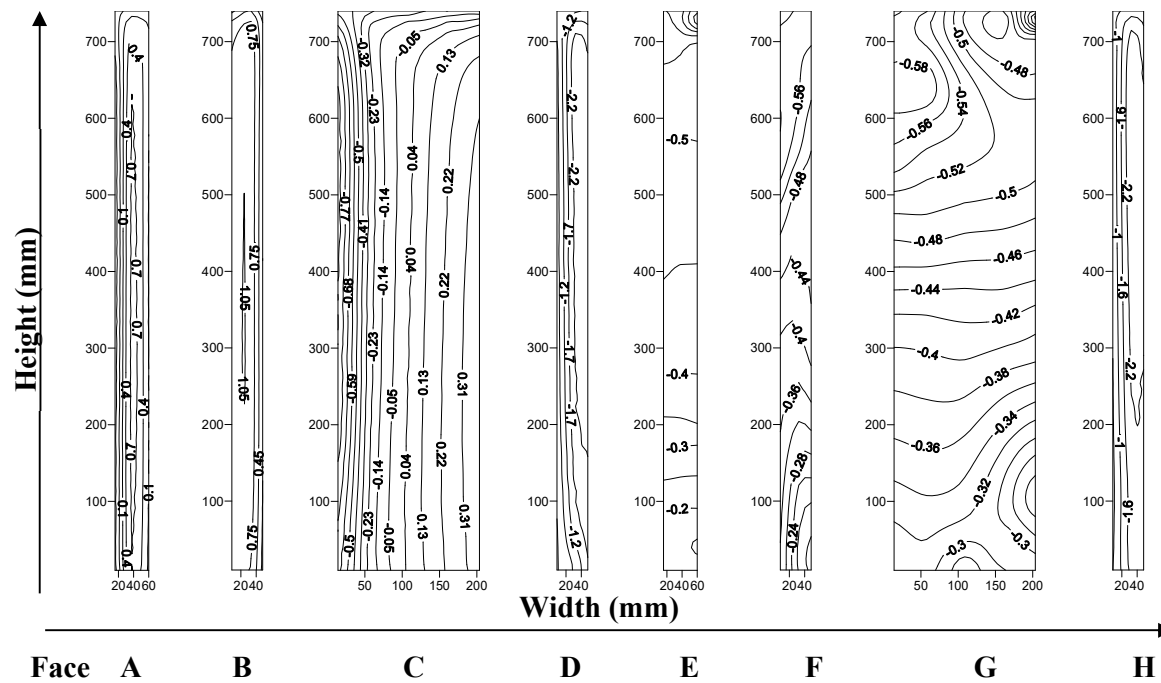


Figure 4.37 Distribution of wind pressure coefficient on the rectangle with fillet corner at  $45^\circ$  wind incidence angle



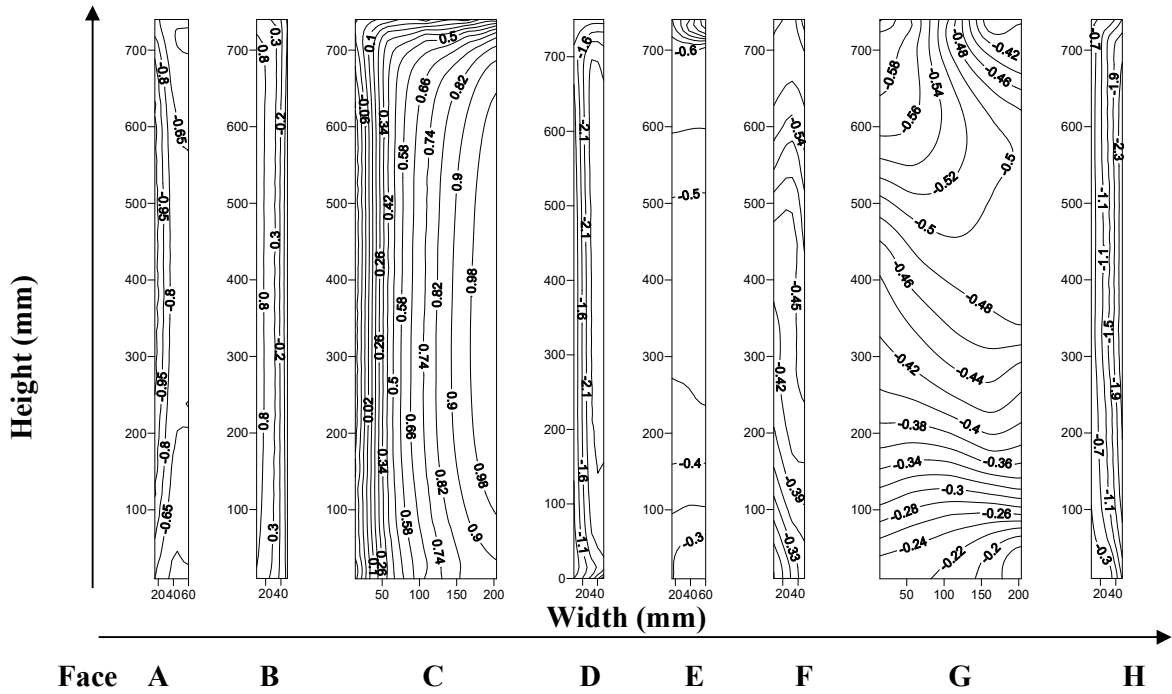


Figure 4.38 Distribution of wind pressure coefficient on the rectangle with fillet corner at  $60^\circ$  wind incidence angle

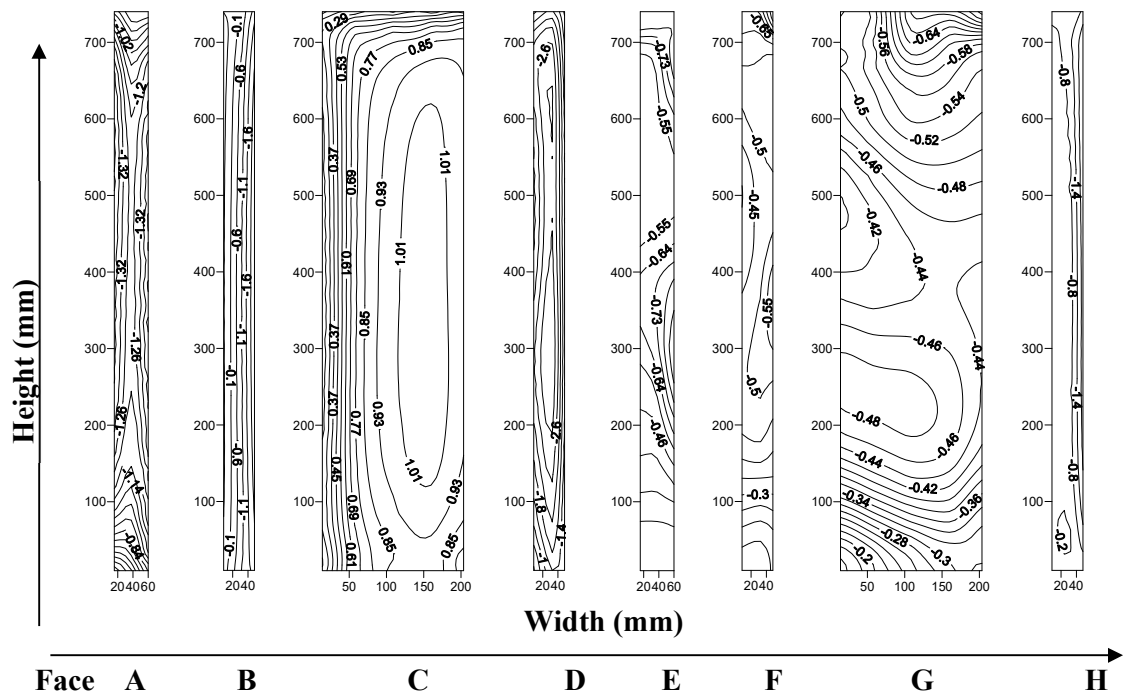
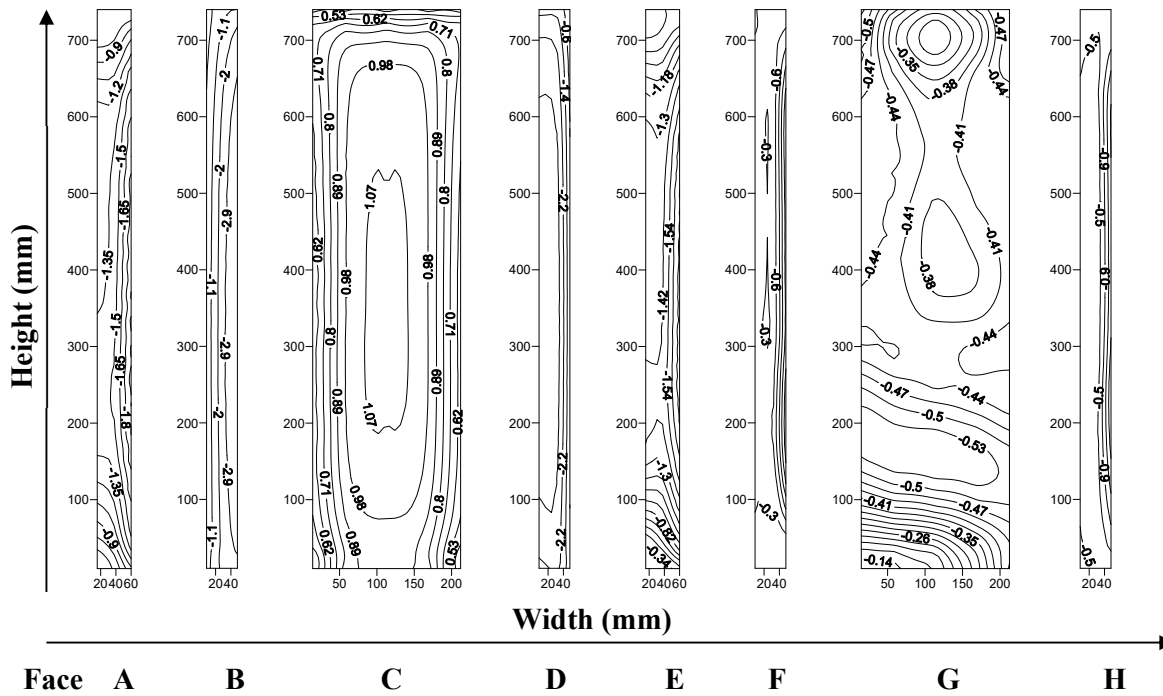


Figure 4.39 Distribution of wind pressure coefficient on the rectangle with fillet corner at  $75^\circ$  wind incidence angle



**Figure 4.40 Distribution of wind pressure coefficient on the rectangle with fillet corner at  $90^\circ$  wind incidence angle**

The pressure varies from positive to negative. Mainly the positive pressure is found on the wind ward face where the pressure is more than the static pressure or because the wind is directly acting on such faces while the other surfaces of the building model is having various distribution pattern and the same can be understood with the help of pressure contours.

**4.5.2 Vertical Pressure Distribution along the Height of Building**

Pressure distribution on the center line along the height of each face is presented graphically in Figure 4.41 Mean pressure distribution on the vertical centre line for rectangle with fillet corner, these line are drawn on each face of the building model and these lines indicate the central pressure characteristics like positive and neagtive. The pressure lies is between 0.84 to -1.17, the maximum postive pressure is found on face- A around the height of 250 mm to 600 mm from the base while the other faces are in suction for the case of  $0^\circ$  wind incidence angle. When wind is incident on the model at  $15^\circ$  the postive pressure is observed on face-A and face-B while for the other faces the vertical pressure distribution is found negative that is suction. The pressure for the wind incidence angle of  $30^\circ$  lies in between 0.76 to -2.07, this pressure distribution along the center line with height is depicted.

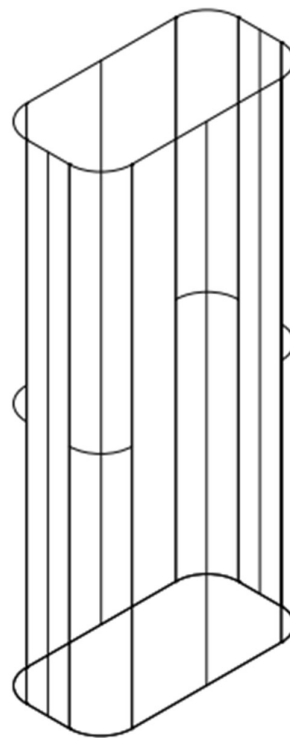
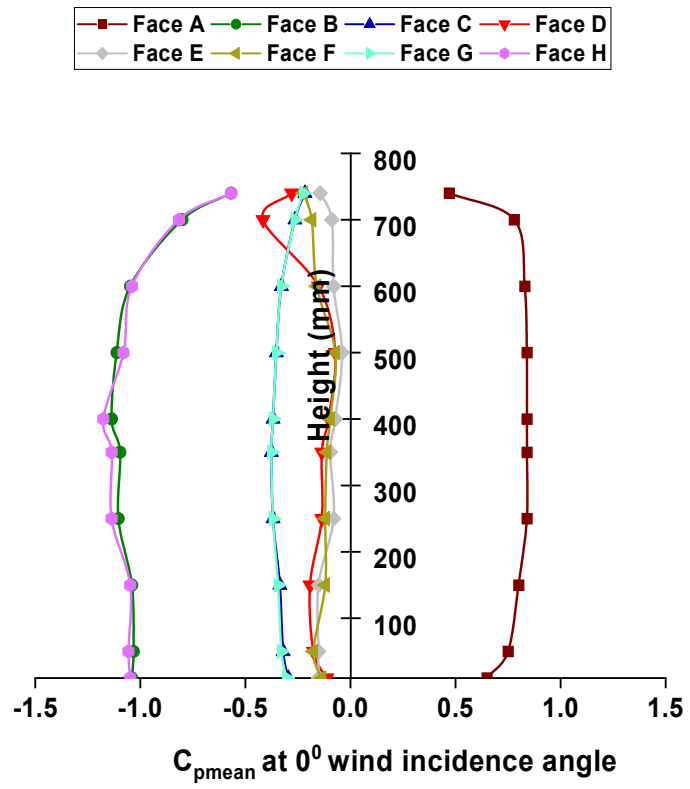


Figure 4.41 (contd.) Mean pressure distribution on the vertical centre line for rectangle with fillet corner

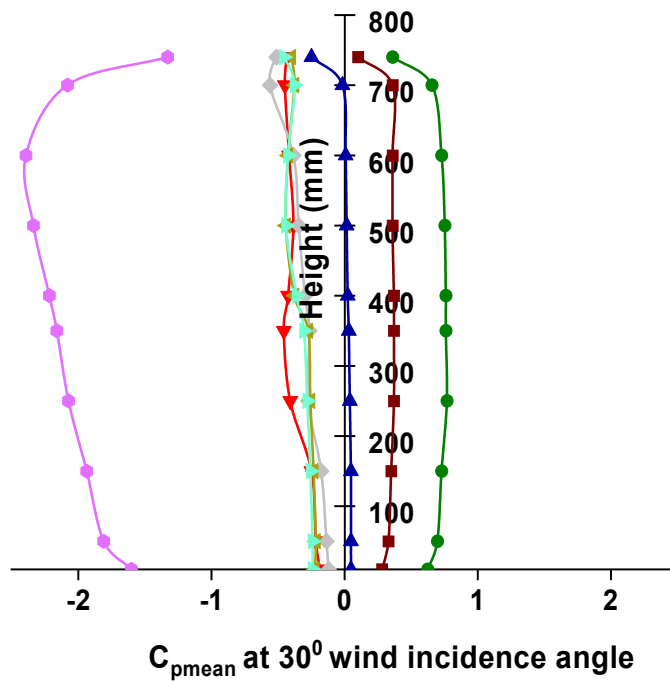
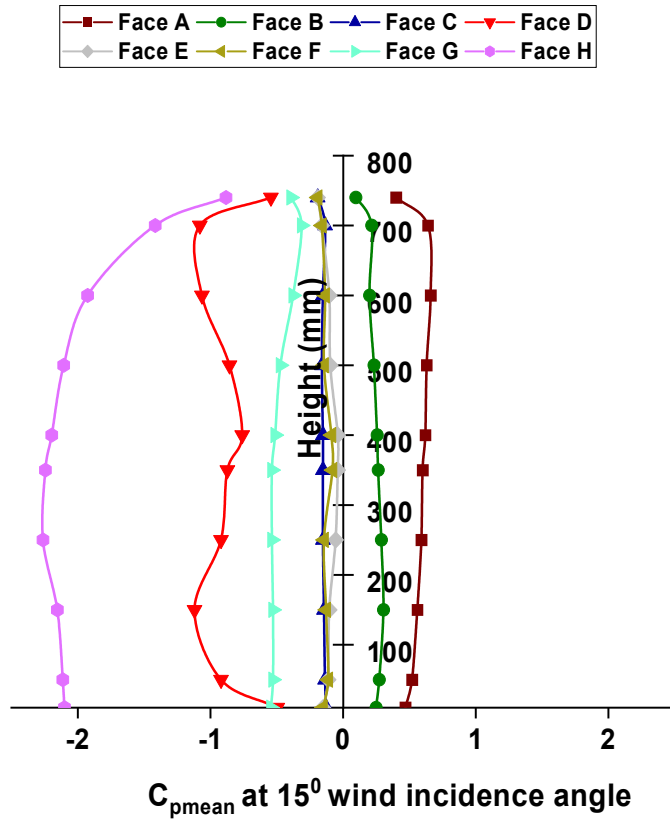


Figure 4.41(contd.) Mean pressure distribution on the vertical centre line for rectangle with fillet corner

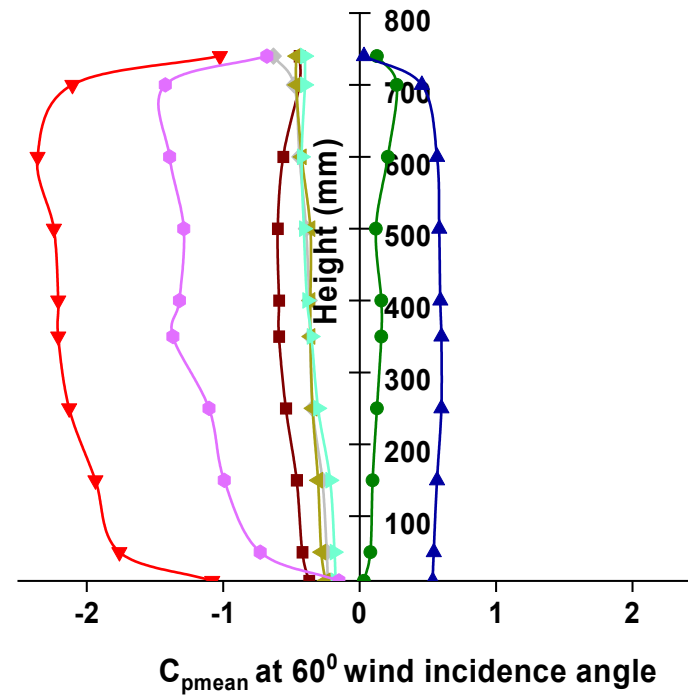
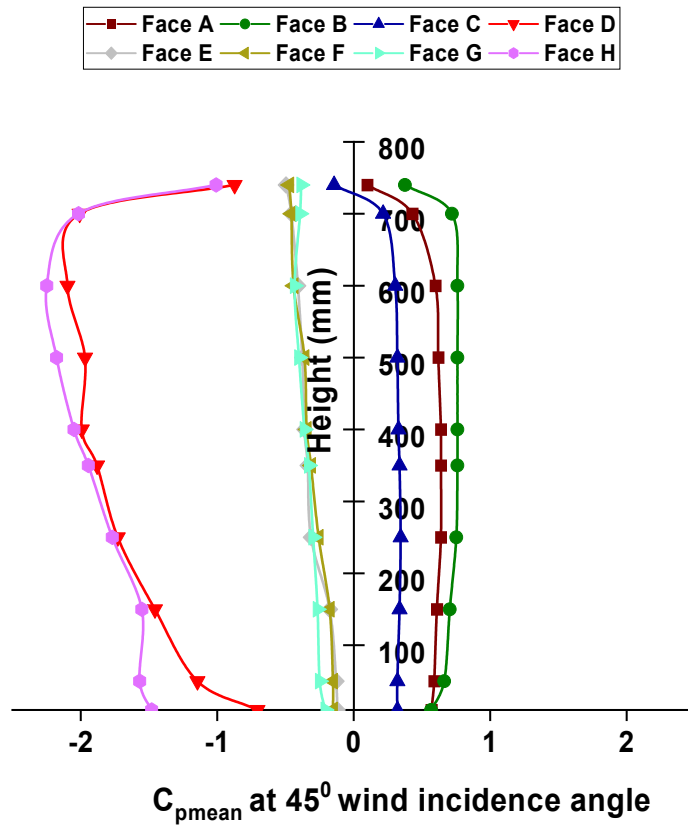


Figure 4.41(contd.) Mean pressure distribution on the vertical centre line for rectangle with fillet corner

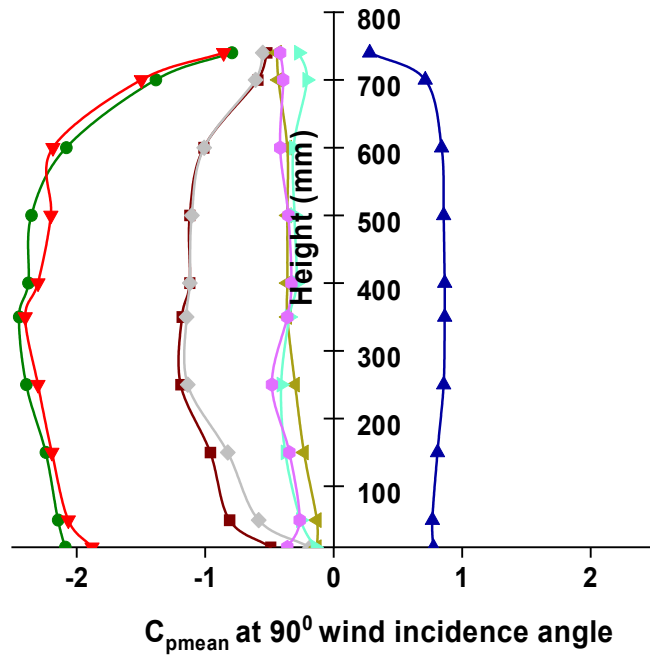
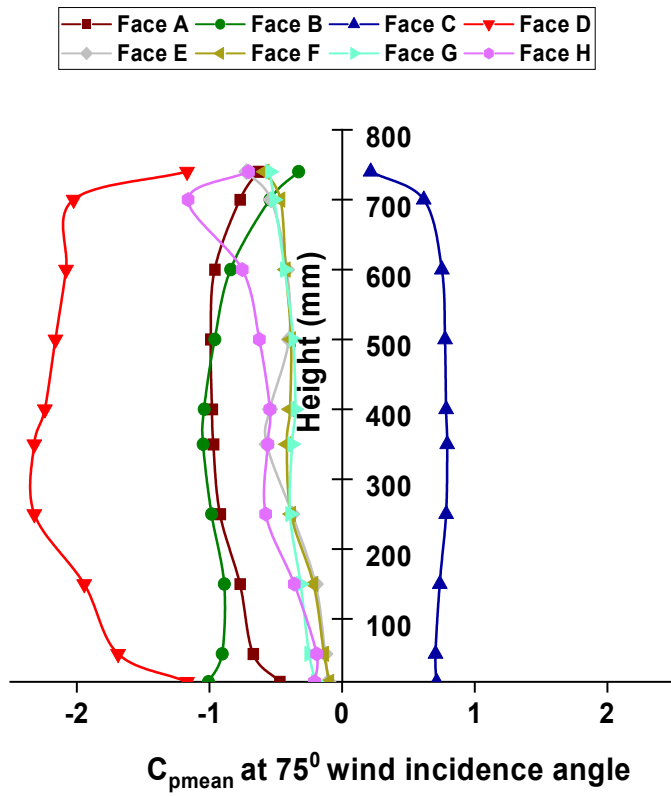


Figure 4.41 Mean pressure distribution on the vertical centre line for rectangle with fillet corner

### **4.5.3 Horizontal Pressure Distribution along the Peripheral Distance of Building**

The pressure distribution along the peripheral distance is observed for the building model which is having the fillet corner into rectangular shape building model and the pressure distribution along the three different level is depicted in Figure 4.42 Mean pressure distribution along the peripheral distance of the rectangle with fillet corner on the building model, three different level are considered at 250 mm that is one third height of the building model, at 375 mm height from the base which is exactly at mid height of the building model and the top one third that is the height of 500 mm from the base of the model. The pressure distribution along the peripheral distance is depicted for the wind incidence angle varying from  $0^{\circ}$  to  $90^{\circ}$  at an interval of  $15^{\circ}$ . The pressure distribution is calculated and depicted after taking into the account various types of flow characteristics like vortex shedding, flow reattachment etc. The pressure lies in the range of 1.05 to -2.2 in the case of  $0^{\circ}$  wind while the wind pressure lies from 1.06 to -1.82 for the wind incidence angle of  $15^{\circ}$  and likewise the pressure distribution for wind incidence angles from  $30^{\circ}$  to  $90^{\circ}$  at an interval of  $15^{\circ}$ .

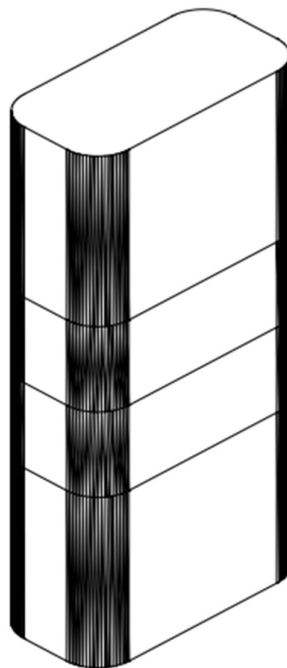
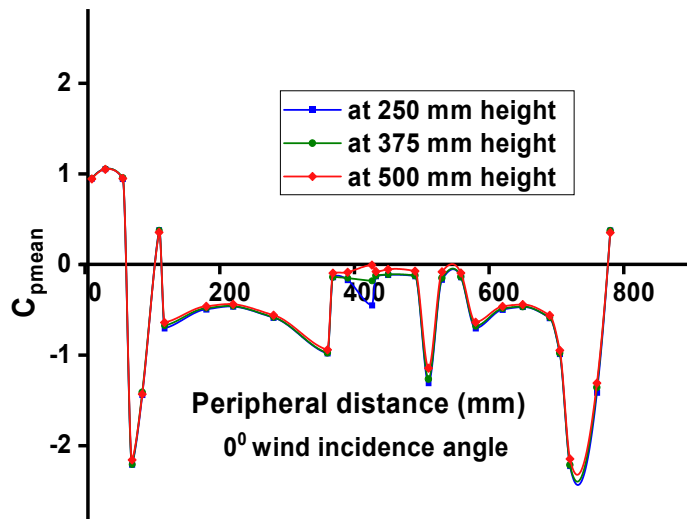


Figure 4.42 (contd.) Mean pressure distribution along the peripheral distance of the rectangle with fillet corner



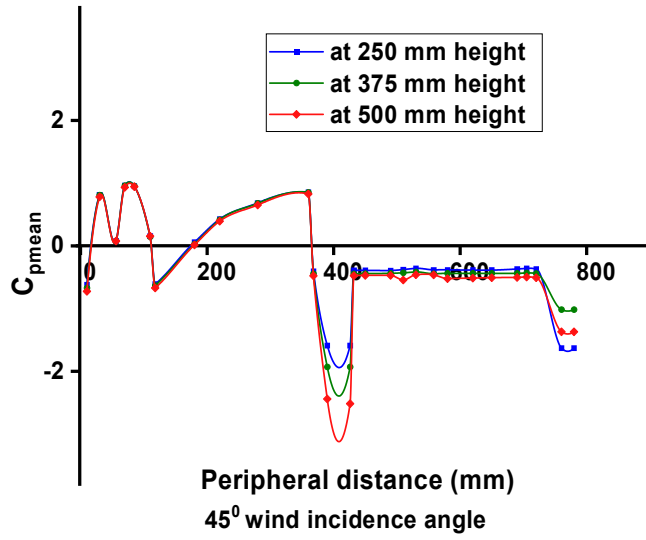
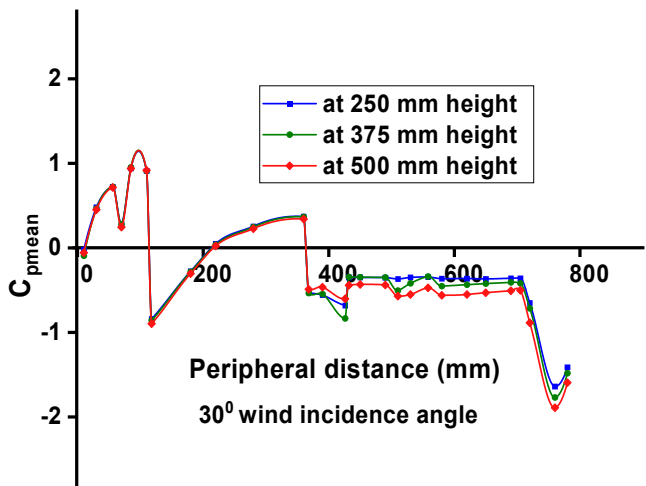
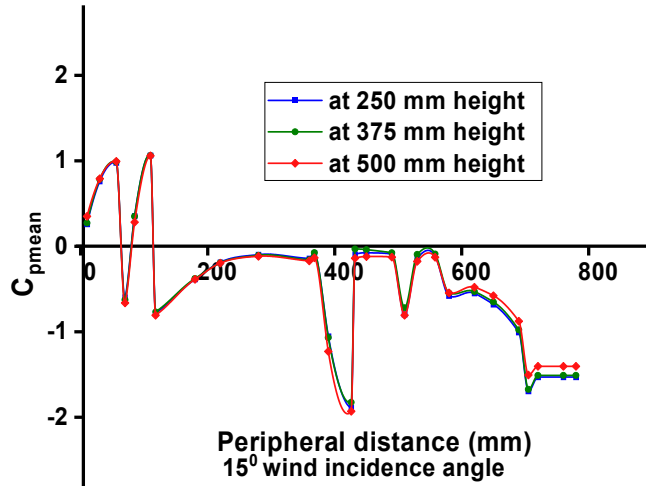


Figure 4.42 (contd.) Mean pressure distribution along the peripheral distance of the rectangle with fillet corner

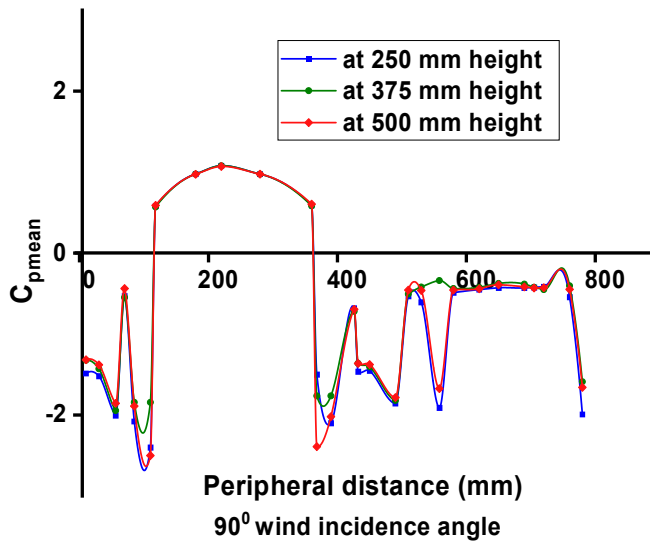
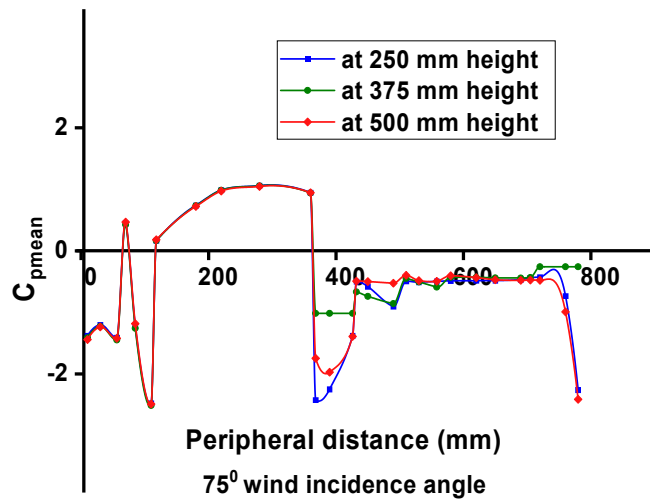
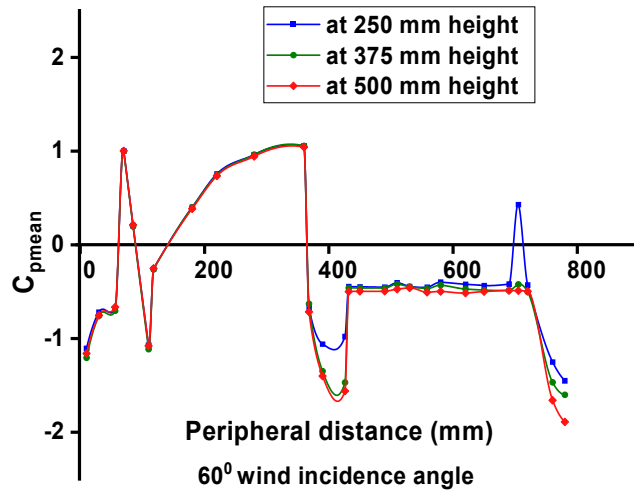


Figure 4.42 Mean pressure distribution along the peripheral distance of the rectangle with fillet corner

### 4.5.4 Force Coefficients

The wind force coefficient is calculated and graphically depicted in the Figure 4.43 Wind Force coefficient of the rectangle with fillet corners. The wind force coefficient in x direction is  $C_{fx}$  and in y-direction is  $C_{fy}$  and it is calculated after performing the numerical simulation on the rectangular model having fillet corners in the cross-sectional area. The maximum  $C_{fx}$  is 1.68 in the case of  $45^\circ$  wind incidence angle while the lowest  $C_{fx}$  is 0.35 when incidence angle is  $15^\circ$ . In the same way the force coefficient in y direction is  $C_{fy}$  and the maximum  $C_{fy}$  is 0.043 in the case of  $0^\circ$  wind incidence angle and the minimum  $C_{fy}$  of -0.98 is observed in the case of  $45^\circ$  wind. The  $C_{fx}$  is drag which acts across wind direction while the  $C_{fy}$  is along the wind direction which is lift force coefficient. The force coefficient is depicted for the wind incidence angle ranging from  $0^\circ$  to  $90^\circ$  at an interval of  $15^\circ$ .

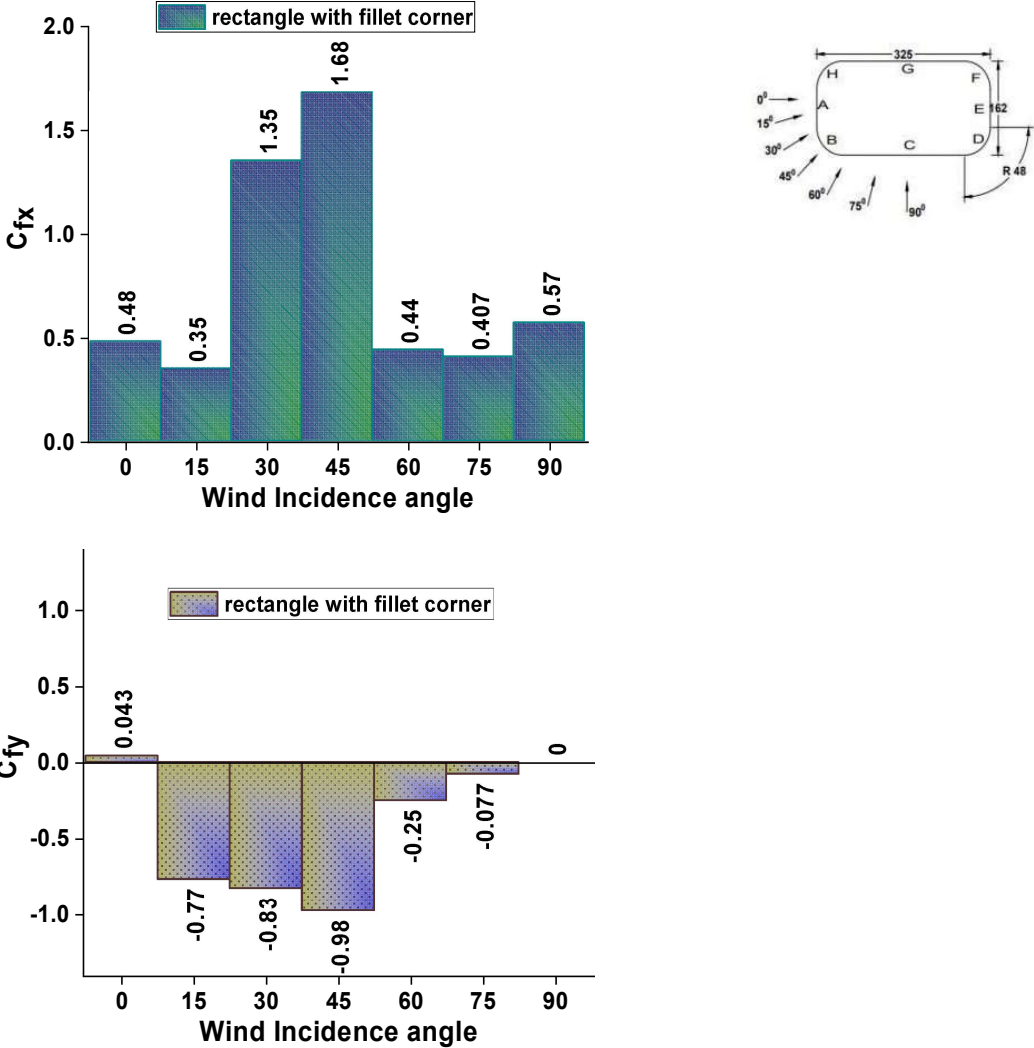


Figure 4.43 Wind Force coefficient of the rectangle with fillet corners

### 4.5.5 Moment Coefficients

The moment coefficient is calculated for building model regular shape having corner modification of fillet these modifications are applied to reduce the wind generated effect on the tall building. The moment coefficient is presented in Figure 4.44 Wind Moment coefficient of the rectangle with fillet corners and is calculated with respect to base force obtained after performing the numerical simulation on the model using ANSYS CFX, the moment coefficient in x-direction is  $C_{mx}$  and in the y-direction this is  $C_{my}$ . The maximum  $C_{mx}$  of 1.06 is observed in the case of  $45^\circ$  wind incidence angle while the minimum  $C_{mx}$  of 0 is found when wind incidence angle is  $0^\circ$  and  $90^\circ$  because along wind force is not acting on this face. It will presents the maximum wind effect on the side faces in the flow reattachment. The maximum  $C_{my}$  is 1.9 in the case of  $45^\circ$  wind while the minimum  $C_{my}$  of 0.39 is spotted in the case of  $15^\circ$  wind incidence angle.

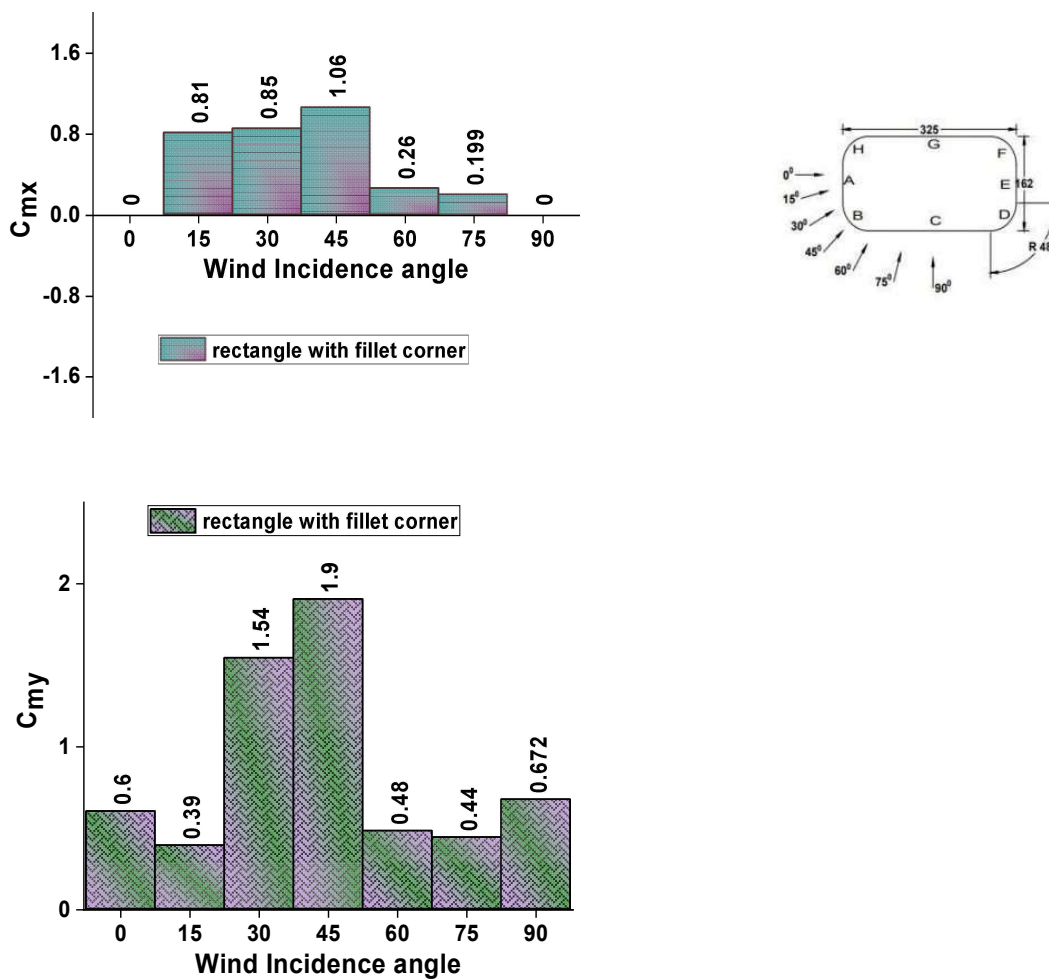


Figure 4.44 Wind Moment coefficient of the rectangle with fillet corners

#### 4.5.6 External Pressure Coefficients

External pressure coefficient is calculated after performing the numerical simulation on the rectangular model having fillet corners and the data obtained is processed as per the procedure provided in the wind tunnel manual and report no 67, this is the average of the pressure effects on the particular face and it is investigated for the wind incidence angle ranging from  $0^{\circ}$  to  $90^{\circ}$  at an interval of  $15^{\circ}$  each. In the case of  $0^{\circ}$  wind the maximum external pressure is 0.71 on face- A and the minimum of -0.76 is on face- H. In the same way the external pressure coefficient in case of  $90^{\circ}$  wind is noted for the maximum value of 0.61 while the minimum is -1.49 on face- B and face-D. The generated data is valuable for the structural designer to reduce the wind effect on the tall building. The mean external pressure coefficient is tabulated in Table: 4.4 External Pressure Coefficient for Building Model-D (Rectangular Fillet).

**Table: 4.4 External Pressure Coefficient for Building Model-D (Rectangular Fillet)**

<b>Model-D ( Rectangular Fillet)</b>							
<b>Face</b>	<b><math>0^{\circ}</math></b>	<b><math>15^{\circ}</math></b>	<b><math>30^{\circ}</math></b>	<b><math>45^{\circ}</math></b>	<b><math>60^{\circ}</math></b>	<b><math>75^{\circ}</math></b>	<b><math>90^{\circ}</math></b>
<b>A</b>	<b>0.71</b>	<b>0.51</b>	0.28	0.05	-0.59	-0.92	-0.99
<b>B</b>	<b>-0.76</b>	0.18	<b>0.50</b>	<b>0.49</b>	<b>0.04</b>	-0.74	<b>-1.49</b>
<b>C</b>	-0.45	-0.24	-0.08	0.19	<b>-1.48</b>	0.56	<b>0.61</b>
<b>D</b>	-0.40	-0.78	-0.39	<b>-1.24</b>	-0.32	<b>-1.48</b>	<b>-1.49</b>
<b>E</b>	-0.11	-0.09	-0.29	-0.31	-0.35	-0.41	-0.99
<b>F</b>	-0.40	-0.23	-0.32	-0.32	-0.35	-0.41	-0.60
<b>G</b>	-0.45	-0.59	-0.32	-0.32	-0.32	-0.34	-0.32
<b>H</b>	<b>-0.76</b>	<b>-1.94</b>	<b>-1.22</b>	<b>-1.24</b>	-1.06	-0.83	-0.60

#### 4.6 Comparative study of $C_{fx}$ at $0^\circ$ and $90^\circ$ wind incidence angles

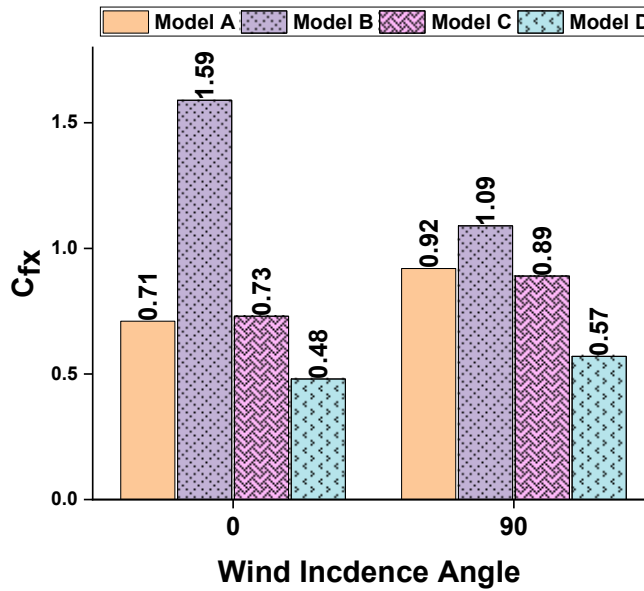


**Figure 4.45  $C_{fx}$  for the regular shape building model**

The  $C_{fx}$  is observed after performing the numerical simulation into ANSYS CFX on the regular shape tall building models. The  $C_{fx}$  for different shape building model is investigated for  $0^\circ$  and  $90^\circ$  degree and a comparative graph is plotted between  $C_{fx}$  and wind incidence angle and is plotted in Figure 4.45  $C_{fx}$  for the regular shape building model. It is observed that the minimum  $C_{fx}$  is for model-D which is having rounded corner in case of  $0^\circ$  wind incidence angle and the maximum  $C_{fx}$  is obtained for model-B having corner cut configuration.

## CHAPTER 5

### Results and Discussion Y-Shape with Corner Configuration

#### 5.1 General

The present study is performed in two parts, the first part explores the wind generated effects on the regular shape building while the second part explains the detailed investigation of wind effects on irregular shape high rise structure. The numerical analysis is performed on different corner configuration of nearly equal area building. The height and the ratio of the modification applied is kept same and results are presented in graphical form using pressure contours, stream lines, vertical centre line and the mean  $C_p$  for different models. Wind is made incident by rotating the model at an interval of  $15^\circ$  in the angle varying in the range of  $0^\circ$  to  $180^\circ$ . The model work as the virtual wind tunnel having the dimension of  $5H$  into sides and inlet while the outlet is kept at  $15H$  and the top of the domain is  $6H$  from the ground,  $H$  defines the height of the building model.

The pressure is obtained by drawing various lines at various faces. The faces which have the dimension greater than  $100\text{ mm}$ , the 5 number lines are drawn in the post processing of the results. The local coordinate frame is also defined at the various faces of the model and results are exported and then the result is calculated and the mean  $C_p$  is tabulated from each building model while the pressure contours with respect to the height of the building model are presented for models having the corner configuration on irregular shape building model.

#### 5.2 Y-shape with simple Corners

The “Y” shape irregular building model is investigated for wind effect and various result of pressure distribution on vertical centre line, horizontal pressure distribution and external mean pressure coefficients and pressure contours are depicted.

##### 5.2.1 Pressure Contours

The pressure contours for different wind incidence angle are presented at every  $15^\circ$  intervals for the angle ranging from of  $0^\circ$  to  $180^\circ$  wind. The pressure contours for each face of building model are presented from Figure 5.1 Distribution of wind pressure coefficient on the Y-shape with simple corner at  $0^\circ$  wind incidence angle to Figure 5.13 Distribution of wind pressure coefficient on the Y-shape with simple corner at  $180^\circ$  wind incidence angle.

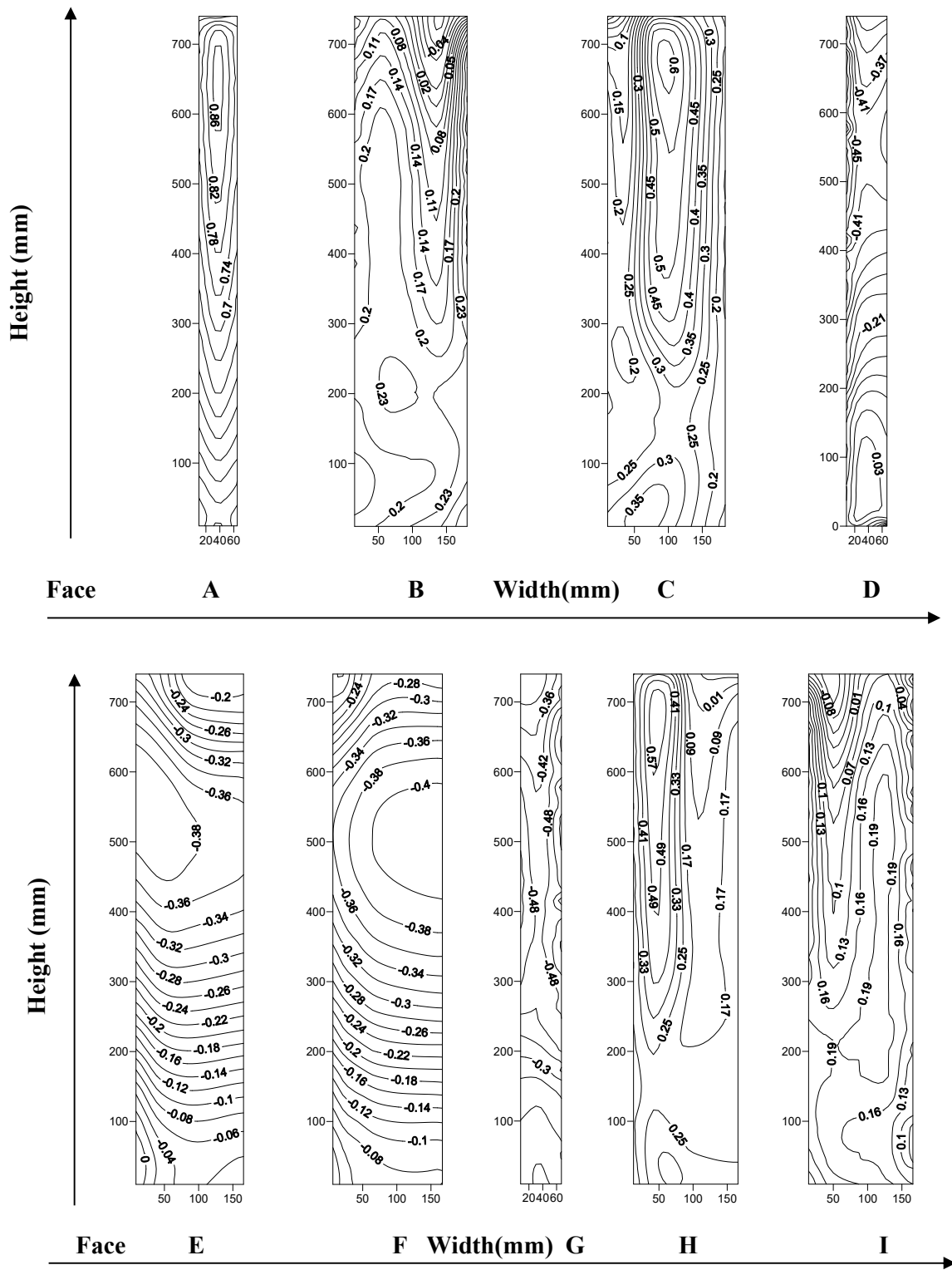


Figure 5.1 Distribution of wind pressure coefficient on the Y-shape with simple corner at  $0^\circ$  wind incidence angle



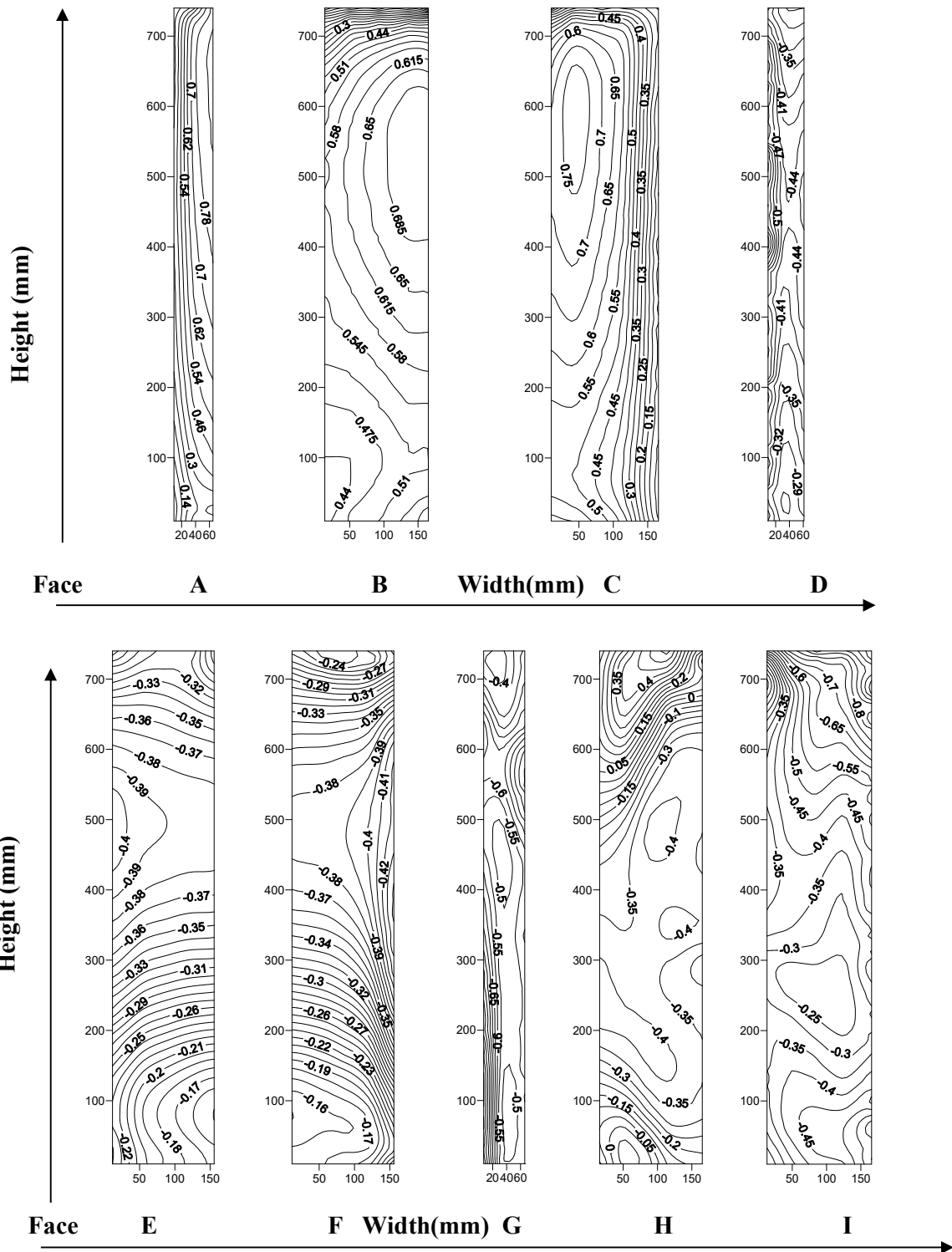


Figure 5.2 Distribution of wind pressure coefficient on the Y-shape with simple corner at 15° wind incidence angle

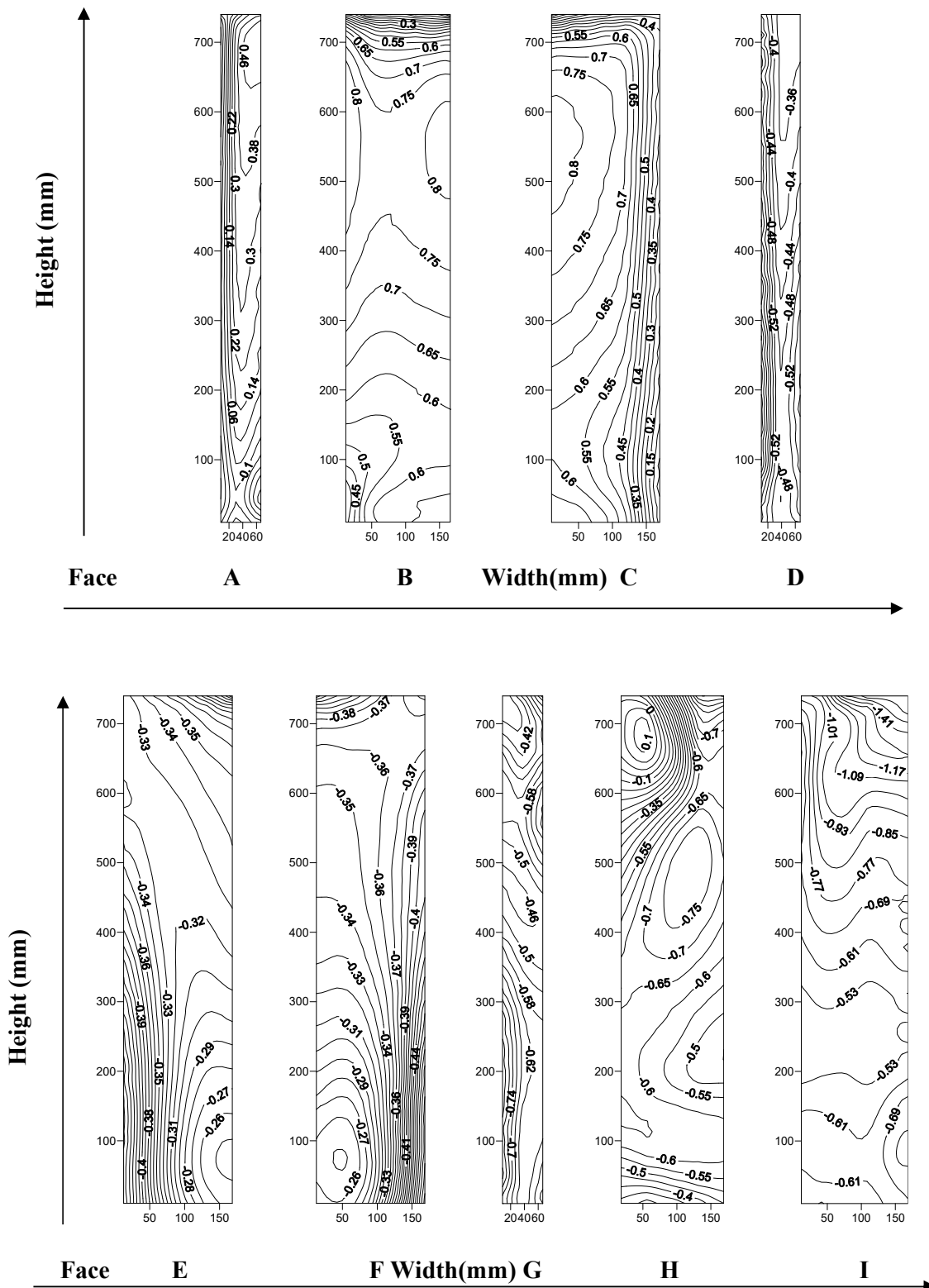


Figure 5.3 Distribution of wind pressure coefficient on the Y-shape with simple corner at  $30^\circ$  wind incidence angle

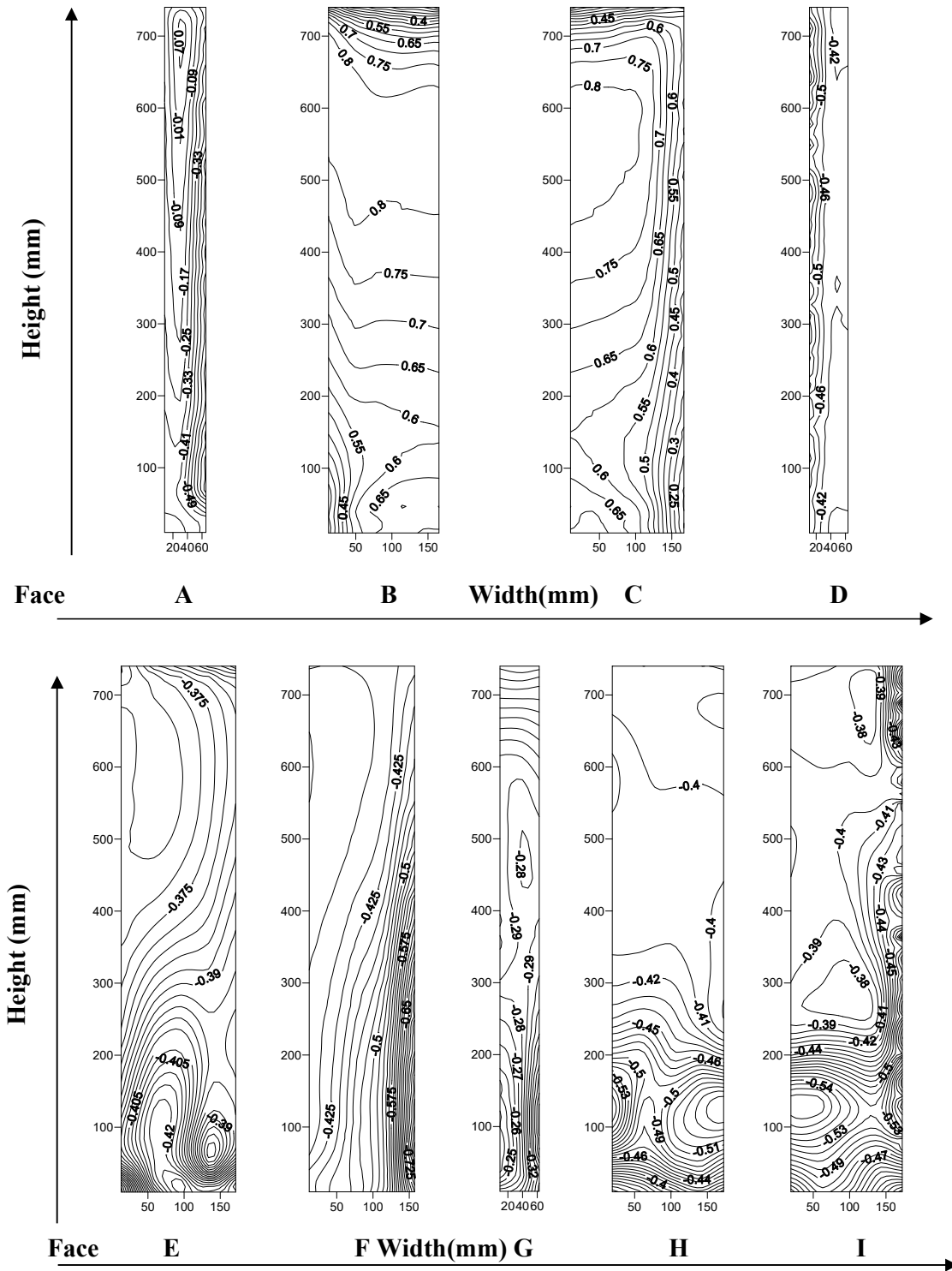


Figure 5.4 Distribution of wind pressure coefficient on the Y-shape with simple corner at  $45^\circ$  wind incidence angle

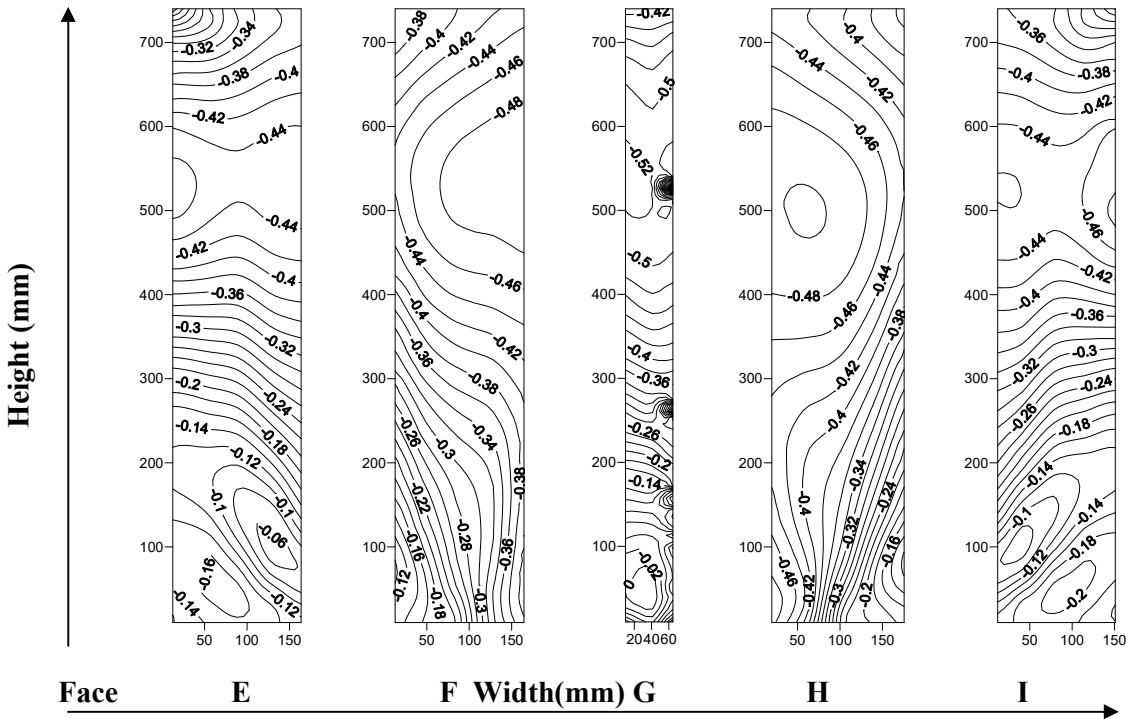
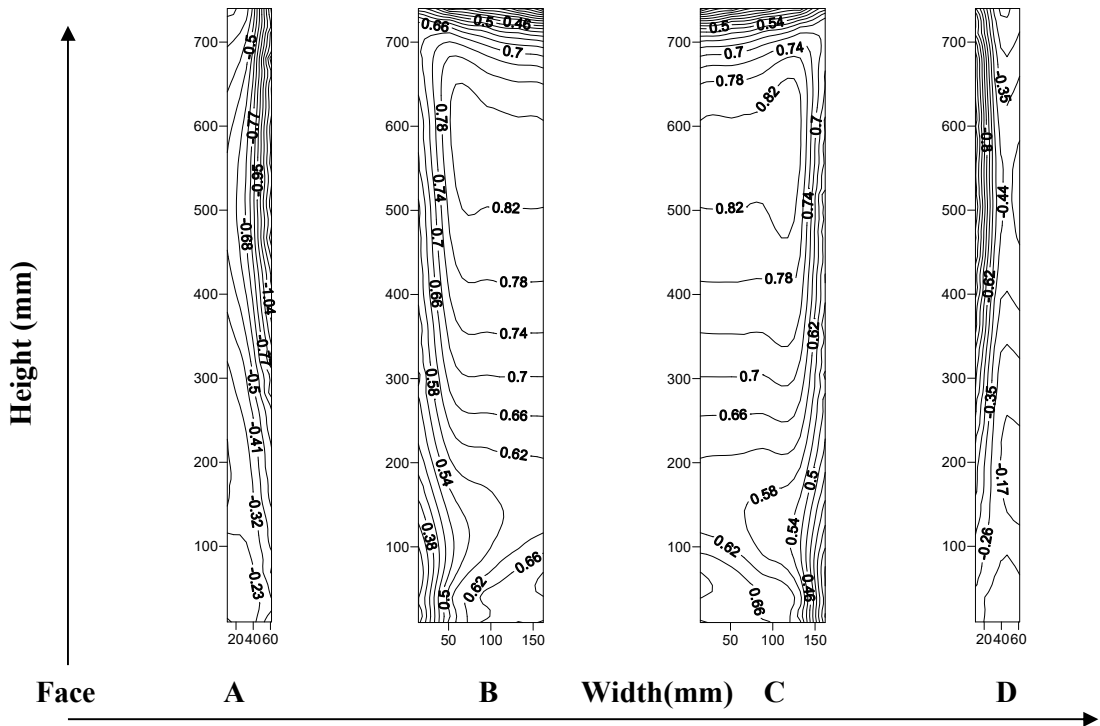


Figure 5.5 Distribution of wind pressure coefficient on the Y-shape with simple corner at 60° wind incidence angle

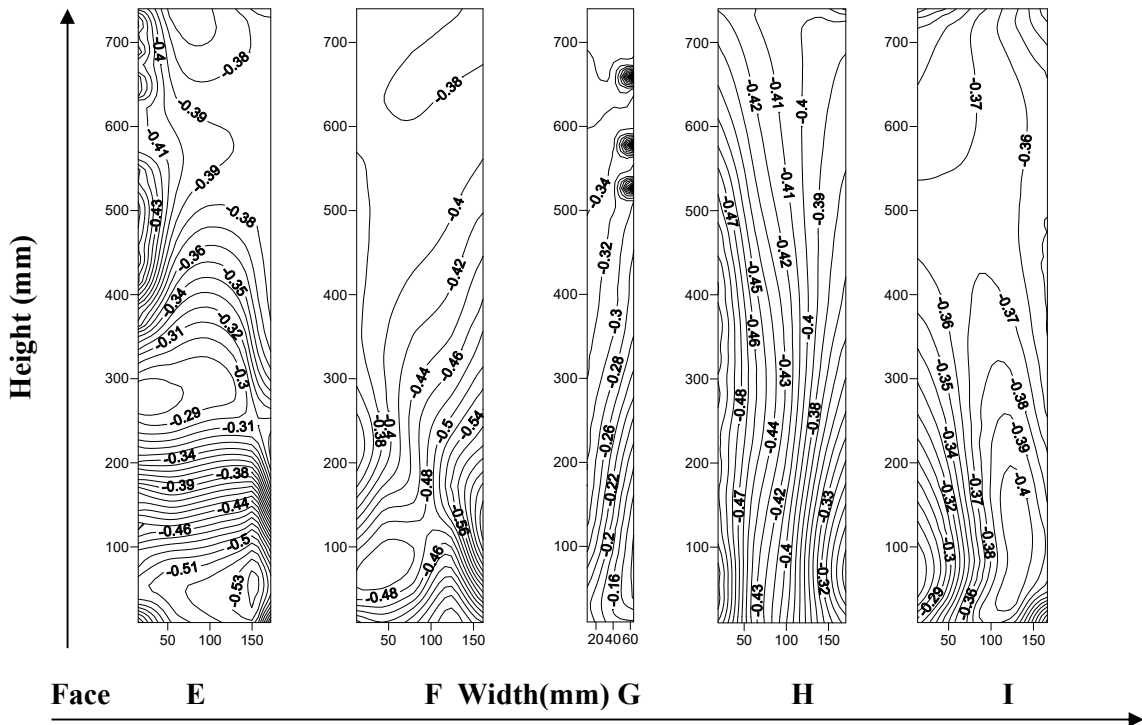
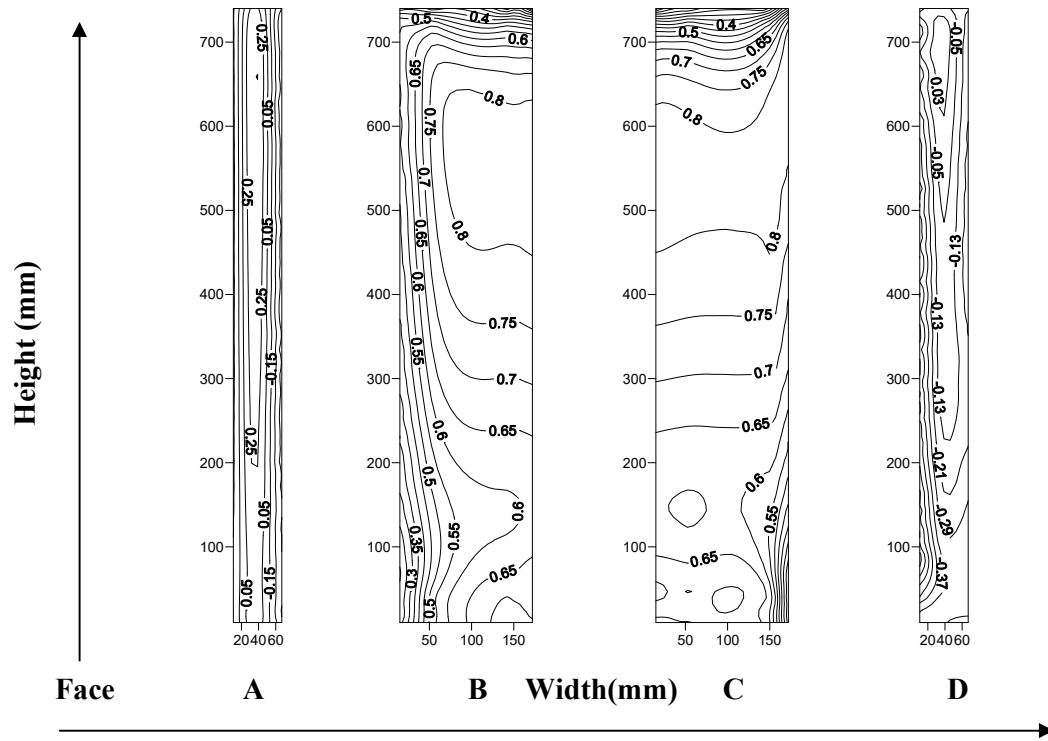


Figure 5.6 Distribution of wind pressure coefficient on the Y-shape with simple corner at 75° wind incidence angle

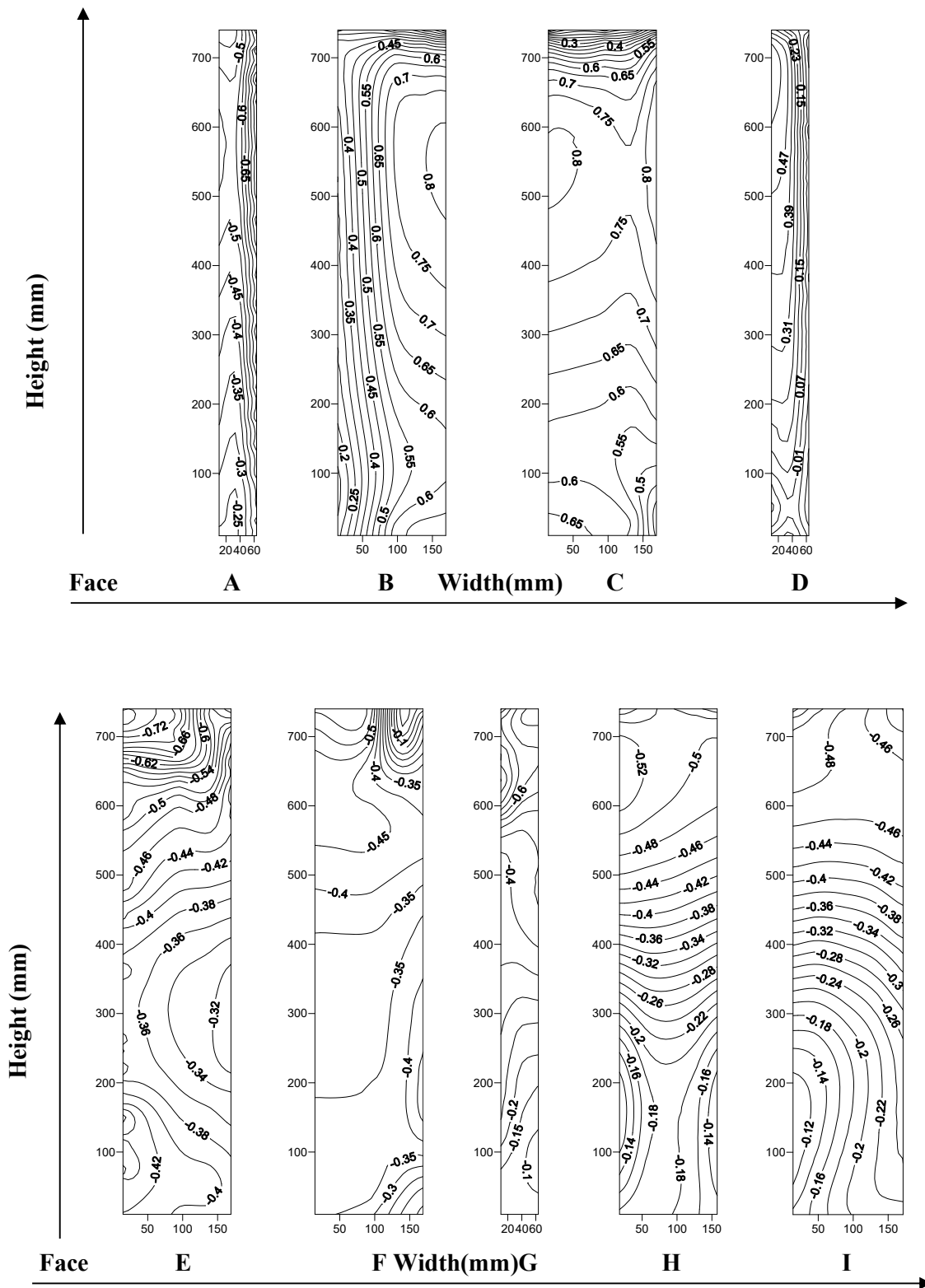


Figure 5.7 Distribution of wind pressure coefficient on the Y-shape with simple corner at  $90^\circ$  wind incidence angle

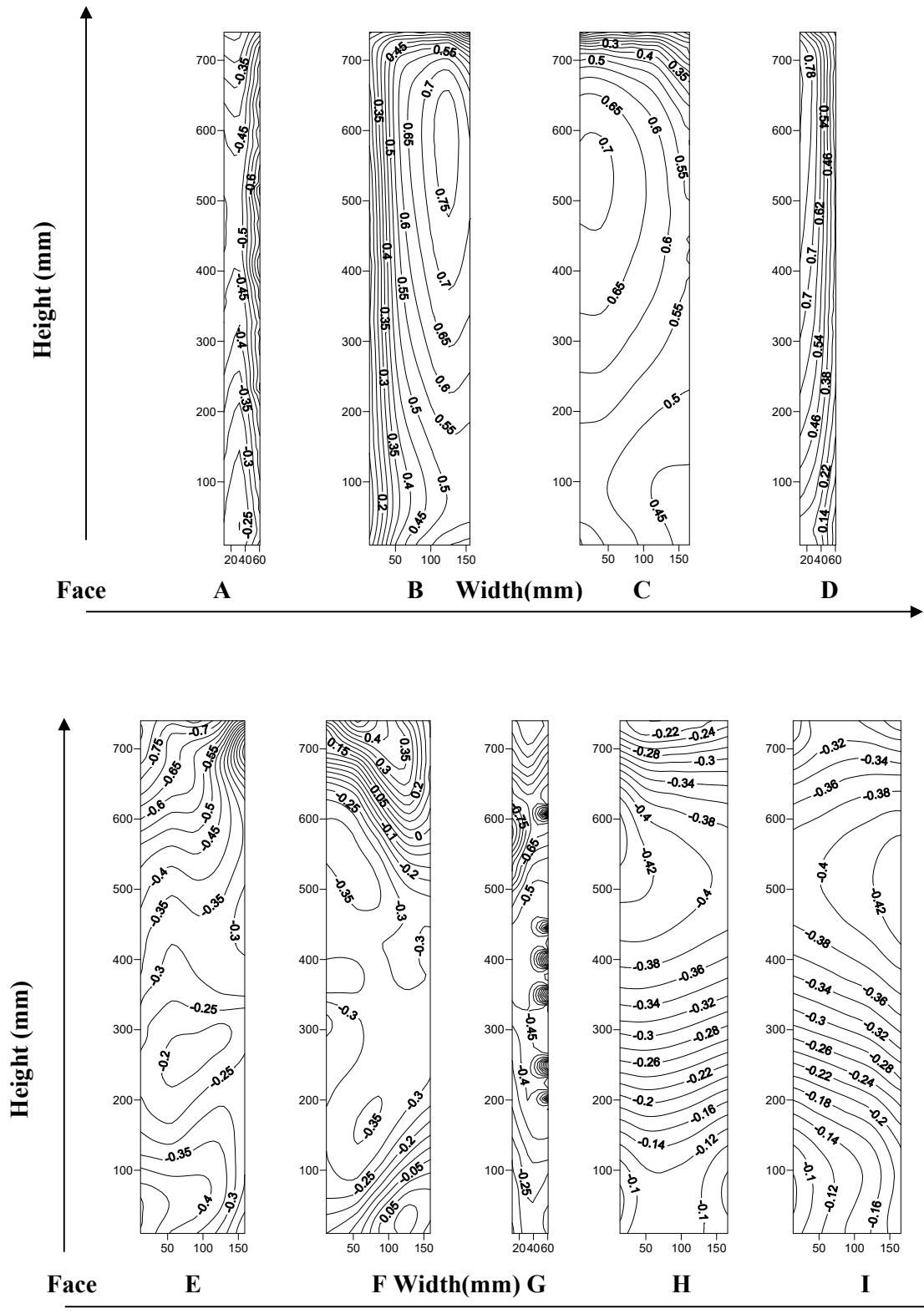


Figure 5.8 Distribution of wind pressure coefficient on the Y-shape with simple corner at  $105^\circ$  wind incidence angle

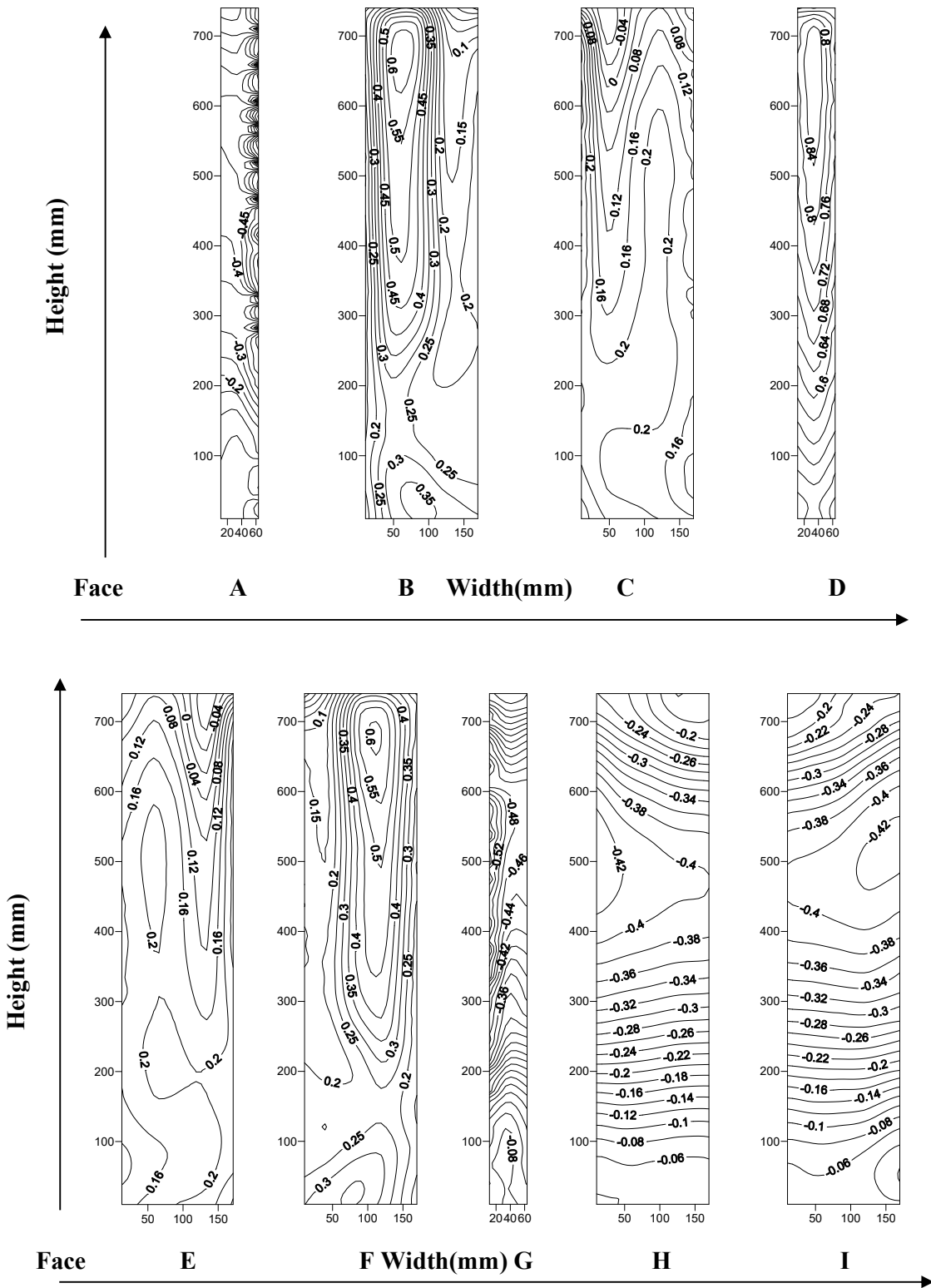


Figure 5.9 Distribution of wind pressure coefficient on the Y-shape with simple corner at 120° wind incidence angle



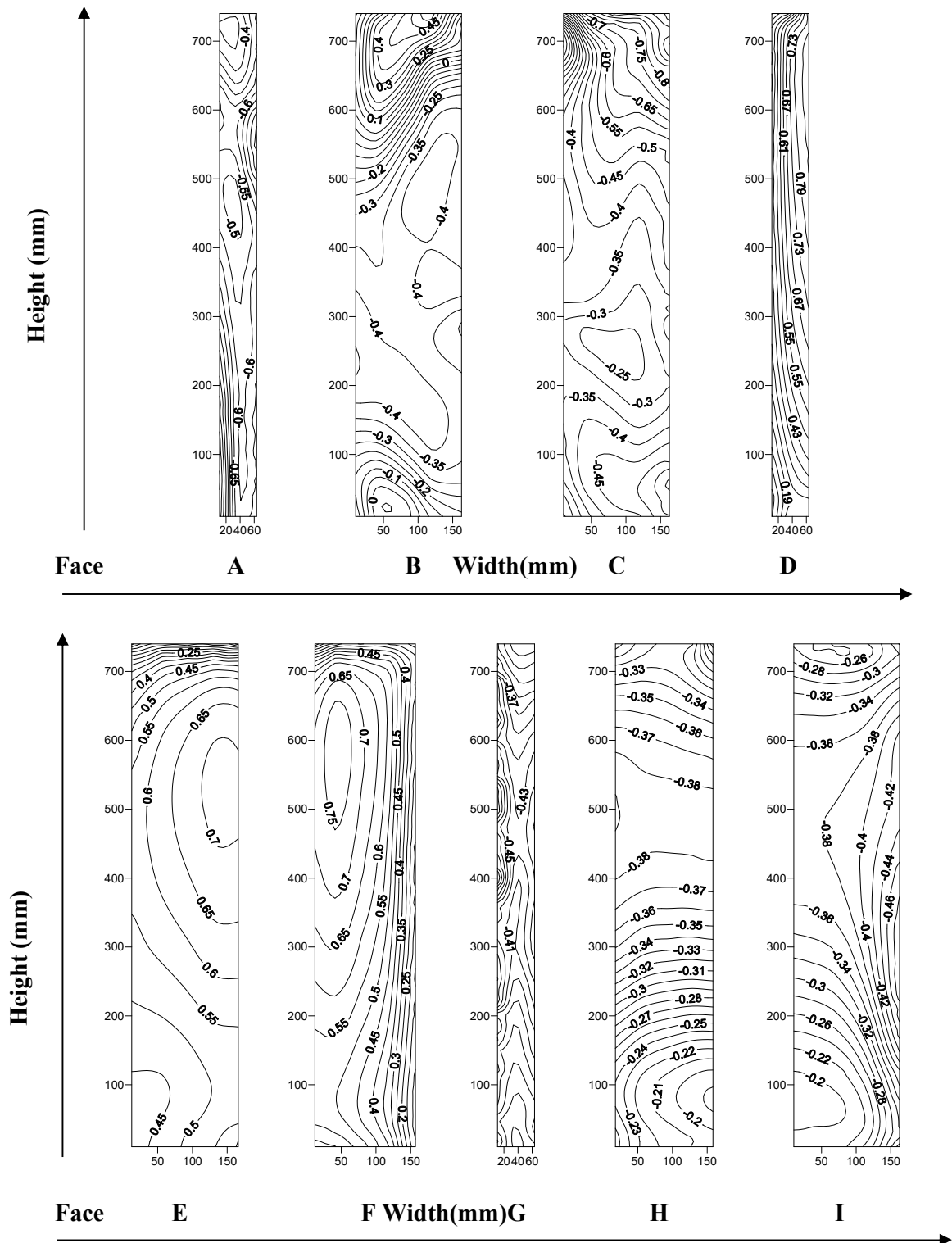


Figure 5.10 Distribution of wind pressure coefficient on the Y-shape with simple corner at 135° wind incidence angle

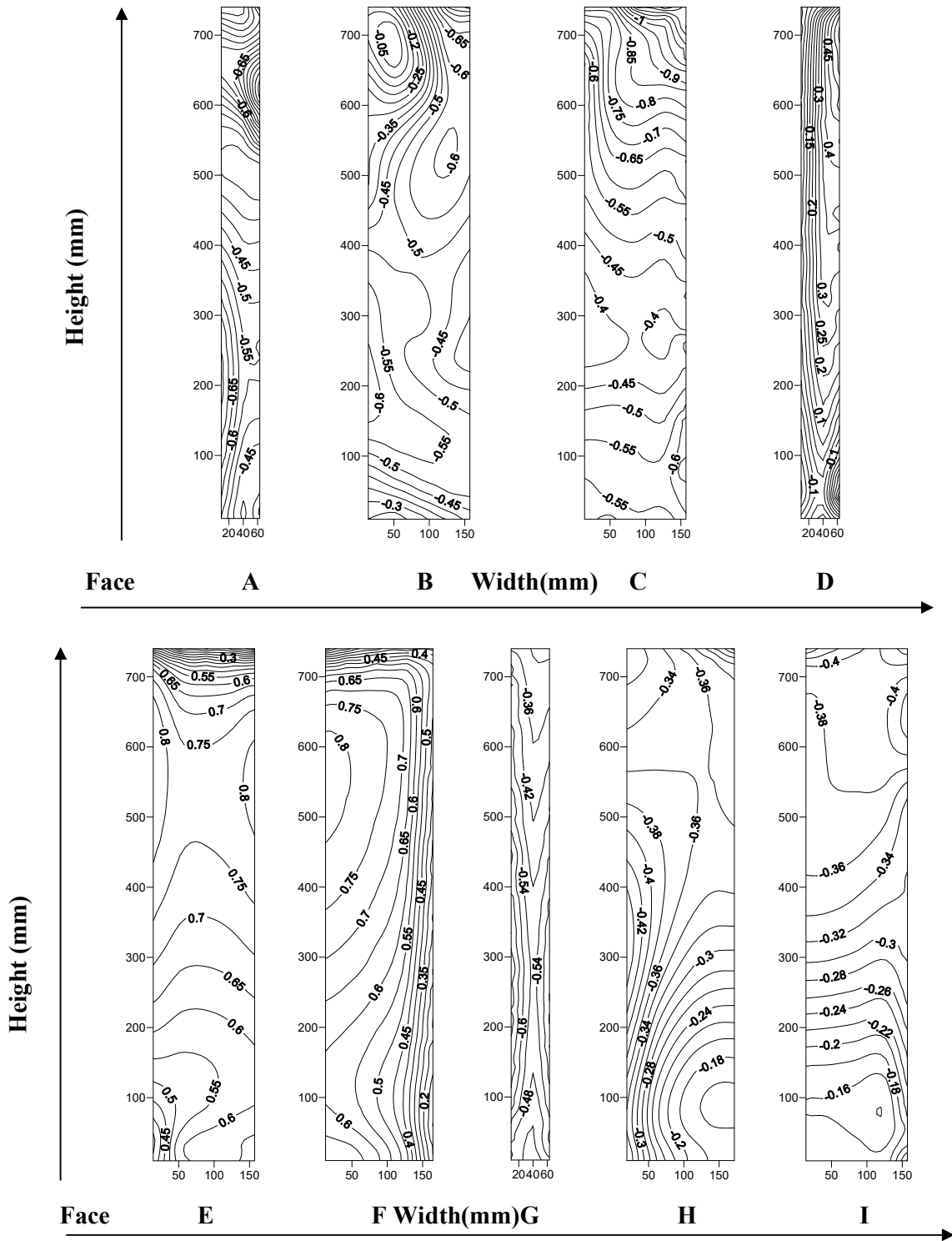


Figure 5.11 Distribution of wind pressure coefficient on the Y-shape with simple corner at  $150^\circ$  wind incidence angle

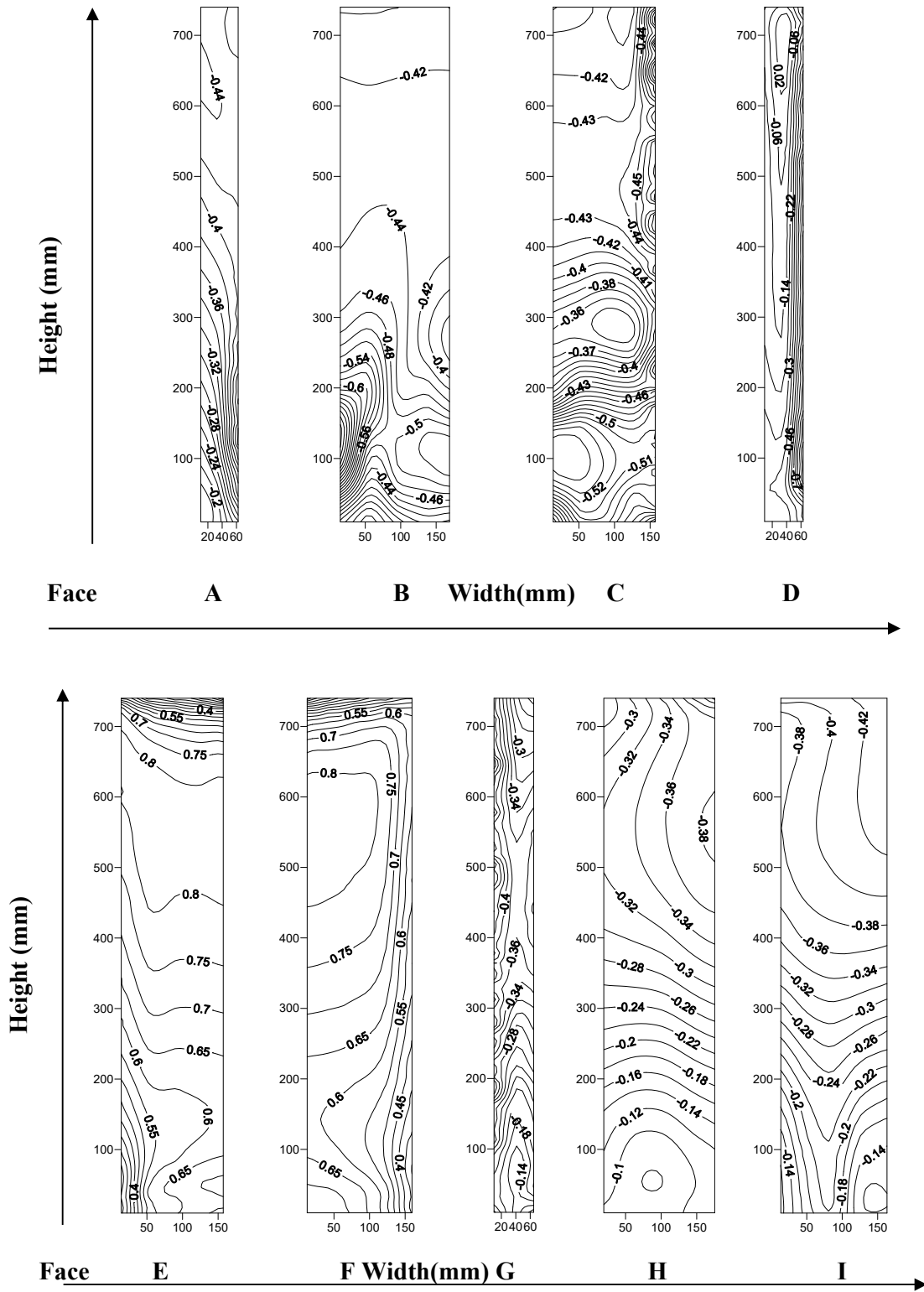


Figure 5.12 Distribution of wind pressure coefficient on the Y-shape with simple corner at 165° wind incidence angle

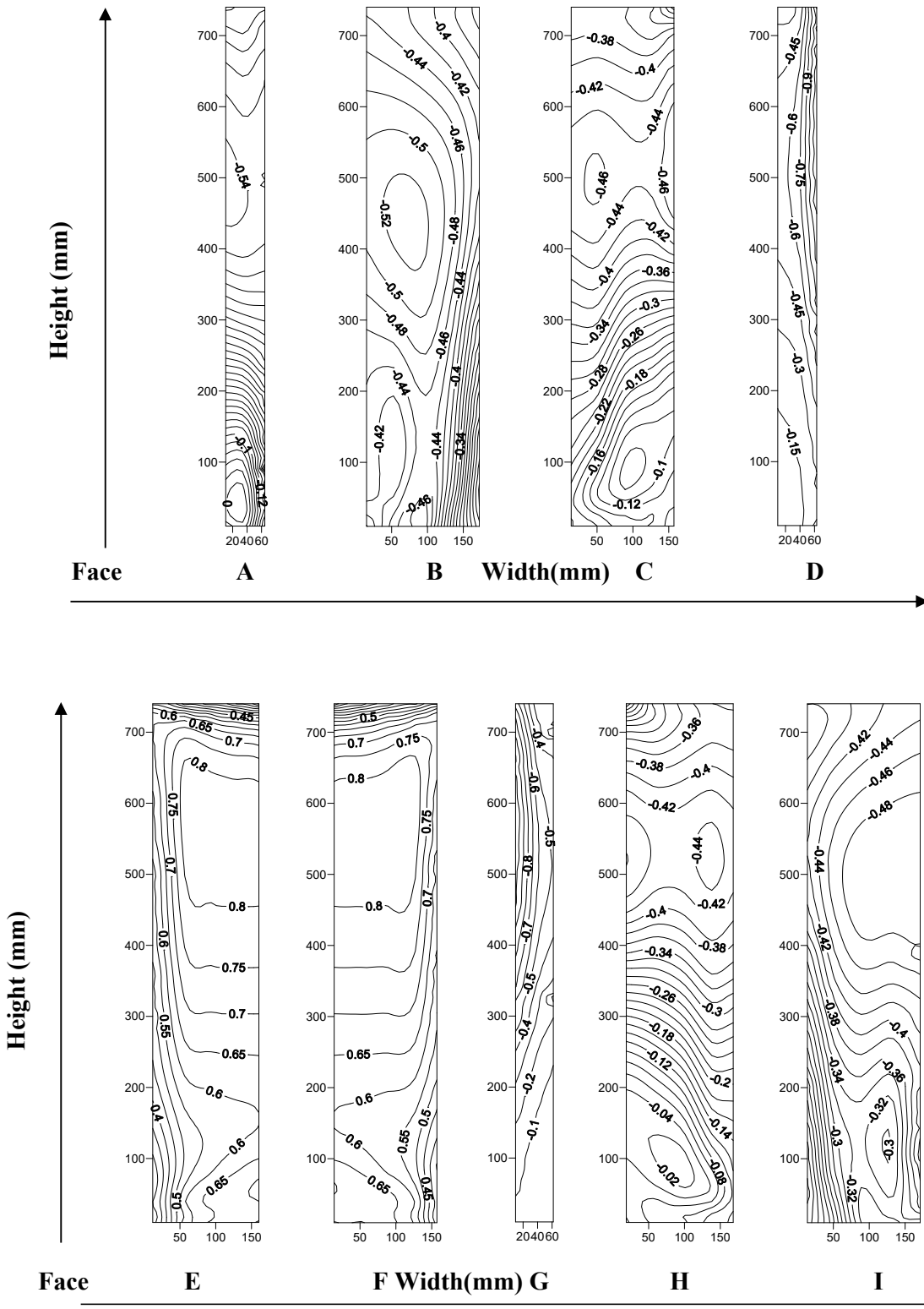


Figure 5.13 Distribution of wind pressure coefficient on the Y-shape with simple corner at 180° wind incidence angle

### 5.2.2 Vertical Pressure Distribution along the Height of the Building

The pressure distribution is presented on the vertical centre line for irregular model of “Y” shaped without any corner configuration as presented in Figure 5.14 Mean pressure distribution on the vertical centre line for Y shape with simple corner . Face-A has maximum  $C_p$  at  $0^\circ$  and minimum is at  $75^\circ$ , from  $0^\circ$  to  $45^\circ$  a fixed pattern of pressure distribution has flowed and it is decreasing in magnitude. From  $0^\circ$  to  $30^\circ$  face-A is under the influence of positive pressure, then as the wind incidence angle changes,  $C_p$  on the vertical centre line is also increases in negative magnitude from  $75^\circ$  to  $135^\circ$ . Face -G is the only face that is under the influence of negative pressure, i.e., suction for all studied wind incidence angles. Face- D and face- A has more or less invariable pressure distribution. Face-C and face-E having uniform nature of pressure distribution.

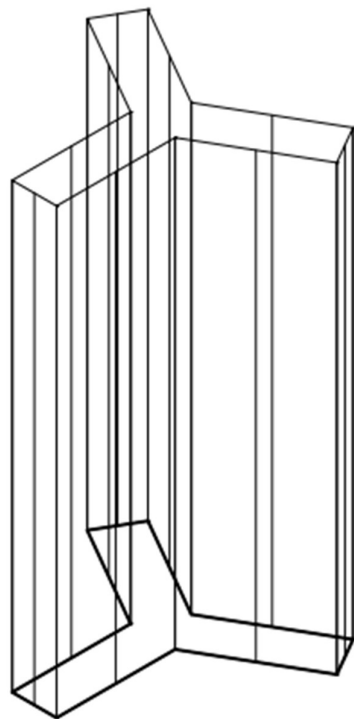
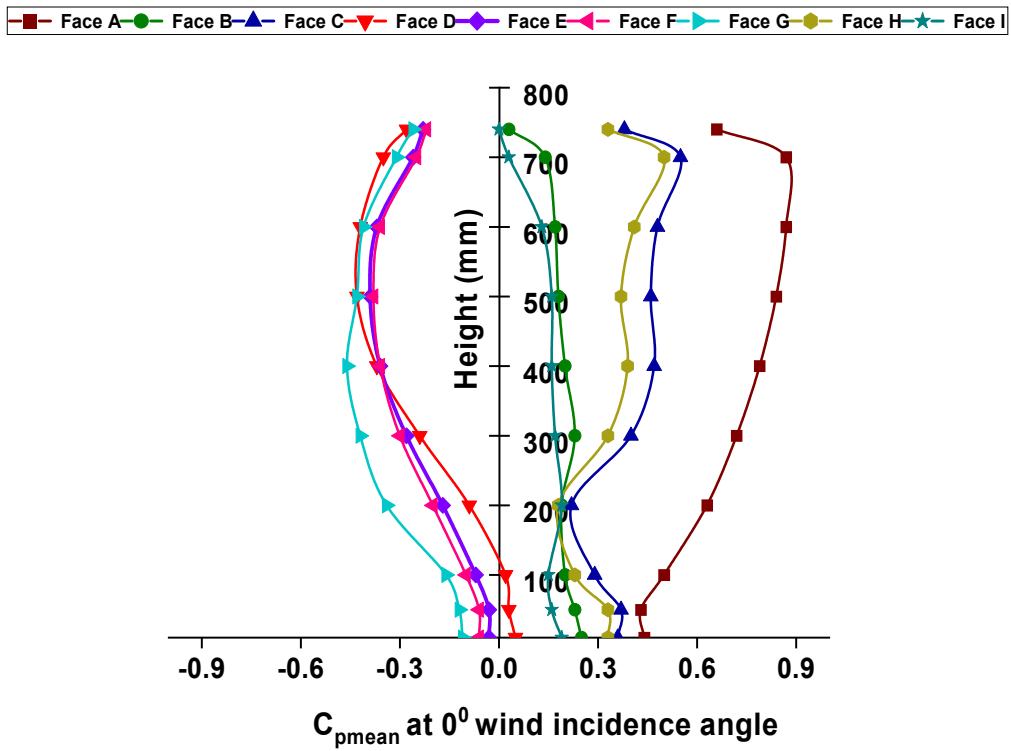


Figure 5.14 (contd.) Mean pressure distribution on the vertical centre line for Y shape with simple corner

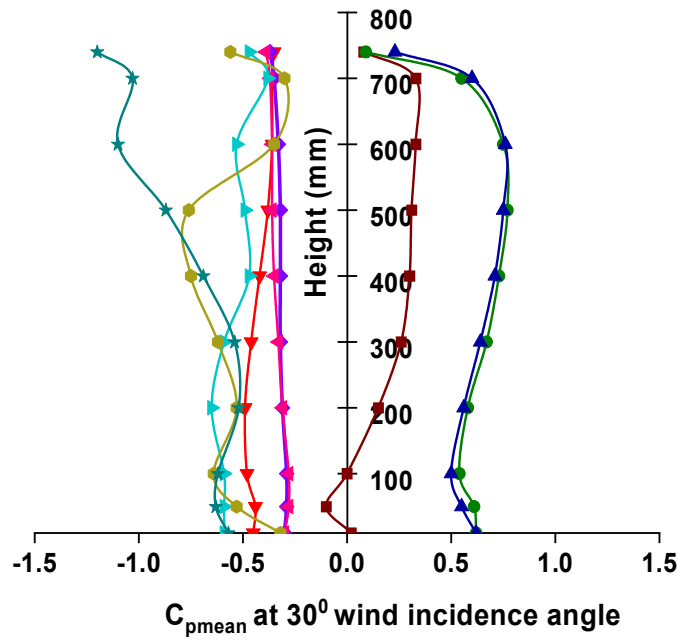
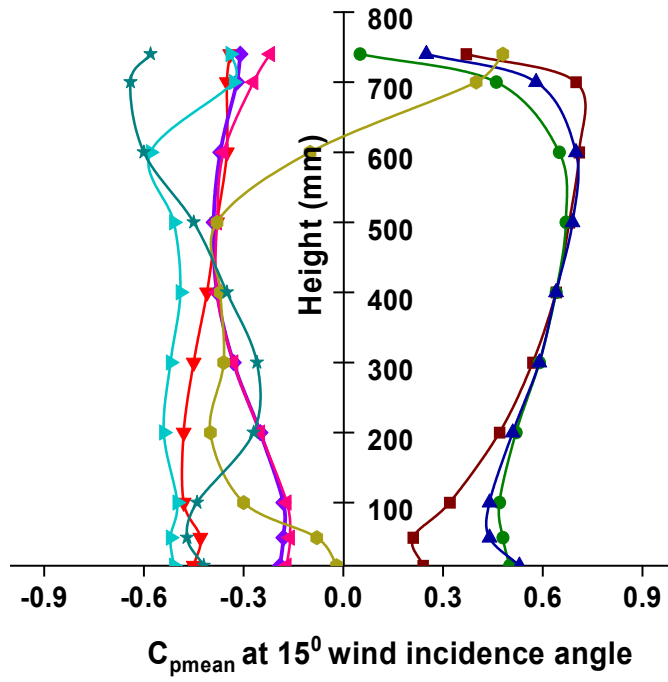
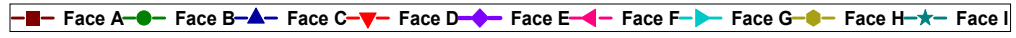


Figure 5.14 (contd.) Mean pressure distribution on the vertical centre line for Y shape with simple corner

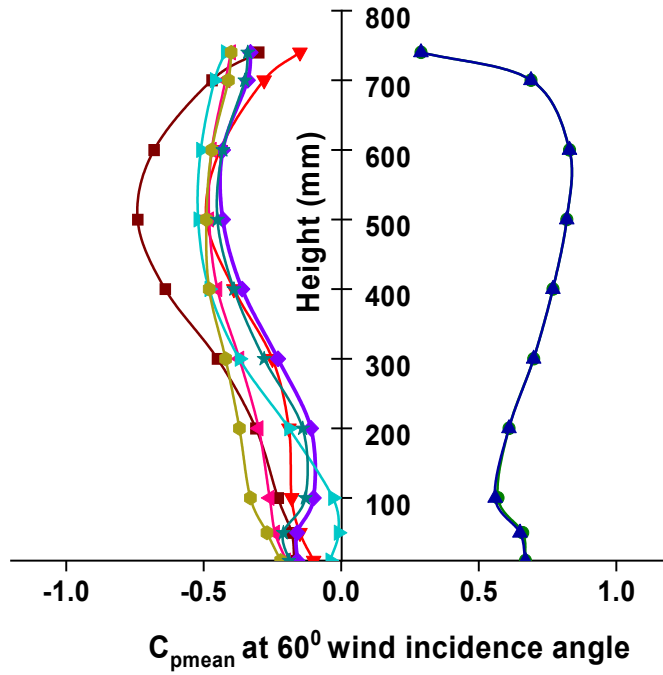
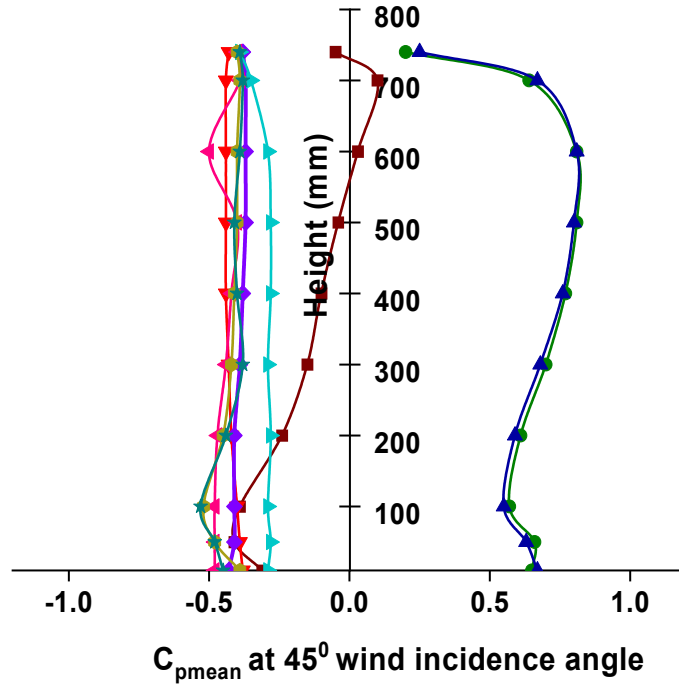
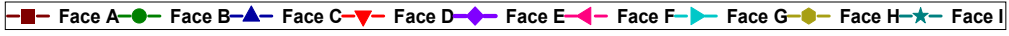


Figure 5.14 (contd.) Mean pressure distribution on the vertical centre line for Y shape with simple corner



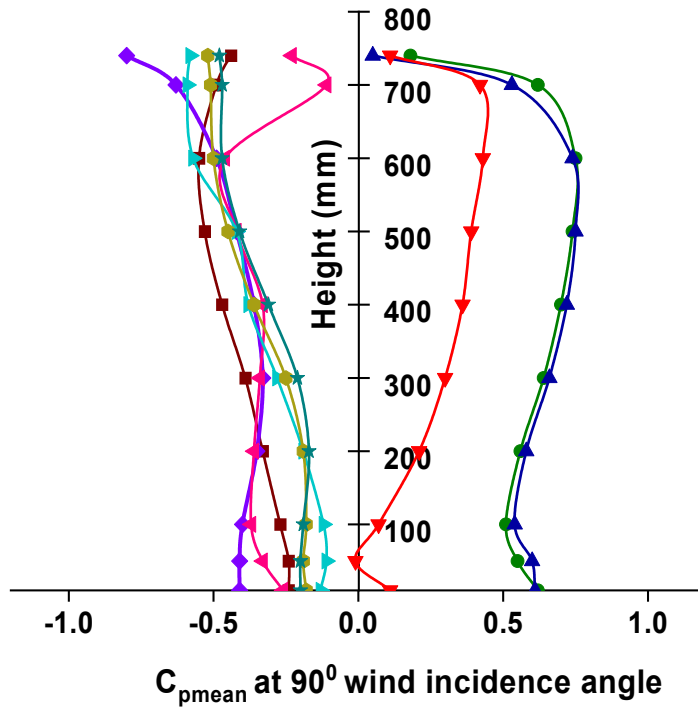
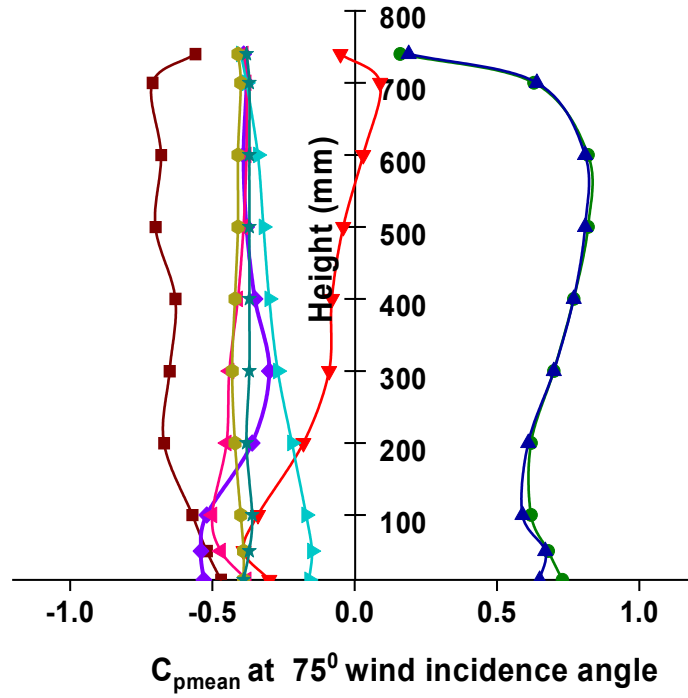
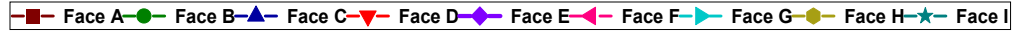


Figure 5.14 (contd.) Mean pressure distribution on the vertical centre line for Y shape with simple corner

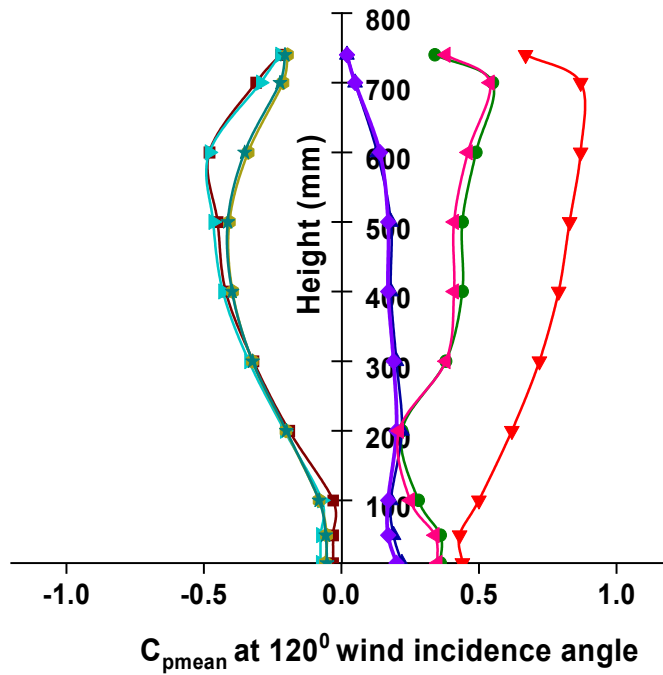
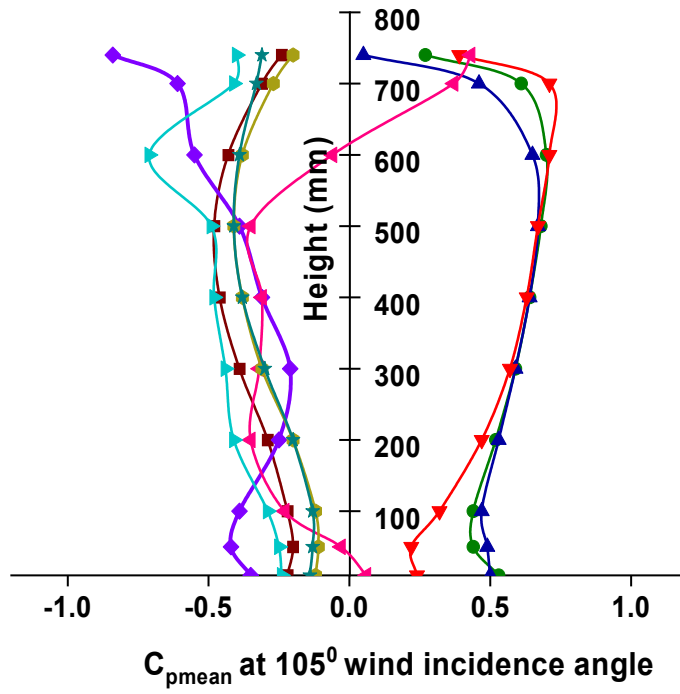
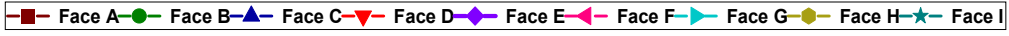


Figure 5.14 (contd.) Mean pressure distribution on the vertical centre line for Y shape with simple corner

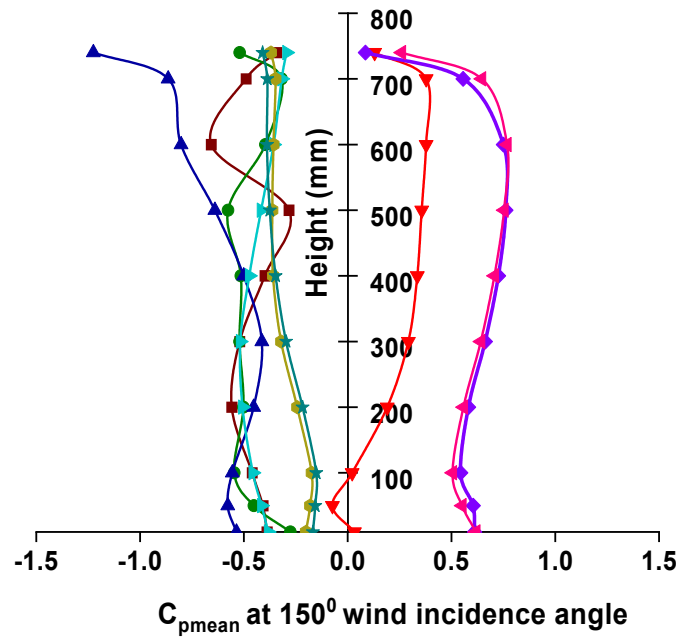
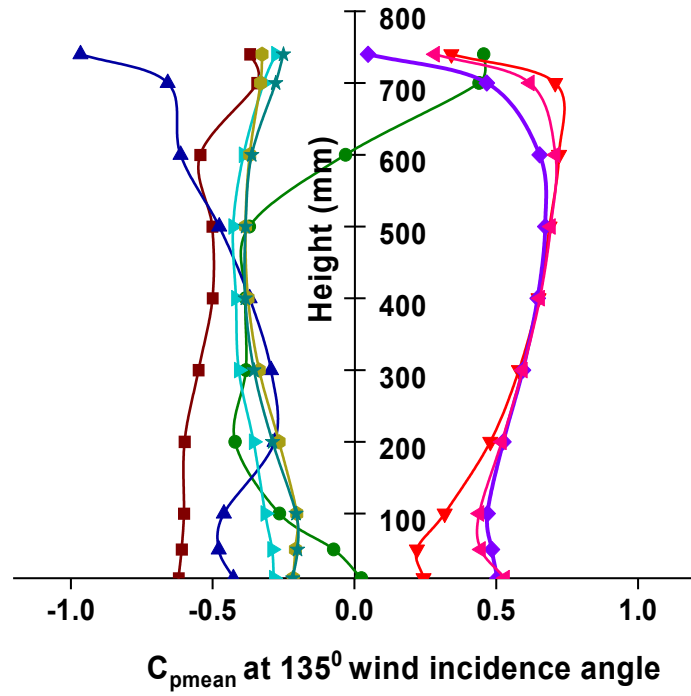
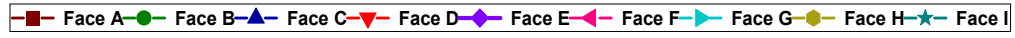


Figure 5.14 (contd.) Mean pressure distribution on the vertical centre line for Y shape with simple corner

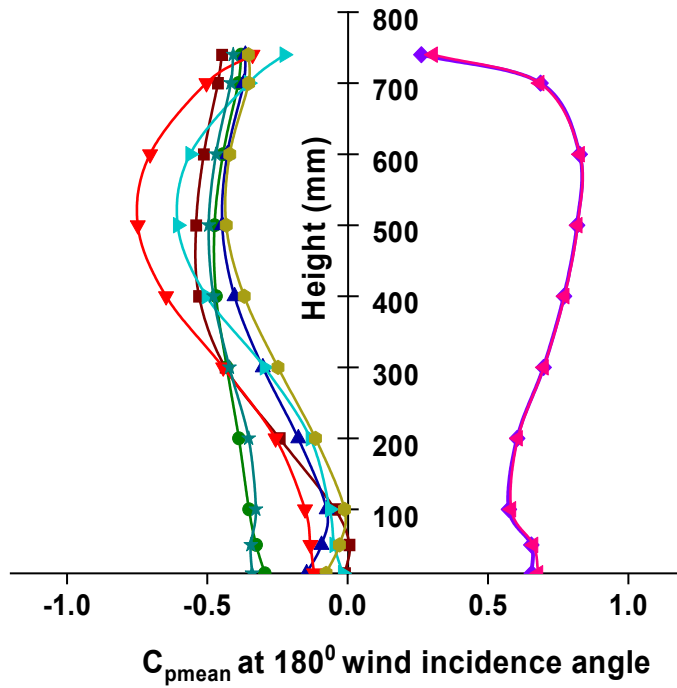
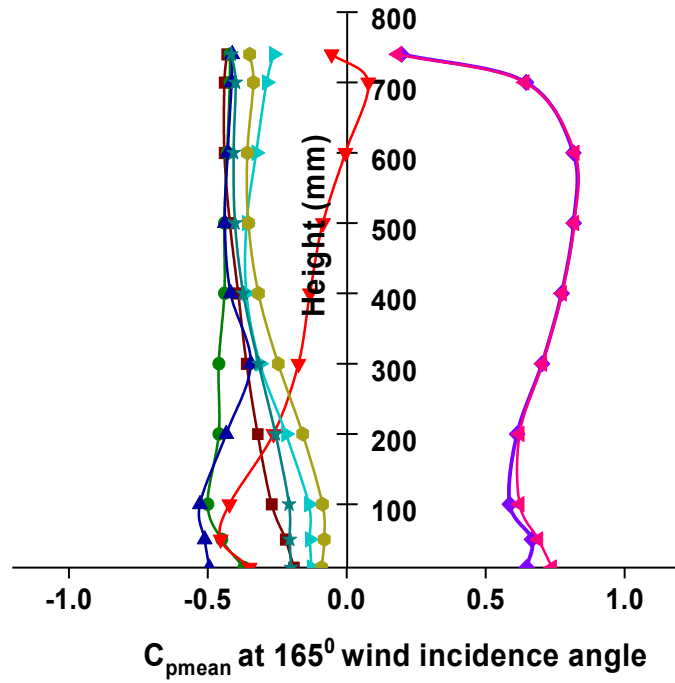
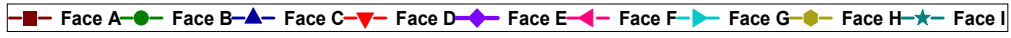


Figure 5.14 Mean pressure distribution on the vertical centre line for Y shape with simple corner

### **5.2.3 Horizontal Pressure Distribution along the Peripheral Distance of Building**

The pressure distribution around the peripheral distance of building model is investigate at three different levels and depicted graphically in Figure 5.15 Mean pressure distribution along the peripheral distance of the Y-shape with simple corner . The pressure distribution around the peripheral distance at one third height of 250 mm from the base of the model, mid-height at 375 mm from the base, two third height of building that is 500 mm from the base of a building model is presented. The maximum pressure of 0.67 is noted on face-A at 37 mm while the least pressure of -0.48 is observed on face-G at 680 mm perpherial distance in the case of  $0^0$  wind incidence angle for one third height of the model. The pressure distibution varies from 0.67 to -0.75 while for mid height of building the pressure lies between +0.77 to -1.07 and for the two third height of model such range varies from +0.84 to -1.35.

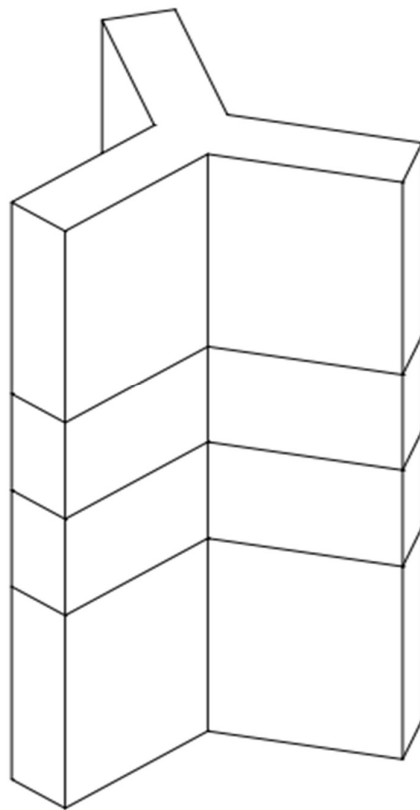
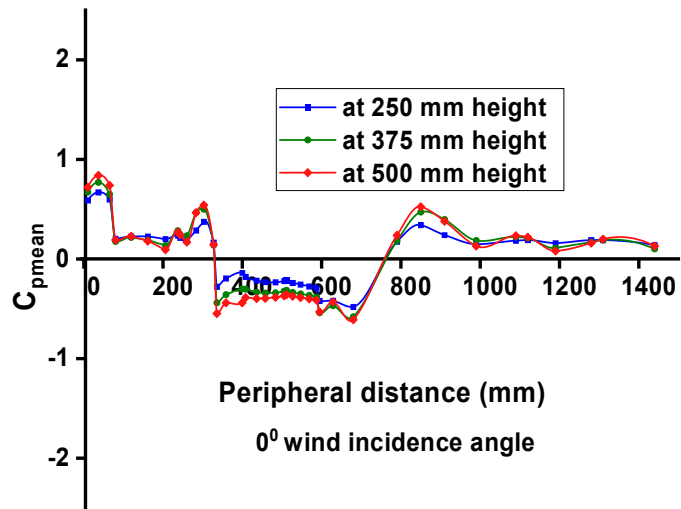


Figure 5.15 (contd.) Mean pressure distribution along the peripheral distance of the Y-shape with simple corner

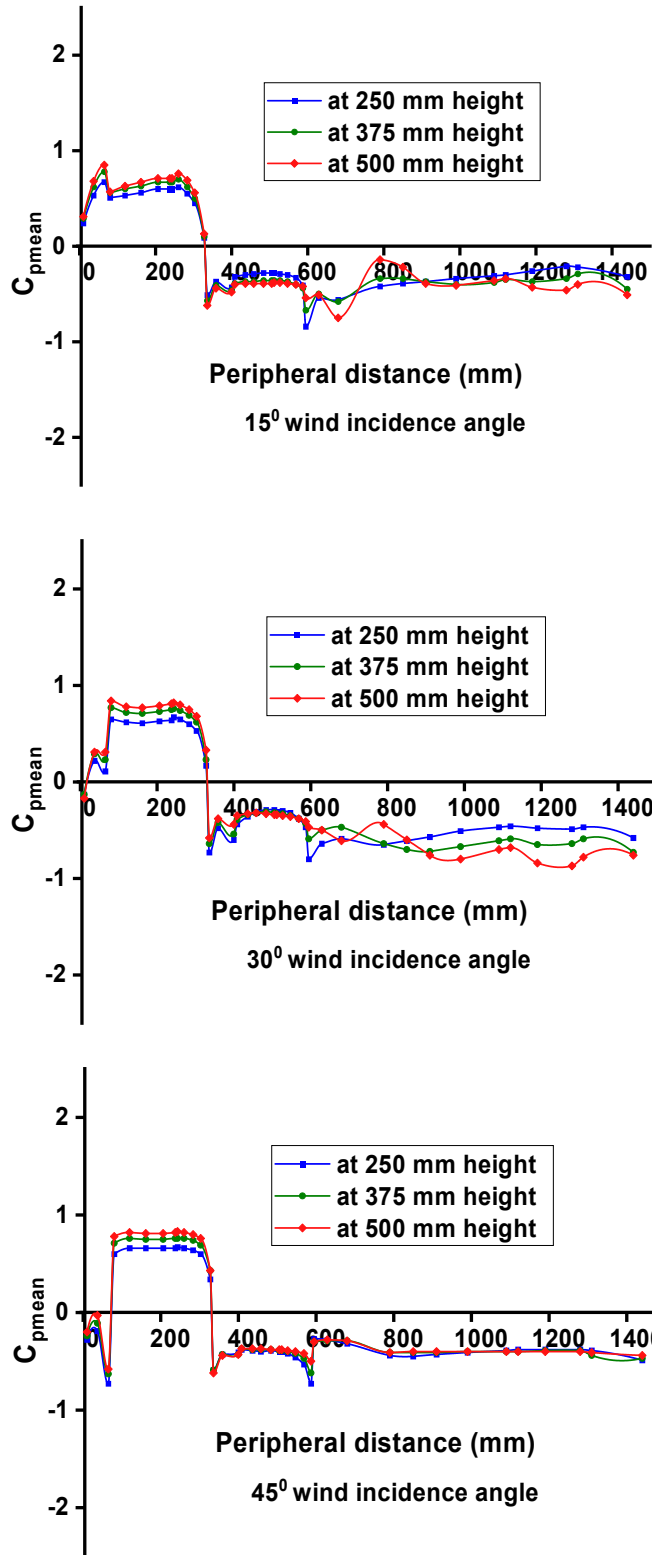


Figure 5.15 (contd.) Mean pressure distribution along the peripheral distance of the Y-shape with simple corner

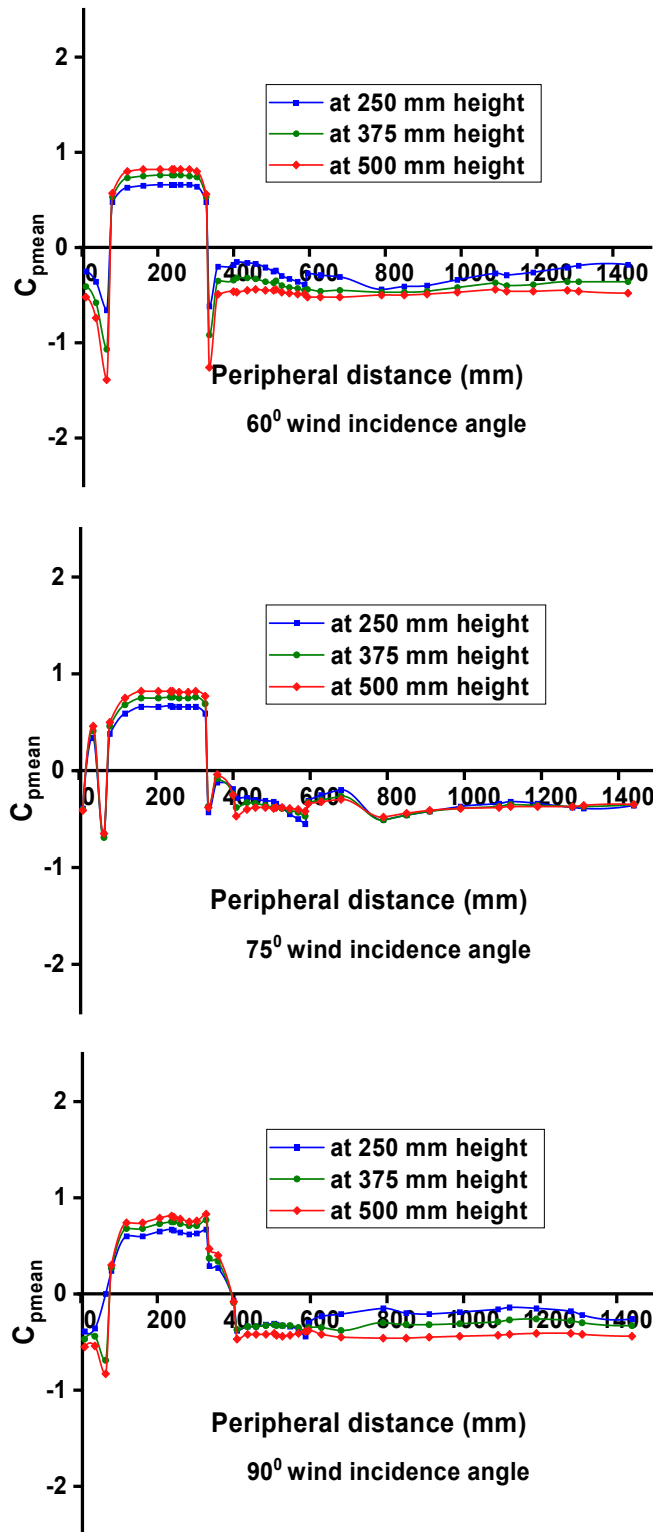


Figure 5.15 (contd.) Mean pressure distribution along the peripheral distance of the Y-shape with simple corner



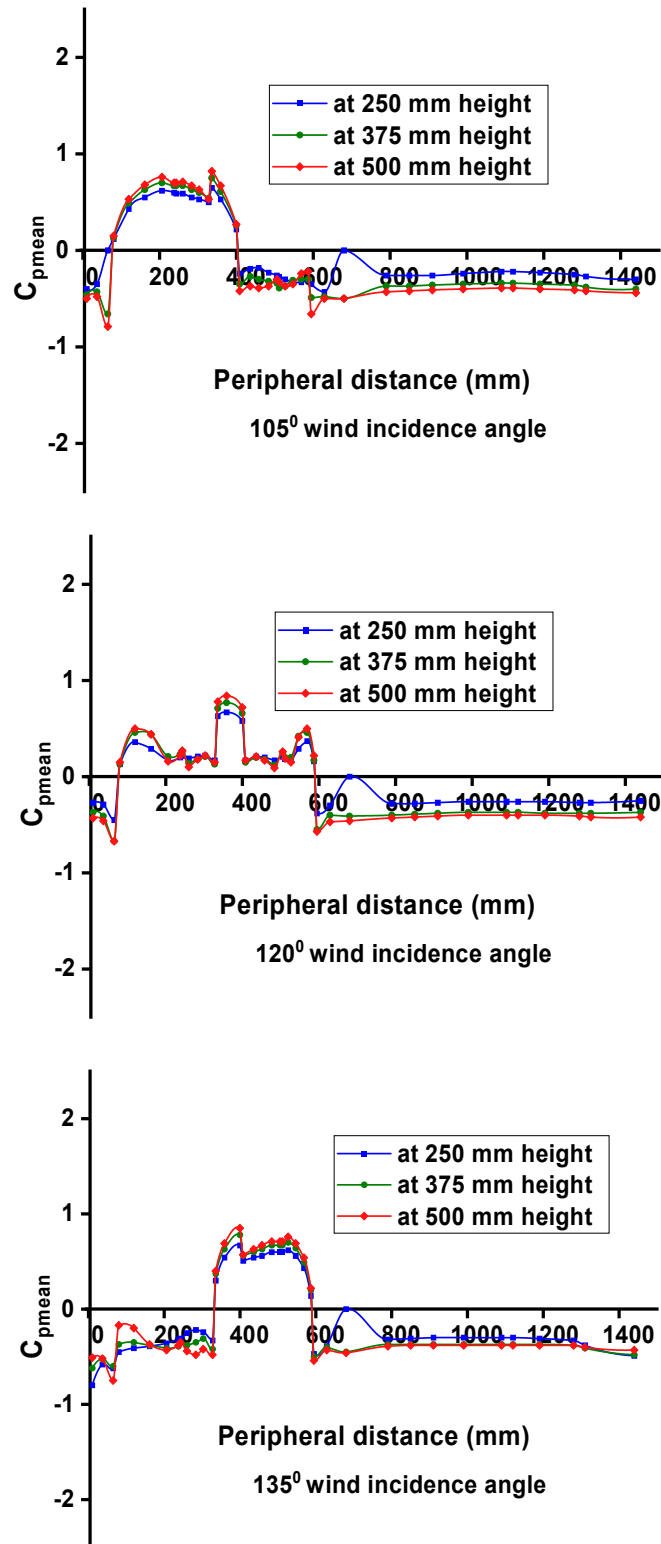


Figure 5.15 (contd.) Mean pressure distribution along the peripheral distance of the Y-shape with simple corner

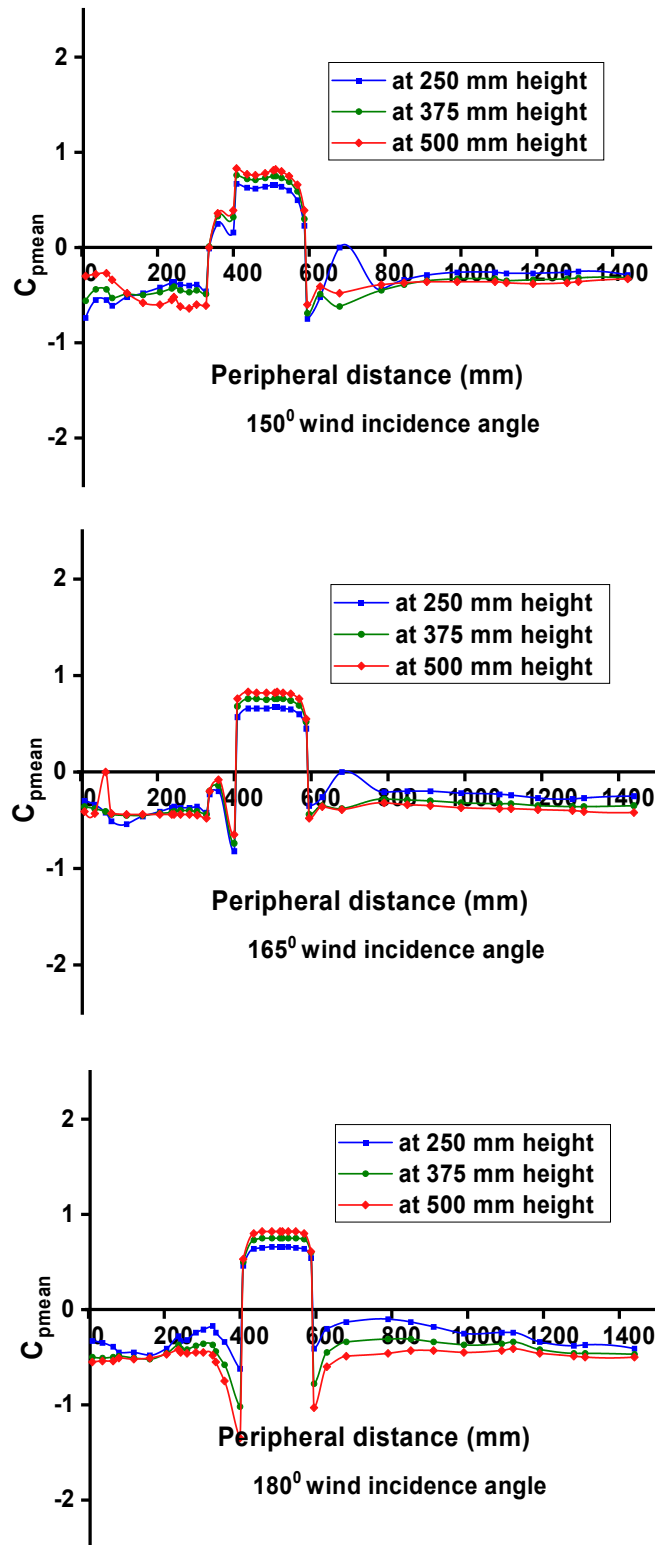


Figure 5.15 Mean pressure distribution along the peripheral distance of the Y-shape with simple corner

### 5.2.4 Force Coefficients

Force coefficient in different direction are explored using numerical simulation performed on “Y” shape building model for  $0^{\circ}$  to  $180^{\circ}$  at an interval of  $15^{\circ}$  and plotted in Figure 5.16 Wind force coefficient of the Y-shape with simple corners. The force coefficient in X and Y directions are  $C_{fx}$  and  $C_{fy}$  and is presented. The value of force in different direction X and Y are  $F_x$  and  $F_y$  and are obtained from ANSYS post and is calculated as per the steps explained in the wind tunnel manual. The  $C_{fx}$  is varies from 0.20 to 1.09 and the least  $C_{fx}$  is noted for  $60^{\circ}$  and the most is observed at  $30^{\circ}$  wind incident. The  $C_{fy}$  lies in the range of - 0.046 to + 0.41.

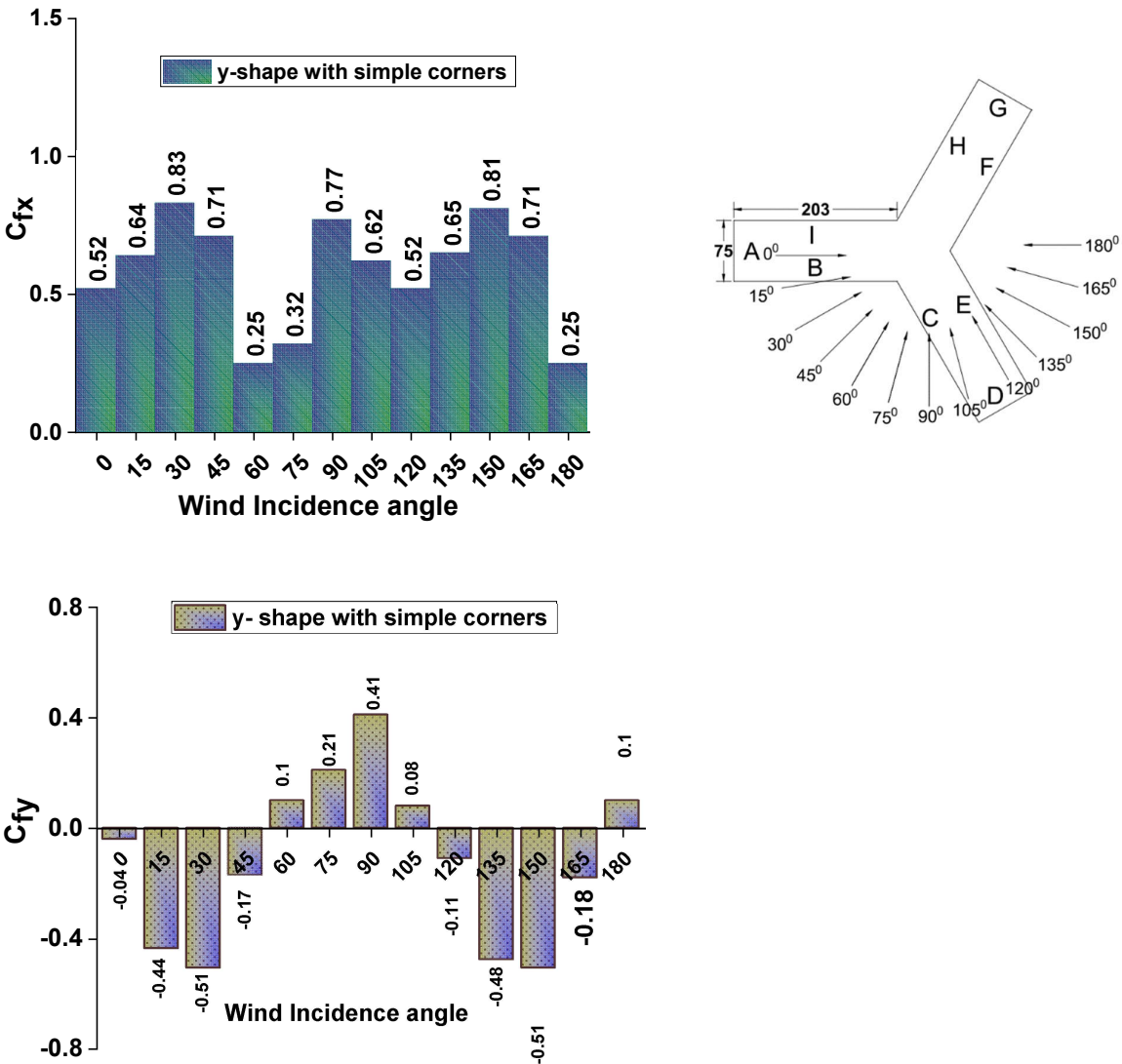


Figure 5.16 Wind force coefficient of the Y-shape with simple corners

### 5.2.5 Moment Coefficients

The moment coefficient in  $C_{mx}$  and  $C_{my}$  direction is calculated and presented in the graphical form in Figure 5.17 Wind moment coefficient of the Y-shape with simple corners. The value of  $M_x$  and  $M_y$  are obtained using ANSYS post and the wind generated moment coefficient that is  $C_{mx}$  and  $C_{my}$  is presented and the value of  $C_{mx}$  varies in the range of -0.16 to +0.29 while the  $C_{my}$  is in the range of 0.20 to 0.48. The moment coefficient is investigated from  $0^\circ$  to  $180^\circ$  at an interval of  $15^\circ$ .

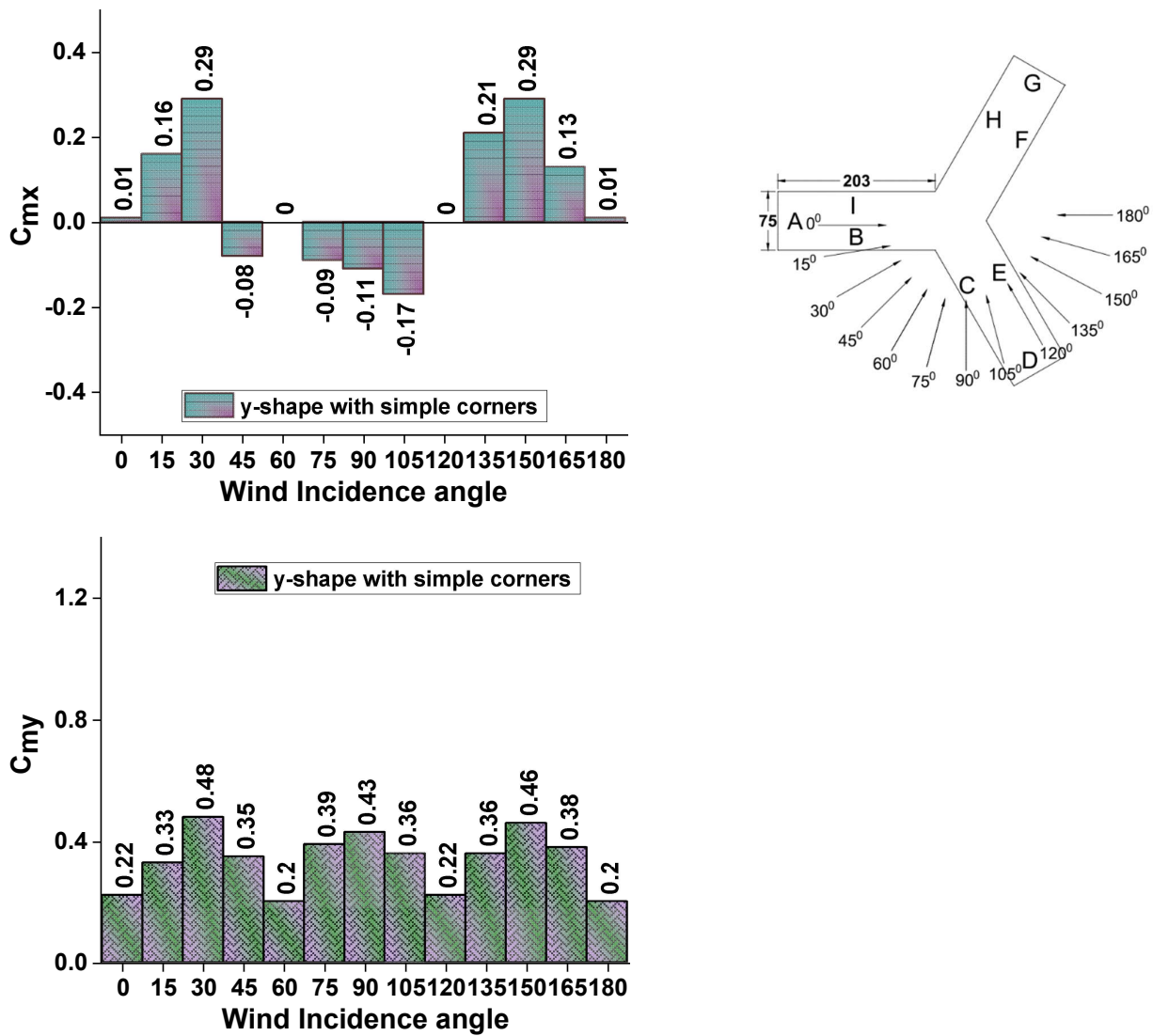


Figure 5.17 Wind moment coefficient of the Y-shape with simple corners

### 5.2.6 External Pressure Coefficients

The external pressure coefficient is noted for irregular “Y” shape model, the wind incidence angle varies from  $0^{\circ}$  to  $180^{\circ}$  at an interval of  $15^{\circ}$ . The average external pressure coefficient is tabulated for each face of model in the tabular form in Table: 5.1 External Pressure Coefficients for model-E (Y-Shape). It is observed that building with irregular shape has a maximum external pressure coefficient of 0.68 on faces-B, C, and face-E at  $45^{\circ}$ ,  $75^{\circ}$ , and  $165^{\circ}$  respectively, while minimum of - 0.73 is observed at face-I in the case of  $30^{\circ}$  wind incidence angle.

The pressure coefficient is obtained after drawing the lines on each face and the coordinate frame is also defined at every face at each studied wind angle. The evolution of maximum and minimum wind external pressure is represented in the tabular form for the model having no corner configuration in irregular plan shape building model which is having the height of 750 mm. The entire numerical simulation is performed by utilizing the k- $\epsilon$  turbulence model. The numerical simulation performed to investigate the wind effects on the high-rise building performed best for complex fluid problems.

**Table: 5.1 External Pressure Coefficients for model-E (Y-Shape)**

Model-E (Y-shape)													
Face	0°	15°	30°	45°	60°	75°	90°	105°	120°	135°	150°	165°	180°
<b>A</b>	<b>0.66</b>	0.49	0.06	-0.33	<b>-0.51</b>	-0.18	<b>-0.48</b>	-0.42	<b>-0.33</b>	<b>-0.62</b>	-0.50	-0.35	-0.38
<b>B</b>	0.18	<b>0.56</b>	<b>0.67</b>	<b>0.68</b>	<b>0.66</b>	0.63	0.58	0.49	0.27	-0.22	-0.47	<b>-0.45</b>	-0.41
<b>C</b>	0.29	0.49	0.56	0.62	<b>0.66</b>	<b>0.68</b>	<b>0.66</b>	<b>0.55</b>	0.16	-0.42	<b>-0.59</b>	-0.44	-0.29
<b>D</b>	<b>-0.41</b>	-0.42	-0.52	<b>-0.47</b>	<b>-0.51</b>	-0.25	0.17	0.48	<b>0.66</b>	0.50	0.14	-0.35	<b>-0.49</b>
<b>E</b>	-0.26	-0.31	-0.34	-0.38	-0.30	-0.39	-0.43	-0.37	0.16	<b>0.56</b>	0.66	<b>0.68</b>	<b>0.66</b>
<b>F</b>	-0.26	-0.31	-0.36	-0.46	-0.37	<b>-0.43</b>	-0.36	-0.18	0.27	0.50	<b>0.57</b>	0.65	<b>0.66</b>
<b>G</b>	<b>-0.41</b>	<b>-0.61</b>	-0.59	-0.30	-0.34	-0.28	-0.35	<b>-0.44</b>	<b>-0.33</b>	-0.37	-0.51	-0.31	<b>-0.49</b>
<b>H</b>	0.29	-0.21	-0.55	-0.43	-0.40	-0.41	-0.32	-0.28	-0.27	-0.32	-0.32	-0.26	-0.29
<b>I</b>	0.18	-0.42	<b>-0.73</b>	-0.44	-0.30	-0.36	-0.31	-0.29	-0.27	-0.34	-0.30	-0.31	-0.41

### **5.3 Y-shape with Corner Cuts**

The land available is in the form of irregular shape hence the building which are designed are in the form of irregular shape hence the tall building of irregular shape is coming up. The wind load on building is increasing with the increment in the height of the building. To avoid such problems in the design of tall building, structures with various modifications are constructing all around the world. The tall building needs its evaluation for wind generated effect and same can be investigated either by wind tunnel test or by numerical testing. In this study different models are investigated for wind resistant design and the various types of modifications are applied in the cross-sectional plan geometry. The area and height is kept same for comparison to find the best model among all studied model for various wind incidence angles.

The irregular building model are very common but usually all of them are mostly without any modification hence this study investigates the wind effect for wind incidence angle  $0^{\circ}$  to  $180^{\circ}$  at an interval of  $15^{\circ}$ . Model is extensively investigated using numerical simulation technique ANSYS. Various result is presented graphically in different forms like pressure contours,  $C_p$ , mean Pressure distribution on vertical centre line of each face and pressure distribution along the building periphery at three different levels.

#### **5.3.1 Pressure Contours**

The pressure on irregular “Y” shape model with corner cut is presented in the form of pressure contours in from Figure 5.18 Distribution of wind pressure coefficient on the Y-shape with corner cut at  $0^{\circ}$  wind incidence angle to Figure 5.30 Distribution of wind pressure coefficient on the Y-shape with corner cut at  $180^{\circ}$  wind incidence angle and the behaviour of the distribution of pressure can be identified by various contours plots at different faces of model for different wind incidence angles. The nature of positive pressure and negative pressure can be visualized with the help of the pressure contours which represent the size of every particular face with respect to height.

The positive pressure is obtained for the face which is resting the direct wind pressure while the leeward and side faces are under the effect of negative pressure. The symmetrical faces found to have same nature of pressure distribution. The building model is rotated for different wind incidence angles while the domain is kept at same location, domain act as virtual wind tunnel for the numerical simulation.





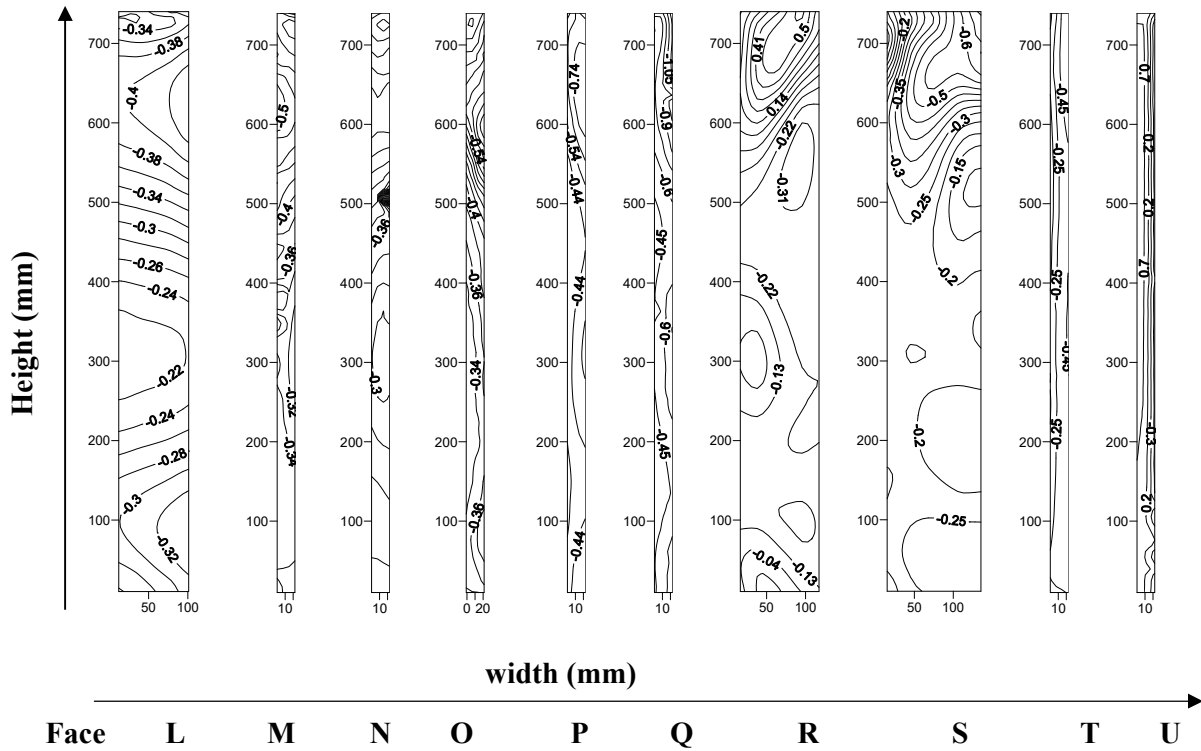
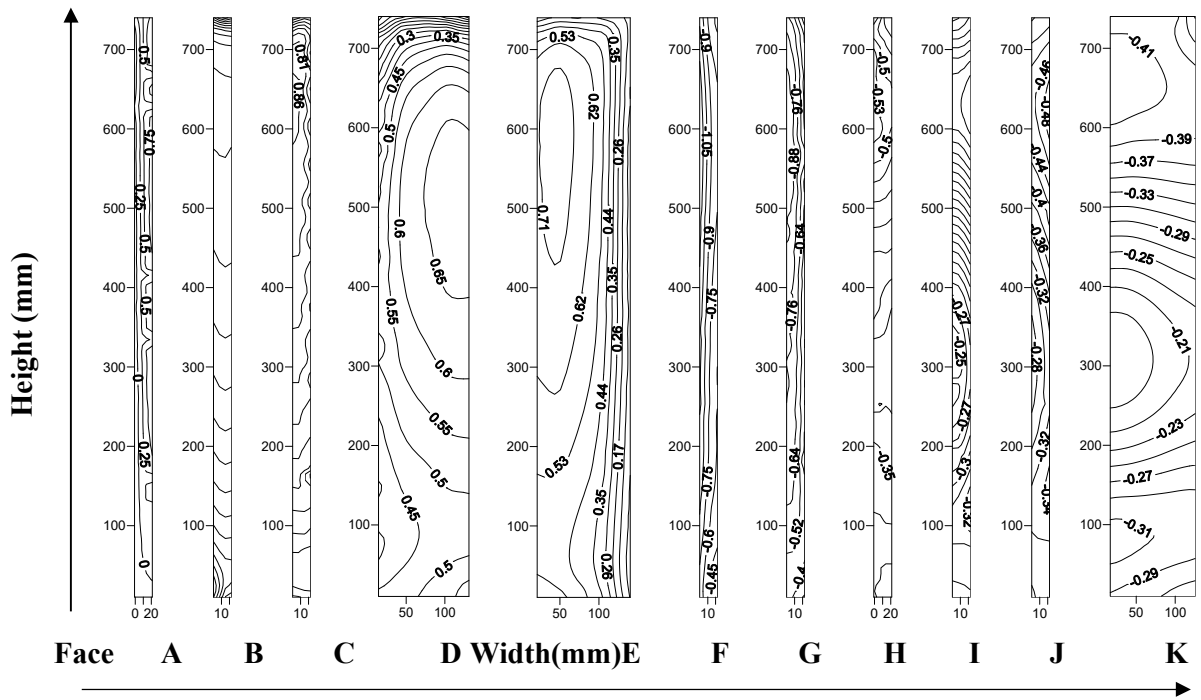


Figure 5.19 Distribution of wind pressure coefficient on the Y-shape with corner cut at  $15^\circ$  wind incidence angle

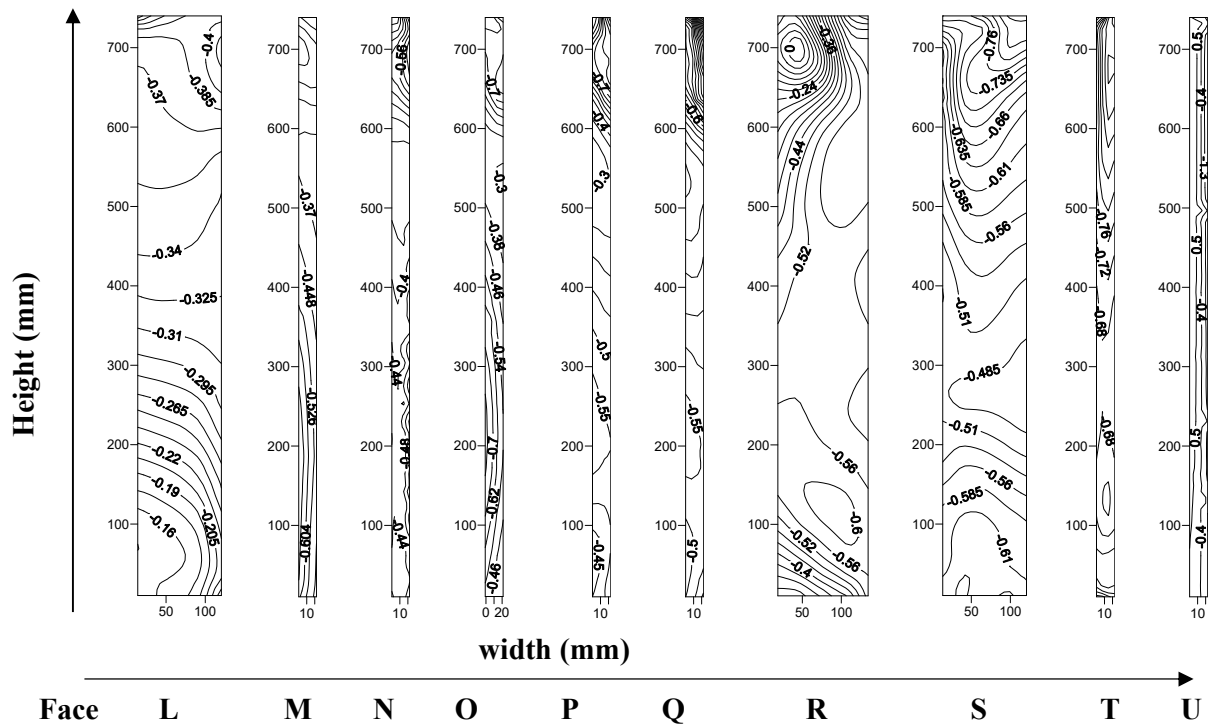
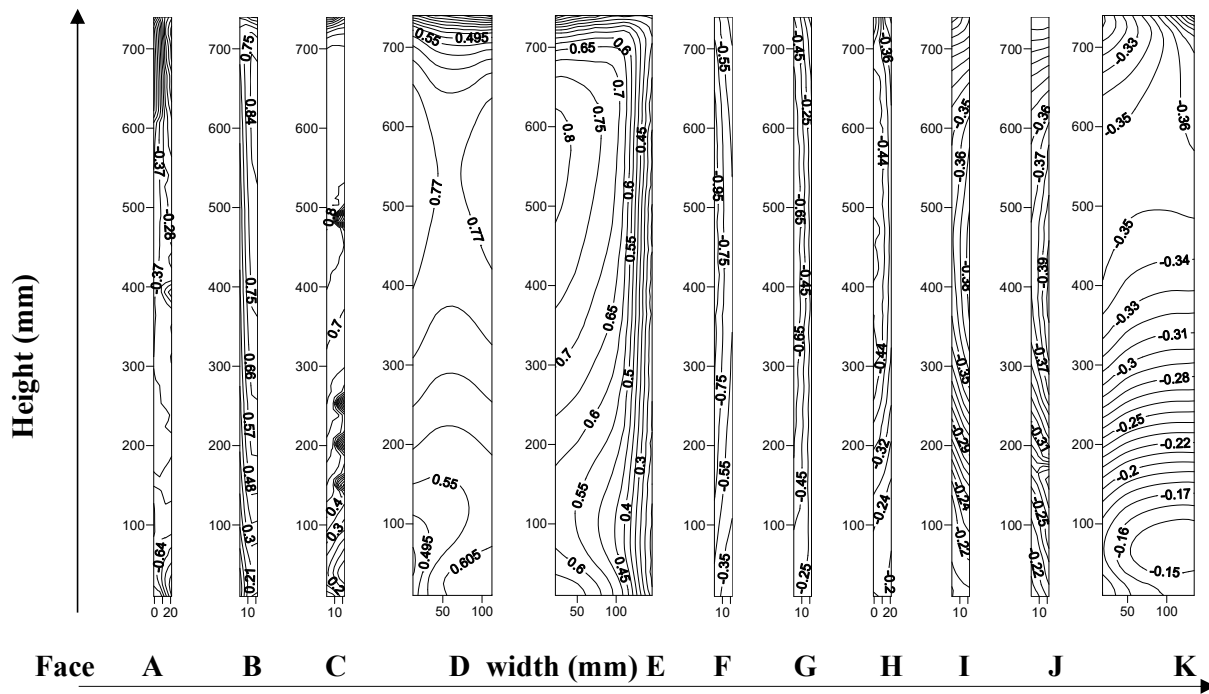


Figure 5.20 Distribution of wind pressure coefficient on the Y-shape with corner cut at  $30^\circ$  wind incidence angle

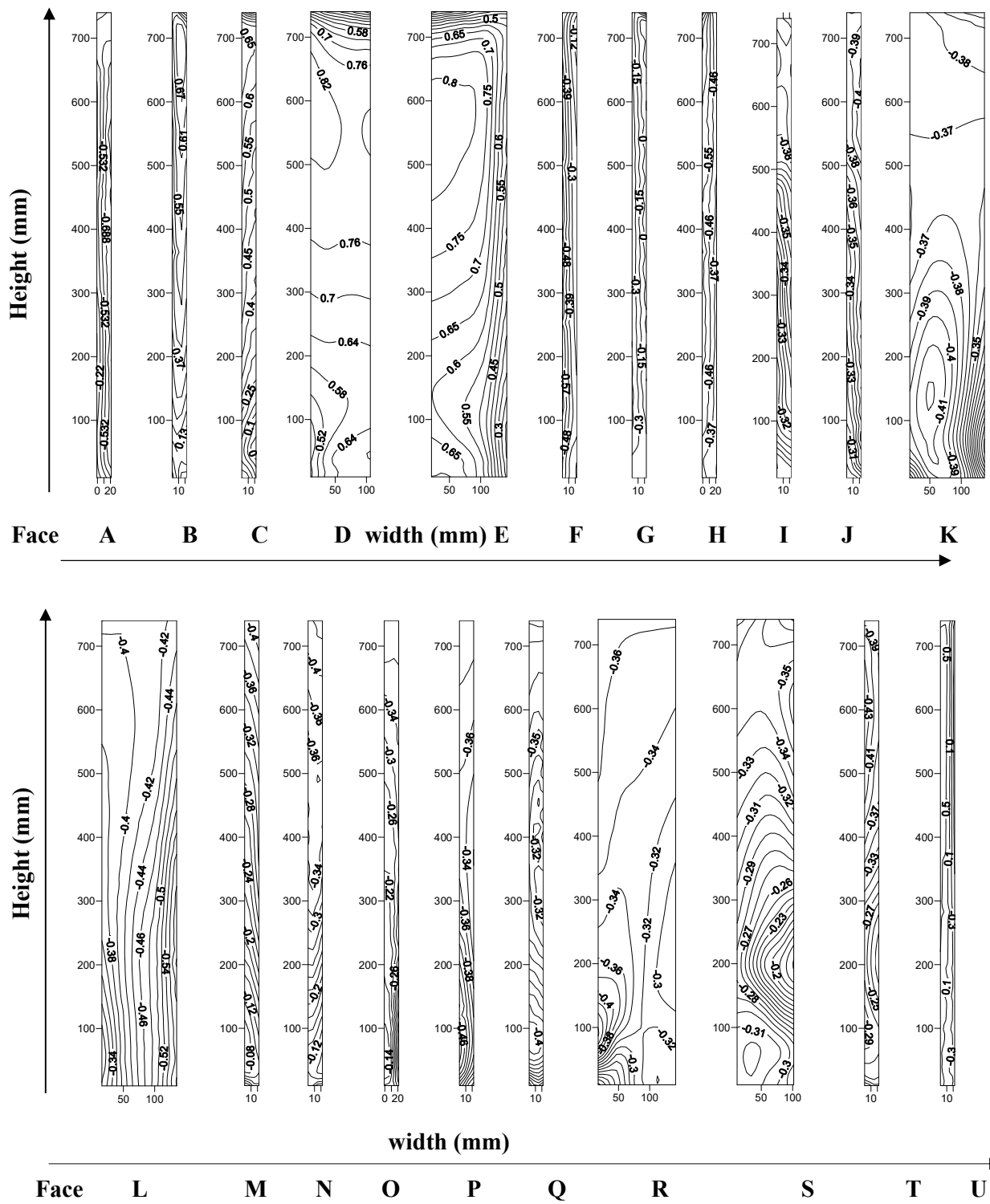


Figure 5.21 Distribution of wind pressure coefficient on the Y-shape with corner cut at 45° wind incidence angle

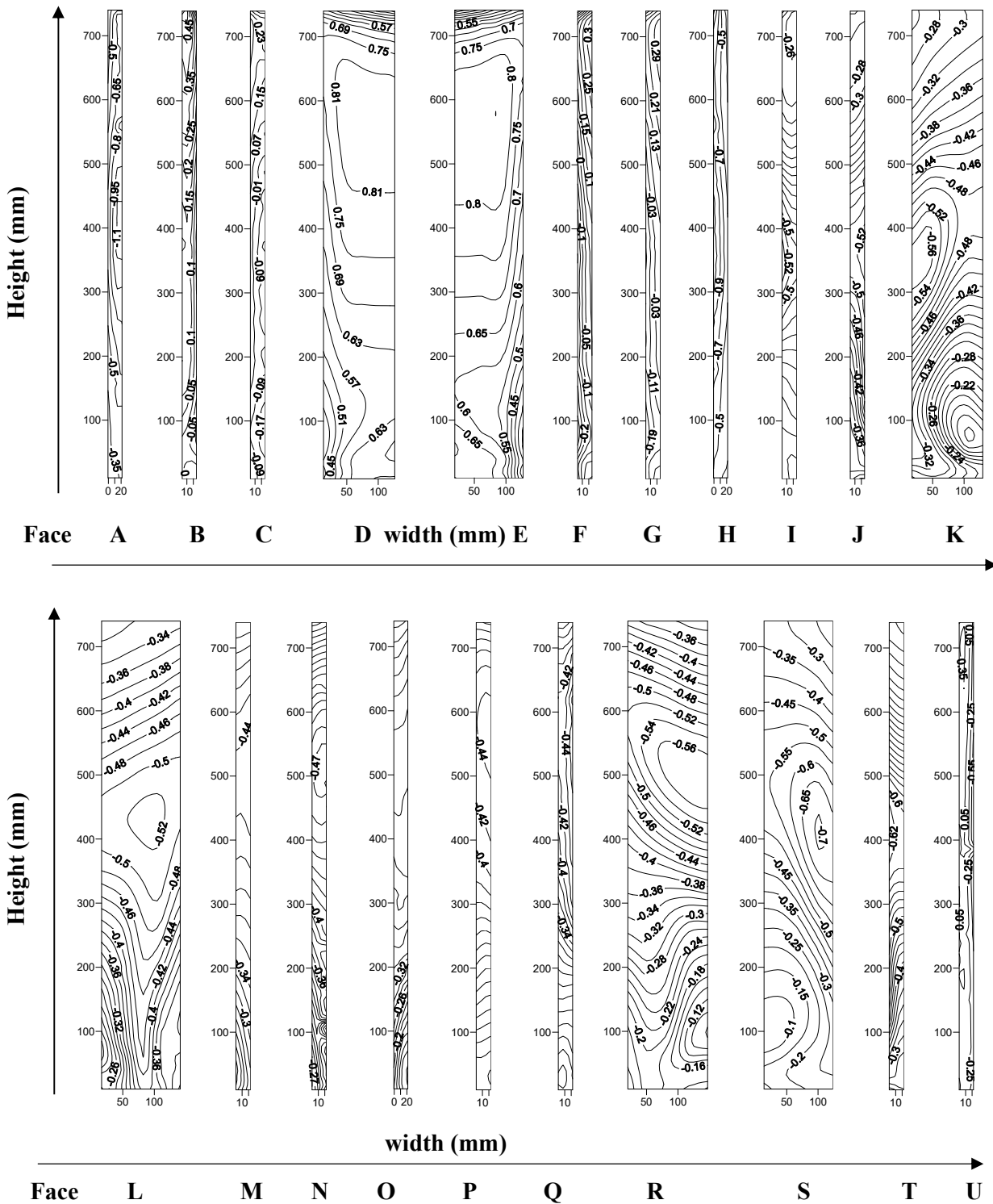


Figure 5.22 Distribution of wind pressure coefficient on the Y-shape with corner cut at 60° wind incidence angle

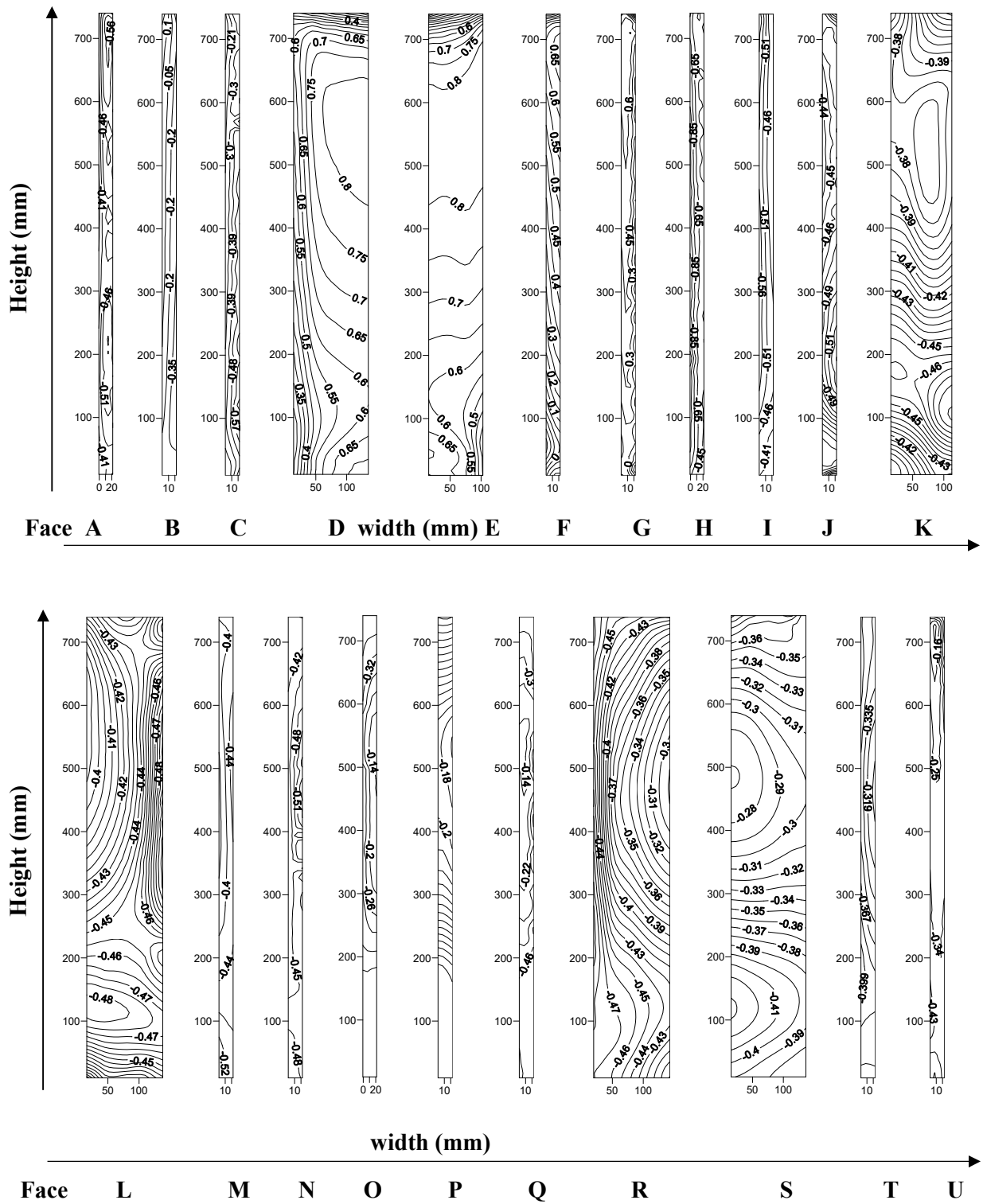


Figure 5.23 Distribution of wind pressure coefficient on the Y-shape with corner cut at  $75^\circ$  wind incidence angle

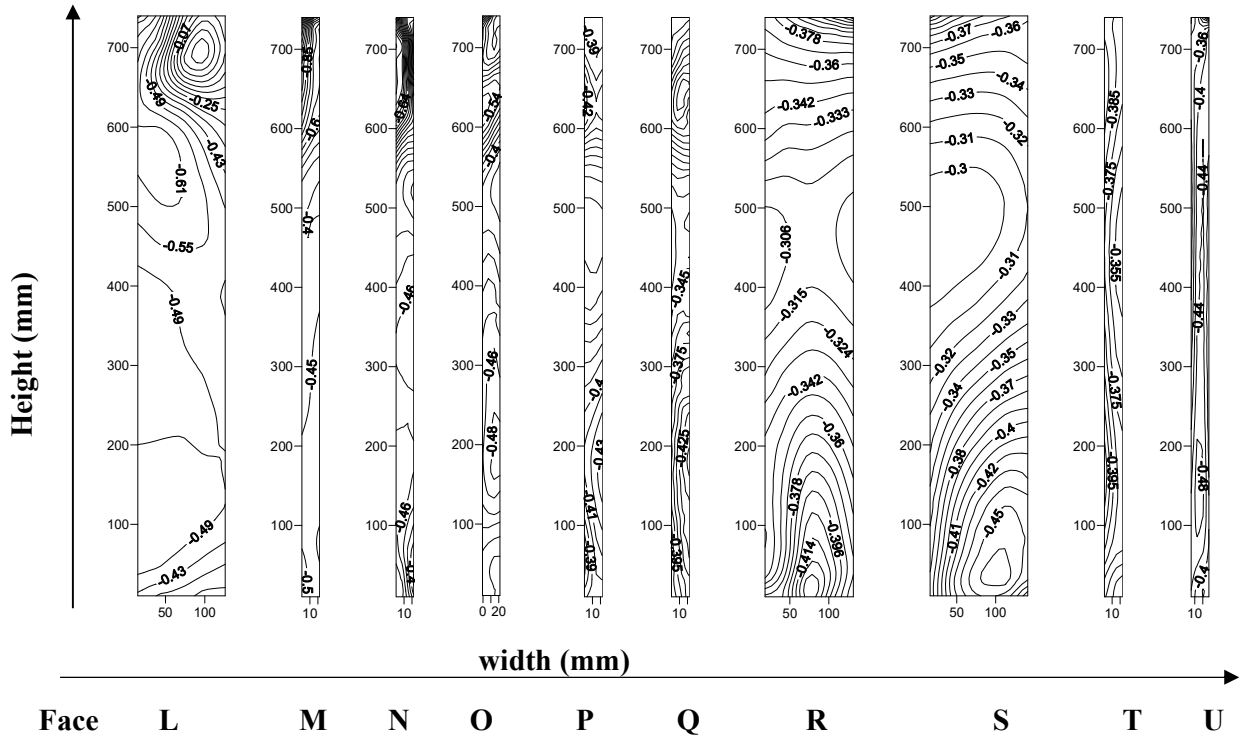
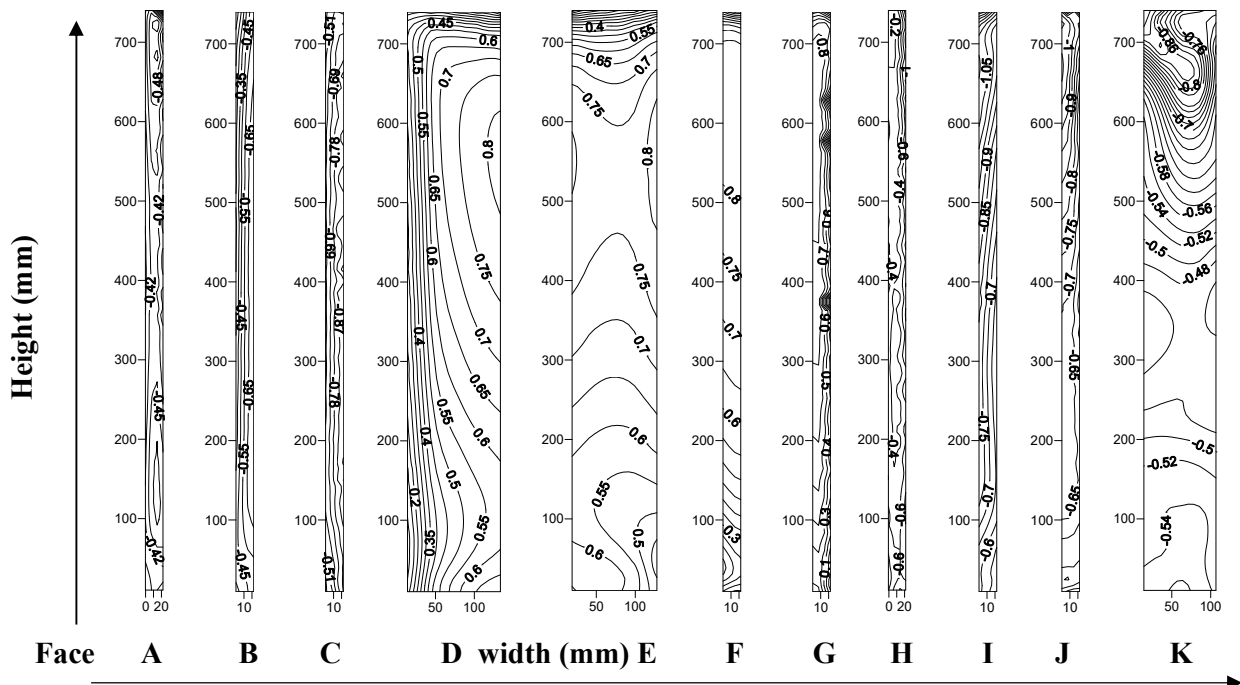


Figure 5.24 Distribution of wind pressure coefficient on the Y-shape with corner cut at  $90^\circ$  wind incidence angle

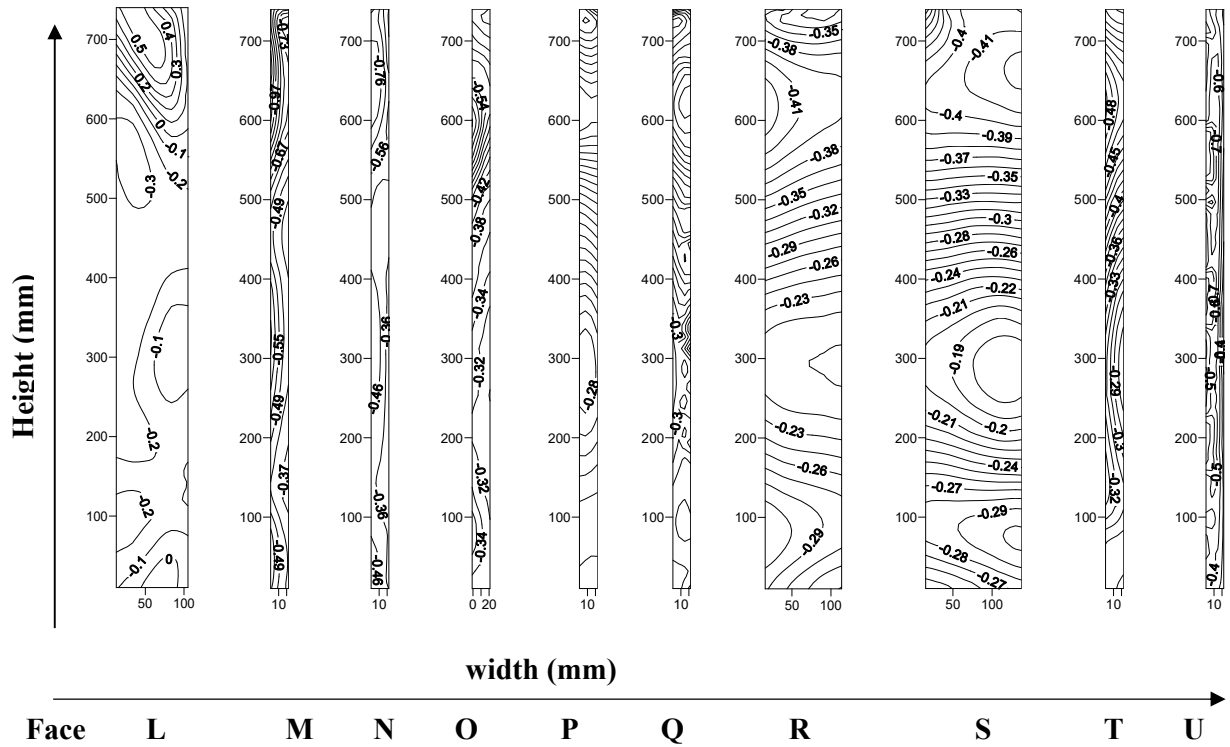
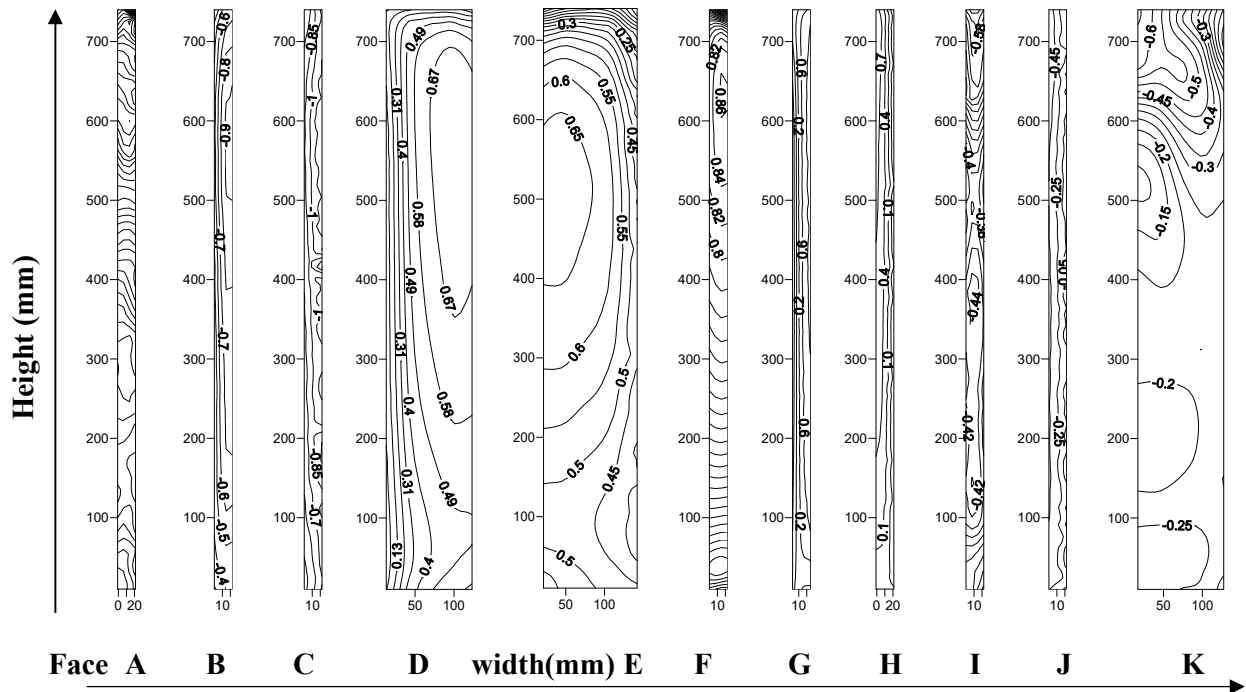


Figure 5.25 Distribution of wind pressure coefficient on the Y-shape with corner cut at  $105^\circ$  wind incidence angle

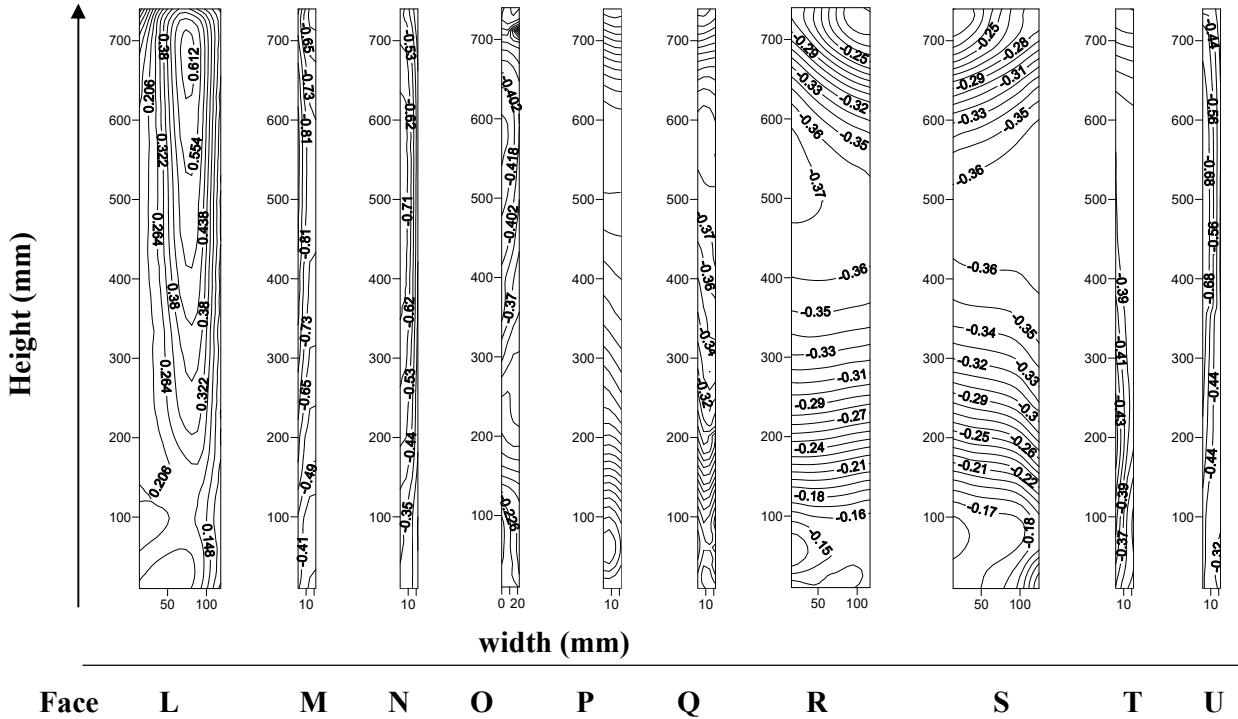
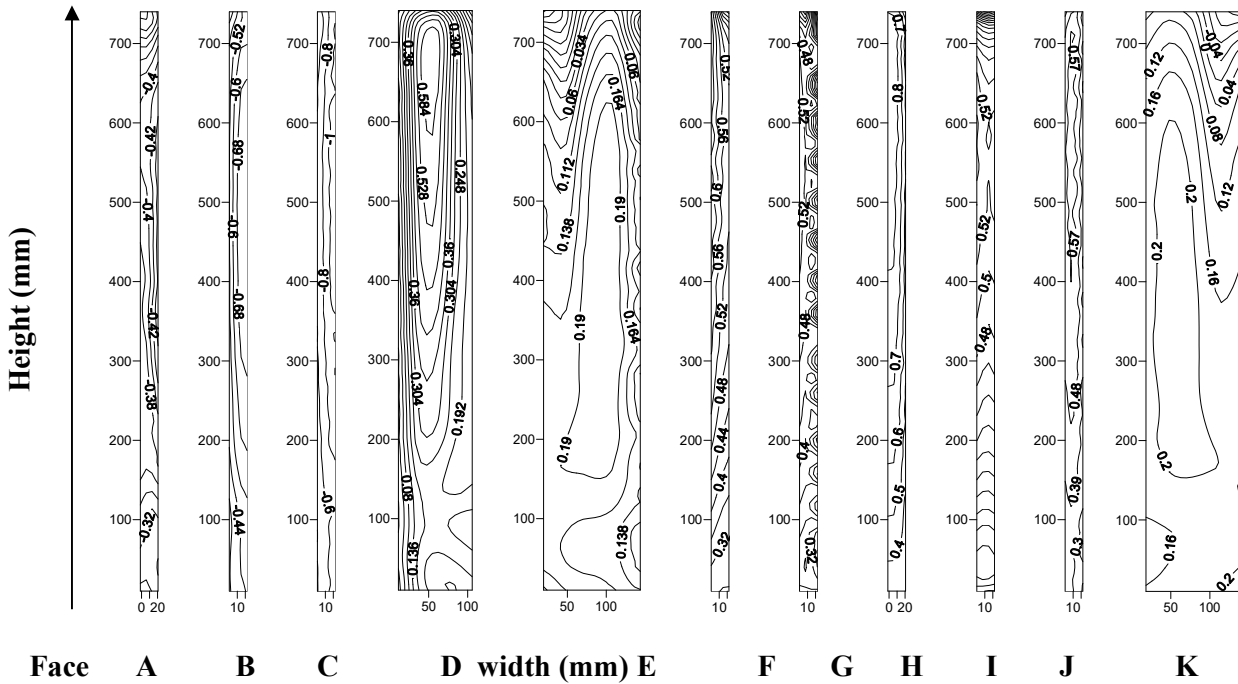


Figure 5.26 Distribution of wind pressure coefficient on the Y-shape with corner cut at  $120^\circ$  wind incidence angle



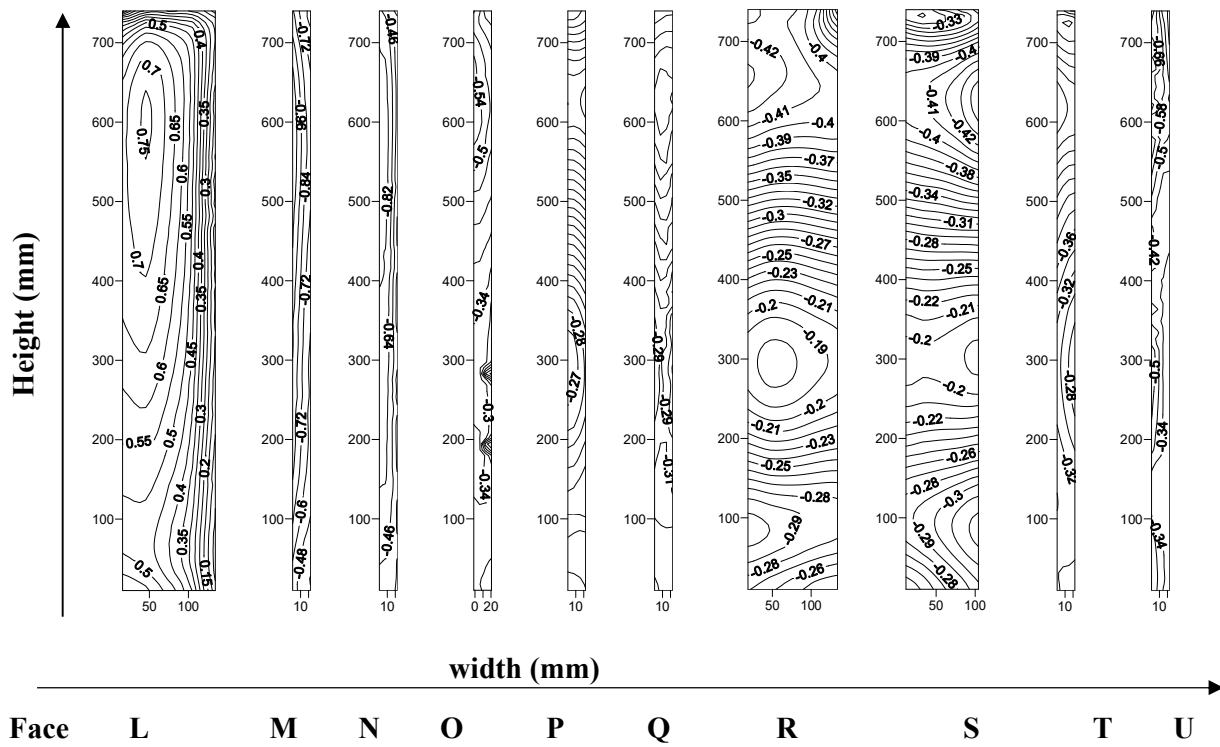
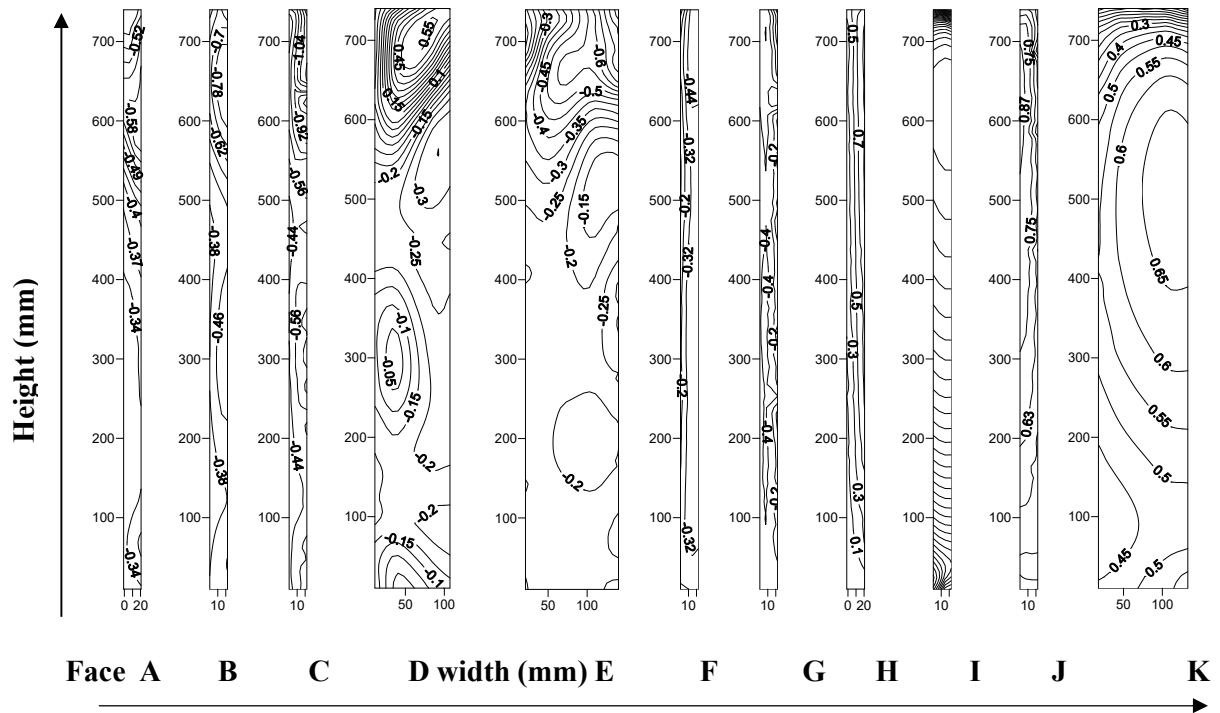


Figure 5.27 Distribution of wind pressure coefficient on the Y-shape with corner cut at  $135^\circ$  wind incidence angle

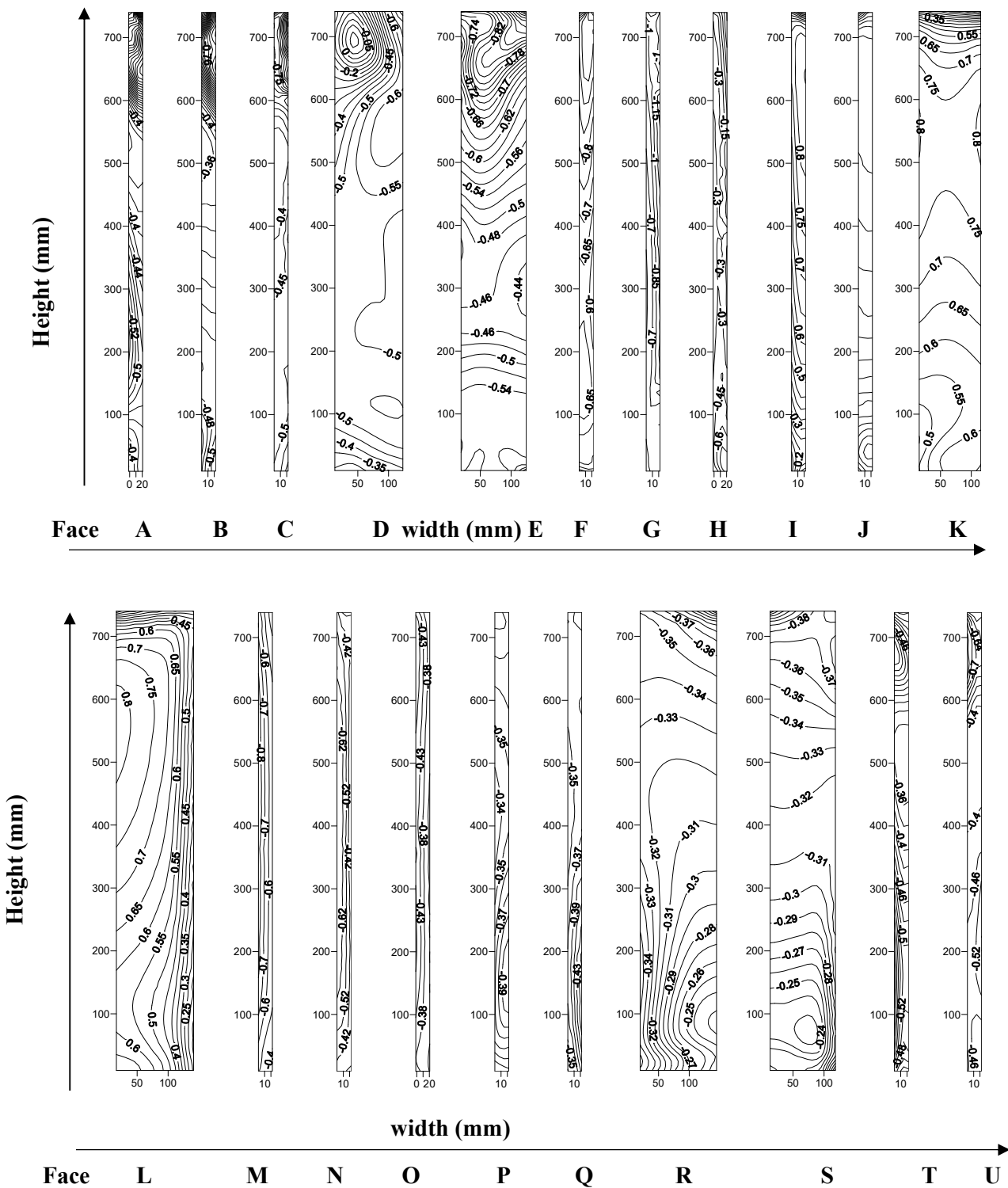


Figure 5.28 Distribution of wind pressure coefficient on the Y-shape with corner cut at  $150^\circ$  wind incidence angle

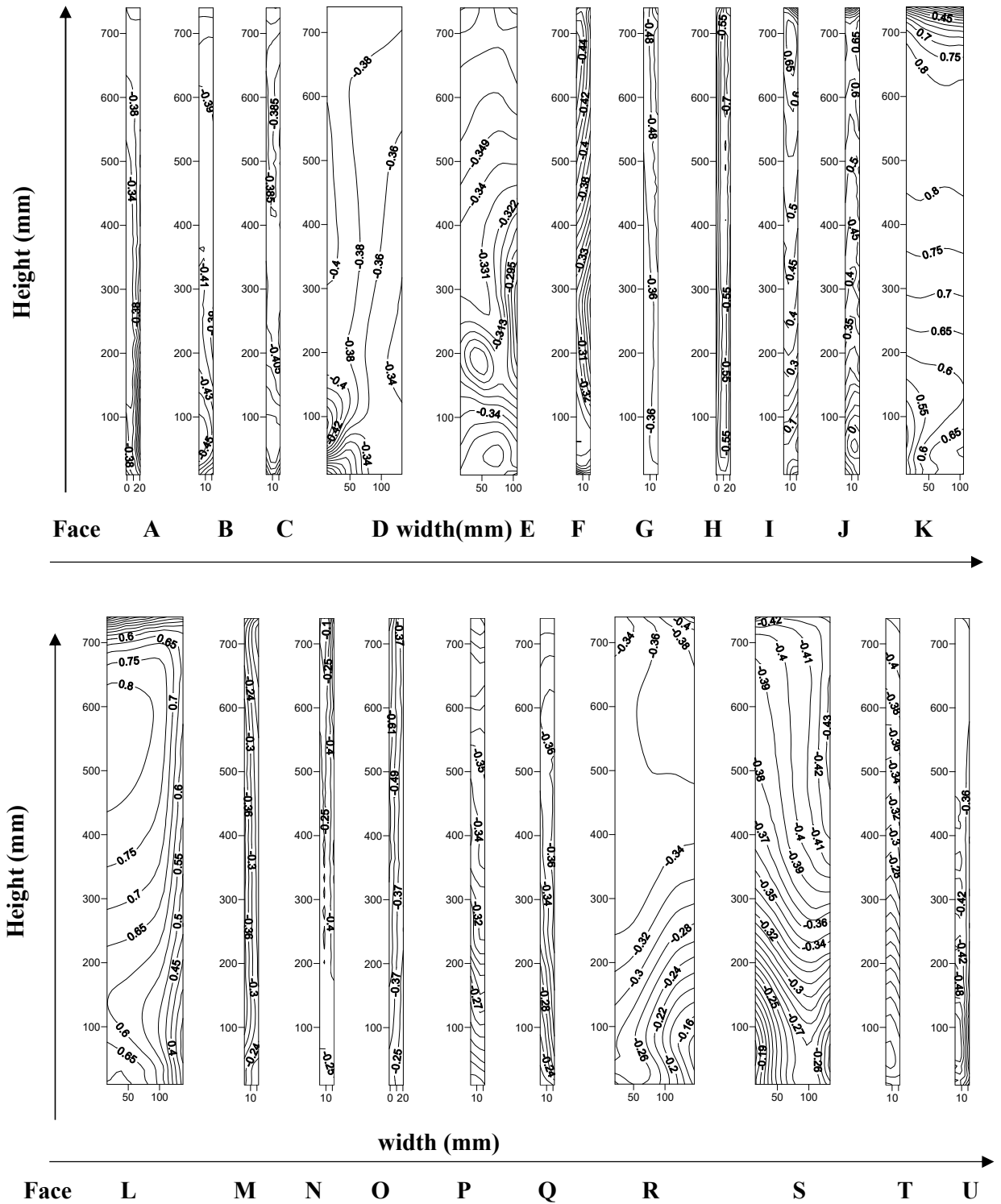


Figure 5.29 Distribution of wind pressure coefficient on the Y-shape with corner cut at 165° wind incidence angle

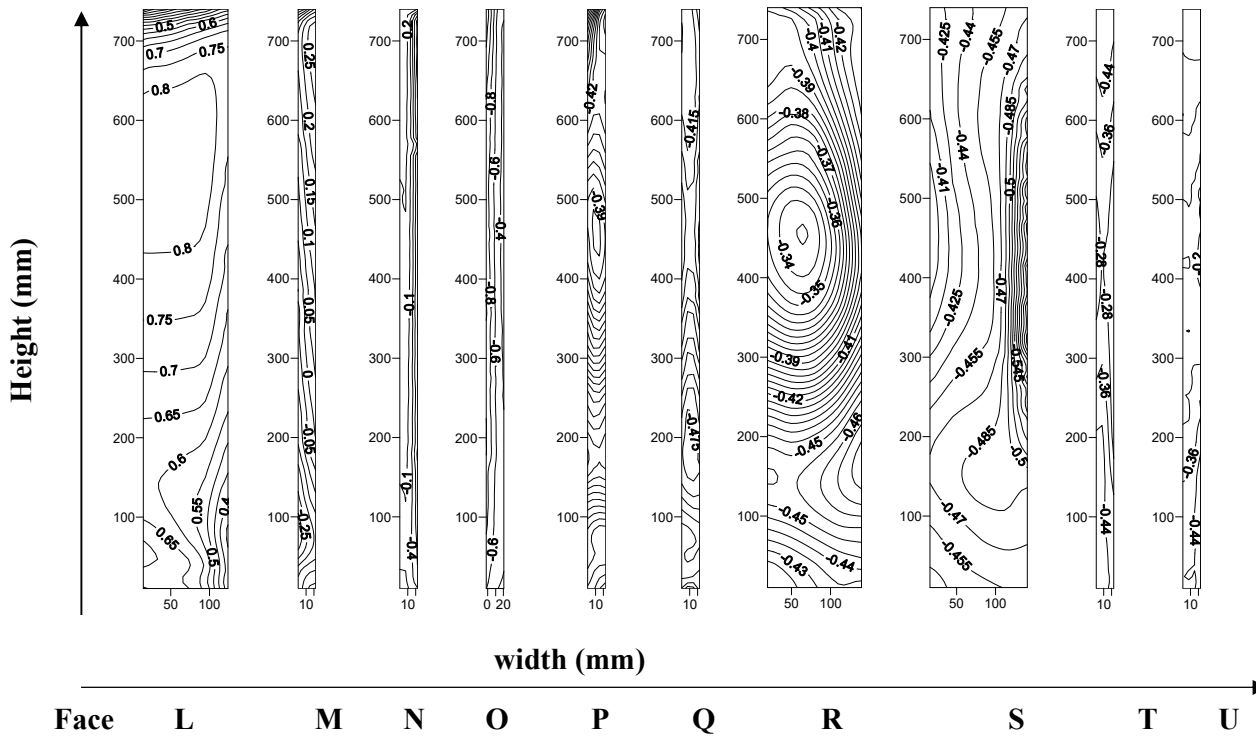
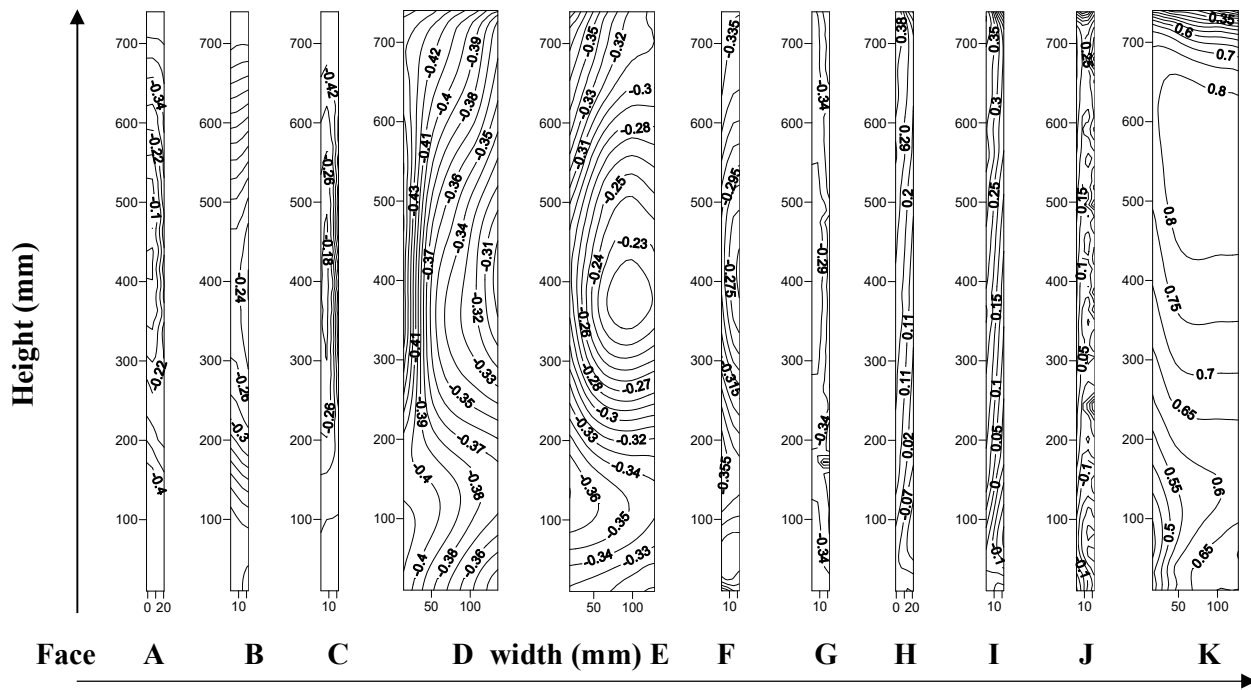


Figure 5.30 Distribution of wind pressure coefficient on the Y-shape with corner cut at  $180^\circ$  wind incidence angle

### **5.3.2 Vertical Pressure Distribution along the Height of the Building**

The  $C_{p,mean}$  distribution along the centre line of each face for building model of irregular “Y” shape which is having the corner cut, the pressure distribution pattern is graphically depicted in Figure 5.31 Mean pressure distribution on the vertical centre line for Y shape with corner cut for wind incidence angle from  $0^0$  to  $180^0$  at an interval of  $15^0$ . The pressure on each face at each wind incidence angle is presented. The minimum pressure on face-A of  $-0.95$  at  $60^0$  wind incidence angle near 600 mm height of the model while the greatest of  $0.89$  at  $0^0$  is observed above 500 mm height. The pressure is diversified in nature at certain faces and the pressure is noted positive while the other faces are under the impact of negative pressure. Likewise, the pressure distribution pattern is represented for all faces for all wind incidence angle.

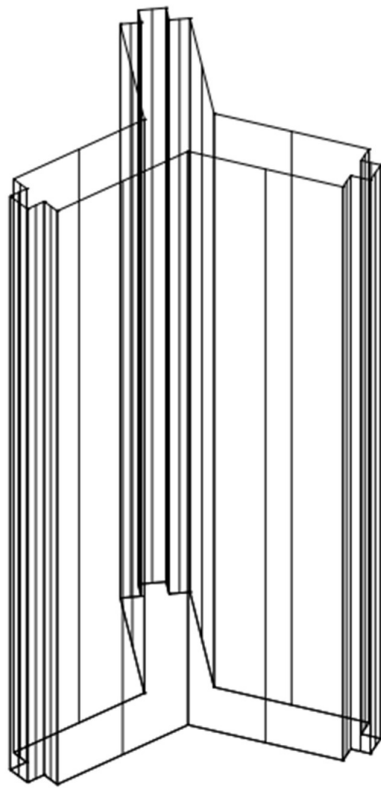
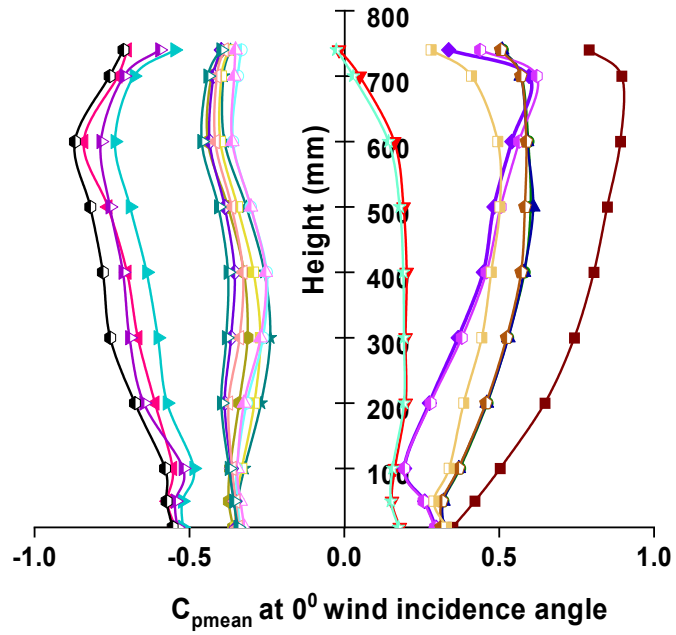


Figure 5.31(contd.) Mean pressure distribution on the vertical centre line for Y shape with corner cut

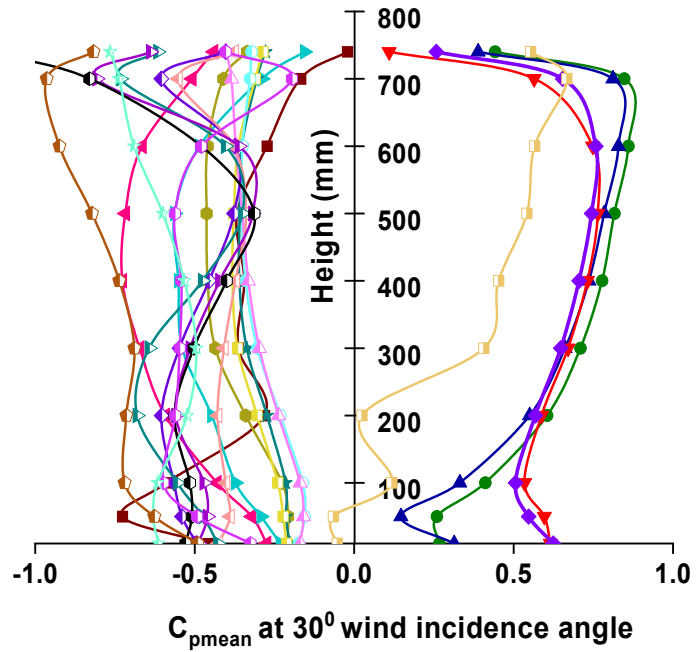
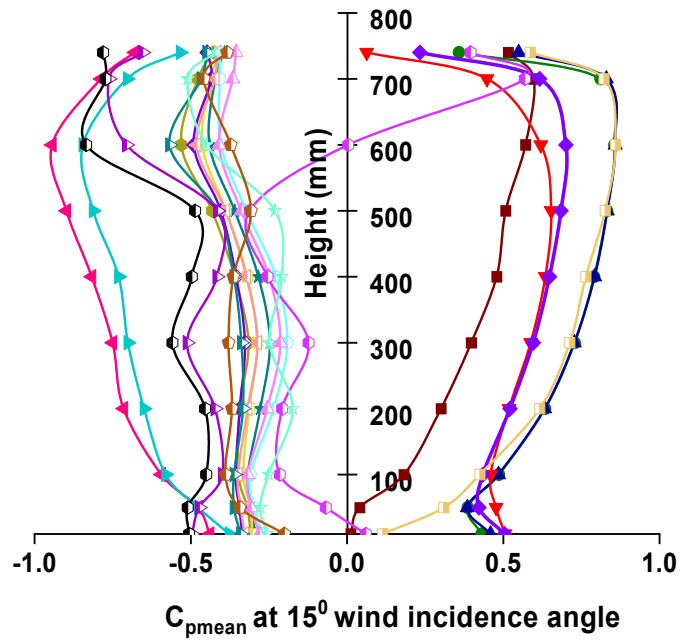


Figure 5.31(contd.) Mean pressure distribution on the vertical centre line for Y shape with corner cut

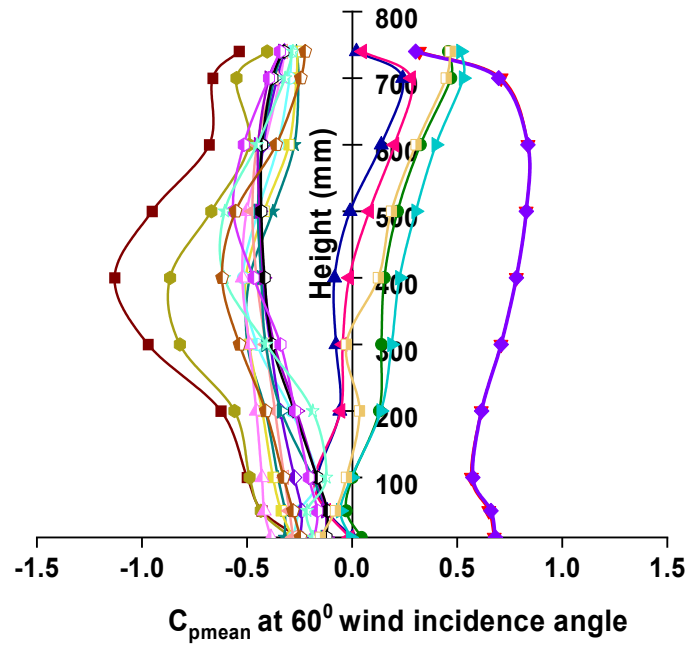
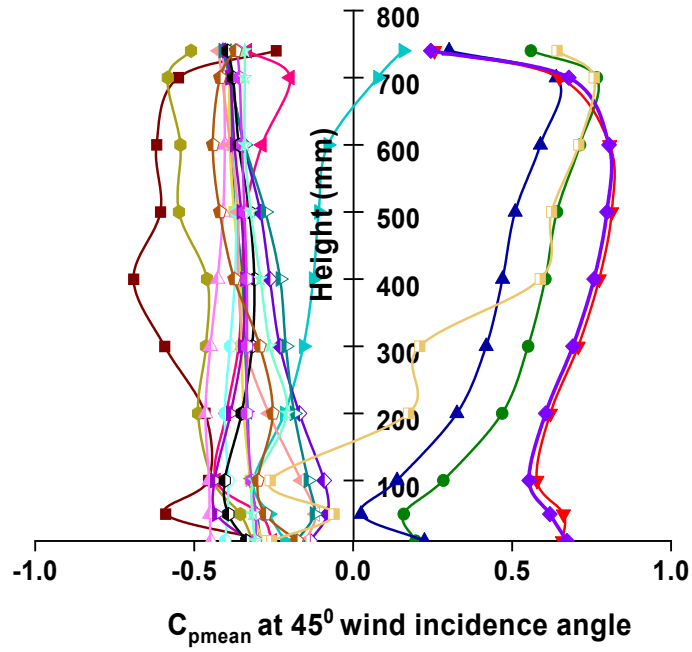
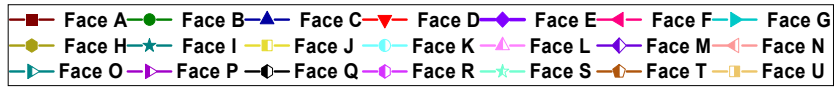


Figure 5.31 (contd.) Mean pressure distribution on the vertical centre line for Y shape with corner cut



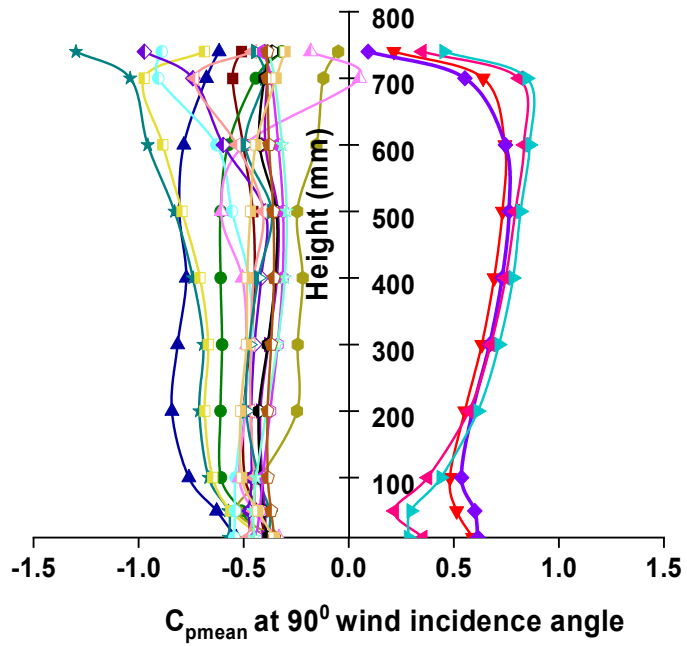
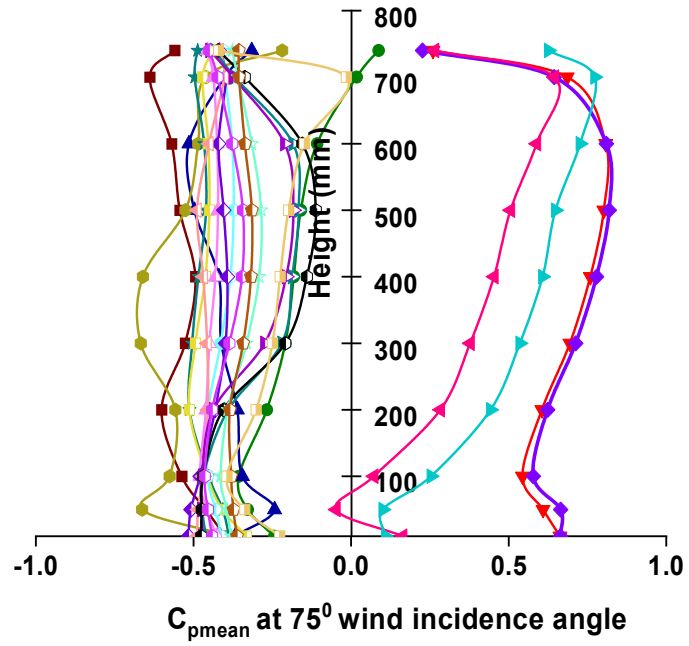
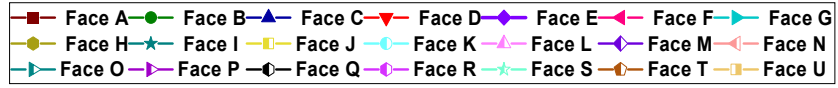


Figure 5.31(contd.) Mean pressure distribution on the vertical centre line for Y shape with corner cut

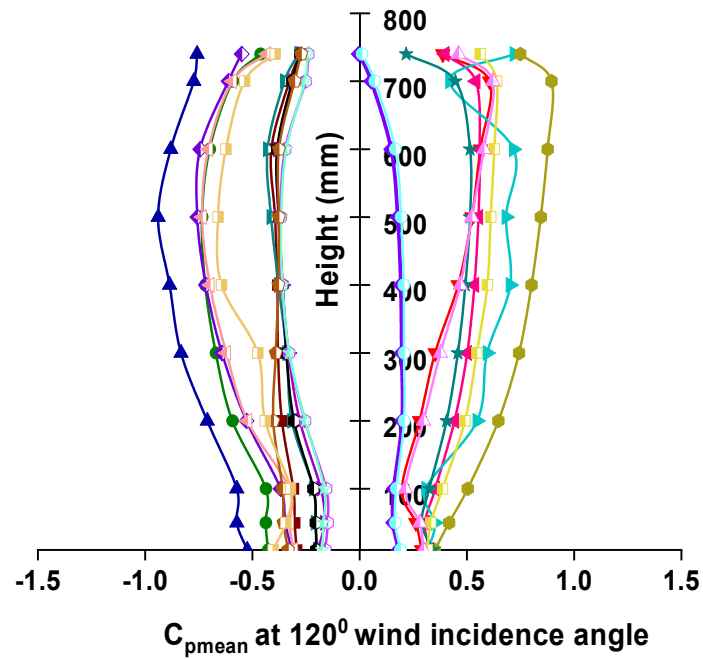
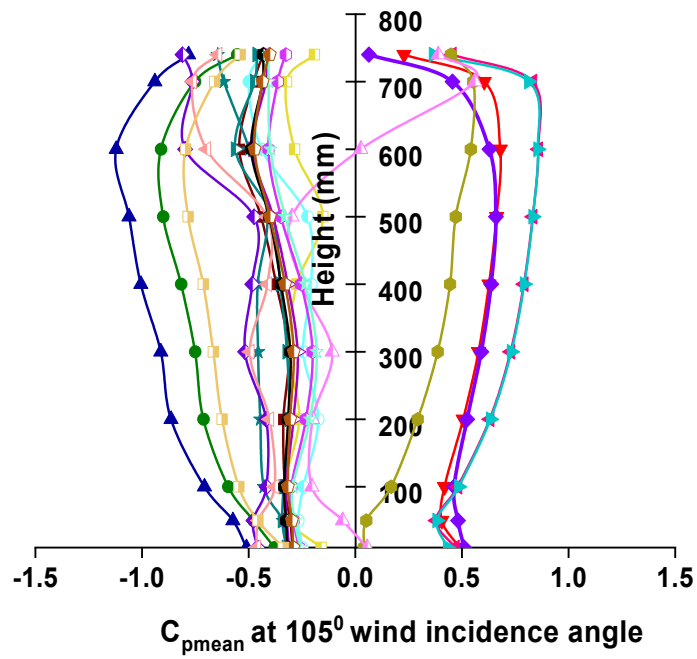


Figure 5.31 (contd.) Mean pressure distribution on the vertical centre line for Y shape with corner cut

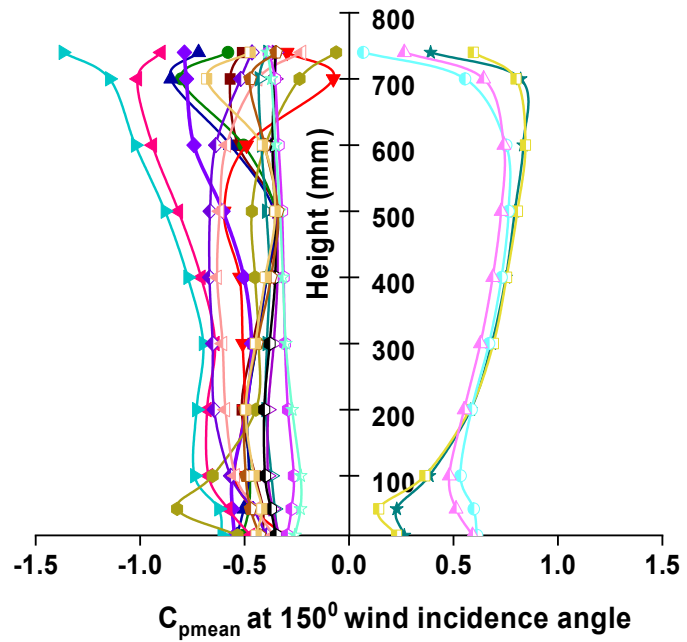
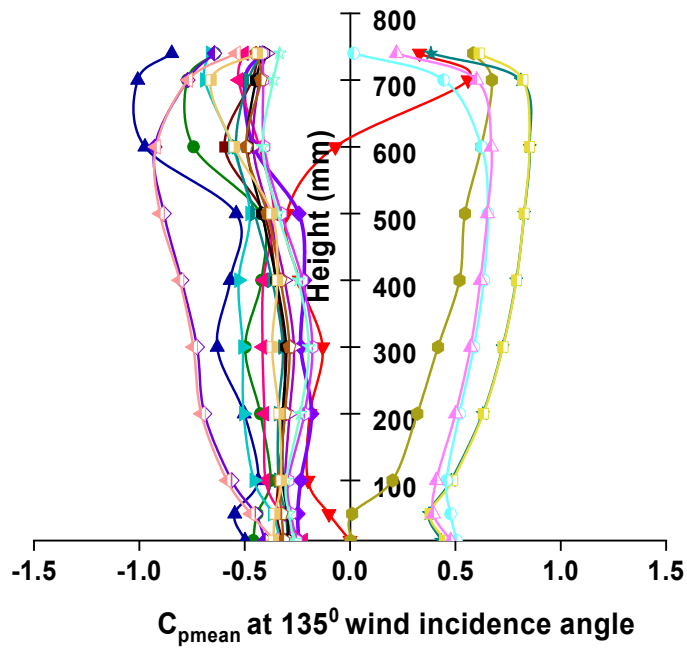


Figure 5.31(contd.) Mean pressure distribution on the vertical centre line for Y shape with corner cut

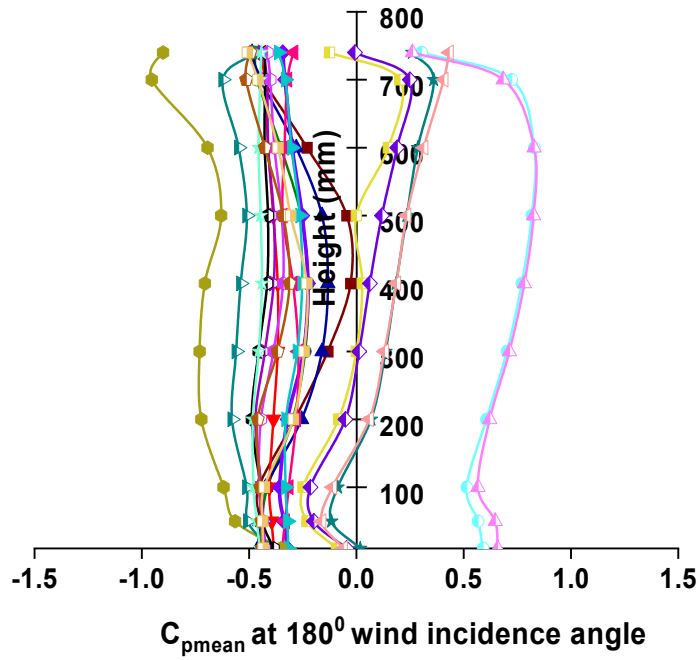
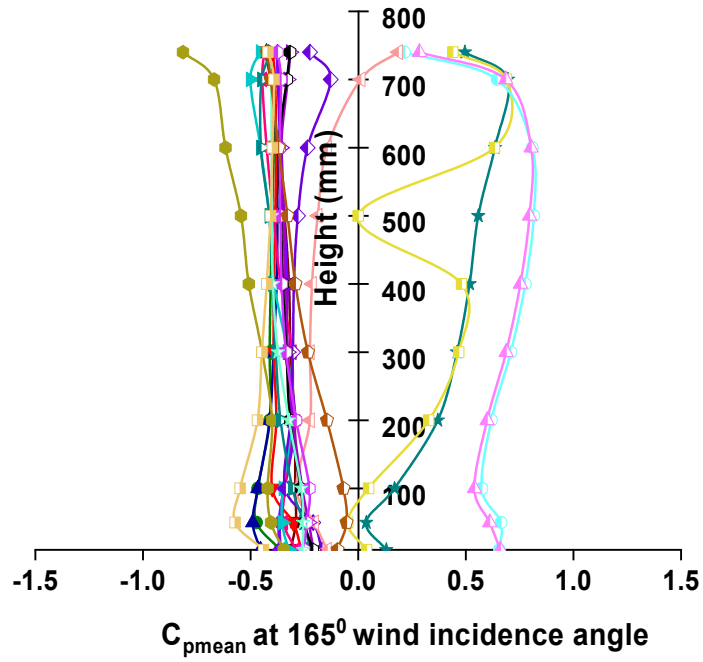
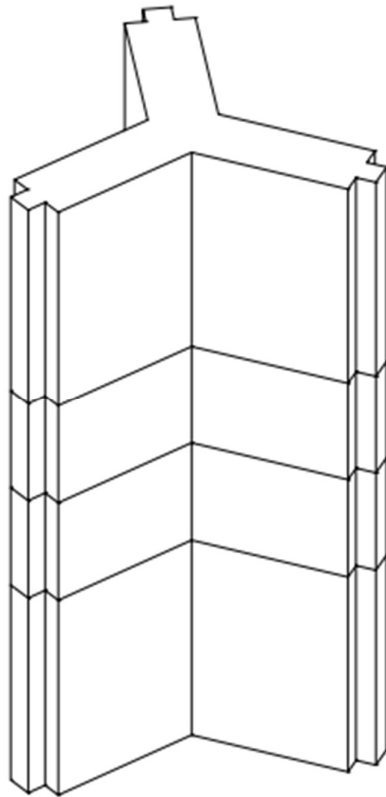
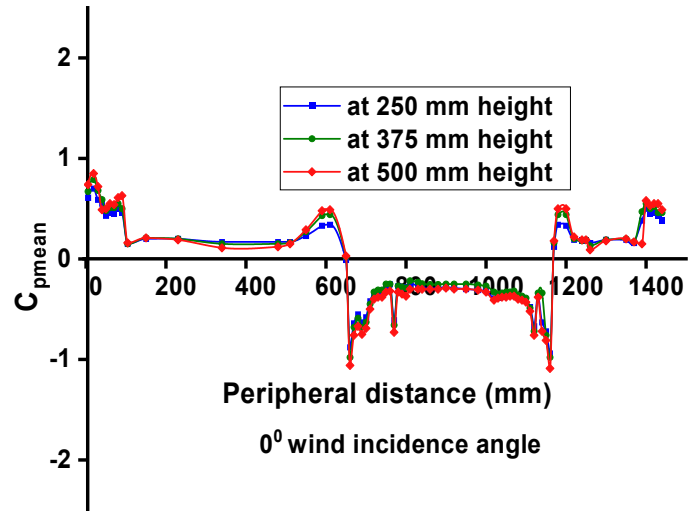


Figure 5.31 Mean pressure distribution on the vertical centre line for Y shape with corner cut

### **5.3.3 Horizontal Pressure Distribution along the Peripheral Distance of Building**

The pressure distribution around the model helps to evaluate the influence of external pressure at different levels in Figure 5.32 Mean pressure distribution along the peripheral distance of the Y-shape with corner cut, in this study the investigation of pressure distribution along the horizontal peripheral distance is plotted graphically at three different levels that are one third height of the building, mid height of the building, and two third height of the height of the building model. The pressure has diversified nature like for the faces which are under the direct exposure to wind having the positive pressure while other faces have different characteristics of wind like separation, reattachment and vortex shedding that is why the wind effect investigation is necessary for the high rise projects.



**Figure 5.32(contd.) Mean pressure distribution along the peripheral distance of the Y-shape with corner cut**

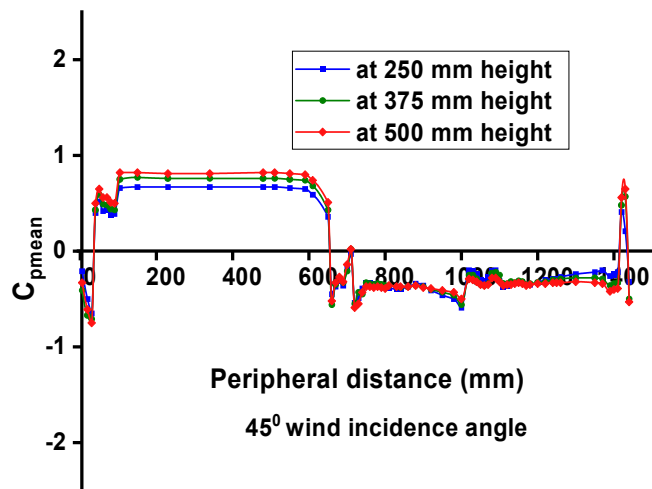
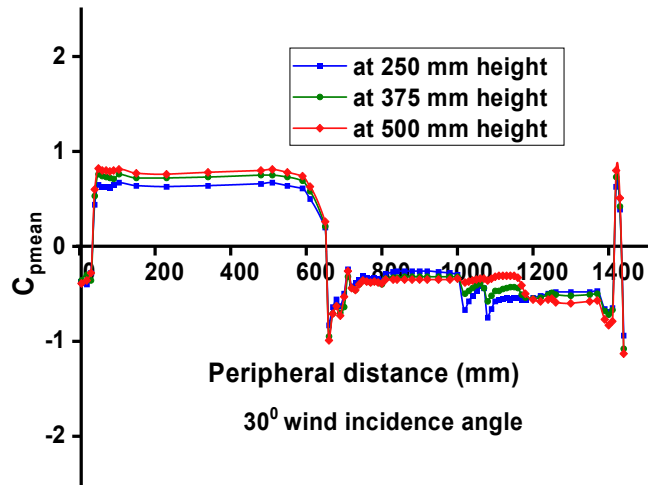
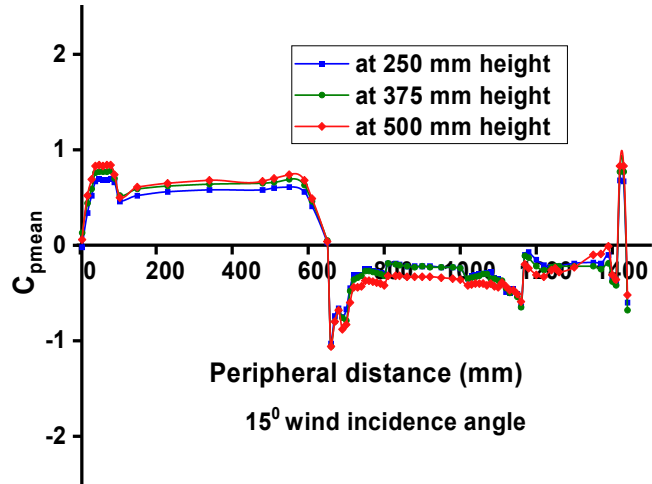


Figure 5.32(contd.) Mean pressure distribution along the peripheral distance of the Y-shape with corner cut

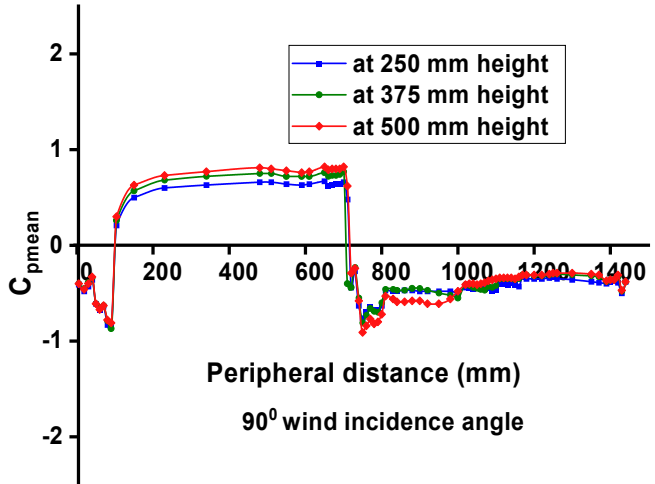
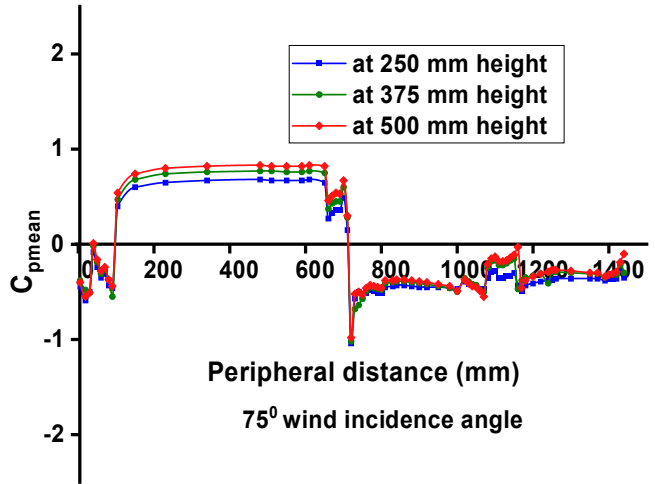
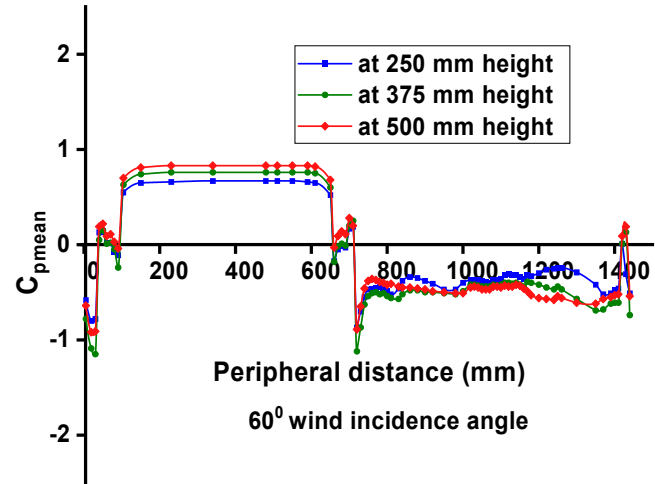


Figure 5.32(contd.) Mean pressure distribution along the peripheral distance of the Y-shape with corner cut



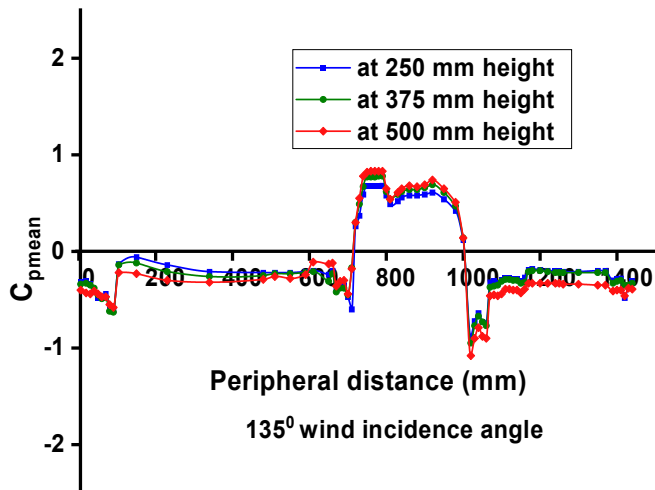
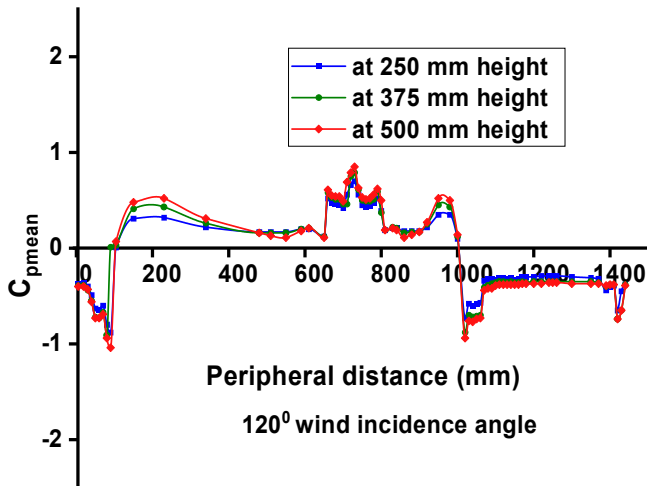
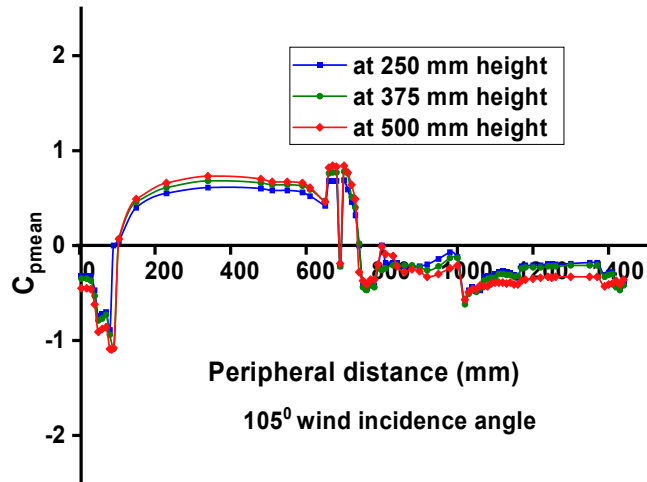


Figure 5.32(contd.) Mean pressure distribution along the peripheral distance of the Y-shape with corner cut

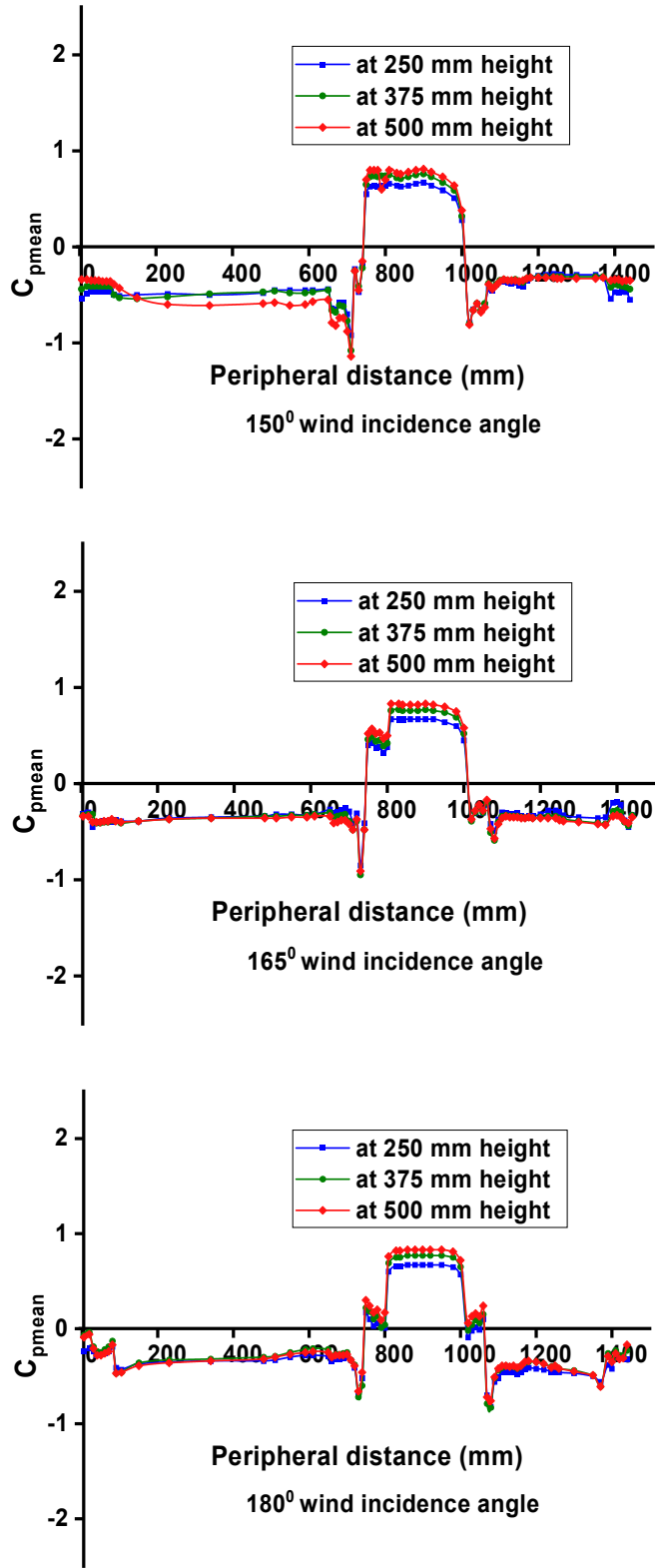


Figure 5.32 Mean pressure distribution along the peripheral distance of the Y-shape with corner cut

### 5.3.4 Force Coefficients

The wind force coefficient in X and Y direction are  $C_{fx}$  and  $C_{fy}$  as presented graphically in Figure 5.33 Wind force coefficient of the Y-shape with corner cut for irregular model of “Y” shape which is having the corner cut in the corners. The  $C_{fx}$  is maximum for  $90^\circ$  wind incidence angle while minimum  $C_{fx}$  is noted in the case of  $135^\circ$  wind incidence angle. The  $C_{fy}$  is maximum in  $90^\circ$  winds whereas the minimum  $C_{fy}$  of -0.62 is observed for  $30^\circ$  wind incidence angle.

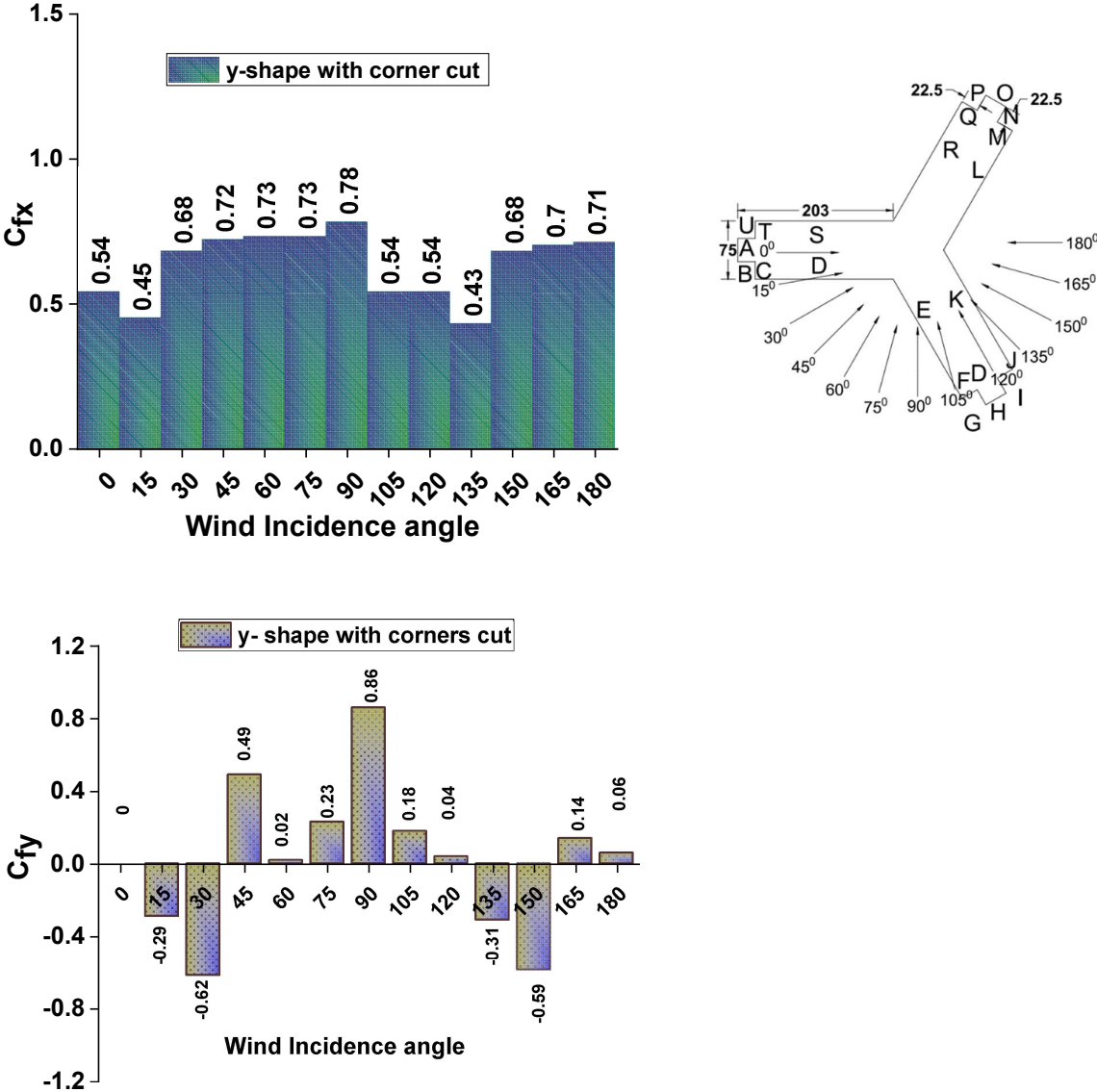


Figure 5.33 Wind force coefficient of the Y-shape with corner cut

### 5.3.5 Moments Coefficients

The moment coefficient in X and Y direction are calculated after performing the numerical simulation for investigating the wind generated effects for irregular model of “Y” shape which is having the corner cut. The moment coefficient is investigated by the steps provided in the wind tunnel manual. The maximum  $C_{mx}$  of 0.30 is noted at  $30^\circ$  winds while the minimum  $C_{mx}$  of -0.29 is found at  $90^\circ$  winds. The greatest  $C_{my}$  of 0.38 is noted in the case of  $45^\circ$  wind while least  $C_{my}$  of 0.31 is spotted at  $0^\circ$  wind. Maximum moment coefficient in x- direction is more or less same with the minimum moment coefficient in x direction but the different is found one is in positive and another is into the negative. Moment coefficient is presented in Figure 5.34 Wind moment coefficient of the Y-shape with corner cut.

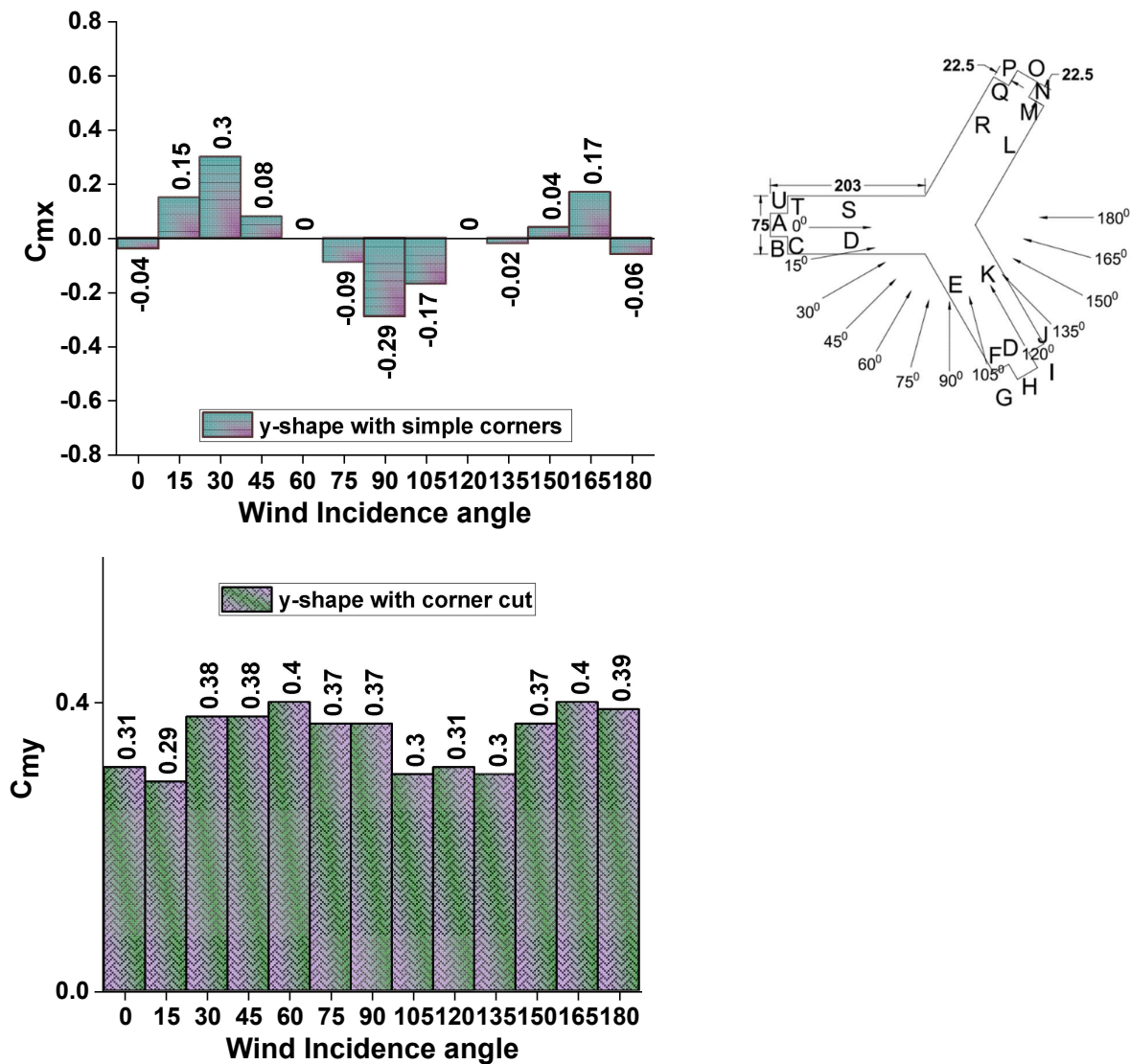


Figure 5.34 Wind moment coefficient of the Y-shape with corner cut

### 5.3.6 External Pressure Coefficients

The external pressure coefficient is investigated and tabulated in Table-5.2 External Pressure Coefficients for model-F (Y- Shape Corner-Cut) at each face for wind angle varies in between  $0^{\circ}$  to  $180^{\circ}$  at the interval of  $15^{\circ}$ . The external pressure coefficient is obtained after drawing the lines into the geometry and for each face a local coordinate frame is defined. The data for pressure is exported on those lines with respect to the local coordinate frame defined. The calculation are made into the excel and the mean external pressure on each face is tabulated. The maximum external pressure is 0.70 on face-B at  $15^{\circ}$ , face-E at  $75^{\circ}$  and face-K at  $165^{\circ}$  while the minimum external pressure is of -0.83 and is observed on face-C at  $105^{\circ}$  and face-G at  $150^{\circ}$ .

**Table-5.2 External Pressure Coefficients for model-F (Y- Shape Corner-Cut)**

Model-F (Y-Shape Corner-Cut)													
Face	0°	15°	30°	45°	60°	75°	90°	105°	120°	135°	150°	165°	180°
<b>A</b>	<b>0.66</b>	0.30	-0.39	<b>-0.52</b>	<b>-0.64</b>	-0.48	-0.44	-0.39	-0.35	-0.40	-0.47	-0.37	-0.27
<b>B</b>	0.46	<b>0.70</b>	0.60	0.01	0.14	-0.18	-0.51	0.67	-0.54	-0.50	-0.49	-0.41	-0.34
<b>C</b>	0.49	0.69	0.62	0.47	0.01	-0.31	-0.73	<b>-0.83</b>	<b>-0.69</b>	-0.55	-0.48	-0.40	-0.35
<b>D</b>	0.14	0.52	<b>0.66</b>	0.42	0.68	0.63	0.55	0.46	0.26	-0.11	-0.47	-0.37	-0.42
<b>E</b>	0.26	0.46	0.56	<b>0.70</b>	<b>0.68</b>	<b>0.70</b>	<b>0.66</b>	0.52	0.15	-0.27	-0.57	-0.34	-0.35
<b>F</b>	<b>-0.75</b>	<b>-0.82</b>	-0.64	-0.37	0.01	0.37	0.64	<b>0.70</b>	0.48	-0.33	-0.73	-0.36	-0.40
<b>G</b>	-0.55	-0.62	-0.43	-0.17	0.14	0.39	0.58	0.41	0.46	-0.35	<b>-0.83</b>	-0.41	-0.39
<b>H</b>	-0.40	-0.38	-0.37	-0.47	<b>-0.64</b>	<b>-0.68</b>	-0.45	0.22	<b>0.66</b>	0.42	-0.33	<b>-0.57</b>	<b>-0.59</b>
<b>I</b>	-0.40	-0.33	-0.31	-0.35	-0.23	-0.49	<b>-0.79</b>	-0.44	0.46	<b>0.69</b>	0.62	0.43	0.16
<b>J</b>	-0.38	-0.36	-0.32	-0.35	-0.31	-0.45	-0.72	-0.27	0.48	0.66	0.63	0.37	0.04
<b>K</b>	-0.31	-0.30	-0.29	-0.37	-0.38	-0.41	-0.57	-0.26	0.15	0.53	<b>0.66</b>	<b>0.70</b>	<b>0.68</b>
<b>L</b>	-0.31	-0.31	-0.30	-0.44	-0.39	-0.44	-0.46	-0.10	0.26	0.47	0.57	0.64	<b>0.68</b>
<b>M</b>	-0.38	-0.37	-0.50	-0.25	-0.35	-0.43	-0.52	-0.57	<b>-0.69</b>	<b>-0.77</b>	-0.63	-0.28	0.04
<b>N</b>	-0.40	-0.36	-0.43	-0.30	-0.35	-0.46	-0.49	-0.48	-0.54	-0.63	-0.52	-0.30	0.16
<b>O</b>	-0.40	-0.39	-0.54	-0.26	-0.35	-0.31	-0.44	-0.39	-0.35	-0.39	-0.40	-0.41	<b>-0.59</b>
<b>P</b>	-0.55	-0.50	-0.49	-0.37	-0.35	-0.32	-0.38	-0.35	-0.40	-0.35	-0.36	-0.31	-0.39
<b>Q</b>	-0.75	-0.59	-0.52	-0.30	-0.35	-0.27	-0.31	-0.31	-0.34	-0.36	-0.37	-0.33	-0.40
<b>R</b>	0.26	-0.10	-0.49	-0.34	-0.39	-0.41	-0.34	-0.30	-0.29	-0.29	-0.32	-0.32	-0.35
<b>S</b>	0.14	-0.26	-0.58	-0.30	-0.38	-0.34	-0.35	-0.30	-0.29	-0.30	-0.31	-0.35	-0.42
<b>T</b>	0.49	-0.30	<b>-0.75</b>	-0.33	-0.41	-0.35	-0.38	-0.36	-0.34	-0.37	-0.45	-0.26	-0.35
<b>U</b>	0.46	0.28	0.01	-0.12	-0.23	-0.28	-0.41	-0.53	-0.40	-0.43	-0.48	-0.41	-0.34

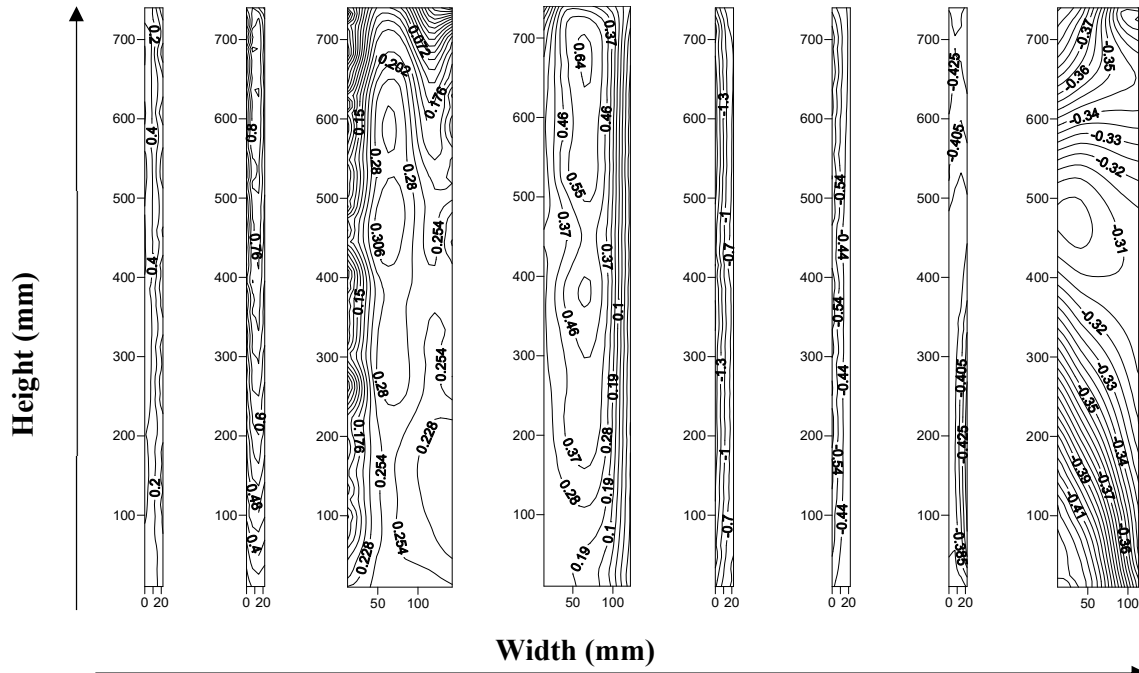
## **5.4 Y-shape with Chamfer Corners**

The land is in different irregular shape and to design the building in such irregular shape is possible through different shape such as “N”, “Y” or different shape and in this study the tri axial symmetry building of “Y” shape is done. Reduction of the wind effects on such types of building is done through the various corner configuration like corner cut, chamfer and filet etc. Wind effects are investigated using numerical simulation and results are generated and calculated using the procedure provided in wind tunnel manual and report no 67. The procedure applied is as per the IS code 875 part 3:2015. The wind is applied as per power law in the numerical simulation and the result are explained in the form of pressure contours, pressure distribution on the vertical centre line and pressure distribution on the horizontal line along the peripheral distance at various level like one third, two third and mid height. The result of force coefficient and moment coefficient are also obtained and explained into details in various forms.

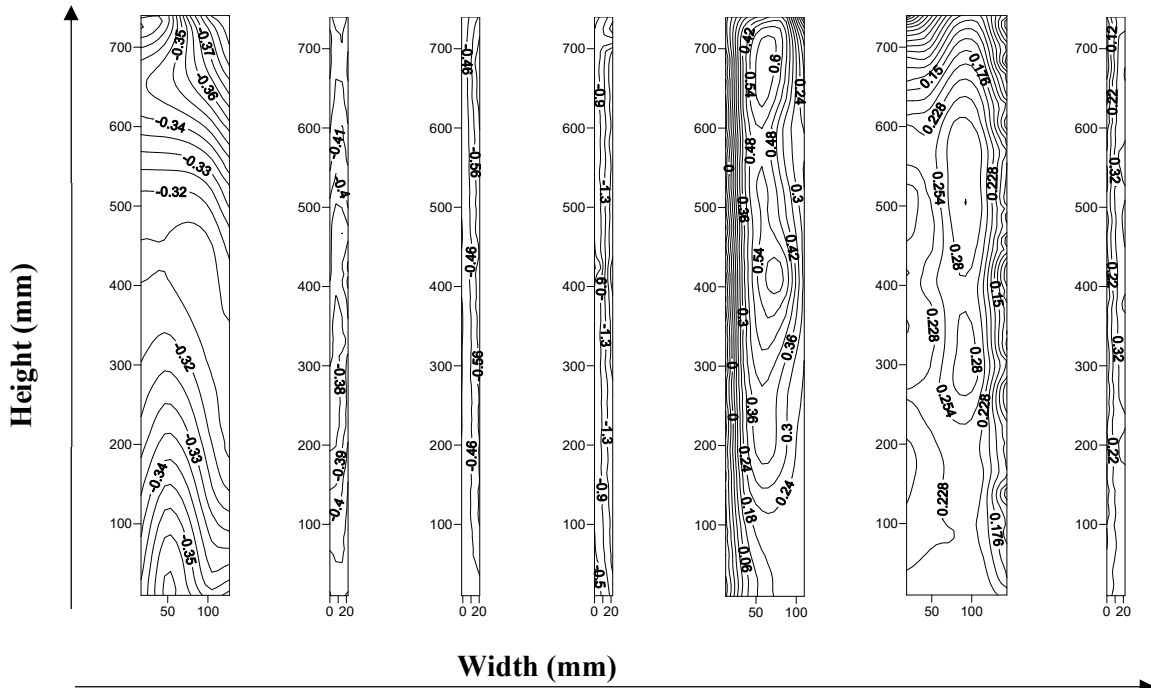
### **5.4.1 Pressure Contours**

Pressure contours depict the pressure along the height and width of the face of model having chamfer corner into Y-shape. Pressure is investigated for the wind incidence angle from  $0^0$  to  $180^0$  at an interval of  $15^0$ . Pressure is investigated after accounting the wind effects like vortex shedding, up wash down wash and various other phenomena. The pressure on the wind ward is positive pressure because wind is directly acting on the face of the model and pressure acting is more than the reference pressure. Also since pressure is positive while the other faces are having the wind characteristics which are different because the flow is trapped in some of the wind incidence angle and also since wind is on some faces are attaching and detaching the wind at different condition. Pressure contours are presented from Figure 5.35 Distribution of wind pressure coefficient on the Y-shape with chamfer corner at  $00$  wind incidence angle to Figure 5.47 Distribution of wind pressure coefficient on the Y-shape with chamfer corner at  $1800$  wind incidence angle.

Wind is having various phenomena and the behaviors of wind pressure is depicted in the form of pressure contours and the pressure with respect to height and width is varied and same can be understood more precisely with the help of such pressure contours. The pressure is varied from positive to negatives, mainly pressure is found negative in the downstream faces and this is because of the vortices that are generated in the wake. The wake region is also varied for the building model having chamfer corners and negative pressure that is suction is found in between the different limbs of Y-shape model.



Face A B C D E F G H



Face I J K L M N O

Figure 5.35 Distribution of wind pressure coefficient on the Y-shape with chamfer corner at  $0^\circ$  wind incidence angle



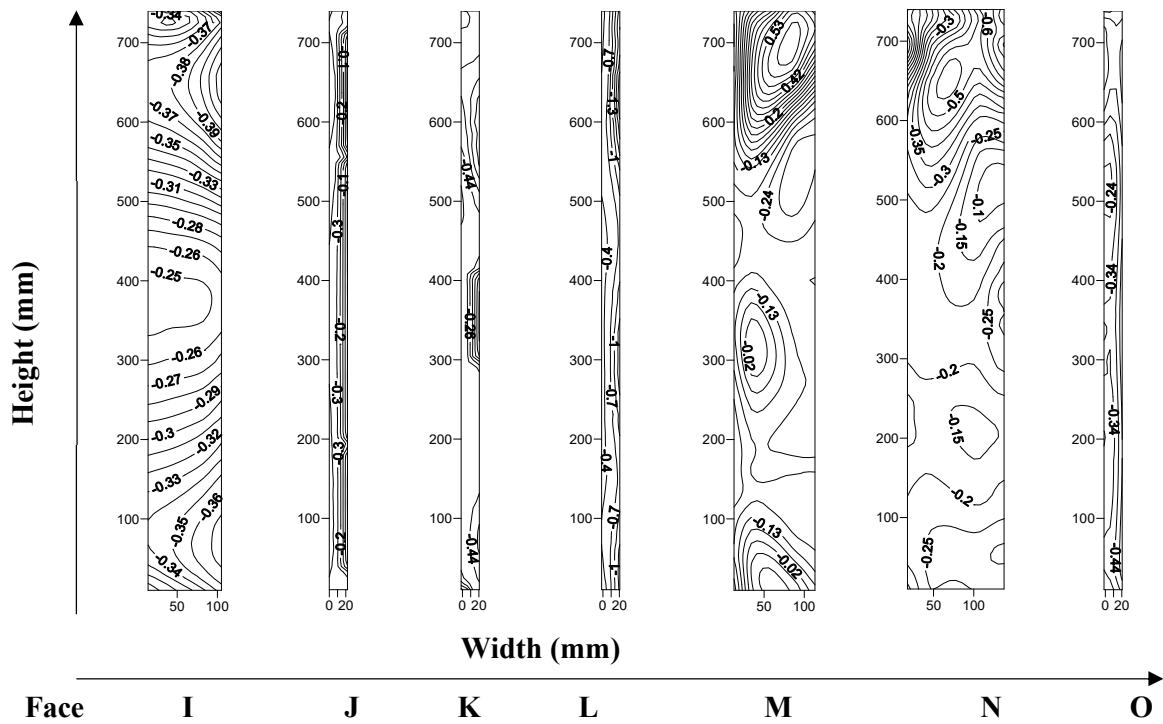
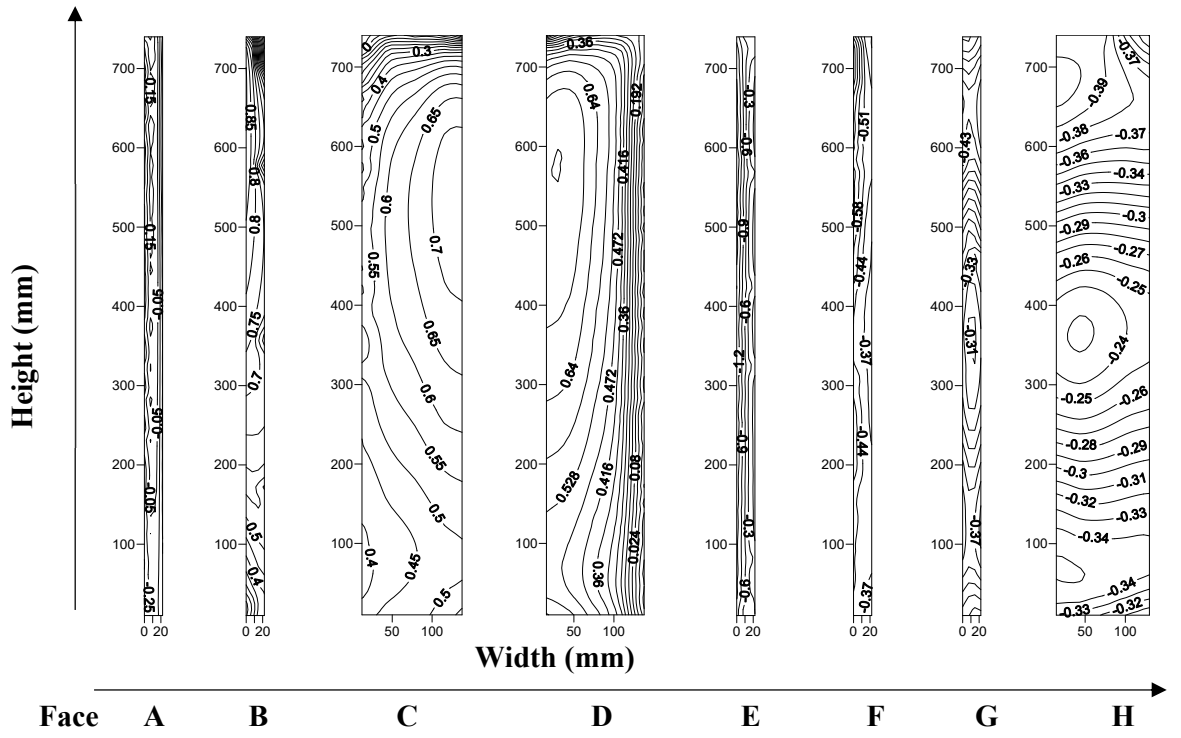


Figure 5.36 Distribution of wind pressure coefficient on the Y-shape with chamfer corner at 15° wind incidence angle

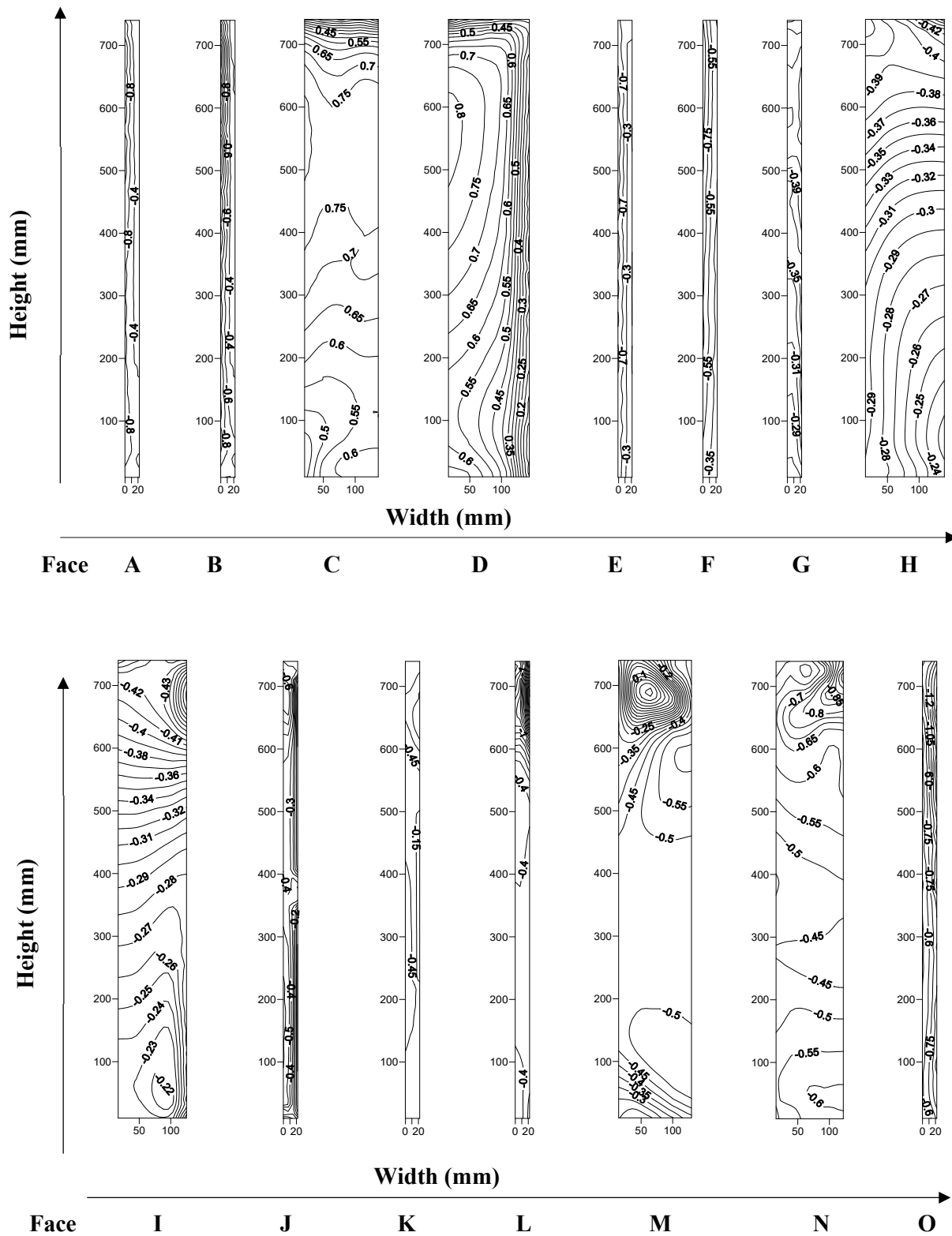


Figure 5.37 Distribution of wind pressure coefficient on the Y-shape with chamfer corner at 30° wind incidence angle

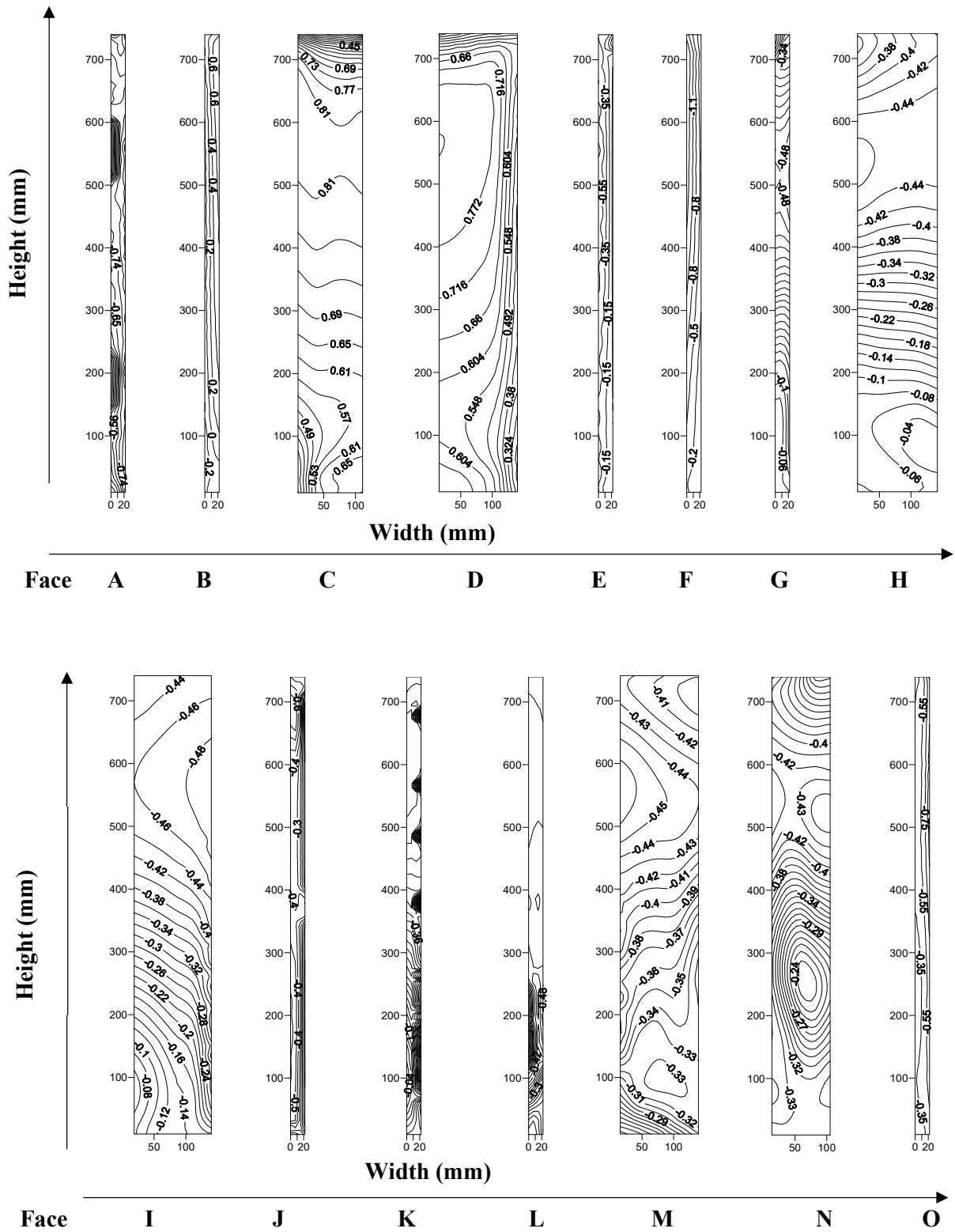


Figure 5.38 Distribution of wind pressure coefficient on the Y-shape with chamfer corner at 45° wind incidence angle

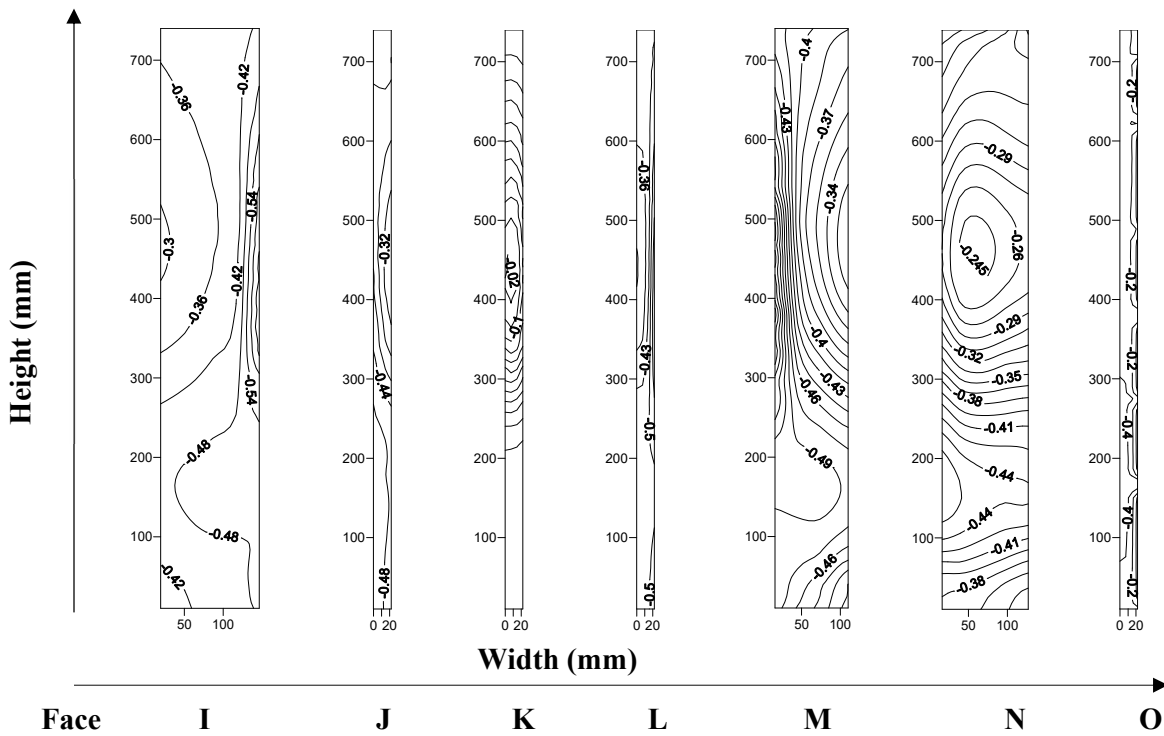
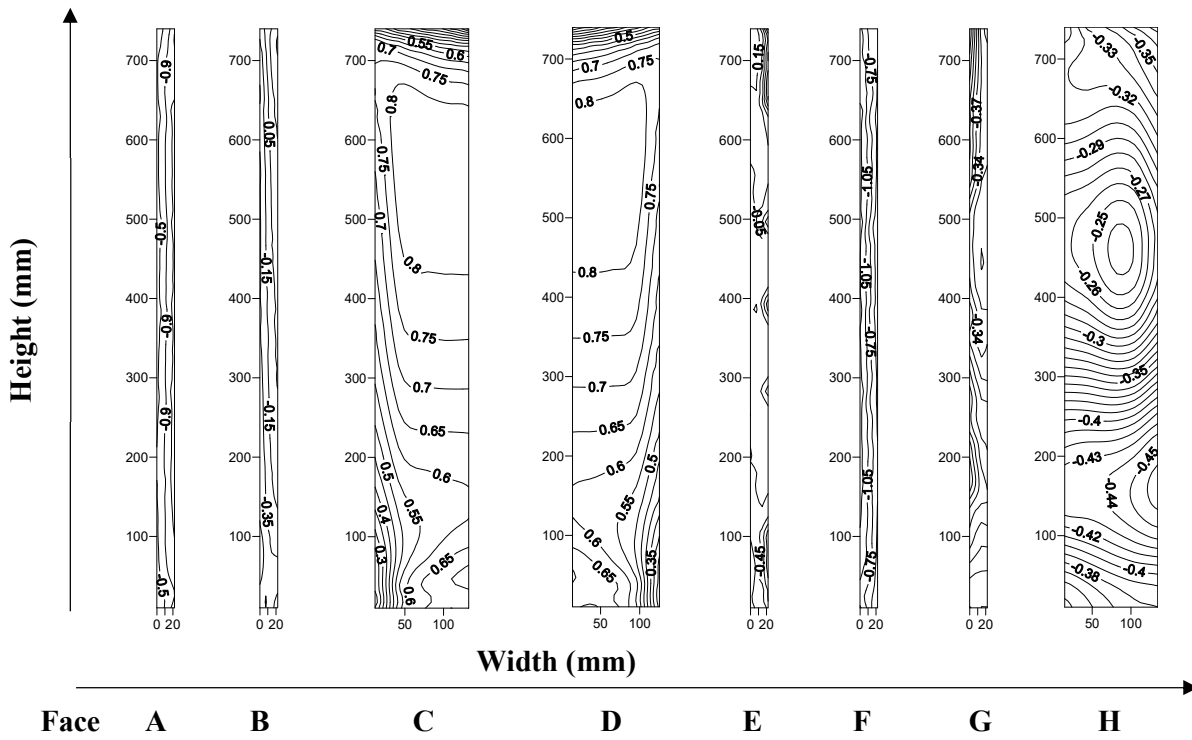


Figure 5.39 Distribution of wind pressure coefficient on the Y-shape with chamfer corner at  $60^\circ$  wind incidence angle

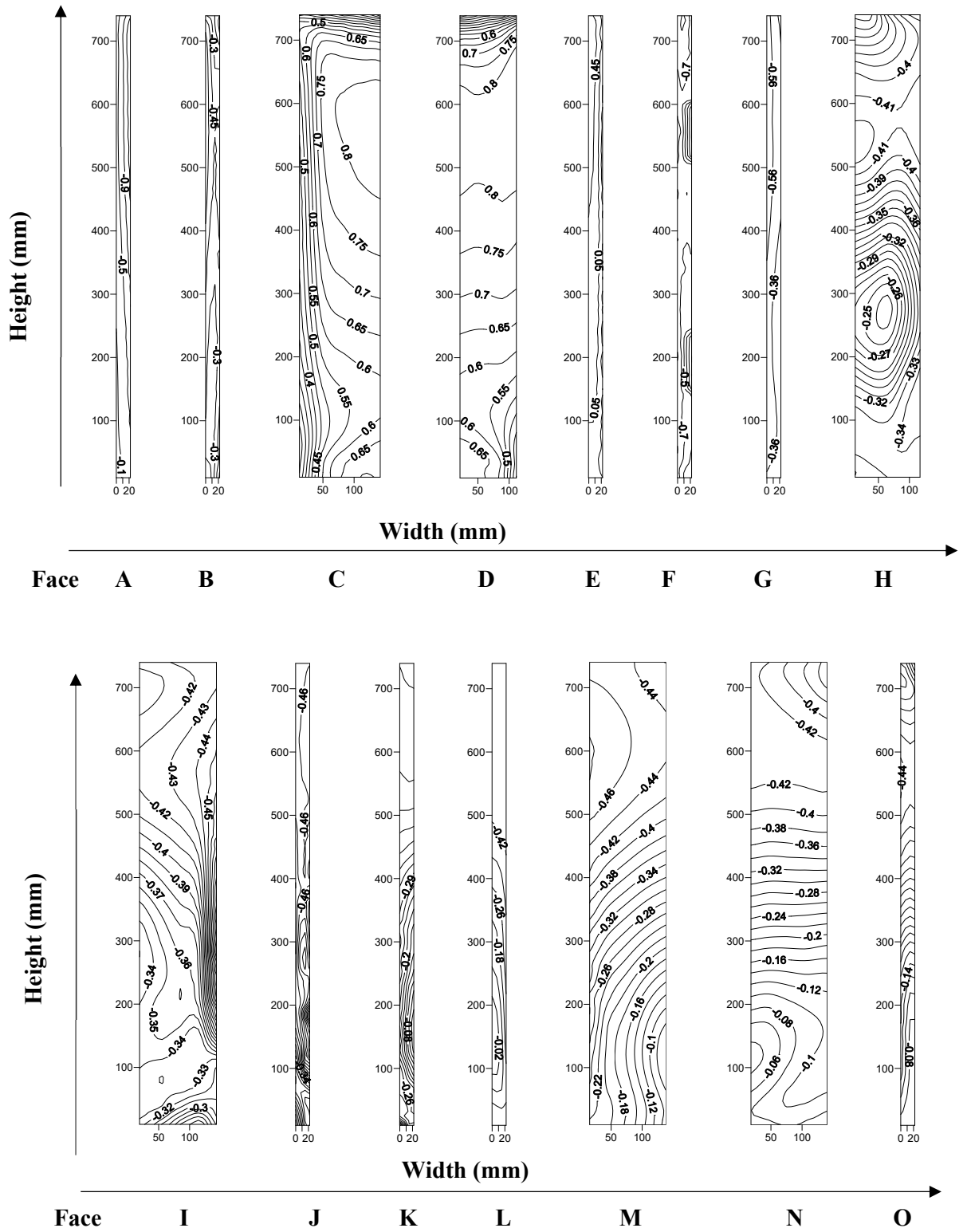


Figure 5.40 Distribution of wind pressure coefficient on the Y-shape with chamfer corner at 75° wind incidence angle

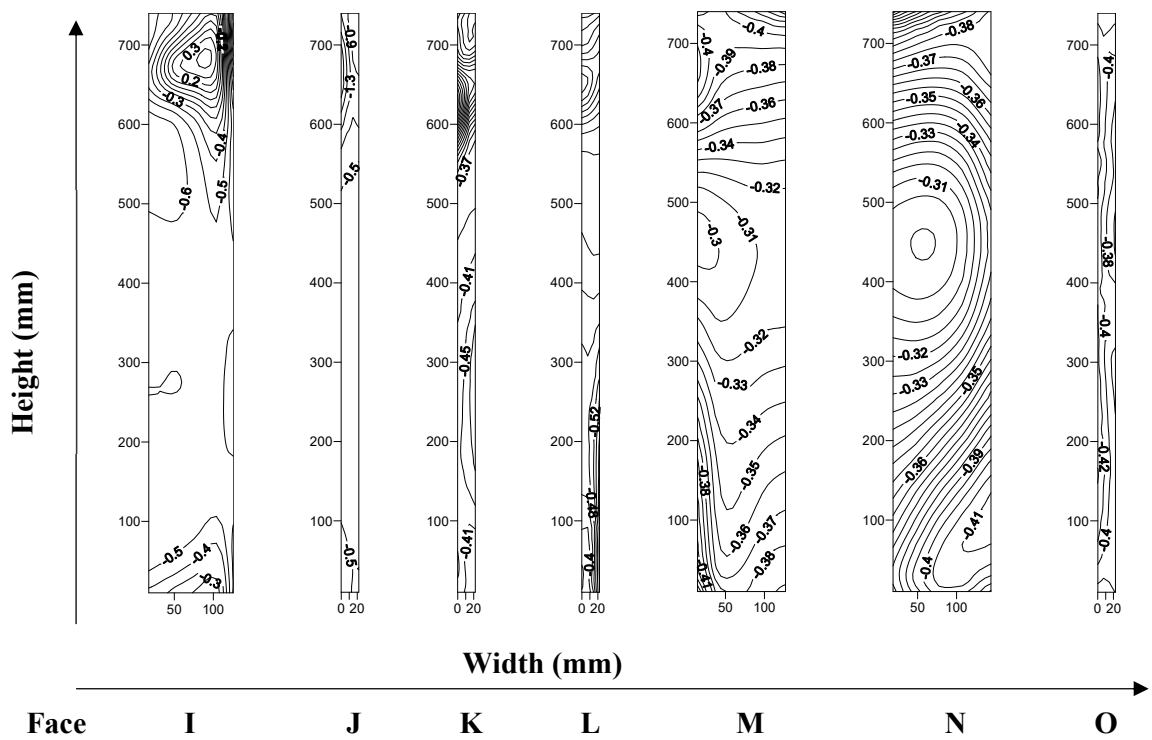
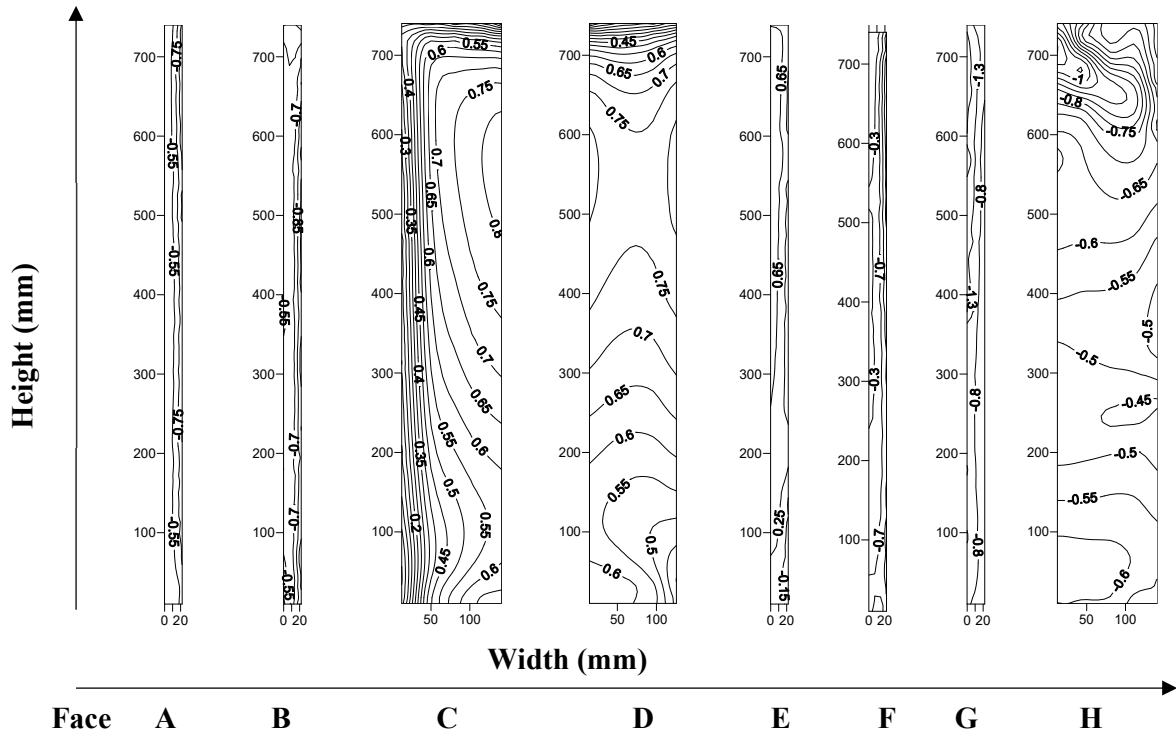


Figure 5.41 Distribution of wind pressure coefficient on the Y-shape with chamfer corner at 90° wind incidence angle

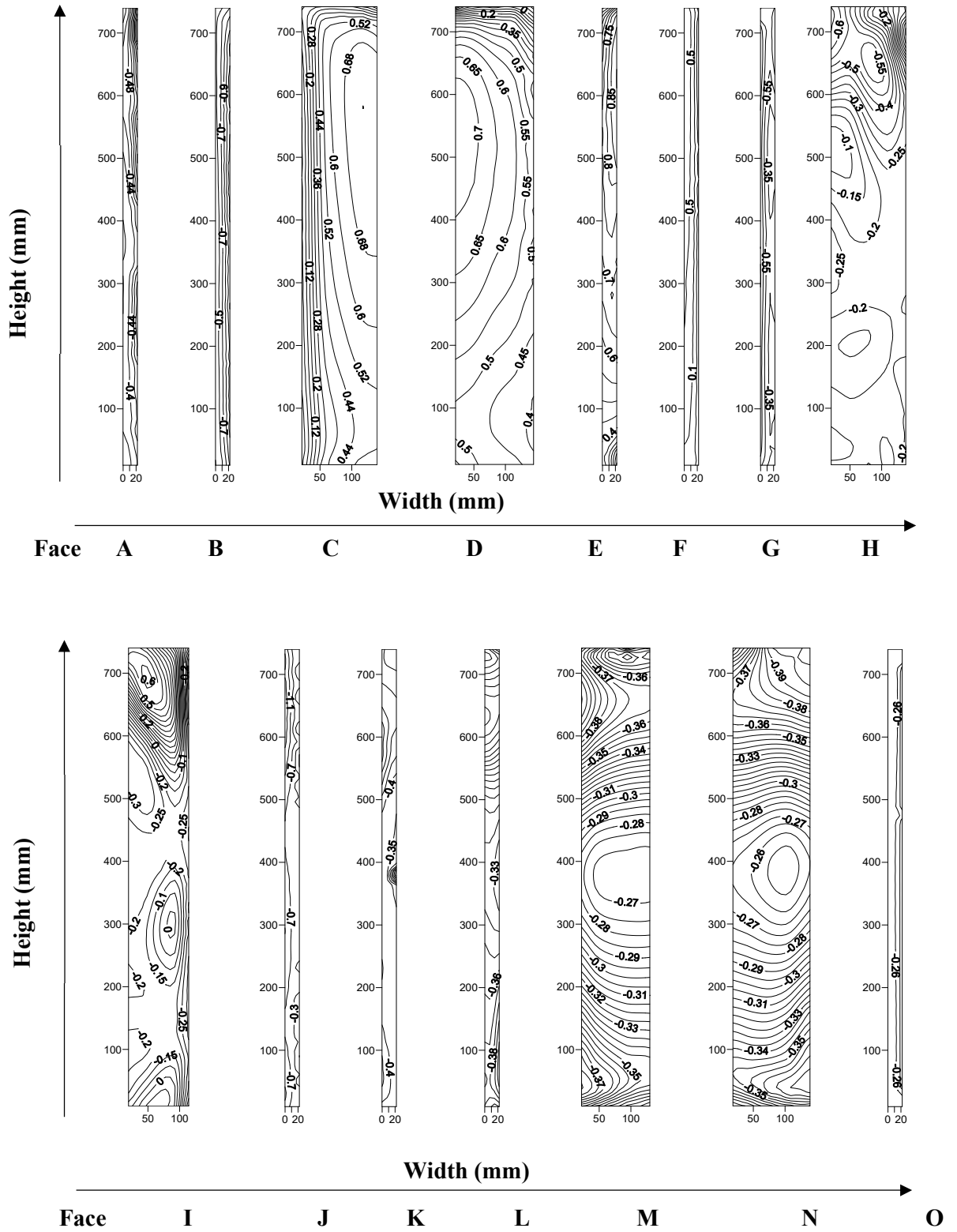


Figure 5.42 Distribution of wind pressure coefficient on the Y-shape with chamfer corner at 105° wind incidence angle

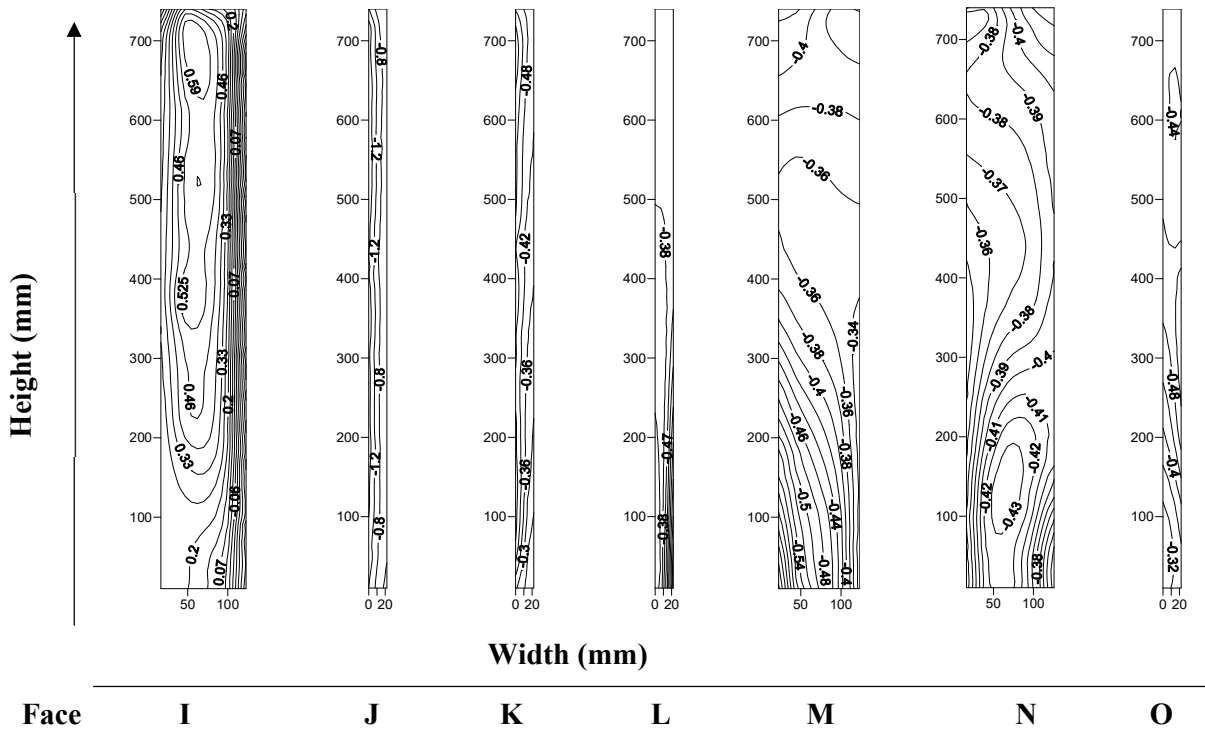
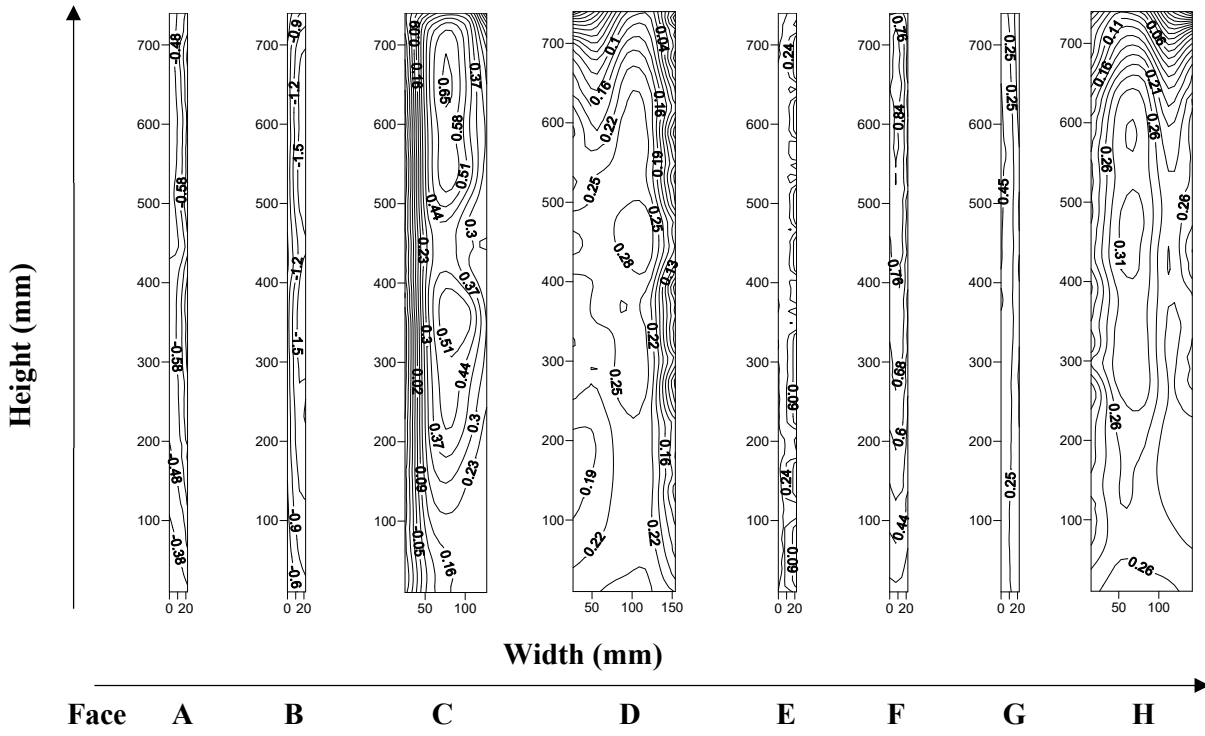


Figure 5.43 Distribution of wind pressure coefficient on the Y-shape with chamfer corner at  $120^\circ$  wind incidence angle



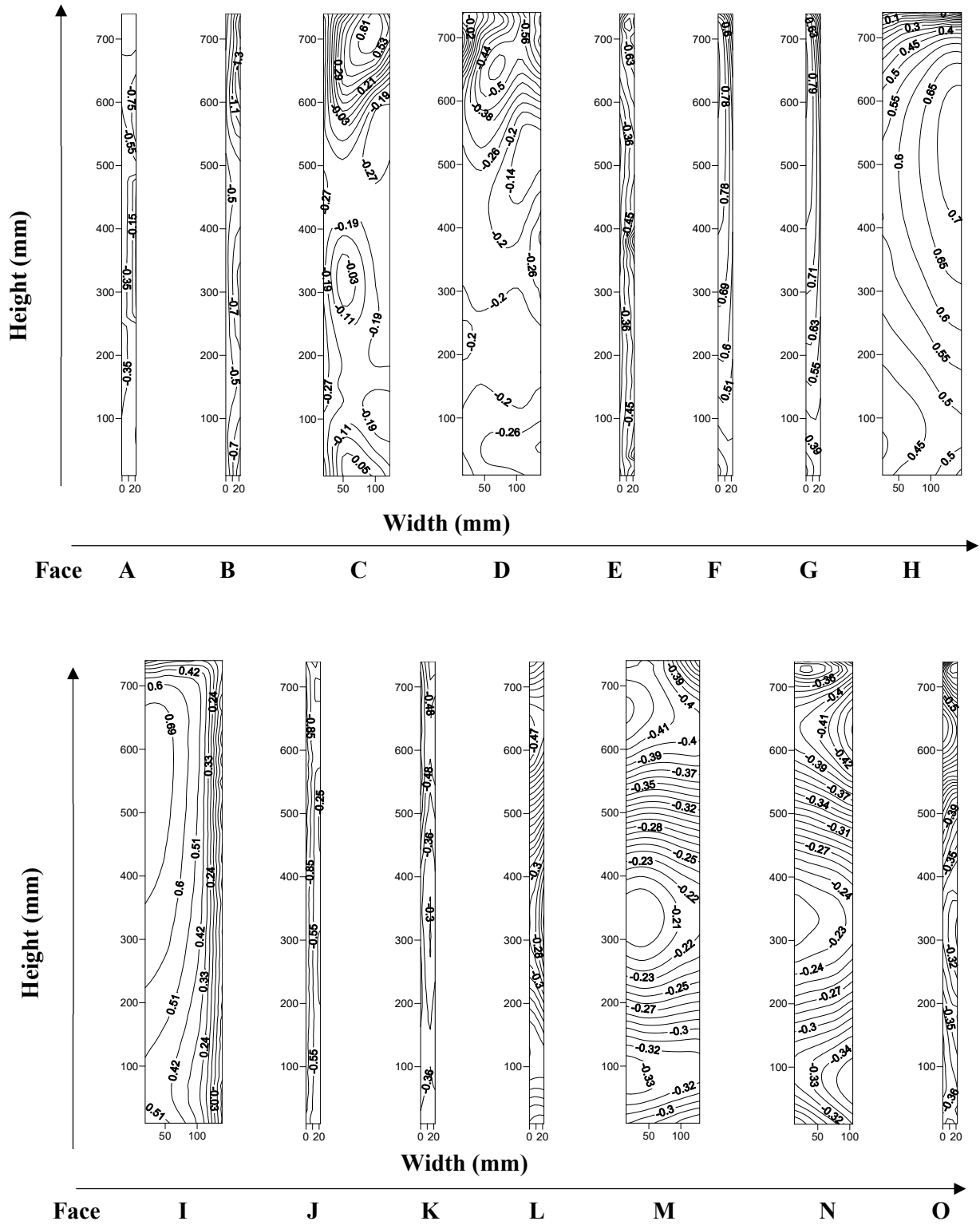


Figure 5.44 Distribution of wind pressure coefficient on the Y-shape with chamfer corner at  $135^\circ$  wind incidence angle

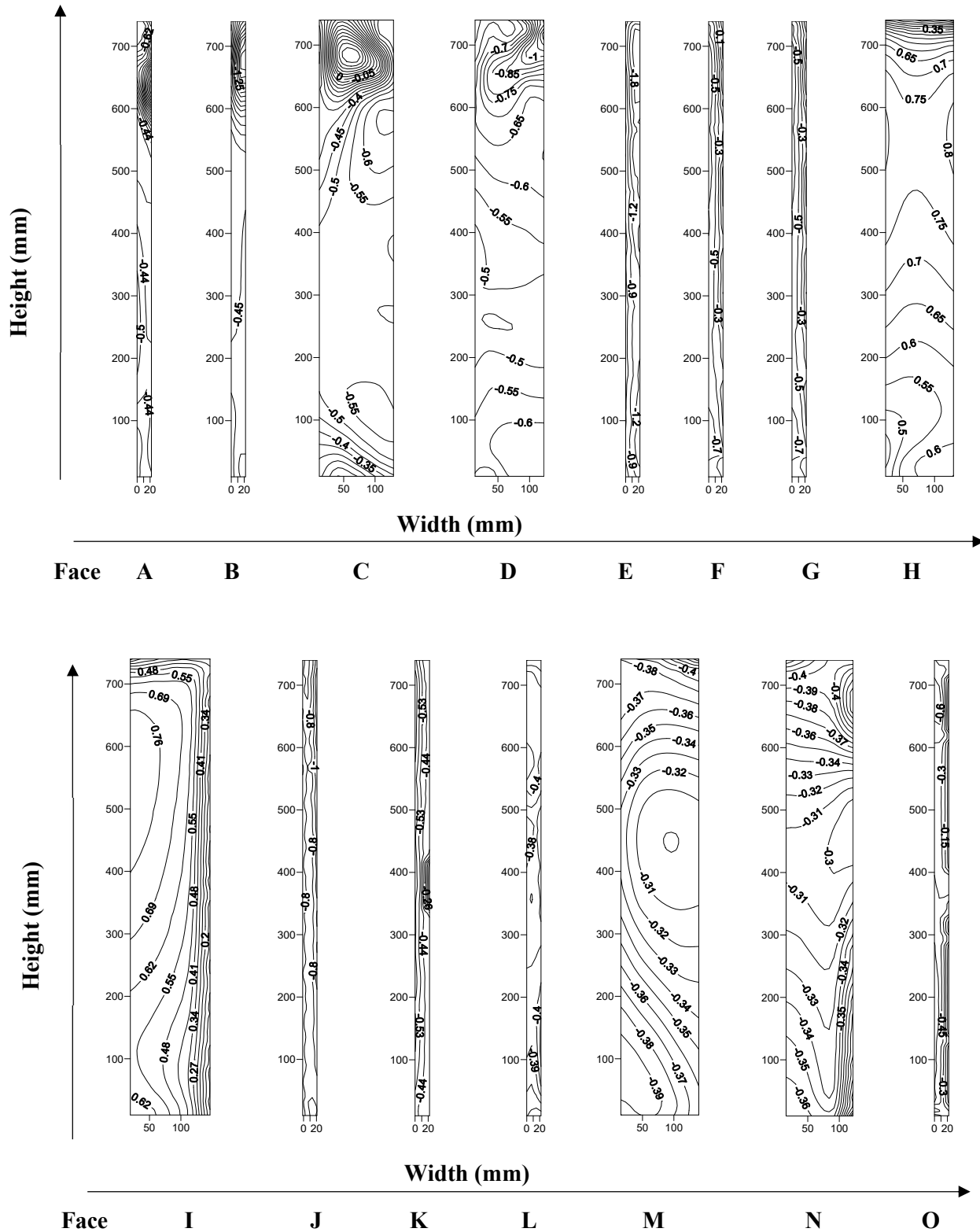


Figure 5.45 Distribution of wind pressure coefficient on the Y-shape with chamfer corner at 150° wind incidence angle

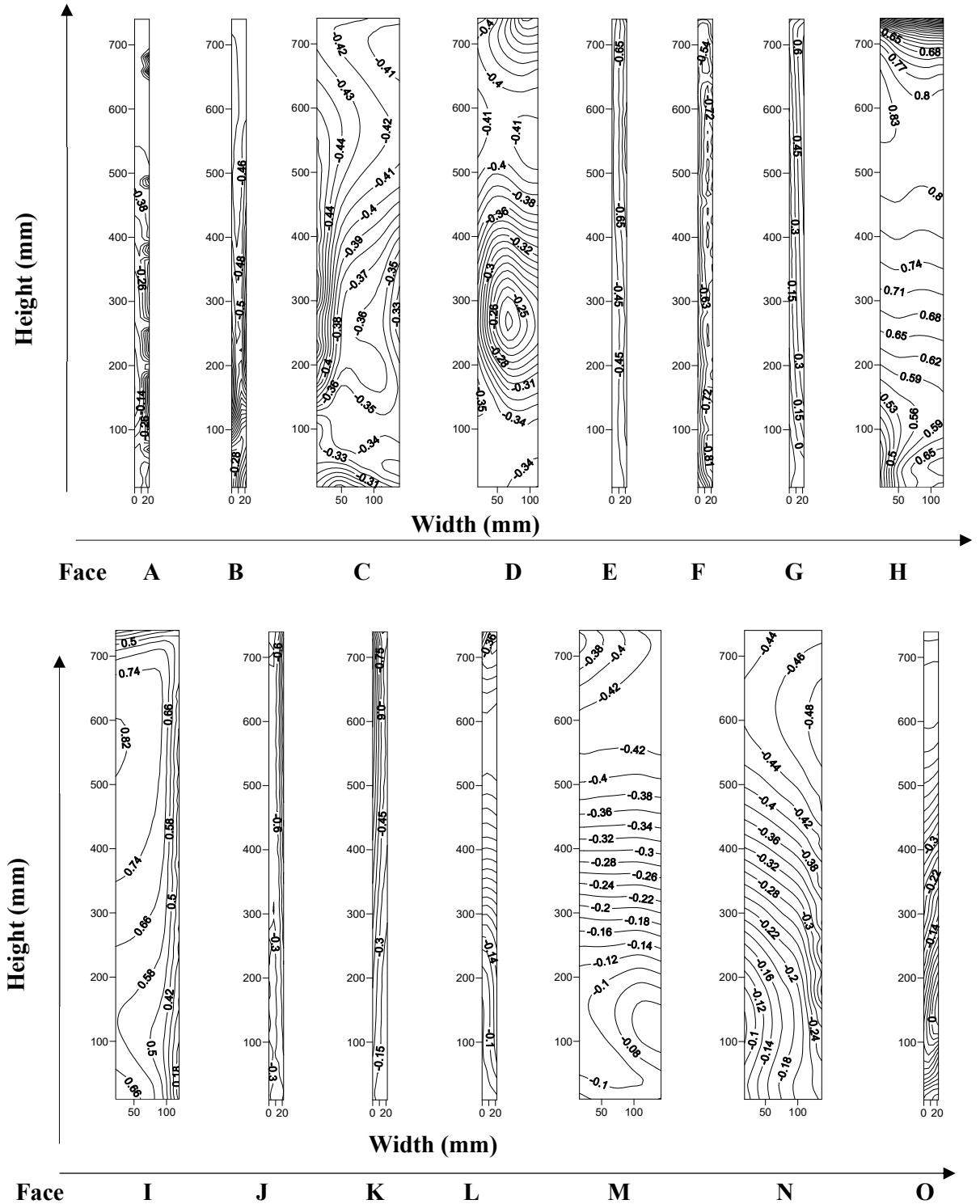


Figure 5.46 Distribution of wind pressure coefficient on the Y-shape with chamfer corner at 165° wind incidence angle

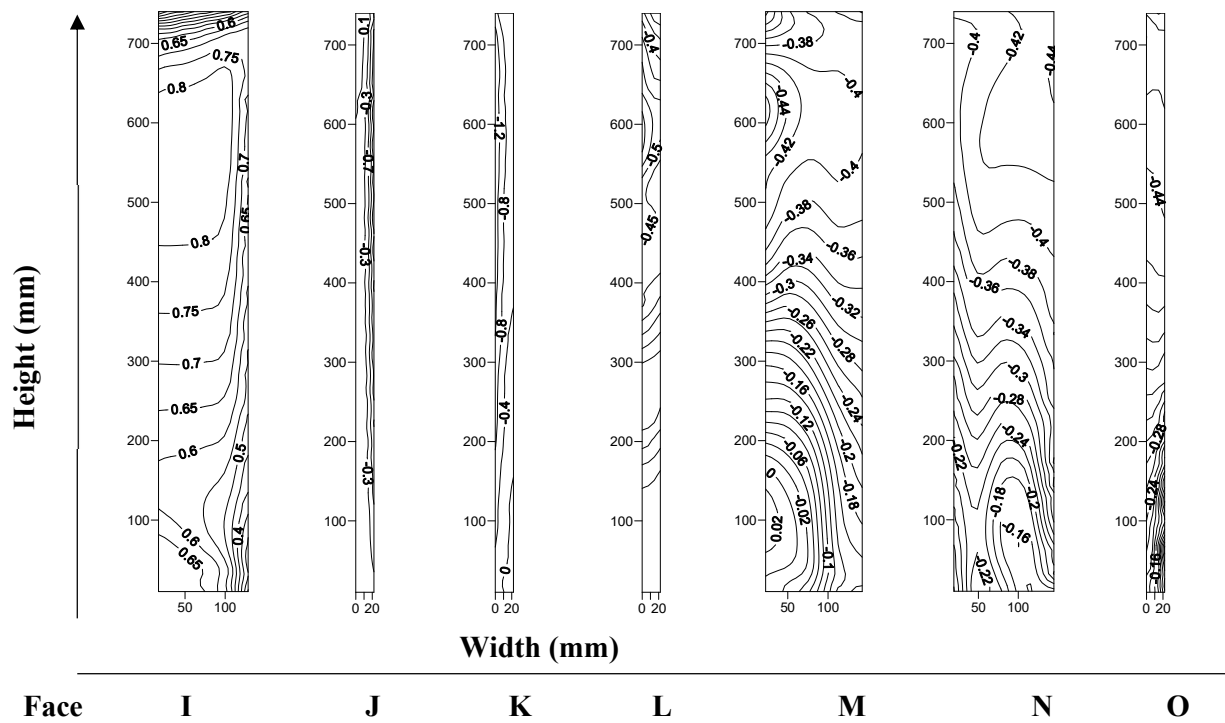
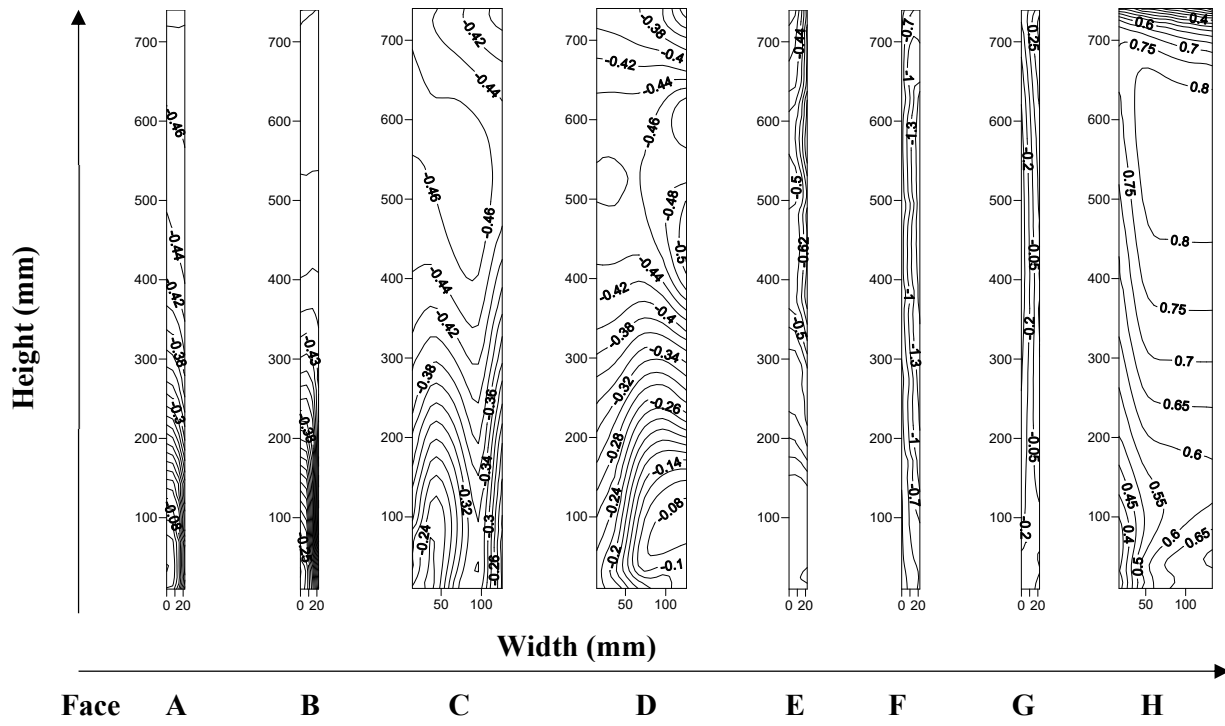


Figure 5.47 Distribution of wind pressure coefficient on the Y-shape with chamfer corner at  $180^{\circ}$  wind incidence angle

The pressure contour is depicted after extracting the pressure values from the numerical simulation after drawing the lines on each surface of building model along the height and then this data is process as per the procedure provided in wind tunnel manual. This data is processed in the form of a grid after that these pressure contours are depicted where the pressure data is showing the distribution along with the magnitude of pressure with respect to height and width of the face.

#### **5.4.2 Vertical Pressure Distribution along the Height of the building**

Pressure distribution is depicted in the Figure 5.48 (contd.) Mean pressure distribution on the vertical centre line for Y shape with chamfer corner is for vertical centre line on each face and it is observed for wind incidence angle ranging from  $0^{\circ}$  to  $180^{\circ}$  at an interval of  $15^{\circ}$ . It is clearly demonstrated that wind pressure in the case of  $0^{\circ}$  wind is positive for very few faces such as A, B, C, D, M, N and O while the pressure on vertical line is range from positive to negative. Range of pressure positive is mainly found on wind ward faces while the negative pressure is observed on the faces where surface pressure is less than the reference pressure likewise the distribution on each centre line of the faces is observed and depicted.

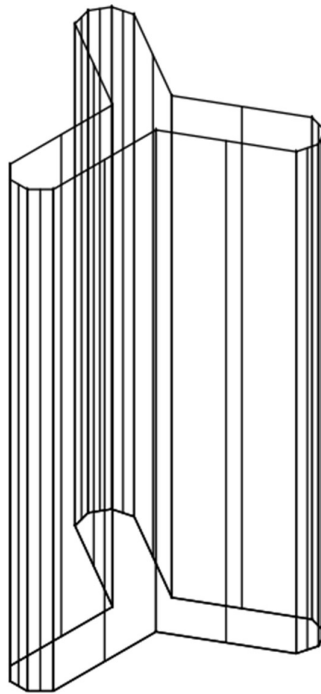
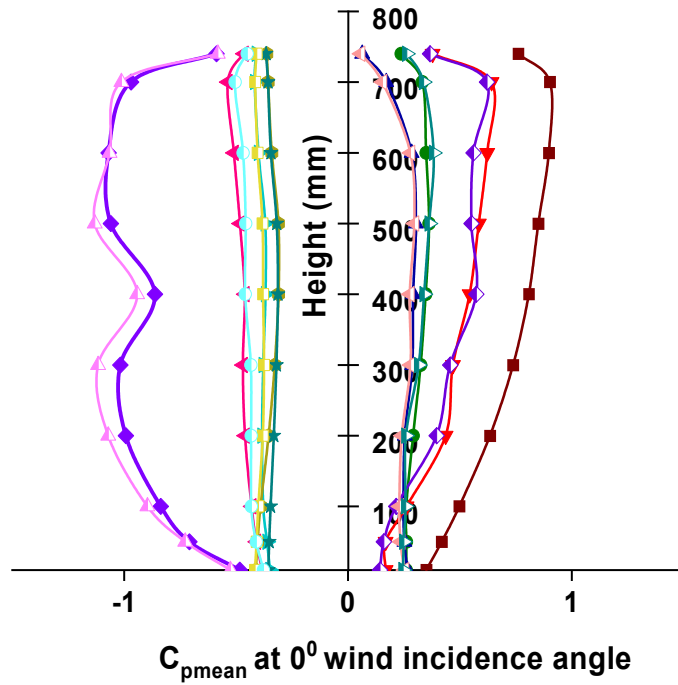
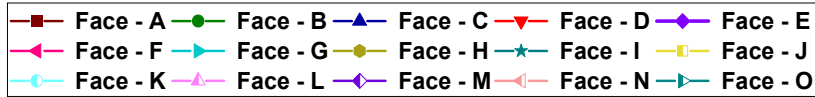


Figure 5.48 (contd.) Mean pressure distribution on the vertical centre line for Y shape with chamfer corner

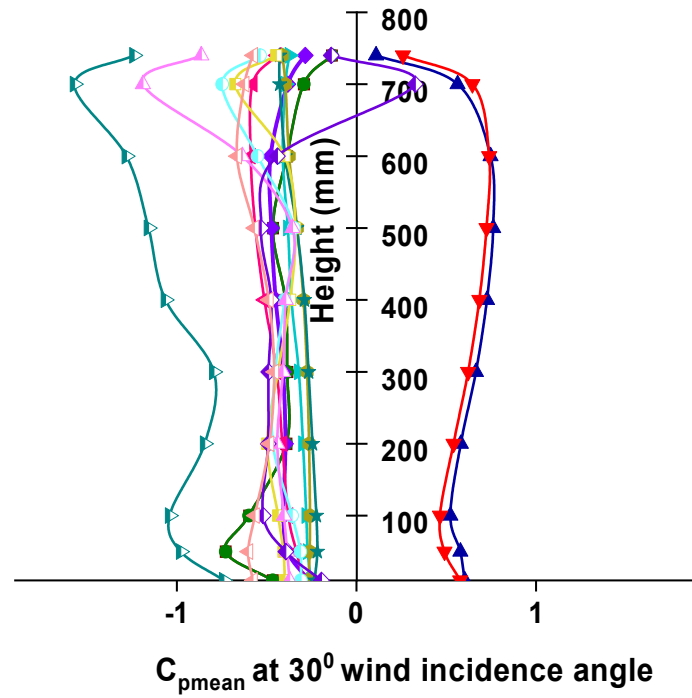
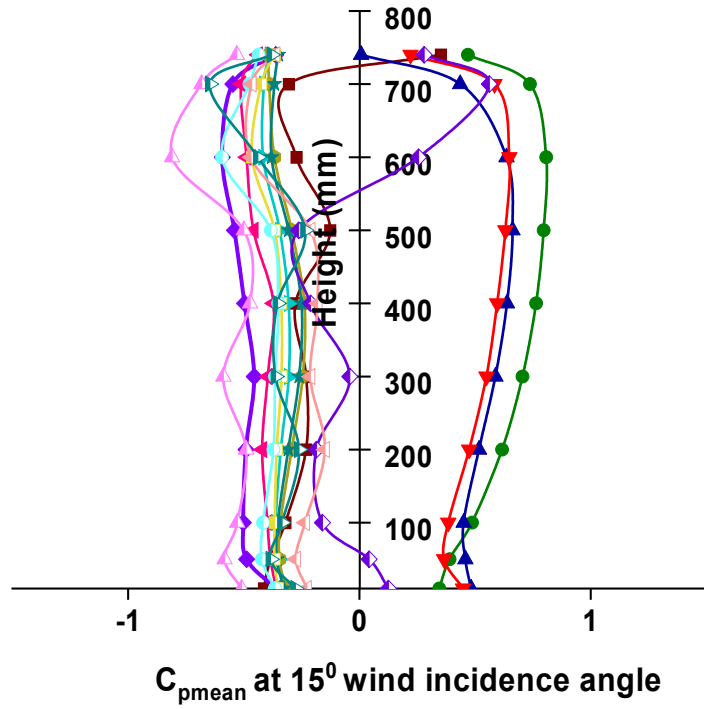
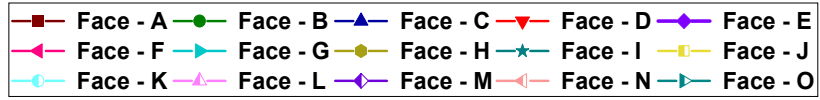


Figure 5.48 (contd.) Mean pressure distribution on the vertical centre line for Y shape with chamfer corner

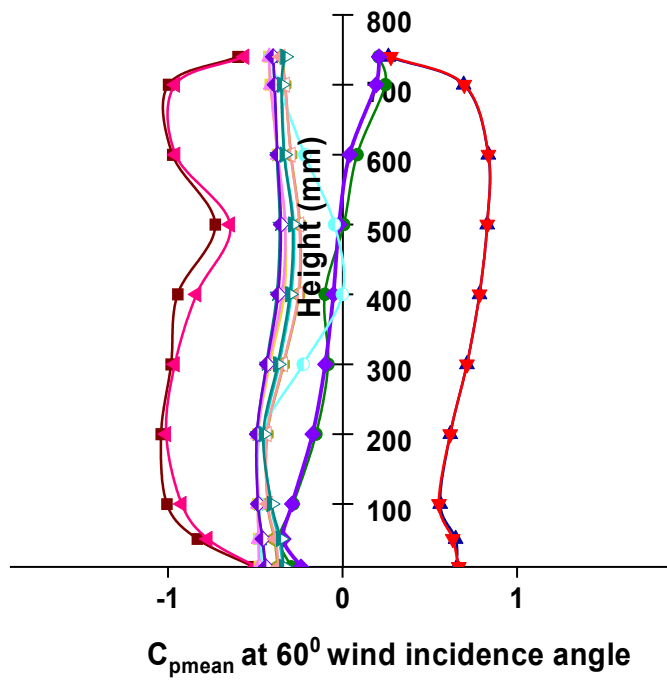
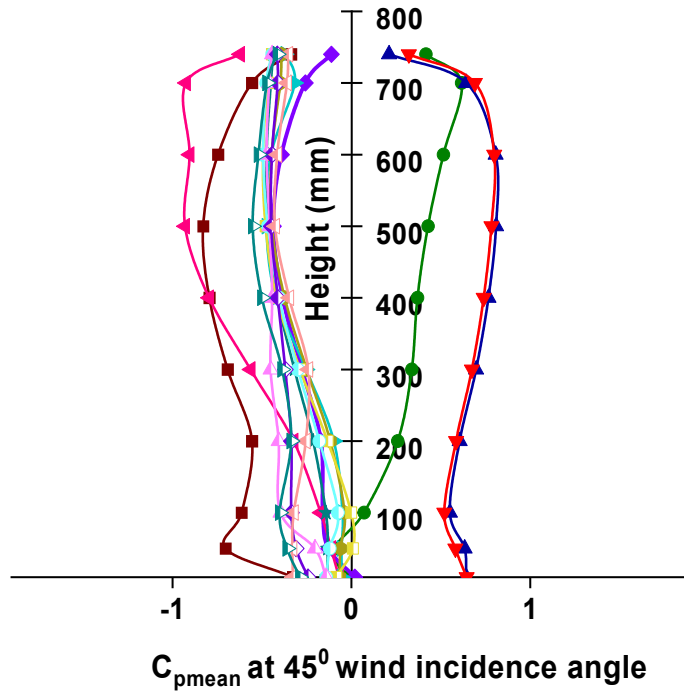


Figure 5.48 (contd.) Mean pressure distribution on the vertical centre line for Y shape with chamfer corner



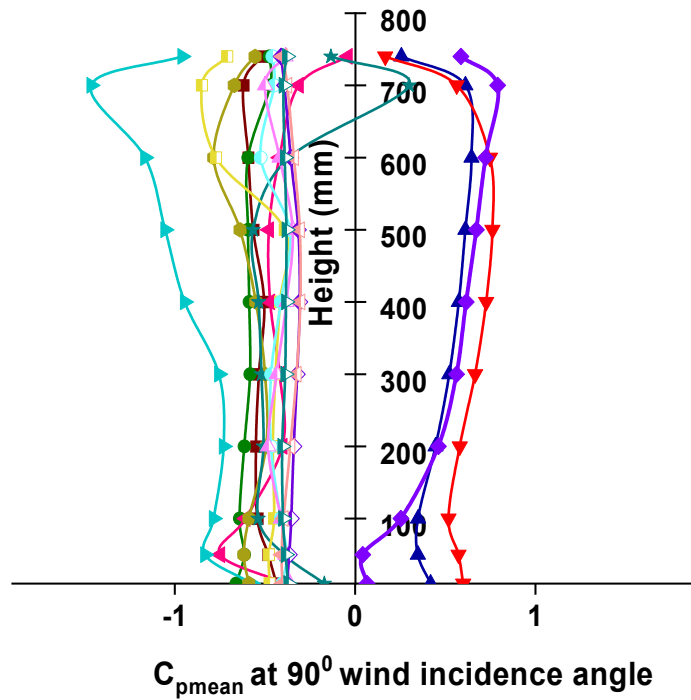
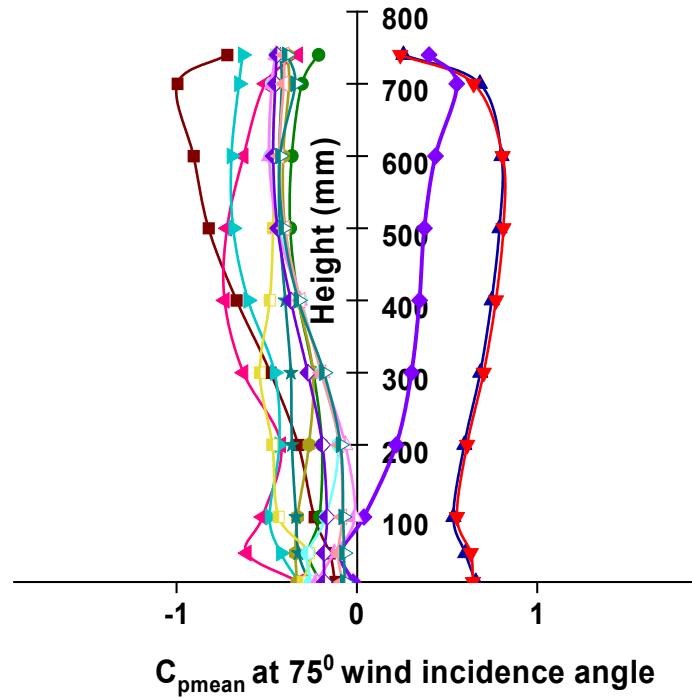


Figure 5.48 (contd.) Mean pressure distribution on the vertical centre line for Y shape with chamfer corner

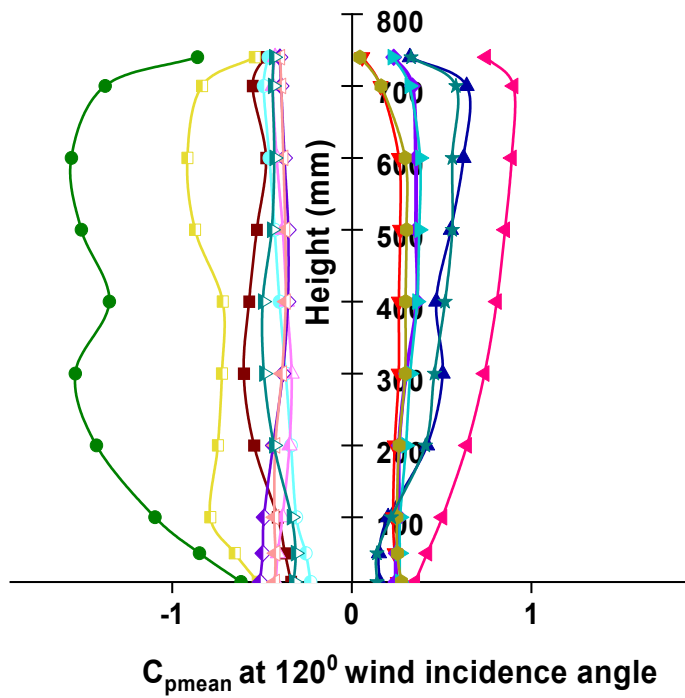
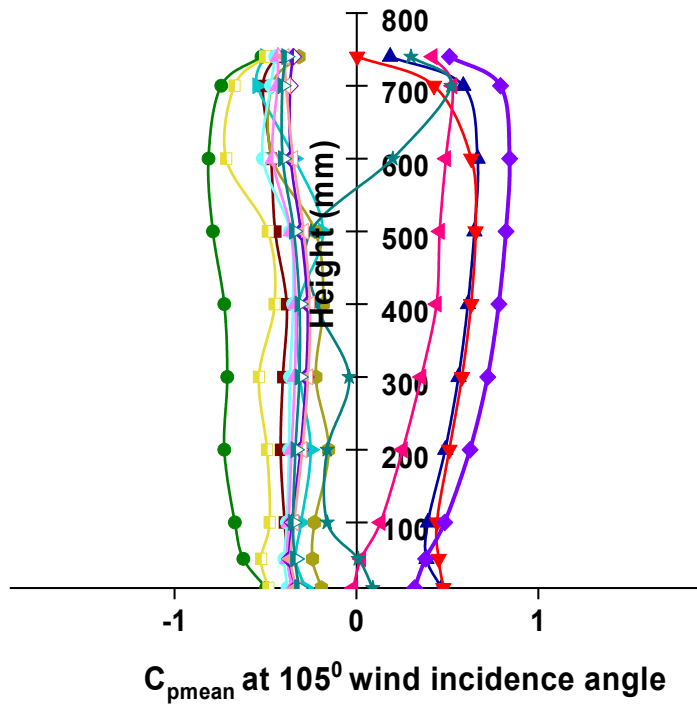
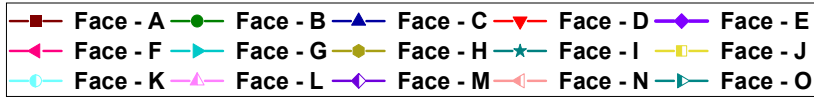


Figure 5.48 (contd.) Mean pressure distribution on the vertical centre line for Y shape with chamfer corner

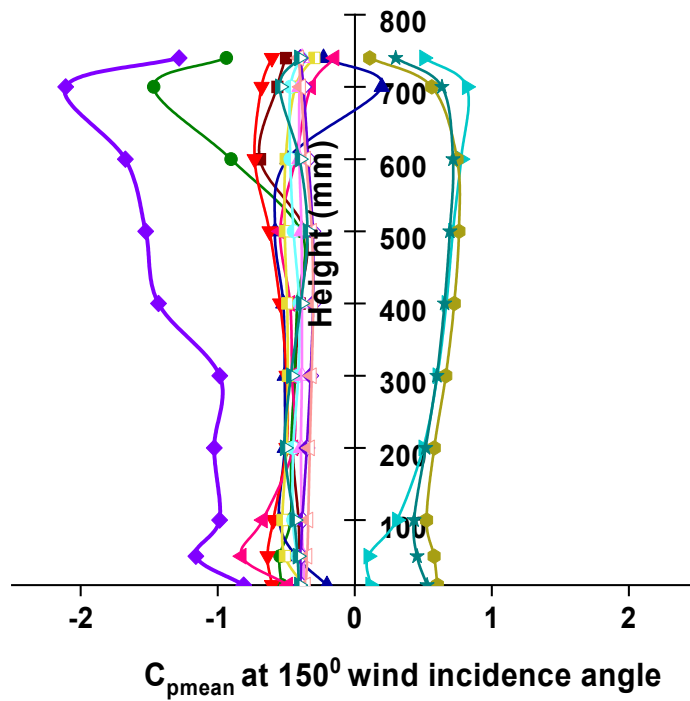
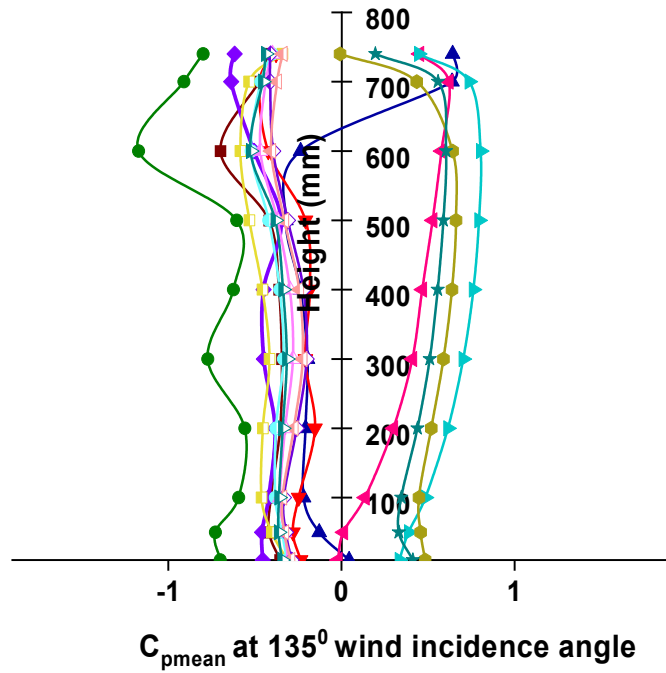
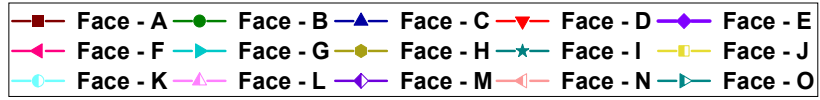


Figure 5.48 (contd.) Mean pressure distribution on the vertical centre line for Y shape with chamfer corner

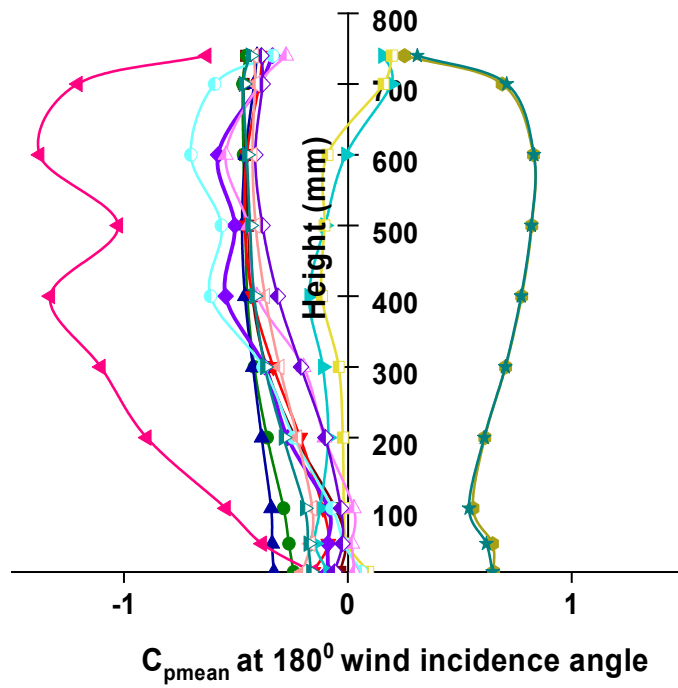
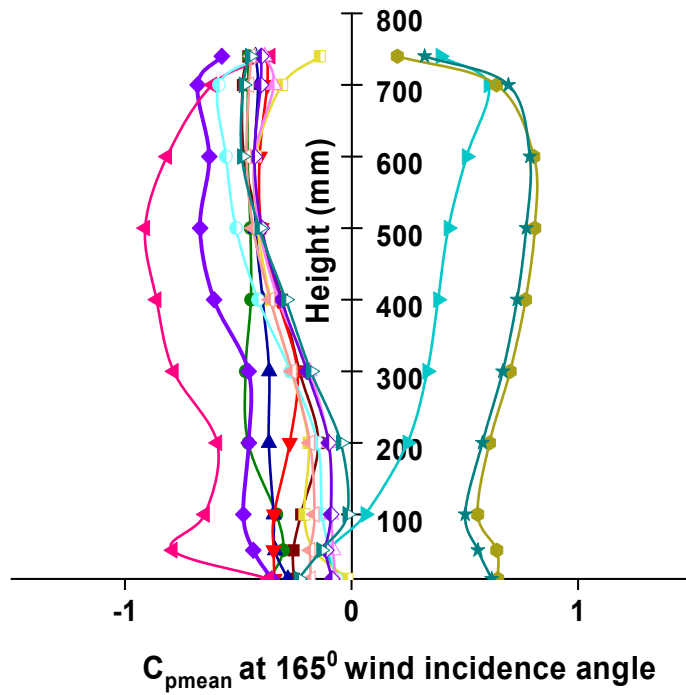
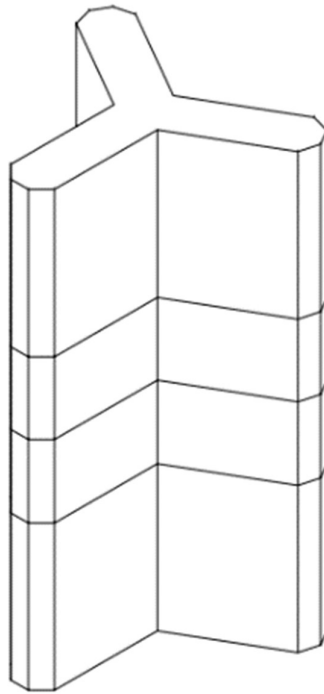
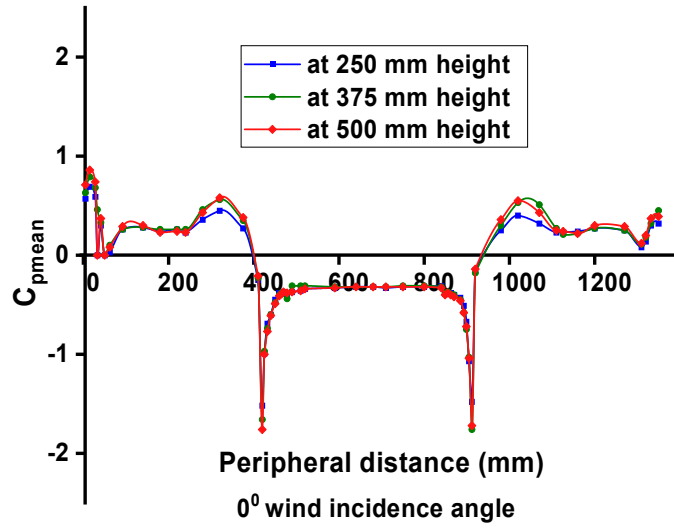


Figure 5.48 Mean pressure distribution on the vertical centre line for Y shape with chamfer corner

### 5.4.3 Horizontal Pressure Distribution along the Peripheral Distance of Building

The wind pressure distribution is clearly demonstrated on three different level at 250 mm, 375 mm and 500 mm height from the base of the model along the peripheral distance of the model. In the lower one third level the maximum pressure is 1.05 found at 30 mm, and the least pressure of -1.30 is observed on 510 mm from the starting point. At different level of mid height of peripheral distance of building model, it is found that the maximum pressure of 1.05 at 30 mm from the starting point and the maximum negative pressure of -1.26 is observed on 510 mm from the starting point likewise the pressure distribution is depicted in graphical presentation from  $0^{\circ}$  to  $180^{\circ}$  at an interval of  $15^{\circ}$ .

The pressure distribution is presented in Figure 5.49 (contd.) Mean pressure distribution along the peripheral distance of the Y-shape with chamfer corner at three level is more or less same and the pressure is observed at the location where there is some minor and major changes into the geometry. The pressure along the peripheral distance shows the nature of response of tall structure like when the pressure on top is more than the modification in the geometrical shape can be applied to reduce the load of wind on the structure likewise the pressure distribution behaviour along the peripheral distance is observed with the help of numerical simulation and result is presented in the graphical form.



**Figure 5.49 (contd.) Mean pressure distribution along the peripheral distance of the Y-shape with chamfer corner**

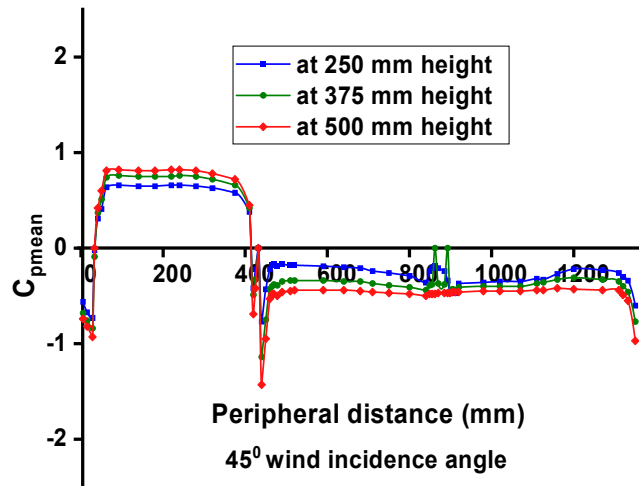
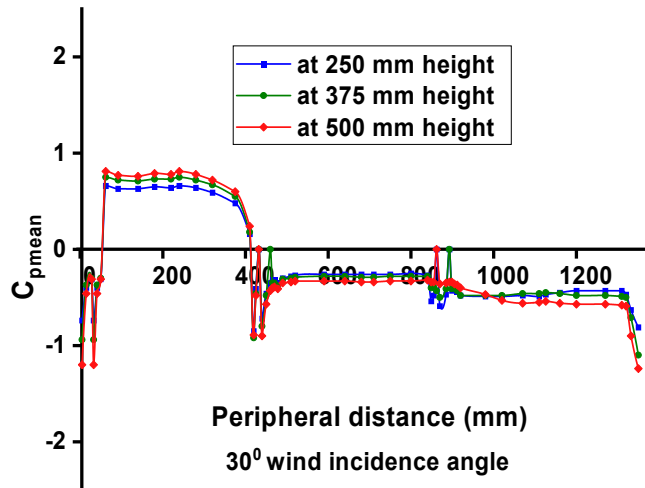
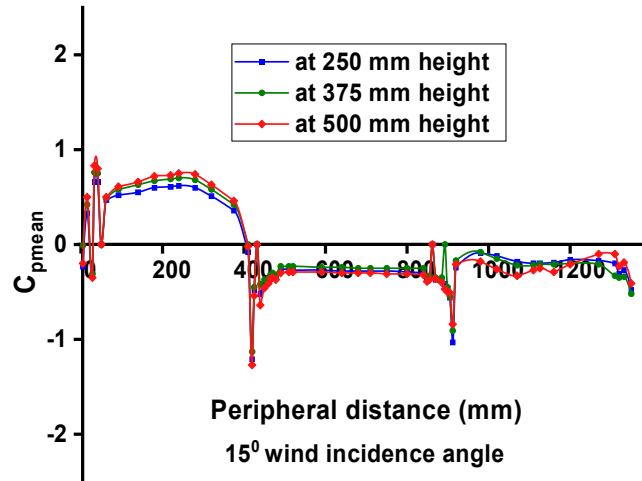


Figure 5.49 (contd.) Mean pressure distribution along the peripheral distance of the Y-shape with chamfer corner

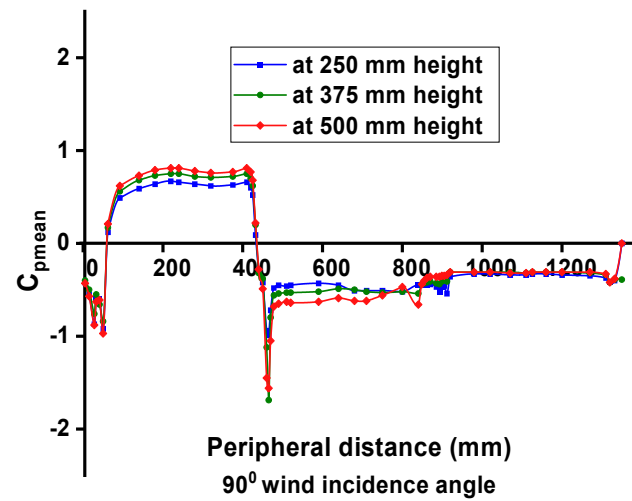
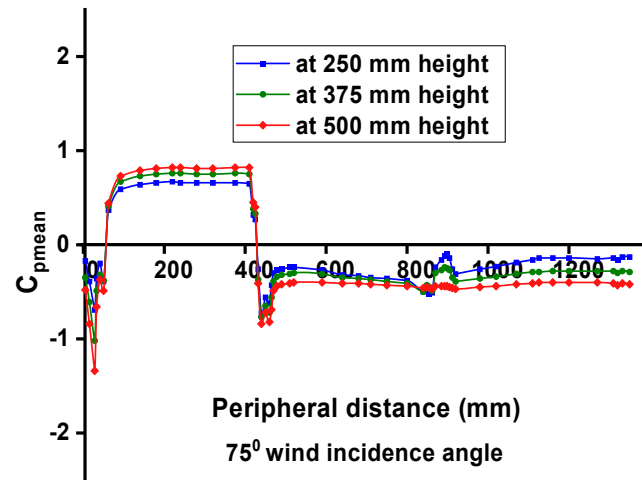
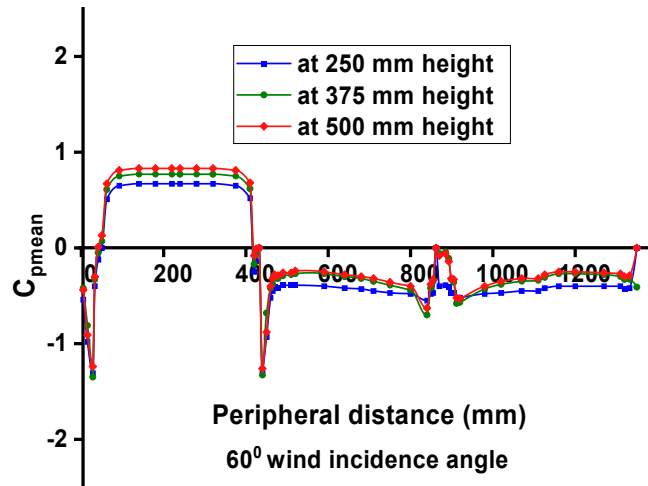


Figure 5.49 (contd.) Mean pressure distribution along the peripheral distance of the Y-shape with chamfer corner



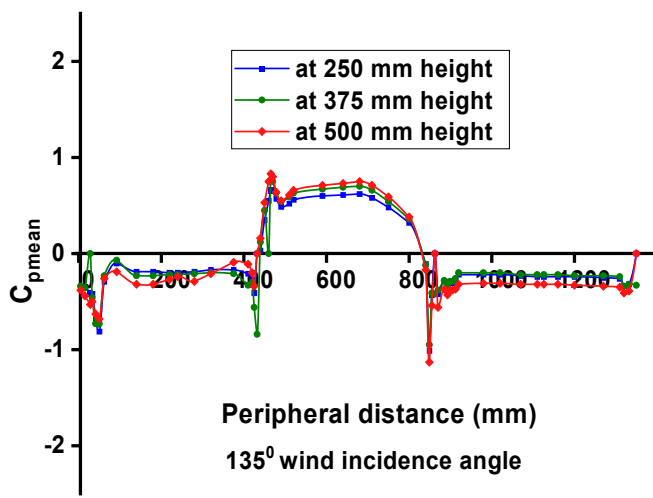
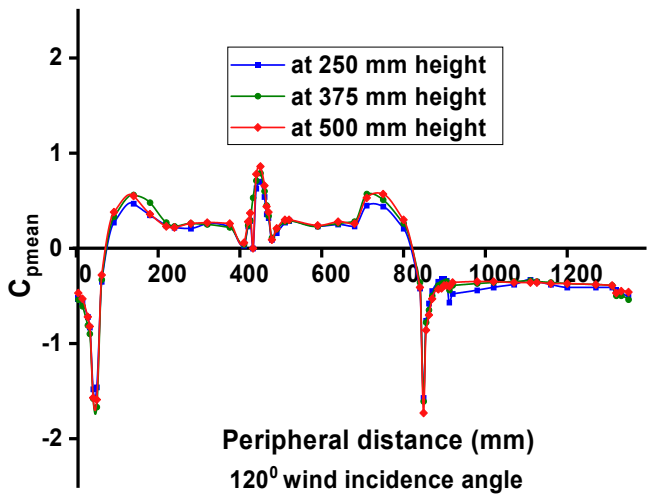
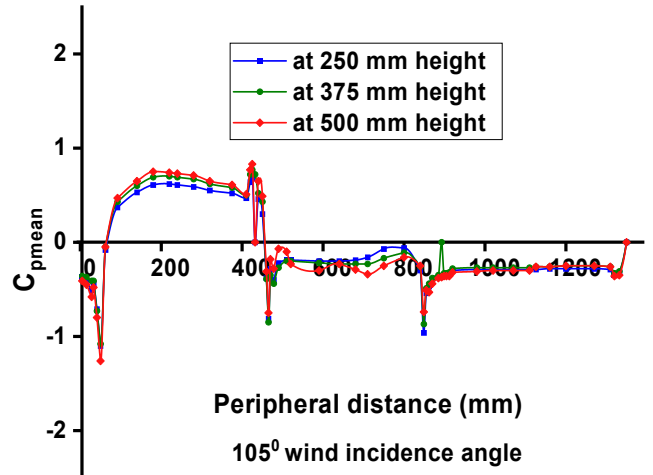


Figure 5.49 (contd.) Mean pressure distribution along the peripheral distance of the Y-shape with chamfer corner

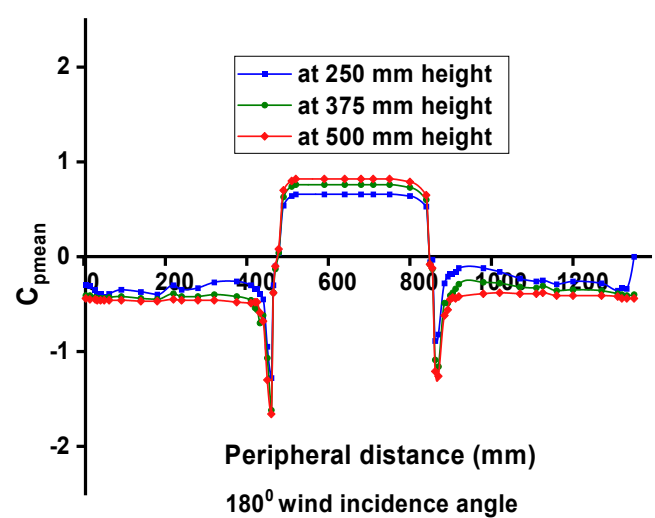
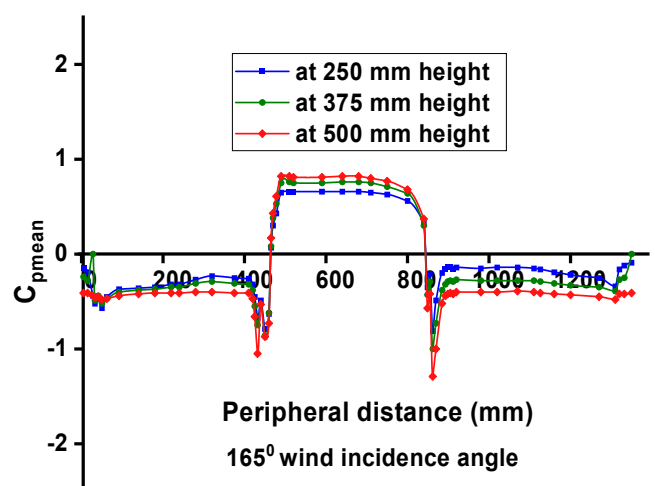
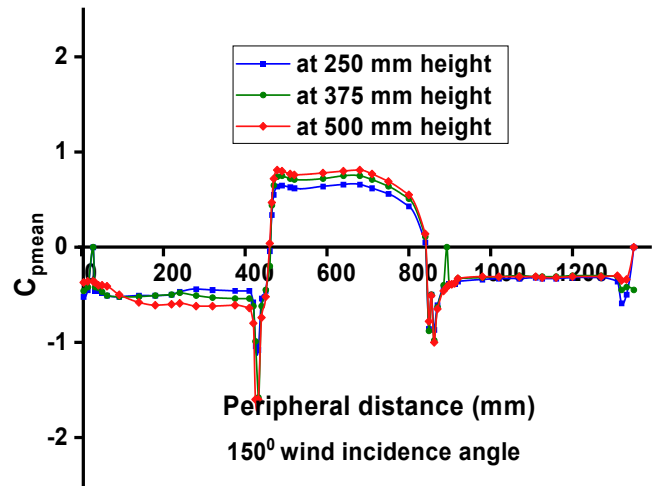


Figure 5.49 Mean pressure distribution along the peripheral distance of the Y-shape with chamfer corner

### 5.4.4 Force Coefficients

The wind force coefficient in X and Y direction is calculated and presented graphically in Figure 5.50 Wind force coefficient of the Y-shape with chamfer corner also these forces are calculated after taking the wind flow characteristics into account. The force coefficient in X direction is  $C_{fx}$  and in Y direction is  $C_{fy}$ . It is also observed that the  $C_{fx}$  is maximum (0.65) at  $60^\circ$  and  $180^\circ$  while the minimum  $C_{fx}$  (0.35) in the case of  $30^\circ$  and  $150^\circ$  wind is spotted on the base of entire building model. The wind force coefficient in y direction is  $C_{fy}$  and it is found maximum (0.58) in the case of  $90^\circ$  wind incidence angle while the minimum  $C_{fy}$  (-0.58) is spotted in the case of  $150^\circ$  wind incidence angle.

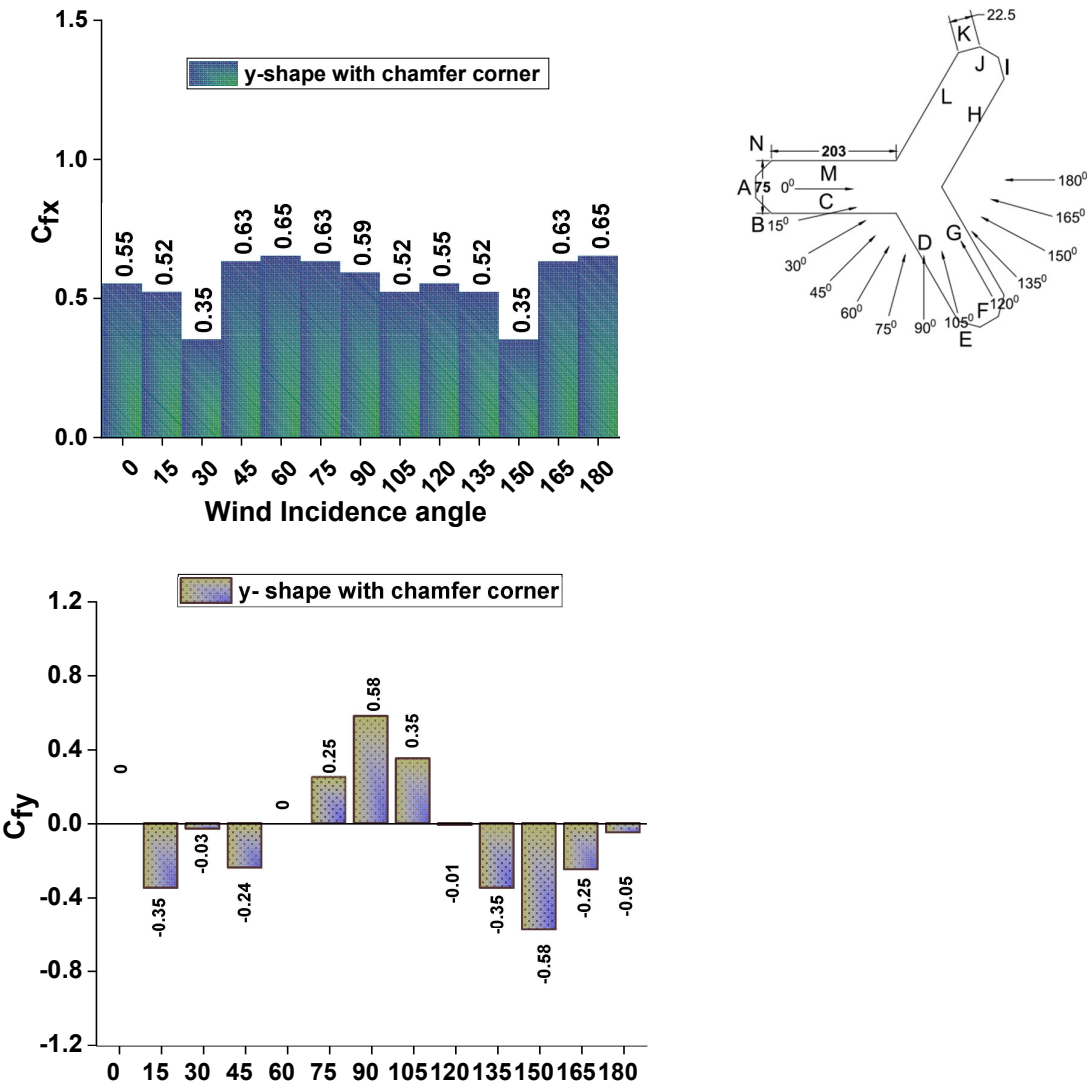


Figure 5.50 Wind force coefficient of the Y-shape with chamfer corner

### 5.4.5 Moment Coefficients

From the moment coefficient on the building model which is having the corner configuration in the form of chamfer corner, it is found that the moment coefficient from Figure 5.51 Wind moment coefficient of the Y-shape with chamfer corner in x direction is  $C_{mx}$  and the maximum of 0.307 is noticed at  $150^\circ$  wind incidence angle while the moment coefficient in y direction is  $C_{my}$  and the maximum of 0.36 is observed at  $90^\circ$  wind incidence angle and the minimum  $C_{mx}$  of -0.30 is found when wind is hitting the model at  $90^\circ$  while the minimum  $C_{fy}$  of 0.19 is detected at  $30^\circ$  and  $150^\circ$  wind incidence angle.

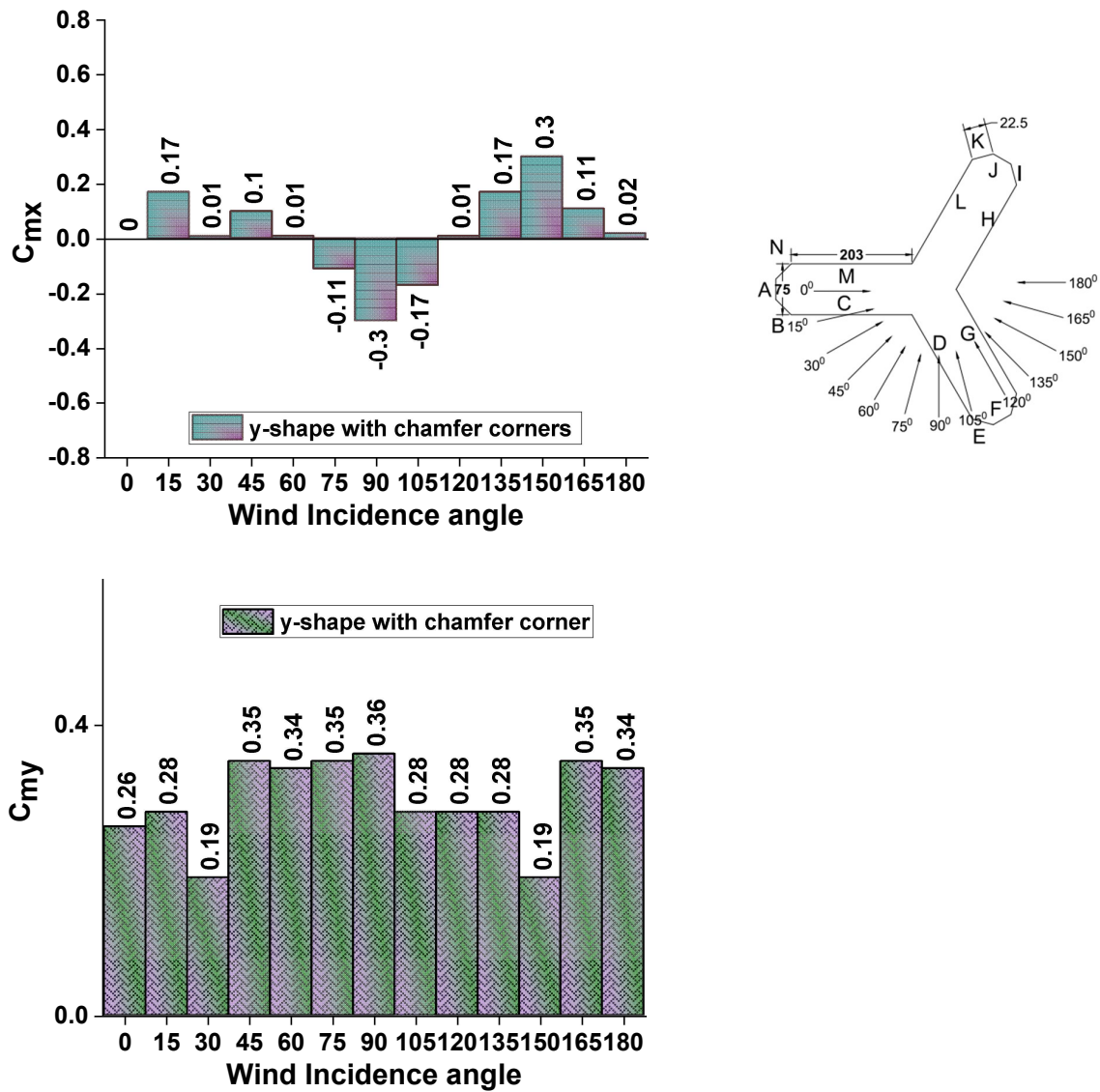


Figure 5.51 Wind moment coefficient of the Y-shape with chamfer corner

#### 5.4.6 External Pressure Coefficients

The pressure coefficient on each surface of building model is calculated for wind incidence angle ranging from  $0^{\circ}$  to  $180^{\circ}$  wind at an interval of  $15^{\circ}$ . The pressure coefficient is calculated after drawing the lines on the geometry of the building model which act like a pressure tapping along the height of the model and the pressure data is extracted after the completion of the numerical simulation performed on the model. The data is then processed as per the wind tunnel manual and report no 67 by ASCE. After that the final values are tabulated for each face of the model. It is observed in the case of  $0^{\circ}$ , the maximum pressure of 0.65 is on face-A and the minimum pressure of -1.06 is spotted on face-E and face -L, likewise the pressure are in tabulated form for each wind incidence angle and the critical values for each wind incidence angle are marked in bold. The mean external pressure coefficient is tabulated in Table: 5.3 External Pressure Coefficient for Building Model-G (Y-shape Chamfer).

**Table: 5.3 External Pressure Coefficient for Building Model-G (Y-shape Chamfer)**

Model-G (Y-shape Chamfer)													
Face	0°	15°	30°	45°	60°	75°	90°	105°	120°	135°	150°	165°	180°
<b>A</b>	<b>0.65</b>	-0.06	-0.60	<b>-0.66</b>	<b>-0.87</b>	-0.62	-0.60	-0.45	-0.45	-0.41	-0.45	-0.32	-0.34
<b>B</b>	0.19	0.47	-0.60	0.26	-0.14	-0.38	-0.69	<b>-0.77</b>	<b>-1.08</b>	<b>-0.71</b>	-0.60	-0.46	-0.39
<b>C</b>	0.20	<b>0.54</b>	<b>0.66</b>	<b>0.69</b>	<b>0.67</b>	0.62	0.53	0.43	0.20	-0.12	-0.46	-0.39	-0.35
<b>D</b>	0.23	0.43	0.54	0.62	<b>0.67</b>	<b>0.69</b>	<b>0.66</b>	<b>0.53</b>	0.21	-0.25	-0.59	-0.35	-0.30
<b>E</b>	<b>-1.06</b>	-0.59	-0.43	-0.26	-0.14	0.14	0.41	0.51	0.25	-0.29	<b>-1.14</b>	-0.58	-0.15
<b>F</b>	-0.49	-0.46	-0.53	-0.65	<b>-0.87</b>	<b>-0.63</b>	-0.65	0.17	<b>0.66</b>	0.34	-0.42	<b>-0.65</b>	<b>-0.75</b>
<b>G</b>	-0.40	-0.36	-0.36	-0.29	-0.32	-0.44	<b>-0.99</b>	-0.53	0.25	<b>0.63</b>	0.53	0.30	-0.21
<b>H</b>	-0.34	-0.31	-0.31	-0.28	-0.34	-0.35	-0.59	-0.24	0.21	0.54	<b>0.66</b>	<b>0.69</b>	<b>0.66</b>
<b>I</b>	-0.34	-0.32	-0.31	-0.34	-0.45	-0.39	-0.48	-0.11	0.20	0.38	0.50	0.60	<b>0.66</b>
<b>J</b>	-0.40	-0.27	-0.33	-0.27	-0.39	-0.40	-0.60	-0.61	<b>-1.08</b>	-0.60	-0.74	-0.58	-0.21
<b>K</b>	-0.49	-0.41	-0.45	-0.32	-0.29	-0.31	-0.47	-0.41	-0.45	-0.41	-0.47	-0.45	<b>-0.75</b>
<b>L</b>	<b>-1.06</b>	<b>-0.73</b>	-0.58	-0.43	-0.39	-0.29	-0.45	-0.38	-0.44	-0.36	-0.39	-0.26	-0.15
<b>M</b>	0.23	-0.09	-0.42	-0.39	-0.45	-0.32	-0.35	-0.32	-0.39	-0.30	-0.35	-0.26	-0.30
<b>N</b>	0.20	-0.25	-0.56	-0.35	-0.34	-0.26	-0.35	-0.32	-0.39	-0.31	-0.34	-0.32	-0.35
<b>O</b>	0.19	-0.40	<b>-0.84</b>	-0.52	-0.32	-0.26	-0.31	-0.25	-0.44	-0.28	-0.35	-0.25	-0.39

## 5.5 Y-shape with Fillet in Corners

The regular shape building can be designed by structural engineer and architect while the irregular shape building model need detailed investigation for its stability and in the case of tall building such model are subjected to wind load and it is the governing criteria in the design of the tall building. In this study the different “Y” and rectangular shape building are studied to reduce the wind effects on different type of corner configuration when applied. The building model are numerically tested for wind incidence angles ranging from  $0^{\circ}$  to  $180^{\circ}$  wind at an interval of  $15^{\circ}$ .

The building model of “Y” shape with fillet corner is investigated and the wind effect like pressure contour on each surface are presented graphically for each wind incidence angle and the pressure effect on the vertical centre line of every angle are presented while the pressure along the peripheral distance at three different levels of 250 mm, 375 mm and 500 mm from the base of the model is presented which are helpful to design such model and huge data of pressure is generated which is very much valuable to architect and structural engineers for designing such type of tall building model.

### 5.5.1 Pressure Contours

The pressure distribution on the surface of the model is presented in the graphical form of contours from Figure 5.52 Distribution of wind pressure coefficient on the Y-shape with fillet corner at  $0^{\circ}$  wind incidence angle to Figure 5.64 Distribution of wind pressure coefficient on the Y-shape with fillet corner at  $180^{\circ}$  wind incidence angle and these are as per the size of the particular face and in direction represents the width of the face while in the Y direction represents the height of the face. Pressure variation is clearly demonstrated in the graphical form of contours and the label also helps to evaluate the wind effect at a particular location. The wind pressure varies on each surface because of the flow pattern as the “Y” shape building model is trapping the wind into the different limbs in a particular wind incidence angle. The wind flow reattaches the building on down stream side and the wind flow also makes the variation in the wake and that is why such variation of pressure is observed. The pressure on the wind ward side is positive meaning that the pressure which is acting on the wind ward face is more than the static pressure. While on some faces the pressure acting on the particular surface is less than the static pressure in that case wind pressure is negative that is known as suction.

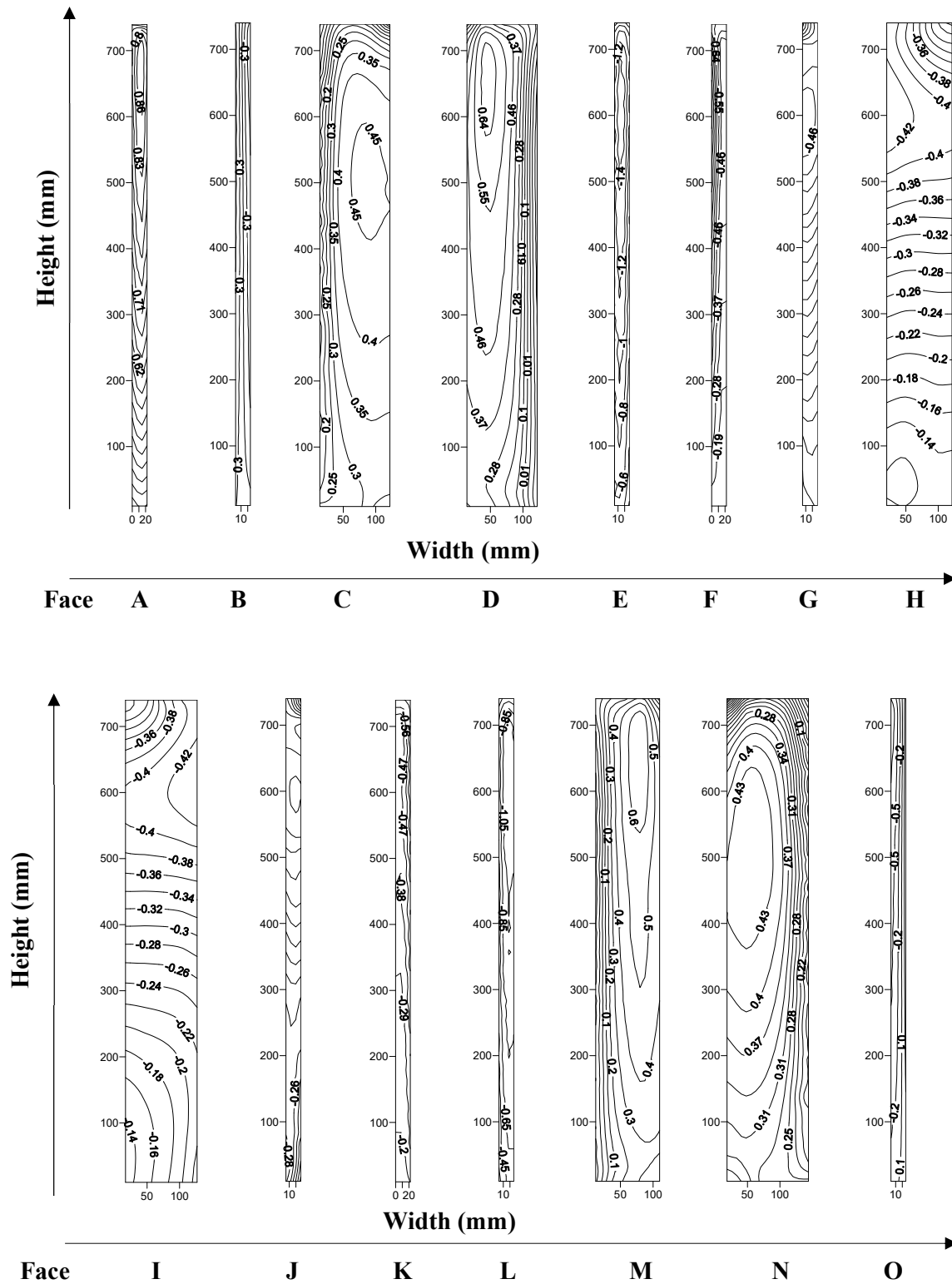


Figure 5.52 Distribution of wind pressure coefficient on the Y-shape with fillet corner at 0° wind incidence angle



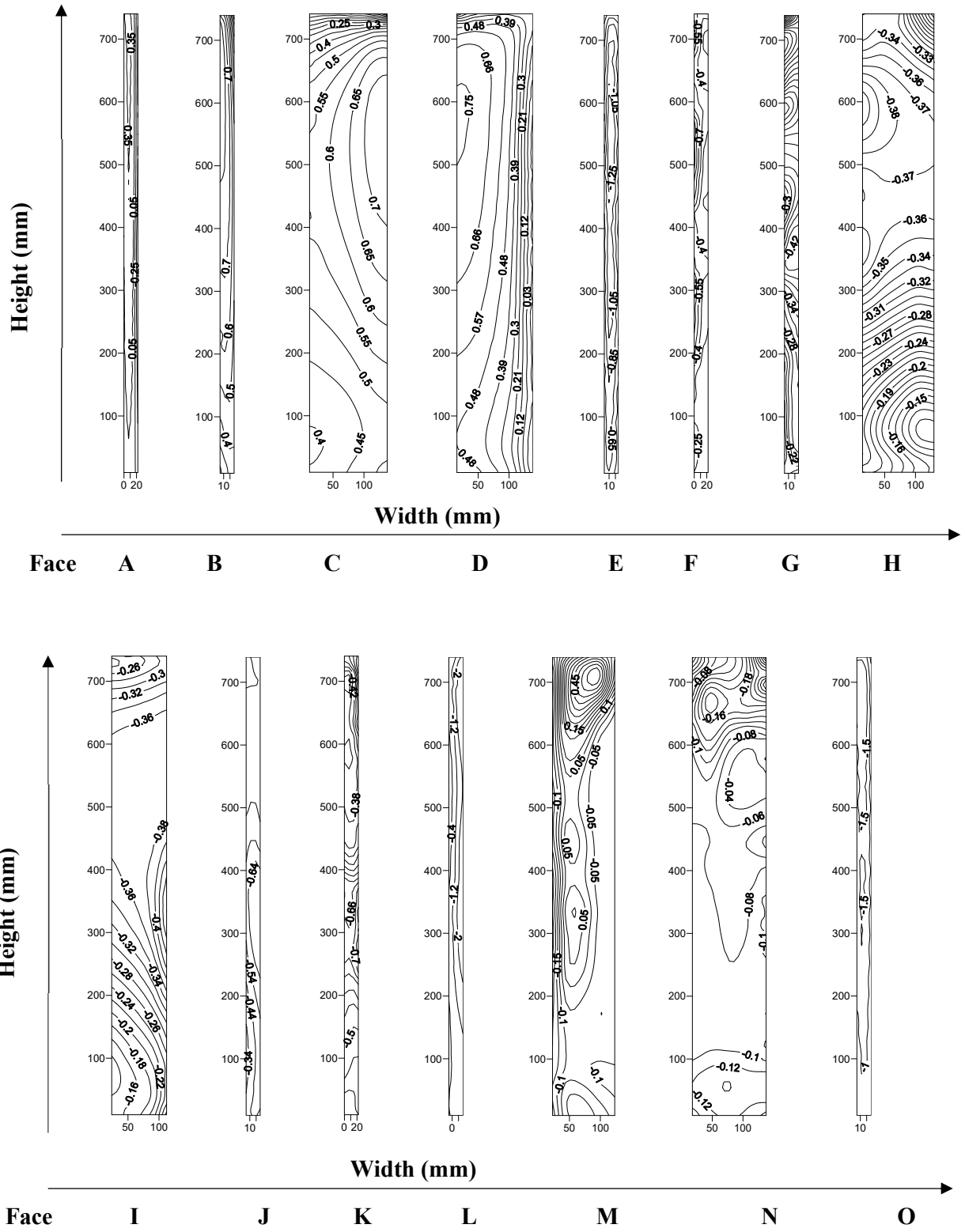


Figure 5.53 Distribution of wind pressure coefficient on the Y-shape with fillet corner at 15° wind incidence angle

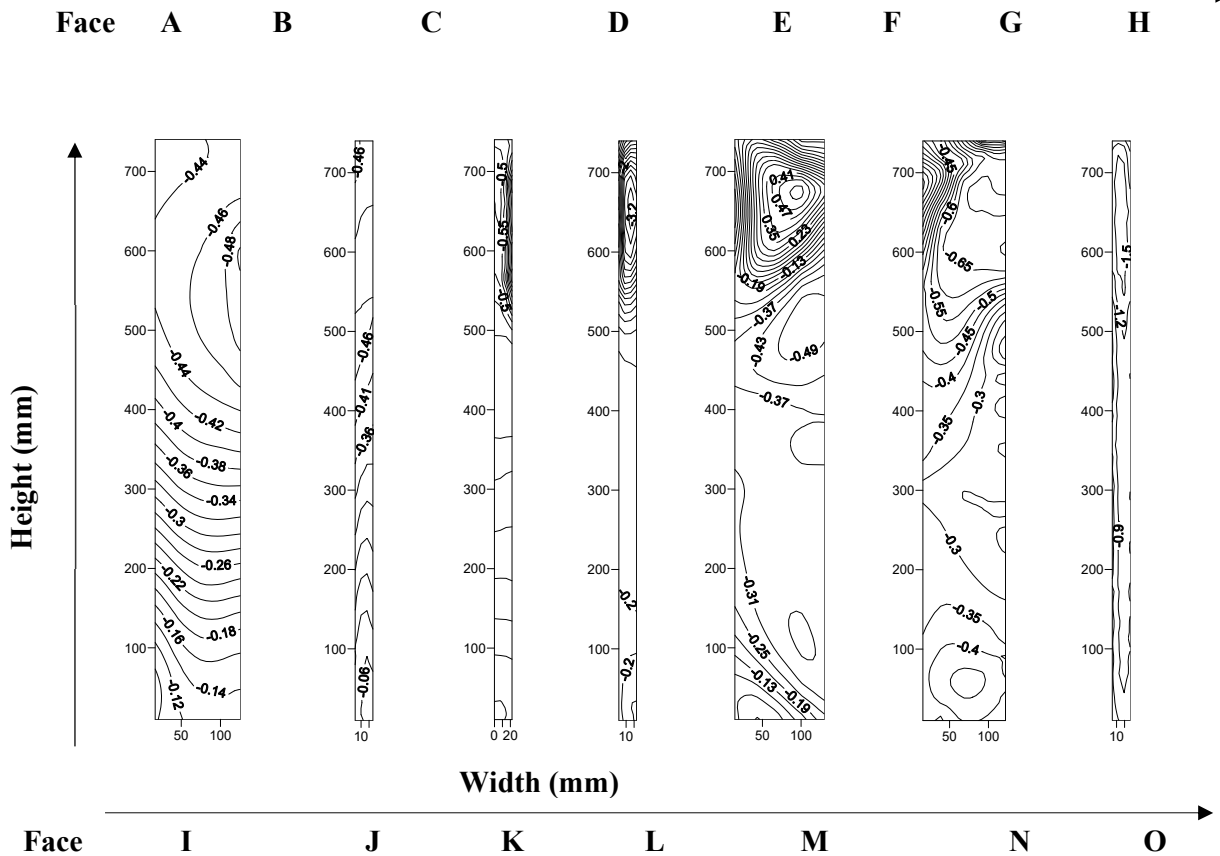
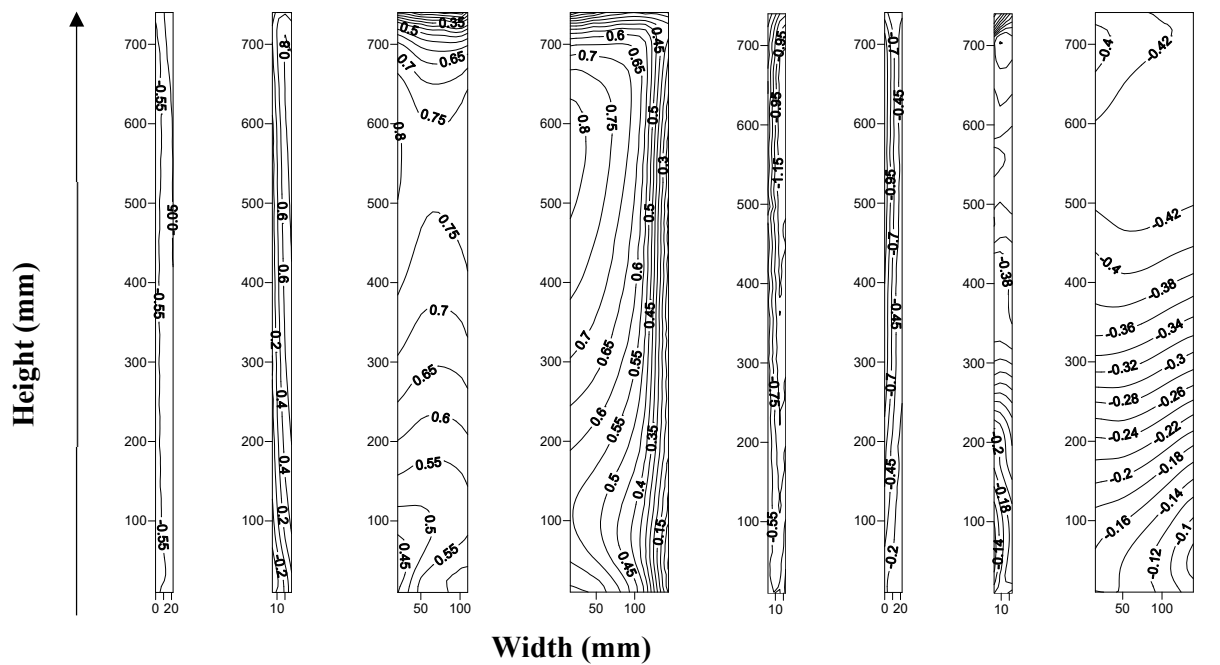


Figure 5.54 Distribution of wind pressure coefficient on the Y-shape with fillet corner at 30° wind incidence angle

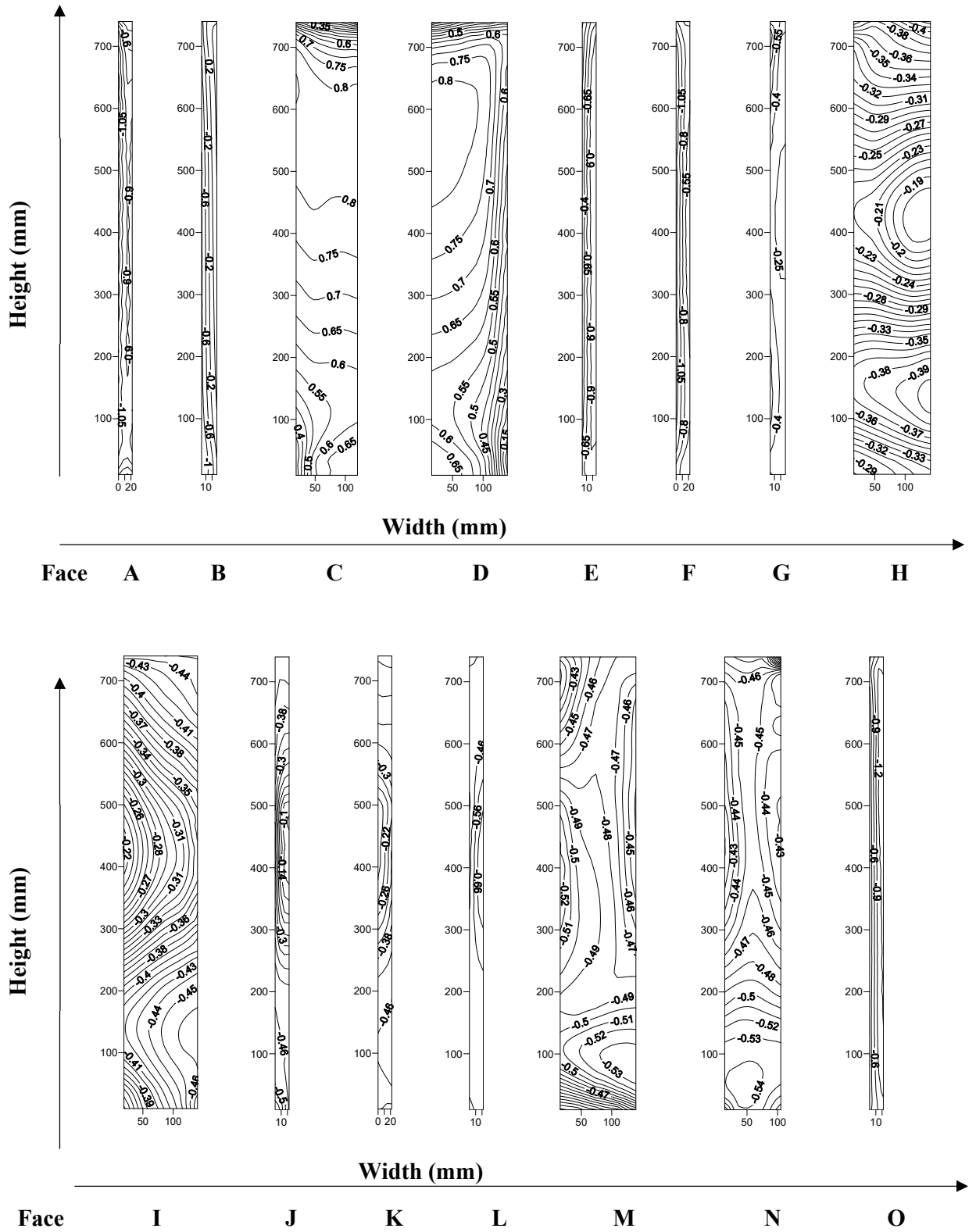


Figure 5.55 Distribution of wind pressure coefficient on the Y-shape with fillet corner at 45° wind incidence angle

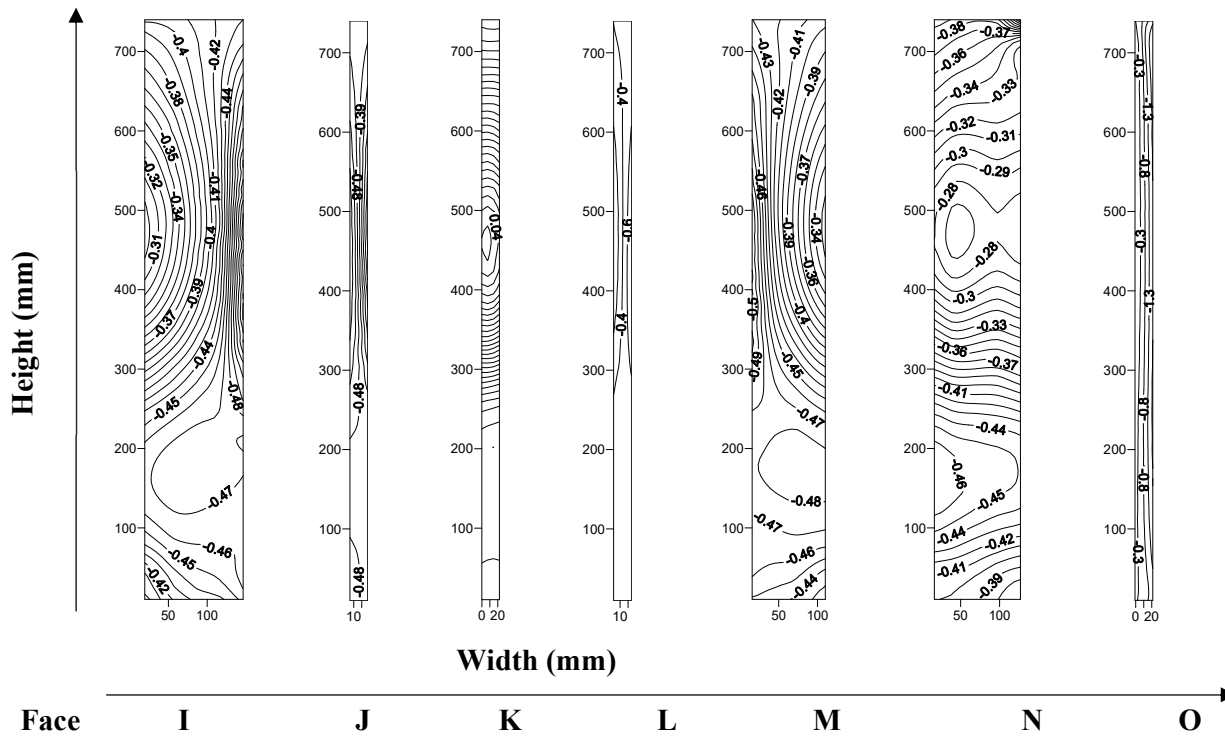
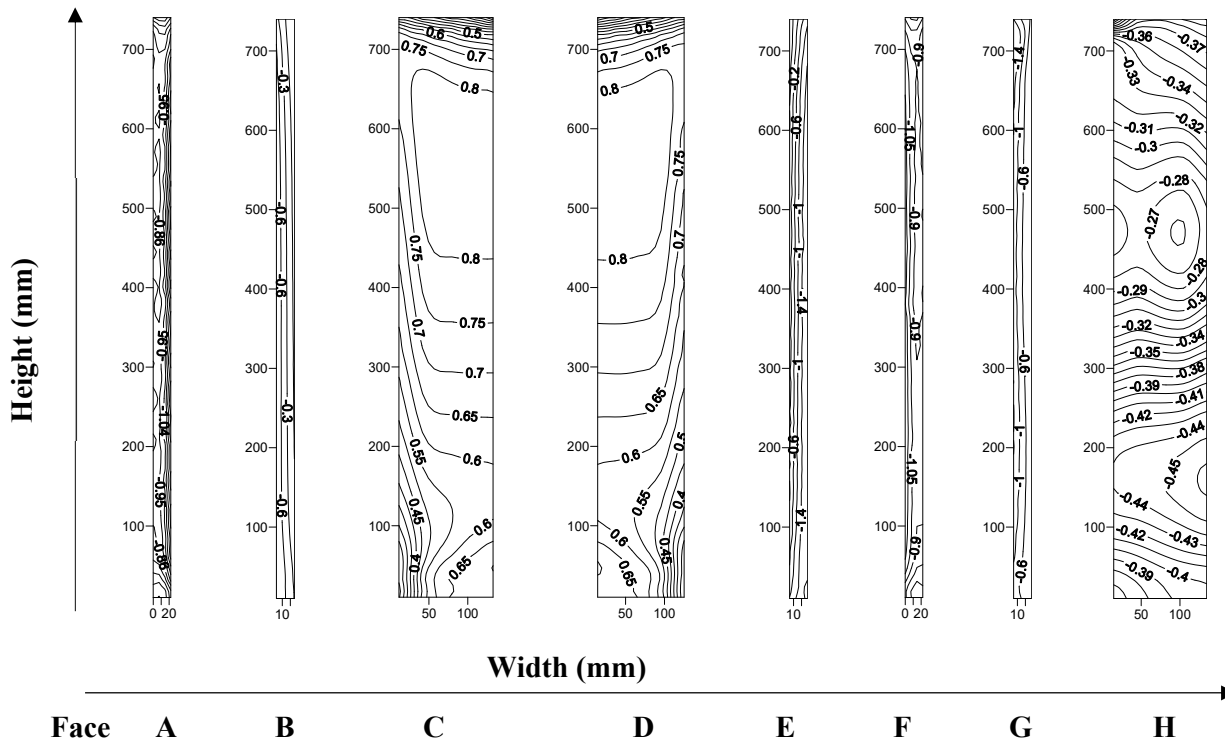


Figure 5.56 Distribution of wind pressure coefficient on the Y-shape with fillet corner at 60° wind incidence angle

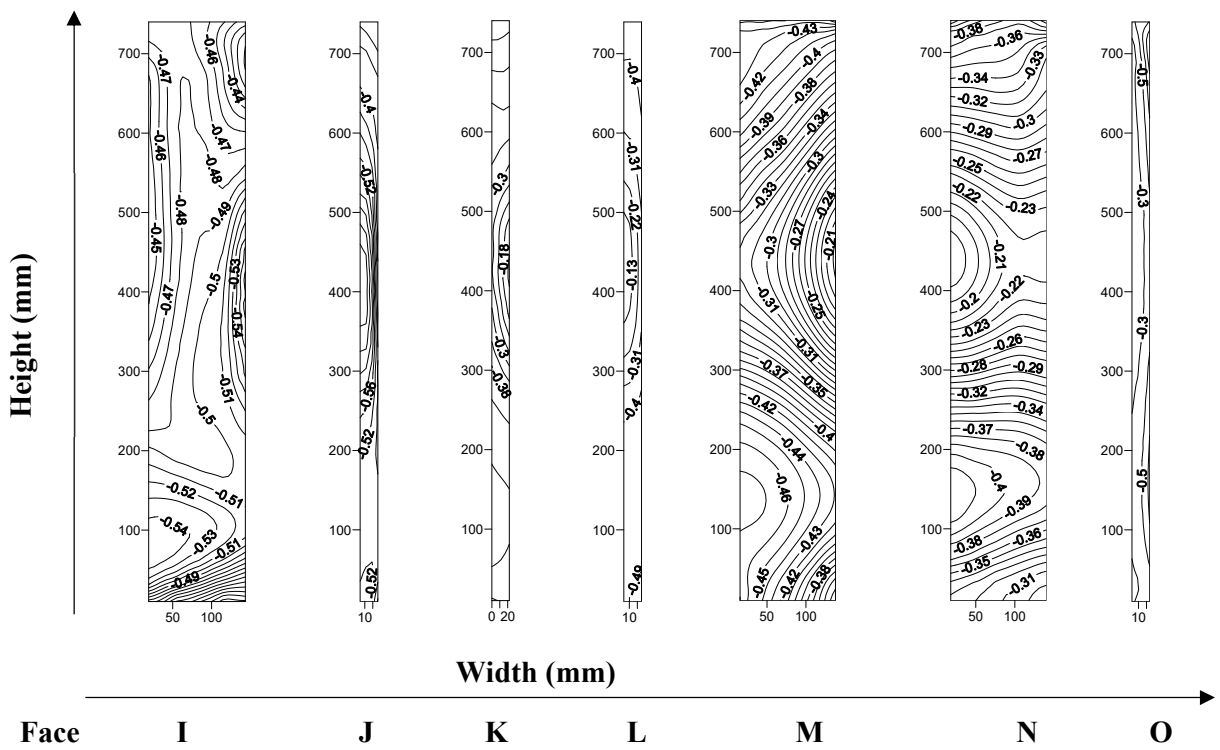
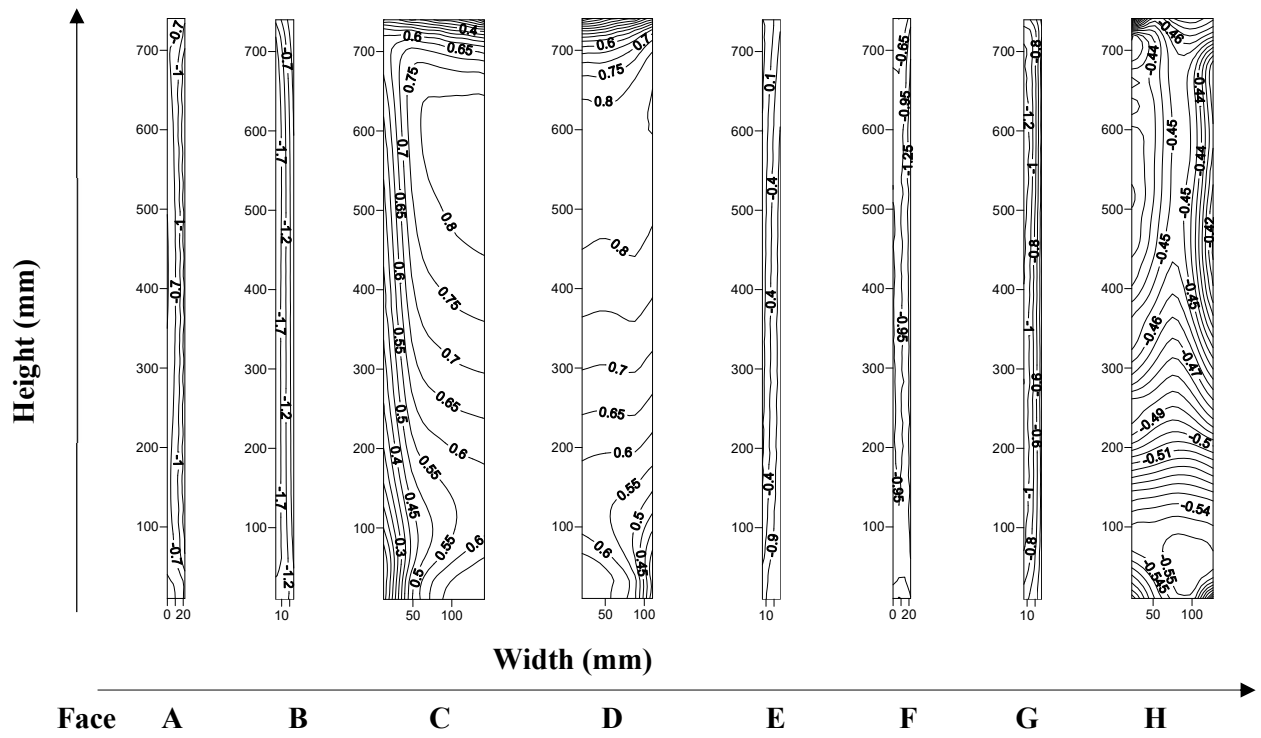


Figure 5.57 Distribution of wind pressure coefficient on the Y-shape with fillet corner at  $75^\circ$  wind incidence angle

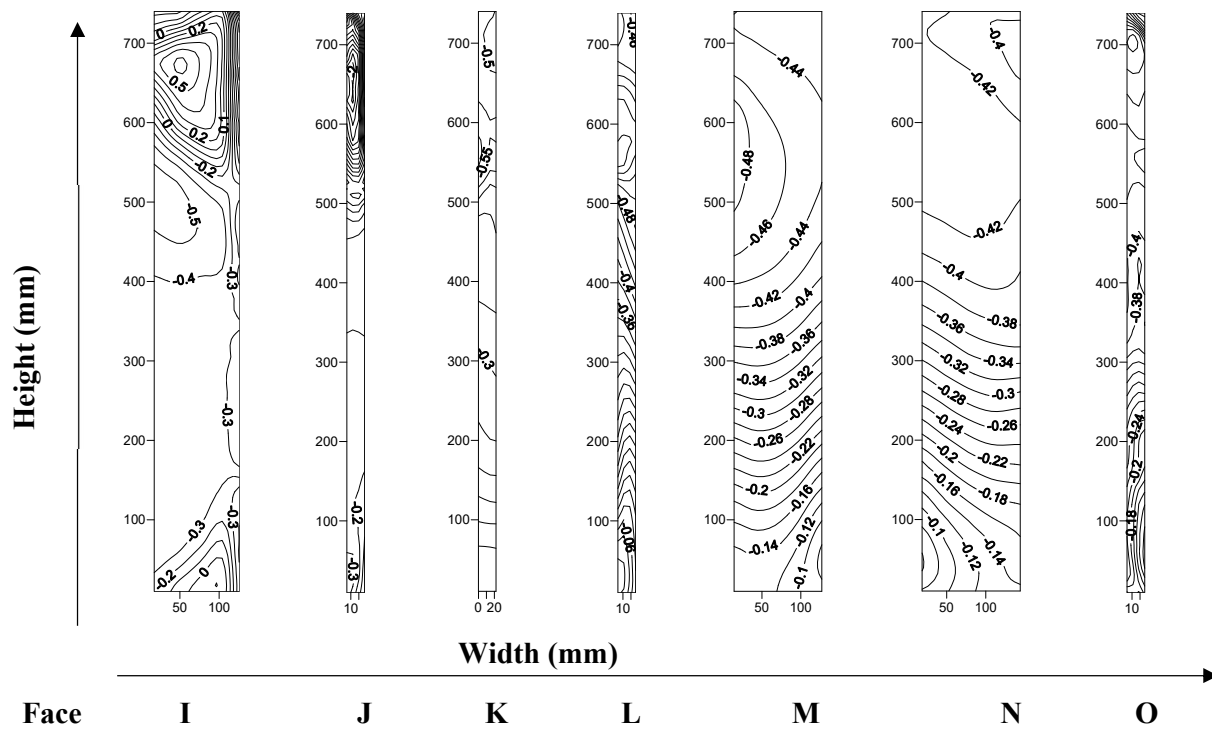
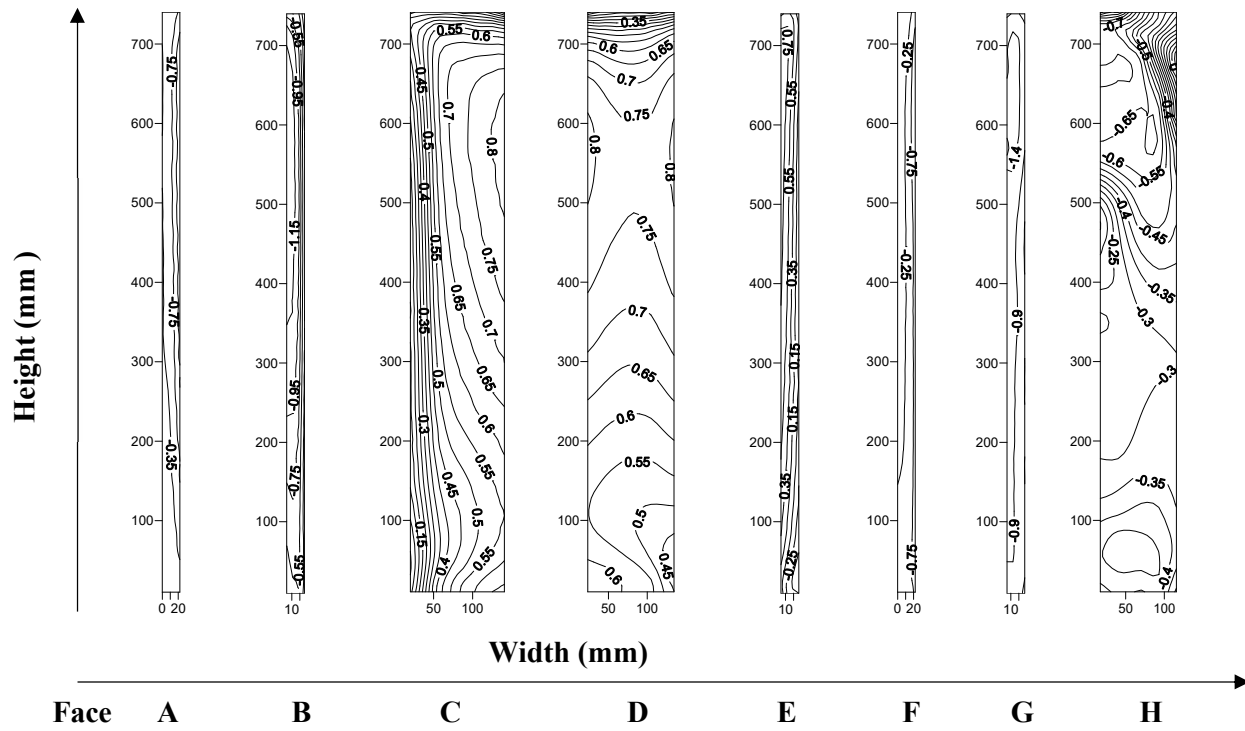


Figure 5.58 Distribution of wind pressure coefficient on the Y-shape with fillet corner at 90° wind incidence angle

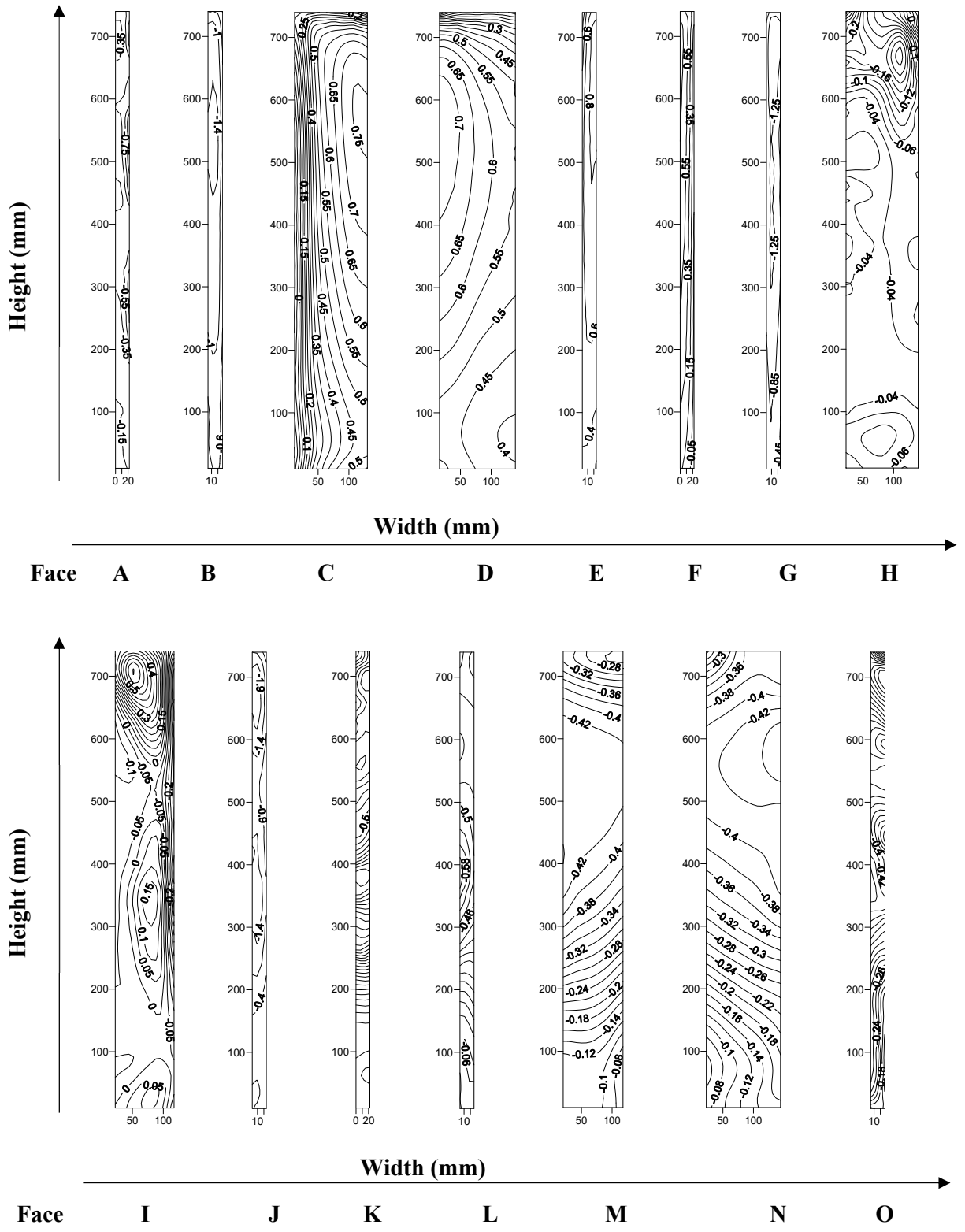


Figure 5.59 Distribution of wind pressure coefficient on the Y-shape with fillet corner at 105° wind incidence angle

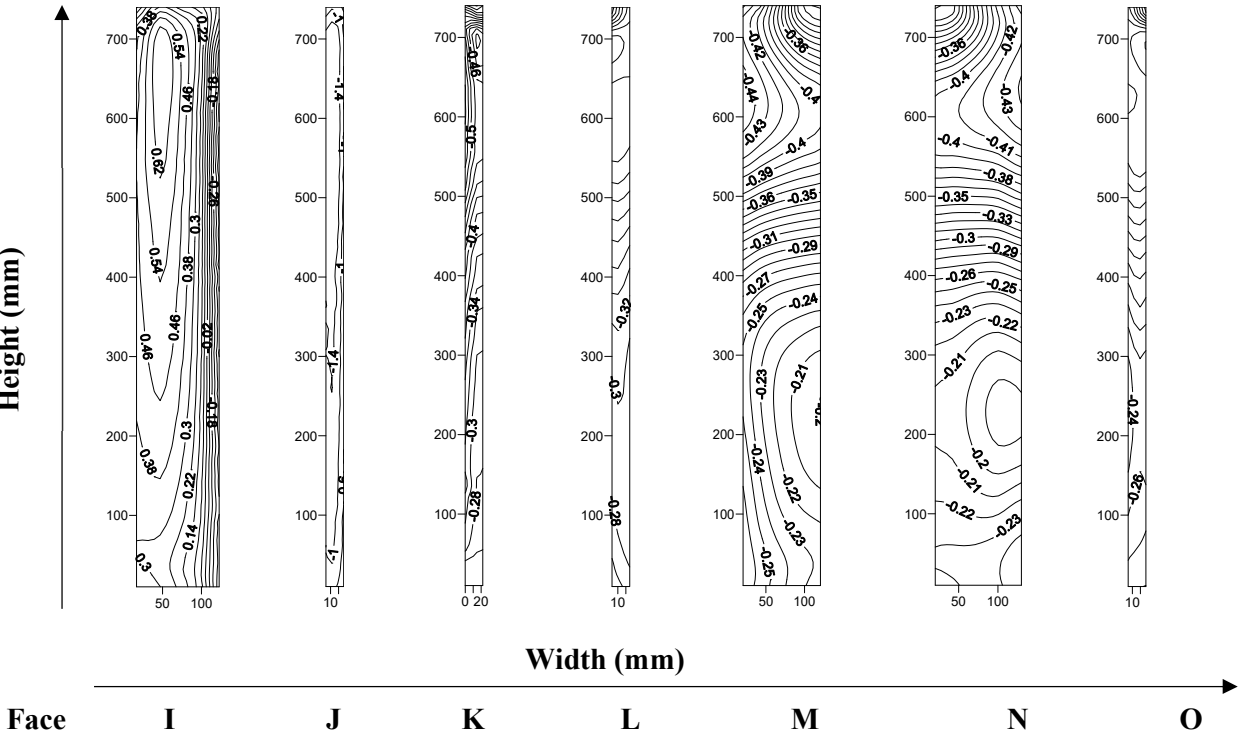
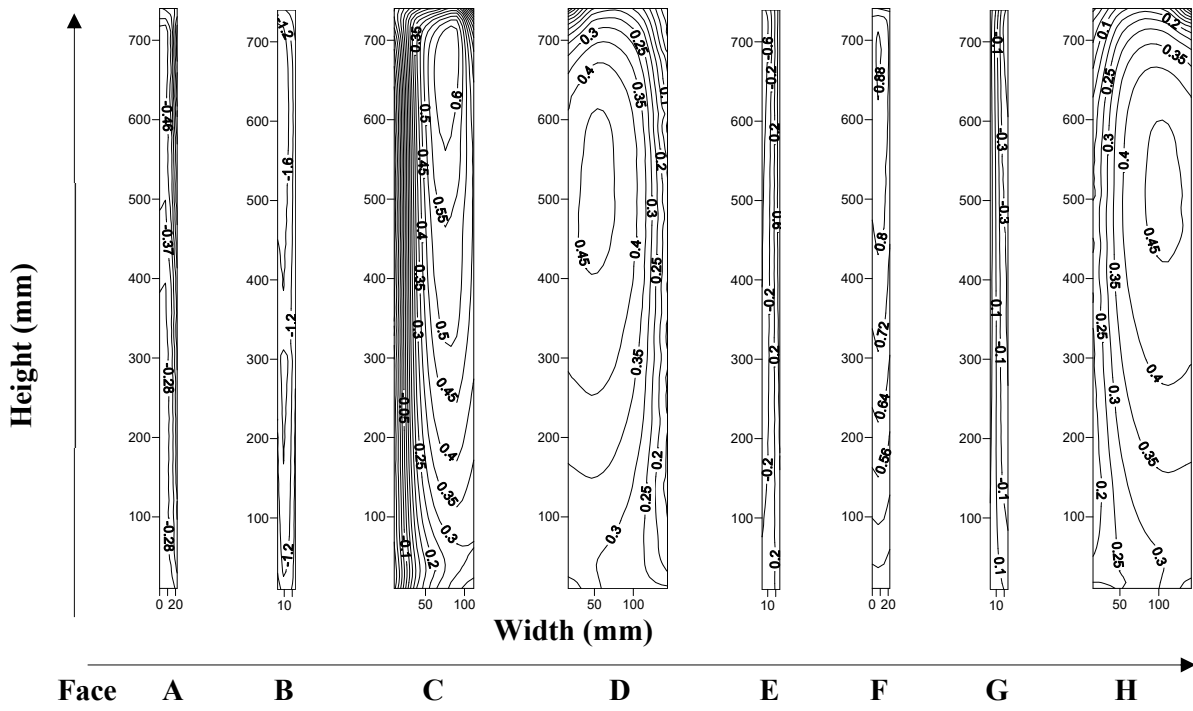


Figure 5.60 Distribution of wind pressure coefficient on the Y-shape with fillet corner at 120° wind incidence angle



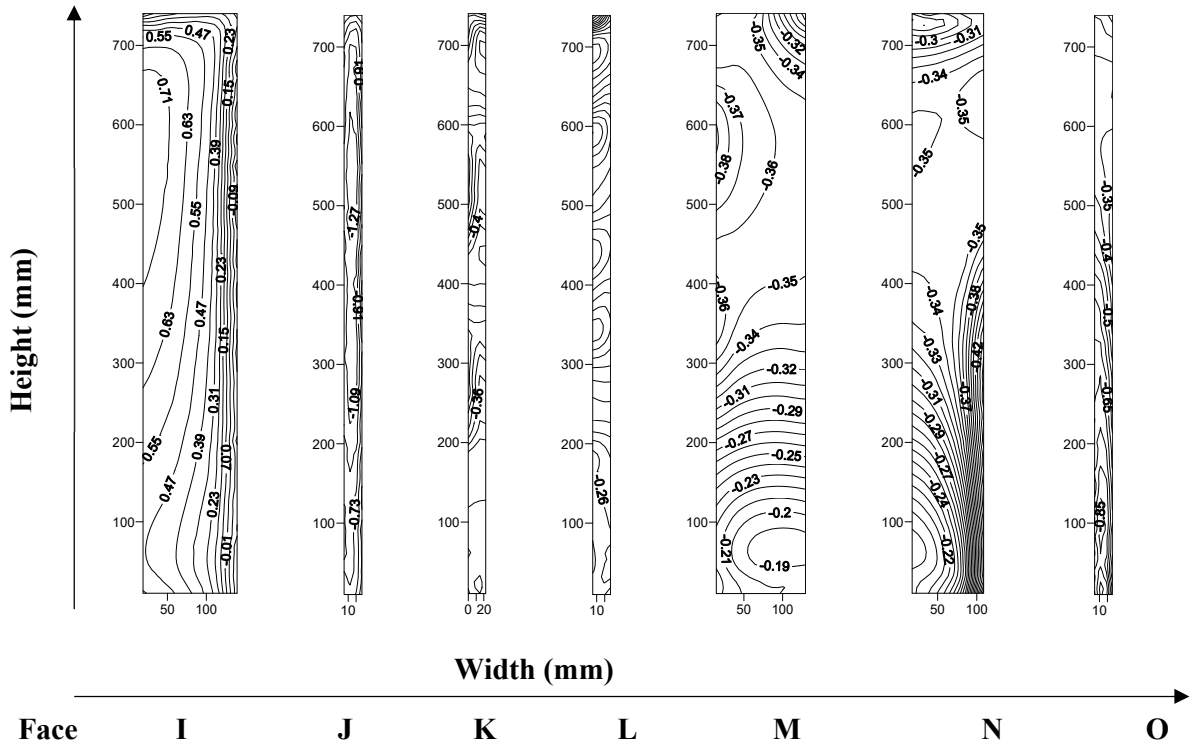
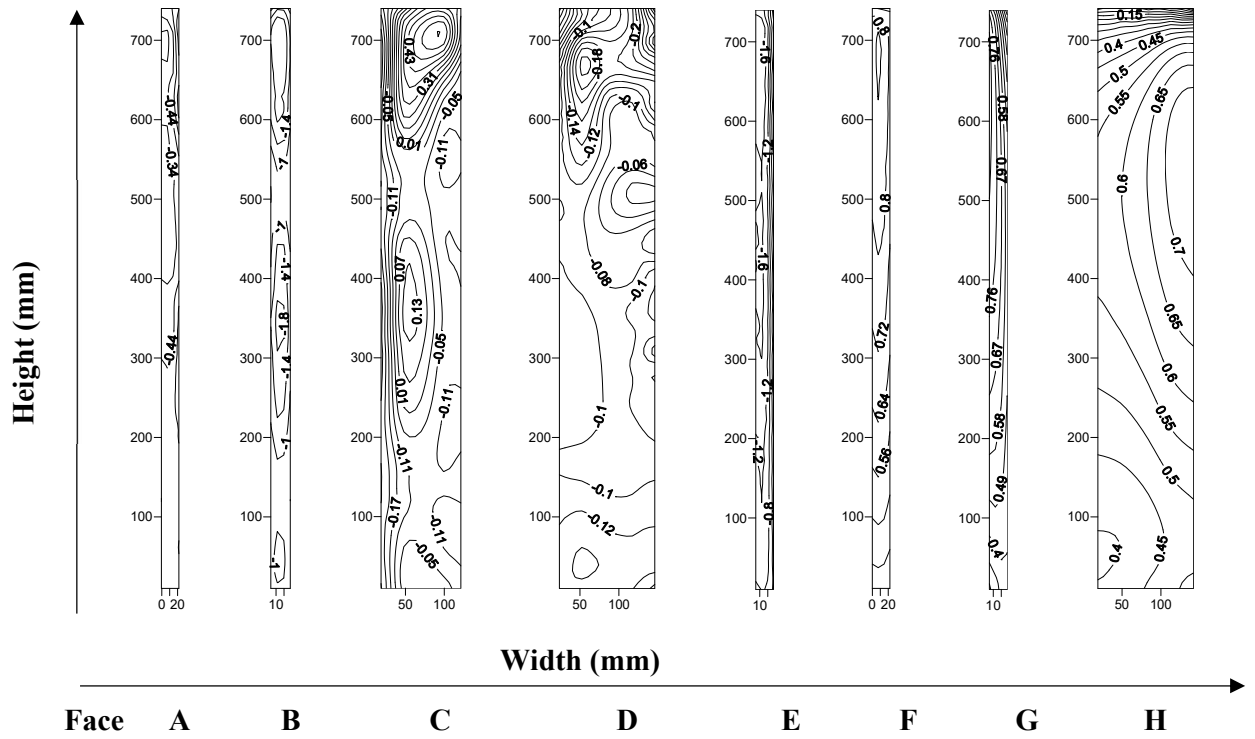


Figure 5.61 Distribution of wind pressure coefficient on the Y-shape with fillet corner at 135° wind incidence angle

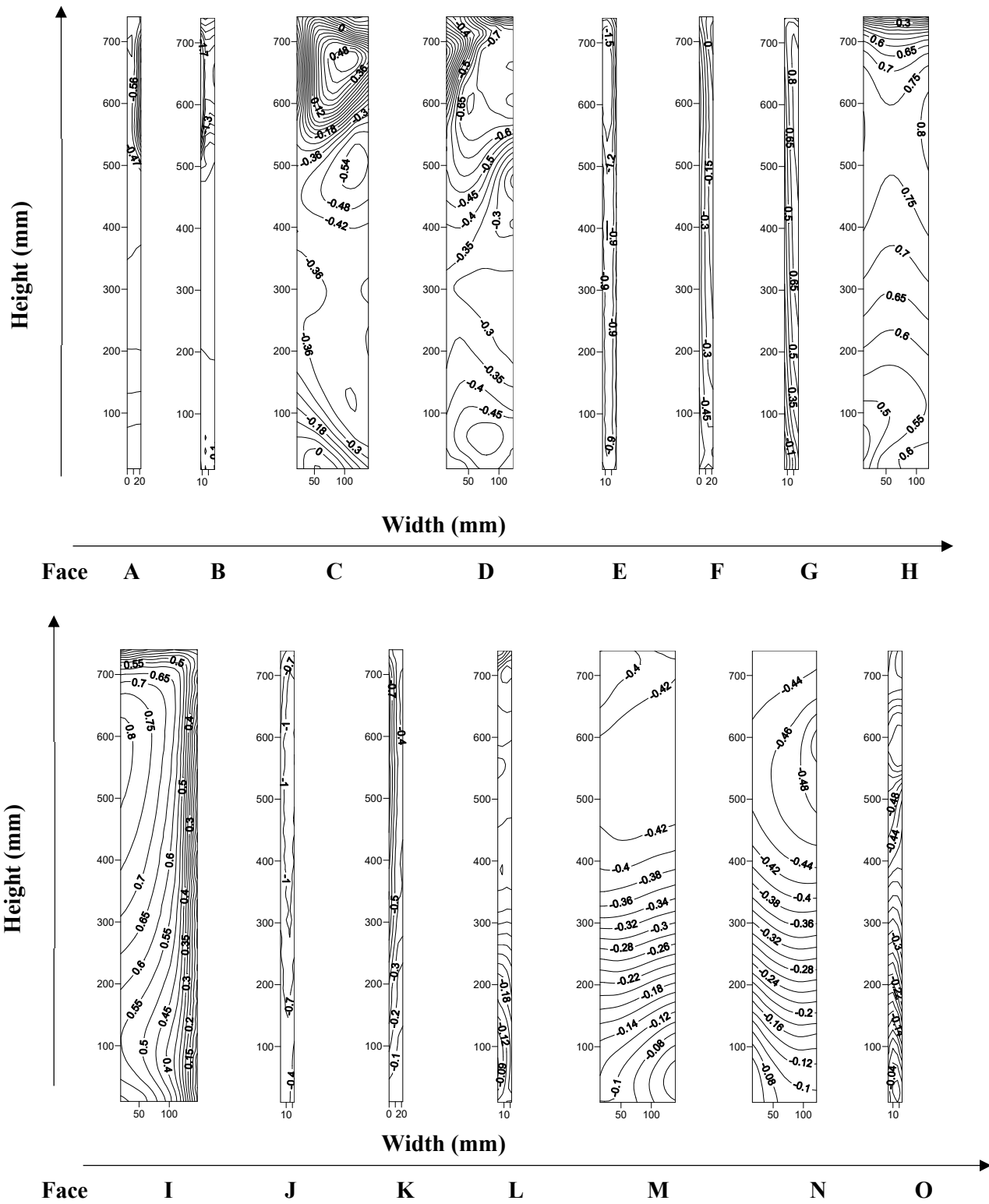


Figure 5.62 Distribution of wind pressure coefficient on the Y-shape with fillet corner at  $150^\circ$  wind incidence angle

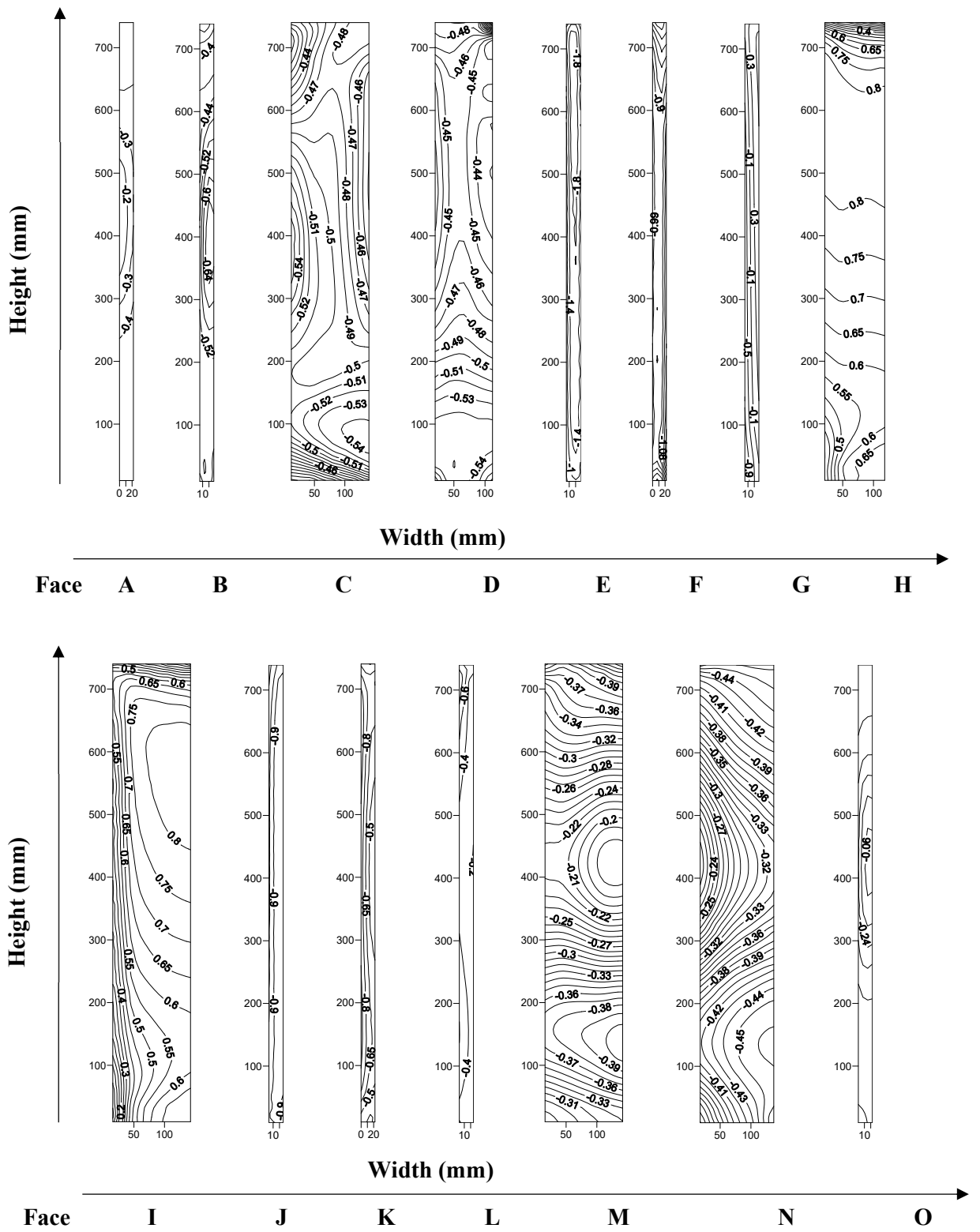


Figure 5.63 Distribution of wind pressure coefficient on the Y-shape with fillet corner at 165° wind incidence angle

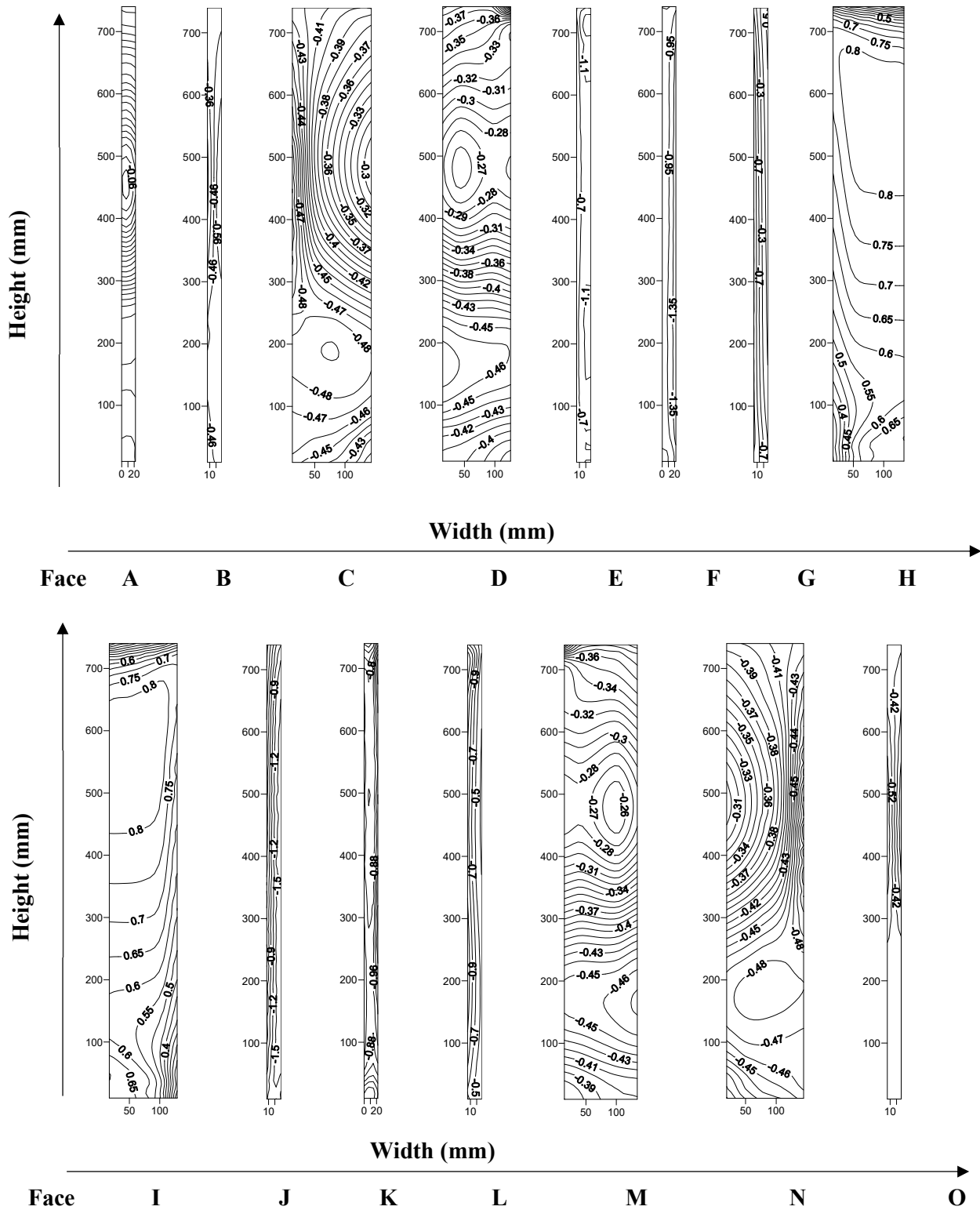


Figure 5.64 Distribution of wind pressure coefficient on the Y-shape with fillet corner at 180° wind incidence angle

The critical value of such pressure is either positive or negative is clearly represented in the form of label on the contour profile for each face of the building model, for the wind incidence angle from  $0^{\circ}$  to  $180^{\circ}$  wind at an interval of  $15^{\circ}$  each. The wind flow is also having different characteristics like vortex shedding etc. and this effect is the main cause for the variation in the pressure also the reduction of wind effects is done on the tall building by investigating the wind effects on building model having chafer corner, fillet corner and recesses corner into the corner configuration of the geometrical shape of the high-rise structure.

### **5.5.2 Vertical Pressure Distribution along the Height of the Building**

The pressure distribution on the central vertical line of each face of model having fillet corners are depicted in the Figure 5.65 (contd.) Mean pressure distribution on the vertical centre line for Y shape with fillet corner and it is clearly demonstrated for each wind incidence angle that how the pressure distribution varies along the centre line and is helpful for designer to provide opening etc. on that particular surface. In this study the wind incidence angle varies from  $0^{\circ}$  to  $180^{\circ}$  wind at an interval of  $15^{\circ}$ . In the case of  $180^{\circ}$  only two faces are under the influence of positive pressure while in the case of  $0^{\circ}$  wind face-A, C, E and N are having positive pressure. And in the same way it is demonstrated more precisely in the form of graph for each wind incidence angle for the angle ranging from  $0^{\circ}$  to  $180^{\circ}$  wind incidence angle.

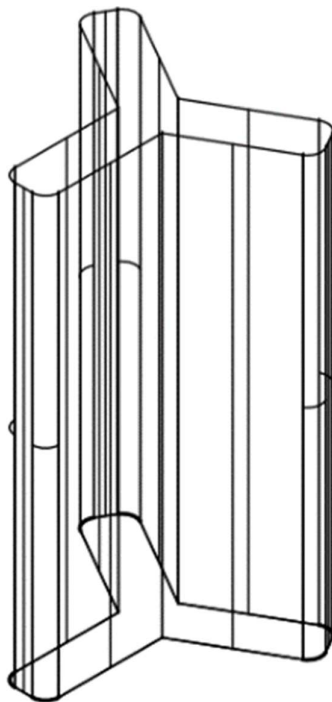
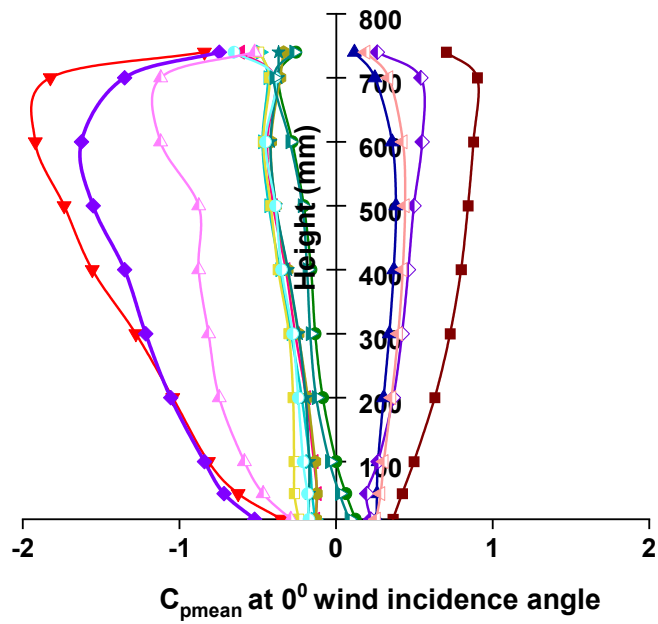
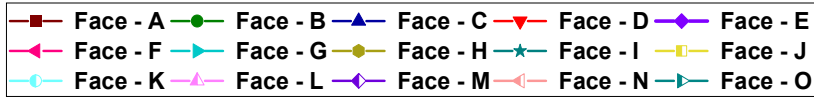


Figure 5.65 (contd.) Mean pressure distribution on the vertical centre line for Y shape with fillet corner

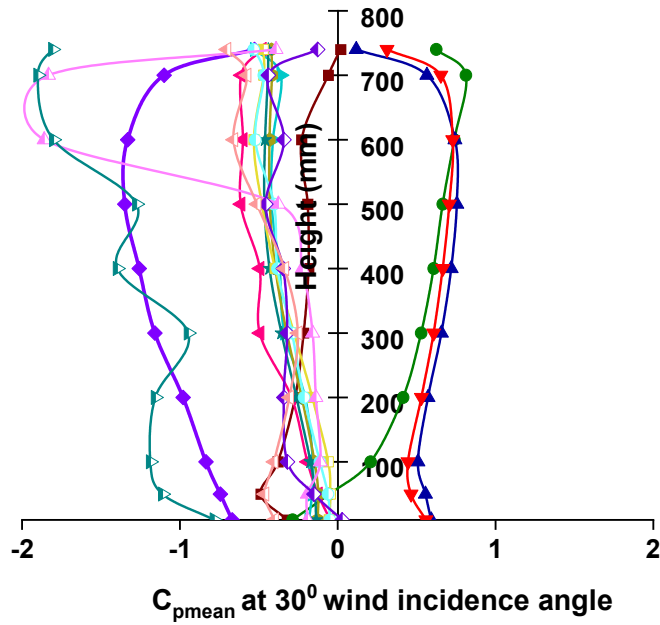
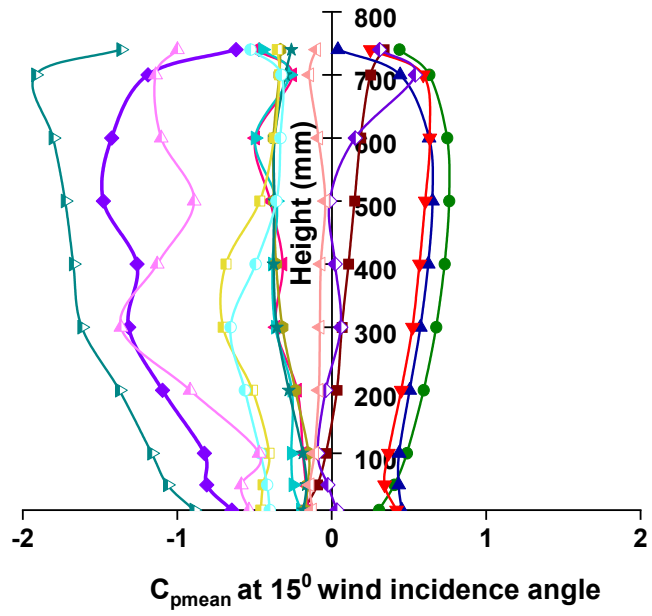
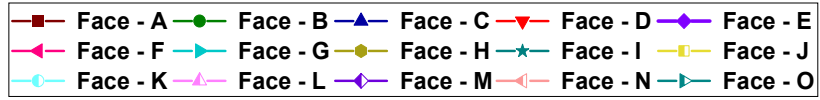


Figure 5.65 (contd.) Mean pressure distribution on the vertical centre line for Y shape with fillet corner

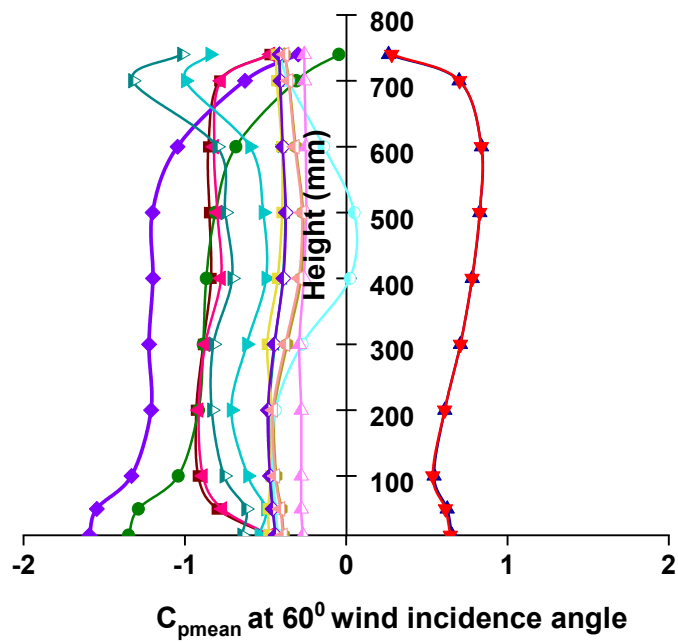
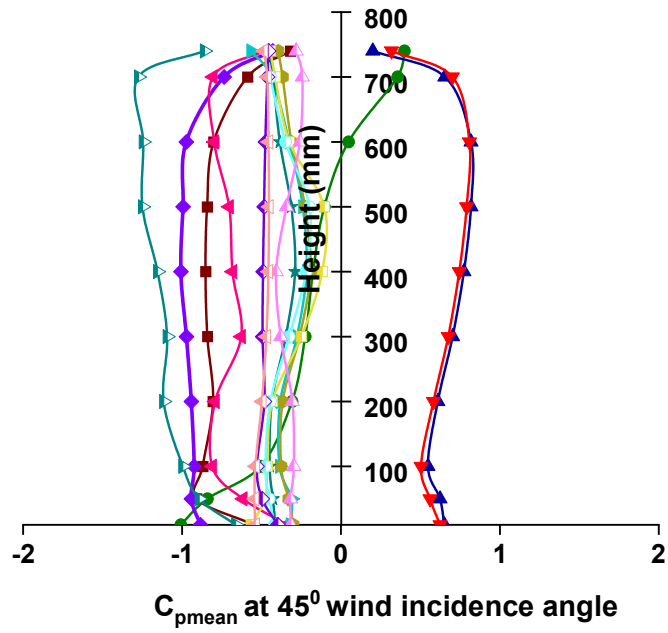
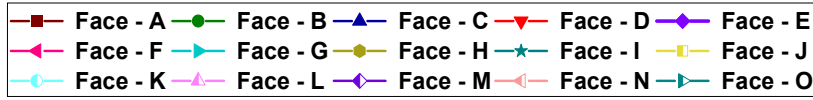


Figure 5.65 (contd.) Mean pressure distribution on the vertical centre line for Y shape with fillet corner



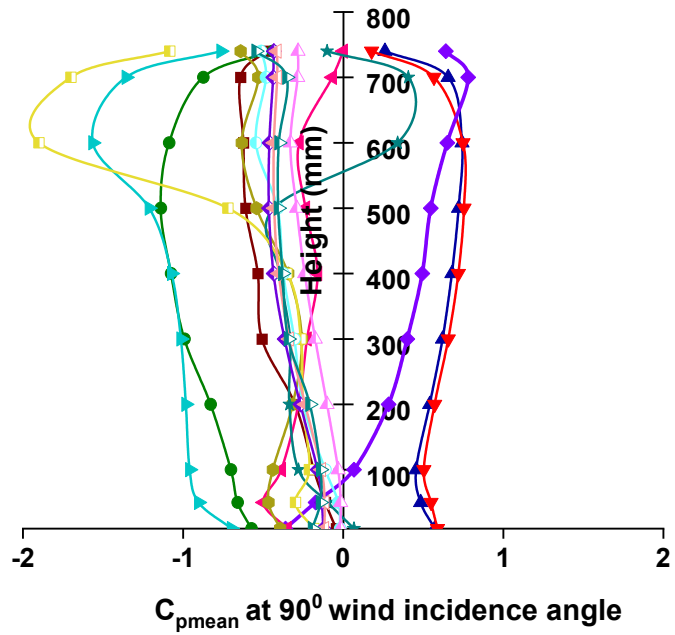
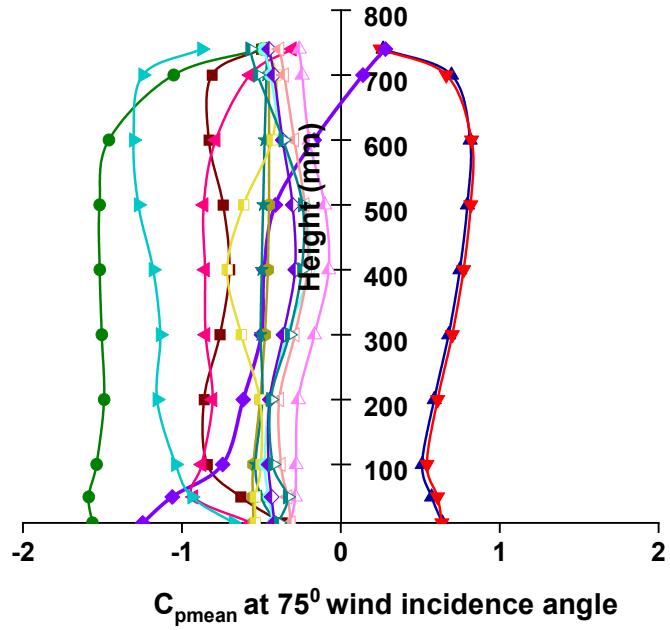


Figure 5.65 (contd.) Mean pressure distribution on the vertical centre line for Y shape with fillet corner

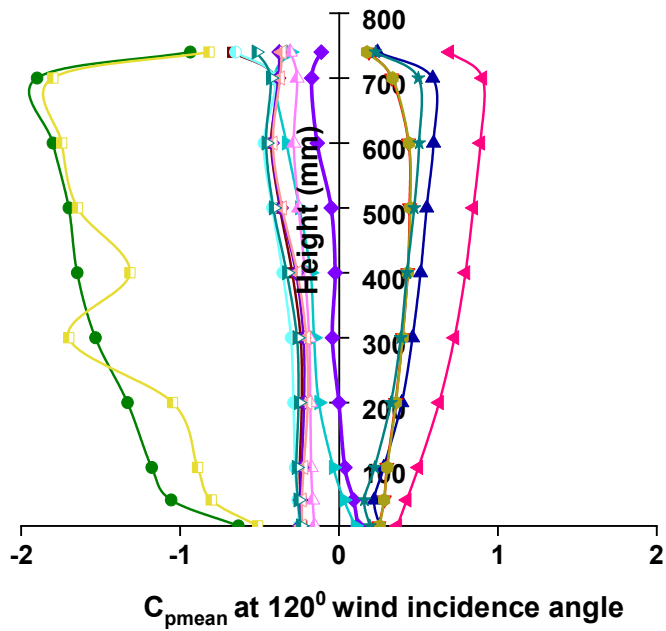
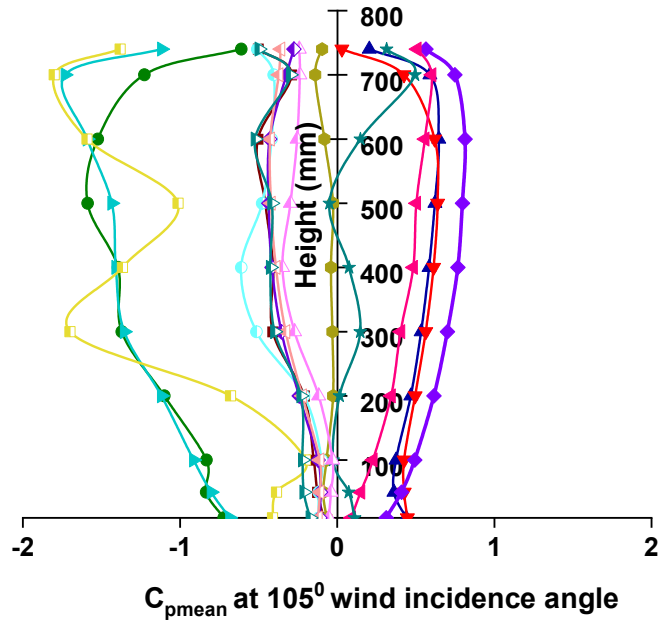
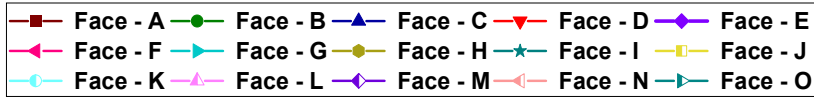


Figure 5.65 (contd.) Mean pressure distribution on the vertical centre line for Y shape with fillet corner

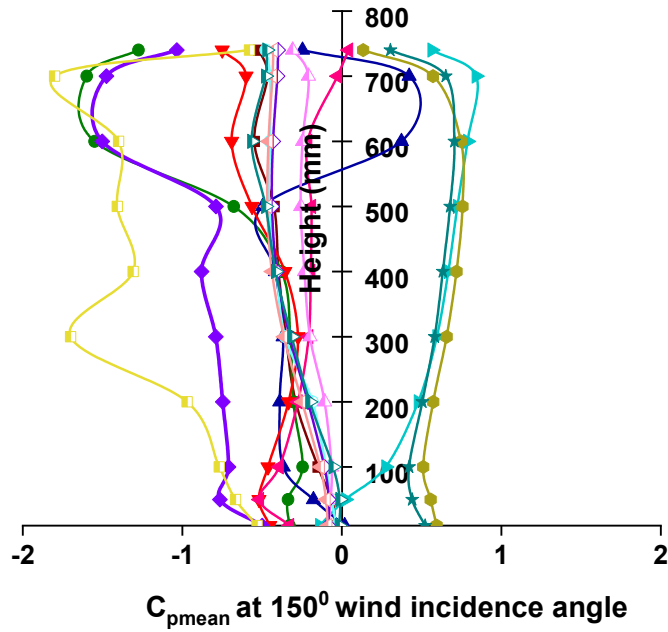
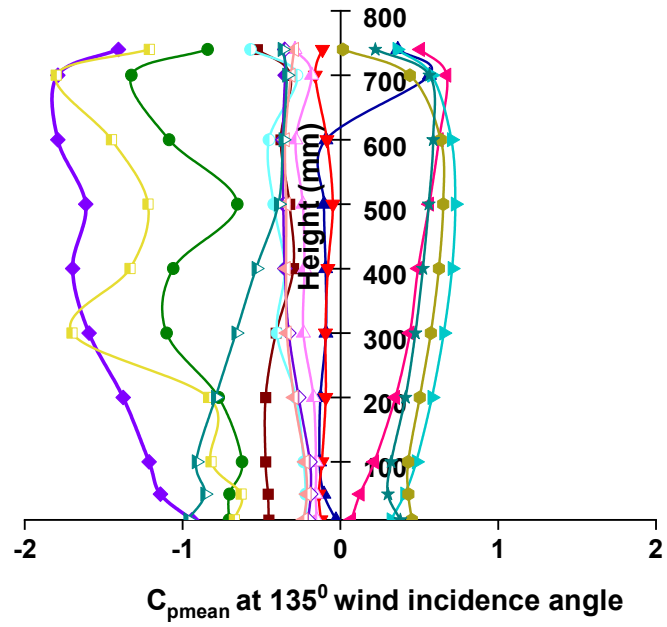
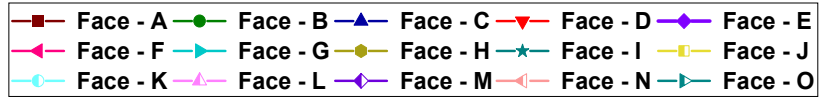


Figure 5.65 (contd.) Mean pressure distribution on the vertical centre line for Y shape with fillet corner

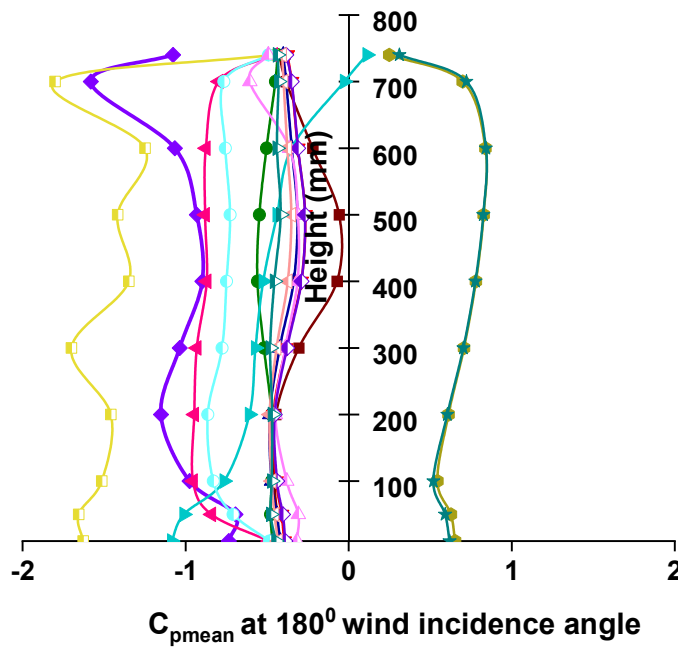
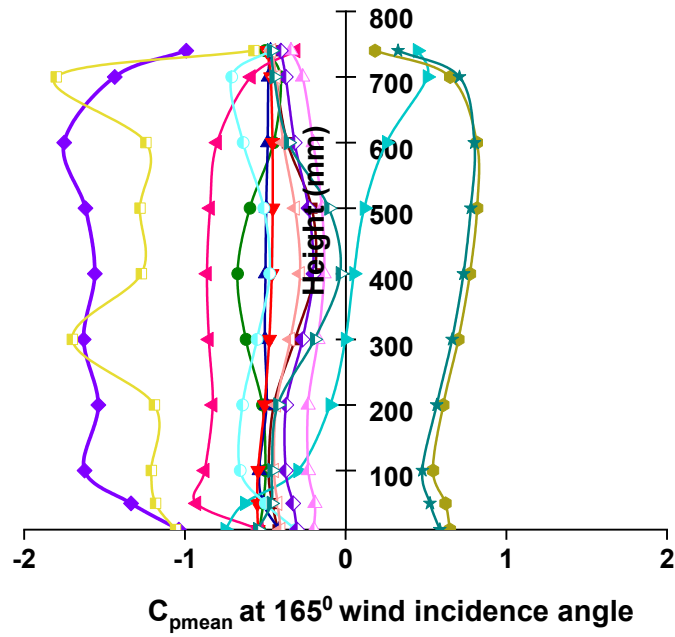
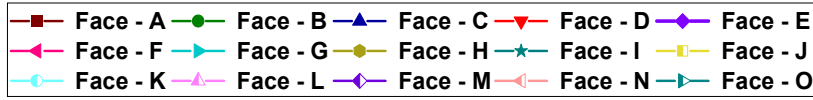


Figure 5.65 Mean pressure distribution on the vertical centre line for Y shape with fillet corner

### **5.5.3 Horizontal Pressure Distribution along the Peripheral Distance of Building**

Pressure distribution around the peripheral distance of building model is presented in Figure 5.66. Mean pressure distribution along the peripheral distance of the Y-shape with fillet corner and is investigated at three different levels of 250 mm, 375 mm and 500 mm height from the base of the model. The point is taken at the places where there is a slight change in the geometry of the model. The graphs depict that the pressure distribution in the case of top two third height of building is more and in bottom one third part it is less than the top one third part meaning it can be concluded that as the height increases pressure will be increased with respect to the height of the model.

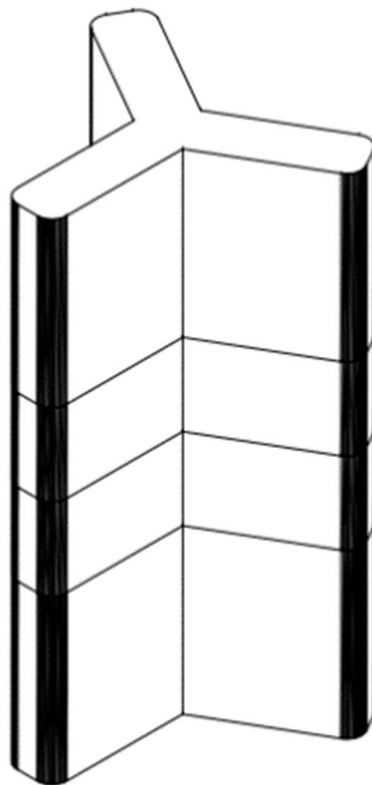
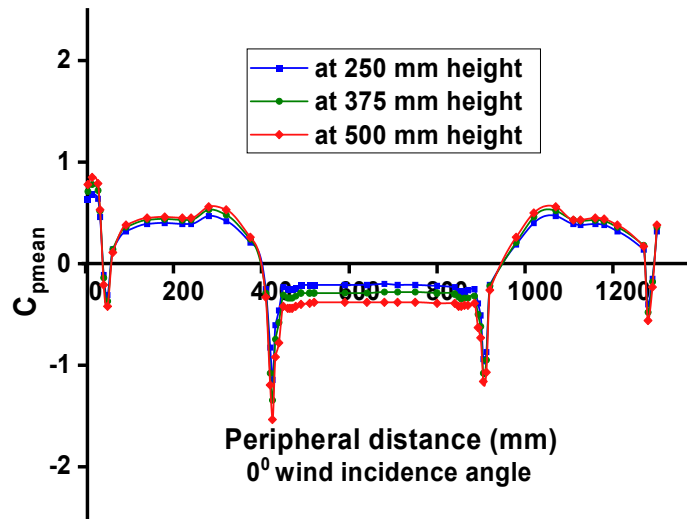


Figure 5.66 (contd.) Mean pressure distribution along the peripheral distance of the Y-shape with fillet corner

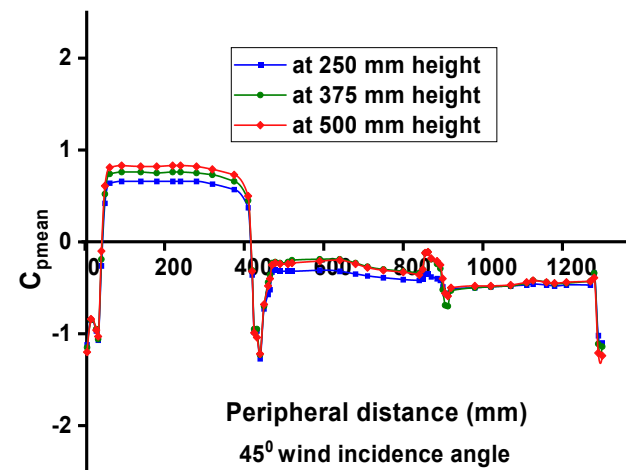
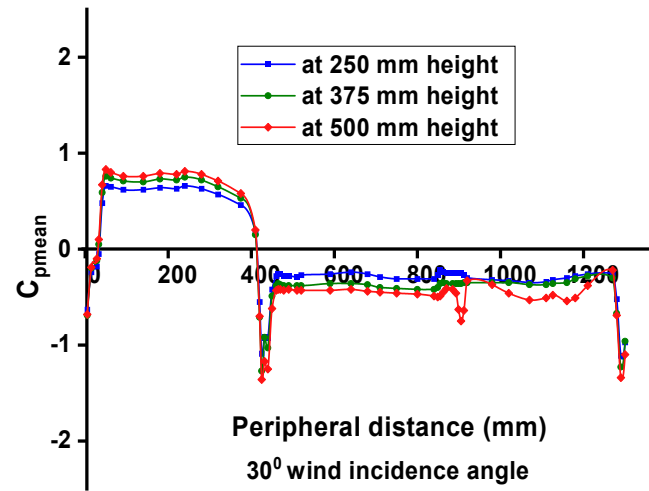
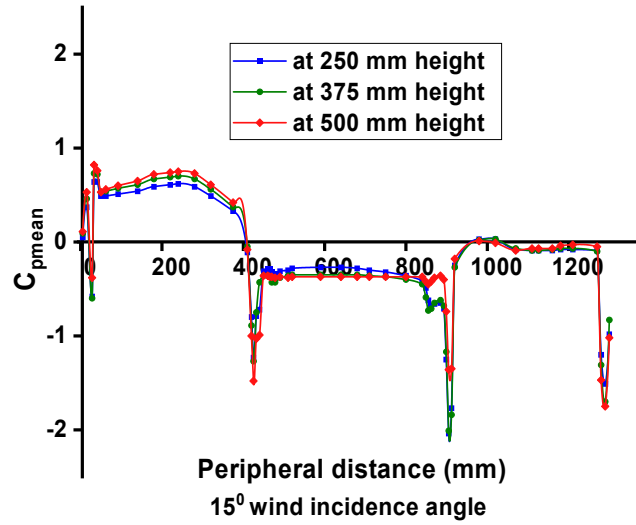


Figure 5.66 (contd.) Mean pressure distribution along the peripheral distance of the Y-shape with fillet corner

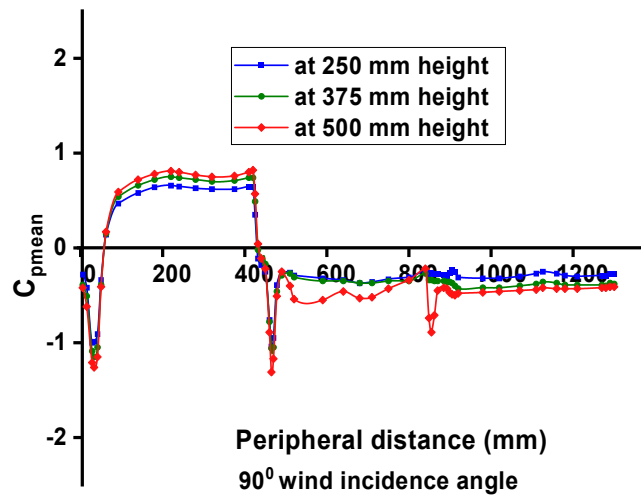
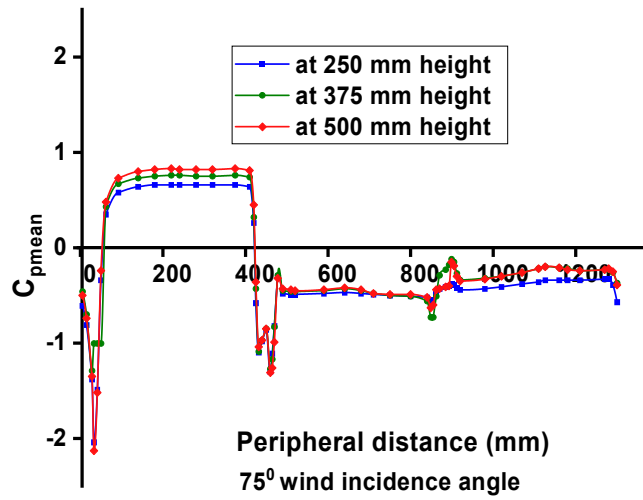
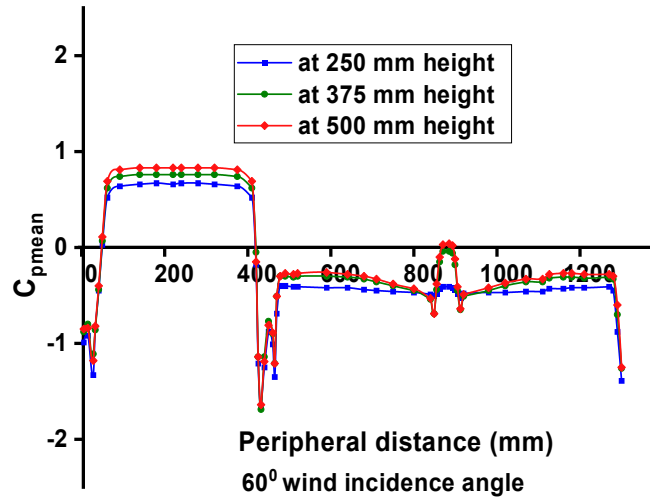


Figure 5.66 (contd.) Mean pressure distribution along the peripheral distance of the Y-shape with fillet corner



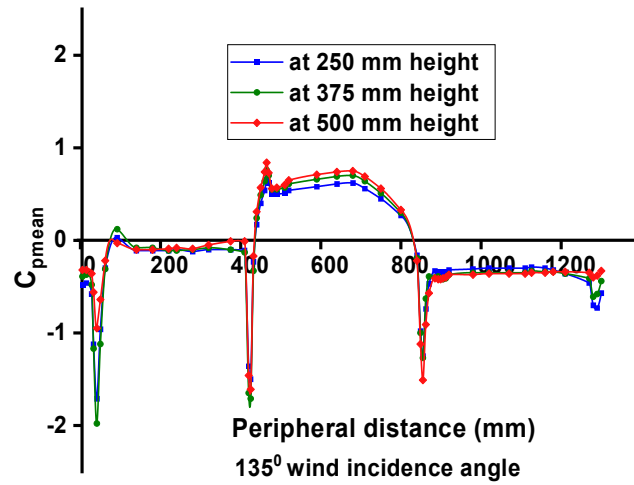
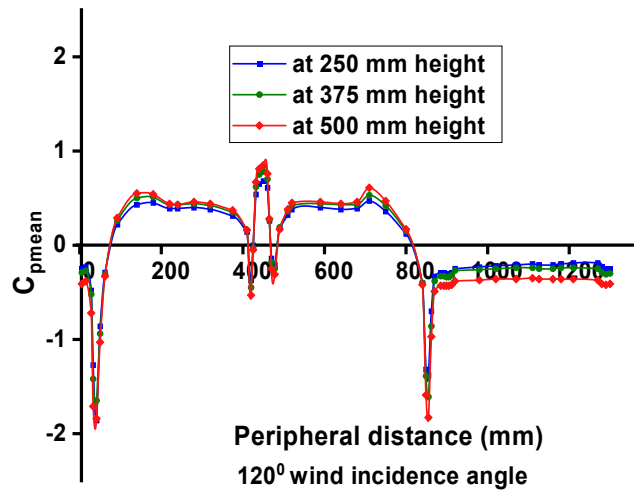
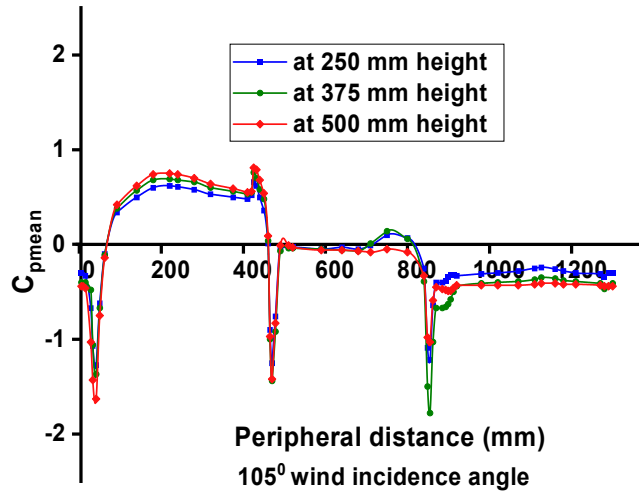


Figure 5.66 (contd.) Mean pressure distribution along the peripheral distance of the Y-shape with fillet corner

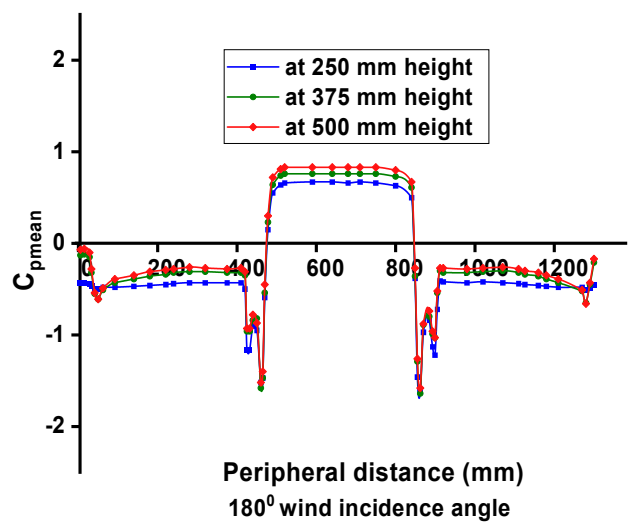
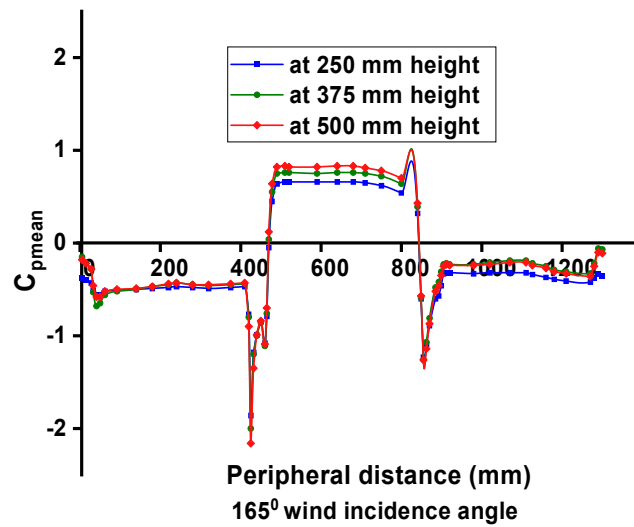
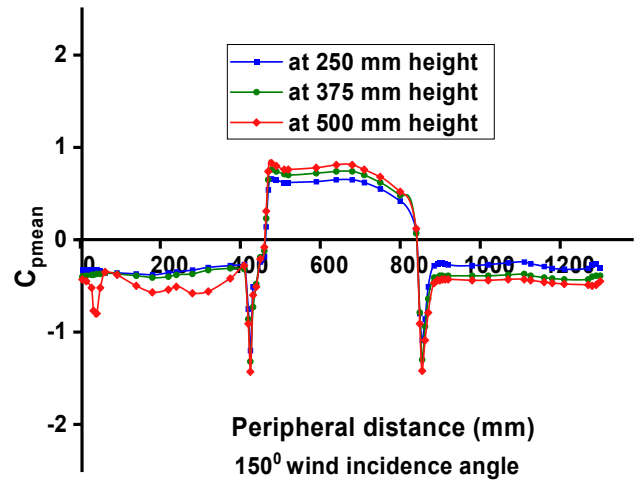


Figure 5.66 Mean pressure distribution along the peripheral distance of the Y-shape with fillet corner

### 5.5.4 Force Coefficients

The wind force coefficient for model having fillet corner is calculated for the wind incidence angle ranging from  $0^{\circ}$  to  $180^{\circ}$  at an interval of  $15^{\circ}$ . The force coefficient is calculated along and across the wind direction, along wind force coefficient is  $C_{fy}$  while the across wind force coefficient is  $C_{fx}$  and it is found that  $C_{fx}$  is maximum of 0.66 for the case of  $60^{\circ}$  and  $180^{\circ}$  wind while the minimum  $C_{fx}$  of 0.41 is obtained in the case of  $120^{\circ}$ . In the same way the  $C_{fx}$  is represented in the graphical form for the all the wind incidence angles. The wind force coefficient is along the wind direction is  $C_{fy}$  and the maximum  $C_{fy}$  of 0.46 in the case of  $90^{\circ}$  wind is spotted while the minimum  $C_{fy}$  of -0.48 is noted for the wind incidence angle of  $150^{\circ}$ . The force coefficient is presented in Figure 5.67 Wind force coefficient of the Y-shape with fillet corner

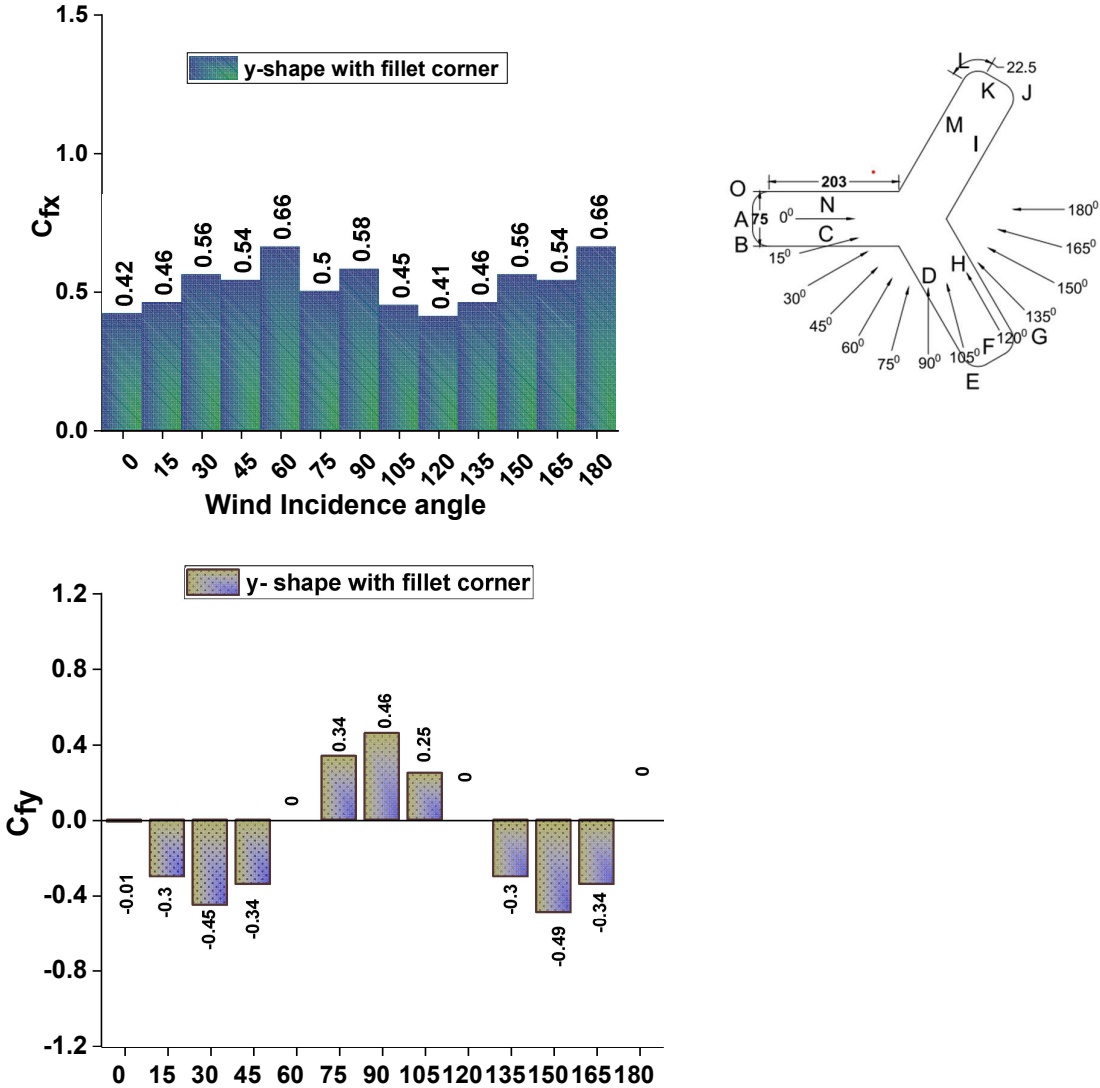


Figure 5.67 Wind force coefficient of the Y-shape with fillet corner

### 5.5.5 Moment Coefficients

The moment coefficient is calculated for the wind incidence angle ranging from  $0^{\circ}$  to  $180^{\circ}$  at an interval of  $15^{\circ}$  for the building model having the geometrical shape of irregular Y-shape with fillet corner. This study is about the corner configuration of the tall building model having the equal area building model of regular and irregular shape. The values of moment are obtained after performing the numerical simulation on the building model into ANSYS CFX. Moment coefficient in x- direction is  $C_{mx}$  while the moment coefficient in y-direction is  $C_{my}$ . It is found that the maximum  $C_{mx}$  of 0.25 is obtained when incidence angle is  $30^{\circ}$  and  $150^{\circ}$  and the minimum  $C_{mx}$  of -0.24 is spotted in the case of  $90^{\circ}$  wind while the moment coefficient in the y- direction is  $C_{my}$  and the maximum  $C_{my}$  of 0.34 is observed in the case of  $30^{\circ}$ ,  $90^{\circ}$  and  $150^{\circ}$  wind while the minimum  $C_{my}$  of 0.24 is found when the incidence angle was  $120^{\circ}$  as in Figure 5.68 Wind moment coefficient of the Y-shape with fillet corner depicting the moment coefficient.

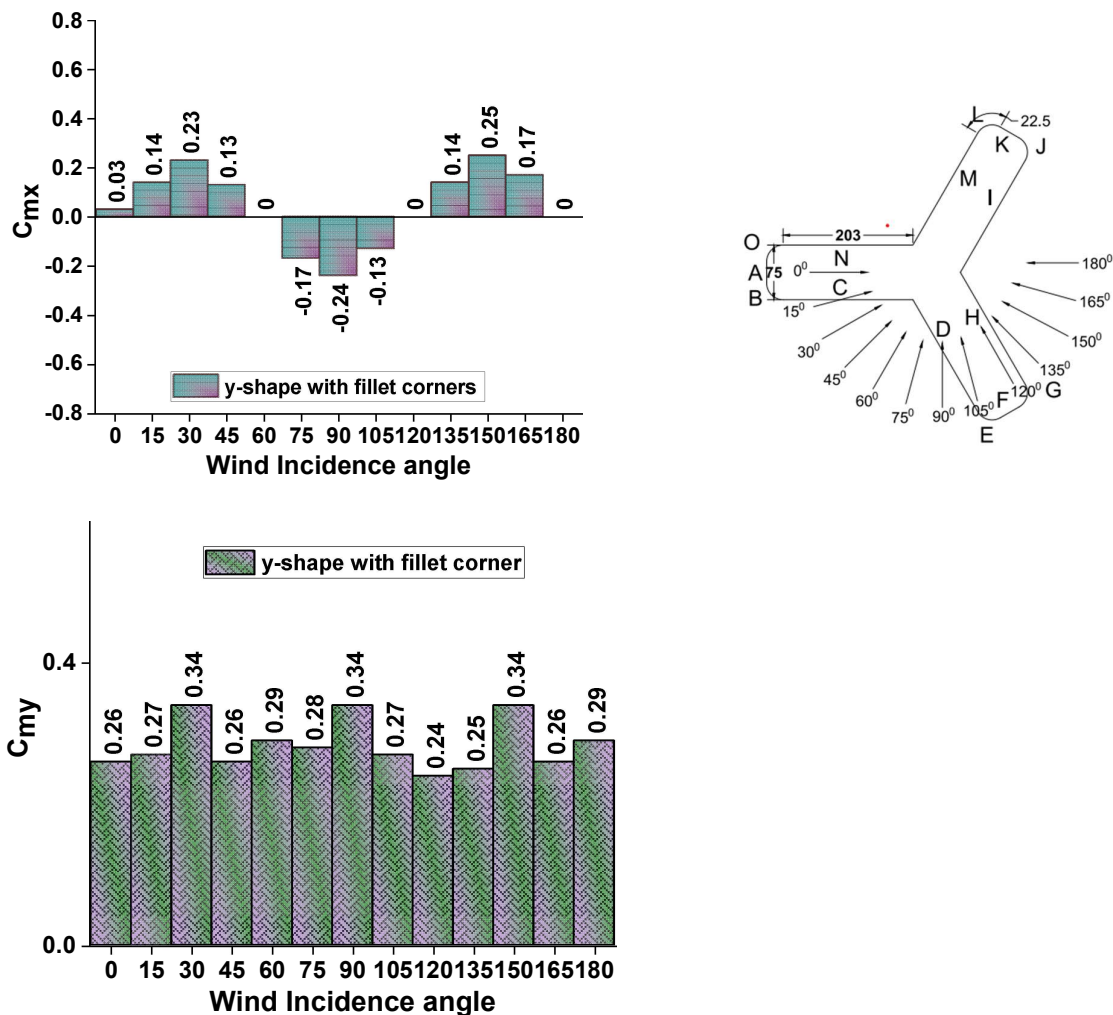


Figure 5.68 Wind moment coefficient of the Y-shape with fillet corner

### 5.5.6 External Pressure Coefficients

The external pressure coefficient for each surface of the building model having irregular shape of Y-having fillet corner, is tabulated in Table:5.4 External Pressure Coefficient for Building Model-H (Y-shape Fillet). This external pressure coefficient is determined after performing the numerical simulation in ANSYS CFX. External pressure coefficient is calculated after drawing the lines along the height and width of the surface here these lines play the role of pressure tapping on the grid lines. After extracting the pressure data, the calculation is performed as per the wind tunnel manual and report no 67. The average of the all-pressure lines is investigated and mean of all points are reported and it is found that in the case of  $0^0$  wind the external pressure coefficient is maximum of 0.69 is on face-A while the minimum of -0.89 is observed on face-E and face-L. In the same way the external pressure coefficient is calculated for the wind incidence angle varies from  $0^0$  to  $180^0$  at an interval of  $15^0$  each. The maximum external pressure coefficient of 0.68 on the face-H and face-I is spotted in the case of  $180^0$  wind while the minimum of -0.96 is observed on face-F and face-K.

**Table:5.4 External Pressure Coefficient for Building Model-H (Y-shape Fillet)**

<b>Model-H (Y-shape Fillet)</b>													
<b>Face</b>	<b>0°</b>	<b>15°</b>	<b>30°</b>	<b>45°</b>	<b>60°</b>	<b>75°</b>	<b>90°</b>	<b>105°</b>	<b>120°</b>	<b>135°</b>	<b>150°</b>	<b>165°</b>	<b>180°</b>
<b>A</b>	<b>0.69</b>	0.01	-0.37	<b>-0.94</b>	<b>-0.96</b>	-0.86	-0.58	-0.41	-0.39	-0.44	-0.39	-0.36	-0.30
<b>B</b>	-0.06	<b>0.58</b>	<b>0.39</b>	-0.25	-0.66	<b>-1.24</b>	-0.76	-0.95	<b>-1.28</b>	<b>-1.18</b>	-0.67	-0.51	-0.46
<b>C</b>	0.31	0.54	0.65	<b>0.69</b>	<b>0.67</b>	0.62	0.53	0.41	0.24	-0.06	-0.26	-0.49	-0.42
<b>D</b>	0.26	0.41	0.53	0.62	<b>0.67</b>	<b>0.69</b>	<b>0.65</b>	0.53	0.32	-0.11	-0.43	-0.48	-0.36
<b>E</b>	-0.89	-0.90	-0.87	-0.74	-0.66	-0.39	0.33	<b>0.60</b>	0.02	-1.07	<b>-0.98</b>	<b>-1.20</b>	-0.77
<b>F</b>	-0.39	-0.39	-0.57	-0.84	<b>-0.96</b>	-0.99	-0.42	0.34	<b>0.69</b>	0.42	-0.31	-0.94	-0.96
<b>G</b>	-0.36	-0.33	-0.32	-0.38	-0.79	-0.79	<b>-0.94</b>	<b>-1.01</b>	0.02	<b>0.59</b>	0.47	-0.07	-0.78
<b>H</b>	-0.29	-0.3	-0.32	-0.3	-0.36	-0.47	-0.4	-0.06	0.32	0.54	<b>0.65</b>	<b>0.69</b>	<b>0.68</b>
<b>I</b>	-0.29	-0.32	-0.35	-0.37	-0.43	-0.49	-0.25	-0.01	0.24	0.37	0.50	0.60	<b>0.68</b>
<b>J</b>	-0.36	-0.48	-0.33	-0.34	-0.44	-0.52	-0.63	<b>-1.01</b>	<b>-1.28</b>	-0.92	-0.9	-0.94	-0.78
<b>K</b>	-0.39	-0.49	-0.35	-0.36	-0.25	-0.36	-0.34	-0.38	-0.39	-0.36	-0.4	-0.66	<b>-0.96</b>
<b>L</b>	<b>-0.89</b>	<b>-1.40</b>	-0.87	-0.51	-0.44	-0.34	-0.33	-0.35	-0.35	-0.35	-0.31	-0.37	-0.77
<b>M</b>	0.26	-0.03	-0.23	-0.48	-0.43	-0.37	-0.35	-0.31	-0.30	-0.31	-0.31	-0.3	-0.36
<b>N</b>	0.31	-0.10	-0.40	-0.47	-0.36	-0.30	-0.32	-0.31	-0.30	-0.33	-0.34	-0.37	-0.42
<b>O</b>	-0.06	-1.23	<b>-1.02</b>	-0.87	-0.79	-0.40	-0.32	-0.35	-0.35	-0.55	-0.34	-0.32	-0.46

### 5.6 Comparative Study of $C_{fx}$ at $0^\circ$ and $180^\circ$ wind incidence angle

The wind can generate a number of varying forces that may have different effects on tall buildings, but the drag force is the one which is most important for tall building design. The term drag force is originated from the physics and fluid dynamics of the forces closely related to stop an object from moving inside the fluid to which it is exposed. A solid item encountering a fluid will cause a force called drag. The solid body must be in touch with the fluid or must block the flow of the fluid for the solid body to produce the drag force. If the fluid is not moving or, in a position of stop then if there is no flow then there will be no drag. The drag force is influenced by the fluid flow characteristics as well as the size, shape, and speed of the wind flow. The drag coefficient  $C_{fx}$  is a dimensionless variable used in fluid dynamics to quantify a drag or resistance to a fluid medium, such as air or water. Drag is a quantity that always includes size and direction is the drag force.

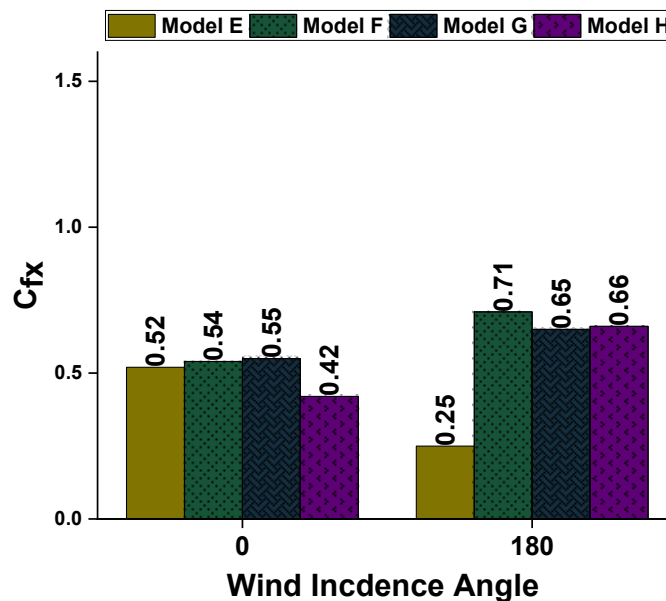


Figure 5.69  $C_{fx}$  for the irregular shape building model

Base shear is derived from the results obtained through the computational fluid dynamic tool ANSYS CFX. The  $C_{fx}$  is calculated on the base and presented in graphical form in Figure 5.69  $C_{fx}$  for the irregular shape building model for the irregular building models considered in this study. The largest  $C_{fx}$  is of 0.55 for model – G, which is more in magnitude than the other model, while the  $C_{fx}$  is more or less identical for model-F, Model-G for the particular case of  $0^{\circ}$  wind incidence angle. As the wind incidence angle changes the wind  $C_{fx}$  acting on the tall building will also change. When wind incidence angle is  $180^{\circ}$  then the maximum  $C_{fx}$  is observed in case of model-F which is Y shaped model having corner cut into the each limb of Y shape and least  $C_{fx}$  is observed in the case of Y shape model-G which is having corner cut into each limb of Y shape building. The  $C_{fx}$  is more or less identical for the model-G (Y shape having chamfer corner into the each the each limb of Y) and model- H (Y shape having fillet corner into the each limb of Y). The maximum  $C_{fx}$  in case of  $0^{\circ}$  wind is obtained for the model-E which is having no corner modification while the maximum  $c_{fx}$  in case of  $180^{\circ}$  wind is obtained for model- F which is having corner cut into each limb of Y plan shape tall building.



## CHAPTER 6

### Conclusion

The significance of wind induced pressure on tall building having different corner configuration on equal area building is investigated using the numerical simulation. The results are compared with available experimental data as well as with various international standards. The wind incidence angle considered in this study are as  $0^{\circ}$ ,  $15^{\circ}$ ,  $30^{\circ}$ ,  $45^{\circ}$ ,  $75^{\circ}$ ,  $90^{\circ}$ ,  $105^{\circ}$ ,  $120^{\circ}$ ,  $135^{\circ}$ ,  $150^{\circ}$ ,  $165^{\circ}$  and  $180^{\circ}$ . The results on validated models are very similar to the experimental values and different international standards. There is very little difference at some locations from experimental values because of the pressure tapping in the experiment cannot be installed at sharp locations and the values for the pressure in this region are either interpolated or extrapolated. However overall, the pressure contours plotted for various wind incidence angle are same for numerical results and other previous studies done in the same area.

#### 6.1 Pressure evaluation

##### Rectangular model

1. Pressure distribution is symmetrical for the symmetric faces.
2. Windward face is always under the positive pressure while the leeward face and side face is under the influence of negative pressure that is suction.
3. The maximum value of  $C_p$  is observed on the wind ward face while the maximum negative  $C_p$  is spotted on the side faces.
4. The value of  $C_p$  on side face is increasing from the upstream to the downstream direction of wind.
5. Leeward face pressure distribution is increasing from the base to the top of the surface.
6. The pressure on wind ward face is increasing from both sides to the central part of the surface.
7. As the wind incidence angle changes positive pressure is shifted to face-A to face-B.
8. The pressure distribution pattern is changes as the wind incidence angle changes.

### **Rectangular Model having Corner cut**

1. The pressure coefficient is mainly affected by the incident wind direction. The influence is more dominant on the windward face for severe wind incidence angle.
2. Corner cut face on the windward side are subjected to suction that is negative pressure.
3. Pressure distribution on the parallel faces is observed in the identical nature of pressure distribution.
4. The negative pressure is spotted more than the rectangular model having no corner configuration.
5. The maximum pressure is observed at one quarter of the top of the building this is because of the upwash.
6. The minimum negative  $C_p$  found less near the base of the building at up stream windward corner while the maximum  $C_p$  is observed at the top of the building on leeward side of downstream wind.
7. Maximum positive pressure in initially start to increase from  $0^\circ$  wind to  $45^\circ$  wind beyond this  $45^\circ$  pressure distribution start to decrease until  $90^\circ$  wind incidence angle.

### **Rectangular Model having Chamfer cuts**

1. Pressure distribution is changes it is pattern from rectangle without any corner modification to the rectangle have chamfer corner cuts.
2. The maximum positive pressure on windward face is lesser in magnitude with respect to the centre portion of the surface.
3. Generally maximum positive pressure is observed in the mid height of the building model.
4. Symmetrical surfaces are having the same pressure distribution pattern.

### **Rectangular Model having Fillet cuts**

1. Pressure distribution is the nature has a little change in the nature of pressure distribution with respect to the chamfer corner.
2. Variation of the corner configuration among the chamfer and fillet mildly affect the pressure coefficient in both the case of positive pressure and negative pressure.
3. Pressure variation on the fillet corner is increases with respect to chamfer corner configuration in both the cases of wind ward and lee ward surfaces with respect to wind incidence angle.
4. Pressure coefficient at the base of the model is lesser in magnitude in case of wind ward face while maximum at the centre part of the surface and again it is start to decreases at the top most part of the building this is because of the upwash of wind.

### **Y-shape model without any corner configuration**

1. Maximum positive pressure shifted to the wind ward face as the wind incidence angle changes as well as maximum negative pressure is shifted as the pressure is shifting.
2. Suction in maximum on lee wards surfaces.
3. Maximum positive pressure on the wind ward surface is increasing from base of the model to the top of the model as the height of the model is increases.
4. Maximum negative pressure on leeward side is also increasing from the base of the building model to the top of the model.
5. Side faces are having maximum pressure on wind wards side while pressure start to decreases as the wind move form wind ward to leeward side.

### **Y-shape model with corner cut configuration**

1. Corner cut model is very efficient to reduce the wind load because the decrease in wind load is higher for the corner cut model than the other corner configuration.
2. Symmetrical surface has same nature of pressure distribution with more or less equal in magnitude.
3. Maximum positive pressure observed on some faces in the top one third portion it is because of the upwash nature in the top one third portion of the building model
4. Maximum suction is observed on some faces in the bottom one third part near to the base of the building model this is because of the downwash of the wind.

### **Y-shape model with chamfer corner configuration**

1. Pressure on wind ward face is positive in nature this is because of the directly wind is acting on these surfaces while the wind pressure is negative in nature on the leeward surface this is because of the various wind characteristics in the wind flow pattern.
2. Maximum positive pressure is noticed in the central part of the surface while it starts to decrease in the top and bottom of the building model.
3. Chamfered corner model is not much efficient to reduce the pressure on the corner regions as the pressure is significant on these corner surfaces.

### **Y-shape model with fillet corner configuration**

1. Pressure on wind ward is lesser in magnitude than the chamfer corners in the Y-Plan shape model while the maximum pressure is observed in the top part of the building model.
2. The pattern on the pressure distribution on side face, wind ward face and leeward face are more or less of same patterns.
3. Maximum negative pressure is on top part of the side surfaces of the model in the wind ward side where as the minimum negative pressure is on the bottom part of the model in the wind ward side.
4. Pressure starts to decreases as the wind moves from wind ward side to the leeward side of the model.

## **6.2 Force evaluation**

### **Rectangular model**

1. Wind force coefficient in x direction is  $C_{fx}$  this is the across wind force which is drag force.
2.  $C_{fx}$  is maximum in the case of  $15^\circ$  and  $90^\circ$  wind incidence angle.
3.  $C_{fx}$  is minimum when wind incidence angle is  $75^\circ$ .
4.  $C_{fy}$  is the wind force coefficient in the Y-direction and this is because of the along wind force which is lift force.
5.  $C_{fy}$  is maximum in case of  $60^\circ$  wind incidence angle.
6. Lift force is negligible in the comparison of the drag force.
7. Moment in X direction is  $C_{mx}$  which is due to the lift force and maximum for the  $0^\circ$  wind incidence angle.
8. Moment in y- direction is because of the drag force and observed maximum in the case of  $15^\circ$  and  $90^\circ$  wind incidence angle.

### **Rectangular Model having Corner cut**

1. Drag Force is maximum when wind incidence angle was  $0^0$  and  $60^0$  wind.
2. Lift force is almost near to zero for all wind incidence angle but critical in the case of  $30^0$  wind.
3.  $C_{mx}$  is almost negligible while maximum is observed in the case of  $60^0$  wind angle.
4.  $C_{my}$  is maximum and equal in magnitude for the wind incidence angle  $0^0$  and  $60^0$  wind.

### **Rectangular Model having Chamfer cuts**

1. Wind force coefficient in X-direction is varies significantly with wind incidence angle.
2. Lift force is lesser in magnitude in comparison to the wind force coefficient in x-direction.
3. Maximum  $C_{fx}$  is observed in the case of  $45^0$  wind while drag force is reducing beyond  $45^0$  wind.
4. Moment coefficient in x-direction is maximum when wind incidence angle was  $30^0$ .
5. Moment coefficient in y-direction is maximum for  $30^0$  and  $45^0$  wind incidence angle.

### **Rectangular Model having Fillet cuts**

1. Drag force is maximum at  $45^0$  wind.
2. Drag force is start to increase from  $0^0$  to  $45^0$  and beyond the  $45^0$  to  $90^0$  wind drag is decreases.
3. Lift force is more for this model in comparison to other regular shape of rectangular plan shape.
4.  $C_{my}$  is maximum in the case of  $45^0$  wind.

### **Y-shape model without any corner configuration**

1. Drag force is maximum when wind incidence angle was  $0^0$  while minimum drag force is noticed in the case of  $60^0$  wind.
2.  $C_{my}$  is positive for all wind incidence angle.
3.  $C_{mx}$  is initially increases from  $0^0$  to  $30^0$  while negative for  $45^0$  to  $135^0$  wind incidence angle.
4. Lift force is maximum negative for  $30^0$  and  $135^0$  wind incidence angle.

### **Y-shape model with corner cut configuration**

1. Wind force coefficient in x-direction is positive for all wind angles.
2. Moment in y direction is due to the drag force and because of that having same nature as that of the across wind force.
3. Lift force is maximum positive on the case of  $90^0$  wind while maximum negative in the case of  $30^0$  and  $150^0$  wind angle.
4. Maximum moment coefficient in x direction is noticed in the case of  $30^0$  and  $165^0$  wind while maximum negative moment coefficient in x-direction is maximum for  $90^0$  wind incidence angle.

### **Y-shape model with chamfer corner configuration**

1. Effect of wind on lift force is almost negligible in comparison to drag force.
2. Maximum drag is noticed in the case of  $75^0$  wind and across wind force coefficient is positive in nature for all wind incidence angles.
3. Along wind force coefficient is  $C_{fy}$  and found maximum positive in the case of  $90^0$  wind while the maximum negative is observed in the case of  $15^0$  and  $150^0$  wind angle.
4. Maximum moment coefficient in x direction is  $C_{mx}$  for  $90^0$  wind angle.

### **Y-shape model with fillet corner configuration**

1. Effect of wind incidence angle on along wind force coefficient is small.
2.  $C_{fx}$  is maximum in the case of  $60^0$  and  $180^0$  wind incidence angles.
3.  $C_{fy}$  is due to the along wind force and noticed maximum in the case of  $90^0$  wind angle.
4. Along wind force having wind force coefficient in y direction is  $C_{fy}$  and moment in x-direction is  $C_{mx}$ .
5.  $C_{my}$  is positive for all wind incidence angles.

### **6.3 RECOMMENDATIONS TO CODE OF PRACTICE**

The available standards are having the pressure coefficient values for the regular shapes only these study aims to find the pressure coefficient for regular and irregular shape building models. Also the pressure values in the IS 875 (pt-3): 2015 is having values for the normal shape while in this study the effect of corner configuration is investigated which can be included in the code of practice so that the designer can choose the best shape among the various corner configurations.

Based on the present numerical investigation the pressure coefficients and force coefficients are investigated for the various wind incidence angles while the code of practice is having such pressure and force coefficient values for the limited wind incidence angles.

### **6.4 RECOMMENDATIONS FOR FUTURE RESEARCH**

The present thesis is a numerical research work carried out on the models of high-rise buildings of various regular and irregular shape in ANSYS CFX to study the influence of geometrical shapes on wind pressure distribution. However, there still exists vast area in which research is required to be carried out in future. Some of the areas which can be explored are listed below.

1. High-rise buildings with rectangular plan are considered in the present study. Buildings with another plan can also be considered.
2. Regular and Irregular shape having same type of corner configuration are studied in the present study while other than the corner cut, chamfer and fillet can be considered for further study.
3. Four types of roof forms namely domical roof, cylindrical roof, north-light roof and hip roof are considered in the present study. Wind pressure distribution on buildings with other roof forms such as conical and skylight roofs can also be investigated.
4. Present study includes clad buildings with different shape but with no openings on walls. Effects of openings on both internal and external wind pressures on such buildings can also be studied.
5. Effects of interference between two and three buildings of same shape and size can be studied for such shapes.
6. Only values of mean wind pressure coefficients are reported in this thesis. Values of fluctuating components of wind pressures can also be investigated and reported.



## REFERENCES

- [1] ASCE: 7-16(2017), *Minimum Design Loads and Associated Criteria for Buildings and Other Structures*. Structural Engineering Institute of the American Society of Civil Engineering, Reston, no. 7 98. 2017.
- [2] IS: 875 (2015), *Indian Standard design loads (other than earthquake) for buildings and structures-code of practice, part 3(wind loads)*. 2015.
- [3] S. 64 (S&T) 2001, “Explanatory Handbook on Indian Standard Code of practice for design loads ( other than earthquake ) For buildings and structures, Part 3 Wind Loads (IS 875 (PART 3): 1987,” *New Delhi Bur. Indian Stand. New Delhi 110002, 2001.*, pp. 1238–1241, 1995.
- [4] AS/NZS:1170.2(2011), *Structural Design Actions - Part 2: Wind actions*. Standards Australia/Standards New Zealand, Sydney. 2011.
- [5] B. European Committe for Standardization, *EN 1991-1-4 (2005) (English): Eurocode 1: Actions on structures - Part 1-4: General actions - Wind actions*, vol. 1, no. 2005. 2011.
- [6] ETHIOPIAN STANDARD, *ES ISO 4354 (2012) (English): Wind actions on structures*, vol. 2012. 2012.
- [7] Hong Kong Building Department, “Code of Practice on Wind Effects in Hong Kong 2019,” 2019.
- [8] R. Sheng, L. Perret, I. Calmet, F. Demouge, and J. Guilhot, “Wind tunnel study of wind effects on a high-rise building at a scale of 1:300,” *J. Wind Eng. Ind. Aerodyn.*, vol. 174, no. September 2017, pp. 391–403, 2018, doi: 10.1016/j.jweia.2018.01.017.
- [9] X. Sun, H. Liu, N. Su, and Y. Wu, “Investigation on wind tunnel tests of the Kilometer skyscraper,” *Eng. Struct.*, vol. 148, pp. 340–356, 2017, doi: 10.1016/j.engstruct.2017.06.052.
- [10] Y. Li, Q. S. Li, and F. Chen, “Wind tunnel study of wind-induced torques on L-shaped tall buildings,” *J. Wind Eng. Ind. Aerodyn.*, vol. 167, no. July 2018, pp. 41–50, 2017, doi: 10.1016/j.jweia.2017.04.013.
- [11] M. Asghari Mooneghi and R. Kargarmoakhar, “Aerodynamic Mitigation and Shape Optimization of Buildings: Review,” *J. Build. Eng.*, vol. 6, pp. 225–235, 2016, doi: 10.1016/j.job.2016.01.009.
- [12] J. Yi and Q. S. Li, “Wind tunnel and full-scale study of wind effects on a super-tall building,” *J. Fluids Struct.*, vol. 58, pp. 236–253, 2015, doi: 10.1016/j.jfluidstructs.2015.08.005.
- [13] L. Carassale, A. Freda, and M. Marrè-Brunenghi, “Experimental investigation on the aerodynamic behavior of square cylinders with rounded corners,” *J. Fluids Struct.*, vol. 44, pp. 195–204, 2014, doi: 10.1016/j.jfluidstructs.2013.10.010.
- [14] D. K. Kwon and A. Kareem, “Comparative study of major international wind codes and standards for wind effects on tall buildings,” *Eng. Struct.*, vol. 51, pp. 23–35, 2013, doi: 10.1016/j.engstruct.2013.01.008.

- [15] E. K. Bandi, Y. Tamura, A. Yoshida, Y. Chul Kim, and Q. Yang, "Experimental investigation on aerodynamic characteristics of various triangular-section high-rise buildings," *J. Wind Eng. Ind. Aerodyn.*, vol. 122, pp. 60–68, 2013, doi: 10.1016/j.jweia.2013.07.002.
- [16] H. Tanaka, Y. Tamura, K. Ohtake, M. Nakai, and Y. Chul Kim, "Experimental investigation of aerodynamic forces and wind pressures acting on tall buildings with various unconventional configurations," *J. Wind Eng. Ind. Aerodyn.*, vol. 107–108, pp. 179–191, 2012, doi: 10.1016/j.jweia.2012.04.014.
- [17] R. Merrick and G. Bitsuamlak, "Shape Effects on the Wind-Induced Response of High-Rise Buildings," *J. Wind Eng.*, vol. 6, no. 2, pp. 1–18, 2009, [Online]. Available: <http://aerodata.ce.nd.edu/interface/>.
- [18] P. A. Irwin, "Bluff body aerodynamics in wind engineering," *J. Wind Eng. Ind. Aerodyn.*, vol. 96, no. 6–7, pp. 701–712, 2008, doi: 10.1016/j.jweia.2007.06.008.
- [19] H. Kawai, "Effect of corner modifications on aeroelastic instabilities of tall buildings," *J. Wind Eng. Ind. Aerodyn.*, vol. 74–76, pp. 719–729, 1998, doi: 10.1016/S0167-6105(98)00065-8.
- [20] A. Zaki, P. Richards, and R. Sharma, "Analysis of airflow inside a two-sided wind catcher building," *J. Wind Eng. Ind. Aerodyn.*, vol. 190, no. August 2018, pp. 71–82, 2019, doi: 10.1016/j.jweia.2019.04.007.
- [21] K. Miyashita *et al.*, "Wind-induced response of high-rise buildings Effects of corner cuts or openings in square buildings," *J. Wind Eng. Ind. Aerodyn.*, vol. 50, no. C, pp. 319–328, 1993, doi: 10.1016/0167-6105(93)90087-5.
- [22] H. Hayashida and Y. Iwasa, "Aerodynamic shape effects of tall building for vortex induced vibration," *J. Wind Eng. Ind. Aerodyn.*, vol. 33, no. 1–2, pp. 237–242, 1990, doi: 10.1016/0167-6105(90)90039-F.
- [23] K. C. S. Kwok, P. A. Wilhelm, and B. G. Wilkie, "Effect of edge configuration on wind-induced response of tall buildings," *Eng. Struct.*, vol. 10, no. 2, pp. 135–140, 1988, doi: 10.1016/0141-0296(88)90039-9.
- [24] B. Bhattacharyya, S. K. Dalui, and A. K. Ahuja, "Wind induced pressure on 'E' plan shaped tall buildings," *Jordan J. Civ. Eng.*, vol. 8, no. 2, pp. 120–134, 2014.
- [25] B. Bhattacharyya and S. K. Dalui, "Investigation of mean wind pressures on 'E' plan shaped tall building," *Wind Struct. An Int. J.*, vol. 26, no. 2, pp. 99–114, 2018, doi: 10.12989/was.2018.26.2.099.
- [26] A. Zaki, P. Richards, and R. Sharma, "The effect of onset turbulent flows on ventilation with a two-sided rooftop windcatcher," *J. Wind Eng. Ind. Aerodyn.*, vol. 225, no. December 2021, p. 104993, 2022, doi: 10.1016/j.jweia.2022.104993.
- [27] K. C. S. Kwok, "Effect of building shape on wind-induced response of tall building," *J. Wind Eng. Ind. Aerodyn.*, vol. 28, no. 1–3, pp. 381–390, 1988, doi: 10.1016/0167-6105(88)90134-1.
- [28] T. Stathopoulos, "Wind environmental conditions around tall buildings with chamfered corners," *J. Wind Eng. Ind. Aerodyn.*, vol. 21, no. 1, pp. 71–87, 1985, doi: 10.1016/0167-

6105(85)90034-0.

- [29] R. P. Lam and L. C. H. Lam, "Mean Wind Pressure Distribution on a Multistorey Building.," *Proc. Inst. Civ. Eng. (London). Part 1 - Des. Constr.*, vol. 71, no. pt 2, pp. 119–129, 1981, doi: 10.1680/iicep.1981.2143.
- [30] R. Raj and A. K. Ahuja, "Wind Loads on Cross Shape Tall Buildings," *J. Acad. Ind. Res.*, vol. 2, no. 2, pp. 111–113, 2013.
- [31] R. . Lam and L. C. . Lam, "Assessment of wind loading on the claddings of high-rise buildings," no. November, pp. 653–666, 1982.
- [32] R. Jozwiak, J. Kacprzyk, and J. A. Zuranski, "Wind tunnel investigation of interference effects on pressure distribution on a building."
- [33] P. A. Blackmore, "The role of wind tunnel testing in the design of building structures," *Proc. Inst. Civ. Eng. Struct. Build.*, vol. 122, no. 3, pp. 253–265, 1997, doi: 10.1680/istbu.1997.29797.
- [34] J. Blessmann and J. D. Riera, "Wind excitation of neighbouring tall buildings," *J. Wind Eng. Ind. Aerodyn.*, vol. 18, no. 1, pp. 91–103, 1985, doi: 10.1016/0167-6105(85)90076-5.
- [35] J. A. Amin and A. K. Ahuja, "Aerodynamic modifications to the shape of the buildings: A review of the state-of-the-art," *Asian J. Civ. Eng.*, vol. 11, no. 4, pp. 433–450, 2010.
- [36] T. Tamura and T. Miyagi, "The effect of turbulence on aerodynamic forces on a square cylinder with various corner shapes," *J. Wind Eng. Ind. Aerodyn.*, vol. 83, no. 1–3, pp. 135–145, 1999, doi: 10.1016/S0167-6105(99)00067-7.
- [37] S. k. Verma, A. K. Ahuja, and A. D. Padey, "Effects of wind incidence angle on wind pressure distribution," *J. Acadmia Ind. Res.*, vol. 1, no. May, pp. 747–752, 2013.
- [38] A. Sharma, H. Mittal, and A. Gairola, "Mitigation of wind load on tall buildings through aerodynamic modifications: Review," *J. Build. Eng.*, vol. 18, no. September 2017, pp. 180–194, 2018, doi: 10.1016/j.job.2018.03.005.
- [39] H. W. Tieleman, "Strong wind observations in the atmospheric surface layer," *J. Wind Eng. Ind. Aerodyn.*, vol. 96, no. 1, pp. 41–77, 2008, doi: 10.1016/j.jweia.2007.03.003.
- [40] S. Ahmad and K. Kumar, "Effect of geometry on wind pressures on low-rise hip roof buildings Shakeel," *J. Wind Eng. Ind. Aerodyn.*, vol. 90, pp. 755–779, 2002, doi: 10.12989/was.2002.5.6.493.
- [41] E. K. Bandi, H. Tanaka, Y. C. Kim, K. Ohtake, A. Yoshida, and Y. Tamura, "Peak Pressures Acting on Tall Buildings with Various Configurations," *Int. J. High-Rise Build.*, vol. 2, no. 3, pp. 229–244, 2013, doi: 10.21022/IJHRB.2013.2.3.229.
- [42] Y. C. Kim, X. Xu, Q. Yang, and Y. Tamura, "Shape effects on aerodynamic and pedestrian-levelwind characteristics and optimization for tall and super-tall building design," *Int. J. High-Rise Build.*, vol. 8, no. 4, pp. 235–253, 2019, doi: 10.21022/IJHRB.2019.8.4.235.
- [43] P. W. Bearman and T. Morel, "Effect of free stream turbulence on the flow around bluff bodies," *Prog. Aerosp. Sci.*, vol. 20, no. 2–3, pp. 97–123, 1983, doi: 10.1016/0376-

0421(83)90002-7.

- [44] S. K. Verma, K. Kumar, and H. Kaur, "Estimation of Coefficient of Pressure in High Rise Buildings Using Artificial Neural Network," *Int. J. Eng. Res. Appl.*, vol. 4, no. 4, pp. 1–6, 2014.
- [45] Y. Tominaga and M. Shirzadi, "Wind tunnel measurement of three-dimensional turbulent flow structures around a building group: Impact of high-rise buildings on pedestrian wind environment," *Build. Environ.*, vol. 206, no. September, p. 108389, 2021, doi: 10.1016/j.buildenv.2021.108389.
- [46] E. Maruta, M. Kanda, and J. Sato, "Effects on surface roughness for wind pressure on glass and cladding of buildings," *J. Wind Eng. Ind. Aerodyn.*, vol. 74–76, pp. 651–663, 1998, doi: 10.1016/S0167-6105(98)00059-2.
- [47] S. Chakraborty, S. K. Dalui, and A. K. Ahuja, "Experimental investigation of surface pressure on '+' plan shape tall building," *Jordan J. Civ. Eng.*, vol. 8, no. 3, pp. 251–262, 2014.
- [48] Y. C. Kim, Y. Tamura, H. Tanaka, K. Ohtake, E. K. Bandi, and A. Yoshida, "Wind-induced responses of super-tall buildings with various atypical building shapes," *J. Wind Eng. Ind. Aerodyn.*, vol. 133, no. October, pp. 191–199, 2014, doi: 10.1016/j.jweia.2014.06.004.
- [49] J. Allegrini and B. Lopez, "The influence of angular configuration of two buildings on the local wind climate," *J. Wind Eng. Ind. Aerodyn.*, vol. 156, pp. 50–61, 2016, doi: 10.1016/j.jweia.2016.07.008.
- [50] S. K. Nagar, R. Raj, and N. Dev, "Experimental study of wind-induced pressures on tall buildings of different shapes," *Wind Struct. An Int. J.*, vol. 31, no. 5, pp. 441–453, 2020, doi: 10.12989/was.2020.31.5.431.
- [51] P. Thool Kushal, A. Ashok K., and Anupam Chakrabarti, "Effect of interference on Wind loads on Tall buildings Thool," *J. Acadmia Ind. Res.*, vol. 1, no. May, pp. 758–760, 2017.
- [52] S. Pal, R. Raj, and S. Anbukumar, "Comparative study of wind induced mutual interference effects on square and fish-plan shape tall buildings," *Sādhanā*, vol. 46, no. 2, p. 86, Jun. 2021, doi: 10.1007/s12046-021-01592-6.
- [53] S. Ahmad and K. Kumar, "Interference effects on wind loads on low-rise hip roof buildings," *Eng. Struct.*, vol. 23, no. 12, pp. 1577–1589, 2001, doi: 10.1016/S0141-0296(01)00057-8.
- [54] S. K. Nagar, R. Raj, and N. Dev, "Proximity effects between two plus-plan shaped high-rise buildings on mean and RMS pressure coefficients," *Sci. Iran.*, pp. 0–0, Jul. 2021, doi: 10.24200/sci.2021.55928.4484.
- [55] M. Yahyai, K. Kumar, P. Krishna, and P. K. Pande, "Aerodynamic interference in tall rectangular buildings," *J. Wind Eng. Ind. Aerodyn.*, vol. 41, no. 1–3, pp. 859–866, 1992, doi: 10.1016/0167-6105(92)90506-6.
- [56] R. Kar and S. K. Dalui, "Wind interference effect on an octagonal plan shaped tall building due to square plan shaped tall buildings," *Int. J. Adv. Struct. Eng.*, vol. 8, no. 1, pp. 73–86, 2016, doi: 10.1007/s40091-016-0115-z.

- [57] S. Pal and R. Raj, "Evaluation of Wind Induced Interference Effects on Shape Remodeled Tall Buildings," *Arab. J. Sci. Eng.*, no. 0123456789, 2021, doi: 10.1007/s13369-021-05923-x.
- [58] S. Pal, R. Raj, and S. Anbukumar, "Bilateral interference of wind loads induced on duplicate building models of various shapes," *Lat. Am. J. Solids Struct.*, vol. 18, no. 5, 2021, doi: 10.1590/1679-78256595.
- [59] X. F. Yu, Z. N. Xie, J. B. Zhu, and M. Gu, "Interference effects on wind pressure distribution between two high-rise buildings," *J. Wind Eng. Ind. Aerodyn.*, vol. 142, pp. 188–197, 2015, doi: 10.1016/j.jweia.2015.04.008.
- [60] S. Hajra and S. K. Dalui, "Numerical investigation of interference effect on octagonal plan shaped tall buildings," *Jordan J. Civ. Eng.*, vol. 10, no. 4, pp. 462–479, 2016.
- [61] J. A. Amin and A. Ahuja, "Wind-induced mean interference effects between two closed spaced buildings," *KSCE J. Civ. Eng.*, vol. 16, no. 1, pp. 119–131, 2012, doi: 10.1007/s12205-012-1163-y.
- [62] R. Paul and S. K. Dalui, "Wind effects on 'Z' plan-shaped tall building: a case study," *Int. J. Adv. Struct. Eng.*, vol. 8, no. 3, pp. 319–335, 2016, doi: 10.1007/s40091-016-0134-9.
- [63] P. Sanyal and S. K. Dalui, "Effects of side ratio for 'Y' plan shaped tall building under wind load," *Build. Simul.*, no. November, 2020, doi: 10.1007/s12273-020-0731-1.
- [64] A. K. Bairagi and S. K. Dalui, "Wind environment around the setback building models," *Build. Simul.*, vol. 14, no. 5, pp. 1525–1541, 2021, doi: 10.1007/s12273-020-0758-3.
- [65] Y. Tominaga, A. Mochida, S. Murakami, and S. Sawaki, "Comparison of various revised k- $\epsilon$  models and LES applied to flow around a high-rise building model with 1:1:2 shape placed within the surface boundary layer," *J. Wind Eng. Ind. Aerodyn.*, vol. 96, no. 4, pp. 389–411, 2008, doi: 10.1016/j.jweia.2008.01.004.
- [66] T. L. Chan, G. Dong, C. W. Leung, C. S. Cheung, and W. T. Hung, "Validation of a two-dimensional pollutant dispersion model in an isolated street canyon," *Atmos. Environ.*, vol. 36, no. 5, pp. 861–872, 2002, doi: 10.1016/S1352-2310(01)00490-3.
- [67] P. K. Goyal, S. Kumari, S. Singh, R. K. Saroj, R. K. Meena, and R. Raj, "Numerical Study of Wind Loads on Y Plan-Shaped Tall Building Using CFD," *Civ. Eng. J.*, vol. 8, no. 02, pp. 263–277, 2022.
- [68] P. Sanyal and S. K. Dalui, "Comparison of aerodynamic coefficients of various types of Y-plan-shaped tall buildings," *Asian J. Civ. Eng.*, vol. 21, no. 7, pp. 1109–1127, 2020, doi: 10.1007/s42107-020-00265-9.
- [69] A. K. Bairagi and S. K. Dalui, "Estimation of Wind Load on Stepped Tall Building Using CFD Simulation," *Iran. J. Sci. Technol. - Trans. Civ. Eng.*, vol. 45, no. 2, pp. 707–727, 2021, doi: 10.1007/s40996-020-00535-1.
- [70] R. Raj, T. Rana, T. Anchalia, and U. Khola, "Numerical study of wind excited action on H Plan-shaped tall building," *Int. J. Emerg. Technol.*, vol. 11, no. 3, pp. 591–605, 2020.
- [71] P. Sanyal and S. K. Dalui, "Effects of courtyard and opening on a rectangular plan shaped tall building under wind load," *Int. J. Adv. Struct. Eng.*, vol. 10, no. 2, pp. 169–188, 2018,

doi: 10.1007/s40091-018-0190-4.

- [72] J. A. Amin and A. K. Ahuja, "Characteristics of wind forces and responses of rectangular tall buildings," *Int. J. Adv. Struct. Eng.*, vol. 6, no. 3, pp. 1–14, 2014, doi: 10.1007/s40091-014-0066-1.
- [73] N. Gaur and R. Raj, "Aerodynamic mitigation by corner modification on square model under wind loads employing CFD and wind tunnel," *Ain Shams Eng. J.*, p. 283, 2021, doi: <https://doi.org/10.1016/j.asej.2021.06.007>.
- [74] P. Sanyal and S. K. Dalui, "Effect of corner modifications on Y' plan shaped tall building under wind load," *Wind Struct. An Int. J.*, vol. 30, no. 3, pp. 245–260, 2020, doi: 10.12989/was.2020.30.3.245.
- [75] R. Raj, S. Jha, S. Singh, and S. Choudhary, "Response analysis of plus shaped tall building with different bracing systems under wind load," *Int. J. Adv. Res. Eng. Technol.*, vol. 11, no. 3, pp. 371–380, 2020, doi: 10.34218/IJARET.11.3.2020.032.
- [76] J. A. Amin and A. K. Ahuja, "Effects of Side Ratio on Wind-Induced Pressure Distribution on Rectangular Buildings," *J. Struct.*, vol. 2013, pp. 1–12, 2013, doi: 10.1155/2013/176739.
- [77] R. Raj, A. Sharma, and S. Chauhan, "Response of Square and Plus Shaped Buildings on Varying Wind Loads," pp. 206–215, 2018, doi: 10.1061/9780784482032.022.
- [78] A. Kumar and R. Raj, "CFD Study of Flow Characteristics and Pressure Distribution on Re-Entrant Wing Faces of L-Shape Buildings," *Civ. Eng. Archit.*, vol. 10, no. 1, pp. 289–304, 2022, doi: 10.13189/cea.2022.100125.
- [79] M. S. Thordal, J. C. Bennetsen, S. Capra, A. K. Kragh, and H. H. H. Koss, "Towards a standard CFD setup for wind load assessment of high-rise buildings: Part 2 – Blind test of chamfered and rounded corner high-rise buildings," *J. Wind Eng. Ind. Aerodyn.*, vol. 205, no. August, p. 104282, 2020, doi: 10.1016/j.jweia.2020.104282.
- [80] L. Shao, S. S. Hons, C. Mcibse, and I. C. Ward, "Building methods pressure coefficients : of three-dimensional," *Build. Serv. Eng. Res. Technol.*, vol. 13, no. 2, pp. 107–111, 1992, doi: <https://doi.org/10.1177/2F014362449201300208>.
- [81] J. Franke *et al.*, "RECOMMENDATIONS ON THE USE OF CFD IN WIND ENGINEERING," *6th UK Wind Eng. Soc. Conf.*, no. January, 2004.
- [82] M. S. Thordal, J. C. Bennetsen, and H. H. H. Koss, "Review for practical application of CFD for the determination of wind load on high-rise buildings," *J. Wind Eng. Ind. Aerodyn.*, vol. 186, no. October 2018, pp. 155–168, 2019, doi: 10.1016/j.jweia.2018.12.019.
- [83] F. Q. Meng, B. J. He, J. Zhu, D. X. Zhao, A. Darko, and Z. Q. Zhao, "Sensitivity analysis of wind pressure coefficients on CAARC standard tall buildings in CFD simulations," *J. Build. Eng.*, vol. 16, no. October 2017, pp. 146–158, 2018, doi: 10.1016/j.jobbe.2018.01.004.
- [84] D. Kumar and S. K. Dalui, "Effect of internal angles between limbs of cross plan shaped tall building under wind load," *Wind Struct. An Int. J.*, vol. 24, no. 2, pp. 95–118, 2017, doi: 10.12989/was.2017.24.2.095.

- [85] Y. Tominaga, "Flow around a high-rise building using steady and unsteady RANS CFD: Effect of large-scale fluctuations on the velocity statistics," *J. Wind Eng. Ind. Aerodyn.*, vol. 142, pp. 93–103, 2015, doi: 10.1016/j.jweia.2015.03.013.
- [86] M. Keerthana and P. Harikrishna, "Application of CFD for assessment of galloping stability of rectangular and H-sections," *J. Sci. Ind. Res. (India)*, vol. 72, no. 7, pp. 419–427, 2013.
- [87] Mahmoud Yahyai, D. Amir Saedi, M. Ziaei, and M. M. Seyed, "Wind effect on milad tower using computational fluid dynamics Mahmoud," *Struct. Des. Tall Spec. Build.*, vol. 20, no. July 2014, pp. 177–189, 2011, doi: 10.1002/tal.
- [88] A. K. Dagnew and G. T. Bitsuamlak, "Computational evaluation of wind loads on buildings: A review," *Wind Struct. An Int. J.*, vol. 16, no. 6, pp. 629–660, 2013, doi: 10.12989/was.2013.16.6.629.
- [89] J. Revuz, D. M. Hargreaves, and J. S. Owen, "On the domain size for the steady-state CFD modelling of a tall building," *Wind Struct. An Int. J.*, vol. 15, no. 4, pp. 313–329, 2012, doi: 10.12989/was.2012.15.4.313.
- [90] B. Blocken, J. Carmeliet, and T. Stathopoulos, "CFD evaluation of wind speed conditions in passages between parallel buildings-effect of wall-function roughness modifications for the atmospheric boundary layer flow," *J. Wind Eng. Ind. Aerodyn.*, vol. 95, no. 9–11, pp. 941–962, 2007, doi: 10.1016/j.jweia.2007.01.013.
- [91] M. G. Gomes, A. Moret Rodrigues, and P. Mendes, "Experimental and numerical study of wind pressures on irregular-plan shapes," *J. Wind Eng. Ind. Aerodyn.*, vol. 93, no. 10, pp. 741–756, 2005, doi: 10.1016/j.jweia.2005.08.008.
- [92] S. Huang, Q. S. Li, and S. Xu, "Numerical evaluation of wind effects on a tall steel building by CFD," *J. Constr. Steel Res.*, vol. 63, no. 5, pp. 612–627, 2007, doi: 10.1016/j.jcsr.2006.06.033.
- [93] A. Okajima, D. Yi, A. Sakuda, and T. Nakano, "Numerical study of blockage effects on aerodynamic characteristics of an oscillating rectangular cylinder," *J. Wind Eng. Ind. Aerodyn.*, vol. 67–68, pp. 91–102, 1997, doi: 10.1016/S0167-6105(97)00065-2.
- [94] T. Stathopoulos, "Computational wind engineering: Past achievements and future challenges," *J. Wind Eng. Ind. Aerodyn.*, vol. 67–68, pp. 509–532, 1997, doi: 10.1016/S0167-6105(97)00097-4.
- [95] M. Tsuchiya, S. Murakami, A. Mochida, K. Kondo, and Y. Ishida, "Development of a new k- $\epsilon$  model for flow and pressure fields around bluff body," *J. Wind Eng. Ind. Aerodyn.*, vol. 67–68, pp. 169–182, 1997, doi: 10.1016/S0167-6105(97)00071-8.
- [96] D. H. Yu and A. Kareem, "Numerical simulation of flow around rectangular prism," *J. Wind Eng. Ind. Aerodyn.*, vol. 67–68, pp. 195–208, 1997, doi: 10.1016/S0167-6105(97)00073-1.
- [97] Y. Meng, M. Matsui, and K. Hibi, "A numerical study of the wind field in a typhoon boundary layer," *J. Wind Eng. Ind. Aerodyn.*, vol. 67–68, pp. 437–448, 1997, doi: 10.1016/S0167-6105(97)00092-5.
- [98] T. Uchida and Y. Ohya, "A numerical study of stably stratified flows over a two-

- dimensional hill - Part I. Free-slip condition on the ground,” *J. Wind Eng. Ind. Aerodyn.*, vol. 67–68, pp. 493–506, 1997, doi: 10.1016/S0167-6105(97)00096-2.
- [99] I. P. Castro, I. R. Cowan, and A. G. Robins, “Numerical considerations for simulations of flow and dispersion around buildings I,” *J. Wind Eng. Ind. Aerodyn.*, vol. 67 & 68, no. 4, pp. 535–545, 1997, doi: 10.1061/(ASCE)0893-1321(1999)12:4(145).
- [100] J. He and C. C. S. Song, “A numerical study of wind flow around the TTU building and the roof corner vortex,” *J. Wind Eng. Ind. Aerodyn.*, vol. 67–68, pp. 547–558, 1997, doi: 10.1016/S0167-6105(97)00099-8.
- [101] S. Kawamoto, “Improved turbulence models for estimation of wind loading,” *J. Wind Eng. Ind. Aerodyn.*, vol. 67–68, pp. 589–599, 1997, doi: 10.1016/S0167-6105(97)00102-5.
- [102] P. J. Richards and R. P. Hoxey, “Appropriate boundary conditions for computational wind engineering models using the k- $\epsilon$  turbulence model,” *J. Wind Eng. Ind. Aerodyn.*, vol. 46–47, no. C, pp. 145–153, 1993, doi: 10.1016/0167-6105(93)90124-7.
- [103] S. Lee and B. Bienkiewicz, “Large-eddy simulation of wind effects on bluff bodies using the finite element method,” *J. Wind Eng. Ind. Aerodyn.*, vol. 67–68, pp. 601–609, 1997, doi: 10.1016/S0167-6105(97)00103-7.
- [104] R. P. Selvam, “Computation of pressures on Texas Tech University building using large eddy simulation,” *J. Wind Eng. Ind. Aerodyn.*, vol. 67–68, pp. 647–657, 1997, doi: 10.1016/S0167-6105(97)00107-4.
- [105] T. Wiik and E. W. M. Hansen, “The assessment of wind loads on roof overhang of low-rise buildings,” *J. Wind Eng. Ind. Aerodyn.*, vol. 67–68, pp. 687–696, 1997, doi: 10.1016/S0167-6105(97)00110-4.
- [106] A. P. Robertson, R. P. Hoxey, P. J. Richards, and W. A. Ferguson, “Full-scale measurements and computational predictions of wind loads on free-standing walls,” *J. Wind Eng. Ind. Aerodyn.*, vol. 67–68, pp. 639–646, 1997, doi: 10.1016/S0167-6105(96)00106-7.
- [107] B. M. Leitl, P. Kastner-Klein, M. Rau, and R. N. Meroney, “Concentration and flow distributions in the vicinity of U-shaped buildings: Wind-tunnel and computational data,” *J. Wind Eng. Ind. Aerodyn.*, vol. 67–68, pp. 745–755, 1997, doi: 10.1016/S0167-6105(97)00115-3.
- [108] G. W. Alminhana, A. L. Braun, and A. M. Loredou-Souza, “A numerical study on the aerodynamic performance of building cross-sections using corner modifications,” *Lat. Am. J. Solids Struct.*, vol. 15, no. 7, 2018, doi: 10.1590/1679-78254871.
- [109] S. Chakraborty, S. K. Dalui, and A. K. Ahuja, “Wind load on irregular plan shaped tall building - A case study,” *Wind Struct. An Int. J.*, vol. 19, no. 1, pp. 59–73, 2014, doi: 10.12989/was.2014.19.1.059.
- [110] R. P. Hoxey, A. P. Robertson, B. Basara, and B. A. Younis, “Geometric parameters that affect wind loads on low-rise buildings: full-scale and CFD experiments,” *J. Wind Eng. Ind. Aerodyn.*, vol. 50, no. C, pp. 243–252, 1993, doi: 10.1016/0167-6105(93)90079-4.
- [111] B. S. Chauhan and A. K. Ahuja, “RESPONSE OF TALL BUILDING SUBJECTED TO WIND LOADS UNDER INTERFERENCE,” vol. 11, no. 2, pp. 156–163, 2020.



- [112] A. K. Bairagi and S. K. Dalui, "Distribution of Wind Pressure Around Different Shape Tall Building," no. July, pp. 31–38, 2020, doi: 10.1007/978-981-15-3254-2\_4.
- [113] A. Zhang, C. Gao, and L. Zhang, "Numerical simulation of the wind field around different building arrangements," *J. Wind Eng. Ind. Aerodyn.*, vol. 93, no. 12, pp. 891–904, 2005, doi: 10.1016/j.jweia.2005.09.001.
- [114] J. Tang, Y. M. Xie, and P. Felicetti, "Conceptual design of buildings subjected to wind load by using topology optimization," *Wind Struct. An Int. J.*, vol. 18, no. 1, pp. 21–35, 2014, doi: 10.12989/was.2014.18.1.021.
- [115] A. K. Bairagi and S. K. Dalui, "Spectral Density at Roof of Setback Tall Building Due to Time Variant Wind Load," no. July, pp. 21–29, 2020, doi: 10.1007/978-981-15-3254-2\_3.
- [116] K. Shahab, "Comparative Study of Aerodynamic Coefficients of Prismatic and Twisted Tall Buildings with various Cross Sections using CFD," *J. Inst. Eng. Ser. C*, 2021, doi: 10.1007/s40032-021-00694-8.
- [117] A. de Macêdo Wahrhaftig and M. A. da Silva, "Using computational fluid dynamics to improve the drag coefficient estimates for tall buildings under wind loading," *Struct. Des. Tall Spec. Build.*, vol. 27, no. 3, pp. 1–12, 2018, doi: 10.1002/tal.1442.
- [118] Y. Abu Zidan, P. Mendis, and T. Gunawardena, "Optimising the computational domain size in CFD simulations of tall buildings," *Heliyon*.
- [119] A. K. Bairagi and S. K. Dalui, "Comparison of Pressure Coefficient Between Square and Setback Comparison of Pressure Coefficient Between Square," no. December, 2018.
- [120] X. Zheng, H. Montazeri, and B. Blocken, "CFD analysis of the impact of geometrical characteristics of building balconies on near-façade wind flow and surface pressure," *Build. Environ.*, vol. 200, no. December 2020, p. 107904, 2021, doi: 10.1016/j.buildenv.2021.107904.
- [121] S. Li, R. Han, P. Gua, X. Wang, and Y. Chu, "Wind tunnel tests of aerodynamic interference effects on two icedt," *Fluid Dyn. Res. Accept.*, no. December 2016, pp. 11–14, 2018.
- [122] Y. Li, Q. Song, C. Li, X. Huang, and Y. Zhang, "Reduction of wind loads on rectangular tall buildings with different taper ratios," *J. Build. Eng.*, vol. 45, no. November 2021, p. 103588, 2021, doi: 10.1016/j.job.2021.103588.
- [123] A. K. Bairagi and S. K. Dalui, "Aerodynamic effects on setback tall building using CFD simulation," *Int. J. Mech. Prod. Eng. Res. Dev.*, no. June, pp. 413–420, 2018, [Online]. Available: [www.tjprc.org](http://www.tjprc.org).
- [124] X. Zheng, H. Montazeri, and B. Blocken, "CFD simulations of wind flow and mean surface pressure for buildings with balconies: Comparison of RANS and LES," *Build. Environ.*, vol. 173, p. 106747, 2020, doi: 10.1016/j.buildenv.2020.106747.
- [125] Y. G. Li, J. H. Yan, Y. Li, C. X. Xiao, and J. X. Ma, "Wind tunnel study of wind effects on 90° helical and square tall buildings: A comparative study," *J. Build. Eng.*, vol. 42, no. August, 2021, doi: 10.1016/j.job.2021.103068.
- [126] N. Jendzelovsky and R. Antal, "CFD and experimental study of wind pressure distribution

on the high-rise building in the shape of an equilateral acute triangle,” *Fluids*, vol. 6, no. 2, 2021, doi: 10.3390/fluids6020081.

- [127] M. Shirzadeh Gerami and H. Eimani Kalehsar, “Numerical investigation of interference effects on the critical wind velocity of tall buildings,” *Structures*, vol. 30, no. January, pp. 239–252, 2021, doi: 10.1016/j.istruc.2021.01.013.
- [128] B. Rocchio, A. Mariotti, and M. V. Salvetti, “Flow around a 5:1 rectangular cylinder: Effects of upstream-edge rounding,” *J. Wind Eng. Ind. Aerodyn.*, vol. 204, no. July, p. 104237, 2020, doi: 10.1016/j.jweia.2020.104237.
- [129] S. Du, M. Li, and Y. Yang, “Effects of turbulence integral scales on characteristics of fluctuating wind pressures,” *J. Wind Eng. Ind. Aerodyn.*, vol. 204, no. September 2019, p. 104245, 2020, doi: 10.1016/j.jweia.2020.104245.
- [130] S. J. Daniels, I. P. Castro, and Z. T. Xie, “Numerical analysis of freestream turbulence effects on the vortex-induced vibrations of a rectangular cylinder,” *J. Wind Eng. Ind. Aerodyn.*, vol. 153, pp. 13–25, 2016, doi: 10.1016/j.jweia.2016.03.007.
- [131] X. Tian, M. C. Ong, J. Yang, and D. Myrhaug, “Unsteady RANS simulations of flow around rectangular cylinders with different aspect ratios,” *Ocean Eng.*, vol. 58, pp. 208–216, 2013, doi: 10.1016/j.oceaneng.2012.10.013.
- [132] N. Ikegaya, S. Morishige, Y. Matsukura, N. Onishi, and A. Hagishima, “Experimental study on the interaction between turbulent boundary layer and wake behind various types of two-dimensional cylinders,” *J. Wind Eng. Ind. Aerodyn.*, vol. 204, no. September 2019, p. 104250, 2020, doi: 10.1016/j.jweia.2020.104250.
- [133] Q. Yang, Z. Liu, Y. Hui, and Z. Li, “Modification of aerodynamic force characteristics on high-rise buildings with arrangement of vertical plates,” *J. Wind Eng. Ind. Aerodyn.*, vol. 200, no. August 2019, p. 104155, 2020, doi: 10.1016/j.jweia.2020.104155.
- [134] M. Lorite-Díez, J. I. Jiménez-González, L. Pastur, O. Cadot, and C. Martínez-Bazán, “Drag reduction on a three-dimensional blunt body with different rear cavities under cross-wind conditions,” *J. Wind Eng. Ind. Aerodyn.*, vol. 200, no. November 2019, 2020, doi: 10.1016/j.jweia.2020.104145.
- [135] Z. Li, G. Huang, X. Chen, Y. Zhou, and Q. Yang, “Wind-resistant design and equivalent static wind load of base-isolated tall building: A case study,” *Eng. Struct.*, vol. 212, no. September 2019, p. 110533, 2020, doi: 10.1016/j.engstruct.2020.110533.
- [136] H. Kataoka, Y. Ono, and K. Enoki, “Applications and prospects of CFD for wind engineering fields,” *J. Wind Eng. Ind. Aerodyn.*, vol. 205, no. August, 2020, doi: 10.1016/j.jweia.2020.104310.
- [137] T. Stathopoulos and H. Alrawashdeh, “Wind loads on buildings: A code of practice perspective,” *J. Wind Eng. Ind. Aerodyn.*, vol. 206, no. August, p. 104338, 2020, doi: 10.1016/j.jweia.2020.104338.
- [138] W. Cui and L. Caracoglia, “Examination of experimental variability in HFFB testing of a tall building under multi-directional winds,” *J. Wind Eng. Ind. Aerodyn.*, vol. 171, no. September, pp. 34–49, 2017, doi: 10.1016/j.jweia.2017.09.001.
- [139] H. Hangan *et al.*, “Novel techniques in wind engineering,” *J. Wind Eng. Ind. Aerodyn.*,

vol. 171, no. June, pp. 12–33, 2017, doi: 10.1016/j.jweia.2017.09.010.

- [140] F. Hou and P. P. Sarkar, “A time-domain method for predicting wind-induced buffeting response of tall buildings,” *J. Wind Eng. Ind. Aerodyn.*, vol. 182, no. June, pp. 61–71, 2018, doi: 10.1016/j.jweia.2018.09.013.
- [141] S. Ahmad, M. Muzzammil, and I. Zaheer, “Numerical prediction of wind loads on low buildings,” *Int. J. Eng. Sci. Technol.*, vol. 3, no. 5, pp. 59–72, 2011, doi: 10.4314/ijest.v3i5.68567.
- [142] K. T. Tse, G. Hu, J. Song, H. S. Park, and B. Kim, “Effects of corner modifications on wind loads and local pressures on walls of tall buildings,” *Build. Simul.*, vol. 14, no. 4, pp. 1109–1126, 2021, doi: 10.1007/s12273-020-0705-3.
- [143] S. Bhattacharya and S. K. Dalui, “Effect of tuned mass damper in wind-induced response of ‘V’ plan-shaped tall building,” *Struct. Des. Tall Spec. Build.*, 2022.
- [144] Q. Yong, J. Chen, and M. Gu, “Aerodynamic interference effects of a proposed taller high-rise building on wind pressures on existing tall buildings,” *Struct. Des. Tall Spec. Build.*, 2019.
- [145] S. Behera, D. Ghosh, A. K. Mittal, Y. Tamura, and W. Kim, “The effect of plan ratios on wind interference of two tall buildings,” *Struct. Des. Tall Spec. Build.*, vol. 29, no. 1, pp. 2–11, 2020, doi: 10.1002/tal.1680.
- [146] T. Deng, J. Y. Fu, Z. N. Xie, Y. L. Pi, and B. Q. Shi, “An experimental study on the wind pressure distribution of tapered super high-rise buildings,” *Struct. Des. Tall Spec. Build.*, vol. 27, no. 13, pp. 1–11, 2018, doi: 10.1002/tal.1483.
- [147] J. Jiménez, “The contributions of A.N. Kolmogorov to the theory of turbulence,” *Arbor*, vol. 178, no. 704, pp. 589–606, 2004, doi: <http://dx.doi.org/10.3989/arbor.2004.i704.550>.
- [148] I. B. Celik, U. Ghia, P. J. Roache, C. J. Freitas, H. Coleman, and P. E. Raad, “Procedure for estimation and reporting of uncertainty due to discretization in CFD applications,” *J. Fluids Eng. Trans. ASME*, vol. 130, no. 7, pp. 0780011–0780014, 2008, doi: 10.1115/1.2960953.
- [149] J. F. Derakhshandeh and M. M. Alam, “Flow structures around rectangular cylinder in the vicinity of a wall,” *Wind Struct. An Int. J.*, vol. 26, no. 5, pp. 293–304, 2018, doi: 10.12989/was.2018.26.5.293.
- [150] R. Raj, “EFFECTS OF CROSS-SECTIONAL SHAPES ON RESPONSE OF TALL BUILDINGS UNDER WIND LOADS,” iit Roorkee, 2015.
- [151] E. Simiu and D. Yeo, *Wind effects on structures*, Fourth Edi. John Wiley & Sons Ltd, 2019.

## LIST OF PUBLICATIONS

### JOURNALS SCI/SCIE

1. Rahul Kumar Meena, Ritu Raj and S. Anbukumar. Effect of wind load on irregular shape tall buildings having different corner configuration. *Sādhanā* 47, 126 (2022). <https://doi.org/10.1007/s12046-022-01895-2>
2. Rahul Kumar Meena, Ritu Raj, S. Anbukumar, "Wind Excited Action around Tall Building Having Different Corner Configurations", *Advances in Civil Engineering*, vol. 2022, Article ID 1529416, 17 pages, 2022. <https://doi.org/10.1155/2022/1529416>
3. Supriya Pal, Rahul Kumar Meena, Ritu Raj, S. Anbukumar (2021), "Wind Tunnel Study of a Fish-Plan Shape Model under Different Isolated Wind Incidences", *Wind and Structures* November 2021, Vol. 33, No. 5 pp 353-366 <https://doi.org/10.12989/was.2021.33.5.353> .
4. Astha Verma, Rahul Kumar Meena, Hrishikesh Dubey, Ritu Raj, S. Anbukumar, "Wind Effects on Rectangular and Triaxial Symmetrical Tall Building Having Equal Area and Height", *Complexity*, vol. 2022, Article ID 4815623, 20 pages, 2022. <https://doi.org/10.1155/2022/4815623>

### SCOPUS Indexed

1. Pradeep K Goyal, Sonia Kumari, Shivani Singh, Rahul Kumar Saroj, Rahul Kumar Meena, and Ritu Raj "Numerical Study of Wind Loads on "Y" Plan Shaped Tall Building Using CFD" February 2022, <https://doi.org/10.28991/CEJ-2022-08-2-06> Civil Engineering Journal
2. Ark Rukhaiyar, Bhagya Jayant, Kunal Dahiya, Rahul Kumar Meena and Ritu Raj (2022), "CFD simulations for evaluating the wind effects on high-rise buildings having varying cross-sectional shape", *Journal of Structural Fire Engineering*, <https://doi.org/10.1108/JSFE-04-2022-0016>
3. Devesh Kasana, Dhawal Tayal, Dhruv Choudhary, S. Anbukumar, Ritu Raj and Rahul Kumar Meena, Evaluation of aerodynamic effects on a tall building with various cross-section shapes having equal area," *Force in Mechanics*, Volume 9, 100134 <https://doi.org/10.1016/j.finmec.2022.100134>

## **Book Chapter**

1. Rahul Kumar Meena, Ritu Raj and S. Anbukumar (2022). Numerical Investigation of Wind Load on Side Ratio of High-Rise Buildings. In: Gupta, A.K., Shukla, S.K., Azamathulla, H. (eds) Advances in Construction Materials and Sustainable Environment. Lecture Notes in Civil Engineering, vol 196. Springer, Singapore. [https://doi.org/10.1007/978-981-16-6557-8\\_76](https://doi.org/10.1007/978-981-16-6557-8_76)
2. Rahul Kumar Meena, Ritu Raj and S. Anbukumar. (2023). Comparative Study of Wind Loads on Tall Buildings of Different Shapes. In: Sharma, D., Roy, S. (eds) Emerging Trends in Energy Conversion and Thermo-Fluid Systems. Lecture Notes in Mechanical Engineering. Springer, Singapore. [https://doi.org/10.1007/978-981-19-3410-0\\_18](https://doi.org/10.1007/978-981-19-3410-0_18)

## **Conference Published/Accepted**

1. Rahul Kumar Meena, Ritu Raj, and S. Anbukumar , "Estimation of air flow around the tall buildings of different shapes", AIP Conference Proceedings 2520, 030020 (2022) <https://doi.org/10.1063/5.0102942>
2. Bhagya Jayant, Rahul Kumar Meena, Aastha Singh, Agyeya Mishra, Navneet Dalal, Rajvir Singh, Shailendra Kumar and Ritu Raj “Evaluation of various Beams Using Computational Tools” accepted for publication in AIP Conference proceeding
3. Payal Devi, Abhishek Prakash Paswan, Hemant Gautam, Ritu Raj and Rahul Kumar Meena, “Aerodynamic Study of Various Tall Building Under Wind Load,” accepted for publication in AIP Conference proceeding
4. Devesh Kasana, Dhawal Tayal, Dhruv Choudhary, S. Anbukumar, Ritu Raj and Rahul Kumar Meena, “Impact of wind effect on high rise building having varying cross sections,” accepted for publication in AIP Conference proceeding

## **Conference Presented**

1. Presented the paper titled, “Analysis of pavements design using fly ash in subgrade soil” into 4th International Conference on Recent Scientific and Technological Trends
2. Presented the paper titled “Analysis of Wind on Different Shape of High- Rise Structure” into International Conference on Sustainable Development and Recent Trends in Civil

Engineering held during 4th – 5th January, 2022 organized by Dr. Akhilesh Das Gupta Institute of Technology & Management and won the Best Paper Award.

3. Presented the paper titled “Evaluation of Various Beams using Computational Tools” into 2nd International Conference on Futuristic and Sustainable Aspects in Engineering and Technology held during 24th-26th December, 2021 organized by GLA university
4. Presented the paper titled “Comparative study of wind load on Tall Buildings of Different Shapes” into International Conference on Energy Conversion and Thermo Fluid system held during 19th – 20th November, 2021 organized by Malviya National Institute of Technology, Jaipur.
5. Presented the paper titled “Estimation of Airflow around the tall buildings of different shapes” into international conference held during 24th to 25th September, 2021 organized by Musaliar College of Engineering and Technology.
6. Presented the paper titled “Numerical Investigation of wind Load on side ratio of High-Rise Buildings” into international conference held during 3rd – 4th June, 2021 organized by Jaypee University of Information Technology.
7. Presented the paper titled “Numerical Investigation of wind Load on side ratio of High-Rise Buildings” into international conference held during 3rd – 4th June, 2021 organized by Jaypee University of Information Technology.

### **Conference Proceeding**

1. Payal Devi, Rahul Kumar Meena and Ritu Raj “Response of tall building with different side ratio under the effect of wind load” in 3rd international online conference on Emerging Trends in Muti-Disciplinary Research “ETMDR-2022” ISBN 987-93-5593-524-3
2. Rahul Kumar Meena, Ritu Raj and S. Anbukumar “Analysis of wind on different shape of high rise structure” in international e- conference on sustainable development and recent trends in civil engineering “ETMDR-2022” ISBN 978-93-5593-431-4

